Report of Activities 2025

Manitoba

REPORT OF ACTIVITIES
2025

Manitoba Business, Mining, Trade and Job Creation
Manitoba Geological Survey

Manitoba

When using information from this publication in other publications or presentations, due acknowledgment should be given to the Manitoba Geological Survey. The following reference format is recommended:

Manitoba Geological Survey 2025: Report of Activities 2025; Manitoba Business, Mining, Trade and Job Creation, Manitoba Geological Survey, 212 p.

Published by:
Manitoba Business, Mining, Trade and Job Creation
Manitoba Geological Survey
360–1395 Ellice Avenue
Winnipeg, Manitoba
R3G 3P2 Canada
Telephone: 1-800-223-5215 (General Enquiry)
204-945-6569 (Publication Sales)
Fax: 204-945-8427
Email: minesinfo@gov.mb.ca
Website: manitoba.ca/minerals

ISBN: 978-0-7711-1657-5

This publication is available to download free of charge at manitoba.ca/minerals

Front cover photo:
MGS geologist Eric Yang taking notes while on field work in the Bird River area.

REPORT OF ACTIVITIES 2025

Minister's Message

I am pleased to present the 2025 Annual Report of Activities for the Manitoba Geological Survey (MGS). This year's report highlights key geoscience research and activities, including twenty-two reports and ten data repositories. Significant wildfires hampered access to some field sites, but MGS staff continued the geoscience work that is vital to understanding Manitoba's geological history and critical mineral future.

The research and data collection conducted by MGS are essential to the exploration and development of Manitoba's mineral resource potential. A key factor in mineral development is the availability of data that are reliable and relevant to both existing and emerging markets. Reliable, nonbiased, geoscience data sets help to increase efficiency, transparency, and accountability during development. Responsible and ethical mineral development attracts investment, furthers reconciliation through partnerships and meaningful consultation with Indigenous communities, and creates good jobs in mining and adjacent economic sectors.

Global trading markets saw a shift in 2025. Canada is forging new international trade alliances, a significant component of which will involve the provision of minerals needed for low-carbon energy, security, defense, and medical technologies. With thirty of thirty-four minerals on Canada's 2024 identified critical minerals list, Manitoba is well-positioned to play a substantial role in the production and delivery of these resources. This changing trade landscape provides Manitoba with an opportunity to further develop its mineral sector as part of a resilient and sustainable economy.

Manitoba's mining history includes extraction of soft and hard minerals, more recent additions such and potash, and exploration to identify potential reserves of critical minerals. Manitoba's Critical Minerals Strategy was developed to position Manitoba as a leader in sustainable critical mineral development by attracting investment, advancing Indigenous partnerships, and supporting the clean energy transition to help bring these resources to market. MGS is fulfilling the geoscience role in the critical minerals value chain not only by searching for deposits via new exploration efforts, but also through re-examination of legacy samples using innovative methods.

Through presentations of geoscience studies at global conferences and fostering partnerships with the public, industry, and academic groups, MGS staff are ensuring that knowledge and awareness of Manitoba's minerals and geoscience are shared both locally and internationally.

Manitoba is building on its mining history and looking to the future. The projects described in this report are products of the expertise, innovation, and diligence of MGS staff. As you read and appreciate the results of their work, please join me in congratulating MGS on a most successful year.

Original signed by

Honourable Jamie Moses

Manitoba Business, Mining, Trade and Job Creation

Rapport d'activités 2025

Message du ministre

J'ai le plaisir de présenter le Rapport d'activités annuel 2025 de la Direction des services géologiques du Manitoba. Le rapport de cette année met en lumière les principales recherches et activités en géosciences, y compris 22 rapports et dix dépôts de données. D'importants feux de forêt ont limité l'accès à certains sites, mais le personnel de la Direction des services géologiques a poursuivi les travaux de géosciences qui sont essentiels pour comprendre l'histoire géologique du Manitoba et l'avenir des minéraux critiques.

La recherche et la collecte de données menées par la Direction des services géologiques jouent un rôle primordial dans l'exploration et la mise en valeur du potentiel en ressources minérales du Manitoba. La disponibilité de données fiables et pertinentes pour les marchés établis et les marchés émergents constitue un facteur clé de la mise en valeur des minéraux. Des ensembles de données géoscientifiques fiables et objectifs renforcent l'efficacité, la transparence et la responsabilisation au cours de la mise en valeur. Une mise en valeur des minéraux responsable et éthique attire les investissements, favorise la réconciliation dans le cadre de partenariats et de consultations constructives avec les communautés autochtones, et crée de bons emplois dans l'industrie minière et les secteurs économiques connexes.

Les marchés commerciaux mondiaux ont connu une transition en 2025. Le Canada noue actuellement de nouvelles alliances commerciales internationales, dont une composante majeure consistera à fournir les minéraux nécessaires à l'énergie à faibles émissions de carbone, à la sécurité, à la défense et aux technologies médicales. En possession de 30 des 34 minéraux figurant sur la liste canadienne des minéraux critiques de 2024, le Manitoba est bien placé pour jouer un rôle important dans la production et la distribution de ces ressources. L'évolution du contexte commercial offre au Manitoba l'occasion de continuer de développer son industrie minière dans le cadre d'une économie résiliente et durable.

L'histoire minière du Manitoba comprend l'extraction de minéraux tendres et durs, des ajouts plus récents comme la potasse et les activités d'exploration pour repérer les réserves potentielles de minéraux critiques. La stratégie sur les minéraux critiques du Manitoba a été élaborée pour positionner le Manitoba comme chef de file en matière d'exploitation durable des minéraux critiques, en attirant des investissements, en améliorant les partenariats avec les Autochtones et en appuyant la transition vers une énergie propre pour faciliter la mise en marché de ces ressources. La Direction des services géologiques assume le rôle géoscientifique dans la chaîne de valeur des minéraux critiques, non seulement en recherchant des gisements au moyen de nouveaux efforts d'exploration, mais également en réexaminant les échantillons existants au moyen de méthodes novatrices.

Grâce à des présentations d'études en géosciences dans des conférences internationales et à l'établissement de partenariats avec le public, l'industrie et le milieu universitaire, le personnel de la Direction des services géologiques assure des activités de sensibilisation et d'information sur les minéraux et les géosciences au Manitoba, à l'échelle locale ainsi qu'internationale.

Le Manitoba mise sur son histoire minière et se tourne vers l'avenir. Les projets décrits dans le présent rapport sont le fruit de l'expertise, de l'innovation et de la rigueur du personnel de la Direction des services géologiques du Manitoba. Avant de découvrir et d'apprécier les résultats de son travail, veuillez vous joindre à moi pour féliciter la Direction des services géologiques du Manitoba pour une année particulièrement fructueuse.

Original signé par

Monsieur Jamie Moses

Ministre du d'Affaires, Mines, Commerce et la Création d'emplois

Foreword

On behalf of the Manitoba Geological Survey (MGS), I am privileged to present the Report of Activities 2025—the annual peer-reviewed volume of geoscience project results by the MGS and its partners.

This year's field season was impacted by the wildfires that affect the Province causing most projects to pivot, be cancelled or re-scheduled. Sadly, the fires destroyed our Baker's Narrows Core facility, and it is now permanently closed. On a positive note, The Pas core library roof was upgraded to metal as part of the core facilities ongoing maintenance, and the Thompson core facility relocated to an enclosed building, ensuring long-term protection of our archived core from the elements.

Our participation in national and international events continued with oral and poster presentations. The MGS attended and exhibited at GeoConvention 2025 in Calgary, where staff presented in three sessions and had five abstracts accepted. The MGS also presented at the Williston Basin Petroleum Conference in Regina, during which staff gave presentations on critical minerals in crude oil and our new water chemistry dataset. Additionally, MGS staff attended the Dr. Don Kent core workshop, which allowed for the viewing of equivalent stratigraphy to that of Manitoba, Saskatchewan, and North Dakota. The Geological Association of Canada (GAC), in concert with the Mineralogical Association of Canada (MAC) annual conference was held in Ottawa this year, during which the MGS gave presentations on Quaternary geology, Manitoba's alkaline and carbonatite magmatism, and the impact of the Target Geoscience Initiative program in growing the geological knowledge of Manitoba.

This year, the MGS hosted a day of technical presentations on the fringes of the Central Canadian Mineral Exploration Convention (CCMEC) 2025. Manitoba Spotlight showcased our work and provided an opportunity for the public to meet our team and gain firsthand accounts of our contributions to Manitoba's geological knowledge.

The 2025 issue of the Report of activities features 22 articles that cover a diverse range of themes and geographic locations, including field observations, drill core logging, ongoing compilation, updates to our mineral deposit datasets, and the potential for pore space resources. The MGS continued to participate in multi-jurisdictional partnerships and collaborations with several universities, the Geological Survey of Canada, as well as with industry stakeholders and independent consultants. We look forward to ongoing collaborations with all the stakeholders to complement our capacity to produce world-class geoscience investigations. This year's Report of Activities continues to highlight the critical mineral potential of Manitoba. The Duperow Formation revealed some interesting finds, including the discovery that the mudstone intervals in the formation may be contributors to lithium in basin brines. Helium and hydrocarbons have been identified consistently throughout the Stony Mountain Formation of the Interlake Group. The Survey's drones acquired photogrammetry in support of geological field mapping in recently burnt forested terrains. The data gathered shows the potential of photogrammetry to contribute to more efficient geological bedrock mapping approaches.

The magnetotelluric resistivity data will serve as regional reconnaissance tools for mineral exploration in the Province. The MGS will use this data to produce a 3D model of the lithosphere, and conductive anomalies will be interpreted within the framework of mineral systems. I encourage you to read more about the Precambrian section activities. The section's ability to publish during a difficult field season is a testament to their resilience and dedication to providing geological information to Manitobans.

There are nine Data Repository Items published with this volume resulting from continuing work on pore space commodities, drill core logging, and field-based ice-flow indicators from the multidisciplinary study in southeastern Manitoba.

Our staffing saw some changes:

- Heather Patterson joined us as a Geoscience and Research Analyst with the Resource Center Section.
- James Macdonald joined us as the Structural Geologist in the Precambrian Section.
- Ethan Ralph joined us as our new Expeditor and Field Support person with the Core libraries and Labs Section.
- Mark Pacey retired after 30 years with the government. His contribution included mentoring youth and colleagues, resource planning, mapping, policy analysis and many other responsibilities.
- Jerrold Rentz, Aggregate Geologist took another position elsewhere within the government.

The production of the Report of Activities and other MGS publications is a collective achievement made possible by the dedicated efforts of our entire team. I want to extend a special mention to Colin Epp, Paul Belanger, and Ethan Ralph for their outstanding field and expediting support, as well as their meticulous maintenance of our equipment throughout the year. Their efforts formed the backbone of our field program, providing clients with access to our core library facilities. I acknowledge Greg Keller and his team of GIS specialists and geologists for their support with our GIS products and services. I also want to recognize Delaney O'Hara for her leadership in designing the report's layout and in meeting our publication deadlines and peer review requirements — special thanks to Bob Davie and his team from R&D Technical for their outstanding professional technical editing services. I sincerely thank every member of the MGS team for their contributions to this year's publication.

Tafa Kennedy, Ph.D., P.Geo.

Director, Manitoba Geological Survey

Avant-propos

Au nom de la Direction des services géologiques du Manitoba (la Direction), j'ai l'honneur de présenter le rapport d'activités de 2025, un recueil annuel évalué par les pairs compilant les résultats de projets géoscientifiques exécutés par la Direction et ses partenaires.

La saison de travaux de prospection de cette année a été perturbée par les incendies échappés qui ont touché la province, entraînant la modification, l'annulation ou le report de la plupart des projets. Malheureusement, les incendies ont détruit notre installation de stockage de carottes de Bakers Narrows, qui est désormais définitivement fermée. Sur une note positive, le toit de la carothèque de The Pas a été remplacé par un toit métallique dans le cadre de l'entretien continu des installations de stockage de carottes, et l'installation de stockage de carottes de Thompson a été transférée dans un bâtiment à construction fermée, assurant ainsi la protection à long terme de nos carottes stockées contre les intempéries.

Notre participation à des événements nationaux et internationaux s'est poursuivie avec des présentations orales et des présentations par affiches. La Direction a participé et exposé à la GéoConvention 2025 à Calgary, où son personnel a présenté trois séances et vu cinq résumés acceptés. La Direction a également fait une présentation lors de la Williston Basin Petroleum Conference à Regina, au cours de laquelle le personnel a fait des exposés sur les minéraux critiques présents dans le pétrole brut et sur notre nouvel ensemble de données sur la chimie de l'eau. De plus, le personnel de la Direction a participé à l'atelier de M. Don Kent, Ph. D., qui a permis d'observer une stratigraphie équivalente à celle du Manitoba, de la Saskatchewan et du Dakota du Nord. La conférence annuelle de l'Association géologique du Canada, en collaboration avec l'Association minéralogique du Canada, s'est tenue cette année à Ottawa. Au cours de cette conférence, la Direction a présenté des exposés sur la géologie du Quaternaire, le magmatisme alcalin et carbonatitique du Manitoba, ainsi que l'incidence du programme de l'Initiative géoscientifique ciblée sur l'enrichissement des connaissances géologiques du Manitoba.

Cette année, la Direction a organisé une journée de présentations techniques en marge du Central Canadian Mineral Exploration Convention 2025. Manitoba Spotlight a présenté notre travail et a permis au public de rencontrer notre équipe et d'obtenir des témoignages directs sur notre contribution aux connaissances géologiques du Manitoba.

Le rapport d'activités de 2025 comprend 22 articles qui couvrent un large éventail de thèmes et de zones géographiques, notamment des observations sur le terrain, la diagraphie de forage, la compilation en cours, les mises à jour de nos ensembles de données sur les gisements minéraux et le potentiel des ressources en espace poral. La Direction a continué de participer à des partenariats et à des collaborations pluri-gouvernementaux avec plusieurs universités, la Commission géologique du Canada, ainsi qu'avec des parties prenantes de l'industrie et des consultants indépendants. Nous nous réjouissons à l'idée de collaborer de façon continue avec tous les intervenants pour renforcer notre capacité de produire des études géoscientifiques de calibre mondial. Le rapport d'activités de cette année continue de mettre en évidence le potentiel en minéraux critiques du Manitoba. La formation de Duperow a révélé des découvertes intéressantes, notamment le fait que les intervalles de mudstone dans la formation pourraient contribuer à la présence de lithium dans les saumures de bassin. De l'hélium et des hydrocarbures ont été identifiés de manière constante dans toute la formation de Stony Mountain du groupe d'Interlake. Les drones de la Direction ont acquis des données photogrammétriques afin de faciliter la cartographie géologique sur le terrain dans les zones forestières récemment brûlées. Les données recueillies montrent le potentiel de la photogrammétrie pour contribuer à des approches plus efficaces de cartographie géologique du substrat rocheux.

Les données de résistivité magnétotellurique serviront d'outils de reconnaissance régionale pour l'exploration minière dans la province. La Direction utilisera ces données pour produire un modèle 3D de la lithosphère, et les anomalies conductrices seront interprétées dans le cadre des systèmes minéraux. Je vous encourage à vous renseigner davantage sur les activités de la section du Précambrien. La capacité de la section à publier pendant une saison difficile sur le terrain témoigne de sa résilience et de son dévouement à fournir des renseignements géologiques aux Manitobains.

Neuf éléments d'entrepôt de données sont publiés dans ce volume, résultat des travaux continus sur les substances utiles contenues dans l'espace poral, la diagraphie de forage et les marques d'écoulement glaciaire sur le terrain issues de l'étude multidisciplinaire menée dans le sud-est du Manitoba.

Notre personnel a connu quelques changements :

- Heather Patterson nous a rejoints en tant qu'analyste en géosciences et recherche au sein de la section du Centre de ressources.
- James Macdonald nous a rejoints en tant que géologue structuraliste au sein de la section du Précambrien.
- Ethan Ralph nous a rejoints en tant que nouvel agent d'ordonnancement et de soutien sur le terrain au sein de la section des carothèques et des laboratoires.
- Mark Pacey a pris sa retraite après 30 ans de service au gouvernement. Sa contribution comprenait le mentorat des jeunes et de ses collègues, la planification des ressources, la cartographie, l'analyse des politiques et de nombreuses autres responsabilités.
- Jerrold Rentz, géologue spécialisé dans les agrégats, a accepté un autre poste au sein du gouvernement.

La production du rapport d'activités et d'autres publications de la Direction est une réalisation collective rendue possible grâce aux efforts dévoués de toute notre équipe. Je tiens à remercier tout particulièrement Colin Epp, Paul Belanger et Ethan Ralph pour leur soutien exceptionnel sur le terrain et leur rapidité d'exécution, ainsi que pour l'entretien méticuleux de notre équipement tout au long de l'année. Leurs efforts ont

constitué l'épine dorsale de notre programme sur le terrain et ont permis aux clients d'avoir accès à nos installations de stockage de carottes de forage. Je souhaite remercier Greg Keller et son équipe de spécialistes et de géologues du système d'information géographique (SIG) de leur soutien à l'égard de nos produits et services SIG. Je tiens également à remercier Delaney O'Hara pour son leadership dans la conception de la mise en page du rapport et pour avoir respecté nos délais de publication et nos exigences en matière d'évaluation par les pairs. Je remercie tout particulièrement Bob Davie et son équipe de R&D Technical pour leurs services de révision technique professionnels exceptionnels. Je remercie sincèrement chacun des membres de l'équipe de la Direction de leur contribution à la publication de cette année.

La directrice des services géologiques du Manitoba,
Tafa Kennedy, Ph.D., P.Geo.

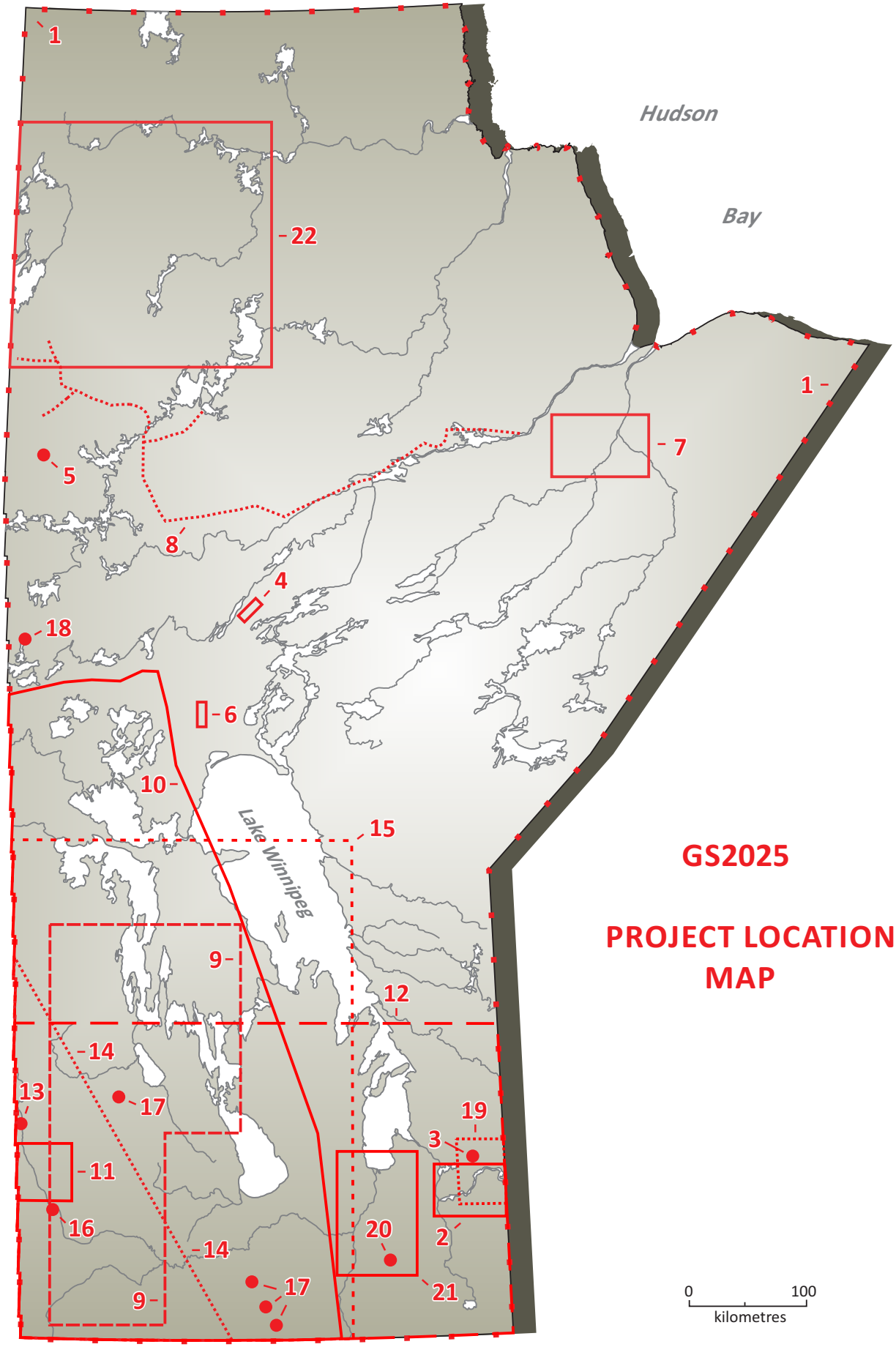

GS2025

PROJECT LOCATION MAP

Table of Contents

PRECAMBRIAN

PHANEROZOIC

QUATERNARY

PUBLICATIONS

GS2025-1

Progress report on the Manitoba Mineral Deposits Database

by M.L. Rinne

Summary

Ongoing updates to the Manitoba Mineral Deposits Database have resulted in significant improvements to mineral-occurrence data across the province. Changes since 2024 include the addition of new occurrence data across parts of the Superior province, the consolidation or deletion of several redundant and irrelevant entries, and the addition of a simplified commodities-group category, allowing for a provincial-scale breakdown of occurrences, primarily by commodity type. The latest version of the Mineral Deposits Database includes approximately 17 000 occurrences, with location data, and is provided in GeoFile 5-2025 published by the Manitoba Geological Survey.

In Brief:

- The Mineral Deposits Database contains data regarding mineral occurrences, including mine sites, in Manitoba
- Recent updates to the database include thousands of fixes, deletions, and additions of new mineral occurrence data across the Superior province
- The 2025 release contains new fields allowing for a province-scale breakdown of occurrences by commodity type

Citation:
Rinne, M.L. 2025: Progress report on the Manitoba Mineral Deposits Database; in Report of Activities 2025, Manitoba Business, Mining, Trade and Job Creation, Manitoba Geological Survey, p. 1–6.

Introduction

A mineral occurrence is a concentration of a commodity or mineral of scientific or economic interest (Cox and Singer, 1986). Where mineral occurrences are of sufficient size or grade to be mined (or potentially mined), they are termed mineral deposits. The Mineral Deposits Database (MDD) is Manitoba's principal data repository for bedrock-hosted mineral occurrences. It also serves as a partial record of other geological findings relating to past-producing brine wells, glaciolacustrine clay and peat quarries, impact craters and helium in natural gas. The occurrence data in the MDD include site locations, selected geochemical analyses, descriptions of deposits (including mines and occurrences with resource estimates), and other mineral findings reported in industry and government sources. Alongside other geoscience datasets such as bedrock geology maps, comprehensive mineral-occurrence data are critical for informing mineral-potential evaluations, exploration strategies and evidence-based land-use planning or resource-management decisions.

Updates to the MDD have been ongoing since 2020 and are described in past annual reports, beginning in 2020 (e.g., Rinne, 2020; 2024a). In this report, changes made to the MDD since the release of GeoFile5-2024 (Rinne, 2024b) in November 2024 are described. Much work remains to be done to clean and populate the database, particularly across the Flin Flon–Snow Lake region and the Thompson Nickel belt. However, for the first time since updates began in 2020, the mineral-occurrence data are now sufficiently organized to allow for province-wide depictions of mineral occurrences by commodity and, to some extent, by relative degree of economic importance (Rinne, 2025).

Summary of 2025 updates

Since last year's update, further georeferencing work has led to the addition of approximately 900 mineral-occurrence records, mostly across parts of the Superior province, based on data collected from geochemistry results and mineral findings reported in nonconfidential assessment reports prepared for industry. Several new occurrences were added, using data from company websites and other public sources, along with new information, such as updated resource estimates, added for existing records.

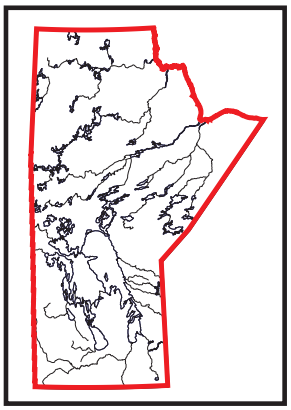

Approximately 2900 existing occurrence records were deleted or merged with other records, contributing to a total of 6050 records marked for deletion since updates began in 2020. Nearly all of the deletions apply to results that were later found to be redundant or duplicated in a combination of Mineral Inventory Card records (a database of earlier analogue records), past MDD records (Conley et al., 2009) and assessment report data. Most of the occurrences marked for deletion in the past year relate to multiple occurrences of the same commodity in the same drillhole and many of those duplicated results were due to drillhole identifications that were inconsistently recorded across multiple sources. While there may be some value in retaining several geochemistry results from the same drillhole, the intended process in the MDD updates, as outlined in Rinne (2021), is to record for each drillhole only the highest recorded value for each commodity.

Also in 2024, continued review of past MDD records compiled by Conley et al. (2009) resulted in a further 240 occurrences being marked for deletion—and many others downgraded to the 'discretion-

ary occurrence' category—after determining that they do not meet the occurrence criteria listed in Rinne (2021). Most of these deleted occurrences from the 2009 version of the MDD relate to findings of minor disseminated pyrite or pyrrhotite in rocks for which there are insufficient geochemical data or that lack other indications of mineralization.

Location errors were corrected for hundreds of existing occurrences derived from many sources, including some significant errors relating to quarries and historical mines, such as the Moose Horn mine, which was incorrectly recorded as occurring at the community of Moosehorn in mine location data collected by the Mines Branch decades ago. Several thousand minor corrections (some identified through user feedback) were applied to existing records in other fields, particularly in the 'Comments/occurrence description' and 'Drillhole ID' fields.

The 'Sample medium' field has been expanded to include: subsurface bedrock, surface outcrop, boulder, sediment (panned), lake sediment, till, glaciolacustrine clay (in the case of four clay quarries recorded in the Mineral Inventory Cards), beach clast, peat (in the case of three peat quarries recorded in the Mineral Inventory Cards) and natural gas well (relating only to helium occurrences in natural gas). The MDD is not designed or intended to provide an inventory of petroleum or natural gas resources, nor does it currently reflect all records pertaining to quarries in Manitoba. Sample-medium information has also been added to many of the earlier occurrence records and work continues to populate this field for future updates.

The 'Mineral deposit model' field has been further populated and now includes 25 categories. A deposit model—intended to follow, to the extent possible, the classification scheme of Hofstra et al. (2021)—has now been assigned to all of the active and most of the historical mine sites in Manitoba, along with most of the larger or more important occurrences with resource estimates. The mineral-deposit models were assigned on the basis of geological setting, hostrocks and ore-mineral associations. As in 2024, the deposit-model field will remain blank in the majority of cases that lack the context or detailed information needed to inform a genetic deposit model.

A simplified 'Commodities group' field has been added and populated to allow for a rough breakdown of known mineral occurrences by commodity or, in some cases, by rock type at the provincial scale (Figures GS2025-1-1 to -3). Although past versions of the MDD (including Conley et al., 2009) contain fields relating to commodity types and deposit types, the information entered in these fields did not allow for this level of commodity-specific breakdown. Furthermore, versions prior to 2009 did not consistently distinguish deposits (i.e., occurrences with resource estimates, historical mines and active mines, as shown in Figure GS2025-1-1) from smaller or less-documented occurrences (i.e., occurrences and discretionary occurrences, shown alongside selected quarry records in Figures GS2025-1-2, -3).

In these preliminary commodity-group classifications, an occurrence is classified as primarily gold ('Au [±Ag, Cu, Zn, Pb, W, Bi, Te]'), where Au (ppm) exceeds 2 x (Cu+Zn[%]). Among the occurrences that do not meet this requirement, but that contain >0.5 ppm Au, most are classified as primarily base-metal occurrences ('Cu, Zn, or Pb [±Fe, Au, Ag]'). Alternatively, users can opt to ignore the preliminary 'Commodities group' field, or test different classifications using the geochemical data columns in GeoFile5-2025 (Rinne, 2025).

Depending on the intended application or the commodity of interest, users may prefer to further subdivide mineral occurrences in the MDD based on other information, such as by selected geochemical data columns. For example, the 'Li, Ta, Cs, Rb, Sn, Be, or related pegmatites' group is a wide-ranging category; most of the pegmatite occurrences assigned to this group have sufficient information to indicate that they are not simple pegmatites, but not enough to further classify into NYF- or LCT-type pegmatites (either enriched in niobium, yttrium and fluorine or in lithium, cesium and tantalum, respectively). However, some occurrences contain enough mineralogical or geochemical data to allow for further classification.

Economic considerations

The ongoing expansion of, and improvements to, the MDD provide a far more comprehensive picture of the spatial distribution of various mineral commodities across Manitoba. The mineral-occurrence data shared in GeoFile5-2025 (Rinne, 2025) are directly applicable to mineral-potential assessments and related land-use decisions; they can be used to inform mineral exploration strategies targeting specific areas or commodities, to identify regions of under-recognized mineral potential, or to support long-term mineral development and related infrastructure planning in partnership with First Nations communities.

Acknowledgments

The author thanks J. Janssens, who continues to provide expert assistance with many aspects of the Mineral Deposits Database updates, particularly in georeferencing a backlog of new occurrence data derived from assessment reports. The author also thanks D. O'Hara for her contribution to the formatting and publication of this volume along with GeoFile5-2025; X.M. Yang and J. Macdonald for their helpful peer review; and external users, including H. Sawatzky, for their help in identifying errors in the 2024 database.

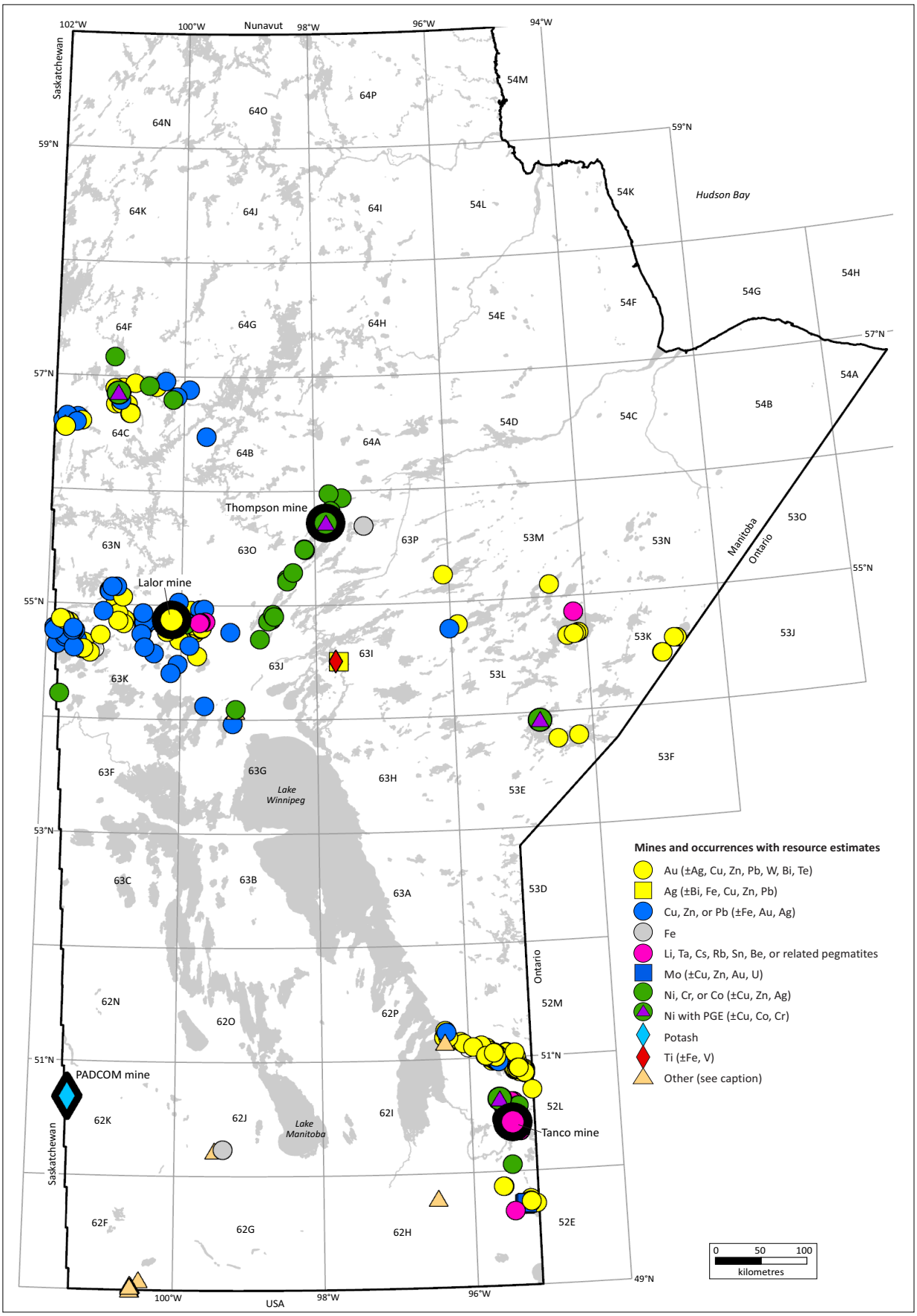

Figure GS2025-1-1

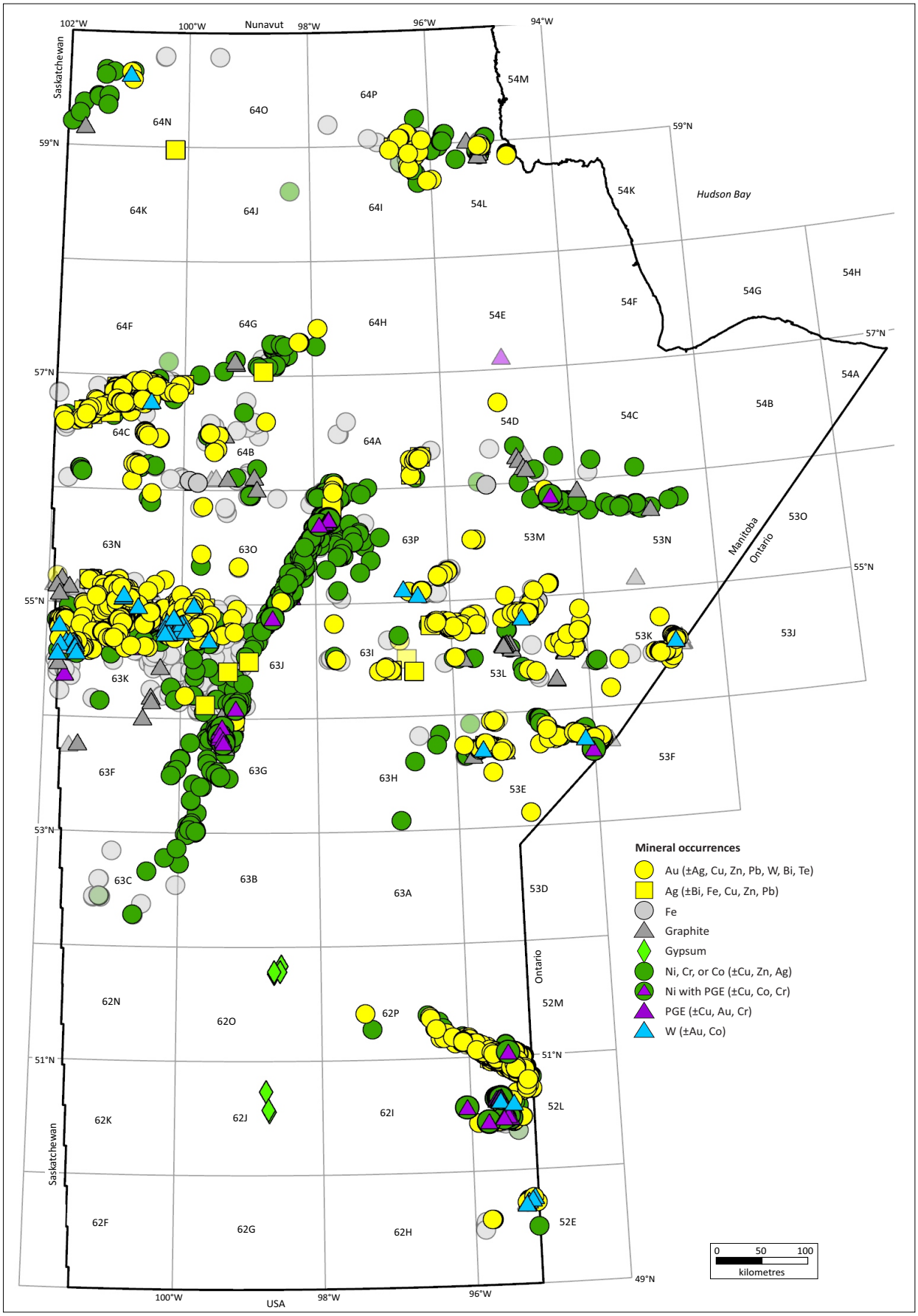

Figure GS2025-1-2

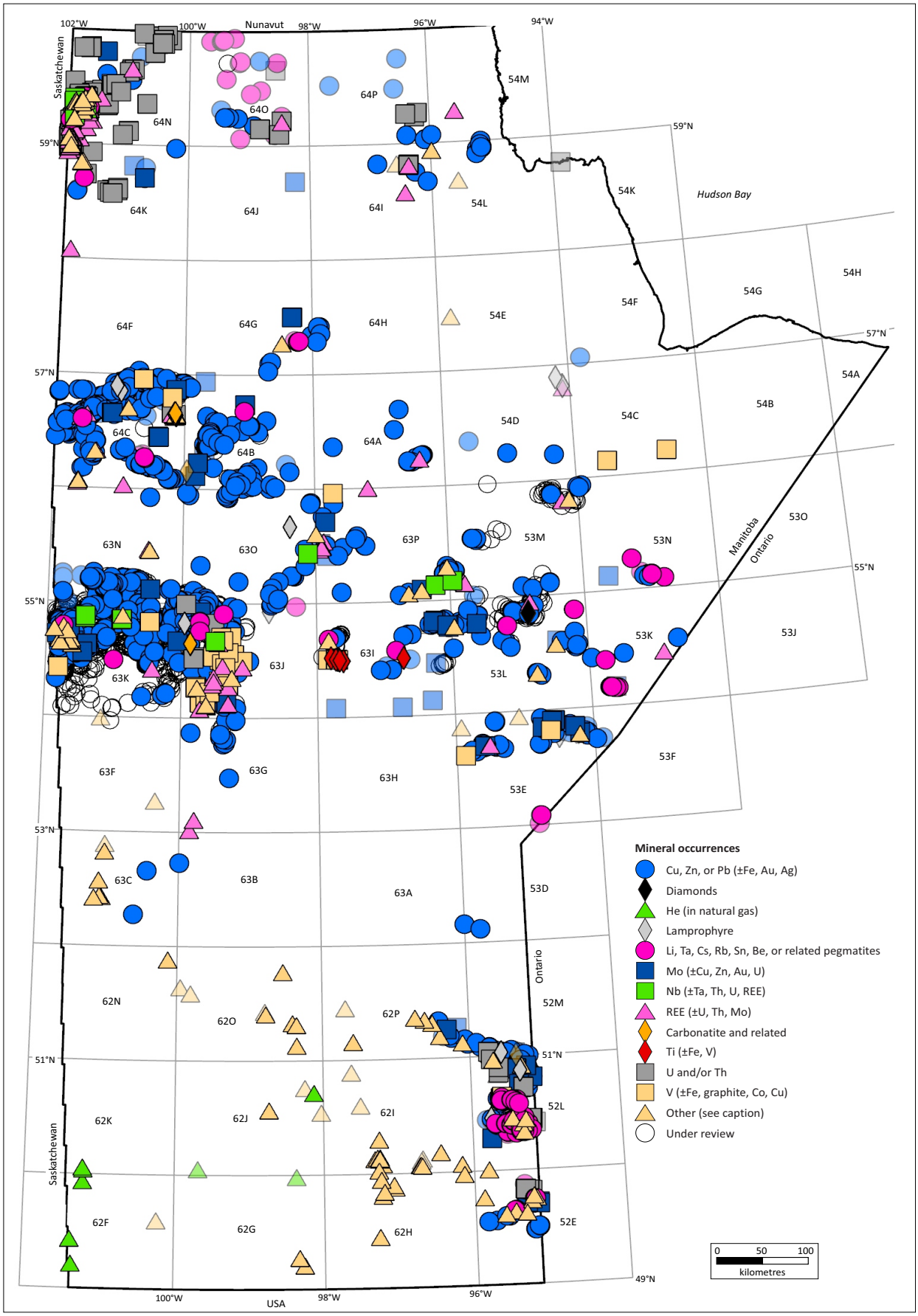

Figure GS2025-1-3

Figures

Figure GS2025-1-1: *Map of Manitoba, showing only active mines (labeled symbols with thick black outlines), historical mines and mineral occurrences with resource estimates in the 2025 version of the Mineral Deposits Database (Rinne, 2025). Occurrences classified as 'Other' are: historical coal mines in NTS area 62F; a past-producing NaCl brine well in 62J; and selected locations relating to high-purity silica sand deposits of the Winnipeg Formation in 62P and 62H.*

Figure GS2025-1-2: *Map of Manitoba, showing mineral occurrences (excluding mines and larger occurrences) including Au, Ni, platinum-group element (PGE) and other commodities listed in the map legend. Occurrences classified as discretionary occurrences (mostly tentative or unconfirmed findings) are indicated with semitransparent symbols and relate mostly to drillcore intersections of elevated iron or graphite concentrations, with uncertain (or not yet determined) total thickness of the mineralized interval. Water bodies are omitted for clarity. The gypsum occurrences are quarries based mostly on previously compiled Mineral Inventory Cards (an earlier analogue archive); note that the Mineral Deposits Database (Rinne, 2025) does not yet contain all quarry-related records in Manitoba.*

Figure GS2025-1-3: *Map of Manitoba, showing mineral occurrences (excluding mines and larger occurrences) including Cu, Zn, Li, rare-earth elements (REE), Ti, V and other commodities listed in the map legend. Occurrences classified as discretionary occurrences in the Mineral Deposits Database (Rinne, 2025) are indicated with semitransparent symbols. Water bodies are omitted for clarity. Some of the REE occurrences are from carbonatite samples with insufficient sample information; partial overlap between carbonatite occurrences and the REE commodities group may be resolved as more sample information is gathered in future updates. Occurrences classified as 'Other' are: a series of commodities including P, Ga, Ge and Hf that are broadly associated with REE-, Mo- and U-enriched samples across parts of NTS areas 64K and 64N; findings of elevated Ga, Ge and Zr concentrations associated with REE-enriched samples from the Eden Lake carbonatite complex in 64C; quarries including limestone, clays and peat across much of NTS 62; and many other findings of elevated Mn, Bi, Sb, Tl and other less common commodities. The 'Other' category also includes some findings that are more significant from an academic rather than economic perspective, such as impact craters (two confirmed and one tentative), gemstone-quality minerals and amber clasts. For more details regarding each occurrence, see GeoFile5-2025 (Rinne, 2025).*

References

Conley, G.G., Heine, T.H., Prouse, D.E. and Leskiw, P.D. 2009: Mineral Deposits Database; Manitoba Science, Technology, Energy and Mines, Manitoba Geological Survey, URL <https://manitoba.ca/iem/geo/gis/databases.html> [October 2024].

Cox, D.P. and Singer, D.A. (ed.) 1986: Mineral deposit models; U.S. Geological Survey Bulletin 1693, 379 p., URL <https://doi.org/10.3133/b1693>.

Hofstra, A., Lisitsin, V., Corriveau, L., Paradis, S., Peter, J., Lauzière, K., Lawley, C., Gadd, M., Pilote, J.-L., Honsberger, I., Bastrakov, E., Champion, D., Czarnota, K., Doublier, M., Huston, D., Raymond, O., VanDerWielen, S., Emsbo, P., Granitto, M. and Kreiner, D. 2021: Deposit classification scheme for the Critical Minerals Mapping Initiative Global Geochemical Database: U.S. Geological Survey, Open-File Report 2021–1049, 60 p.

Rinne, M.L. 2020: Progress report on updates to the Manitoba Mineral Deposits Database, east-central Manitoba (NTS 53E, F); *in* Report of Activities 2020, Manitoba Agriculture and Resource Development, Manitoba Geological Survey, p. 9–12.

Rinne, M.L. 2021: Updates to the Manitoba Mineral Deposits Database, east-central and northwestern Manitoba (NTS 53E, F, 64J, K, N, O); *in* Report of Activities 2021, Manitoba Agriculture and Resource Development, Manitoba Geological Survey, p. 1–7, URL <https://manitoba.ca/iem/geo/field/roa21pdfs/GS2021-1.pdf> [September 2025].

Rinne, M.L. 2024a: Progress report on the Manitoba Mineral Deposits Database; *in* Report of Activities 2024, Manitoba Economic Development, Investment, Trade and Natural Resources, Manitoba Geological Survey, p. 1–3.

Rinne, M.L. 2024b: Updates to the Manitoba Mineral Deposits Database; Manitoba Economic Development, Investment, Trade and Natural Resources, Manitoba Geological Survey, GeoFile 5-2024, Microsoft® Excel file®

Rinne, M.L. 2025: Updates to the Manitoba Mineral Deposits Database; Manitoba Business, Mining, Trade and Job Creation, Manitoba Geological Survey, GeoFile 5-2025, Microsoft® Excel file®.

GS2025-2

Unveiling high-heat–production granites in the terrane boundary zone between the Bird River and Winnipeg River domains, southeastern Manitoba (parts of NTS 52L3–6, 62I8): a gamma-ray spectrometry approach

by X.M. Yang, D.R. Lentz[1] and T. Martins

In Brief:

- High-heat–production granites (HHPGs) occur in the terrane boundary zone between the Bird River and Winnipeg River domains
- HHPGs can be identified quickly by combined (U+Th) contents above 40 ppm using a hand-held gamma-ray spectrometer in the field
- HHPGs are potential targets for heavy rare-earth elements, uranium, thorium, niobium, tin and tungsten

Citation:
Yang, X.M., Lentz, D.R. and Martins, T. 2025: Unveiling high-heat–production granites in the terrane boundary zone between the Bird River and Winnipeg River domains, southeastern Manitoba (parts of NTS 52L3–6, 62I8): a gamma-ray spectrometry approach; *in* Report of Activities 2025, Manitoba Business, Mining, Trade and Job Creation, Manitoba Geological Survey, p. 7–19.

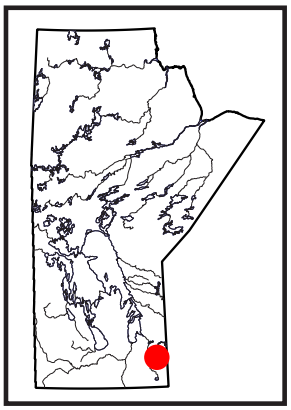

Summary

As the global economy shifts toward greener practices, high-heat–production granites are emerging as valuable exploration targets as they represent potential sources of geothermal energy and critical minerals, such as heavy rare-earth elements, uranium, thorium, niobium, tin and tungsten. It is worth noting that thorium is a particularly critical material for the next generation of clean and safe energy systems due to its use in thorium-based molten-salt nuclear reactors. Furthermore, occurrences of high-heat–production granites provide valuable insights into surface heat flow and the regional thermal gradient, which are crucial for assessing geothermal energy potential. Despite this, there is limited scientific information currently available regarding the occurrence and distribution of high-heat–production granites in Manitoba and across the Canadian shield.

In the summer of 2025, the Manitoba Geological Survey, in collaboration with the University of New Brunswick, conducted a reconnaissance survey using a hand-held gamma-ray spectrometer to assess the concentrations of heat-producing radioactive elements (U, Th and K) in Archean granitoid intrusions in the terrane boundary zone between the Bird River and Winnipeg River domains of the western Superior province in southeastern Manitoba. The results indicate significant variability in U and Th concentrations both within individual intrusions and between different intrusions, whereas K concentrations are less variable. High concentrations of the heat-producing elements are primarily observed in younger, massive, evolved I-type to A-type granites and associated pegmatites that cut older gneissic tonalite-trondhjemite-granodiorite suites. These are identified as high-heat–production granites based on them being characterized by radiogenic heat-production values (A) ≥5 μWm^{-3} or by combined (U+Th) contents exceeding 40 ppm. Magmatic fractionation, along with fluid-related processes, contributes to the enrichment of U and Th in high-heat–production granites. Furthermore, S-type granites constitute part of the Marijane Lake pluton, in the central part of the Bird River domain. Although S-type granite intrusions characterized by low Th/U ratios and elevated K abundances register low radiogenic heat-production values, they are a valuable geological indicator of the occurrence of lithium-cesium-tantalum pegmatites, which are genetically linked to S-type granites.

Introduction

Gamma-ray spectrometry is a powerful tool for geological mapping and mineral exploration, leveraging the distinct radiometric signatures of rocks, ore deposits and hydrothermal alteration zones (e.g., Lentz, 1991, 1994; Rickard et al., 1998; Shives et al., 2000; Ford, 2001; Long et al., 2010; Shives, 2015; Thomas et al., 2016; Dostal, 2017; Regelous et al., 2021). In addition, this technique is valuable for assessing radiogenic heat production in rocks (Rybach, 1988; Bücker and Rybach, 1996; Jefferson et al., 2007; Abbady et al., 2018; Sanjurjo-Sánchez et al., 2022)—an important geophysical parameter for understanding continental crust and lithosphere dynamics (Bücker and Rybach, 1996; Artemieva et al., 2017; Hasterok and Webb, 2017; Hasterok et al., 2018). Whereas granite heat-production capacity has varied over geological time, Archean granites typically exhibit relatively low global heat production, which may have contributed to the preservation of cratonic lithosphere (e.g., Artemieva et al., 2017). Nevertheless, the heat-generation capacity of granites depends primarily upon their petrogenetic type, rather than their age (e.g., Kromkhun, 2010).

The Archean western Superior Province, in southeastern Manitoba, is dominantly underlain by diverse types of granitic rocks. These include I-type, S-type, sanukitoid and tonalite-trondhjemite-granodiorite (TTG) suites, and associated pegmatites (e.g., Černý et al., 1981; Goad and Černý, 1981;

[1] Department of Earth Sciences, University of New Brunswick, Fredericton, New Brunswick

Bannatyne, 1985; Wang, 1993; Bailes et al., 2003; Van Lichtervelde et al., 2008; Anderson, 2013; Yang, 2014, 2023; Yang, and Houlé, 2020; Martins et al., 2024; Nambaje et al., 2024), which differ from post-Archean granites in their geochemical compositions (e.g., Janoušek et al., 2020). However, information on the distribution and occurrences of high-heat–production granites (HHPGs) in this region has been limited so far. These granites are significant in mineral exploration as they are associated with critical-metal mineralization, including heavy rare-earth elements (HREEs), uranium, thorium, niobium, tin and tungsten (Long et al., 2010; Dostal, 2017; Liu et al., 2023; Carvalhêdo et al., 2025). Characterized by relatively high concentrations of radioactive elements (U, Th and K), HHPGs typically exhibit radiogenic heat-production values (A) exceeding 5 μWm^{-3} (Kromkhun, 2010; Artemieva et al., 2017; Pleitavino et al., 2021). Consequently, they represent not only targets for geothermal exploration but also crucial factors in defining the thermal configuration of the continental crust and lithosphere (Vilà et al., 2010; Artemieva et al., 2017; Abbady and Al-Ghamdi, 2018). More importantly, thorium is considered a critical material for the next generation of clean and safe energy systems (i.e., using thorium-based molten-salt nuclear reactors; e.g., Cai et al., 2016; Dai, 2017; Zhou et al., 2019).

In the summer of 2025, the Manitoba Geological Survey (MGS) performed a two-week ground gamma-ray spectrometric survey at a reconnaissance scale, in collaboration with the University of New Brunswick, focusing on well-exposed granite plutons in the Lac du Bonnet region of southeastern Manitoba. The objective of this work was to explore the occurrences and characteristics of HHPGs, and their relationships with associated rocks in the region. Since HHPGs contain relatively high concentrations of heat-producing radioactive elements (U, Th and K), they can be quickly recognized and measured using a hand-held gamma-ray spectrometer (GRS) in the field. During fieldwork, 314 GRS measurements were acquired from 148 outcrops in 6 composite intrusions (see below). Each outcrop was thoroughly examined to document field relationships, texture, mineral assemblage and alteration. Outcrop locations were recorded in UTM coordinates using a GPS device (Garmin), with an accuracy of better than ±10 m. Detailed GRS data acquired in the field are available in MGS Data Repository Item DRI2025031 (Yang et al., 2025)[1]. Additionally, 11 representative whole-rock samples were collected for subsequent laboratory analysis.

Field descriptions of the granitic rocks

The granitoid plutons examined and measured using GRS in this study are shown in Figure GS2025-2-1. From north to south, they are the Maskwa Lake batholith, Marijane Lake pluton, Lac du Bonnet batholith, Pointe du Bois batholith, Rennie River plutonic suite and Big Whiteshell Lake pluton. The gneissic granites of the Maskwa Lake and Pointe du Bois batholiths constitute the main components of TTG suites in the region and were emplaced into supracrustal sequences of the Bird River and Winnipeg River domains before the northward accretion and final consolidation of the Superior Province (ca. 2.72–2.68 Ga; Bailes et al., 2003; Percival et al., 2006, 2012; Yang et al., 2019). The Marijane Lake pluton is a large composite intrusion that intruded greywacke of the Flanders Lake formation in the Bird River domain and extends east into Ontario (Gilbert et al., 2008; Rinne and Martins, 2024). Massive to weakly foliated granites in the Lac du Bonnet batholith, Rennie River plutonic suite and Big Whiteshell Lake pluton are situated in the terrane boundary zone between the Bird River and Winnipeg River domains (Figure GS2025-2-1; Percival et al., 2006, 2012; Gilbert et al., 2008), and likely welded and stitched these domains.

Marijane Lake pluton

The Marijane Lake pluton consists of granodiorite, garnet-bearing biotite-muscovite granite, pegmatitic granite and pegmatite. Monazite from the more homogeneous phase of medium-grained granodiorite yielded a U-Pb crystallization age of 2645.6 ±1.3 Ma determined by isotope dilution–thermal ionization mass spectrometry (ID-TIMS) techniques (Gilbert et al. 2008). This age is identical within measurement uncertainty to the age of the Tanco pegmatite, which hosts giant rare-metal (Li, Cs, Ta) deposits (e.g., Kremer, 2010, p. 79; Camacho et al., 2012).

Massive, fine- to coarse-grained, equigranular granodiorite to granite occurs in the northern part of the Marijane Lake pluton, with pegmatitic pods that commonly contain biotite and, more rarely, muscovite (Figure GS2025-2-2a). In the southern part of the pluton, two-mica granite and related pegmatitic differentiates are common and appear variably seriate-textured at the outcrop scale, from fine-, medium-, coarse- to very coarse-grained to pegmatitic (Figure GS2025-2-2b). The two-mica granite consists primarily of quartz, K-feldspar and small amounts of sodic plagioclase, biotite, muscovite and garnet. Locally, pale greenish beryl and apatite crystals occur in pegmatitic pods or patches (or segregations) in the two-mica granite. Although the granites appear massive and undeformed, strongly foliated greywacke xenoliths or slivers are commonly found within the pluton, particularly near the contact zone.

Lac du Bonnet batholith

The Lac du Bonnet batholith (Černý et al., 1981; Goad and Černý, 1981) has an ID-TIMS U-Pb zircon crystallization age of 2660 ±3 Ma (Wang; 1993) and consists dominantly of massive, pinkish to reddish, medium- to coarse-grained biotite granite (Figure GS2025-2-2c, d), and leucogranite. Locally, seriate to

[1] MGS Data Repository Item DRI2025031, containing the data or other information sources used to compile this report, is available online to download free of charge at https://manitoba.ca/iem/info/library/downloads/index.html, or on request from minesinfo@gov.mb.ca, or by contacting the Resource Centre, Manitoba Business, Mining, Trade and Job Creation, 360-1395 Ellice Avenue, Winnipeg, Manitoba R3G 3P2, Canada.

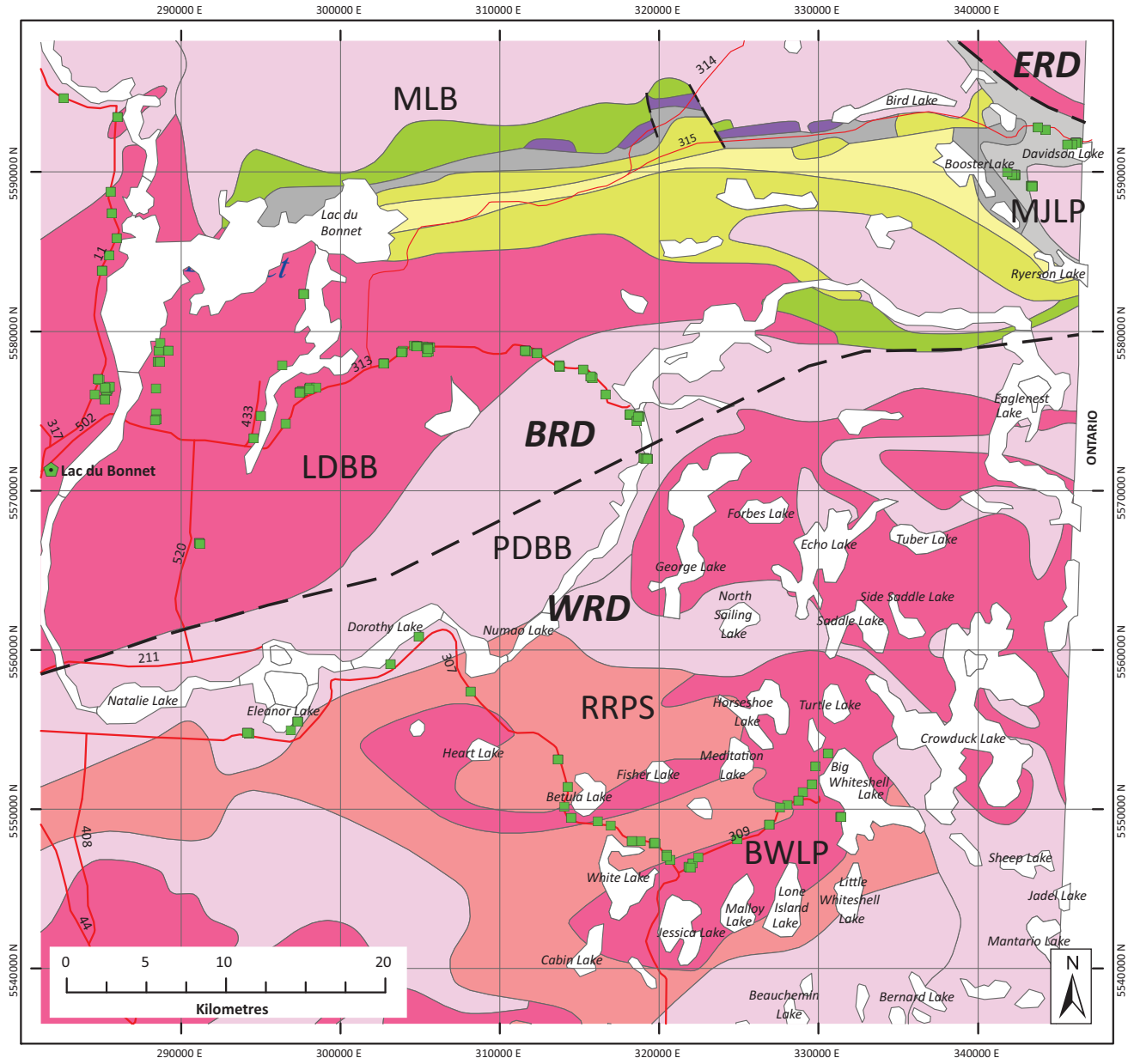

Legend

Archean intrusive rocks

- Granite, minor granodiorite
- Granodiorite, minor tonalite and migmatite
- Tonalite, minor granodiorite, granite, related gneiss
- Ultramafic rocks

Archean supracrustal rocks

- Greywacke, conglomerate, arkose, arenite
- Greywacke, mudstone, conglomerate, arkose, banded iron formation
- Basalt, minor andesite, minor sedimentary and mafic intrusive rocks
- Felsic to intermediate, volcanic and volcaniclastic rocks; minor intrusive and sedimentary rocks

Pluton key

BWLP, Big Whiteshell Lake pluton
LDBB, Lac du Bonnet batholith
MJLP, Marijane Lake pluton
MLB, Maskwa Lake batholith
PDBB, Pointe du Bois batholith
RRPS, Rennie River plutonic suite

BRD, Bird River domain
ERD, English River domain
WRD, Winnipeg River domain

Domain boundary

Station location

315 Provincial highway

Figure GS2025-2-1: *Geology of granitoid intrusions emplaced into the terrane boundary zone between the Bird River and Winnipeg River domains, showing their spatial distribution and relationship with the supracrustal sequence of the Bird River greenstone belt and the station locations of the study area. Terminology on domains are after Gilbert et al. (2008) and Stott et al. (2010). Co-ordinates are in UTM Zone 15, NAD83.*

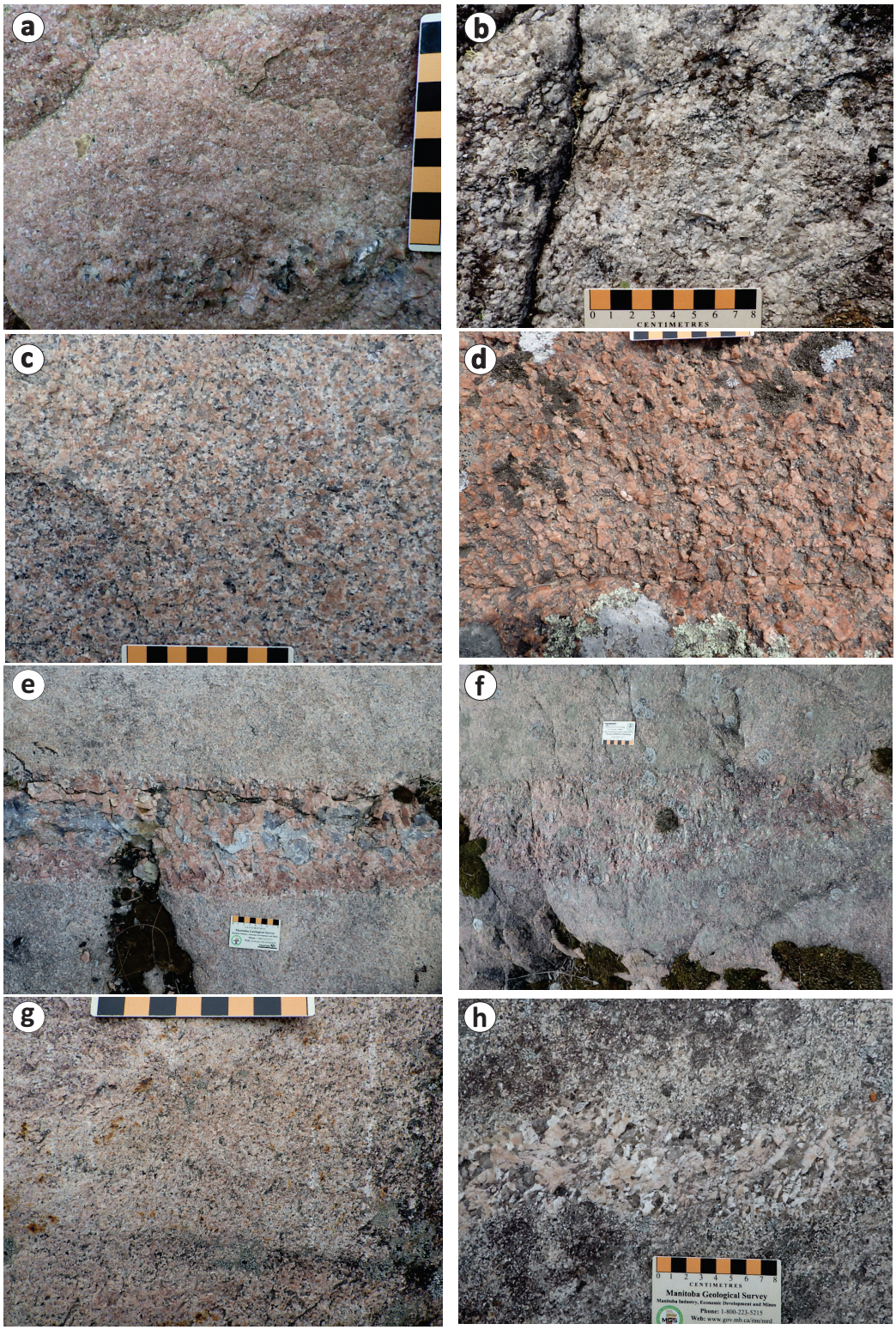

Figure GS2025-2-2: *Field photographs of outcrops of typical granitoid rocks in the Bird River domain:* ***a)*** *medium-grained, massive granite with pegmatite pods, Marijane Lake pluton (347242E, 5591897N);* ***b)*** *garnet-bearing biotite-muscovite granite with heterogeneous texture, Marijane Lake pluton (343329E, 5589124N);* ***c)*** *medium- to coarse-grained biotite granite (285309E, 5576438N), Lac du Bonnet batholith;* ***d)*** *massive, coarse-grained granite (288557E, 55530985N), Lac du Bonnet batholith;* ***e)*** *simple pegmatite dike, with a fine-grained margin, cutting K-feldspar–phyric biotite granite (305501E, 5578897N), Lac du Bonnet batholith;* ***f)*** *fine- to medium-grained biotite granite cut by a hematitic pegmatite dike 15–30 cm wide and striking 100° (297698E, 5582325N), Lac du Bonnet batholith;* ***g)*** *pinkish, medium-grained granite (282630E, 5594624N), Maskwa Lake batholith;* ***h)*** *grey foliated, medium-grained, granodiorite with a pegmatitic vein 4–6 cm wide (286022E, 5593457N), Maskwa Lake batholith. All co-ordinates of locations are in UTM Zone 15, NAD83, except for outcrops shown in (c), (g) and (h) that are in UTM Zone 14, NAD83 (recorded originally by a GPS as 712586E, 5576353N; 708450E, 5594263N; 711925E, 5593374N, respectively).*

K-feldspar–phyric textures are also present, as are small amounts of quartz diorite and monzonite. Pegmatitic pods in massive, pink granite are common. Locally, simple pegmatite dikes composed of quartz, K-feldspar and small amounts of biotite, muscovite and tourmaline, cut K-feldspar–phyric biotite granite. Notably, some pegmatite dikes show internal zonation from fine-grained margins to quartz core (Figure GS2025-2-2e). Some pegmatite dikes show pervasive hematitic alteration or metasomatism, as indicated by grey albite replacing reddish K-feldspar (Figure GS2025-2-2f).

Maskwa Lake batholith

The western part of the Maskwa Lake batholith is composed mainly of pinkish, fine- to medium-grained granite (Figure GS2025-2-2g) that is massive to weakly foliated; and of grey, foliated, medium-grained tonalite to granodiorite (Figure GS2025-2-2h). An ID-TIMS U-Pb zircon crystallization age of 2725 ±6 Ma (Wang et al., 1993) was determined for the pinkish granite that intrudes the grey, foliated granitoid rocks, which constitute part of the TTG suite of the batholith (Yang and Houlé, 2020; Yang, 2023).

Pointe du Bois batholith

The Pointe du Bois batholith was emplaced into the boundary zone between the Bird River and Winnipeg River domains. It consists mainly of gneissic tonalite, granodiorite and granite that are cut by pinkish grey, massive equigranular granite dated at 2729 ±8.7 Ma by Wang (1993) using zircon ID-TIMS U-Pb techniques. At the contact zone with the Lac du Bonnet batholith in the Bird River domain, a northwest-trending pegmatite dike (K-feldspar–quartz–biotite±muscovite±tourmaline), up to 5 m in width, cuts pinkish, medium-grained biotite granite. The pinkish granite cuts grey gneissic granodiorite (Figure GS2025-2-3a) intruding mafic volcanic rocks (amphibole-biotite-plagioclase schist). In places, pinkish aplite-pegmatite dikes commonly crosscut the gneissic tonalite to granodiorite (Figure GS2025-2-3b).

Rennie River plutonic suite

The Rennie River plutonic suite is composed dominantly of pinkish, massive to weakly foliated granodiorite to granite that displays variable textures at outcrop scale, such as seriate, equigranular and megacrystic textures. Notably, subhedral to euhedral K-feldspar phenocrysts (2–3 cm in length) occur together with rare quartz phenocrysts (up to 2 cm in size) in a medium- to coarse-grained groundmass of quartz, K-feldspar, plagioclase and biotite (Figure GS2025-2-3c). Pegmatitic pods, consisting of K-feldspar, quartz and small amounts of biotite (Figure GS2025-2-3d), are common in places.

Big Whiteshell Lake pluton

The Big Whiteshell Lake pluton consists largely of reddish to pink, medium-grained granodiorite to granite and a coarse- to very coarse-grained granite. The medium-grained granite (Figure GS2025-2-3e) is mostly massive and slightly foliated, with local pegmatitic pods, whereas the very coarse-grained granite (Figure GS2025-2-3f) is more homogeneous and contains a foliation defined by aligned K-feldspar laths. The very coarse-grained granite rarely contains pegmatitic pods and is cut by medium-grained granodiorite.

Methodology

Concentrations of heat-producing radioactive elements U, Th and K in natural outcrops and/or roadcuts were measured with a portable GRS equipped with a 103 cm^3 sodium-iodide detector (model RS 125; Radiation Solutions Inc., 2008). The calibration of the GRS was conducted by Radiation Solutions Inc., following the procedure described in Grasty et al. (1991). In the field, the GRS was calibrated twice daily using a ^{137}Cs source to correct for counting drift. Measurements were taken in the 'assay-mode' over a 120 s interval. The abundances of K, equivalent (e) U and eTh were determined from the intensities of ^{40}K (l.46 MeV), ^{214}Bi (1.76 MeV) and ^{208}Tl (2.62 MeV), respectively. The eU and eTh contents are proportional respectively to the concentrations of the daughter nuclides, if parent-daughter nuclide equilibrium is maintained (i.e., ^{214}Bi–^{238}U, ^{208}Tl–^{232}Th). Radioactivity of ^{40}K is measured directly by the GRS (Killeen and Cameron, 1977; Lentz, 1994). Analytical precision was based on replicate analyses of a target. Given the measured target contains 5 wt. % K, 10 ppm eU and 10 ppm eTh, their precision is ±0.1 (1 σ) wt. %, ±1 and ±3.5 ppm, respectively; such uncertainties should be treated as relative because they depend on K, U and Th contents in the target, geometry and counting time (Radiation Solutions Inc., 2008). For the sake of brevity, the 'e' in eU and eTh is omitted in this report.

At each outcrop visited, GRS measurements were conducted based on the specific lithologies present and their field relationships. Each distinct lithology was measured at least once, and sometimes multiple times, depending on the characteristics and dimensions of the outcrop.

Radiogenic heat-production value (or rate), A (μWm^{-3}), of a rock is calculated using the equation of Rybach (1988) as shown below:

$$A\ (\mu Wm^{-3}) = \rho \times (9.52C_U + 2.56C_{Th} + 3.48C_K) \times 10^{-5}$$

where ρ is density in kg/m^3; C_U is uranium concentration in ppm; C_{Th} is thorium concentration in ppm; C_K is potassium concentration in weight percentage (wt. %), as determined by the GRS. Density of 2700 kg/m^3 is used for calculating the heat-production rate of granitic rocks. It should be noted that changing density from 2700 to 2650 kg/m^3 would result in an uncertainty in the heat-production rate of about 2% (Artemieva et al., 2017); more-

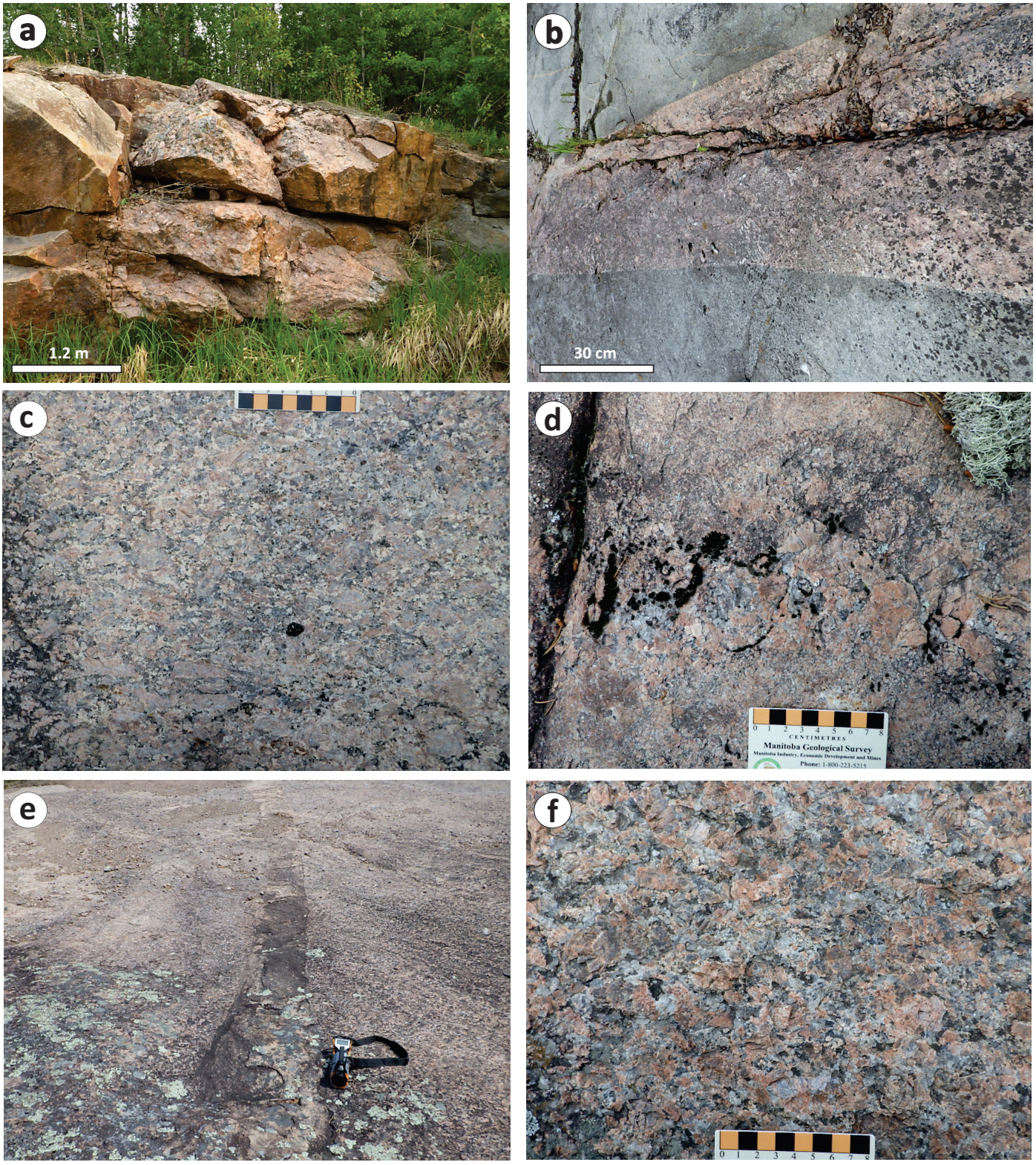

Figure GS2025-2-3: *Field photographs of outcrops of typical granitoid rocks in the boundary zone between the Bird River and Winnipeg River domains:* ***a)*** *a 4–5 m wide pegmatite dike (311595E, 5578747N) consisting of K-feldspar and quartz, with small amounts of biotite and tourmaline, trends northwest and cuts medium-grained biotite granite that intrudes grey gneissic granodiorite at the contact zone between the Lac du Bonnet batholith and Pointe du Bois batholith (to the west);* ***b)*** *grey, medium-grained gneiss cut by a 1.2 m wide granitic aplite to pegmatite dike (318699E, 5574636N) trending 210°, Pointe du Bois batholith;* ***c)*** *foliated, megacrystic K-feldspar granite (308178E, 5557389N), Rennie River plutonic suite;* ***d)*** *weakly foliated, coarse-grained granite, with simple pegmatitic pod (313666E, 55530985N), Rennie River plutonic suite;* ***e)*** *massive, medium-grained granite dike (330594E, 5553481N), approximately 0.5 m wide and trending 260°, cutting coarse- to very coarse-grained granite, Big Whiteshell Lake pluton;* ***f)*** *weakly foliated, coarse- to very coarse-grained granite (329802E, 5552684N), Big Whiteshell Lake pluton. Co-ordinates of locations are in UTM Zone 15, NAD83.*

over, about 85% of heat production is contributed by U and Th in rocks, and 15% by K (Vilà et al., 2010).

Results

A summary of the abundances of heat-producing elements (U, Th and K), Th/U ratios and radiogenic heat-production A-values of granitic rocks is tabulated in Table GS2025-2-1. Details of the GRS measurements are listed in DRI2025031 (Yang et al., 2025). This dataset shows that U and Th concentrations exhibit considerable variability both within single intrusions and across different intrusions, whereas potassium levels tend to remain comparatively consistent. The following plots illustrate the dataset and highlight significant variations in radioactive elements both within and between intrusions.

Radiometric features of the Marijane Lake pluton

The GRS data (Table GS2025-2-1) show that U, Th and K contents in the granitic phases of Marijane Lake pluton range from 1.0 to 25.6 ppm (average 9.1 ±6.4 ppm; n = 26), 0.3 to 17.8 ppm (5.3 ±4.6 ppm) and 1.8 to 6.0 wt. % (4.4 ±1.2 wt. %), respectively, with Th/U ratios of 0.1 to 2.6 (0.7 ±0.5). The pegmatites associated with this pluton have 1.0 to 21.1 ppm U (6.4 ±5.1 ppm; n = 16), 0.6 to 12.1 ppm Th (6.0 ±3.3 ppm), Th/U ratios of 0.1 to 5.7 (1.7 ±2.0) and 2.8 to 6.2 wt. % K (4.6 ±0.9 wt. %). Greywacke of the Flanders formation intruded by the Marijane Lake pluton displays 1.8 to 4.4 ppm U (2.8 ±1.4 ppm; n = 3), 11.3 to 12.8 ppm Th (12.1 ±0.8 ppm), Th/U ratios of 2.9 to 6.3 (4.9 ±1.8) and consistent 2.1 wt. % K (Yang et al., 2025).

The Th/U ratios are mostly lower than the average ratio determined for the upper continental crust (4.2) and increase with increasing Th abundances (Figure GS2025-2-4a) but decrease with increasing U (Figure GS2025-2-4b). There is no discernible correlation of the Th/U rations with K contents in granites and pegmatites of the Marijane Lake pluton (not shown).

The granites display radiogenic heat-production A-values of 1.0 to 7.4 (average 3.1 ±1.9; n = 26) μWm^{-3} (Table GS2025-2-1). The differentiated pegmatites have A-values of 1.0 to 6.6 (2.5 ±1.4; n = 16) μWm^{-3} (Table GS2025-2-1). The greywackes

Table GS2025-2-1: Summary of radioactive-element (U, Th and K) abundances, Th/U ratios and radiogenic heat-production A-values of granitic rocks in the Lac du Bonnet region.

		MJLP			LDBB		MLB		PDBB			RRPS		BWLP	
		Granite	Pegmatite	Greywacke	Massive granite	Pegmatite	Gneissic granite	Red granite	Gneissic granite	Granite	Pegmatite	Granite	Pegmatite	Granite	Pegmatite
		n = 26	n = 16	n = 3	n = 91	n = 40	n = 3	n = 3	n = 17	n = 19	n = 39	n = 21	n = 6[1]	n = 26	n = 3
U (ppm)	Max	25.6	21.1	4.4	35.2	37.9	2.5	7.7	6.0	27.6	105.3	24.7	40.0	8.1	8.6
	Min	1.0	1.0	1.8	0.3	0.4	0.7	5.1	0.5	0.8	0.5	0.8	1.0	0.5	1.8
	AV	9.1	6.4	2.8	7.8	11.1	1.6	6.7	2.6	8.2	11.7	5.3	15.1	2.8	5.2
	SD	6.4	5.1	1.4	6.9	9.7	1.3	1.4	1.8	7.1	17.0	8.3	18.4	2.0	4.8
Th (ppm)	Max	17.8	12.1	12.8	119.3	169.7	26.7	61.8	24.7	153.7	178.7	137.4	444.4	73.7	128.4
	Min	0.3	0.6	11.3	5.0	11.9	20.3	34.2	3.8	14.5	3.5	4.8	15.4	3.9	58.6
	AV	5.3	6.0	12.1	33.9	42.7	23.5	43.7	13.5	46.6	34.7	34.5	119.0	30.8	93.5
	SD	4.6	3.3	0.8	21.7	45.8	4.5	15.7	5.1	34.8	37.5	40.3	195.5	18.2	49.4
K (wt. %)	Max	6.0	6.2	2.1	6.9	6.9	4.0	4.9	3.8	5.7	7.1	4.9	5.1	5.1	4.6
	Min	1.8	2.8	2.1	1.9	2.7	3.6	3.7	1.1	1.9	1.6	2.4	3.4	3.0	4.4
	AV	4.4	4.6	2.1	4.0	4.6	3.8	4.1	2.4	4.2	4.1	3.8	4.4	3.9	4.5
	SD	1.2	0.9	0.0	0.8	0.9	0.3	0.7	0.8	0.9	1.4	0.6	0.7	0.5	0.1
Th/U	Max	2.6	5.7	6.3	118.6	424.3	38.1	12.1	49.4	71.9	71.9	45.8	28.7	84.7	71.3
	Min	0.1	0.1	2.9	0.8	0.5	8.1	4.6	2.2	1.3	0.6	0.6	1.3	4.2	6.8
	AV	0.7	1.7	4.9	9.7	27.6	23.1	7.1	9.6	11.6	8.6	11.6	13.2	16.2	39.1
	SD	0.5	2.0	1.8	15.7	83.9	21.2	4.3	12.2	16.1	13.8	12.3	12.0	17.3	45.6
A (μWm^{-3})	Max	7.4	6.6	2.2	12.1	15.5	2.4	5.9	2.8	13.4	37.3	16.3	39.9	7.6	9.8
	Min	1.0	1.0	1.4	1.4	1.7	2.4	4.7	0.7	2.1	0.6	0.9	2.0	0.8	6.7
	AV	3.1	2.5	1.8	4.7	6.2	2.4	5.1	1.8	5.7	5.7	4.1	12.5	3.2	8.2
	SD	1.9	1.4	0.4	2.5	3.9	0.0	0.7	0.6	3.1	6.2	4.7	16.7	1.7	2.2

[1] One measure on a pegmatite dike returned results of 0 ppm U, 710 ppm Th and 1.3 wt. % K, which appears to be abnormal, and it was therefore excluded from the statistical analysis

Abbreviations: AV, average; BWLP, Big Whiteshell Lake pluton; LDBB, Lac du Bonnet batholith; MJLP, Marijane Lake pluton; MLB, Maskwa Lake batholith; n, number of measures; PDBB, Pointe du Bois batholith; RRPS, Rennie River plutonic suite; SD, standard deviation.

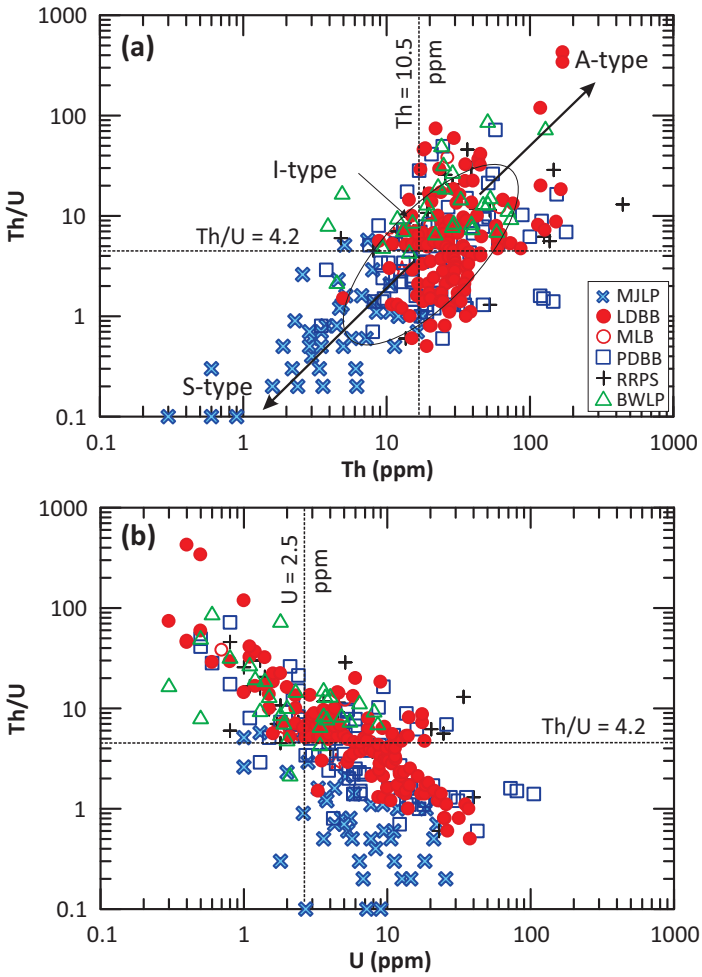

Figure GS2025-2-4: *Plots of* ***a)*** *Th/U versus Th (ppm) and* ***b)*** *Th/U versus U (ppm) for the granitoid rocks from the study area in the terrane boundary zone between the Bird River and Winnipeg River domains. Variation trend of A-, I- and S-type granites from Regelous et al. (2021). Average Th (10.5 ppm) and U (2.5 ppm) abundances as well as Th/U ratio (4.2) of the upper continental crust from Artemieva et al. (2017). Abbreviations: BWLP, Big Whiteshell Lake pluton; LDBB, Lac du Bonnet batholith; MJLP, Marijane Lake pluton; MLB, Maskwa Lake batholith; PDBB, Pointe du Bois batholith; RRPS, Rennie River plutonic suite.*

have lower A-values, ranging from 1.4 to 2.2 (1.8 ±0.4; n = 3) μWm^{-3}, than the granitic rocks (Table GS2025-2-1; Yang et al., 2025). Most GRS measurements of the granites and associated pegmatites (Figure GS2025-2-5a, b) yielded A-values ≤5 μWm^{-3}, falling in the category of normal granites in terms of radiogenic heat production (Kromkhun, 2010; Artemieva et al., 2017; Pleitavino et al., 2021).

Radiometric features of the Lac du Bonnet batholith

Massive to weakly foliated granites and associated pegmatites present as dikes and/or pegmatitic pods in the Lac du Bonnet batholith show a large range of U contents from 0.3 to 37.9 ppm (average of 8.8 ±8.0 ppm; n = 131), Th contents from 5.0 to 169.7 ppm (36.6 ±31.1 ppm), and a narrower range of K from 1.9 to 6.9 wt. % (4.2 ±0.9 wt. %). The Th/U ratios are elevated generally with increasing Th abundances (Figure GS2025-2-4a) but decrease with increasing U (Figure GS2025-2-4b) in the Lac du Bonnet batholith.

The Lac du Bonnet batholith granites have 0.3 to 35.2 ppm U (average 7.8 ±6.9 ppm; n = 91) U, 5.0 to 119.3 ppm Th (33.9 ±21.7 ppm) and 1.9 to 6.9 wt. % K (4.0 ±0.8 wt. %). They display Th/U ratios of 0.8 to 118.6, averaging 9.7 ±15.7 (Table GS2025-2-1). The pegmatitic rocks have 0.4 to 37.9 ppm U (average 11.1 ±9.7 ppm; n = 40), 11.9 to 169.7 ppm Th (42.7 ±45.8 ppm) and 2.7 to 6. wt. % K (4.6 ±0.9 wt. %), with Th/U ratios ranging from 0.5 to 424.3, averaging 27.6 ±83.9.

The radiogenic heat-production A-values of the granites (1.4 to 12.1 μWm^{-3}; average 4.7 ±2.5, n = 91) and pegmatites (1.7 to 15.5 μWm^{-3}; 6.2 ±3.9, n = 40) are increasing consistently with (U+Th) abundances. A large portion (~43%) of GRS measurements of the Lac du Bonnet batholith granites and associated pegmatites (Figure GS2025-2-5a, b) yielded A-values ≥5 μWm^{-3}, classifying them as HHPGs (Kromkhun, 2010; Artemieva et al., 2017; Pleitavino et al., 2021).

Radiometric features of the Maskwa Lake batholith

Reddish, weakly foliated, medium-grained granite cuts grey gneissic (or foliated) granitoid rocks of the Maskwa Lake batholith. The reddish granite contains higher radioactive elements (average 6.7 ppm U, 43.7 ppm Th and 4.1 wt. % K) and lower Th/U ratios (7.1) than the foliated granitoid rocks (Table GS2025-2-1). The granite has an average radiogenic heat-production A-value of 5.1 μWm^{-3}, whereas the grey gneissic granitoid has an average A-value of 2.4 μWm^{-3}.

Radiometric features of the Pointe du Bois batholith

In the Pointe du Bois batholith, gneissic diorite to granodiorite contains 0.5 to 6.0 ppm U (average 2.6 ±1.8 ppm; n = 17), 3.8 to 24.7 ppm Th (13.5 ±5.1 ppm), with Th/U ratios of 2.2 to 49.4 (9.6 ±12.2) and 1.1 to 3.8 wt. % K (2.4 ±0.8 wt. %; Table GS2025-2-1). Pink massive, weakly foliated granites have varied and relatively high U contents ranging from 0.8 to 27.6 ppm (8. ±7.1 ppm; n = 19), Th contents from 14.5 to 153.7 ppm(46.6 ±34.8 ppm), with Th/U ratios of 1.3 to 71.9 (11.6 ±16.1) and K from 1.9 to 5.7 wt. % (4.2 ±0.9 wt. %).

Pegmatite dikes cutting foliated grey granitoids and/or occurring as fractionated pods in the pink granites show a wide range of U contents of 0.5 to 105.3 ppm (average 11.7 ±17.0 ppm; n = 39), Th contents of 3.5 178.7 ppm (34.7 ±37.5 ppm), with Th/U ratios of 0.6 to 71.9 (8.6 ±13.8) and K of 1.6 to 7.1 wt. % (4.1 ±1.4 wt. %). Overall, Th/U ratios appear more scattered when plotted against Th contents but are negatively correlated with U concentrations (Figure GS2025-2-4a, b).

The Pointe du Bois batholith gneissic granitoids have a low range of heat-production A-values of 0.7 to 2.8 (average 1.8 ±0.6) μWm^{-3}, whereas the pinkish granites and pegmatites

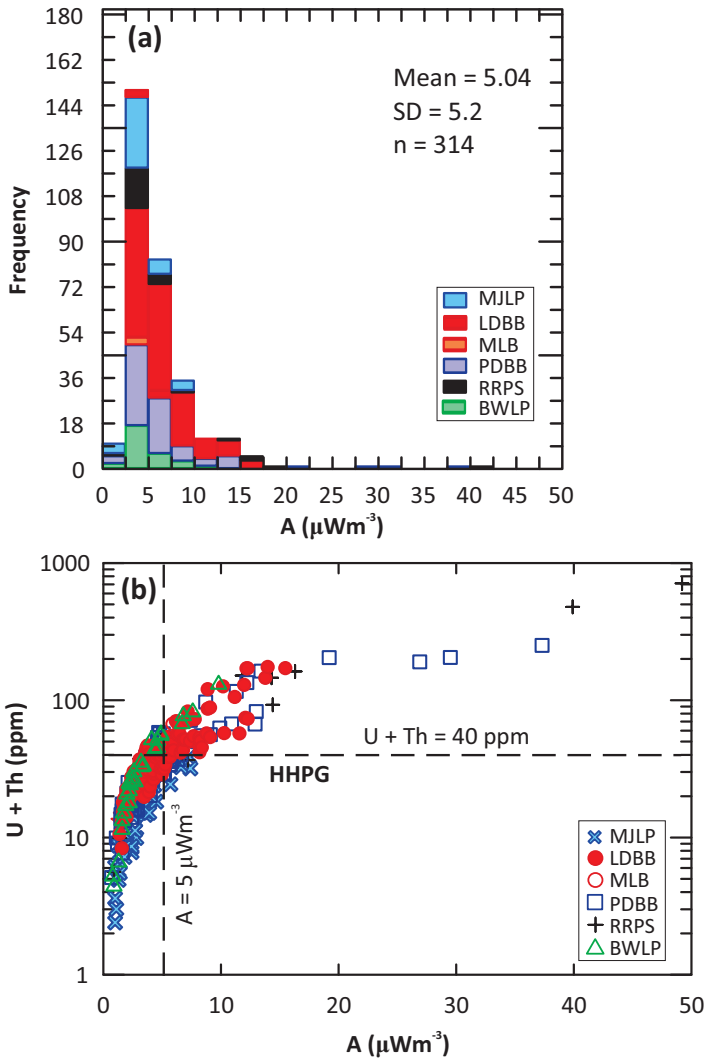

Figure GS2025-2-5: *Radiogenic heat production of the granitoid rocks from the study area in the terrane boundary zone between the Bird River and Winnipeg River domains:* ***a)*** *histogram of radiogenic heat-production A-values (µWm^{-3});* ***b)*** *plot of (U+Th) in ppm versus A (µWm^{-3}). Note that A >5 µWm^{-3} is equivalent to (U+Th) >40 ppm, which can be used for identification of high-heat–production granites. Abbreviations: BWLP, Big Whiteshell Lake pluton; HHPG, high-heat–production granite; LDBB, Lac du Bonnet batholith; MJLP, Marijane Lake pluton; MLB, Maskwa Lake batholith; n, number; PDBB, Pointe du Bois batholith; RRPS, Rennie River plutonic suite; SD, standard deviation.*

yield higher and varied A-values of 2.1 to 13.4 (5.7 ±3.1) and 0.6 to 37.3 (5.7 ±6.2) µWm^{-3}, respectively. It should be noted that about 43% of GRS measurements on pegmatitic rocks returned A-values >5 µWm^{-3}.

Radiometric features of the Rennie River plutonic suite

Granites in the Rennie River plutonic suite returned results of 0.8 to 24.7 ppm U (average 5.3 ±8.3 ppm; n = 21), 4.8 to 137.4 ppm Th (34.5 ±40.3 ppm), with Th/U ratios of 0.6 to 45.8 (11.6 ±12.3) and 2.4 to 4.9 wt. % K (3.8 ±0.6 wt. %). Compared to the granites, pegmatites contain relatively higher U ranging from 1.0 to 40.0 ppm (average 15.1 ±18.4 ppm; n = 6), Th contents of 15.4 to 444.4 ppm (119.0 ±195.5 ppm), with Th/U ratios of 1.3 to 28.7 (13.2 ±12.0) and K of 3.4 to 5.1 wt. % (4.4 ±0.7 wt. %). It should be noted that one measure on a pegmatite dike returned results of 0 ppm U and 710 ppm Th, and 1.3 wt. % K; this appears to be abnormal and it was therefore excluded from the statistical analysis.

Radiogenic heat-production A-values of the Rennie River plutonic suite granites range from 0.9 to 16.3 (4.1 ±4.7) µWm^{-3}, whereas the pegmatites show higher A-values of 2.0 to 39.9 (12.5 ±16.7) µWm^{-3}.

Radiometric features of the Big Whiteshell Lake pluton

The Big Whiteshell Lake pluton granites have 0.5 to 8.1 ppm U (average 2.8 ±2.0 ppm; n = 26), 3.9 to 73.7 ppm Th (30.8 ±18.2 ppm), with Th/U ratios of 4.2 to 84.7 (16.2 ±17.3) and 3.0 to 5.1 wt. % K (3.9 ±0.5 wt. %). Pegmatite dikes associated with the granites have 1.8 to 8.6 ppm U (5.2 ±4.8 ppm; n = 3), 58.6 to 128.4 ppm Th (93.5 ±49.4 ppm), with Th/U ratios of 6.8 to 71.3 (39.1 ±45.6) and 4.4 to 4.6 wt. % K (4.5 ±0.1 wt. %).

The granites display relatively lower heat-production A-values of 0.8 to 7.6 µWm^{-3} (average 3.2 ±1.7) than their associated pegmatites that have returned A-values of 6.7 to 9.8 µWm^{-3} (8.2 ±2.2; n = 3; Table GS2025-2-1).

Discussion

High-heat–production potential

Granites and associated pegmatites in the terrane boundary zone (Yang, 2014; Yang et al., 2019) between the Bird River and Winnipeg River domains show elevated U, Th and K contents compared to the upper-continental–crust values (e.g., Plant et al., 1999; Artemieva et al., 2017). Both intra- and inter-intrusion variations in element abundances and Th/U ratios are observed (Figure GS2025-2-4; Table GS2025-2-1). Pegmatites have U and Th contents typically higher than the massive granites, which intrude grey, gneissic or foliated granitoids that are older and characterized by lower Th/U abundances (e.g., Pointe du Bois batholith). These differences likely reflect magmatic fractionation or varying source materials. Older gneissic granitoids may have originated from partial melting of the lower crust (Yang, 2023), whereas the younger granites may have formed via relamination (Hacker et al., 2011) or remelting of granitoid rocks. Further data, such as precise U-Pb zircon ages, are needed to clarify interintrusion differences, especially in the Lac du Bonnet, Maskwa Lake and Pointe du Bois batholiths.

Granite and pegmatite petrogenesis

Variations in U and Th abundances in granites are mainly linked to source differences and petrogenesis, whereas K shows less variability (Table GS2025-2-1). During magmatic to hydrothermal evolution, U and Th can separate as U^{6+} preferentially

enters fluids under relatively oxidizing conditions, whereas Th^{4+} stays in the melt (e.g., Plant et al., 1999). This process may have led to the fractionation of U from Th, and the negative correlation between Th/U and U content in the granitic melt (Figure GS2025-2-4b). Postemplacement U^{6+} mobility may be driven by fluid circulation, aided by structural activity and radiogenic heat. The U^{6+} in the fluids would be reduced to U^{4+} and precipitated in upper-level faults and/or fractures, where reducing agents are present. High U content is also observed in hematitic alteration zones or patches in massive pink granites and hematitic pegmatites (e.g., Figure GS2025-2-2f). This higher concentration of U is probably due to the infiltration of U^{6+}-bearing fluids, which may have interacted with magnetite to form hematite and uraninite (e.g., Lentz, 1991; Plant et al., 1999; Jefferson et al., 2007).

Younger evolved granites and pegmatites contain high levels of heat-producing elements, classifying them as HHPGs with A-values ≥5 μWm^{-3} (Figure GS2025-2-5a, b). Granites with combined (U+Th) contents >40 ppm typically fall into this category, as these elements account for 85% of total heat production (Vilà et al., 2010). Figure 2025-2-5b also shows two apparent trends: one following magmatic fractionation (indicated by the lower trend) and another representing more evolved granitic to pegmatitic melts (as shown by the upper trend). These two trajectories appear to merge when (U+Th) contents equal 40 ppm and A-values equal 5 μWm^{-3}.

Whole-rock Th/U ratios provide a robust means of differentiating S-, I- and A-type granites (Regelous et al., 2021). The systematic decrease in Th/U ratios from S-, I- to A-types is mainly ascribed to magmatic fractionation, source heterogeneity and, sometimes, to U mobilization (Regelous et al., 2021) and/or fixation via a process of absorption by clay minerals in sedimentary rocks that are source rocks of S-type granites (e.g., Chappell and White, 1974, 2001). Compared with the Th/U ratios versus Th and U variation trends as described in Regelous et al. (2021), the massive granites with high Th/U ratios in this study (Figure 2025-2-4a, b) most closely resemble evolved I- to A-type granites that are emplaced at relatively shallow levels of the crust because of high quartz (or silica) concentrations (e.g., Yang, 2017; Yang et al., 2021). This agrees with their mineral assemblage (magnetite, biotite, red and/or pink K-feldspar) and the Nb/Y, La/Yb trace-element systematics (e.g., Whalen et al., 1987; Eby, 1990, 1992; Whalen and Hildebrand, 2019; Yang, 2023). Thus, the HHPGs may have been emplaced into late- to postorogenic settings (e.g., Pearce et al., 1984; Christiansen and Keith, 1996; Pearce, 1996) during accretionary tectonics leading to terrane juxtaposition in the western Superior province (Percival et al., 2006, 2012).

The garnet-bearing two-mica granite in the Marijane Lake pluton has K, Th and U abundances and Th/U ratios indistinguishable from S-type granites (Regelous et al., 2021), which is consistent with its primary mineral assemblage (muscovite, garnet, Fe-rich biotite), low magnetic susceptibility values ($<0.1 \times 10^{-3}$) and peraluminous affinity, as reported in Yang (2023). Although these granites have relatively low A-values (<5 μWm^{-3}), belonging to normal granites in terms of radiogenic heat production, they could potentially be the source from which lithium-cesium-tantalum (LCT) pegmatite dikes are derived in the region. This is hypothesized based on potential pegmatite genetic relationship with S-type granites emplaced into collisional zones at a relatively shallow level (Černý and Ercit, 2005; Yang, 2017; Yang et al., 2019, 2021) as well as on the coincidence in timing of emplacement with that of the Tanco pegmatite, which hosts giant rare-metal (Li, Cs, Ta) deposits (e.g., Kremer, 2010; Camacho et al, 2012). Such a genetic association is substantial, notwithstanding the ongoing debate regarding the source rocks and petrogenesis of Archean Li-Cs-Ta pegmatites such as the Tanco pegmatite (e.g., Koopmans et al., 2024; Smithies et al., 2025) and their potential association with economic gold skarn and orogenic gold mineralization in Archean greenstone belts (e.g., Zhou et al., 2012, 2016; Yang and Houlé, 2020; Mueller, 2025).

Significant findings and future work

A significant number of the younger massive granites and associated pegmatite dikes in the terrane boundary zone (Yang, 2014; Yang et al., 2019) between the Bird River and Winnipeg domains are identified as HHPGs. They significantly influence the geothermal gradient and crustal heat budget in the region, and could be geothermal targets. The gamma-ray spectrometer measurements recorded in the field, showing the combined (U+Th) contents above 40 ppm, allow for a rapid identification of HHPGs.

To determine if the HHPGs in different batholiths or plutons share a common timing of emplacement, magmatic processes and sources, acquiring additional U-Pb zircon and trace Sm-Nd isotope data is essential.

Economic considerations

The presence of HHPGs suggests a considerable potential for HREEs, uranium, thorium, niobium, tin and tungsten mineralization. Of greater importance to mineral exploration is the fact that these granites are identified as evolved I- to A-type that were likely emplaced into the terrane boundary zone during late- to postorogenic events. Thorium is a particularly strategic metal for the next generation of clean and safe energy due to its use in thorium-based molten-salt nuclear reactors. The work presented here highlights the importance of proceeding with further evaluation of potential Th resources in Manitoba and elsewhere in Canada.

Lithium-cesium-tantalum (LCT) pegmatites, including the Tanco pegmatite mine, are well-known to occur in the Bird River domain (Černý et al, 1981; Bannatyne, 1985), although the source(s) and petrogenesis of these pegmatites have been debated for decades. This report indicates that part of the Marijane Lake pluton belongs to S-type granites that are thought to be associated genetically with LCT pegmatites, spurring a need for further evaluation of the potential for LCT mineralization in the region.

Acknowledgments

The authors thank Z. Rahabi for providing enthusiastic field assistance, E. Ralph for logistic support, J. Marks for converting radiometric images, H. Adediran for GIS support, as well as C. Epp and P. Belanger for assistance in processing and cataloguing samples. Constructive reviews by J. MacDonald and K. Reid, technical editing by M.-F. Dufour at RnD Technical and report layout by D. O'Hara are appreciatively acknowledged.

References

Abbady, A.G.E. and Al-Ghamdi, A.H. 2018: Heat production rate from radioactive elements of granite rocks in north and southeastern Arabian shield Kingdom of Saudi Arabia; Journal of Radiation Research and Applied Sciences, v. 11, p. 281–290.

Anderson, S.D. 2013: Geology of the Garner–Gem lakes area, Rice Lake greenstone belt, southeastern Manitoba (parts of NTS 52L11, 14); Manitoba Mineral Resources, Manitoba Geological Survey, Geoscientific Report GR2013-1, 135 p., URL <https://manitoba.ca/iem/info/libmin/GR2013-1.zip> [December 2022].

Artemieva, I.M., Thybo, H., Jakobsen, K., Sørensen, N.K. and Nielsen, L.S.K. 2017: Heat production in granitic rocks: global analysis based on a new data compilation GRANITE2017; Earth-Science Reviews, v. 172, p. 1–26.

Bailes, A.H., Percival, J.A., Corkery, M.T., McNicoll, V.J., Tomlinson, K.Y., Sasseville, C., Rogers, N., Whalen, J.B. and Stone, D. 2003: Geology and tectonostratigraphic assemblages, West Uchi map area, Manitoba and Ontario; Manitoba Geological Survey, Open File OF2003-1, Geological Survey of Canada, Open File 1522, Ontario Geological Survey, Preliminary Map P. 3461, scale 1:250 000.

Bannatyne, B.B. 1985: Industrial minerals in rare-element pegmatites of Manitoba; Manitoba Energy and Mines, Geological Services, Economic Geology Report ER84-1, 96 p., URL <https://manitoba.ca/iem/info/libmin/ER84-1.pdf> [September 2023].

Bücker, C. and Rybach, L. 1996: A simple method to determine heat production from gamma-ray logs; Marine and Petroleum Geology, v. 13, p. 373–375.

Cai, X.-Z., Dai, Z.-M. and Xu, H.-J. 2016: Thorium molten salt reactor nuclear energy system; Physics, v. 45, p. 578–590, URL <https://doi.org/10.7693/wl20160904>.

Camacho, A., Baadsgaard, H., Davis, D.W. and Černý, P. 2012: Radiogenic isotope systematics of the Tanco and Silverleaf pegmatites, Winnipeg River pegmatite district, Manitoba; The Canadian Mineralogist, v. 50, p. 1775–1792.

Carvalhêdo, A.L., Carmelo, A.C. Lima, J.P.D., Botelho, N.F. and Chornobay, A. 2025: Investigation of radiogenic heat production in granites of the Goiás Tin Province, Central Brazil; Geothermics, v. 125, art. 103183, URL <https://doi.org/10.1016/j.geothermics.2024.103183>.

Černý, P. and Ercit, T.S. 2005: The classification of granitic pegmatites revisited; The Canadian Mineralogist, v. 43, p. 2005–2026, URL <http://doi.org/10.2113/gscanmin.43.6.2005>.

Černý, P., Trueman, D.L., Ziehlke, D.V., Goad, B.E. and Paul, B.J. 1981: The Cat Lake–Winnipeg River and the Wekusko Lake pegmatite fields, Manitoba; Manitoba Department of Energy and Mines, Mineral Resources Division, Economic Geology Report ER80-1, 216 p., URL <https://manitoba.ca/iem/info/libmin/ER80-1.zip> [December 2022].

Chappell, B.W. and White, A.J.R. 1974: Two contrasting granite types; Pacific Geology, v. 8, p. 173–174.

Chappell, B.W. and White, A.J.R. 2001: Two contrasting granite types: 25 years later; Australian Journal of Earth Sciences, v. 48, p. 489–499, URL <https://doi.org/10.1046/j.1440-0952.2001.00882.x>.

Christiansen, E.H. and Keith, J.D., 1996: Trace-element systematics in silicic magmas: a metallogenic perspective; *in* Trace Element Geochemistry of Volcanic Rocks: Applications for Massive Sulfide Exploration, D.A. Wyman (ed.), Geological Association of Canada, Short Course Notes, v. 12, p. 115–151.

Dai, Z. 2017: Thorium molten salt reactor nuclear energy system (TMSR); *in* Molten Salt Reactors and Thorium Energy, T.J. Dolan (ed.), Woodhead Publishing, New Delhi, India, p. 531–540, URL <https://doi.org/10.1016/B978-0-08-101126-3.00017-8.>.

Dostal, J. 2017. Rare earth element deposits of alkaline igneous rocks; Resources, v. 6, art. 34, URL <https://doi.org/10.3390/resources6030034>.

Eby, G.N. 1990: The A-type granitoids: a review of their occurrence and chemical characteristics and speculations on their petrogenesis; Lithos, v. 26, p. 115–134.

Eby, G.N. 1992: Chemical subdivision of the A-type granitoids: petrogenetic and tectonic implications; Geology, v. 20, p. 641–644.

Ford, K.L., 2001: Reconnaissance gamma-ray spectrometry studies of the Paleoproterozoic Piling Group and adjacent Archean basement rocks, central Baffin Island, Nunavut; Geological Survey of Canada, Current Research 2001-E4, 12 p.

Gilbert, H.P., Davis, D.W., Duguet, M., Kremer, P.D., Mealin, C.A. and MacDonald, J. 2008: Geology of the Bird River Belt, southeastern Manitoba (parts of NTS 52L5, 6); Manitoba Science, Technology, Energy and Mines, Manitoba Geological Survey, Geoscientific Map MAP2008-1, scale 1:50 000, URL <https://manitoba.ca/iem/info/libmin/MAP2008-1.zip> [December 2022].

Goad, B.E. and Černý, P. 1981: Peraluminous pegmatitic granites and their pegmatite aureoles in the Winnipeg River district, southeastern Manitoba; The Canadian Mineralogist, v. 19, p. 177–194.

Grasty, R.L., Holman, P.B. and Blanchard, Y.B. 1991: Transportable calibration pads for ground and airborne Gamma-ray spectrometers; Geological Survey of Canada, Paper 90-23, 25 p.

Hacker, B.R., Kelemen, P.B. and Behn, M.D. 2011: Differentiation of the continental crust by relamination; Earth and Planetary Science Letters, v. 307, p. 501–516.

Hasterok, D. and Webb, J. 2017: On the radiogenic heat production of igneous rocks; Geoscience Frontiers, v. 8, p. 919–940.

Hasterok, D., Gard, M. and Webb, J. 2018: On the radiogenic heat production of metamorphic, igneous, and sedimentary rocks; Geoscience Frontiers, v. 9, p. 1777–1794.

Janoušek, V., Bonin, B., Collins, W.J., Farina, F. and Bowden, P. 2020: Post-Archean granitic rocks: contrasting petrogenetic processes and tectonic environments; Geological Society of London, Special Publications, v. 491, p. 1–8.

Jefferson, C.W., Thomas, D.J., Gandhi, S.S., Ramaekers, P., Delaney, G., Brisbin, D., Cutts, C., Quirt, D., Portella, P. and Olson, R.A. 2007: Unconformity-associated uranium deposits of the Athabasca Basin, Saskatchewan and Alberta; *in* Mineral Deposits of Canada: a Synthesis of Major Deposit-Types, District Metallogeny, the Evolution of Geological Provinces, and Exploration Methods, W.D. Goodfellow (ed.), Geological Association of Canada, Mineral Deposits Division, Special Publication No. 5, p. 273–305.

Killeen, P.G. and Cameron, G.W., 1977: Computation of in situ potassium, uranium, and thorium concentrations from portable gamma-ray spectrometer data; *in* Report of Activities Part A, Geological Survey of Canada, Paper 77-1A, p. 91–-92.

Koopmans, L., Martins, T., Linnen, R., Gardiner, N.J., Breasley, C.M., Palin, R.M., Groat, L.A., Silva, D. and Robb, L. J. 2024: The formation of lithium-rich pegmatites through multi-stage melting; Geology, v. 52, p. 7–11, URL <https://doi.org/10.1130/G51633.1>.

Kremer, P.D. 2010: Structural geology and geochronology of the Bernic Lake area in the Bird River greenstone belt, Manitoba: evidence for syn-deformational emplacement of the Bernic Lake pegmatite group; M.Sc. thesis, University of Waterloo, Waterloo, Ontario, 91 p.

Kromkhun, K. 2010: Petrogenesis of high heat production granite: implications for the Mt Painter Province, South Australia; Ph.D. thesis, The University of Adelaide, Adelaide, Australia, p. 1–64.

Lentz, D. 1991: Radioelement distribution in U, Th, Mo, and rare-earth-element pegmatites, skarns, and veins in a portion of the Grenville Province, Ontario and Quebec; Canadian Journal of Earth Sciences, v. 28, p. 1–12.

Lentz, D.R. 1994: A gamma-ray spectrometric study of the footwall felsic volcanic and sedimentary rocks around Brunswick No. 6 massive sulphide deposit, northern New Brunswick; *in* Current Research 1994-D, Geological Survey of Canada, p. 135–141.

Liu, X., Zhang, D., Yang, J., Xiao, C. and Zhang, T. 2023: High heat producing granites and prolonged extraction of tungsten and tin from melts; Geochimica et Cosmochimica Acta, v. 348, p. 340–354.

Long, K.R., Van Gosen, B.S., Foley, N.K. and Cordier, D. 2010: The principal rare earth elements deposits of the United States—A summary of domestic deposits and a global perspective; U.S. Geological Survey Scientific Investigations Report 2010–5220, 96 p., URL <http://pubs.usgs.gov/sir/2010/5220/> [August 2025].

Martins, T., Breasley, C., Groat, L., Linnen, R., Deveau, C. and Rankmore, S. 2024: The Tanco pegmatite: geological setting, internal zonation, mineralogy and mining of a world-class rare-element pegmatite deposit; Manitoba Business, Mining, Trade and Job Creation, Manitoba Geological Survey, Open File OF2024-3, 16 p, URL <https://www.manitoba.ca/iem/info/libmin/OF2024-3.pdf> [May 2025].

Mueller, A.G. 2025: Granite-pegmatite-related gold skarns and associated Li-Cs-Ta pegmatites in the Archean Yilgarn Craton, Western Australia; Mineralium Deposita, v. 60, p. 835–867.

Nambaje, C., Martins, T., McFarlane, C.R.M., Kaczmer, M., Rinne, M.L. and Groat, L. 2024: Preliminary results from field investigations in the Cat Lake–Winnipeg River pegmatite field, southeastern Manitoba (parts of NTS 52L5, 6, 11, 12); *in* Report of Activities 2024, Manitoba Economic Development, Investment, Trade and Natural Resources, Manitoba Geological Survey, p. 10–26, URL <https://www.manitoba.ca/iem/geo/field/roa24pdfs/GS2024-3.pdf> [November 2024].

Pearce, J.A. 1996: Sources and settings of granitic rock; Episodes, v. 19, p. 120–125.

Pearce, J.A., Harris, N.B.W. and Tindle, A.G. 1984: Trace element discrimination diagrams for the tectonic interpretation of granitic rocks; Journal of Petrology, v. 25, p. 956–983.

Percival, J.A., Sanborn-Barrie, M., Skulski, T., Stott, G.M., Helmstaedt, H. and White, D.J. 2006: Tectonic evolution of the western Superior province from NATMAP and Lithoprobe studies; Canadian Journal of Earth Sciences, v. 43, p. 1085–1117, URL <https://doi.org/10.1139/e06-062>.

Percival, J.A., Skulski, T., Sanborn-Barrie, M., Stott, G.M., Leclair, A.D., Corkery, M.T. and Boily, M. 2012: Geology and tectonic evolution of the Superior province, Canada; *in* Tectonic Styles in Canada: The Lithoprobe Perspective, J.A. Percival, F.A. Cook and R.M. Clowes (ed.), Geological Association of Canada, Special Paper No. 49, p. 321–378.

Plant, J.A., Simpson, P.R., Smith, B. and Windley, B.F. 1999: Uranium ore deposits—products of the radioactive Earth; Reviews in Mineralogy, v. 38, p. 255–319.

Pleitavino, M., Carro Pérez, M.E., García Aráoz, E. and Cioccale, M.A. 2021: Radiogenic heat production in granitoids from the Sierras de Córdoba, Argentina; Geotherm Energy, v. 9, art. 16, URL <https://doi.org/10.1186/s40517-021-00198-9>.

Radiation Solutions Inc., 2008: RS-125 Super-SPEC handheld gamma-ray spectrometer; Radiation Solutions Inc., Users Manual, URL <https://manualslib.com/maanuaal/1370682/Radiation-Solutions-Rs-125.html> [October 2025].

Regelous, A., Scharfenberg, L. and De Wall, H. 2021: Origin of S-, A- and I-type granites: petrogenetic evidence from whole rock Th/U ratio variations; Minerals, v. 11, art. 672., URL <https://doi.org/10.3390/min11070672>.

Rickard, J., Lentz, D.R., Ford, K. and Taylor, R.P. 1998: Gamma-ray spectrometric applications to volcanogenic massive sulfide exploration in the Heath Steele Mines Area, Bathurst camp, New Brunswick; Exploration and Mining Geology, v. 7, p. 287–297.

Rinne, M.L. and Martins, T. 2024: Updated structural interpretations in the Bird River domain, southeastern Manitoba (parts of NTS 52L5, 6, 11, 12); *in* Report of Activities 2024, Manitoba Economic Development, Investment, Trade and Natural Resources, Manitoba Geological Survey, p. 4–9, URL <https://www.manitoba.ca/iem/geo/field/roa24pdfs/GS2024-2.pdf> [December 2024].

Rybach, L. 1988: Determination of heat production rate; *in* Handbook of Terrestrial Heat Flow Density Determination, R. Hänel, L. Rybach and L. Stegena (ed.), Springer, Dordrecht, Netherlands, p. 125–142.

Sanjurjo-Sánchez, J., Barrientos Rodríguez, V., Arce Chamorro, C. and Alves, C. 2022: Estimating the radioactive heat production of a granitic rock in the University of A Coruña (Galicia, Northwest Spain) by gamma-ray spectrometry; Applied Science, v. 12, art. 11965, URL <https://doi.org/10.3390/app122311965>.

Shives, R.B.K. 2015: Using gamma ray spectrometry to find rare metals; *in* Symposium on Strategic and Critical Materials Proceedings, G.J. Simandl and M. Neetz (ed.), November 13–14, 2015, Victoria, British Columbia, British Columbia Ministry of Energy and Mines, British Columbia Geological Survey Paper 2015-3, p. 199–209.

Shives, R.B.K., Charbonneau, B.W. and Ford, K.L. 2000: The detection of potassic alteration by gamma-ray spectrometry—recognition of alteration related to mineralization; Geophysics, v. 65, p. 2001–2011.

Smithies, R.H., Lu, Y., Champion, D.C., Sweetapple, M.T., Lowrey, J.R., Bowman, N.H., Cassidy, K.F., Ivanic, T.J., Kemp, A.I.S., Turnbull, R.E., Gessner, K., Korhonen, F.J.2025: Giant lithium-rich pegmatites in Archean cratons form by remelting refertilised roots of greenstone belts; Communications Earth & Environment, v. 6, art. 630, URL <https://doi.org/10.1038/s43247-025-02622-5>.

Stott, G.M., Corkery, M.T., Percival, J.A., Simard, M. and Goutier, J. 2010: A revised terrane subdivision of the Superior Province; *in* Summary of Field Work and Other Activities 2010, Ontario Geological Survey, Open File Report 6260, p. 20-1–20-10.

Thomas, M.D., Ford, K.L. and Keating, P. 2016: Review paper: exploration geophysics for intrusion-hosted rare metals; Geophysical Prospecting, v. 64, p. 1275–1304.

Van Lichtervelde, M., Grégoire, M., Linnen, R.L., Béziat, D. and Salvi, S. 2008: Trace element geochemistry by laser ablation ICP-MS of micas associated with Ta mineralization in the Tanco pegmatite, Manitoba, Canada; Contributions to Mineralogy and Petrology, v. 155, p. 791–806.

Vilà, M., Fernández, M. and Jiménez-Munt, I. 2010: Radiogenic heat production variability of some common lithological groups and its significance to lithospheric thermal modeling; Tectonophysics, v. 490, p. 152–164.

Wang, X. 1993: U-Pb zircon geochronology study of the Bird River greenstone belt, southeastern Manitoba; M.Sc. thesis, University of Windsor, Windsor, Ontario, 96 p.

Whalen, J.B. and Hildebrand, R.S. 2019: Trace element discrimination of arc, slab failure, and A-type granitic rocks; Lithos, v. 348–349, art. 105179, URL <https://doi.org/10.1016/j.lithos.2019.105179>.

Whalen, J.B., Currie, K.L. and Chappell, B.W. 1987: A-type granites: geochemical characteristics, discrimination and petrogenesis; Contributions to Mineralogy and Petrology, v. 95, p. 407–419.

Yang, X.M. 2014: Granitoid rocks in southeastern Manitoba: preliminary results of reconnaissance mapping and sampling; *in* Report of Activities 2014, Manitoba Mineral Resources, Manitoba Geological Survey, p. 49-63, URL <https://manitoba.ca/iem/geo/field/roa14pdfs/GS-4.pdf> [December 2022].

Yang, X.M. 2017: Estimation of crystallization pressure of granite intrusions; Lithos, v. 286–287, p. 324–329, URL <https://doi.org/10.1016/j.lithos.2017.06.018>.

Yang, X.M. 2023: Progress report on the study of granitoids in Manitoba: petrogenesis and metallogeny; Manitoba Economic Development, Investment and Trade, Manitoba Geological Survey, Open File OF2022-3, 119 p., URL <https://www.gov.mb.ca/iem/info/libmin/OF2022-3.zip> [March 2023].

Yang, X.M. and Houlé, M.G. 2020: Geology of the Cat Creek−Euclid Lake area, Bird River greenstone belt, southeastern Manitoba (parts of NTS 52L11, 12); Manitoba Department of Agriculture and Resource Development, Manitoba Geological Survey, Geoscientific Report GR2020-1, 105 p., plus 1 map at 1:20 000 scale, URL <https://manitoba.ca/iem/info/libmin/GR2020-1.zip> [October 2021].

Yang, X.M., Drayson, D. and Polat, A. 2019: S-type granites in the western Superior Province: a marker of Archean collision zones; Canadian Journal of Earth Sciences, v. 56, p. 1409–1436, URL <https://doi.org/10.1139/cjes-2018-0056>.

Yang, X.M., Lentz, D.R. and Chi, G. 2021: Ferric-ferrous iron oxide ratios: effect on crystallization pressure of granites estimated by Qtz-geobarometry; Lithos, v. 380–381, art. 105920, URL <https://doi.org/10.1016/j.lithos.2020.105920>.

Yang, X.M., Lentz, D.R. and Martins, T. 2025: Gamma-ray spectrometric data of granitoid rocks and related rocks from the terrane boundary zone between the Bird River and Winnipeg River domains, southeastern Manitoba (parts of NTS 52L3–6, 62I8); Manitoba Business, Mining, Trade and Job Creation, Manitoba Geological Survey, Data Repository Item DRI2025031, Microsoft® Excel® file.

Zhou, X., Li, Z., Lu, Y., Huang, H., He, Z., Dai, Z. and Xu, H. 2019: Development strategy for thorium molten salt reactor materials; Strategic Study of Chinese Academy of Engineering, v. 21, p. 29-38, URL <https://doi.org/10.15302/J-SSCAE-2019.01.005>.

Zhou, X., Lin, S. and Anderson, S.D. 2012: Structural study of the Ogama-Rockland gold deposit, southeastern margin of the Ross River pluton, Rice Lake greenstone belt, southeastern Manitoba (NTS 52L14); *in* Report of Activities 2012, Manitoba Innovation, Energy and Mines, Manitoba Geological Survey, p. 59–67, URL <https://manitoba.ca/iem/geo/field/roa12pdfs/GS-5.pdf> [December 2022].

Zhou, X., Lin, S. and Anderson, S.D. 2016: Stratigraphy, structure and lode gold system at the Central Manitoba mine trend, Rice Lake greenstone belt, Archean Superior Province, Manitoba, Canada; Precambrian Research, v. 281, p. 80–100, URL <https://doi.org/10.1016/j.precamres.2016.05.020>.

GS2025-3

Preliminary investigations into mica, cesium and quartz mineralization in the Cat Lake–Winnipeg River pegmatite field, southeastern Manitoba (parts of NTS 52L6, 11)

by Z. Rahabi[1], T. Martins, D.R. Lentz[1] and L. Groat[2]

In Brief:

- High Cs grades in drill core from the Cat Lake-Winnipeg River pegmatite field are limited to strongly foliated, biotite-rich country rock along pegmatite contacts
- The quartz and pollucite zones of the Tanco pegmatite have highly variable contacts, locally marked by spodumene and quartz intergrowths
- The habits and distribution of micas were described at the Tanco pegmatite and are highly variable

Citation:
Rahabi, Z., Martins, T., Lentz, D.R. and Groat, L. 2025: Preliminary investigations into mica, cesium and quartz mineralization in the Cat Lake–Winnipeg River pegmatite field, southeastern Manitoba (parts of NTS 52L6, 11); *in* Report of Activities 2025, Manitoba Business, Mining, Trade and Job Creation, Manitoba Geological Survey, p. 20–32.

Summary

Details of the preliminary results of an investigation into cesium and quartz mineralization at the Tanco pegmatite and other selected pegmatites in the Cat Lake–Winnipeg River pegmatite field during the 2025 field season are given in this report. This project is a collaboration between the Manitoba Geological Survey, the University of New Brunswick, The University of British Columbia, New Age Metals Inc. and the Tantalum Mining Corporation of Canada Limited-Sinomine Resource Group Co., Ltd. Included within this report is an overview of the different varieties of mica present at the Tanco mine, an investigation into high-cesium (>1000 ppm) intervals in drillcore from the Cat Lake–Winnipeg River pegmatite field, and preliminary characterizations of the quartz and pollucite zones hosted within the Tanco pegmatite. Notable preliminary results of these investigations include: the observation that high-grade cesium intervals in the Cat Lake–Winnipeg River pegmatite field are limited to strongly foliated, biotite-rich country-rock intervals along pegmatite contacts; the identification of a distinct striped or banded pattern and local colour/opacity zonation within the quartz zone of the Tanco pegmatite; and the identification of internally zoned quartz±albite veinlets within the pollucite zone of the Tanco pegmatite. In future studies, the causes of these phenomena will be investigated, with the goal of characterizing the relationship between quartz and pollucite mineralization in the Tanco pegmatite, and their relationship to the late-stage magmatic-hydrothermal system documented in many highly fractionated pegmatites.

Introduction

Canadian rare-element pegmatites are known sources of 'critical minerals' (e.g., Cs, Li, Nb, Ta, Sn and rare-earth elements) considered essential for Canada's economic or national security (Natural Resources Canada, 2025), as well as of industrial minerals such as high-purity quartz and feldspars (e.g., London, 2018). However, the way such pegmatites form and become enriched in these resources is currently not fully understood.

The Tanco pegmatite in southeastern Manitoba is a rare-element–Li subclass, complex type, petalite subtype pegmatite of the Li-Cs-Ta (LCT) family (classification after Černý and Ercit, 2005), which is currently being mined for Cs and Li and used to be mined for Ta (Martins et al., 2024). At one point, the Tanco mine was estimated to contain approximately 80% of current global reserves of Cs (Gilbert et al., 2008). The Tanco pegmatite is a part of the larger Cat Lake–Winnipeg River pegmatite field, which is overall considered prospective for many critical and industrial minerals (Černý et al., 1981). The Tanco pegmatite and Cat Lake–Winnipeg River pegmatite field have historically been the subject of many local- and regional-scale studies (e.g., Černý et al., 1981; 1996; London, 1985; Morgan and London, 1987; Stilling, 1998; Stilling et al., 2006; Camacho et al., 2012; Breasley et al., 2022; 2024; 2025; Martins et al., 2024; Nambaje et al., 2024); however, few of these studies have focused on Cs mineralization in the region, despite its abundance at the Tanco mine and its prospectivity elsewhere in the Cat Lake–Winnipeg River pegmatite field.

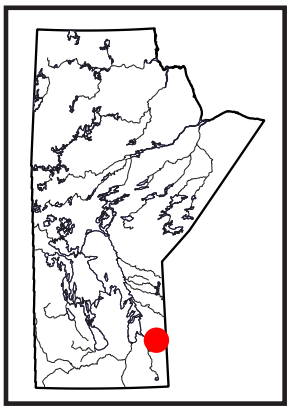

The Tanco pegmatite displays complex internal zonation of mineral assemblages, including a 'pollucite zone', which comprises up to 75% pure pollucite, as well as a 'quartz zone' that occurs as massive lenses of essentially monomineralic quartz and represents a highly evolved pegmatitic core (Černý et al., 1996). These two zones are commonly found in direct contact with each other (Černý et al., 1996; Stilling et al., 2006; Martins et al., 2024), suggesting a possible genetic relationship between the two. The existence of an extensive zone of massive pollucite has interesting implications for late-

[1] Department of Earth Sciences, University of New Brunswick, Fredericton, New Brunswick, zanealdeen.rahabi@unb.ca
[1] Department of Earth Sciences, University of New Brunswick, Fredericton, New Brunswick, dlentz@unb.ca
[2] Department of Earth, Ocean and Atmospheric Sciences, The University of British Columbia, Vancouver, British Columbia

stage magmatic-hydrothermal processes in the Tanco pegmatite area, given the strong incompatibility of Cs, as well as the potential involvement of fluid immiscibility and/or late-stage hydrothermal processes in the formation of massive pollucite (Dittrich et al., 2019). The aim of this project is to investigate the nature, distribution and controls on quartz and Cs mineralization within the Tanco deposit, including the potential involvement of fluid immiscibility processes (London, 1986; London et al., 1998). This includes a study of the various forms of mica present at the Tanco mine, to gain insight into the complex magmatic-hydrothermal processes responsible for the formation of the deposit, as well as a study of pegmatite-related Cs mineralization elsewhere in the Cat Lake–Winnipeg River pegmatite field, to more generally investigate the behavior of Cs in local pegmatite systems.

Access to the Tanco mine for the 2025 season was delayed due to wildfires in the area. As a result, fieldwork began with the process of compiling a comprehensive list of different mica varieties at the Tanco mine based on samples from the University of Manitoba. This was followed by examination and sampling of recent pegmatite-bearing drillcore from the Cat Lake–Winnipeg River pegmatite field, with drillcore data and core-yard access provided by New Age Metals Inc. Once access to the Tanco mine was granted, fieldwork for the rest of the season consisted mostly of logging and sampling drillcore that crosscut the quartz and pollucite zones of the Tanco pegmatite, based on cross-section and historical core logs.

In total, 18 drillcores (Tantalum Mining Corporation of Canada Limited-Sinomine Resource Group Co., Ltd., unpublished data) recovered from the Tanco pegmatite were logged, with 146 quartz samples and 28 pollucite samples selected. Samples were collected from an additional 10 drillcores, but they were not logged in full. In addition to these samples, an additional 14 non-quartz or pollucite drillcore samples were selected, comprising material which could prove useful in future studies. Limited underground access was also granted, allowing for the collection of 14 mine samples, mostly comprising pollucite-zone or wall-zone material.

Geological setting

The Cat Lake–Winnipeg River pegmatite field is in the Neoarchean Bird River greenstone belt (BRGB) of the western Superior Province in southeastern Manitoba. The BRGB is situated between the English River basin and Winnipeg River terrane, and forms part of an east-trending supracrustal belt, which extends for 150 km from Lac du Bonnet in the west to Separation Lake (Ontario) in the east (Figure GS2025-3-1; Gilbert et al., 2008; Yang and Houlé, 2020). Mineral deposits within the BRGB include shear-hosted gold, magmatic Ni–Cu–Cr–platinum-group element and Li-Cs-Ta rare-element pegmatites (e.g., Černý et al., 1981, Nambaje et al., 2024).

The Cat Lake–Winnipeg River pegmatite field is divided into two districts, these being the Winnipeg River and the Cat Lake–

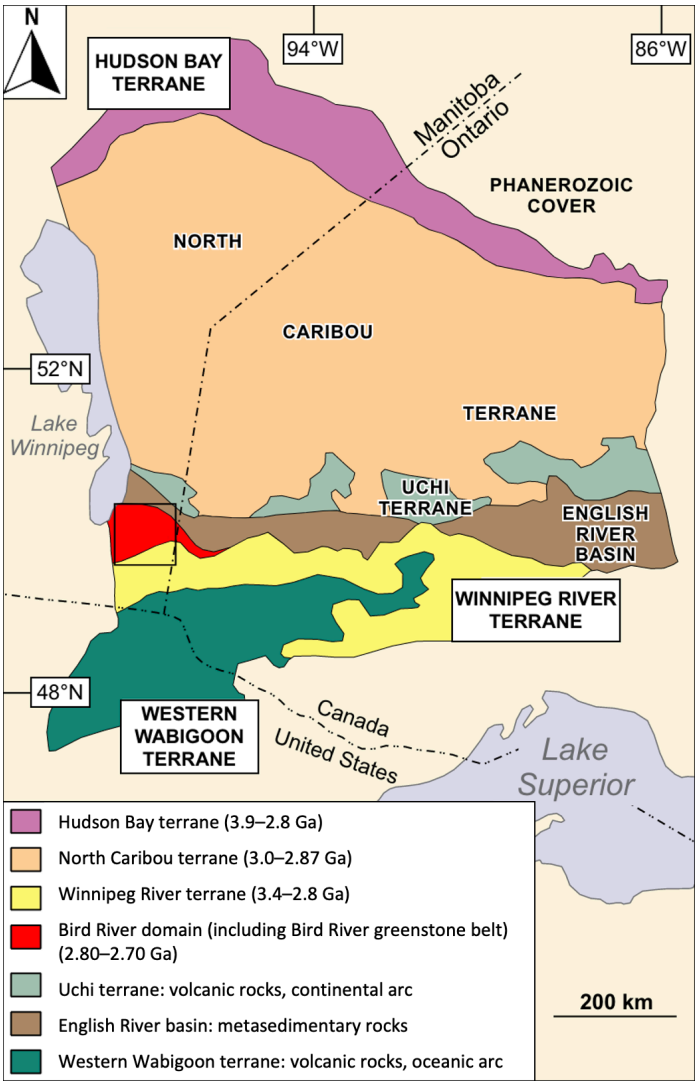

Figure GS2025-3-1: *Simplified geology of the western Superior Province showing the location of the Bird River greenstone belt (modified from Gilbert et al., 2008; Yang and Houlé, 2020), with the area of Figure GS2025-3-2 outlined in black.*

Maskwa Lake districts (Černý et al., 1981). Pegmatites of these districts are then further divided into several distinct pegmatite groups, including the Greer Lake, Eagle-Irgon, Rush Lake and Bernic Lake groups, the latter of which includes the Tanco pegmatite (Černý et al., 1981). Pegmatites investigated and sampled in this study include the Tanco pegmatite, as well as the Silverleaf pegmatite of the Greer Lake group, the Eagle and Magpie pegmatites of the Eagle-Irgon group and the RL-7 pegmatite of the Rush Lake group (Figure–GS2025-3-2). These pegmatites are briefly described below, with a separate section dedicated to the larger and more complex Tanco pegmatite.

The Tanco pegmatite

The Tanco pegmatite (Bernic Lake group; Figure GS2025-3-2) is hosted by the Tanco gabbro, dated at 2723.1 ±0.8 Ma (Gilbert et al., 2008). This gabbro is part of the larger Bernic Lake forma-

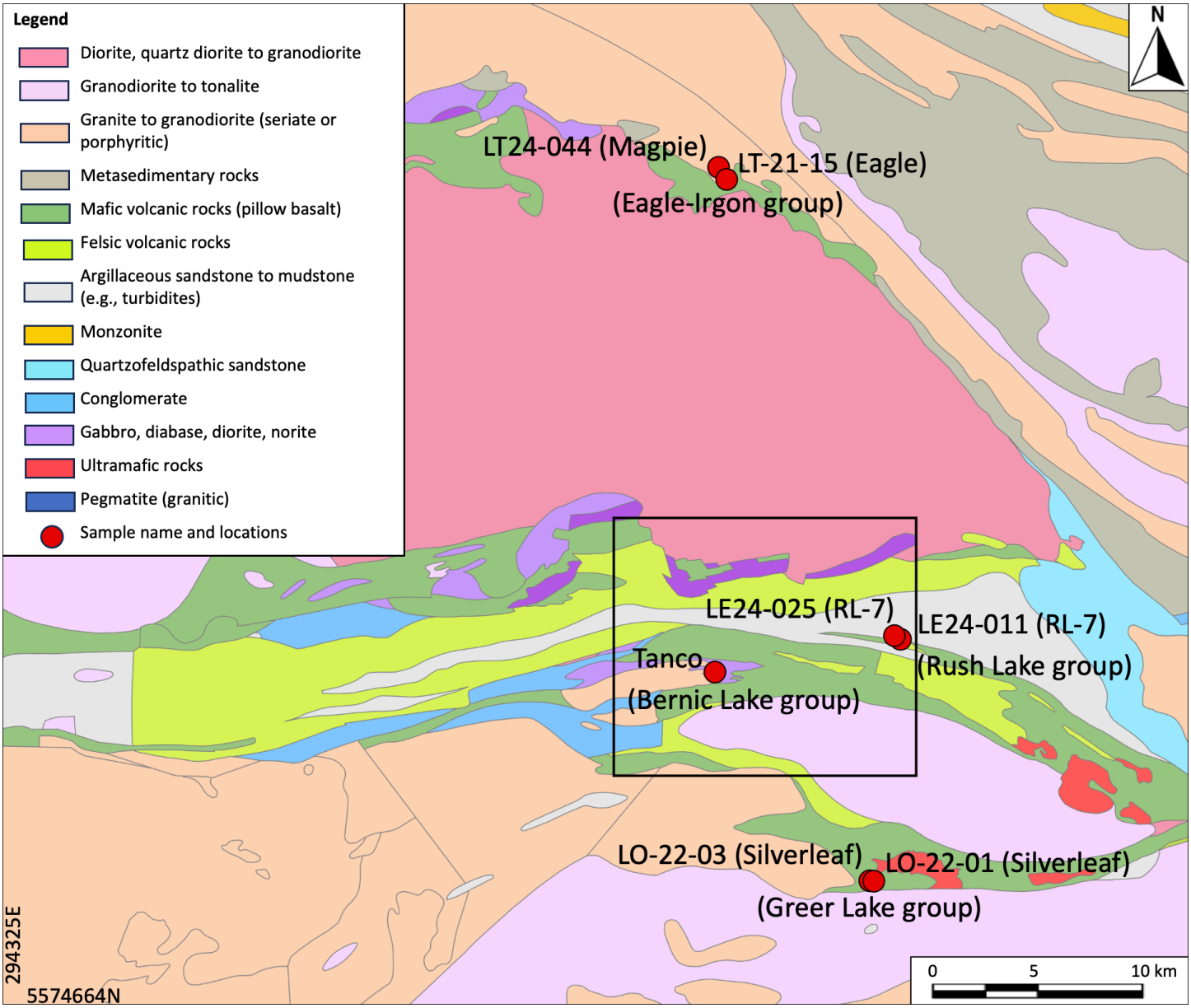

Figure GS2025-3-2: *Geology of the Bird River greenstone belt (modified from Manitoba Geological Survey, 2022; Nambaje et al., 2024), with names and locations of sampled drillcores and pegmatites, as well as their respective pegmatite groups. The area of Figure GS2025-3-3 is outlined in black.*

tion, which is characterized by a dominantly mafic, volcanic-rich unit dated at 2724.6 ±1 Ma located in the southern portion of the BRGB (Figure GS2025-3-3; Gilbert et al., 2008). The Tanco gabbro and Bernic Lake formation are metamorphosed to greenschist and amphibolite facies (Černý et al., 1981).

The Tanco pegmatite is a subhorizontal, essentially undeformed, bilobate, saddle-shaped body about 1520 m long, 1060 m wide and up to 100 m thick. Its volume has been estimated as approximately 21 850 000 m³, with a mass of approximately 57 430 000 tonnes and an average density of 2.63 g/cm³ (Stilling et al., 2006). Uranium-lead dating of tantalite minerals from the pegmatite has yielded intrusive ages ranging from 2647.4 ±1 Ma (Kremer, 2010) to 2641 ±3 Ma (Camacho et al., 2012).

The Tanco pegmatite displays a complex internal zonation of mineral assemblages (Figure GS2025-3-4b), with nine major zones described in total, as well as several subzones and transitional zones. The mineralogy and petrography of all zones is described in detail by several authors (e.g., Stilling et al., 2006; Breasley et al., 2022; Martins et al., 2024) and is briefly outlined below, with a focus on the major zones of the pegmatite.

The hostrock of the Tanco pegmatite is commonly referred to as 'amphibolite' but is synonymous with the Tanco gabbro. It generally comprises 54% hornblende, 37% plagioclase, 4% ilmenite, 4% quartz and 1% apatite, with minor epidote, biotite, chlo-

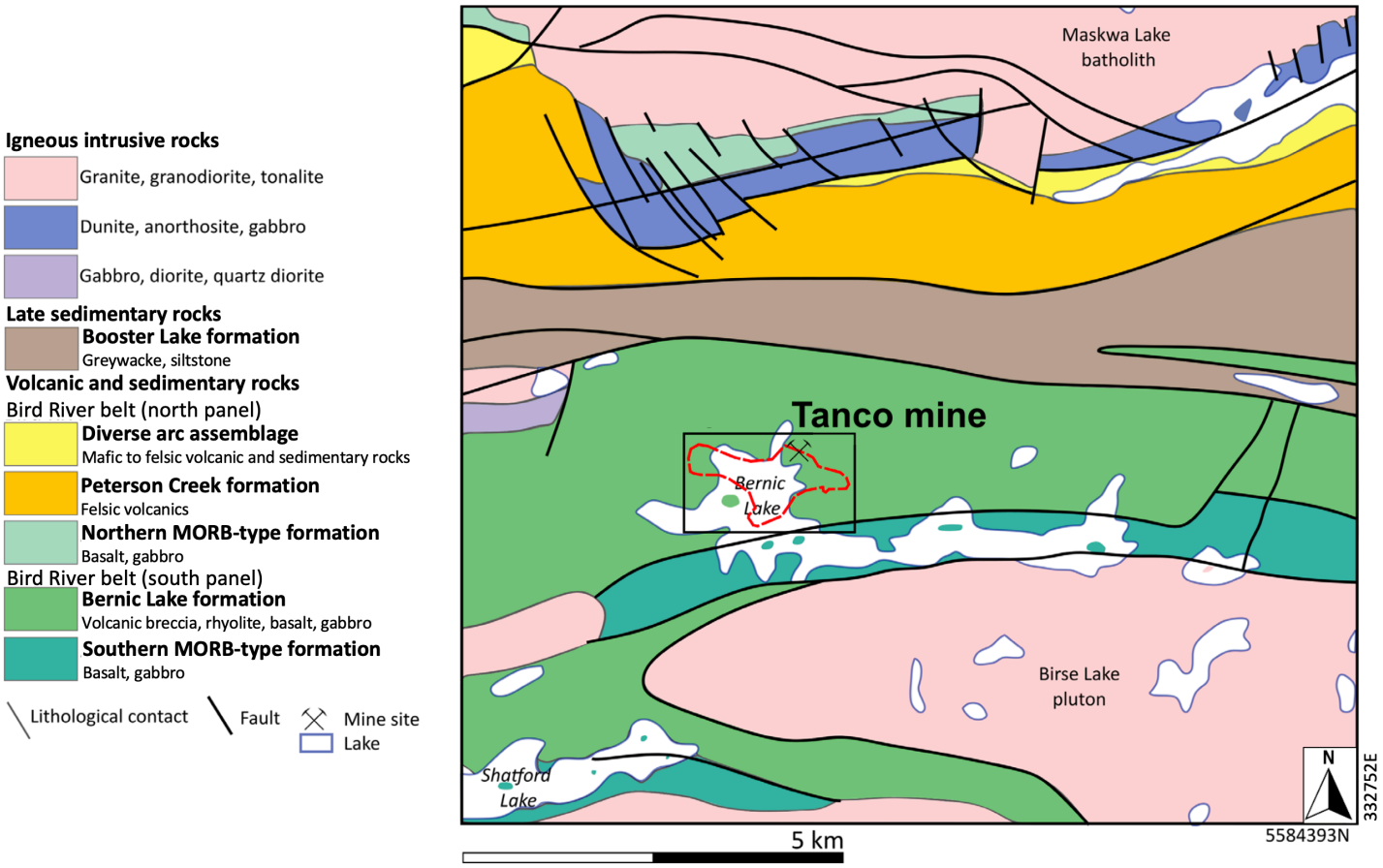

Figure GS2025-3-3: *Location and surrounding geology of the Tanco pegmatite (surface projection of the deposit indicated by dashed red line; Stilling et al., 2006) of the Cat Lake–Winnipeg River pegmatite field (modified from Gilbert, 2008; Breasley et al., 2021, 2022, 2024). The location of the Tanco mine is labeled and the area of Figure GS2025-20-4a is outlined in black. Abbreviation: MORB, mid-ocean–ridge basalt.*

rite and almandine (Morgan and London, 1987; Breasley et al., 2022; Martins et al., 2024).

The border zone of the Tanco pegmatite represents the portion of the pegmatite that crystallized first along the hostrock contact. It comprises a <30 cm thick zone of fine-grained quartz and albite and locally includes minor apophyses, which intrude into the hostrock (Stilling et al., 2006; Breasley et al., 2022; Martins et al., 2024).

The wall zone (zone 20; Figure GS2025-3-4b) comprises simple pegmatite up to 35 m thick, which roughly approximates the Tanco pegmatite's bulk composition. It is composed of megacrystic microcline-perthite, quartz, albite and Li-muscovite. Minor components include beryl, tourmaline and muscovite (Černý, 2005; Breasley et al., 2022; Martins et al., 2024).

The aplitic albite zone (zone 30; Figure GS2025-3-4b) is locally up to 16 m thick, and generally comprises aplitic albite, quartz and muscovite, with minor Ta-oxides, beryl, apatite, tourmaline, cassiterite, ilmenite, zircon and sulphides. It has a distinct pale blue-white colour, with local dark brown to black clots of Ta/Nb-bearing minerals (Černý et al., 1996; Breasley et al., 2022; Martins et al., 2024).

The lower intermediate zone (zone 40; Figure GS2025-3-4b) is up to 25 m thick and is also known as the 'mixed zone' due to its highly variable mineralogy. It comprises medium- to coarse-grained perthite, albite, quartz, amblygonite and spodumene (including spodumene and quartz intergrowths [SQUI]). Minor components include Li muscovite, lithiophilite, lepidolite, petalite and Ta-oxides. It is distinguished from zone 50 (see below) by the presence of abundant feldspars (Černý et al., 1996; Breasley et al., 2022; Martins et al., 2024).

The upper intermediate zone (zone 50; Figure GS2025-3-4b) is up to 24 m thick and is the most enriched in Li mineralization, comprising giant (up to 13 m long) crystals of spodumene, quartz and amblygonite. Minor components include microcline-perthite, pollucite, lithiophilite, petalite, eucryptite, Ta-oxides, albite and Li muscovite. The presence of minor quartz pods, triphylite and apatite is noted in historical drill logs (Černý et al., 1996; Breasley et al., 2022; Martins et al., 2024).

The central intermediate zone (zone 60; Figure GS2025-3-4b) is up to 45 m thick and is thought to be entirely metasomatic in origin. Known as the 'muscovite and quartz alteration after microcline' (MQM) zone, it is also the most enriched in

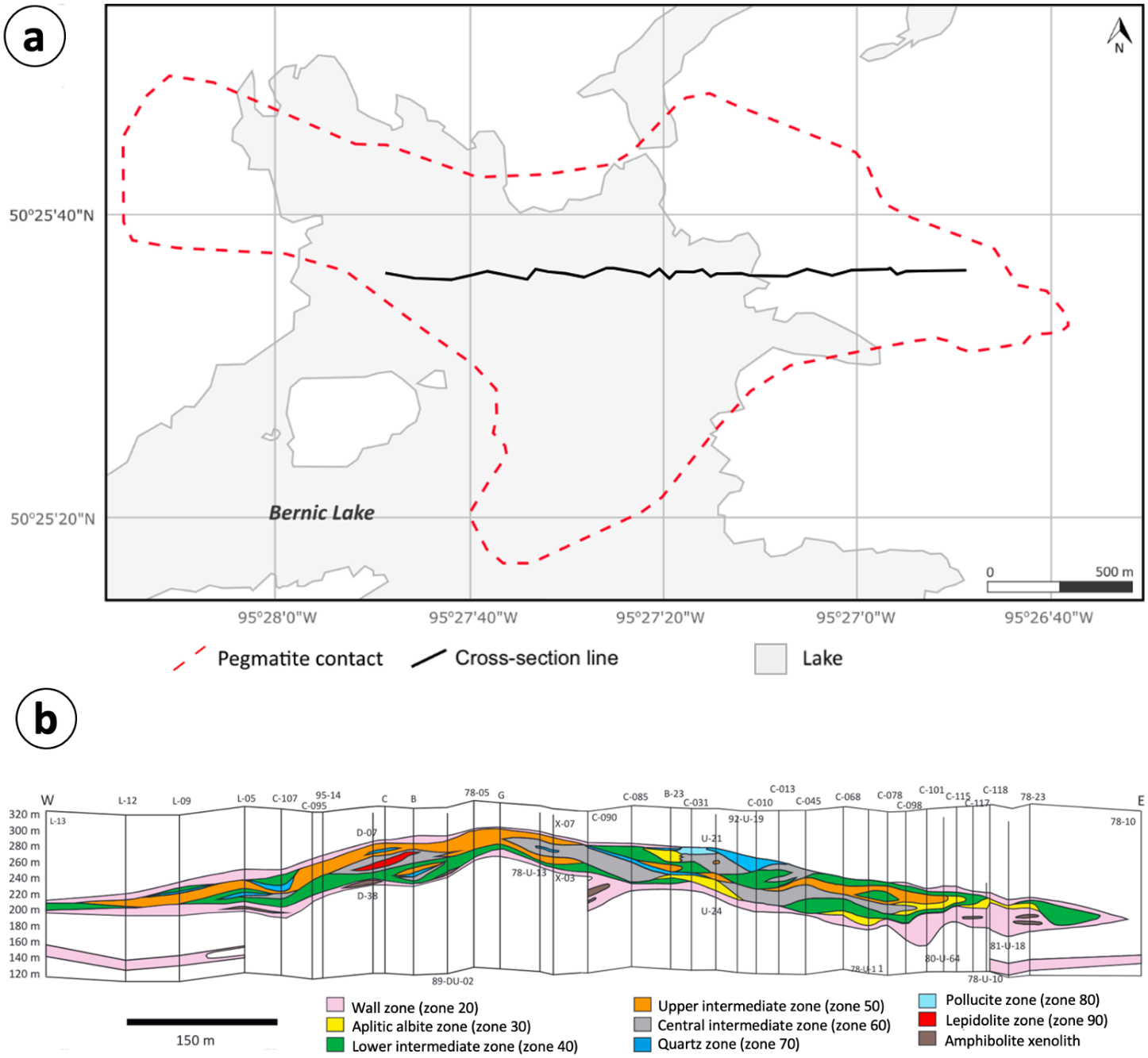

Figure GS2024-3-4: *The Tanco pegmatite of the Cat Lake–Winnipeg River pegmatite field:* ***a)*** *location of the deposit (projected to surface) and path of cross-section shown in (b), modified from Stilling et al. (2006) and Breasley et al. (2022);* ***b)*** *east-west cross-section (looking north) of the Tanco pegmatite, showing major zones (based on drillcore data), and drillcore names and locations (modified from Stilling et al., 2006; Breasley et al., 2022; Martins et al., 2024).*

Ta mineralization. It also comprises medium- to coarse-grained microcline-perthite, quartz, albite and muscovite, with minor beryl, Ta-oxides, zircon, ilmenite, spodumene, sulphides, lithiophilite, apatite and cassiterite (Černý et al., 1996; Breasley et al., 2022; Martins et al., 2024).

The quartz zone (zone 70; Figure GS2025-3-4b) represents a highly evolved pegmatitic core and comprises massive monomineralic quartz lenses, with minor amblygonite, spodumene and possible petalite (Stilling et al., 2006; Breasley et al., 2022; Martins et al., 2024).

The pollucite zone (zone 80; Figure GS2025-3-4b) comprises up to 75% pure pollucite, with minor quartz, spodumene, petalite, muscovite, lepidolite, albite, microcline and apatite (Černý et al., 1996; Breasley et al., 2022; Martins et al., 2024). Alteration of pollucite to adularia and clay minerals in this zone has resulted in a characteristic texture known as the 'tapioca' texture (Černý et al., 1981, Figure 90).

The lepidolite zone (zone 90; Figure GS2025-3-4b) is <18 m thick and is thought to have formed due to metasomatism. It features abundant fine-grained to saccharoidal Li-muscovite as

replacement of primary feldspar. The zone comprises dominantly Li-muscovite, lepidolite and microcline-perthite, with minor albite, quartz, beryl, cassiterite, zircon and Ta-oxides (including abundant microlite; Černý et al., 1996; Breasley et al., 2022; Martins et al., 2024).

Other pegmatites studied during the 2025 season

The Silverleaf pegmatite (Greer Lake group; Figure GS2025-3-2) is a metabasalt-hosted, Li-bearing pegmatite with a surface exposure of approximately 80 m by 45 m. It comprises spodumene, quartz, feldspar, muscovite, lepidolite, garnet and apatite (Bannatyne, 1985; Nambaje et al., 2024). Uranium-lead isotopic ages for zircon megacrystic fragments from the Silverleaf pegmatite range from about 2660 to 2600 Ma (Camacho et al., 2012). A more detailed description of mineral assemblages in the Silverleaf pegmatite can be found in Bannatyne (1985).

The Eagle pegmatite (Eagle-Irgon group; Figure GS2025-3-2) is a metagranodiorite-hosted Li-mineralized pegmatite comprising several dikes with thicknesses varying between 10 cm and 9 m. Its mineralogy is mostly uniform, consisting of varying modal percentages of feldspar (hematized plagioclase±K-feldspar), quartz, green spodumene and white micas, with minor apatite, beryl and lepidolite (Roush et al., 2023; Nambaje et al., 2024).

The Magpie pegmatite (Eagle-Irgon group; Figure GS2025-3-2) is located north-northwest of the Eagle pegmatite. It is noted to contain localized spodumene zones, based on drillcore from New Age Metals Inc. (New Age Metals Inc., 2024). Little additional information is available.

The RL-7 pegmatite (Rush Lake group; Figure GS2025-3-2) comprises abundant microcline and quartz, subordinate albite, and rare biotite, muscovite and schorl (black tourmaline). It is unzoned but becomes increasingly coarse grained toward the centre (Černý et al., 1981). Little additional information is available regarding this pegmatite.

Micas of the Tanco pegmatite

Micas (e.g., muscovite, biotite, lepidolite) are common components of most peraluminous granitic pegmatites and are one of several minerals that can be used to quantify the evolution of such pegmatites via incompatible trace-element mineral chemistry. The trace-element contents of micas can range from tens of parts per million to high weight-percent values, and as such they are particularly useful as a window into the complex magmatic-hydrothermal processes in pegmatites (e.g., Benn et al., 2022).

Micas of the Tanco pegmatite are highly variable in terms of grain size, colour and crystal habit, with certain variations being local to specific zones of the pegmatite. Past studies of micas of the Tanco pegmatite, for example Rinaldi et al. (1972) and Van Lichtervelde et al. (2008), focused on Li-Rb-Cs micas and micas associated with Ta mineralization, respectively. The latter study found that micas of the Tanco pegmatite can contain up to 2.15 wt. % Cs_2O. Higher weight-percent values were found to be associated with coarser grained, more highly fractionated primary or magmatic-metasomatic event-derived micas, whereas fine-grained micas associated with later aqueous fluid-derived metasomatism were shown to be less evolved, with lower Cs_2O contents (Van Lichtervelde et al., 2008). The relationship between Cs concentrations, fractionation and metasomatic fluids demonstrated by micas of the Tanco pegmatite suggests that a review of these highly variable micas could shed light on Cs-enrichment processes in the pegmatite.

Zone 20 commonly contains pegmatitic (i.e., >2.5 cm) tabular crystals or 'books' of greenish to silver muscovite (Figure GS2025-3-5a). Biotite is also locally observed and this zone is seemingly the only zone of the Tanco pegmatite in which biotite appears. Curvilamellar to botryoidal masses of mica in the Tanco pegmatite produce a particularly common texture, which is colloquially referred to as 'ball-peen' texture. In cross-section, ball-peen micas are observed to form radial masses and are commonly associated with radial to tabular cleavelandite, suggesting a possible paragenetic relationship. Ball-peen silver muscovite and lavender Li-muscovite are common within zone 20. Most micas within zone 20 appear to be primary; however, local fine-grained, green muscovite is also present, which may represent a secondary alteration product after K-feldspar.

Micas within zone 30 are saccharoidal and are generally incorporated into the aplite, which makes up most of this zone. The micas consist of green muscovite and purple lepidolite, with the latter being locally incorporated into the banded textures that are common in this zone (Figure GS2025-3-5b). It is possible that saccharoidal micas within zone 30 represent later metasomatic alteration of the aplite or, alternatively, represent compositional variations in the melt during episodic aplite crystallization.

Micas within zone 40 are highly varied, and include muscovite, Li-muscovite, paragonite and lepidolite. Muscovite locally exhibits a likely primary, pegmatitic, tabular habit within this zone, but is also a common component of later alteration assemblages. These include muscovite+Li-muscovite after rubellite (Figure GS2025-3-5c), fine-grained muscovite+cookeite after spodumene and fine- to medium-grained pale green to yellow-green muscovite+paragonite after feldspar, with local ball-peen habit. Muscovite also occurs as rims on amblygonite-montebrasite crystals in association with apatite within zone 40. In addition to being part of the alteration assemblage after rubellite, Li-muscovite also occurs as likely primary, grey to lavender curvilamellar masses (Figure GS2025-3-5d). Lepidolite in zone 40 locally shows both medium- to coarse-grained tabular and ball-peen habits (Figure GS2025-3-5e).

Micas within zone 50 mostly comprise different varieties of muscovite and share some similar modes of occurrence with those of zone 40, including muscovite+cookeite after spodumene, muscovite+paragonite after feldspar and muscovite+apatite rims on amblygonite-montebrasite. In addition to the above, micas within zone 50 include medium- to coarse-grained, late-stage

Figure GS2025-3-5*: Assorted micas from the Tanco pegmatite of the Cat-Lake–Winnipeg River pegmatite field:* ***a)*** *pegmatitic muscovite (+albite) from zone 20;* ***b)*** *saccharoidal lepidolite (+aplitic albite, quartz) from zone 30, showing compositional banding;* ***c)*** *muscovite+Li-muscovite after rubellite (+quartz) from zone 40;* ***d)*** *coarse-grained ball-peen Li-muscovite (+quartz, albite) from zone 40;* ***e)*** *coarse-grained tabular lepidolite (+quartz, K-feldspar) from zone 40;* ***f)*** *coarse-grained late-stage green muscovite (+primary lepidolite, albite, quartz) from zone 50;* ***g)*** *massive saccharoidal grey muscovite from zone 50;* ***h)*** *saccharoidal pale green muscovite after microcline+quartz and wodginite (black specks) from zone 60;* ***i)*** *coarser grained green mica veining microcline and aplitic albite from zone 60;* ***j)*** *saccharoidal lepidolite veining in pollucite from zone 80;* ***k)*** *saccharoidal lepidolite (+Ta-oxides) from zone 90. Coin diameter is 3 centimetres.*

green muscovite (Figure GS2025-3-5f), as well as fine-grained muscovite, quartz and albite intergrowths. Several varieties of saccharoidal-textured muscovite are found within zone 50, including saccharoidal green to purple muscovite veins in pollucite, as well as saccharoidal grey muscovite associated with wodginite mineralization (Figure GS2025-3-5g).

Zone 60 is defined by the presence of abundant very fine grained to saccharoidal, metasomatic green muscovite after microcline feldspar, which is locally associated with Ta-oxides (Figure GS2025-3-5h). Green mica within zone 60 may also occur as a coarser grained variety in the matrix of apparent hydrothermal breccias (Figure GS2025-3-5i), with local ball-peen habit. Purple Li-muscovite and lepidolite are locally present within zone 60, generally as coarse-grained tabular to curvilamellar masses. Coarse-grained Li-muscovite within zone 60 was noted by Van Lichtervelde et al. (2008) to be relatively geochemically evolved and possibly representative of magmatic metasomatism associated with Ta mineralization. However, fine-grained green muscovite after microcline was noted to be less evolved and was linked to later aqueous fluid-derived metasomatism.

No samples from zone 70 are included within the Tanco collection of the University of Manitoba, but observations conducted as part of this study show that rare lenses of SQUI and K-feldspar within zone 70 are locally associated with dark green, yellow-green and grey muscovite.

A few mica-bearing samples from zone 80 are included within the Tanco collection of the University of Manitoba. These

samples locally feature Li-Rb muscovite veining or alteration of pollucite. In an investigation regarding paragenetic relationships between zones 80 and 90 of the Tanco pegmatite, Breasley et al. (2024) also showed that mesh-like veining of lepidolite within zone 80 (Figure GS2025-3-5j) is found close to the contact with zone 90.

Finally, in addition to previously mentioned, fine-grained to saccharoidal lepidolite and Li-muscovite present within zone 90 (Figure GS2025-3-5k), samples from the Tanco collection also show the presence of local coarser grained Li-muscovite within zone 90.

Cesium in the Cat Lake–Winnipeg River pegmatite field

In addition to the investigation into mica variations in the Tanco pegmatite, an investigation into Cs mineralization in granitic pegmatites of the Cat Lake–Winnipeg River pegmatite field was initiated as part of this project. Drillcores were selected based on the presence of high-grade Cs intervals (>1000 ppm), with some intervals grading over 5000 ppm Cs. In total, six drillcores were studied and sampled (Figure GS2025-3-2).

It was noted that high-grade Cs intervals consistently comprised metasedimentary or metabasaltic hostrock adjacent to pegmatite, rather than the actual pegmatite dikes themselves (Figure GS2025-3-6a–f). Even in drillcores from the generally granodiorite-hosted Eagle-Irgon group, it was observed that high-grade Cs intervals occurred specifically in strongly foliated amphibolite lenses within the host granodiorite, rather than within the granodiorite itself (Figure GS2025-3-6a, f).

Restriction of high-grade Cs intervals to metamorphic hostrocks was interpreted to represent metasomatism by Cs-bearing hydrothermal fluids, which could have separated from pegmatitic melts due to fractionation processes (e.g., London et al., 1998). Preliminary geochemical analysis shows that high-grade Cs intervals are consistently associated with low K/Rb ratios, supporting an origin linked to metasomatism by highly evolved fluids.

In most cases, no visible change in hostrock colour or mineralogy appeared to accompany Cs enrichment; therefore, it is difficult to determine how far from the pegmatite the enrichment extends into the hostrock, particularly given the large (generally 0.5–1 m) assay intervals. However, in some cases, Cs-enriched

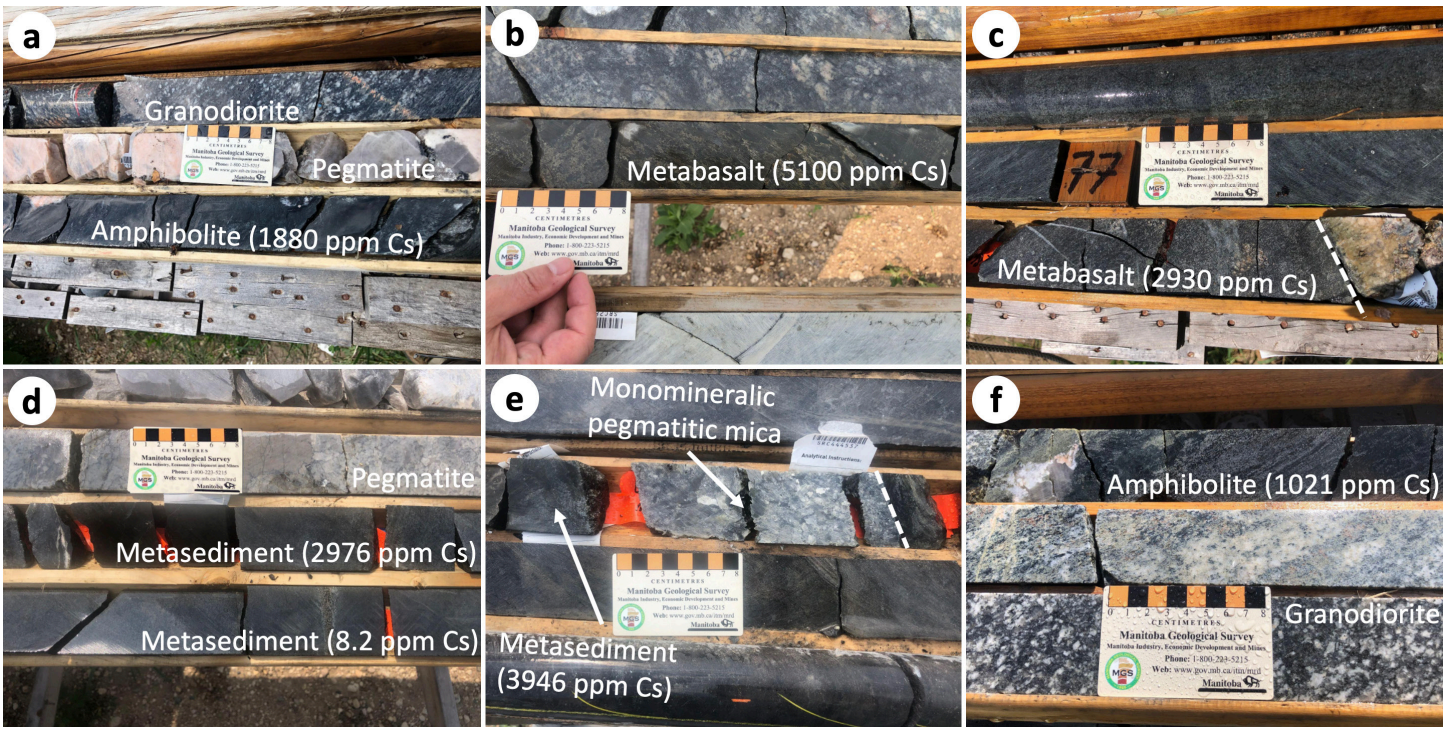

***Figure GS2025-3-6**: Photographs of samples from drillcores recovered from the Cat Lake–Winnipeg River pegmatite field: **a)** a primarily granodiorite-hosted pegmatite immediately underlain by a high-grade Cs amphibolite interval from drillhole LT-21-15 (Eagle pegmatite, Eagle-Irgon group); **b)** a particularly high-grade Cs metabasalt interval underlying a zone of strongly metasomatically altered rock from drillhole LO-22-01 (Silverleaf pegmatite, Greer Lake group); **c)** an interval of high-grade Cs metabasalt immediately above a pegmatite contact from drillhole LO-22-03 (Silverleaf pegmatite, Greer Lake group); **d)** metasedimentary rock underlying a pegmatite from drillhole LE24-011 (RL-7 pegmatite, Rush Lake group), with the interval directly adjacent to the pegmatite containing significant Cs concentrations not seen in the more distal interval; **e)** high-grade Cs metasedimentary rock immediately above a minor pegmatite dike comprising monomineralic greenish mica from drillhole LE24-025 (RL-7 pegmatite, Rush Lake group); **f)** a high-grade Cs amphibolite lens within granodiorite from drillhole LT24-044 (Magpie pegmatite, Eagle-Irgon group). Scale bar is in centimetres.*

hostrock was visibly crosscut by veins (Figure GS2025-3-6c, f) or was visibly altered (Figure GS2025-3-6b). All high-grade Cs intervals were observed to contain biotite as a major modal component. It is theorized that Cs is primarily contained within biotite, which is known to readily incorporate Cs into its crystal structure via adsorption, given the negative surface charge, specific surface area and frayed edge sites of biotite (Kwon et al., 2021; 2024).

Quartz zone of the Tanco pegmatite

Based on the logged drillcores, the quartz zone of the Tanco pegmatite has an apparent thickness ranging from 35 cm to 39 m. A common property of the quartz zone appears to be internal zonation of quartz colours, with grey intervals up to 10 cm along the contacts, zoning inward to more common translucent white, colourless, or pinkish quartz. Such zoned intervals may also locally have opaque, milky white to very pale yellow intervals up to 2.3 m long at their centre, which were interpreted to potentially represent cryptic amblygonite inclusions or pods. Conversely, quartz from other zones tends to be grey or 'smoky' in colour. Another characteristic property of zone 70 quartz appears to be the local presence of a striped or banded texture. These textures were generally restricted to zone 70 quartz but were locally observed within large quartz crystals from zone 20 as well.

Local SQUI pods are common within the quartz zone. These SQUI pods have an apparent thickness of up to 2.5 m and tend to have sharp contacts with surrounding quartz, suggesting that they may represent later veining. Contacts between the quartz and SQUI pods also tend to be associated with abundant dark green to yellow-green muscovite. The muscovite is generally restricted to the SQUI pods themselves and is not present in the surrounding quartz. Local lenses of K-feldspar are also present within the quartz zone and show a similar association with green to grey muscovite. Quartz within these lenses is generally grey, rather than white.

Contact relationships

The quartz zone of the Tanco pegmatite contacts many of the previously described zones, with contacts varying from sharp to gradational. However, contacts between the quartz zone and hostrock are consistently sharp (Figure GS2025-3-7a).

Sharp contacts between zones 70 and 20 are locally marked by brownish green muscovite, or by cleavelanditic albite oriented orthogonally to the contact and growing alongside quartz. Gradational contacts between the two are locally marked by the presence of coarse-grained SQUI, associated with minor green muscovite (Figure GS2025-3-7b). Both types of contacts locally show gradation from grey quartz of zone 20 into white quartz of zone 70.

Contacts between zones 70 and 30 vary from sharp to gradational. Sharp contacts are locally marked by SQUI veins associated with yellow-green muscovite, whereas gradational contacts may be marked by extensive zones of intermixed quartz+albite mottling. Both types of contacts locally show gradation from grey to white quartz. It was noted that along one contact, grey quartz appeared to take on a saccharoidal texture.

Contacts between zones 70 and 40 vary from sharp to gradational. Sharp contacts commonly feature orthogonal cleavelanditic albite growths, resembling those described in zone 20, and are locally associated with cleavelandite and lepidolite intergrowths. Gradational contacts commonly feature intermixed quartz and K-feldspar or albite mottling like those described in zone 30; they are locally associated with green muscovite. Other contact associations observed between zones 70 and 40 include local compositionally banded albite, quartz and grey muscovite-bearing aplite above gradational contacts (Figure GS2025-3-7c), as well as sharp to gradational contacts between zone 40 SQUI and zone 70 quartz.

Contacts between zones 70 and 50 vary from sharp to gradational but are consistently marked by SQUI mineralization plus or minus green muscovite. Contacts between zones 70 and 60 also vary from sharp to gradational and are commonly marked by K-feldspar and/or fine-grained green muscovite veining in zone 70 quartz. Sharper contacts between the two zones locally contain white beryl. Only one instance of zone 70 in contact with zone 80 was observed in the core from the study area, with a sharp contact marked by greenish SQUI. Similarly, one instance of zone 70 in sharp contact with zone 90 was observed.

Pollucite zone of the Tanco pegmatite

Based on the logged drillcores, pollucite-zone lenses of the Tanco pegmatite range from 0.55 to 12.7 m in apparent thickness. This agrees with the findings of Černý et al. (1996), who noted that the largest pollucite-zone body associated with the pegmatite is 12 m thick. Zone 80 pollucite ranges from colourless to white to light grey and is recognizable due to its distinct 'tapioca' texture, which is characterized by a speckled appearance caused by alteration to adularia, muscovite and spodumene (Černý et al., 1996). From conversations held with geologists working at the Tanco mine, it would appear that not all pollucite of the Tanco pegmatite shows the tapioca texture and that this texture may be restricted to zone 80 pollucite.

In addition to pollucite, zone 80 lenses were commonly veined by micas, including lepidolite and/or grey to yellow-green muscovite (Figure GS2025-3-8a, b). Another common observation was the presence of thin, grey quartz veinlets, with local albite rims (Figure GS2025-3-8c). Local lenses of cleavelandite+spodumene, SQUI, grey quartz or white K-feldspar were also observed. Small blue apatite crystals were locally observed scattered throughout zone 80 pollucite and were sometimes associated with quartz veins or K-feldspar lenses.

Zone 80 was observed in contact with zones 20, 40, 50 and 70 (Figure GS2025-3-8d, e, f). Contacts between zone 80 and other zones are invariably sharp and locally marked by white

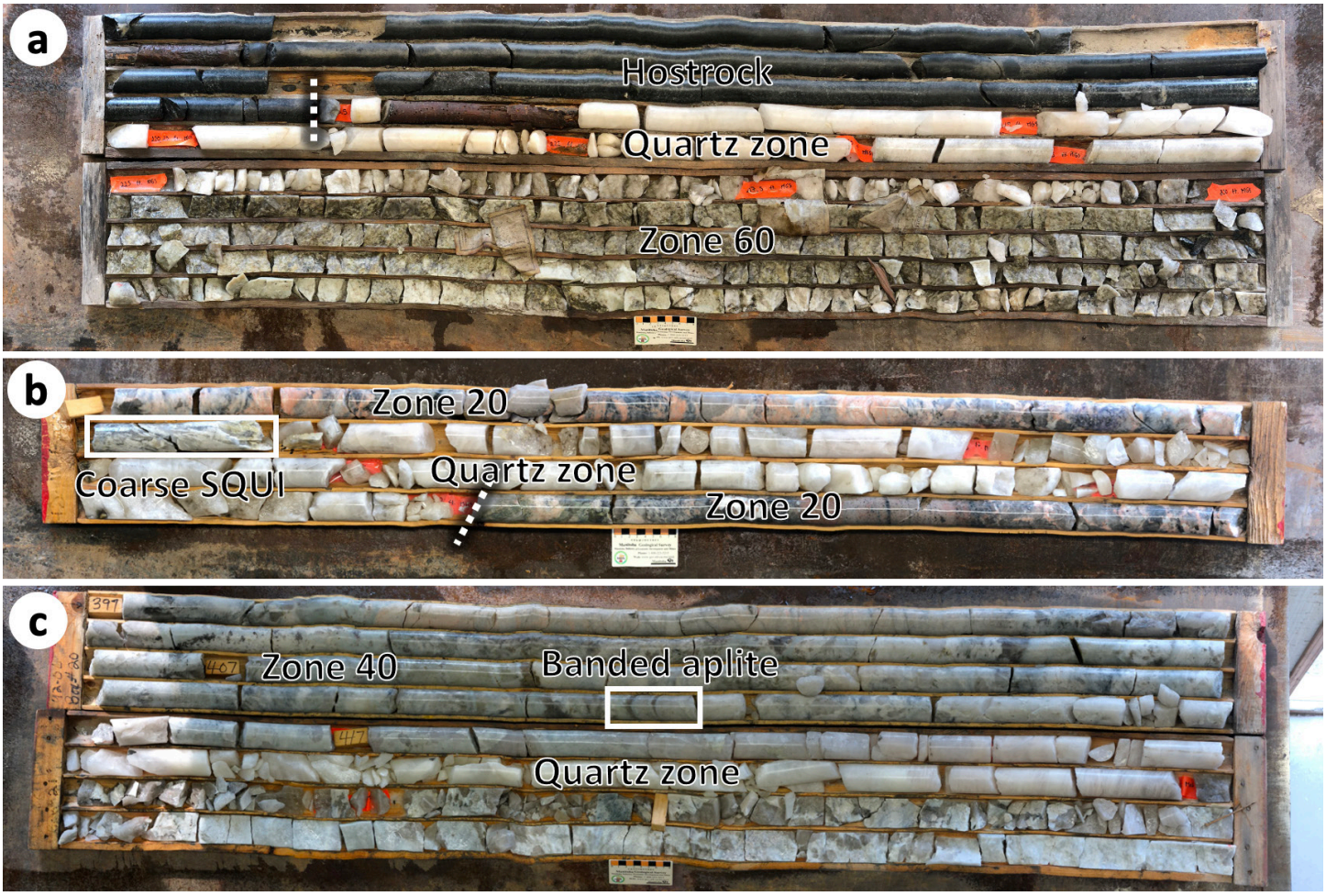

Figure GS2025-3-7*: Core box photographs of drillcore from the Tanco pegmatite of the Cat Lake–Winnipeg River pegmatite field showing quartz-zone contacts:* ***a)*** *sharp upper contact (dashed white line) with the hostrock and gradational lower contact with zone 60 marked by green muscovite veining in quartz;* ***b)*** *gradational upper contact with zone 20 marked by coarse SQUI (box outlined in white) and sharp lower contact (dashed white line) also with zone 20;* ***c)*** *compositionally banded aplite (box outlined in white) along the upper contact of the quartz zone with zone 40. Scale bar is in centimetres.*

to dark green SQUI. In one drillcore, zone 80 is underlain by a 7.4 m long interval of alternating SQUI and pollucite lenses in approximately equal parts, with local K-feldspar, quartz and mica. This was interpreted to possibly represent the 'low-grade pollucite zone' or 'zone 58', which locally surrounds zone 80 (Breasley et al., 2022; Martins et al., 2024); this interval featured a sharp contact with the underlying zone 40, marked by smoky quartz.

Future work

Future investigations into mica, quartz and pollucite at Tanco will make use of the observations described here in tandem with selected samples. The goal of these studies will be to fully understand and characterize the nature and distribution of quartz and cesium mineralization in the Tanco pegmatite. This will include an investigation into possible relationships between quartz and cesium mineralization and the complex magmatic-hydrothermal processes indicated by the variable mica compositions and habits of the Tanco pegmatite. These investigations will comprise detailed petrography, micro X-ray fluorescence spectrometry, electron probe microanalysis, scanning electron microscopy, laser-ablation inductively coupled plasma–mass spectrometry, scanning electron microscope-cathodoluminescence, fluid- and melt-inclusion analyses, as well as temperature determination using the Ti-in-quartz (TitaniQ) geothermometer (see Wark and Watson, 2006).

Economic considerations

The Cat Lake–Winnipeg River pegmatite field is considered prospective for both critical minerals such as Cs, Li and Ta, as well as for industrial minerals such as high-purity quartz and feldspar (Černý et al., 1981). In particular, the Tanco mine was once estimated to contain approximately 80% of current global reserves of Cs (Gilbert et al., 2008). Although not currently exploited as a resource at the Tanco mine, the presence of massive, potentially high-purity quartz within zone 70 of the Tanco pegmatite could also be of economic interest at some point in the future. Detailed spatial and geochemical characterizations of zones 70

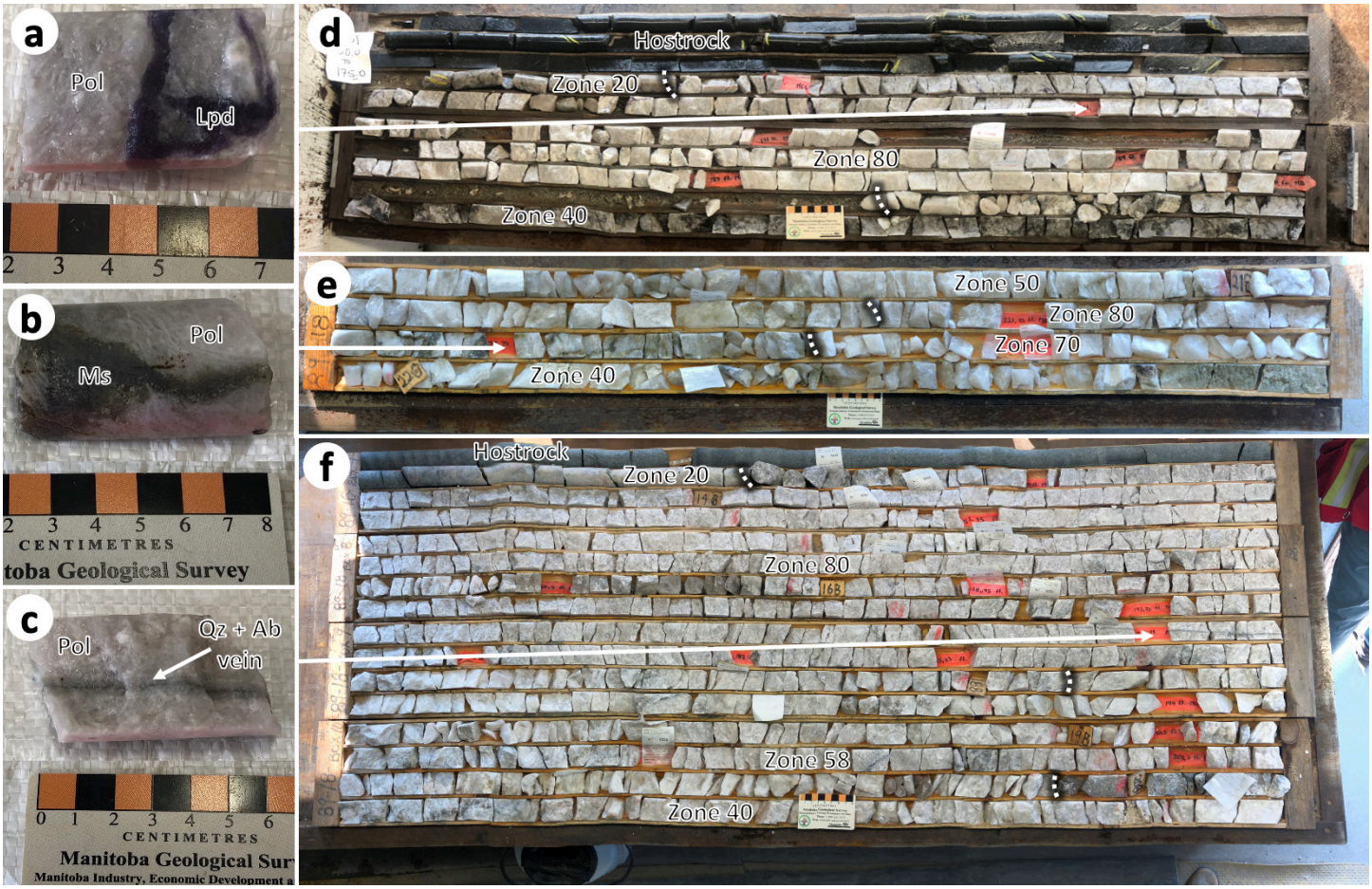

Figure GS2025-3-8*: Sample and core box photographs of various drillcores from the Tanco pegmatite of the Cat Lake–Winnipeg River pegmatite field containing zone 80 (sharp contacts indicated by dashed white lines):* ***a)*** *pollucite sample showing lepidolite (Lpd) veining in zone 80 pollucite (Pol);* ***b)*** *pollucite sample showing green muscovite (Ms) veining in zone 80 pollucite (Pol);* ***c)*** *pollucite sample showing a zoned quartz (Qz)+albite (Ab) vein in zone 80 pollucite (Pol);* ***d)*** *pollucite zone showing sharp contacts with zones 20 and 40;* ***e)*** *zone 80 showing sharp contacts with zones 50 and 70;* ***f)*** *zones 80 and 58 showing sharp contacts with zones 20 and 40.*

and 80 of the Tanco pegmatite will be conducted at a future point in this project, with the potential to both facilitate exploitation of high-purity zone 70 quartz as a new resource for the mine and to enable more efficient mining of Cs ore at the Tanco mine, as well as other Cs deposits in Cs-bearing pegmatites.

Acknowledgments

The authors thank the Tantalum Mining Corporation of Canada Limited-Sinomine Resource Group Co., Ltd. team for their support, most notably S. Rankmore and J. Champagne. All employees at the Tanco mine are also deserving of thanks, particularly B. Ducharme for assistance with historical drillcore logs. The authors extend their gratitude to New Age Metals Inc. for allowing access to their drilling data and core yard. Thanks are due to the Manitoba Geological Survey for their logistical and field support throughout the 2025 field season. Finally, the authors also extend their gratitude to N. Palacios-Montenegro for valuable field assistance.

References

Bannatyne, B.B. 1985: Industrial minerals in rare-element pegmatites of Manitoba; Manitoba Energy and Mines, Geological Services, Economic Geology Report ER84-1, 96 p.

Benn, D., Martins, T. and Linnen, R. 2022: Fractionation and enrichment patterns in white mica from Li pegmatites of the Wekusko Lake pegmatite field, Manitoba, Canada; The Canadian Mineralogist, v. 60, no. 6, p. 933–956.

Breasley, C.M., Martins, T., Groat, L.A. and Linnen, R.L. 2021: Results of a preliminary investigation into the lithium mineralization, distribution trends and remobilization in the Tanco pegmatite, southeastern Manitoba (part of NTS 52L6); *in* Report of Activities 2021, Manitoba Agriculture and Resource Development, Manitoba Geological Survey, p. 8–17.

Breasley, C.M., Martins, T., Linnen, R.L. and Groat, L.A. 2022: Investigating textural and geochemical relations of lithium mineralization in the Tanco pegmatite, southeastern Manitoba (part of NTS 52L6); *in* Report of Activities 2022, Manitoba Natural Resources and Northern Development, Manitoba Geological Survey, p. 25–35.

Breasley, C.M., Martins, T., Linnen, R.L. and Groat, L.A. 2024: Paragenetic relationships between zones 80 and 90 at the Tanco pegmatite, southeastern Manitoba (part of NTS 52L6); *in* Report of Activities 2024, Manitoba Economic Development, Investment, Trade and Natural Resources, Manitoba Geological Survey, p. 27–32.

Breasley, C.M., Martins, T., Linnen, R.L., Deveau, C., Groat, L.A., Koopmans, L., Landry, E. and Moser, D. 2025: The geochemistry, origins and metallurgical implications of different textural types of spodumene-quartz intergrowths (SQUI) from the Tanco pegmatite, Manitoba, Canada; Ore Geology Reviews, v. 180, 18 p.

Camacho, A., Baadsgaard, H., Davis, D.W. and Černý, P. 2012: Radiogenic isotope systematics of the Tanco and Silverleaf granitic pegmatites, Winnipeg River pegmatite district, Manitoba; The Canadian Mineralogist, v. 50, p. 1775–1792.

Černý, P. 2005: The Tanco rare-element pegmatite deposit, Manitoba: Regional context, internal anatomy, and global comparisons; *in* Rare-element Geochemistry and Mineral Deposits, R.L. Linnen and I.M. Samson (ed.), Geological Association of Canada, GAC Short Course Notes 17, p. 127–158.

Černý, P. and Ercit, T.S. 2005: The classification of granitic pegmatites revisited; The Canadian Mineralogist, v. 43, p. 2005–2026.

Černý, P., Ercit, T. and Vanstone, P. 1996: Petrology and mineralization of the Tanco rare-element pegmatite, southeastern Manitoba (Field Trip A3); Geological Association of Canada–Mineralogical Association of Canada, Joint Annual Meeting, May 27–29, 1996, Winnipeg, Manitoba, 63 p.

Černý, P., Trueman, D.L., Ziehlke, D.V., Goad, B.E. and Paul, B.J. 1981: The Cat Lake–Winnipeg River and the Wekusko Lake pegmatite fields, Manitoba; Manitoba Department of Energy and Mines, Mineral Resources Division, Economic Geology Report ER80-1, 216 p.

Dittrich, T., Seifert, T., Schulz, B., Hagemann, S., Gerdes, A. and Pfänder, J. 2019: Archean Rare-Metal Pegmatites in Zimbabwe and Western Australia: Geology and Metallogeny of Pollucite Mineralisations; Springer Briefs in World Mineral Deposits, Springer International Publishing, Cham, Switzerland, 125 p.

Gilbert, H.P. 2008: Stratigraphic investigations in the Bird River greenstone belt, Manitoba (part of NTS 52L5, 6); *in* Report of Activities 2008, Manitoba Science, Technology, Energy and Mines, Manitoba Geological Survey, p. 121–138.

Gilbert, H.P., Davis, D.W., Duguet, M., Kremer, P.D., Mealin, C.A. and MacDonald, J. 2008: Geology of the Bird River Belt, southeastern Manitoba (parts of NTS 52L5, 6); Manitoba Science, Technology, Energy and Mines, Manitoba Geological Survey, Geoscientific Map MAP2008-1, scale 1:50 000.

Kremer, P. 2010: Structural geology and geochronology of the Bernic Lake area in the Bird River greenstone belt, Manitoba: evidence for syn-deformational emplacement of the Bernic Lake pegmatite group; M.Sc. Thesis, University of Waterloo, Waterloo, Ontario, 91 p.

Kwon, S., Kim, Y. and Roh, Y. 2021: Cesium removal using acid- and base-activated biotite and illite; Journal of Hazardous Materials, v. 401, 12 p.

Kwon, S., Seoung, D., Jung, E., Park, J., Lim, J., Park, B., Cho, Y., Kim, P., Kim, H. and Lee, Y. 2024: Eco-friendly natural mineral biotite as a cesium adsorbent: utilizing low-concentration acid and hydrogen peroxide; Chemosphere, v. 353, 11 p.

London, D. 1985: Origin and significance of inclusions in quartz; a cautionary example from the Tanco Pegmatite, Manitoba; Economic Geology, v. 80, p. 1988–1995.

London, D. 1986: Magmatic-hydrothermal transition in the Tanco rare-element pegmatite: evidence from fluid inclusions and phase-equilibrium experiments; American Mineralogist, v. 71, p. 376–395.

London, D. 2018: Ore-forming processes within granitic pegmatites; Ore Geology Reviews, v. 101, p. 349–383.

London, D., Morgan, G.B., IV and Icenhower, J. 1998: Stability and solubility of pollucite in the granite system at 200 MPa H_2O; The Canadian Mineralogist, v. 36, no. 2, p. 497–510.

Manitoba Geological Survey 2022: New edition of the 1:250 000 scale Precambrian bedrock geology compilation map of Manitoba; Manitoba Natural Resources and Northern Development, Manitoba Geological Survey, GeoFile 3-2022.

Martins, T., Breasley, C., Groat, L., Linnen, R., Deveau, C. and Rankmore, S. 2024: The Tanco pegmatite: geological setting, internal zonation, mineralogy and mining of a world-class rare-element pegmatite deposit; Manitoba Business, Mining, Trade and Job Creation, Manitoba Geological Survey, Open File OF2024-3, 16 p.

Morgan, G.B., VI and London, D. 1987: Alteration of amphibolitic wallrocks around the Tanco rare-element pegmatite, Bernic Lake, Manitoba; American Mineralogist, v. 72, p. 1097–1121.

Nambaje, C., Martins, T., McFarlane, C.R.M., Kaczmer, M., Rinne, M.L. and Groat, L. 2024: Preliminary results from field investigations in the Cat Lake–Winnipeg River pegmatite field, southeastern Manitoba (parts of NTS 52L5, 6, 11, 12); *in* Report of Activities 2024, Manitoba Economic Development, Investment, Trade and Natural Resources, Manitoba Geological Survey, p. 10–26.

Natural Resources Canada 2025: Canada's Critical minerals; Natural Resources Canada, Critical Minerals Centre of Excellence, URL <https://www.canada.ca/en/campaign/criticalminerals-in-canada/critical-minerals-an-opportunity-for-canada. html> [July 2025].

New Age Metals Inc., 2024: New Age Metals provides update on the winter drilling program and detailed geophysical study at the Winnipeg River–Cat Lake lithium project; New ge Metals Inc., press release, March 4, 2024, URL <https://newagemetals.com/new-age-metals-provides-update-on-the-winter-drilling-program-and-detailed-geophysical-study-at-the-winnipeg-river-cat-lake-lithium-project/> [October 2025].

Rinaldi, R., Černý, P. and Ferguson, R.B. 1972: The Tanco pegmatite at Bernic Lake, Manitoba. VI. Lithium-rubidium-cesium micas; Canadian Mineralogist, v. 11, p. 690–707.

Roush, J., Martins, T., McFarlane, C.R.M., Rinne, M.L. and Groat, L. 2023: Preliminary examination of the Tappy, Eagle and F.D. No. 5 pegmatites in the Cat Lake–Winnipeg River pegmatite field, southeastern Manitoba (parts of NTS 52L5, 11); *in* Report of Activities 2023, Manitoba Economic Development, Investment, Trade and Natural Resources, Manitoba Geological Survey, p. 20–26.

Stilling, A. 1998: Bulk composition of the Tanco pegmatite at Bernic Lake, Manitoba, Canada; M.Sc. thesis, University of Manitoba, Winnipeg, Manitoba, 76 p.

Stilling, A., Černý, P. and Vanstone, P.J. 2006: The Tanco pegmatite at Bernic Lake, Manitoba. XVI. Zonal and bulk compositions and their petrogenetic significance; The Canadian Mineralogist, v. 44, p. 599–623.

Van Lichtervelde, M., Grégoire, M., Linnen, R.L., Béziat, D. and Salvi, S. 2008: Trace element geochemistry by laser ablation ICP-MS of micas associated with Ta mineralization in the Tanco pegmatite, Manitoba, Canada; Contributions to Mineralogy and Petrology, v. 155, p. 791–806.

Wark, D.A. and Watson, E.B. 2006: TitaniQ: a titanium-in-quartz geothermometer; Contributions to Mineralogy and Petrology, v. 152, p. 743–754.

Yang, X.M. and Houlé, M.G. 2020: Geology of the Cat Creek–Euclid Lake area, Bird River greenstone belt, southeastern Manitoba (parts of NTS 52L11, 12); Manitoba Agriculture and Resource Development, Manitoba Geological Survey, Geoscientific Report GR2020-1, 105 p., plus 1 map at 1:20 000 scale.

GS2025-4

Lithogeochemistry and isotopic analyses of rocks from the Halfway Lake area, Thompson nickel belt, central Manitoba (parts of NTS 63O1, 2)

by C.G. Couëslan

In Brief:

- Supracrustal rocks at Halfway Lake are geochemically and stratigraphically similar to the Ospwagan group
- Whole-rock Nd-model ages of Pipe-Setting formations clastic rocks are anomalously young for Ospwagan group rocks
- Many ultramafic bodies in the Halfway Lake area occur at the Thompson formation-Pipe formation boundary, which correlates to the mine horizons at the Pipe and Birchtree mines

Citation:
Couëslan, C.G. 2025: Lithogeochemistry and isotopic analyses of rocks from the Halfway Lake area, Thompson nickel belt, central Manitoba (parts of NTS 63O1, 2); *in* Report of Activities 2025, Manitoba Business, Mining, Trade and Job Creation, Manitoba Geological Survey, p. 33–47.

Summary

A mapping project, initiated at Halfway Lake in 2022, continued with the examination of lithogeochemical and isotopic analyses of outcrop and drillcore samples collected during the 2022–2025 field seasons. Mafic volcanic rocks collected from south-central Halfway Lake share a geochemical affinity with mid-ocean–ridge basalts and are likely correlative with the Bah Lake assemblage of the Ospwagan group. Amphibolite layers contained within the sedimentary rocks at Halfway Lake likely represent mafic dikes or sills and have a mid-ocean–ridge to back-arc–basalt affinity. They are assumed to be correlative with mafic intrusions of the ca. 1880 Ma Molson dike swarm. A monzonitic pluton located along the southeastern shore of Halfway Lake has a high-K calcalkaline affinity and is geochemically and isotopically similar to the ca. 1835 Ma Bucko pluton south of Wabowden. A garnet-bearing granite–tonalite pluton that occurs in western Halfway Lake shares an affinity with FII felsic rocks and was likely derived by melting of shallow- to mid-level crust in an extensional environment. The garnet-bearing pluton could be contemporaneous with Bah Lake assemblage or Molson swarm mafic–ultramafic magmatism.

The sedimentary stratigraphy at Halfway Lake appears to be correlative with the Ospwagan group and is similar to the Thompson mine sequence. Clastic rocks from the upper part of the sequence (P3 member of the Pipe formation and Setting formation) are geochemically similar to Pipe formation pelite; however, Nd-model ages are anomalously young for Ospwagan group rocks. Detrital zircon recovered from the upper sequence yield dominant age-nodes that coincide with metamorphism in the adjacent Pikwitonei domain of the Superior craton. Calcareous semipelite of the Thompson formation may be correlative to the T2 member, but shares geochemical similarities with Paint sequence rocks. A Nd-model age calculated for the calcareous semipelite is considered typical for Ospwagan group rocks.

Ultramafic rocks at Halfway Lake are frequently emplaced near sulphidic horizons at the boundary between the Thompson and Pipe formations, which coincides with the ore horizons at the Pipe and Birchtree mines. Although whole-rock Sm-Nd isotope geochemistry has been proposed as an exploration tool for differentiating rock units in the northern Thompson nickel belt, the presence of anomalously young Nd-model ages for upper sequence Ospwagan group rocks at Halfway Lake suggests a cautious approach should be taken. The FII felsic rock affinity of the garnet-bearing pluton could suggest a notional potential for volcanogenic massive-sulphide or epithermal mineralization.

Introduction

A mapping project at Halfway Lake in the Thompson nickel belt (TNB) was initiated in the summer of 2022 with shoreline mapping (Figure GS2025-4-1). Significant discrepancies were found between previous mapping and the 2022 results, which led to the logging of archival and recent drillcore from the area in 2023, 2024 and 2025 (Couëslan, 2022a, 2023). The drillcore data suggests a correlation between the metasedimentary rocks at Halfway Lake and the Ospwagan group, with close similarities to the stratigraphic sequence at the Thompson mine (cf. Bleeker, 1990; Couëslan, 2023). Samples of metasedimentary rocks, along with all of the major rock units at Halfway Lake, were submitted for lithogeochemical and isotopic analyses to better characterize and strengthen this correlation with the Ospwagan group. The main focus of this report is the analytical results for mafic, metasedimentary and granitoid rocks. The geochemical results and analytical methods can be found in Couëslan and Janssens (2025b) and in Data Repository Item DRI2025029 (Couëslan and Janssens, 2025c)[1]. The

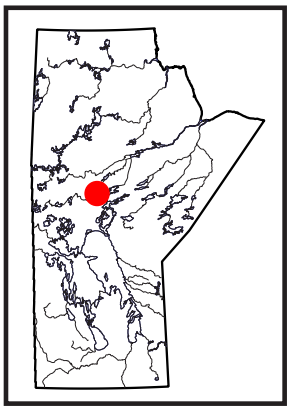

[1] MGS Data Repository Item DRI2025029, containing the data or other information sources used to compile this report, is available online to download free of charge at https://manitoba.ca/iem/info/library/downloads/index.html, or on request from minesinfo@gov.mb.ca, or by contacting the Resource Centre, Manitoba Business, Mining, Trade and Job Creation, 360-1395 Ellice Avenue, Winnipeg, Manitoba R3G 3P2, Canada.

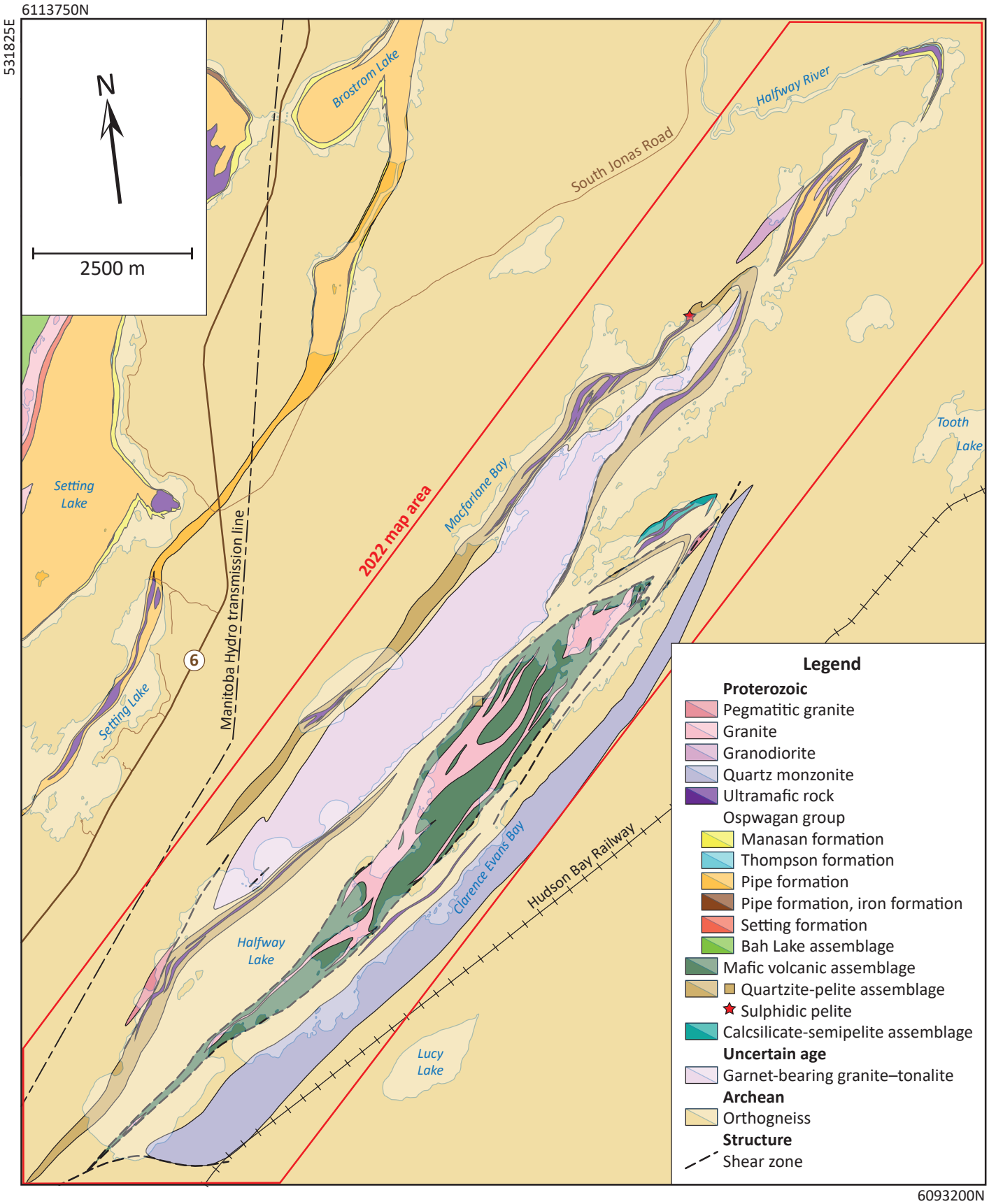

Figure GS2025-4-1: *Bedrock geology of the Halfway Lake area, central Manitoba (modified from Couëslan, 2022a). Lighter shade of colour indicates a body of water. Geology outside of the 2022 map area is from Macek et al. (2006). All co-ordinates are in UTM Zone 14, NAD83.*

U-Pb zircon data can be found in Couëslan (2025). For a review of the project objectives, as well as the regional and local geology, the reader is referred to Couëslan (2022a). All rocks reported in this study were subjected to amphibolite-facies metamorphism; however, the 'meta-' prefix is not used for rock names in an effort to simplify the text.

Whole-rock lithogeochemistry and Sm-Nd isotope geochemistry

Mafic rocks

Heterogeneous amphibolites, interpreted as volcanic rocks, form a large continuous unit in south-central Halfway Lake and are believed to be correlative with the Bah Lake assemblage (Figure GS2025-4-1). They are characterized by intermediate Mg# values (molar $Mg/[Fe^T+Mg]$; 0.41–0.62). Silica contents range from 46.58 to 52.16 wt. %, total alkalis (Na_2O+K_2O) range from 2.20 to 4.02 wt> % and molar K_2O/Na_2O ratios range from 0.11 to 0.23. Chondrite-normalized rare-earth element (REE) profiles are relatively flat ($[La/Yb]_N$ = 0.87–1.88), with the exception of a single sample ($[La/Yb]_N$ = 3.60; Figure GS2025-4-2a). Primitive mantle-normalized multi-element profiles are relatively smooth, with variable enrichment at Th and variable depletion at Nb (Figure GS2025-4-2b). No spatial pattern is associated with the variations in Nb anomalies; however, the two most enriched samples are both located toward the southern end of the heterogeneous amphibolite package.

Layers of garnet amphibolite occur within the clastic rocks of the upper sequence (Pipe and Setting formations) of the Ospwagan group. The amphibolites are interpreted as mafic dikes or sills that intruded the sedimentary sequence. The Mg# values range from 0.28 to 0.64, with SiO_2 contents of 45.51–53.89 wt. %. Total alkali content is generally low (0.95–1.97 wt. %), except for one sample that contains 3.40 wt. %. Molar K_2O/Na_2O ratios range from 0.12 to 1.50. Chondrite-normalized REE profiles are relatively flat ($[La/Yb]_N$ = 1.00–1.90), and primitive mantle-normalized profiles are characterized by variable to no enrichment at Th and variable anomalies at Nb (Figure GS2025-4-2c, d).

Layers of homogeneous amphibolite occur within the Archean orthogneiss and Ospwagan group, and are interpreted as Paleoproterozoic mafic dikes or sills. The Mg# values range from 0.38 to 0.65, with SiO_2 contents of 48.01–52.13 wt. %. Total alkali content ranges from 1.72 to 4.00 wt. %, with molar K_2O/Na_2O ratios of 0.16 to 0.58. Chondrite-normalized REE profiles are relatively flat ($[La/Yb]_N$ = 1.14–1.67), with one sample displaying a more negative slope ($[La/Yb]_N$ = 2.52; Figure GS2025-4-2e). Primitive mantle-normalized profiles show minor to no enrichment at Th and minor to no depletion at Nb (Figure GS2025-4-2f).

Granitoids

A variety of granitoids are present in the Halfway Lake area, ranging from pegmatitic granite dikes that are present in almost all outcrops, to kilometre-scale bodies of monzonite and granite–granodiorite. Only more substantial intrusions were investigated for geochemistry.

A monzonite pluton roughly 13 km long occurs along the southeastern shore of Halfway Lake (Figure GS2025-4-1). Samples of monzonite have Mg# values of 0.64–0.66, and contain 59.71–61.23 wt. % SiO_2, 180–200 ppm Cr and 90–110 ppm Ni. The monzonite is metaluminous (alumina saturation index, ASI = 0.77–0.78; Figure GS2025-4-3), contains 7.13–7.33 wt. % total alkalis, with K_2O/Na_2O ratios of 0.61–0.70, and is enriched in other large-ion lithophile-elements (LILEs; 2396–2417 ppm Ba, 1031–1064 ppm Sr). Chondrite-normalized REE profiles have steep negative slopes ($[La/Yb]_N$ = 46.3–60.5) and primitive mantle-normalized profiles are characterized by enrichment in LILEs and light rare-earth elements (LREEs), and relatively depleted in high-field strength elements (HFSEs; Figure GS2025-4-4a, b). A sample of monzonite yielded an initial εNd value of –1.77, assuming a crystallization age of ca. 1835 Ma (see Discussion) and a depleted-mantle Nd-model age (T_{DM}) of ca. 2.34 Ga (Table GS2025-4-1).

A garnet-bearing pluton at least 12 km long occurs along the western shore of Halfway Lake and ranges from granitic in the south to tonalitic in the north (Figure GS2025-4-1). The age of intrusion is not well constrained. It is characterized by a weak gneissosity and previous mapping suggests that it is intruded by mafic dikes of the ca. 1880 Ma Molson swarm (Macek et al., 2006; Heaman et al., 2009). The pluton becomes increasingly ferruginous from tonalite (Mg# = 0.19–0.25) to granite (Mg# = 0.11–0.12). Similar trends are observed with many of the LILEs, with the total alkalis increasing from the tonalite (3.86–4.13 wt. %) to the granite (6.98–7.08 wt. %), as the pluton becomes more enriched in potassium (K_2O/Na_2O = 0.08–0.15 and 1.05–1.09, respectively) and Ba increasing from 179–229 ppm to 1488–1664 ppm, respectively. Alumina saturation also increases from the tonalite (ASI = 0.85–0.94) to the granite (ASI = 1.03–1.08; Figure GS2025-4-3). However, no trend is observed related to the SiO_2 content, which varies from 71.95 to 75.64 wt. %, and Sr concentrations are relatively uniform from tonalite to granite (159–264 ppm). Chondrite-normalized REE profiles are characterized by negative-sloping LREEs ($[La/Sm]_N$ = 2.40–4.12) and relatively flat heavy rare-earth elements (HREEs; $[Gd/Yb]_N$ = 0.89–1.11; Figure GS2025-4-4c). Primitive mantle-normalized multi-element profiles are characterized by depletion at Nb, P, Ti and V (Figure GS2025-4-4d). Both tonalitic and granitic profiles are relatively enriched in Th; however, granitic and granodioritic profiles are also enriched in Ba and K.

A folded pluton or series of granodioritic to granitic intrusions with a combined length of at least 2.5 km underlies a series of points, islands and reefs in northern Halfway Lake (Figure GS2025-4-1). The pluton grades from biotite-bearing to hornblende-bearing. The Mg# values range from 0.27 to 0.33, with 69.97–70.55 wt. % SiO_2. The rocks are weakly peraluminous (ASI = 1.00–1.05; Figure GS2025-4-3) with 8.56–8.87 wt. % total

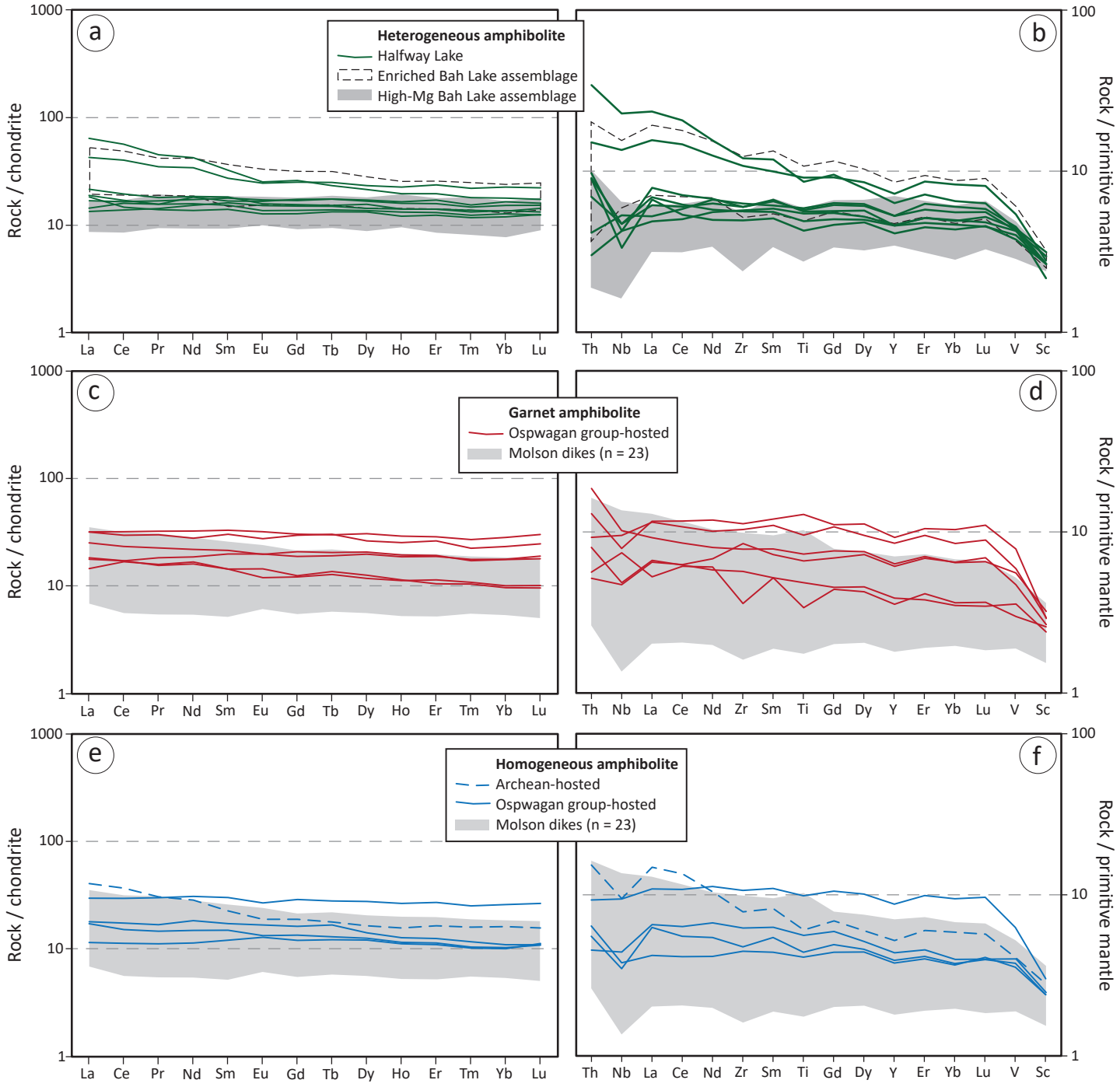

Figure GS2025-4-2: *Chondrite-normalized rare-earth element profiles (left column) and primitive mantle-normalized multi-element profiles (right column) for mafic rocks from the Halfway Lake area:* ***a), b)*** *heterogeneous amphibolite;* ***c), d)*** *garnet amphibolite;* ***e), f)*** *homogeneous amphibolite. Normalizing values for chondrite and primitive mantle are from McDonough and Sun (1995). Reference values for Bah Lake assemblage area are from Zwanzig (2005). Reference values for Molson dikes are for analyses with 1 <$(La/Yb)_N$ <3 and are sourced from Burnham et al. (2009), Heaman et al. (2009), Ciborowski et al. (2017) and Couëslan (2016, 2021a, b; unpublished data, 2014).*

alkalis, K_2O/Na_2O ratios of 0.45–0.56, and high concentrations of Sr and Ba (1857–2306 ppm and 4381–5266 ppm, respectively). Chondrite-normalized REE profiles have negative slopes ($[La/Yb]_N$ = 16.8–45.8), with variable enrichment of Eu ($[Eu/Eu^*]_N$ = 0.88–1.66; Figure GS2025-4-4e). Primitive mantle-normalized profiles display relative enrichments at Ba, K, Sr and Zr, and relative depletions at Nb, P, Ti and V (Figure GS2025-4-4f).

A granite–granodiorite pluton or series of intrusions is intercalated with rocks of the Bah Lake assemblage in south-central Halfway Lake. The Mg# values range from 0.26 to 0.33, with 70.89–72.91 wt. % SiO_2. The rocks are weakly peraluminous (ASI = 1.00–1.02; Figure GS2025-4-3) with 8.12–8.42 wt. % total alkalis and K_2O/Na_2O ratios of 0.29–0.64. Barium concentrations are enriched but vary considerably from 1606 to 4110 ppm,

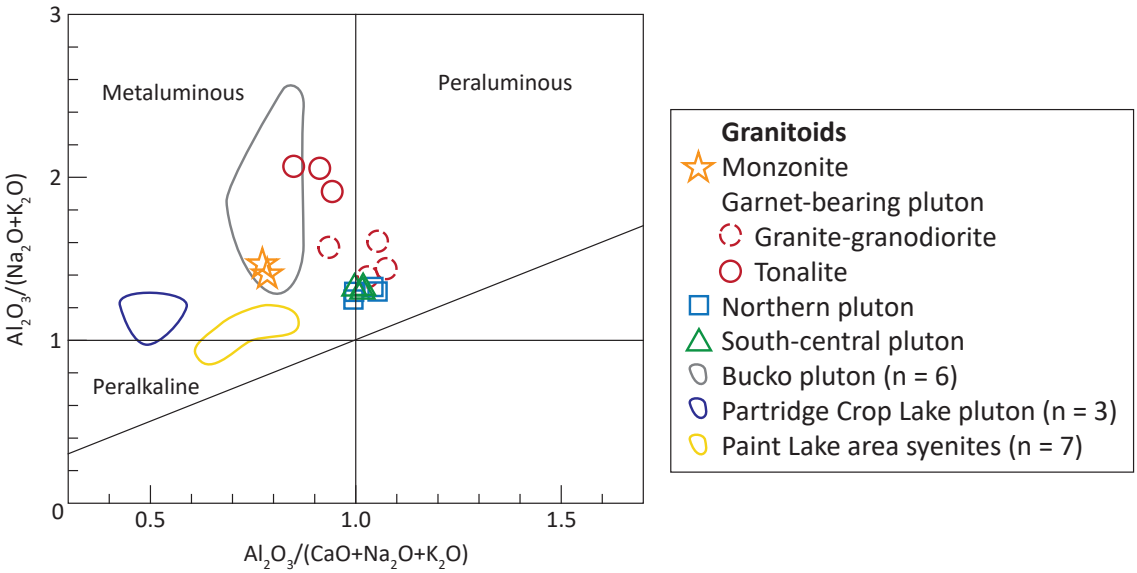

Figure GS2025-4-3: *Granitoids from the Halfway Lake area and syenitic to monzonitic rocks from the Thompson nickel belt plotted on the alumina saturation-index diagram (Maniar and Piccoli, 1989). Reference values for the Bucko pluton are from Burnham et al. (2009) and H.V. Zwanzig (unpublished data, 2003). Reference values for the Partridge Crop Lake pluton are from Couëslan and Janssens (2025a) and C.G. Couëslan (unpublished data, 2014). Reference values for the Paint Lake area syenites are from Couëslan (2016).*

whereas Sr is more consistent at 1104–1302 ppm. Chondrite-normalized REE profiles have negative slopes ($[La/Yb]_N$ = 3.60–18.3), with variable enrichment or depletion at Eu ($[Eu/Eu^*]_N$ = 0.55–1.65; Figure GS2025-4-4g). Primitive mantle-normalized profiles are characterized by relative enrichments at Ba, K, Sr and Zr, and relative depletions at Nb, P, Ti and V (Figure GS2025-4-4h).

Sedimentary rocks

The Setting formation of the Ospwagan group is defined as the clastic sedimentary rocks deposited above the uppermost iron formation of the P3 member of the Pipe formation (Zwanzig et al., 2007). The stratigraphy of the P3 member of the Pipe formation at Halfway Lake is similar to that of the Thompson mine and consists largely of interbedded quartzite, wacke and pelite, with only local iron formation. This makes differentiating Setting formation from Pipe formation clastic rocks difficult. Therefore, clastic rocks of the P3 member and Setting formation will be referred to simply as 'upper sequence' rocks in this report. Multi-element profiles normalized to the average P2 member pelite (Zwanzig et al., 2007) are relatively flat for upper sequence pelites, with minor variability for Th, K and LREEs (Figure GS2025-4-5a, b). The P2 pelite-normalized profiles of upper sequence wacke are typically flat; however, one sample is notably depleted in Th and LREEs and enriched in HREEs (Figure GS2025-4-5c, d). Two wacke samples from the upper sequence yielded T_{DM} ages of ca. 2.46 Ga and 2.71 Ga (Table GS2025-4-1).

The lower Thompson formation at Halfway Lake consists largely of calcareous semipelite, locally interlayered with calcsilicate (Couëslan, 2023). The semipelite is similar to the T2 member as described by Bleeker (1990) and Zwanzig et al. (2007), which occurs as a relatively thin (1–4 m) unit at the Thompson mine. This suggests that unlike elsewhere in the TNB, the T2 member could make up a significant portion of Thompson formation stratigraphy in the Halfway Lake area. The P2 pelite-normalized profiles of the calcareous semipelite are flat to weakly negative sloping, with relative depletions at K, Zr and Ti, and strong enrichment at Sr and P (Figure GS2025-4-5e, f). A sample of Thompson formation calcareous semipelite yielded a T_{DM} of ca. 2.94 Ga (Table GS2025-4-1).

Detrital zircon U-Pb geochronology

Two samples of upper sequence clastic rocks were submitted for detrital zircon U-Pb isotope analyses. The results and description of the methods can be found in Couëslan (2025). For this report, analyses were filtered to results of detrital-core analyses (no rims or mixed core-rim analyses) that are <5% discordant, with $^{207}Pb/^{206}Pb$ age errors <100 Ma (2σ). Sample 108-22-118 consists dominantly of arkose and was collected from a point in southwestern Halfway Lake. The outcrop is composed of interlayered arkose and arkosic wacke, with local pegmatite dikes and boudinaged layers of plagioclase amphibolite. The sample yielded zircon grains of variable size and morphology. Most grains consist of rounded to subrounded, equant to elongate crystals and crystal fragments. A total of 112 analyses were made on detrital zircon grains with 90 analyses considered after filtering. A probability-density distribution (PDD) curve of the $^{207}Pb/^{206}Pb$ ages defines a dominant node at ca. 2640 Ma, with minor Paleoproterozoic nodes older than ca. 2215 Ma and minor Meso- to Paleoarchean nodes as old as ca. 3480 Ma (Figure GS2025-4-6a). A cumulative distribution curve of the detrital zircon ages yields

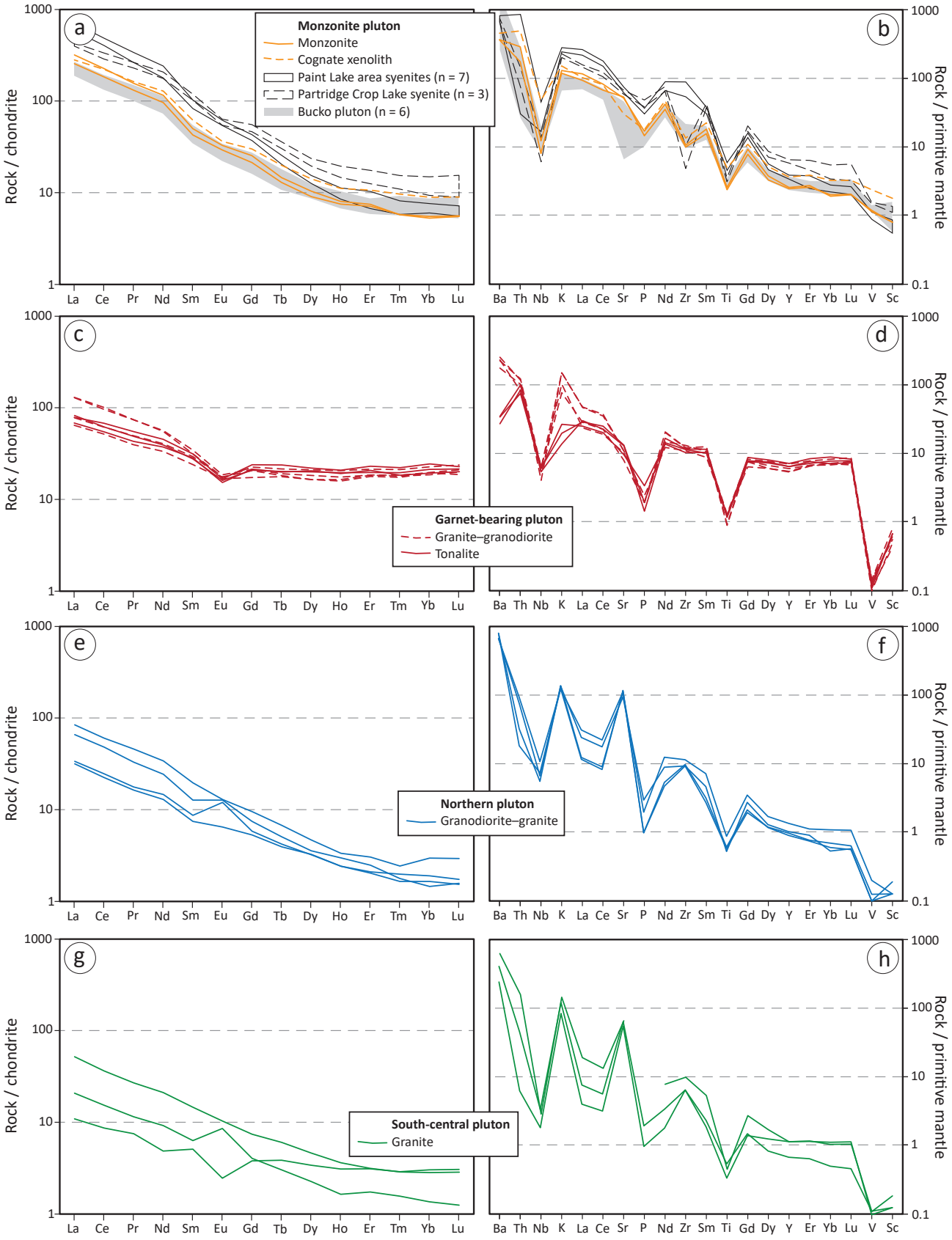

Figure GS2025-4-4: *Chondrite-normalized rare-earth element profiles (left column) and primitive mantle-normalized multi-element profiles (right column) for granitoids from the Halfway Lake area:* ***a)***, ***b)*** *monzonite compared with syenites from the Paint Lake and Partridge Crop Lake areas and the Bucko pluton;* ***c)***, ***d)*** *garnet-bearing pluton;* ***e)***, ***f)*** *granodiorite–granite from northern Halfway Lake;* ***g)***, ***h)*** *granite from south-central Halfway Lake. Data sources: Bucko pluton, Burnham et al. (2009) and H.V. Zwanzig (unpublished data, 2003); Paint Lake area syenites, Couëslan (2016); Partridge Crop Lake syenite, Couëslan and Janssens (2025a) and C.G. Couëslan (unpublished data, 2014).*

Table GS2025-4-1: Summary of Sm-Nd isotopic data for selected samples from the Halfway Lake area.

Sample number	Rock type	Sm (ppm)	Nd (ppm)	$^{147}Sm/^{144}Nd$[1]	$^{143}Nd/^{144}Nd$[2]	2σ abs. uncert.	T_{DM}[3] (Ga)	εNd[4]
108-22-039	Archean Bt-Hbl gneiss	2.00	10.92	0.11108	0.511025	0.000010	3.12	-1.64
108-22-097	Monzonite	6.52	41.28	0.0954	0.511325	0.000010	2.34	-1.77
108-22-111	Thompson formation calcareous semi-pelite	4.86	32.17	0.0913	0.510766	0.000010	2.94	
108-22-118	Ospwagan group, upper sequence arkose	5.30	31.47	0.1018	0.511328	0.000010	2.46	
108-22-157A	Ospwagan group, upper sequence arkosic wacke	1.50	10.08	0.0898	0.510928	0.000010	2.71	

[1] Estimated error is better than 1.0%

[2] Presented relative to $^{143}Nd/^{144}Nd = 0.512095$ for the JNdi-1 standard

[3] Depleted-mantle Nd-model ages (T_{DM}) calculated according to the linear model of Goldstein et al. (1984)

[4] ε_{Nd} values at 2700 Ma for 108-22-039 and 1835 Ma for 108-22-097, calculated using present-day chondritic ratios of $^{143}Nd/^{144}Nd = 0.512638$ and $^{147}Sm/^{144}Nd = 0.1967$

Sample locations can be found in Couëslan and Janssens (2025b)

Abbreviations: abs., absolute; uncert., uncertainty

an interquartile range (middle 50% of data) of 2600–2700 Ma (Figure GS2025-4-6b).

Sample 108-22-157A consists of interbedded arkosic wacke and arkose. It was collected from an island in central Halfway Lake. The outcrop consists of arkosic quartzite with interbeds of arkosic wacke and local boudins of plagioclase amphibolite. Local veins of pseudotachylite cut the compositional layering at a low-angle. A total of 118 detrital zircon grains were analyzed with 96 analyses considered after filtering. A PDD curve of the $^{207}Pb/^{206}Pb$ ages defines a dominant node at ca. 2650 Ma, with minor Paleoproterozoic nodes as young as ca. 1940 Ma and Mesoarchean nodes as old as ca. 2955 Ma (Figure GS2025-4-6c). The interquartile range of the detrital zircon ages is relatively narrow (2623–2692 Ma; Figure GS2025-4-6d).

Discussion

Mafic rocks

The volcanic rocks from Halfway Lake all plot within the ocean-floor field in the Zr-Ti-Y diagram (Figure GS2025-4-7a); however, the normalized profiles appear to define two trends. One trend is relatively flat, whereas the other is more enriched and negative sloping (Figure GS2025-4-2a, b). Two trends are also evident in the Zr-Nb-Y and La-Y-Nb discrimination diagrams, with the majority of samples plotting within the normal mid-ocean–ridge basalt (N-MORB) field and back-arc–basalt fields, and two samples trending toward increasing enrichment into the enriched mid-ocean–ridge basalt (E-MORB) and continental basalt fields (Figure GS2025-4-7b, c). Previous work on the Bah Lake assemblage of the Ospwagan group by Zwanzig (2005) subdivided the volcanic rocks into an N-MORB–like high-Mg suite and an E-MORB–like enriched suite (Figure GS2025-4-2a, b). The profiles of the two suites are similar to the two trends defined by the mafic volcanic rocks at Halfway Lake and support the interpretation that they could be correlative with the Bah Lake assemblage.

The normalized profiles of the garnet-bearing mafic dikes are relatively flat and suggestive of a MORB affinity (Figure GS2025-4-2c, d), and are similar to the profiles of homogeneous amphibolite samples hosted in Ospwagan group rocks (Figure GS2025-4-2e, f). Variable anomalies at Th and Nb could indicate interaction with more evolved crust. Samples of garnet amphibolite and homogeneous amphibolite plot within the ocean-floor–basalt and MORB fields of the discrimination diagrams of Pearce and Cann (1973) and Meschede (1986), and overlap with the back-arc–basalt field of Cabanis and Lecolle (1989; Figure GS2025-4-7a–c). The normalized profiles and results from discrimination diagrams are similar to those of mafic dikes of the Molson swarm, which have been interpreted as the result of a mantle plume, passive mantle upwelling or back-arc magmatism (Figure GS2025-4-2c–f; Figure GS2025-4-7a–c; Heaman et al., 2009; Ciborowski et al., 2017). The main difference between the garnet amphibolite and the homogeneous amphibolite appears to be related to alkali content. The garnet amphibolite typically contains <2 wt. % total alkalis with a K_2O/Na_2O ratio typically >0.3, whereas the homogeneous amphibolite typically contains >2 wt. % total alkalis with a K_2O/Na_2O ratio <0.2.

The homogeneous appearance of the Archean-hosted amphibolite suggests that it is likely of Paleoproterozoic age. The normalized profiles of the samples have notably steeper negative slopes than the other amphibolite samples ($[La/Yb]_N = 2.5$ vs. 1.14–1.66), as well as negative anomalies at Nb and Ti, which could suggest an arc affinity (Figure GS2025-4-2e, f). However, the Archean-hosted sample is also characterized by a relatively flat normalized HREE profile ($[Gd/Yb]_N = 1.16$), which is similar to the other homogeneous amphibolite and garnet amphibolite

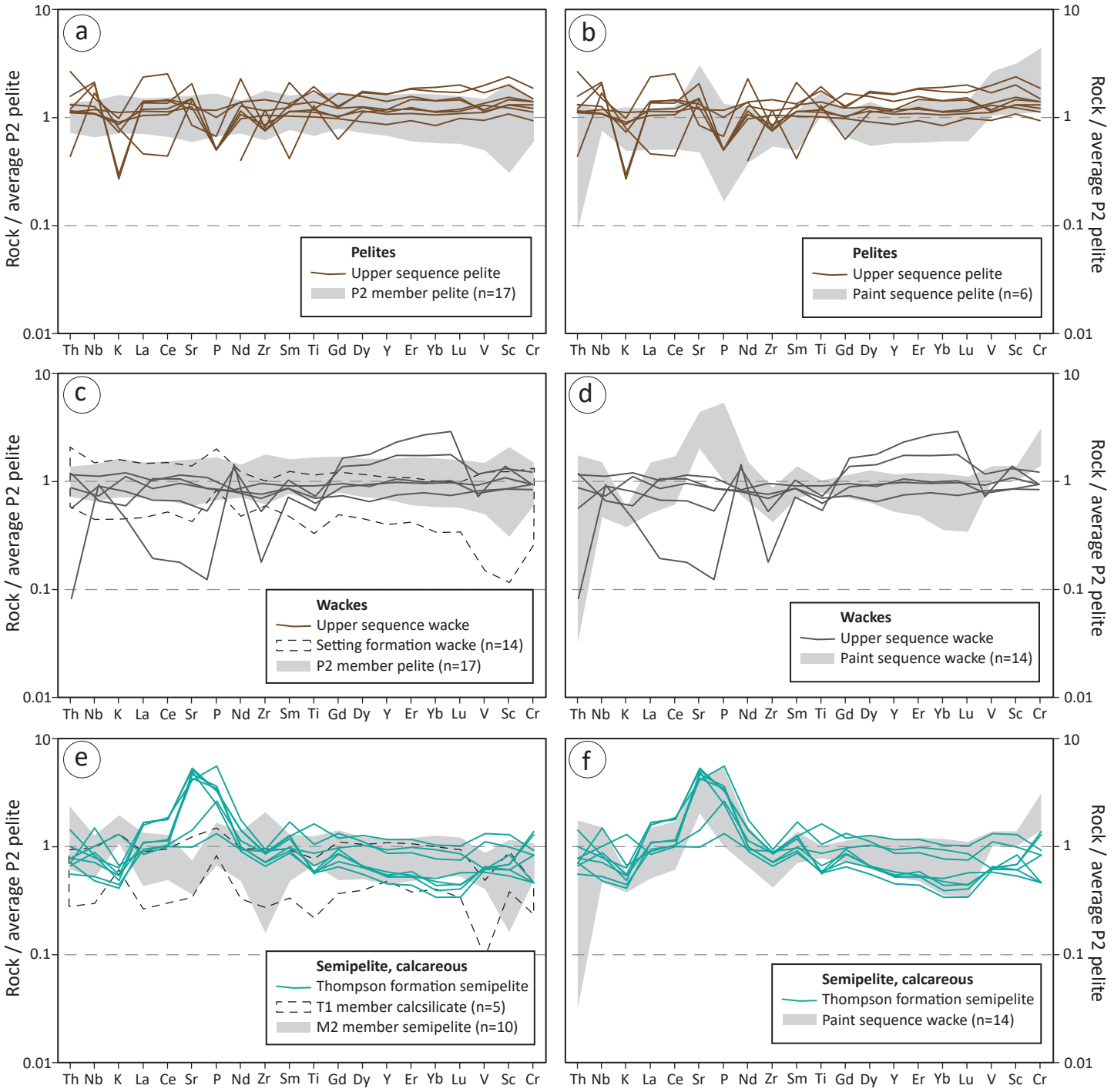

Figure GS2025-4-5: *Average P2 member pelite-normalized multi-element profiles for sedimentary rocks from the Halfway Lake area compared with other sedimentary rocks from the Thompson nickel belt:* ***a)*** *upper sequence pelite and P2 member pelite;* ***b)*** *upper sequence pelite and Paint sequence pelite;* ***c)*** *upper sequence wacke, Setting formation wacke and P2 member pelite;* ***d)*** *upper sequence wacke and Paint sequence wacke;* ***e)*** *Thompson formation semipelite, calcsilicate and M2 member semipelite;* ***f)*** *Thompson formation semipelite and Paint sequence wacke. Normalizing values are from Zwanzig et al. (2007). Reference values for pelite from the P2 member of the Pipe formation, wacke from the Setting formation and semipelite from the M2 member of the Manasan formation are from Zwanzig et al. (2007) and Couëslan (2016). Reference values for the Paint sequence pelite and wacke are from Couëslan (2016) and Couëslan and Janssens (2025a). Reference values for the calcsilicate from the T1 member of the Thompson formation are from Couëslan (2003), Zwanzig et al. (2007) and Couëslan (2021b).*

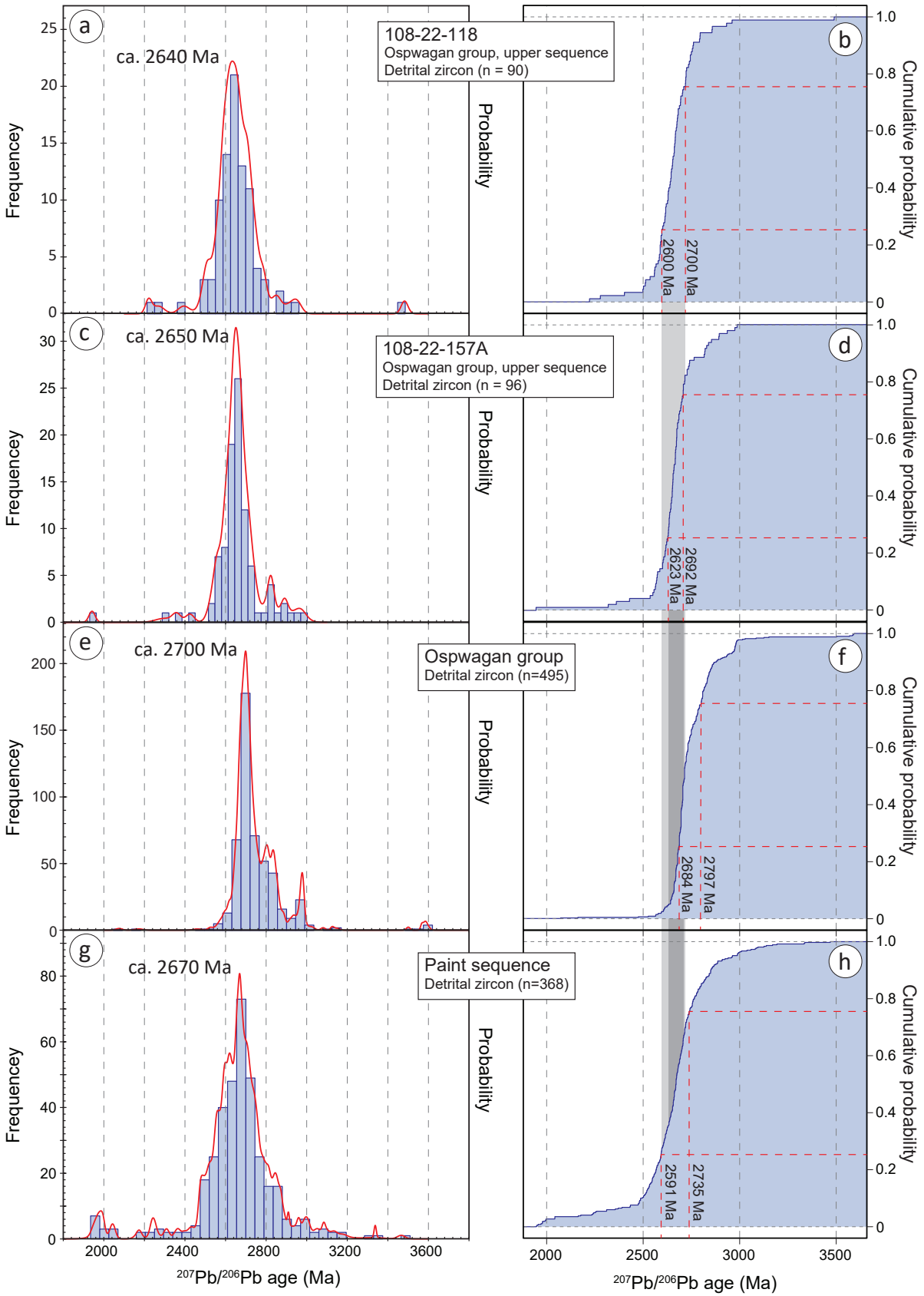

Figure GS2025-4-6: *Combined frequency histogram and probability-density distribution curves (left column) and cumulative distribution curves (right column) of $^{207}Pb/^{206}Pb$ detrital zircon ages for sedimentary rocks from the Thompson nickel belt:* ***a), b)*** *Halfway Lake sample 108-22-118;* ***c), d)*** *Halfway Lake sample 108-22-157A;* ***e), f)*** *compilation of Ospwagan group rocks;* ***g), h)*** *compilation of Paint sequence rocks. Data sources: Ospwagan group, Rayner et al. (2006), Zwanzig et al. (2021), Couëslan (2022c); Paint sequence, Couëslan (2016, 2022b, 2025). The interquartile ranges of the Halfway Lake samples are projected in grey for comparison with the Ospwagan group and Paint sequence cumulative distribution curves.*

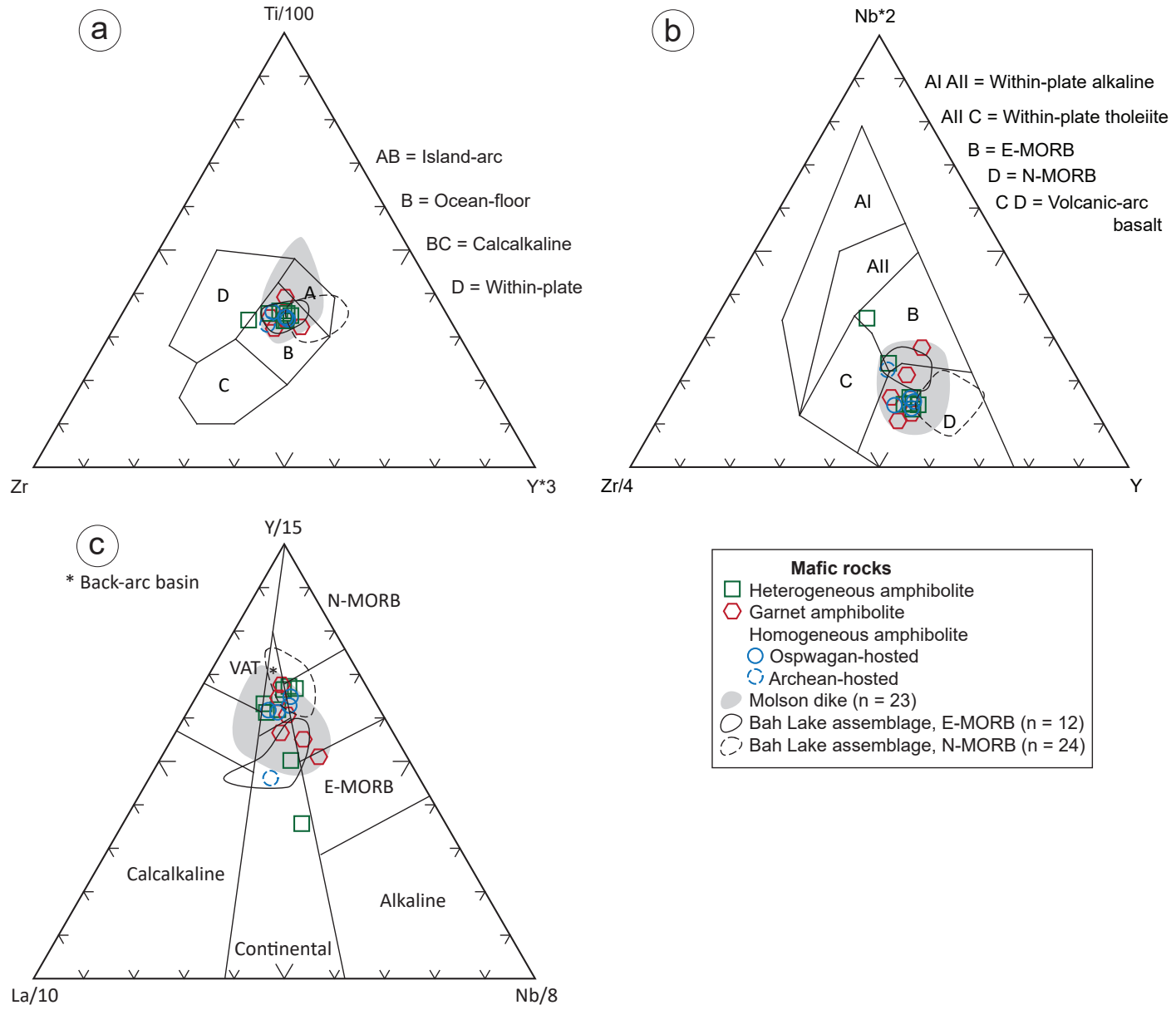

Figure GS2025-4-7: *Geochemical discrimination diagrams for mafic rocks from Halfway Lake:* ***a)*** *Zr-Ti-Y diagram (after Pearce and Cann, 1973);* ***b)*** *Zr-Nb-Y diagram (after Meschede, 1986);* ***c)*** *La-Y-Nb diagram (after Cabanis and Lecolle, 1989). Reference values for Molson dikes are for analyses with 1 <$(La/Yb)_N$ <3 and are sourced from Burnham et al. (2009), Heaman et al. (2009), Ciborowski et al. (2017), Couëslan (2016, 2021a, b; unpublished data, 2014). Reference values for Bah Lake assemblage area from Zwanzig (2005). Abbreviation: VAT, volcanic arc tholeiite.*

samples ($[Gd/Yb]_N$ = 1.06–1.48). The enrichment in LREEs and Th could be the result of crustal interaction/assimilation, possibly combined with a slightly more enriched mantle source, similar to the enriched Bah Lake assemblage sample discussed above. This interpretation is consistent with discrimination diagrams in which the Archean-hosted sample plots toward the E-MORB and continental basalt fields (Figure GS2025-4-7b, c).

Granitoids

The primitive mantle-normalized profiles of granitoids from the Halfway Lake area are typical of arc or crustal-derived melts (Figure GS2025-4-4b, d, f, h). The garnet-bearing granite–tonalite pluton is geochemically distinct from the other granitic to granodioritic intrusions in that it defines a trend from tholeiitic to calcalkaline affinity on the K_2O–SiO_2 diagram (Figure GS2025-4-8a). All other granitoids plot in the calcalkaline field(s). The garnet-bearing pluton is also characterized by flat HREE profiles ($[Gd/Yb]_N$ = 0.89–1.11 compared with >1.25 for other granitoids; Figure GS2025-4-4c). This is a characteristic of FII felsic rocks, which are interpreted to form from mid-level, high-temperature partial melting of crust in extensional environments (Figure GS2025-4-8b, c; Hart et al., 2004; Piercey, 2011). The garnet-bearing tonalite also shares some characteristics with FIII felsic rocks, including high SiO_2 content (>75 wt. %), and a tholeiitic affinity, which are characteristic of partial melts generated at higher crustal levels (Hart et al., 2004; Piercey, 2011). Partial melting in extensional environments is typically driven by mantle upwelling

and the emplacement of mafic to ultramafic magmas. Emplacement of the garnet-bearing pluton could therefore be contemporaneous with magmatism related to the Bah Lake assemblage or the Molson dike swarm. Samples were collected from drillcore for U–Pb zircon geochronology in June 2025 to test this theory.

A number of syenitic to monzonitic plutons occur within the TNB in the Paint Lake area, Bucko-Resting lakes area and at Partridge Crop Lake. The plutons in the Paint Lake area and at Partridge Crop Lake are typically more magnesian (Mg# = 0.65–0.76), enriched in Cr (270–460 ppm), Ni (100–280 ppm) and LILEs (Na_2O+K_2O = 7.32–9.99 wt. %, 1166–1479 ppm Sr, 4299–5377 ppm Ba) than the Halfway Lake monzonite (Couëslan, 2016; Couëslan and Janssens, 2025a; C.G. Couëslan, unpublished data, 2014). The Paint Lake and Partridge Crop Lake plutons also have a lower peralkalinity index (molar $Al_2O_3/[Na_2O+K_2O]$ = 0.91–1.2 compared with >1.4) and a more shoshonitic affinity (Figure GS2025-4-3; Figure GS2025-4-8a, d). The Paint Lake syenite yielded a U-Pb zircon age of 1883 ±5 Ma, which is interpreted as a magmatic crystallization age (Couëslan, 2016). The plutons from the Paint Lake area and Partridge Crop Lake are characterized by strongly negative εNd values of –14.3 to –15.0 (calculated at 1880 Ma) and relatively old depleted-mantle Nd-model ages of ca. 3.09–3.36 Ga (Couëslan, 2016; unpublished data, 2017), which contrast with the much less evolved Sm-Nd isotope geochemistry of the Halfway Lake pluton (sample 108-22-097, Table GS2025-4-1).

The Bucko pluton is a relatively large monzodioritic to monzonitic pluton that stretches approximately 25 km from the Bucko Lake area in the north to the Manibridge mine area in the south. The Bucko pluton has a high-K calcalkaline affinity, and has Mg# values (0.57–0.62) and concentrations of Cr and Ni (90–141 ppm and 52–71 ppm, respectively) that are similar to the Halfway Lake pluton (Figure GS2025-4-8a, d). The Bucko pluton is also characterized by similar total alkali contents (Na_2O+K_2O = 6.35–7.84 wt. %) and ASI values (0.76–0.83) as the Halfway Lake pluton (Figure GS2025-4-3). The Bucko pluton has a magmatic crystallization age of ca. 1835 Ma (Bleeker et al., 1995), with an εNd value of –1.4 (calculated at ca. 1845 Ma) and a depleted-mantle Nd-model age of ca. 2.49 Ga (Percival et al., 2004). Given the similarities in geochemistry and Nd-model ages, a similar magmatic crystallization age could be assumed for the Halfway Lake pluton, which results in an εNd value of –1.77 (Table GS2025-4-1). An εNd value, calculated at 1835 Ma, of –1.77 Ga suggests a weakly evolved source or that the monzonite was derived from a juvenile magma that interacted with evolved crust.

Similarities were noted between the Bucko pluton and Archean sanukitoids (Percival et al., 2004); however, they also have characteristics that are transitional between the high-silica and low-silica adakites of Martin et al. (2005). Sanukatoid and adakite magmas are typically associated with subduction zone processes. This challenges current understanding of the subduction polarity at ca. 1835 Ma, which places the Superior craton as the under-riding plate (Bleeker, 1990; White et al., 2002).

Sedimentary rocks

One of the original intentions behind the mapping project at Halfway Lake was to investigate if Paint sequence rocks were present along strike from the Phillips–Paint lakes area (Couëslan, 2016, 2022b). A method using average P2 member pelite-normalized multi-element profiles to compare and contrast sedimentary rock units in the TNB was devised by Zwanzig et al. (2007). Average P2-normalized profiles of pelite from Halfway Lake are relatively flat and more similar to the profiles of pelite from the P2 member than pelite from the Paint sequence, which can be characterized by relative depletions at Th and P, and relative enrichments at Sr, V, Sc and Cr (Figure GS2025-4-5a, b). The majority of wacke samples from the upper sequence at Halfway Lake have similarly flat normalized multi-element profiles (Figure GS2025-4-5c). This contrasts with normalized profiles of the Paint sequence wacke, which can have negative slopes and be relatively depleted in Th and K, and is typically enriched in Sr, P and Cr (Figure GS2025-4-5d).

The calcareous semipelite of the Thompson formation at Halfway Lake is assumed to consist of a clastic component (likely siltstone or wacke) along with a calcareous component (sedimentary carbonate). A multi-element profile could therefore be expected with characteristics falling between those of the M2 member semipelite of the underlying Manasan formation and those of the Thompson formation calcsilicate (Figure GS2025-4-5e). Instead, the normalized profile of the calcareous semipelite can appear more similar to that of the Paint sequence wacke, with relative depletions in K and enrichments in Sr, P and, in some cases, Cr (Figure GS2025-4-5f). This could imply a similar clastic source is shared by Thompson formation rocks at Halfway Lake and the Paint sequence, whether or not it suggests a direct stratigraphic relationship (e.g., lateral facies change). However, it should also be noted that Thompson formation calcsilicates and marbles from the Halfway Lake area display similar relative enrichments in P, which could imply that P is part of the calcareous sedimentary component rather than the clastic component (Couëslan and Janssens, 2025b).

The T_{DM} of the Thompson formation calcareous semipelite (ca. 2.94 Ga) is typical for Ospwagan group rocks (ca. 2.82–3.16 Ga) and near the lower end for analyzed Paint sequence rocks (ca. 2.95–3.57 Ga; Figure GS2025-4-9). In contrast, the T_{DM} ages for the upper sequence wackes from Halfway Lake are significantly younger (ca. 2.46–2.71 Ga) than previous model ages determined for the Ospwagan group and overlap with model ages of the Burntwood group of the adjacent Kisseynew domain (ca. 2.13–2.62 Ga). The younger model ages for the upper sequence wacke suggest a less evolved (possibly younger) crustal component than observed elsewhere in the Ospwagan group. Recent work suggests that there may be a general younging of Paint sequence Nd-model ages toward the south (Figure GS2025-4-9; Couëslan, 2022b). Initial results suggest a similar relationship may exist in the Archean basement, with generally older model ages in the north (possibly coinciding with Hudson Bay terrain-

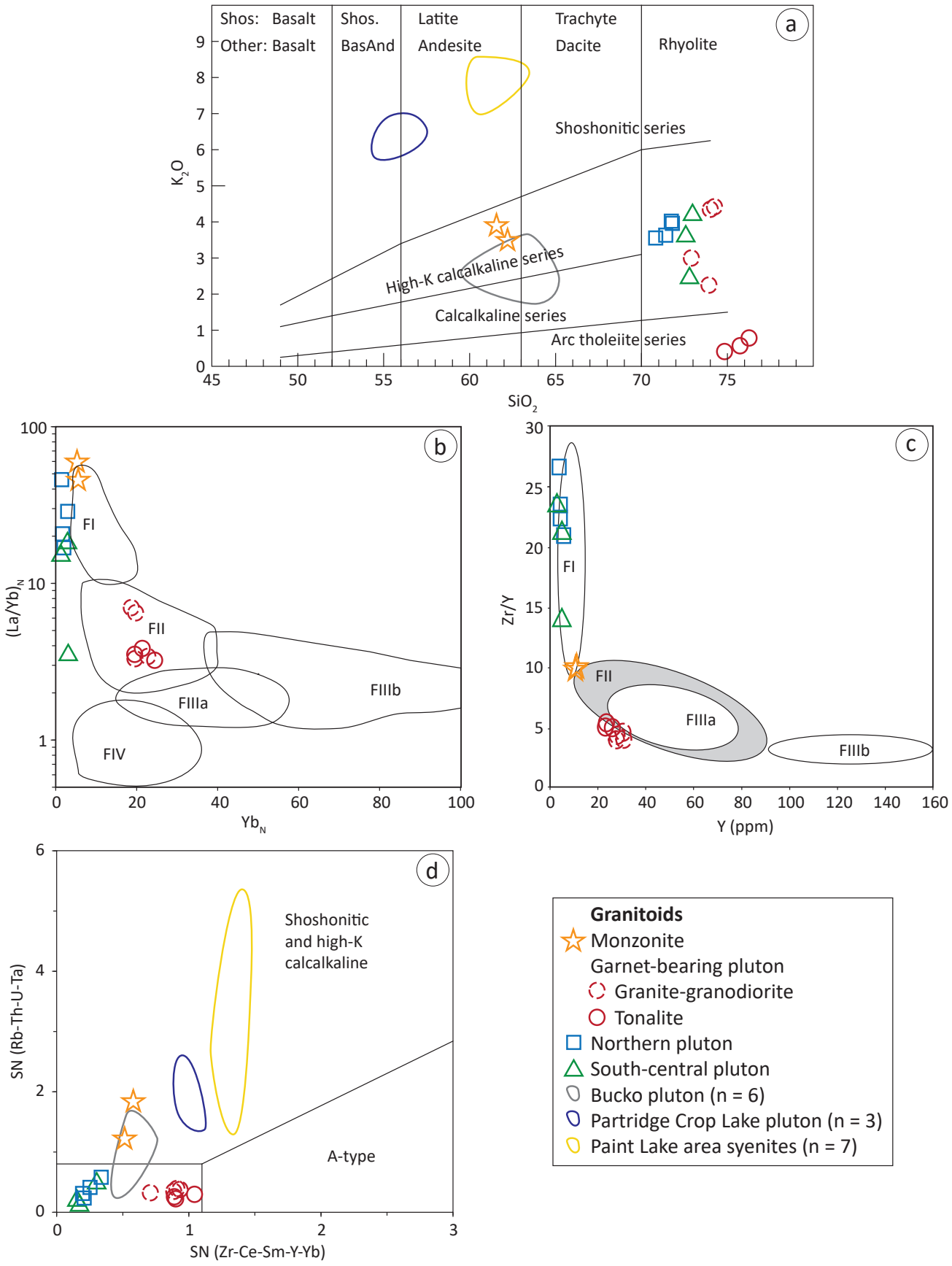

Figure GS2025-4-8: *Geochemical discrimination diagrams for granitoid rocks from Halfway Lake:* ***a)*** *K_2O-SiO_2 diagram of Peccerillo and Taylor (1976);* ***b)*** *$(La/Yb)_N$-Yb_N diagram of Hart et al. (2004; modified after Lesher et al., 1986);* ***c)*** *Zr/Y-Y diagram of Lesher et al. (1986);* ***d)*** *sliding normalization (SN) diagram of Liégeois et al. (1998). Abbreviations: BasAnd, basaltic andesite; Shos., shoshonite.*

derived crust) and younger model ages in the south (possibly coinciding with North Caribou terrain-derived crust; Couëslan, 2021a, 2022b). It is possible that the same pattern could exist within the Ospwagan group, with older model ages in the north and younger model ages in the south; however, more sampling of all the rock suites in the south is required to provide a statistically robust dataset to confirm this hypothesis.

The dominant detrital zircon age nodes for the upper sequence wacke samples 108-22-118 and 108-22-157A are 2640 Ma and 2650 Ma, respectively (Figure GS2025-4-6a, c). These nodes coincide with U-Pb metamorphic zircon and monazite ages from the adjacent Pikwitonei granulite domain of the Superior craton (Heaman et al., 2011; Guevara et al., 2020; Couëslan, 2021a). This supports previous interpretations that the clastic detritus that formed the Ospwagan group was sourced mainly from the Superior craton (Bleeker, 1990; Bleeker and Hamilton, 2001; Rayner et al., 2006; Böhm et al., 2007; Zwanzig et al., 2007). However, these dominant age nodes are significantly younger than the dominant age node for a compilation of previously analyzed Ospwagan group detrital zircon (ca. 2700 Ma; Figure GS2025-4-6e). Although there is overlap of the interquartile ranges between the Ospwagan group compilation (2684–2797 Ma) and the upper sequence rocks of Halfway Lake (2600–2700 Ma and 2623–2692 Ma; Figure GS2025-4-6b, d, f), it is relatively minor. The dominant node and interquartile ranges of the Halfway Lake rocks are closer to those of the compilation of Paint sequence detrital zircon (Figure GS2025-4-6g, h).

Economic considerations

The stratigraphic relationships and lithogeochemistry of the supracrustal rocks at Halfway Lake suggest that they are correlative with the Ospwagan group rather than the Paint sequence (Couëslan, 2023; this study). Although not discussed in this study, many of the ultramafic bodies at Halfway Lake appear to be emplaced near sulphidic horizons at the boundary between the Thompson and Pipe formations, which coincides with the ore horizons at the Pipe and Birchtree mines (Couëslan, 2023). Conductors along this horizon, with or without significant ultramafic rock and that have been thickened along regional fold hinges, are prospective targets for Ni exploration (Bleeker, 1990; Lightfoot et al., 2017).

Böhm et al. (2007) demonstrated the use of Sm-Nd whole-rock geochemistry as an exploration tool for distinguishing Ospwagan group rocks from the less prospective Archean basement and Burntwood group in the northern TNB. However, the Nd-model age results from this study included two samples considerably younger than previous analyses from the Ospwagan group, one of which could be considered typical of the Burntwood group (Figure GS2025-4-9). These results underline the importance of collecting a suitable sample size. Further work is required to see if there could be a shift to younger Nd-model ages in Ospwagan group rocks toward the south in the TNB, which could restrict the use of Sm-Nd isotope geochemistry as an exploration tool to the northern portions of the TNB.

The garnet-bearing granite–tonalite pluton in western Halfway Lake shares a geochemical affinity with FII felsic rocks, which

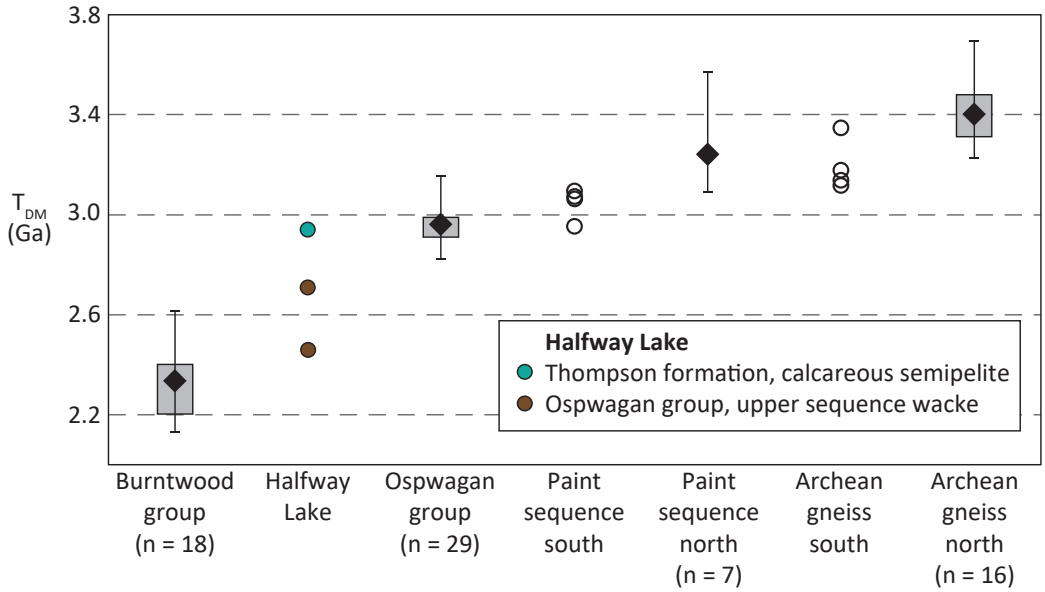

Figure GS2025-4-9: *Range of crustal-residence Nd-model ages for rocks from the Thompson nickel belt and adjacent Kisseynew domain. Diamonds indicate median values, circles indicate individual model ages for units with limited datasets and grey bars indicate the interquartile range (middle 50% of the data). Data sources: Burntwood group, Böhm et al. (2007) and Murphy and Zwanzig (2021); Ospwagan group and Archean gneiss, Böhm et al. (2007) and Manitoba Geological Survey (2022); Paint sequence, Couëslan (2016, 2022b).*

can be spatially associated with VMS systems. If the pluton was emplaced contemporaneously with the mafic–ultramafic magmatism of the Bah Lake volcanic assemblage, it would imply at least a notional potential for VMS mineralization. Outside of the submarine volcanic environment, FII felsic rocks can be found associated with epithermal deposits in extensional/rift environments (Hart et al., 2004). However, epithermal mineralization is considered to form at shallow crustal levels (<1000 m; Panteleyev, 1988), and would likely have poor preservation potential in the relatively high metamorphic-grade rocks of the TNB.

Acknowledgments

The author thanks S. Anthony and C. Ducharme of CaNickel Mining Limited for access to drillcore and storage facilities in Wabowden, and M. Urbatsch and C. Glew, formerly of Core Nickel Corporation, for access to drillcore. Thanks to P. Belanger, C. Epp, J. Macdonald, N. Palacios Montenegro and W. Sharpe for their help with moving, photographing, and sampling drillcore. The author also thanks M. Rinne and X.M. Yang for reviewing previous drafts of this report.

References

Bleeker, W. 1990: Evolution of the Thompson Nickel Belt and its nickel deposits, Manitoba, Canada; Ph.D. thesis, University of New Brunswick, Fredericton, New Brunswick, 400 p.

Bleeker, W. and Hamilton, M.A. 2001: New SHRIMP U-Pb ages for the Ospwagan Group: implications for the SE margin of the Trans-Hudson Orogen; Geological Association of Canada–Mineralogical Association of Canada, Joint Annual Meeting 2001, May 27–30, 2001, St. John's, Newfoundland, Abstracts, v. 26, p. 15.

Bleeker, W., Nägerl, P. and Machado, N. 1995: The Thompson Nickel Belt, Manitoba: some new U-Pb ages; *in* Geological Association of Canada–Mineralogical Association of Canada, Joint Annual Meeting 1995, May 17–19, 1995, Victoria, British Columbia, Program with Abstracts, p. A-8.

Böhm, C.O., Zwanzig, H.V. and Creaser, R.A. 2007: Sm-Nd isotope technique as an exploration tool: delineating the northern extension of the Thompson Nickel Belt, Manitoba, Canada; Economic Geology, v. 102, p. 1217–1231.

Burnham, O.M., Halden, N., Layton-Matthews, D., Lesher, C.M., Liwanag, J., Heaman, L., Hulbert, L., Machado, N., Michalak, D., Pacey, M., Peck, D.C., Potrel, A., Theyer, P., Toope, K. and Zwanzig, H. 2009: CAMIRO project 97E-02, Thompson Nickel Belt: final report, March 2002, revised and updated 2003; Manitoba Science, Technology, Energy and Mines, Manitoba Geological Survey, Open File OF2008-11, 434 p. plus appendices and GIS shape files for use with ArcInfo®.

Cabanis, B. and Lecolle, M. 1989: Le diagramme La/10-Y/15-Nb/8: un outil pour la discrimination des séries volcaniques et la mise en évidence des processus de mélange et/ou de contamination crustale; Comptes Rendus de l'Académie des Sciences, v. 309, p. 2023–2029.

Ciborowski, T.J.R., Minifie, M.J., Kerr, A.C., Ernst, R.E., Baragar, B. and Millar, I.L. 2017: A mantle plume origin for the Palaeoproterozoic Circum-Superior Large Igneous Province; Precambrian Research, v. 294, p. 189–213.

Couëslan, C.G. 2003: Petrogenesis of the Thompson Formation T1 Member, Thompson Nickel Belt, Manitoba, Canada; B.Sc. thesis, Brandon University, Brandon, Manitoba, 125 p.

Couëslan, C.G. 2016: Geology of the Paint and Phillips lakes area, Thompson nickel belt, central Manitoba (parts of NTS 63O1, 8, 9, 63P5, 12); Manitoba Growth, Enterprise and Trade, Manitoba Geological Survey, Geoscientific Report GR2016-1, 44 p., 1 map at 1:50 000 scale.

Couëslan, C.G. 2021a: Bedrock geology of the central Sipiwesk Lake area, Pikwitonei granulite domain, central Manitoba (part of NTS 63P4); Manitoba Agriculture and Resource Development, Manitoba Geological Survey, Geoscientific Report GR2021-1, 47 p. plus 1 appendix and 1 map at 1:20 000 scale.

Couëslan, C.G. 2021b: Lithogeochemistry of iron formation, calcsilicate, marble, and mafic dikes from the Thompson nickel belt, central Manitoba (NTS 63O8, 9, 63P5, 12, 15); Manitoba Agriculture and Resource Development, Manitoba Geological Survey, Data Repository Item DRI2021016, Microsoft® Excel® file.

Couëslan, C.G. 2022a: Bedrock mapping in the Halfway Lake area, Thompson nickel belt, central Manitoba (parts of NTS 63O1, 2); *in* Report of Activities 2022, Manitoba Natural Resources and Northern Development, Manitoba Geological Survey, p. 12–24.

Couëslan, C.G. 2022b: Characterization of ultramafic-hosting metasedimentary rocks and implications for nickel exploration at Phillips Lake, Thompson nickel belt, central Manitoba (part of NTS 63O1); Manitoba Natural Resources and Northern Development, Manitoba Geological Survey, Geoscientific Paper GP2022-1, 33 p.

Couëslan, C.G. 2022c: Laser-ablation inductively coupled plasma–mass spectrometry analyses of detrital zircon grains from metasedimentary rocks of the Ospwagan group, Thompson nickel belt, Manitoba (parts of NTS 63O8, 9; 63P12); Manitoba Natural Resources and Northern Development, Manitoba Geological Survey, Data Repository Item DRI2022008, Microsoft® Excel® file.

Couëslan, C.G. 2023: Logging of archived drillcore from the Halfway Lake area, Thompson nickel belt, central Manitoba (parts of NTS 63O1, 2); *in* Report of Activities 2023, Manitoba Economic Development, Investment and Trade, Manitoba Geological Survey, p. 27–39.

Couëslan, C.G. 2025: Laser-ablation inductively coupled plasma–mass spectrometry analyses of detrital zircon grains from metasedimentary rocks of the Thompson nickel belt, Manitoba (parts of NTS 63O1; 63P5, 12); Manitoba Business, Mining, Trade and Job Creation, Manitoba Geological Survey, Data Repository Item DRI2025001, Microsoft® Excel® file.

Couëslan, C.G. and Janssens, J. 2025a: Lithogeochemistry of samples from the Thompson nickel belt, central Manitoba (parts of NTS 63P5, 12; 63O8); Manitoba Business, Mining, Trade and Job Creation, Manitoba Geological Survey, Data Repository Item DRI2025014, Microsoft® Excel® file.

Couëslan, C.G. and Janssens, J. 2025b: Whole-rock lithogeochemistry and assays for samples from the Halfway Lake area, Thompson nickel belt, central Manitoba (part of NTS 63O1, 2); Manitoba Business, Mining, Trade and Job Creation, Manitoba Geological Survey, Data Repository Item 2025011, Microsoft® Excel® file.

Couëslan, C.G. and Janssens, J. 2025c: Whole-rock lithogeochemistry and assays for drillcore samples from the Halfway Lake area, Thompson nickel belt, central Manitoba (part of NTS 63O1, 2); Manitoba Business, Mining, Trade and Job Creation, Manitoba Geological Survey, Data Repository Item 2025029, Microsoft® Excel® file.

Goldstein, S.L., O'Nions, R.K. and Hamilton, P.J. 1984: A Sm-Nd study of atmospheric dusts and particulates from major river systems; Earth and Planetary Science Letters, v. 70, p. 221–236.

Guevara, V.E., MacLennan, S.A., Dragovic, B., Caddick, M.J., Schoene, B., Kylander-Clark, A.R.C. and Couëslan, C.G. 2020: Polyphase zircon growth during slow cooling from ultrahigh temperature: an example from the Archean Pikwitonei Granulite Domain; Journal of Petrology, v. 61, no. 1, egaa021, URL <https://doi.10.1093/petrology/egaa021>.

Hart, T.R., Gibson, H.L. and Lesher, C.M. 2004: Trace element geochemistry and petrogenesis of felsic volcanic rocks associated with volcanogenic massive Cu-Zn-Pb sulfide deposits; Economic Geology, v. 99, p. 1003–1013.

Heaman, L.M., Peck, D. and Toope, K. 2009: Timing and geochemistry of 1.88 Ga Molson Igneous Events, Manitoba: insights into the formation of a craton-scale magmatic and metallogenic province; Precambrian Research, v. 172, p. 143–162.

Heaman, L.M., Böhm, Ch.O., Machado, N., Krogh, T.E., Weber, W. and Corkery, M.T. 2011: The Pikwitonei Granulite Domain, Manitoba: a giant Neoarchean high-grade terrane in the northwest Superior Province; Canadian Journal of Earth Sciences, v. 48, p. 205–245, URL <https://doi.org/10.1139/E10-058>.

Lesher, G.M., Goodwin, A.M., Campbell, I.H. and Gorton, M.P. 1986: Trace-element geochemistry of ore-associated and barren, felsic metavolcanic rocks in the Superior Province, Canada; Canadian Journal of Earth Sciences, v. 23, p. 222–237.

Liégeois, J.–P., Navez, J., Hertogen, J. and Black, R. 1998: Contrasting origin of post-collisional high-K calc-alkaline and shoshonitic versus alkaline and peralkaline granitoids. The use of sliding normalization; Lithos, v. 45, p. 1–28.

Lightfoot, P.C., Stewart, R., Gribbon, G. and Mooney, S.J. 2017: Relative contribution of magmatic and post-magmatic processes in the genesis of the Thompson Mine Ni-Co sulfide ores, Manitoba, Canada; Ore Geology Reviews, v. 83, p. 258–286.

Macek, J.J., Zwanzig, H.V. and Pacey, J.M. 2006: Thompson Nickel Belt geological compilation map, Manitoba (parts of NTS 63G, J, O, P and 64A and B); Manitoba Industry, Economic Development and Mines, Manitoba Geological Survey, Open File Report OF2006-33, digital map on CD.

Maniar, P.D. and Piccoli, P.M. 1989: Tectonic discrimination of granitoids; Geological Society of America, Bulletin, v. 101, p. 635–643.

Manitoba Geological Survey 2022: Compilation of Sm-Nd isotope results from the Manitoba Geological Survey 2021/2022 field season; Manitoba Natural Resources and Northern Development, Manitoba Geological Survey, Data Repository Item DRI2022003, Microsoft® Excel® file.

Martin, H., Smithies, R.H., Rapp, R., Moyen, J.-F. and Champion, D. 2005: An overview of adakite, tonalite-trondhjemite-granodiorite (TTG), and sanukitoid: relationships and some implications for crustal evolution; Lithos, v. 79, p. 1–24, URL <https://doi.org/10.1016/j.lithos.2004.04.048>.

McDonough, W.F. and Sun, S.-s. 1995: The composition of the Earth; Chemical Geology, v. 120, p. 223–253.

Meschede, M. 1986: A method of discriminating between different types of mid-ocean ridge basalts and continental tholeiites with the Nb-Zr-Y diagram; Chemical Geology, v. 56, p. 207–218.

Murphy, L.A. and Zwanzig, H.V. 2021: Geology of the Wuskwatim–Granville lakes corridor, Kisseynew domain, Manitoba (parts of NTS 63O, P, 64A–C); Manitoba Agriculture and Resource Development, Manitoba Geological Survey, Geoscientific Report GR2021-2, 94 p.

Panteleyev, A. 1988: A Canadian Cordilleran model for epithermal gold-silver deposits; *in* Ore Deposit Models, R.C. Roberts and P.A. Sheahan (ed.), Geoscience Canada, Reprint Series 3, p. 31–43.

Pearce, J.A. and Cann, J.R. 1973: Tectonic setting of basic volcanic rocks determined using trace element analyses; Earth and Planetary Science Letters, v. 19, p. 290–300.

Peccerillo, A. and Taylor, S.R. 1976: Geochemistry of Eocene calc-alkaline volcanic rocks from the Kastamonu area, Northern Turkey; Contributions to Mineralogy and Petrology, v. 58, p. 63–81.

Percival, J.A., Whalen, J.B. and Rayner, N. 2004: Pikwitonei–Snow Lake, Manitoba transect (parts of NTS 63J, O and P), Trans-Hudson Orogen–Superior Margin Metallotect Project: initial geological, isotopic and SHRIMP U-Pb results; *in* Report of Activities 2004, Manitoba Industry, Economic Development and Mines, Manitoba Geological Survey, p. 120–134.

Piercey, S.J. 2011: The setting, style, and role of magmatism in the formation of volcanogenic massive sulphide deposits; Mineralium Deposita, v. 46, p. 449–471.

Rayner, N., Zwanzig, H.V. and Percival, J.A. 2006: Detrital zircon provenance of the Pipe Formation, Ospwagan Group, Thompson Nickel Belt, Manitoba, NTS 63O8; *in* Report of Activities 2007, Manitoba Science, Technology, Energy and Mines, Manitoba Geological Survey, p. 116–124.

White, D.J., Lucas, S.B., Bleeker, W., Hajnal, Z., Lewry, J.F. and Zwanzig, H.V. 2002: Suture-zone geometry along an irregular Paleoproterozoic margin: the Superior boundary zone, Manitoba, Canada; Geology, v. 30, p. 735–738.

Zwanzig, H.V. 2005: Geochemistry, Sm-Nd isotope data and age constraints of the Bah Lake assemblage, Thompson Nickel Belt and Kisseynew Domain margin: relation to Thompson-type ultramafic bodies and a tectonic model (NTS 63J, O and P); *in* Report of Activities 2005, Manitoba Industry, Economic Development and Mines, Manitoba Geological Survey, p. 40–53.

Zwanzig, H.V., Macek, J.J. and McGregor, C.R. 2007: Lithostratigraphy and geochemistry of the high-grade metasedimentary rocks in the Thompson Nickel Belt and adjacent Kisseynew Domain, Manitoba: implications for nickel exploration; Economic Geology, v. 102, p. 1197–1216.

Zwanzig, H.V., Böhm, C.O. and Couëslan, C.G. 2021: Laser-ablation, multicollector, inductively coupled plasma–mass spectrometry U-Pb isotopic analyses of detrital zircon grains from the Ospwagan group, Setting formation metagreywacke sample 12-04-4462, Setting Lake, central Manitoba (part of NTS 63O2); Manitoba Agriculture and Resource Development, Manitoba Geological Survey, Data Repository Item DRI2021013, Microsoft® Excel® file.

GS2025-5

Geochronology and isotope geochemistry results from Russell Lake, northwestern Manitoba (parts of NTS 64C5, 6)

by T. Martins and C.G. Couëslan

Summary

Results from geochronological and radiogenic isotope analyses are presented here for the mapping project at Russell Lake, northwestern Manitoba. Geological bedrock mapping at a scale of 1:20 000 was conducted during the 2019 and 2020 field seasons. Outcrops at Russell Lake are dominated by the coeval sedimentary rocks of the Burntwood and Sickle groups, as well as by volcanic rocks and granodioritic intrusions. The Sm-Nd results for both the Burntwood and Sickle groups fit the range presented by previous authors. The four samples studied yield similar U-Pb dates, which suggests that the sediments from the Burntwood and Sickle groups were eroded from the same terrane. The Burntwood group samples seem to have less Archean zircon than the Sickle group, but this could be explained by the small number of samples targeting zircon cores.

In Brief:

- Geochronology and radiogenic isotopes are presented for the mapping project at Russell Lake
- Outcrops at Russell Lake are dominated by the coeval sedimentary rocks of the Burntwood and Sickle groups, as well as volcanic rocks and granodiorite intrusions
- The Sm-Nd results and the U-Pb dates for both the Burntwood and Sickle groups fit the range presented by previous workers

Citation:
Martins, T. and Couëslan, C.G. 2025: Geochronology and isotope geochemistry results from Russell Lake, northwestern Manitoba (parts of NTS 64C5, 6); *in* Report of Activities 2025, Manitoba Business, Mining, Trade and Job Creation, Manitoba Geological Survey, p. 48–58.

Introduction

A multidisciplinary mapping project was undertaken by the Manitoba Geological Survey (MGS) at Russell Lake during 2019 and 2020, which generated contributions in the annual report series and preliminary bedrock maps (Martins and Couëslan, 2019a, b, 2020a, b). The Quaternary geology of the area was also studied as part of this project and results include new sampling for till geochemistry and kimberlite indicator minerals as well as for ice-flow mapping (Hodder, 2019a, b, 2020, 2021). In this report, the results from geochronological and isotopic studies of representative rock units from the study area are presented.

Although the stratigraphy of the region is known (e.g., Zwanzig and Bailes, 2010), U-Pb zircon and whole-rock Sm-Nd results are scarce, especially along the north flank of the Kisseynew paleobasin. Representative samples from the metamorphosed mafic and sedimentary rock units were targeted for whole-rock Sm-Nd isotope geochemistry. Samples selected for detrital-zircon U-Pb geochronology are representative of the two major metasedimentary rock packages mapped at Russell Lake (Burntwood and Sickle groups). Gathering this type of information is important because it provides insight into the timing of deposition of the rocks in the study area, their provenance and the manner in which they compare with correlative units in other parts of the basin. The main objective for the detrital-zircon geochronology study is to better characterize the detrital sources of the Burntwood and Sickle groups along the northern margin of the Kisseynew domain (Figure GS2025-5-1).

All rocks in the study area were metamorphosed to at least upper-amphibolite–facies conditions (Lenton, 1981; Martins and Couëslan, 2019b); however, for the sake of brevity, the ‘meta’ prefix has been omitted from rock names. Where possible, protolith interpretation was used in the naming of rock units.

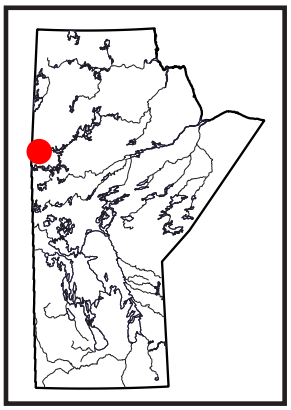

Previous work

The Russell–McCallum lakes area was previously mapped by Downie (1936) of the Geological Survey of Canada (GSC) at a scale of 1:253 440. Later, geological mapping by Hunter (1953) extended the regional coverage into McKnight Lake at a scale of 1:126 720. The MGS mapped the area in the 1970s. McRitchie (1975a, b) mapped Russell Lake on a scale of 1:31 680. The adjoining areas were mapped by Baldwin (1974) and Zwanzig and Wielezynski (1975a, b) at a scale of 1:31 680, and Pollock (1966) at a scale of 1:63 360. The area to the west of Russell–McCallum lakes was mapped by Gilboy (1976) at a scale of 1:100 000. Lenton (1981) mapped the area extending from the Russell–McCallum lakes area to McKnight Lake at a scale of 1:50 000. In 2019, the MGS initiated a multidisciplinary geological mapping project in the Russell–McMallum lakes area. Preliminary results of bedrock mapping at the 1:20 000 scale can be found in Martins and Couëslan (2019a, b, 2020a, b, c) and those from Quaternary studies in Hodder (2019a, b, 2020, 2021).

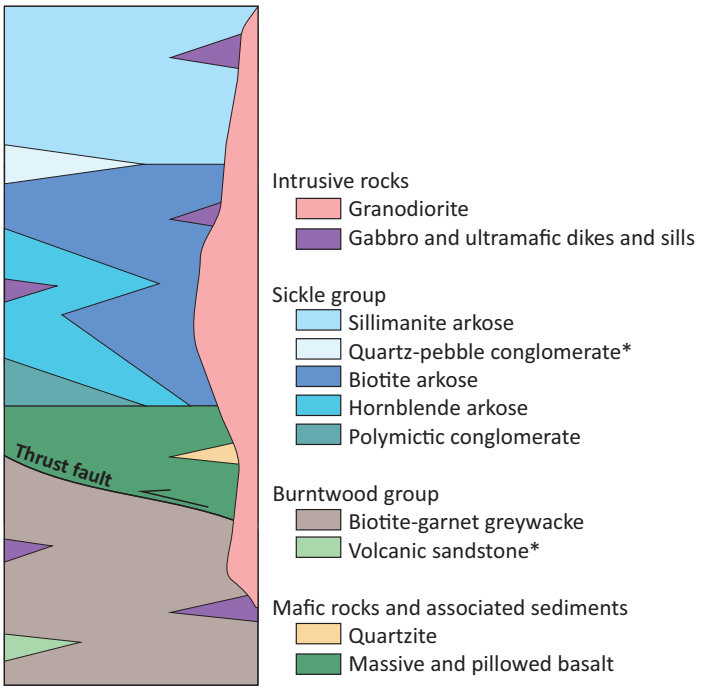

Figure GS2020-5-1: *Idealized, schematic stratigraphic column of the rock units of the Burntwood and Sickle groups at Russell Lake; asterisks indicate rock units not observed in the northern arm of the lake (after Martins and Couëslan, 2020b).*

The Russell Lake area was the target of economic studies focused on base-metal mineralization along the contact zone between rocks of the Burntwood and Sickle groups, the two major stratigraphic units of the area (Baldwin, 1976, 1980). There are records of base-metal exploration work in the area from 1954 until 1983 (e.g., Assessment Files 91616, 93803; Manitoba Business, Mining, Trade and Job Creation, Winnipeg). Airborne electromagnetic surveys located a number of conductors. The airborne anomalies were commonly followed up by diamond-drilling. Base- and precious-metal assay results (e.g., Ni, Au, Ag, Cu) were not promising and led to abandonment of the claims. However, significant graphite mineralization was reported in the majority of drillholes (e.g., Assessment Files 92387, 93001, 93804). For example, graphite was described in Assessment File 90985 submitted by Hudson Bay Exploration and Development Company Limited. The company drilled six drillholes in 1962 and reported up to 2.2 m (7.3 feet) of near-solid to solid graphite, pyrite and pyrrhotite, 1.9 m (6.2 feet) well-mineralized with graphite and 1.2 m (4.1 feet) mineralized with graphite.

Regional geology

The Kisseynew domain (KD) forms the large central part of the predominantly juvenile Paleoproterozoic internides, which make up the Reindeer Zone of the Trans-Hudson orogen (THO) in Manitoba (Figure GS2025-5-2; Stauffer, 1984; Lewry and Collerson, 1990). The KD is dominated by metamorphosed greywacke and mudstone of the Burntwood group, and arkosic rocks of the Sickle group. The provenance of the Burntwood group is interpreted to be the adjacent magmatic-arc terranes. Detritus from the arcs was deposited in coalescing turbidite fans (Bailes, 1980; Zwanzig, 1999). The turbidites were deformed and metamorphosed to amphibolite- and transitional granulite-facies, resulting in migmatization. Rocks from the Sickle group are typically metamorphosed arkosic units interpreted to have been deposited unconformably on the Lynn Lake arc massif (Zwanzig, 2008) and prograded over the Burntwood group prior to, and during, the onset of terminal continental collision. Both Burntwood and Sickle groups are intruded by granitoid rocks, including foliated granitoid bodies ranging from granite to tonalite and later pegmatite (e.g., Lenton, 1981; Zwanzig and Bailes, 2010; Zwanzig, 2019).

The geological setting of the KD is a matter of debate. Some authors (Ansdell, 2005; Corrigan et al., 2005, 2009) favour the interpretation of the KD as a back-arc basin to the Flin Flon volcanic arc that was filled during its opening. However, other authors (e.g., Zwanzig, 1999; Zwanzig and Bailes, 2010) favour an interpretation of a longer lived and dynamic evolution, in which the present geographic distribution of rocks resulted from crustal-scale overturning and oroclinal bending during continental collision.

The Russell Lake area is located within the Kisseynew north flank, a subdivision of the KD introduced by Zwanzig (2008; Figure GS2025-5-2). The Kisseynew north flank is dominated by Paleoproterozoic metasedimentary rocks of the Burntwood and Sickle groups, typically separated by the volcanosedimentary Granville complex, a composite assemblage of predominantly mafic rocks that includes remnants of ocean floor (Murphy and Zwanzig, 2021). The Kisseynew north flank is bounded to the north by the Lynn Lake domain, to the east by the northeastern Kisseynew subdomain and to the south by the central Kisseynew subdomain.

The majority of outcrops in the Russell lake area are dominated by sedimentary rocks of the Burntwood and Sickle groups, volcanic rocks and granodiorite bodies (Figure GS2025-5-3). The Burntwood and Sickle groups are interpreted to be coeval (e.g., Zwanzig and Bailes, 2010); therefore, the succession of units is not to be viewed as a true chronostratigraphic sequence (see Figure GS2025-5-1). For a detailed description of the rock units at Russell Lake, readers are referred to Martins and Couëslan (2019a, b, 2020a, b).

Results of whole-rock Sm-Nd isotope geochemistry

The results for the whole-rock Sm-Nd isotopic analyses of samples from the mapping area were published by Manitoba Agriculture and Resource Development (2020, 2021) but are also presented in Table GS2025-5-1 (sample locations are plotted in Figure GS2025-5-3). The results from this study yield initial εNd (calculated at 1840 Ma) of –1.2 and +0.7; crustal residence Nd-model depleted-mantle model ages (T_{DM}) of 2.39 and 2.29 Ga for

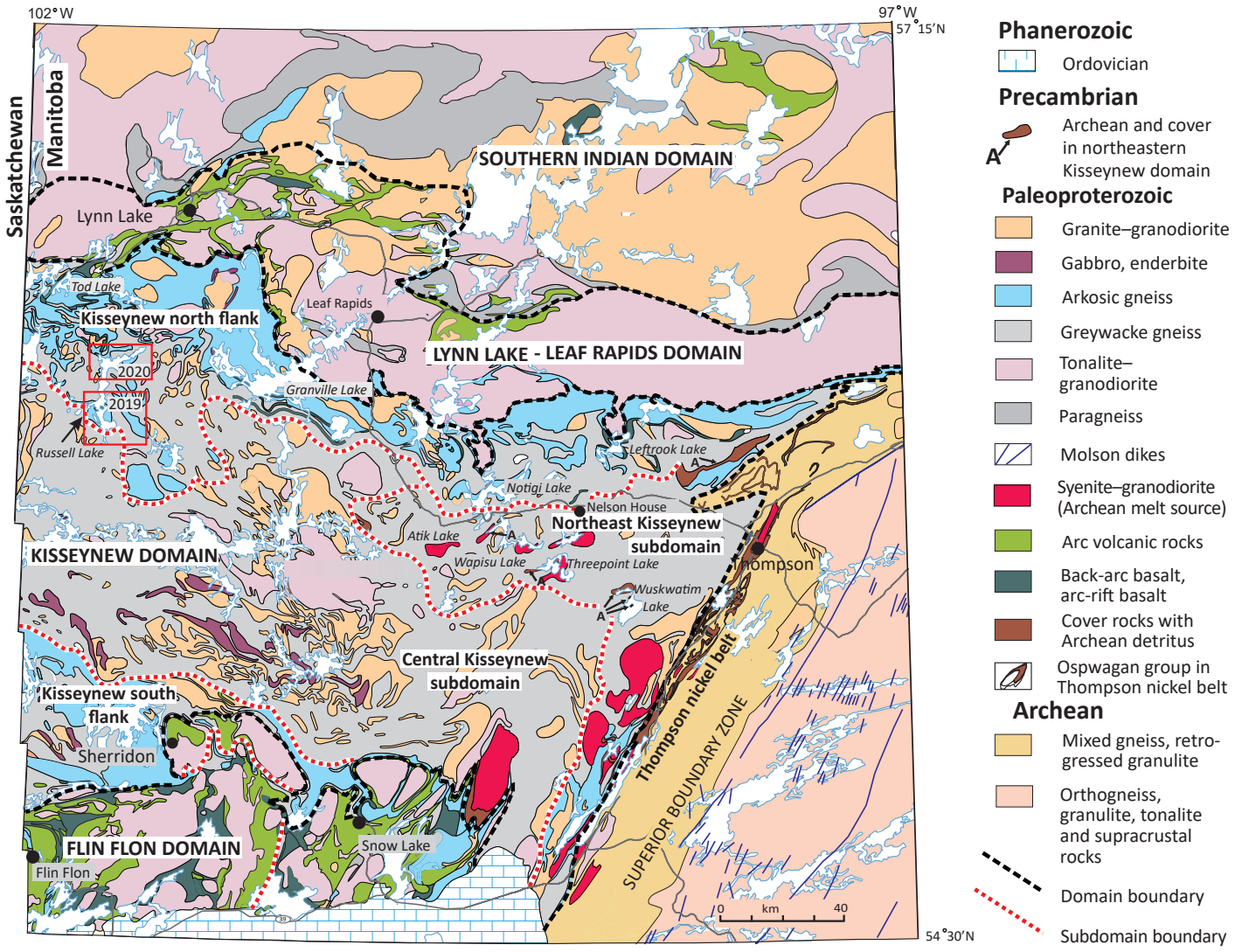

Figure GS2025-5-2: *Regional geology of the Trans-Hudson orogen in Manitoba, indicating the subdivision of the Kisseynew domain proposed by Zwanzig and Bailes (2010). Red rectangles outline the 2020 and 2019 study areas.*

the Burntwood group rocks; and εNd of –1.0 and +1.0, and T_{DM} of 2.36 and 2.33 Ga for the Sickle group rocks.

Results for initial εNd of the pillow basalt (unit 1a of Martins Couëslan, 2019b) mapped in the Russell Lake area were calculated at 1900 Ma and give an εNd(T) of +3.2. The initial εNd for the mafic sills and gabbro were calculated at 1840 Ma because these units intruded rocks of the Sickle and Burntwood groups. The mafic sills (unit 8 of Martins and Couëslan, 2020b) have a εNd(T) varying from +2.7 to +3.2 and the value for gabbro (unit 3 of Martins and Couëslan, 2019b) is +1.3.

Results of detrital-zircon U-Pb geochronology

Four samples were submitted for detrital-zircon U-Pb analyses by laser-ablation inductively coupled plasma–mass spectrometry (LA-ICP-MS) to the Micro-Analysis of Natural Trace-element and Isotope Systematics laboratory at the University of New Brunswick. A detailed method description can be found in Reid (2020).

Both cores and rims of separate zircon grains were targeted for analyses. Results were plotted on kernel density-estimate diagrams at 95%–105% concordance using IsoplotR, a free, open-source R package for geochronology (Vermeesch, 2018), and are reported with errors calculated at the 2σ level of uncertainty. Zircon morphologies from mineral separates recovered from each sample were diverse and ranged from rounded, equant grains, suggesting sedimentary transport, to long, euhedral and undamaged zircon crystals that were likely sourced from nearby rocks of igneous origin. The latter morphology seems to be dominant. Zircon grain sizes ranged from 40 to 150 µm.

A total of 73 analyses were performed on zircon-grains from mineral separates from Burntwood group greywacke sample 113-19-694B. Concentrations of U and Th were 1.65–79.3 ppm and 0.28–61.4 ppm, respectively; Th/U ratios ranged from

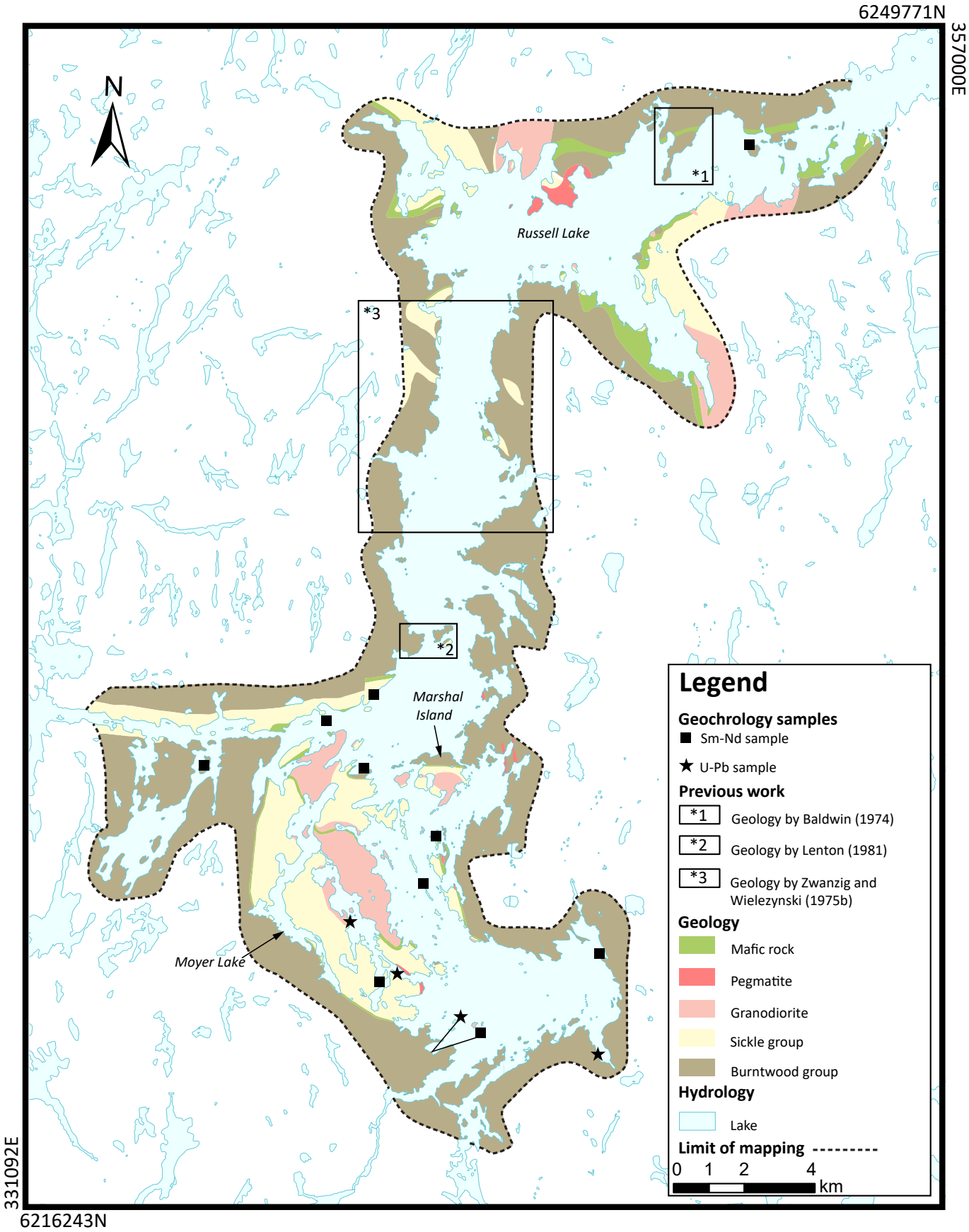

Figure GS2025-5-3: *Simplified geology of the Russell Lake area (after Martins and Couëslan, 2019a, 2020a), with location of samples collected for radiogenic isotope and geochronological studies. Co-ordinates are in UTM Zone 14, NAD83.*

Table GS20255-1: Compilation of Sm-Nd isotopic results from the Russell Lake project.

Sample number	Location	Sample locations (UTM)		Lithology	Sm ppm	Nd ppm	$^{147}Sm/^{144}Nd$	$^{143}Nd/^{144}Nd_0$	Uncertainty*	eNd_0	$^{143}Nd/^{144}Nd_T$	T_{DM} Ga	~T(Ma)	CHUR @ T(Ma)	eNd_T
		Easting	Northing												
113-19-517A	Russell Lake	339502	6230080	pillow basalt	1.594	4.89	0.1969	0.512804	0.000009	3.2	0.510342	n/a	1900	0.510179	3.2
108-19-R029	Russell Lake	340558	6228727	mafic sill intruding Burntwood group	7.544	36.608	0.1246	0.511930	0.000008	-13.8	0.510422	2.10	1840	0.510257	3.2
108-19-R123	Russell Lake	336023	6228817	mafic sill intruding Burntwood group	4.528	19.19	0.1426	0.512127	0.000008	-10.0	0.510400	n/a	1840	0.510257	2.8
108-19-R127	Russell Lake	340985	6222691	mafic sill intruding Sickle group	3.682	14.77	0.1507	0.512221	0.000009	-8.1	0.510396	n/a	1840	0.510257	2.7
108-19-R006	Russell Lake	340829	6230815	mafic sill intruding Sickle group	2.610	10.13	0.1558	0.512284	0.000010	-6.9	0.510397	n/a	1840	0.510257	2.7
113-19-683C	Russell Lake	347226	6223486	gabbro intruding Burntwood group	2.494	12.39	0.1217	0.511798	0.000008	-16.4	0.510324	2.25	1840	0.510257	1.3
108-19-R223	Russell Lake	351451	6246365	greywacke (Burntwood group; aluminous)	5.03	25.9	0.1176	0.511716	0.000007	-18.0	0.510292	2.29	1840	0.510257	0.7
113-19-651A	Russell Lake	342493	6220718	greywacke (Burntwood group; aluminous)	6.38	34.9	0.1106	0.511537	0.000010	-21.5	0.510197	2.39	1840	0.510257	-1.2
108-19-R067	Russell Lake	342592	6226816	hornblende arkose (Sickle group)	4.88	22.4	0.1317	0.511902	0.000008	-14.4	0.510307	2.33	1840	0.510257	1.0
108-19-R017	Russell Lake	342239	6225470	biotite arkose (Sickle group)	6.49	37.3	0.1050	0.511475	0.000006	-22.7	0.510204	2.36	1840	0.510257	-1.0

Depleted-mantle Nd-model (T_{DM}) not calculated for samples with $^{147}Sm/^{144}Nd > 0.14$

All samples relative to LaJolla isotope standard (0.511850) used to measure $^{143}Nd/^{144}Nd$ ratio

* Uncertainty is 2σ on $^{143}Nd/^{144}Nd$.

Depleted-mantle Nd-model ages (T_{DM}) uses the linear model of Goldstein et al. (1984)

Co-ordinates are in UTM Zone 14, NAD83

Abbreviation: CHUR, chondritic uniform reservoir

0.008 to 1.171. Zircon dates from this sample define one prominent peak at 1.85 Ga, with subordinate peaks found at 2.45–2.50 and 2.65–2.75 Ga (Table GS20255-2; Figure GS2025-5-4a). The oldest grain yielded a U-Pb age of ca. 3.33 Ga. A total of 105 analyses were performed on the zircon-grain separates from Burntwood group volcaniclastic sample 113-19-651B3. Concentrations of U and Th were 24.42–3190 ppm and 0.51–1680 ppm, respectively; calculated Th/U ratios ranged from 0.004 to 0.820. Calculated zircon ages from this sample define one prominent peak at 1.86 Ga (Table GS20255-2; Figure GS2025-5-4b).

A total of 105 analyses were carried out on the zircon separates from a sample of Sickle group polymictic conglomerate (108-19-136B). Concentrations of U and Th were 41.94–2264 ppm and 8.56–387.40 ppm, respectively; Th/U ratios ranged from 0.01 to 0.80. The calculated U-Pb ages define one prominent peak at 1.82 Ga and subordinate peaks at 2.25 and 2.35 Ga (Table GS20255-2; Figure GS2025-5-4c). A total of 113 analyses were performed on the zircon separates from the quartz-pebble conglomerate sample (108-19-090B) from the Sickle group. Concentrations of U and Th were 29.09–2290 ppm and 7.25–424 ppm, respectively; Th/U ratios ranged from 0.009 to 1.32. Zircon dates define one prominent peak at 1.86 Ga and subordinate peaks can be found at 2.35–2.68 Ga (Table GS20255-2; Figure GS2025-5-4d).

Discussion of Sm-Nd and U-Pb geochronology results

The results from Sm-Nd isotope analyses for both the Burntwood and Sickle groups fit the range compiled and presented by Murphy et al. (2021). Results from these authors for initial εNd calculated at 1840 Ma for the Burntwood samples from the Wuskwatim corridor vary between –1.34 and +2.66, with a mean Nd-model age of 2.32 Ga (varies between 2.54 to 2.13 Ga; average of 9 samples). For the Sickle group samples, εNd values vary between –1.65 and +3.62, and yield a mean Nd-model age of 2.32 Ga (varies between 2.43 to 2.03 Ga; average of 9 samples). The εNd(T) results for the pillowed basalt and the mafic sills (+2.7 to +3.2) suggest a juvenile magma source with little involvement of evolved crust in the magma petrogenesis. These types of signatures were also observed in rocks of the Lynn Lake greenstone belt (Beaumont-Smith and Böhm, 2002) and in the Granville complex volcanogenic rocks (Murphy and Zwanzig, 2021). The εNd(T) result for the gabbro (+1.3) is slightly more evolved, possibly due to interaction or recycling of some older material.

Regional geochronology studies indicate that 1814 ±1 Ma are dates of suspected metamorphic zircons in the Lynn Lake greenstone belt (Figure GS2025-5-2; Beaumont-Smith and Böhm, 2003). In the KD, east of the study area, ages ranging from 1805 ±3 to 1809 ±4 Ma (Rayner and Percival, 2007) are interpreted to be metamorphic, indicating high-grade metamorphism lasting about 10 million years. Furthermore, in the southern part of the KD, enderbite intruding the Burntwood Group was dated at ca. 1830 Ma (Gordon et al., 1990), providing a local minimum age of sedimentation. Recent work by Lawley et al. (2020) provided the first reproducible maximum depositional age for the Sickle group at 1836 ±15 Ma. For sample 108-19-136B, the polymictic conglomerate of the Sickle group, the prominent peak is at ca. 1.82 Ga (Figure GS2025-5-4c). Available imagery for zircon from this sample indicates that rims were preferentially targeted for analyses. Taking this into account and the known metamorphic ages for the region, the 1.82 Ga date is interpreted as a metamorphic age and not a minimum age of sedimentation.

The unimodal zircon age peak at ca. 1.86 Ga for the volcaniclastic unit (sample 113-19-651B3) effectively dates that section of the Burntwood group. The volcaniclastic material could be derived from younger units of the Wasekwan group of the Lynn Lake greenstone belt. The Wasekwan group comprises a mafic to felsic metavolcanic rock package and associated metasedimentary rocks dated at 1.91–1.85 Ga (e.g., Beaumont-Smith et al., 2006). The dominant peaks at 1.86–1.85 Ga for the remaining two samples could have been sourced from similar volcanic detritus, or either from the 1.86–1.85 Ga Chipewyan batholith (e.g., Meyer et al., 1992; Martins et al., 2019) or the ca. 1.86–1.85 Ga granitoid rocks (e.g., Burge Lake igneous suite; Beaumont-Smith

Table GS20255-2: Summary of geochronological results for the rock samples from the Russell Lake study area.

Sample ID	Rock type	Sample Locations (UTM)		Age range (Ga)	Dominant age peak (Ga)	Subordinate age peaks (Ga)
		Easting	Northing			
113-19-694B	Greywacke; Burntwood group	347177	6220658	3.33–1.72	1.85	2.45–2.50; 2.65–2.75; 3.33
113-19-651B3	Volcanoclastic; Burntwood group	342493	6220718	2.11–1.81	1.86	N/A
108-19-136B	Polymictic conglomerate; Sickle group	340166	6224405	2.36–1.56	1.82	2.25; 2.35
108-19-090B	Quartz-pebble conglomerate; Sickle group	341499	6222938	2.66–1.76	1.86	2.35–2.68

Co-ordinates are in UTM Zone 14, NAD83

Abbreviation: N/A, not applicable.

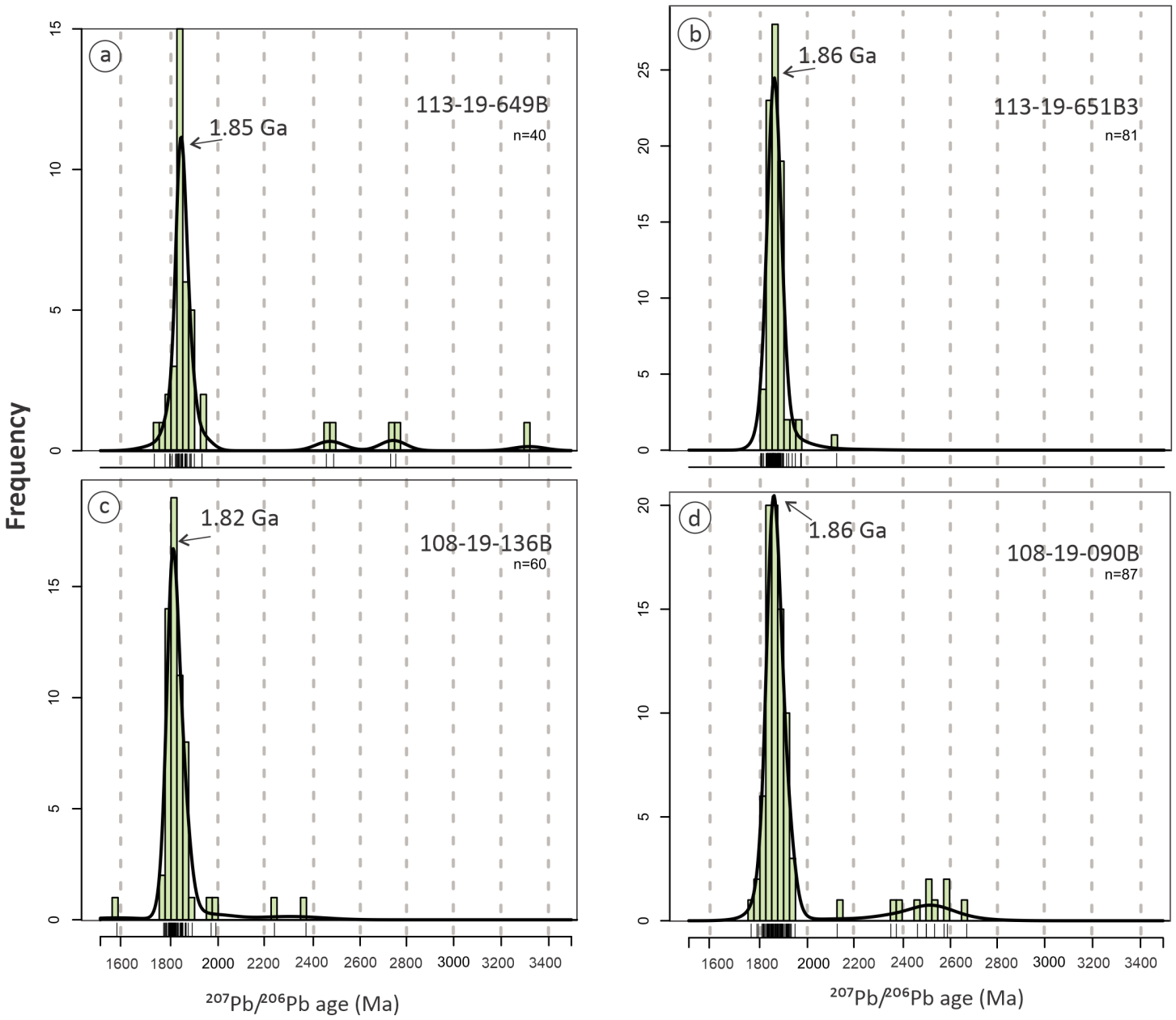

Figure GS2025-5-4: *Kernel density-estimate diagrams for results of detrital zircon U-Pb geochronology of rock samples from Russell Lake:* ***a)*** *sample 113-19-694B, Burntwood group; 347177E/6220658N;* ***b)*** *sample 113-19-651B3, Burntwood group (342493E/6220718N;* ***c)*** *sample 108-19-136B, polymictic conglomerate, Sickle group (340166E/6224405N);* ***d)*** *sample 108-19-090B, quartz-pebble conglomerate, Sickle group (341499E/6222938N). Probability curves are shown in black and histograms in light green, with a bin width of 25 million years. Co-ordinates are in UTM Zone 14, NAD83.*

et al., 2006). Multiple ca. 1.85 Ga zircons within all dated samples suggest not only a common source but also that the 1.86–1.85 Ga plutons were eroding at the time of sedimentation.

Zircon grains yielding ca. 1.89 Ga ages are also present in the samples from the study area. These grains could be derived either from the ca. 1.89–1.87 Ga Pool Lake suite (a variety of mafic, intermediate and felsic plutons) from the nearby Lynn Lake greenstone belt (Turek et al., 2000) or from the older rocks from the Wasekwan group. Another possible but distal source is the Southern Indian domain (Figure GS2025-5-2), where ca. 1.89 Ga felsic and mafic magmatism is recognized (e.g., Martins et al., 2019).

The scatter of ca. 3.33–2.25 Ga zircon ages indicates Meso- to Neoarchean and older Paleoproterozoic sources, possibly from the cratons adjoining the THO (i.e., Hearne and/or Sask). Alternatively, these results could have been sourced from inherited zircons hosted within the eroding Paleoproterozoic igneous intrusions. The Hearne craton is currently geographically located to the north and the Sask craton outcrops to the southwest in Saskatchewan, but its full extent is presently unknown. A crys-

tallization age of a granodiorite gneiss at 2.52 Ga was reported in the Southern Indian domain (Figure GS2025-5-2; e.g., Martins et al., 2019, 2022) and ages of similar range are reflected in the dominant and subdominant detrital zircon populations in most Paleoproterozoic assemblages of that area (e.g., Martins et al., 2019). Zircon ages ranging between 2.55 and 2.45 Ga overlap with known ages from the Sask craton (e.g., Rayner et al., 2005) but were also identified elsewhere in the region further west in Saskatchewan (e.g., Rottenstone domain, Bickford et al., 2001; the Peter Lake domain, Maxeiner and Rayner, 2017; and plutons from the southern Hearne craton, Card et al., 2018). No event is known to have occurred during ca. 2.20–2.00 Ga. Some of the ca. 2.20–2.00 Ga zircon ages could be mixed ages (ablation of multiple age domains). Older zircon ages of ca. 2.12, 2.39, 2.51, 2.73, 3.02 and 3.35 Ga are also reported from Sickle group rocks in the Lynn Lake greenstone belt (Lawley et al., 2020). These grains are interpreted to have come from distal sources because no Paleoproterozoic or Archean rocks from this age range are currently exposed.

The results presented here are similar to the range of detrital zircon ages obtained for the Burntwood group (1896–1847 Ma) and Sickle group (1865–1845 Ma) reported by Murphy and Zwanzig (2021). This is consistent with the interpretation that the groups represent lateral marine and terrestrial facies (Zwanzig and Bailes, 2010) with the same detrital source. The coeval timing of marine and clastic sedimentation is further supported by the youngest detrital zircon $^{207}Pb/^{206}Pb$ ages yielded by samples from the Missi (1837 ±4 Ma) and Burntwood (1842 ±2 Ma) groups, which overlap within the 2σ level of analytical uncertainty (e.g., Ansdell and Norman, 1995).

Three of the four samples yield similar U-Pb dates, which suggests that the sedimentary rocks of the Burntwood and Sickle groups were eroded from the same terrane. Sample 108-19-136B yielded predominantly younger zircon ages, which are interpreted as metamorphic and provide little inheritance-source information. The Burntwood group samples seem to yield fewer Archean grains than the Sickle group, but this could be explained by a lack of targeted zircon cores creating analytical bias, or could be a statistical artifact.

Economic considerations

The timing of deposition for the Sickle group conglomerates and arkosic rocks coincides with the formation of major gold-bearing structures in the adjacent Lynn Lake belt (Lawley et al., 2020).

As pointed out by Martins and Couëslan (2019b), the Russell–McCallum lakes area shows clear evidence and economic potential for graphite mineralization. Natural graphite has several uses including anode material for Li-ion batteries, brake linings, lubricants, powdered metals, refractory applications and steelmaking (U.S. Geological Survey, 2019). Currently, natural graphite is a well-sought commodity mainly due to anticipated demand associated with the production of Li-ion batteries. Graphite is listed in Canada as a critical mineral (Natural Resources Canada, 2024) as well as in other countries such as the United States (U.S. Department of the Interior, 2018) and in Europe (European Commission, 2020).

Assay results from the 2019 field season reveal up to 3.31 wt. % total carbon in Burntwood group rocks (Martins and Couëslan, 2020b). Graphitic horizons can also be associated with enrichments in several transition metals (Couëslan, 2020). A graphitic sulphide-facies iron formation (>5 m thick) on the western shore of McCallum Lake was found to contain 0.82 wt. % total carbon, 63.8 ppm Co, 609 ppm Cu, 377 ppm Ni, 73.8 ppm Mo and 22.2 ppm U (Martins and Couëslan, 2020b).

Acknowledgments

The publications stemming from the Russell Lake project benefited from in-depth discussions with H. Zwanzig (Manitoba Geological Survey, emeritus). His extensive knowledge of the area greatly improved the understanding of the complex geological history of this portion of the Kisseynew domain. J. Janssens helped to produce the figures. Edits by M. Rinne and J. Macdonald helped improve earlier drafts of the manuscript. Technical editing services were provided by RnD Technical. D. O'Hara was responsible for layout and looked after all final editorial duties.

References

Ansdell, K.M. 2005: Tectonic evolution of the Manitoba-Saskatchewan segment of the Paleoproterozoic Trans-Hudson Orogen, Canada; Canadian Journal of Earth Sciences, v. 42, no. 4, p. 741–759.

Ansdell, K. and, Norman, A. 1995: U-Pb geochronology and tectonic development of the southern flank of the Kisseynew Domain, Trans-Hudson Orogen, Canada; Precambrian Research, v. 72, p. 147–167.

Bailes, A.H. 1980: Origin of early Proterozoic volcaniclastic turbidites, south margin of the Kisseynew sedimentary gneiss belt, File Lake, Manitoba; *in* Early Precambrian Volcanology and Sedimentology in the Light of the Recent, E. Dimroth, J.A. Donaldson and J. Veizer (ed.), Precambrian Research, v. 12, no. 1–4, p. 197–225, URL <https://doi.org/10.1016/0301-9268(80)90029-7>.

Baldwin, D.A. 1974: Kadeniuk Lake; Manitoba Department of Mines, Resources and Environmental Management, Mineral Resources Division, Exploration and Geological Survey Branch, Preliminary Map 1974R, scale 1:31 680.

Baldwin, D.A. 1976: The evaluation of disseminated base metal environments; *in* Non-Renewable Resource Evaluation Program (NREP), First Annual Report 1975-1976, Canadian Department of Energy, Mines and Resources and Manitoba Mines, Resources and Environmental Management, Mineral Resources Division, Open File Report 77/1, p. 62-92. Digital re-release November 15, 2017.

Baldwin, D.A. 1980: Disseminated stratiform base metal mineralization along the contact zone of the Burntwood River metamorphic suite and the Sickle Group; Manitoba Energy and Mines, Mineral Resources Division, Economic Geology Report GR79–5, 20 p. plus 2 maps at 1:250 000 scale.

Beaumont-Smith, C.J. and Böhm, C.O. 2002: Structural analysis and geochronological studies in the Lynn Lake greenstone belt and its gold-bearing shear zones (NTS 64C10, 11, 12, 14, 15 and 16), Manitoba; *in* Report of Activities 2002, Manitoba Industry, Trade and Mines, Manitoba Geological Survey, p. 159–170.

Beaumont-Smith, C.J. and Böhm, C.O. 2003: Tectonic evolution and gold metallogeny of the Lynn Lake greenstone belt, Manitoba (NTS 64C10, 11, 12, 14, 15 and 16); *in* Report of Activities 2003, Manitoba Industry, Trade and Mines, Manitoba Geological Survey, p. 39–49.

Beaumont-Smith, C.J., Machado, N., Peck, D.C. 2006: New uranium-lead geochronology results from the Lynn Lake greenstone belt, Manitoba (NTS 64C11–16); Manitoba Science, Technology, Energy and Mines, Manitoba Geological Survey, Geoscientific Paper GP2006-1, 11 p.

Bickford, M.E., Hamilton, M.A., Wortman, G.L. and Hill, B.M. 2001: Archean rocks in the southern Rottenstone Domain: significance for the evolution of the Trans-Hudson Orogen; Canadian Journal of Earth Sciences, v. 38, p. 1017–1025.

Card, C.D., Bethune, K.M., Rayner, N. and Creaser, R.A. 2018: Characterising the southern part of the Hearne Province: a forgotten part of Canada's shield revisited; Precambrian Research, v. 307, p. 51–65.

Corrigan, D., Hajnal, Z., Németh, B. and Lucas, S.B., 2005: Tectonic framework of a Paleoproterozoic arc-continent to continent-continent collisional zone, Trans-Hudson Orogen, from geological and seismic reflection studies; Canadian Journal of Earth Sciences, v. 42, p. 421–434.

Corrigan, D., Pehrsson, S., Wodicka, N. and de Kemp, E. 2009: The Palaeoproterozoic Trans-Hudson Orogen: a prototype of modern accretionary processes; *in* Ancient Orogens and Modern Analogues; J.B. Murphy, J.D. Keppie and A.J. Hynes (ed.), Geological Society of London, Special Publications, v. 327, p 457–479.

Couëslan, C.G. 2020: Geology and interpretation of graphite- and vanadium-enriched drillcore from the Huzyk Creek property, sub-Phanerozoic Kisseynew domain, central Manitoba (NTS 63J6); Manitoba Agriculture and Resource Development, Manitoba Geological Survey, Geoscientific Paper GP2020-1, 29 p.

Downie, D.L. 1936: Granville Lake Sheet, west half, Manitoba; Geological Survey of Canada, Map 343A, 1:253 440 scale, URL <https://doi.org/10.4095/107123>.

European Commission 2020: Communication from the commission to the European Parliament, the Council, the European Economic and Social Committee and the Committee of the Regions on critical raw materials resilience: charting a path towards greater security and sustainability; European Commission, Brussels, Belgium, 23 p., URL <https://eur-lex.europa.eu/legal-content/EN/ TXT/PDF/?uri=CELEX:52017DC0490&qid=1568232381923&from=EN> [September, 2025].

Gilboy, C.F. 1976: Project 8: Reindeer Lake, South (SE quarter) – reconnaissance geological mapping of 64O-1, 2, 7 and 8; *in* Summary of Investigations 1976, Saskatchewan Geological Survey, Saskatchewan Department of Mineral Resources, p. 36–43.

Goldstein, S.L., O'Nions, R.K. and Hamilton, P.J. 1984: A Sm-Nd isotopic study of atmospheric dusts and particulates from major river systems; Earth and Planetary Science Letters, v. 70, p. 221–236.

Gordon, T., Hunt, P., Bailes, A. and Syme, E. 1990: U-Pb zircon ages from the Flin Flon and Kisseynew belt, Manitoba: chronology of crust formation at an Early Proterozoic accretionary margin; *in* The Early Proterozoic Trans-Hudson Orogen of North America, J.F. Lewry and M.R. Stauffer (ed.), Geological Association of Canada, Special Paper, v. 37, p. 177–199.

Hodder, T.J. 2019a: Field-based ice-flow–indicator data, Russell–McCallum lakes area, northwestern Manitoba (parts of NTS 64C3–6); Manitoba Agriculture and Resource Development, Manitoba Geological Survey, Data Repository Item DRI2019005, Microsoft® Excel® file.

Hodder, T.J. 2019b: Till sampling and ice-flow mapping in the Russell–McCallum lakes area, northwestern Manitoba (parts of NTS 64C3–6); *in* Report of Activities 2019, Manitoba Agriculture and Resource Development, Manitoba Geological Survey, p. 90–96.

Hodder, T.J. 2020: Till-matrix geochemistry data, Russell–McCallum Lakes area, northwestern Manitoba (parts of NTS 64C3–6); Manitoba Agriculture and Resource Development, Manitoba Geological Survey, Data Repository Item DRI2020004, Microsoft® Excel® file.

Hodder, T.J. 2021: Kimberlite-indicator-mineral data derived from glacial sediments (till) in the Russell–McCallum lakes area of northwestern Manitoba (parts of NTS 64C3–6); Manitoba Agriculture and Resource Development, Manitoba Geological Survey, Data Repository Item DRI2021020, Microsoft® Excel® file.

Hunter, H.E. 1953: Geology of the McKnight Lake area; Manitoba Mines and Natural Resources, Mines Branch, Publication 52-3, 7 p., plus map at 1:126 720 scale.

Lawley, C.J.M., Yang, X.M., Selby, D., Davis, W., Zhang, S., Petts, D.C. and Jackson, S.E 2020: Sedimentary basin controls on orogenic gold deposits: new constraints from U-Pb detrital zircon and Re-Os sulphide geochronology, Lynn Lake greenstone belt, Canada; Ore Geology Reviews, v. 126, art. 103790, URL <https://doi.org/10.1016/j.oregeorev.2020.103790>.

Lenton, P.G. 1981: Geology of the McKnight–McCallum Lakes area; Manitoba Energy and Mines, Geological Services, Geological Report GR79-1, 39 p. plus 2 maps at 1:50 000scale and 1 map t 1:20 000 scale.

Lewry, J. F. and Collerson, K. D. 1990: The Trans-Hudson Orogen: extent, subdivisions and problems; *in* The Early Proterozoic Trans-Hudson Orogen of North America, J.F. Lewry M.R. Stauffer (ed.), Geological Association of Canada, Special Paper, v. 37, p. 1–14.

Manitoba Agriculture and Resource Development 2020: Compilation of Sm-Nd isotope results from the Manitoba Geological Survey 2019/2020 season; Manitoba Agriculture and Resource Development, Manitoba Geological Survey, Data Repository Item DRI2020011, Microsoft® Excel® file.

Manitoba Agriculture and Resource Development 2021: Compilation of Sm-Nd isotope results from the Manitoba Geological Survey 2020/2021 season; Manitoba Agriculture and Resource Development, Manitoba Geological Survey, Data Repository Item DRI2021005, Microsoft® Excel® file.

Martins, T. and Couëslan, C.G. 2019a: Bedrock geology of Russell Lake, southern half (NTS 64C3–6); Manitoba Agriculture and Resource Development, Manitoba Geological Survey, Preliminary Map PMAP2019-3, scale 1:20 000.

Martins, T. and Couëslan, C.G. 2019b: Geological investigations in the Russell–McCallum lakes area, northwestern Manitoba (parts of NTS 64C3–6); *in* Report of Activities 2019, Manitoba Agriculture and Resource Development, Manitoba Geological Survey, p. 30–41.

Martins, T. and Couëslan, C.G. 2020a: Bedrock geology of Russell Lake, northern arm, northwestern Manitoba (parts of NTS 64C5–6); Manitoba Agriculture and Resource Development, Manitoba Geological Survey, Preliminary Map PMAP2020-1, scale 1:20 000.

Martins, T. and Couëslan, C.G. 2020b: Preliminary results from bedrock mapping in the northern arm of Russell Lake, northwestern Manitoba (parts of NTS 64C5, 6); *in* Report of Activities 2020, Manitoba Agriculture and Resource Development, Manitoba Geological Survey, p. 31–40.

Martins, T. and Couëslan, C.G. 2020c: Whole-rock geochemistry of the Russell Lake mapping project, northwestern Manitoba (parts of NTS 64C3–6); Manitoba Agriculture and Resource Development, Manitoba Geological Survey, Data Repository Item DRI2020001, Microsoft® Excel® file.

Martins, T., Kremer, P.D., Corrigan, D. and Rayner, N. 2019: Geology of the Southern Indian Lake area, north-central Manitoba (parts of NTS 64G1, 2, 7–10, 64H3–6); Manitoba Growth, Enterprise and Trade, Manitoba Geological Survey, Geoscientific Report GR2019-1, 51 p. plus 4 maps at 1:50 000 scale, URL <https://www. manitoba.ca/iem/info/libmin/GR2019-1.zip> [September 2021].

Martins, T., Rayner, N., Corrigan, D. and Kremer P. 2022: Regional geology and tectonic framework of the Southern Indian domain, Trans-Hudson orogen, Manitoba; Canadian Journal of Earth Sciences, v. 59, p. 371–88.

Maxeiner, R.O. and Rayner, N.M. 2017: Geology, U–Pb zircon geochronology, and geochemistry of PGE-bearing Neoarchean and Paleoproterozoic gabbroic rocks of the Peter Lake domain, southern Hearne craton; Canadian Journal of Earth Sciences, v. 54, p. 587–608.

McRitchie, W.D. 1975a: Russell Lake South (parts of NTS 64C-3, 4); *in* Summary of Geological Fieldwork 1975, Manitoba Mines, Resources and Environmental Management, Mineral Resources Division, Exploration and Geological Survey Branch, Geological Paper GP2/75, p. 19–21.

McRitchie, W.D. 1975b: Russell Lake South (parts of NTS 64C-4E; 64C-3); Manitoba Mines, Resources and Environmental Management, Mineral Resources Division, Exploration and Geological Survey Branch, Preliminary Map 1975R-3, scale 1:31 680.

Meyer, M.T., Bickford, M.E. and Lewry, J.F. 1992: The Wathaman Batholith. an Early Proterozoic continental arc in the Trans-Hudson orogenic belt, Canada; Geological Society of America, Bulletin, v. 104, p. 1073–1085.

Murphy, L.A. and Zwanzig, H.V. 2021: Geology of the Wuskwatim–Granville lakes corridor, Kisseynew domain, Manitoba (parts of NTS 63O, P, 64A–C); Manitoba Agriculture and Resource Development, Manitoba Geological Survey, Geoscientific Report GR2021-2, 94 p.

Murphy, L.A., Zwanzig, H.V. and Böhm, C.O. 2021: Lithogeochemical database, Sm-Nd isotopic data and U-Pb geochronological data for the Wuskwatim–Granville–Laurie lakes corridor, Manitoba (parts of NTS 63O, P, 64A–C); Manitoba Agriculture and Resource Development, Manitoba Geological Survey, Data Repository Item DRI2021014, Microsoft® Excel® file.

Natural Resources Canada, 2024: Canada's critical minerals; Natural Resources Canada, Critical Minerals Centre of Excellence, URL <https://www.canada.ca/en/campaign/critical-minerals-in-canada/critical-minerals-an-opportunity-for-canada.html> [September 2025].

Pollock, G.D. 1966: Geology of the Trophy Lake area (west half); Manitoba Mines and Natural Resources, Manitoba Mines Branch, Publication 64-1, 14 p. plus 1 map at 1:63 360 scale.

Rayner, N. and Percival, J.A. 2007: Uranium-lead geochronology of basement units in the Wuskwatim–Tullibee lakes area, northeastern Kisseynew domain, Manitoba (NTS 63O); *in* Report of Activities 2007, Manitoba Science, Technology, Energy and Mines, Manitoba Geological Survey, p. 82–90.

Rayner, N., Stern, R.A. and Bickford, M.E. 2005: Tectonic implications of new SHRIMP and TIMS U-Pb geochronology of rocks from the Sask Craton, Peter Lake Domain, and Hearne margin, Trans-Hudson Orogen, Saskatchewan; Canadian Journal of Earth Sciences, v. 42, p. 635–657.

Reid, K.D. 2020: Laser-ablation inductively coupled plasma–mass spectrometry analyses of detrital zircon grains from metasedimentary rocks in drillcores KUS378 and HAR070 in the Watts, Mitishto and Hargrave river areas, central Manitoba (parts of NTS 63J5, 6, 11–14); Manitoba Agriculture and Resource Development, Manitoba Geological Survey, Data Repository Item DRI2020026, Microsoft® Excel® file.

Stauffer, M.R. 1984: Manikewan and early Proterozoic ocean in central Canada, its igneous history and orogenic closure; Precambrian Research, v. 25, p. 257–281.

Turek, A., Woodhead, J. and Zwanzig, H. 2000: U-Pb Age of the gabbro and other plutons at Lynn Lake (part of NTS 64C); *in* Report of Activities 2000, Manitoba Industry, Trade and Mines, Manitoba Geological Survey, p. 97–104.

U.S. Department of the Interior 2018: Final List of Critical Minerals 2018; Federal Register, The Daily Journal of the United States Government, Notice, May 18, 2018, URL <https://www.federalregister.gov/documents/2018/05/18/2018-10667/final-list-of-critical-minerals-2018> [September 2025].

U.S. Geological Survey, 2019, Mineral commodity summaries 2019: U.S. Geological Survey, 200 p., URL <https://doi.org/10.3133/70202434>.

Vermeesch, P. 2018: IsoplotR: a free and open toolbox for geochronology; Geoscience Frontiers, v. 9, 479–1493, URL <https://doi.org/10.1016/j.gsf.2018.04.001>.

Zwanzig, H.V. 2008: Correlation of lithological assemblages flanking the Kisseynew Domain, Manitoba (parts of NTS 63N, 63O, 64B, 64C): proposal for tectonic/metallogenic subdomains; *in* Report of Activities 2008, Manitoba Science, Technology, Energy and Mines, Manitoba Geological Survey, p. 38–52.

Zwanzig, H.V. 2019: Geology of the southern Granville Lake area, Manitoba (parts of NTS 64C1, 2, 7); Manitoba Growth, Enterprise and Trade, Manitoba Geological Survey, Geoscientific Map MAP2019-1, scale 1:20 00.

Zwanzig, H.V. 1999: Structure and stratigraphy of the south flank of the Kisseynew Domain in the Trans-Hudson Orogen, Manitoba: implications for 1.845–1.77 Ga collision tectonics; *in* NATMAP Shield Margin Project, Volume 2, Canadian Journal of Earth Sciences, v. 36, no. 11, p. 1859–1880.

Zwanzig, H.V. and Bailes, A.H. 2010: Geology and geochemical evolution of the northern Flin Flon and southern Kisseynew domains, Kississing–File lakes area, Manitoba (parts of NTS 63K, N); Manitoba Innovation, Energy and Mines, Manitoba Geological Survey, Geoscientific Report GR2010-1, 135 p.

Zwanzig, H.V. and Wielezynski, P. 1975a: Geology of the Kamuchawie Lake area; *in* Summary of Geological Fieldwork 1975, Manitoba Mines, Resources and Environmental Management, Mineral Resources Division, Exploration and Geological Survey Branch, Geological Paper GP2/75, p. 12–15.

Zwanzig, H.V. and Wielezynski, P. 1975b: Kamuchawie Lake; Manitoba Mines, Resources and Environmental Management, Mineral Resources Division, Exploration and Geological Survey Branch, Preliminary Map 1975R-1, scale 1:31 680.

GS2025-6

Investigation of volcanic rocks along the eastern margin of the sub-Phanerozoic Thompson nickel belt, central Manitoba (part of NTS 63J3) project update: preliminary lithogeochemistry and metamorphic petrology results

by C.G. Couëslan

In Brief:

- Arc basalt has been identified in the northern extension of the sub-Phanerozoic Winnipegosis komatiite belt, accompanied by evidence for local hydrothermal alteration
- Sedimentary rocks spatially associated with the volcanic rocks appear to be sourced from the Superior craton.
- The discovery of additional arc-volcanic rocks along strike from the Tower deposit could expand the area of VMS mineralization potential

Citation:
Couëslan, C.G. 2025: Investigation of volcanic rocks along the eastern margin of the sub-Phanerozoic Thompson nickel belt, central Manitoba (part of NTS 63J3) project update: preliminary lithogeochemistry and metamorphic petrology results; *in* Report of Activities 2025, Manitoba Business, Mining, Trade and Job Creation, Manitoba Geological Survey, p. 59–72.

Summary

An ongoing project to investigate metavolcanic rocks from the sub-Phanerozoic Superior boundary zone in Manitoba continued with geochemical and petrographic analyses of drillcore. The geochemistry of metasedimentary rocks suggests that they are likely sourced from the adjacent Superior craton; however, one sample of 'iron formation' from drillhole MRO-007 appears to be derived from basalt subjected to intense sericite alteration. Mafic rocks from the area can be subdivided into arc affinity and mid-ocean–ridge basalt affinity based on whole-rock geochemistry. The arc-affinity mafic rocks are restricted to an area previously mapped as Winnipegosis komatiite belt. Ultramafic volcanic rocks from drillhole NIM-068, within the Thompson nickel belt, are geochemically similar to aluminum undepleted komatiites.

Metapelite and metabasalt from the area mapped as Thompson nickel belt are characterized by middle amphibolite-facies metamorphic assemblages with a best estimate for pressure and temperature conditions of 3.25–3.5 kbar and 550–650 °C. Mafic rocks from the area mapped as Winnipegosis komatiite belt have mineral assemblages characteristic of the lower- to middle-amphibolite facies, and yield pressure and temperature estimates as low as 2.0–6.5 kbar and 460–540 °C. It is uncertain if a continuous metamorphic field gradient occurs between the Winnipegosis rocks and the rocks of the Thompson belt, or if a sharp, fault-bounded change in metamorphic grade exists.

The Tower deposit is the only known volcanogenic massive-sulphide deposit in the sub-Phanerozoic Superior boundary zone and is associated with arc-affinity volcanic rocks. The discovery of additional arc-affinity volcanic rocks along strike with the Tower deposit could indicate a greater potential for volcanogenic massive-sulphide–style mineralization in the area. The full tectonic significance of arc-affinity volcanics in the sub-Phanerozoic Superior boundary zone remains unknown.

Introduction

During the summer of 2024, a project was initiated in collaboration with HudBay Minerals Inc. to characterize metavolcanic rocks in the sub-Phanerozoic Superior boundary zone of Manitoba. Four drillholes, ranging from 16 to 28 km along strike from the Tower volcanogenic massive-sulphide (VMS) deposit (Figure GS2025-6-1), were selected for relogging to assess their affinities to Thompson nickel belt (TNB) rocks, Winnipegosis komatiite belt (WKB) rocks and the juvenile arc rocks that host the Tower deposit. Results from geochemical and petrographic analyses of the samples collected in 2024 are presented in this report. A more detailed description of the drillcore and the project can be found in Couëslan (2024). All rocks reported in this study were subjected to amphibolite-facies metamorphism; however, the 'meta-' prefix is not used for rock names in an effort to simplify the text.

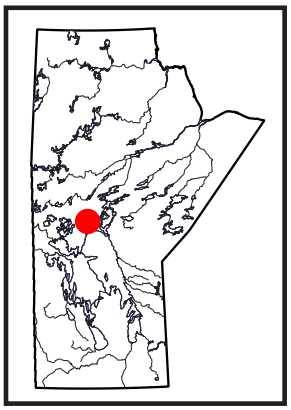

Geochemistry

Representative samples of each of the major rock types were collected for lithogeochemistry from each drillhole that was relogged in 2024. The data collected, and analytical methods used, can be found in Couëslan and Janssens (2025). The geochemistry of the sedimentary and volcanic rocks is discussed below.

Sedimentary rocks

Samples of sedimentary rocks were collected from drillholes MRO-005 and MRO-007 (Assessment File 73174, Manitoba Business, Mining, Trade and Job Creation, Winnipeg), which are interpreted from previous mapping to reside in the TNB and WKB, respectively (Figure GS2025-6-1). Multi-element profiles of pelitic rocks, normalized to the average P2 member pelite of the Ospwagan group

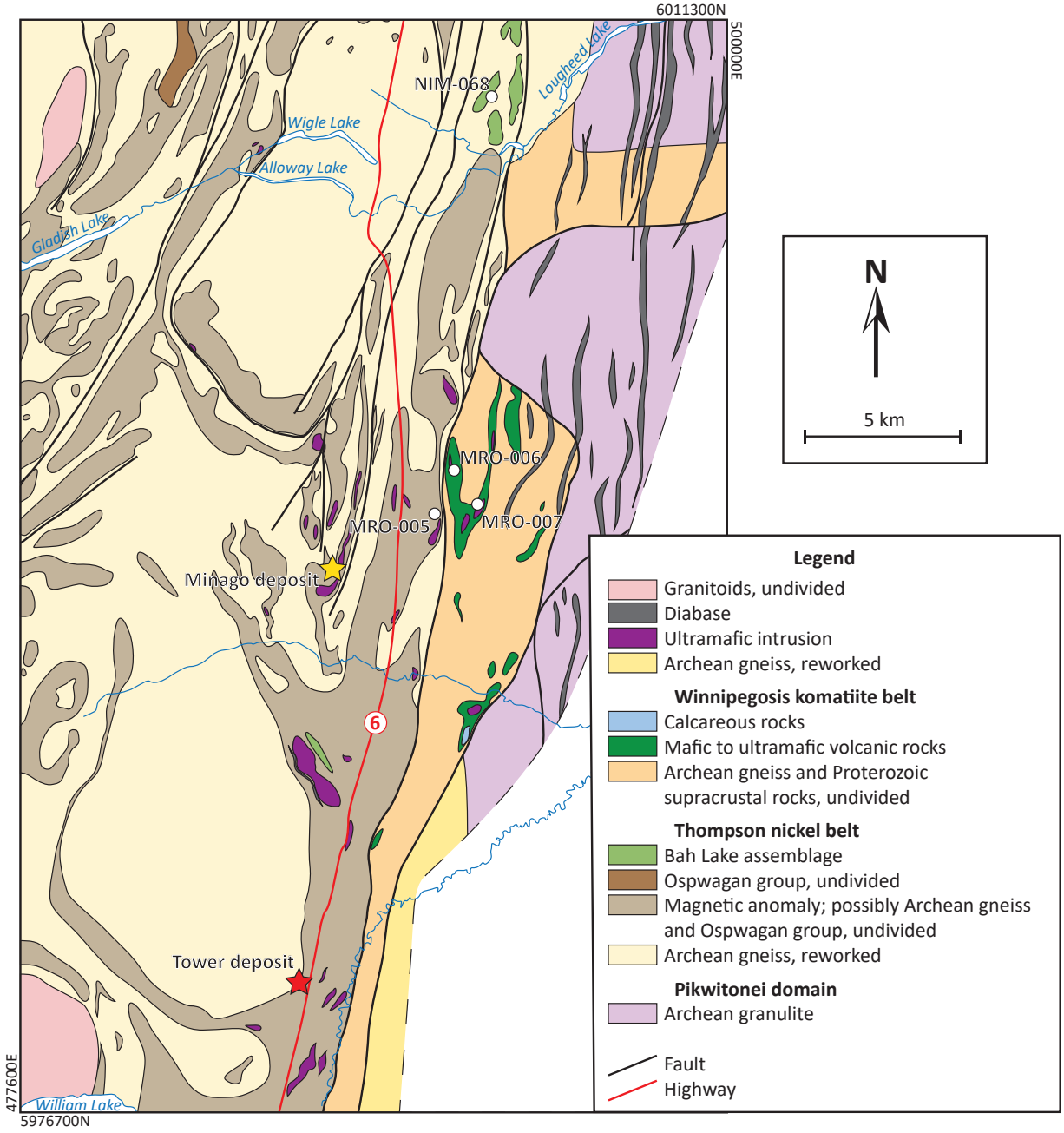

Figure GS2025-6-1: *Geology of the sub-Phanerozoic Superior boundary zone in the Minago River area (modified from Macek et al., 2006). Circles indicate the locations of drillholes from this study; the red star indicates a volcanogenic massive-sulphide deposit and the yellow star indicates a magmatic nickel deposit. All co-ordinates are in UTM Zone 14, NAD83.*

(Figure GS2025-6-2a; Zwanzig et al. 2007), are relatively flat and contrast with the weak positive slope typical of Burntwood group wacke from the Kisseynew domain (Figure GS2025-6-2b). The exception is the black shale from drillhole MRO-005, which is characterized by depletion at Al, Zr and Ti, and enrichment at V. In addition to V (526 ppm), the black shale is enriched in other redox-sensitive metals (280 ppm Ni, 170 ppm Cu, 660 ppm Zn, 46 ppm Mo).

A sample of 'impure chert' (108-24-011) from drillhole MRO-005 is enriched in iron (15.81 wt. % $Fe_2O_3^t$) and although it is characterized by quartz-rich laminations, the rock is not particularly siliceous (59.91 wt. % SiO_2). In addition to quartz, the rock is also biotite rich, which is reflected by a relatively high K_2O content (4.51 wt. %). The rock likely represents a combination of ferruginous, pelitic and siliceous sedimentary components. The normalized multi-element profile is relatively flat, with minor depletions at Th, Zr and Al (Figure GS2025-6-2c, d). The profile shares similarities with both iron formation from the P3 member and pelite from the P2 member of the Pipe formation. This is in strong contrast with the normalized profile of the magnetite-rich

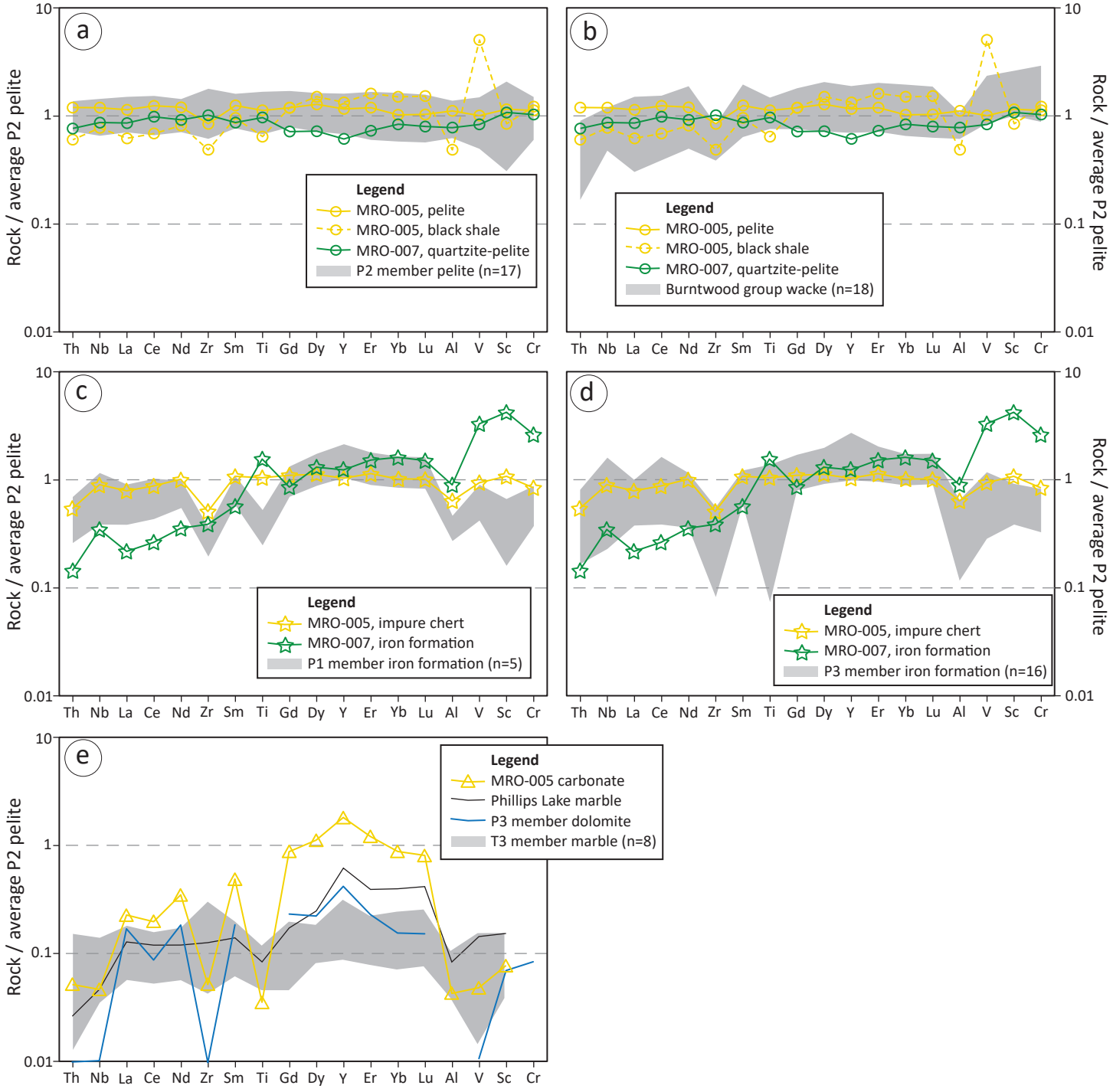

Figure GS2025-6-2: *Multi-element profiles of sedimentary rocks from the study area normalized to the average P2 pelite of Zwanzig et al. (2007) comparing:* ***a)*** *pelitic rocks with pelite from the P2 member of the Pipe formation;* ***b)*** *pelitic rocks with Burntwood group wacke;* ***c)*** *impure chert and iron formation with iron formation from the P1 member of the Pipe formation;* ***d)*** *impure chert and iron formation with iron formation from the P3 member of the Pipe formation;* ***e)*** *carbonate rock with marbles from Phillips Lake, the P3 member of the Pipe formation and the T3 member of the Thompson formation. Data sources: Burntwood group, Zwanzig et al. (2007); iron formations from the P1 and P3 members, Zwanzig et al. (2007) and Couëslan (2021); P2 member pelite, Zwanzig et al. (2007) and Couëslan (2022); P3 member dolomite, Zwanzig et al. (2007); T3 member marble, Zwanzig et al. (2007) and Couëslan (2016, 2021, 2022); Phillips Lake marble, Couëslan (2022).*

iron formation from drillhole MRO-007, which is characterized by a moderate positive slope and relative enrichments at Nb, Ti, V, Sc and Cr. The rock is characterized by abundant quartz-rich laminations and abundant magnetite (20.00 wt. %$Fe_2O_3^t$), which is typical of iron formations; however, it is also muscovite rich, with relatively abundant tourmaline (Figure GS2025-6-3a), and contains 15.87 wt. % Al_2O_3 and 5.91 wt. % K_2O, which is not typical of iron formations.

A second variety of impure chert (108-24-010) from drillhole MRO-005 consists of interlaminated chert and carbonate. This rock is characterized by a concave-down, normalized multi-element profile, with relative depletions at Nb, Zr, Ti, Al, V and Cr (Figure GS2025-6-2e). Although generally more enriched, the normalized profile does share a similar overall shape to that of other carbonate rocks from the TNB.

Mafic and ultramafic rocks

Basalt from drillholes MRO-005 and NIM-068 (Assessment Files 73174 and 73648; TNB; Figure GS2025-6-1) yields intermediate Mg# values (molar Mg/[Fe^T+Mg]; 0.44–0.54), which overlap the high-Fe tholeiite and high-Mg tholeiite fields of Jensen and Pyke (1982; Figure GS2025-6-4a). Chondrite-normalized rare-earth element (REE) profiles of the basalt are relatively flat to shallow sloping ($[La/Yb]_N$ = 0.90–1.79) and primitive mantle-normalized multi-element profiles are relatively flat to slightly concave down (Figure GS2025-6-5a–d). Drillhole NIM-068 also

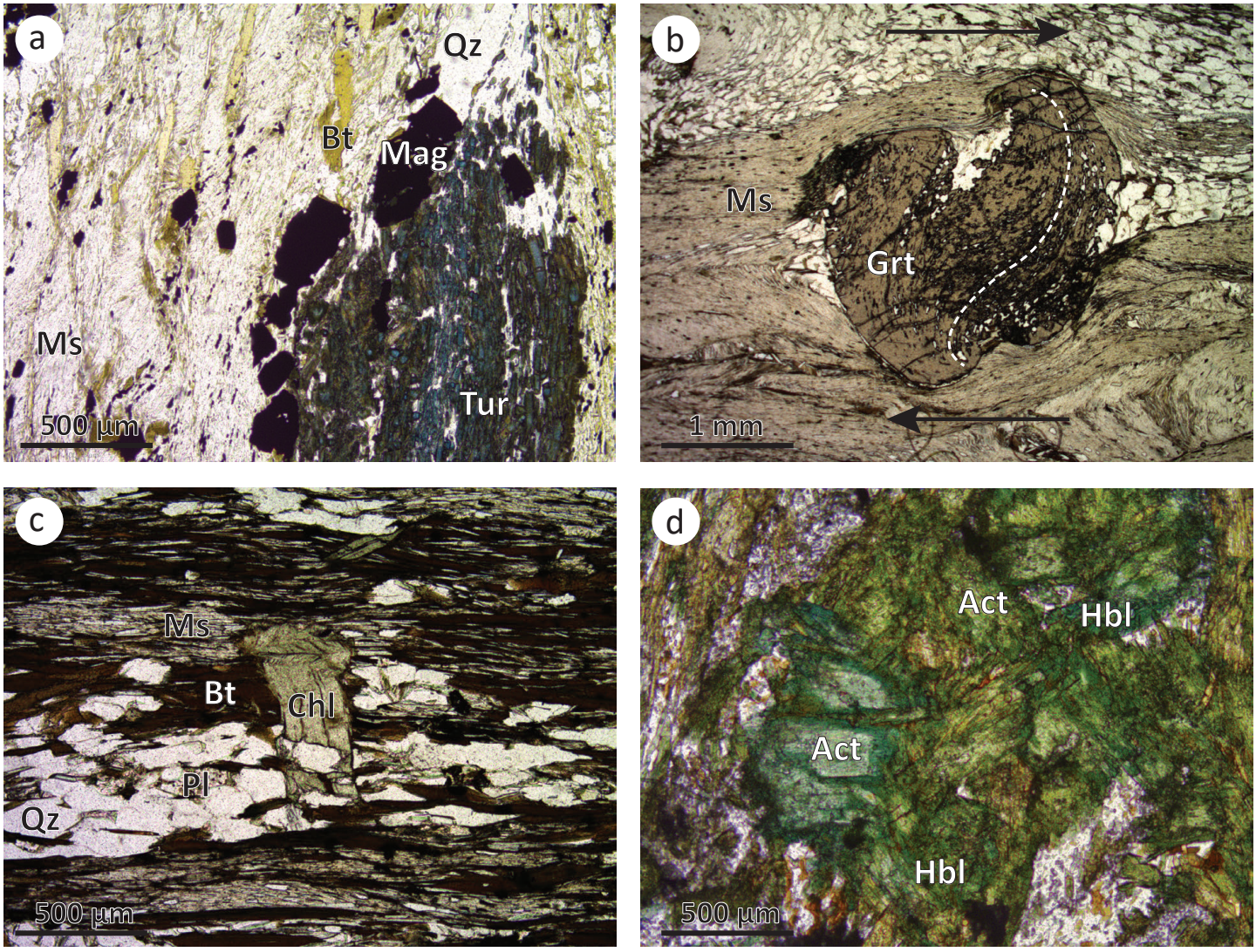

Figure GS2025-6-3: *Photomicrographs in plane-polarized light of samples from the study area:* ***a)*** *iron formation from drillhole MRO-007, with abundant muscovite, magnetite and tourmaline;* ***b)*** *rotated garnet porphyroblast in pelite from drillhole MRO-005, with inclusion-trail fabric in garnet indicated by dashed white line and direction of shear/rotation indicated by arrows;* ***c)*** *late chlorite crosscutting foliation in pelite from drillhole MRO-005, with foliation-parallel kink band present at the top of the chlorite grain;* ***d)*** *amphibole in gabbro from drillhole MRO-007, with pale actinolite cores and darker hornblende rims. Abbreviations: Act, actinolite; Bt, biotite; Chl, chlorite; Grt, garnet; Hbl, hornblende; Mag, magnetite; Ms, muscovite; Pl, plagioclase; Qz, quartz; Tur, tourmaline.*

contains ultramafic volcanic flows with Mg# values of 0.82–0.83, which plot within the komatiite field of Jensen and Pyke (1982; Figure GS2025-6-4a). The TiO_2 content of the ultramafic flows is 0.41–0.42 wt. %, and Al_2O_3/TiO_2 ratios of 15.5–19.5 and $(Gd/Yb)_N$ ratios of 0.91–1.32 are characteristic of aluminum undepleted komatiites (Nesbitt et al., 1979; Sproule et al., 2002). Normalized REE profiles of the ultramafic flows are relatively flat to concave down with negative Eu anomalies ($[La/Yb]_N$ = 1.03–1.14; Eu/Eu^* = 0.62–0.72; Figure GS2025-6-5c). Similarly, normalized multi-element profiles are relatively flat with pronounced positive anomalies at Th and negative anomalies at Nb (Figure GS2025-6-5d).

Three samples of basalt were collected from drillhole MRO-006 (Assessment Files 73174), including a sample with intense carbonate alteration, while one sample of basalt and one sample of gabbro were collected from MRO-007 (WKB; Figure GS2025-6-1). The unaltered basalt from MRO-006 plots within the high-Fe tholeiite field of Jensen and Pyke (1982; Figure GS2025-6-4a) and yields Mg# values of 0.41–0.43, whereas the gabbro and basalt from MRO-007 plot within the high-Mg tholeiite field and have Mg# values of 0.52–0.54.

Chondrite-normalized REE profiles of basalt from MRO-006 are characterized by moderate negative slopes for light REEs (LREEs) and flat to shallow negative slopes for medium and heavy REEs (MREEs and HREEs; $[La/Yb]_N$ = 2.28–2.71; Figure GS2025-6-5e). The carbonate altered basalt yields a similar normalized REE profile with a slight enrichment of LREEs ($[La/Yb]_N$ = 4.22). Primitive mantle-normalized multi-element profiles are characterized by negative slopes with negative anomalies at Nb (Figure GS2025-6-5f). The gabbro from MRO-007 yields normalized REE and multi-element profiles that are similar to the basalt from MRO-006, but with a slightly more pronounced negative slope to the MREEs ($[La/Yb]_N$ = 3.92; Figure GS2025-6-5g, h). In contrast, the basalt from MRO-007 yields a relative flat normalized REE profile ($[La/Yb]_N$ = 0.95) and slightly concave-down normalized multi-element profile (Figure GS2025-6-5g, h).

Discussion of geochemistry

The majority of sedimentary rocks yield normalized multi-element profiles similar to Ospwagan group rocks of the TNB (Figure GS2025-6-2). The similarity in profiles is indicative of a similar detrital source, which in this case is likely the Superior craton; however, it may be premature to assume a direct correlation with the Ospwagan group. As discussed in Couëslan (2024), none of the sequences described from the drillcore make for straightforward correlations with Ospwagan group stratigraphy.

Although the normalized profile of the black shale from MRO-005 bares some similarity to Burntwood group rocks of the Kisseynew domain, the Burntwood group typically occurs as a monotonous succession of turbidite deposits. Volcanogenic rocks, chert and carbonate rocks are rare. In contrast, the black shale occurs as deposits between basalt flows, along with interlaminated chert and carbonate rocks. In addition, the abundance of sulphide and graphite, and negative anomalies at Al, Ti and Zr indicate detritus-starved deposits, which were likely influenced by strongly reducing conditions, as suggested by enrichment in redox-sensitive metals. Chemistry of the black shale could also have been influenced by small amounts of basalt-derived detritus.

The normalized profile of the iron formation from MRO-007 is in strong contrast to the profiles of similar Ospwagan group rocks. The positive slope of the iron formation's profile, along with positive anomalies at Nb, Ti, V and Sc, is indicative of a mafic igneous rock (Figure GS2025-6-2c, d; cf. Couëslan, 2018). The modified Zr/TiO_2-Ni diagram of Couëslan (2018) effectively subdivides the mafic igneous rocks from the sedimentary rocks (Figure GS2025-6-4b). Although it is more enriched in Ni, the iron formation from MRO-007 has a similar Zr/TiO_2 value as the basalts, and would lie close to the projected dividing line between the igneous rock field and the sedimentary rock field. In addition, it plots well outside the field defined by Ospwagan group iron formations. The iron formation also plots tightly clustered with the mafic rocks in the basalt field of the Zr/Ti-Nb/Y diagram of Pearce (1996; Figure GS2025-6-4c), and is distinct from Ospwagan group iron formations and the impure chert from MRO-005. Finally, chondrite- and primitive mantle-normalized profiles of the iron formation from MRO-007 are similar to the profiles of the gabbro from MRO-007 and basalt from MRO-006 (Figure GS2025-6-6a, b).

The atypical mineral assemblage for the iron formation (dominantly quartz+magnetite+muscovite), combined with the geochemical evidence, suggests that it represents a mafic igneous rock that was hydrothermally altered prior to peak metamorphism. Alteration indices were calculated for the iron formation, as well as the mafic and ultramafic igneous rocks of this study, using the NORMAT approach of Piché and Jébrak (2004; Table GS2025-6-1). The technique uses a normative mineral approach to calculate the overall intensity of alteration (IFRAIS), as well as specific normative mineral alteration indices for paragonite (IPARA), sericite (ISER), chlorite (ICHLO), pyrophyllite (IPYRO) and carbonatization (IPAF). The carbonatization index is calculated by comparing the measured loss-on-ignition (LOI) values with the normative LOI values. Because the rocks contain amphibolite-facies mineral assemblages (see Metamorphic petrology section) and the normative calculations are for greenschist-facies assemblages, the IPAF values are likely an underestimate. All samples of mafic and ultramafic rocks yield IFRAIS values of 100, indicating relatively fresh and unaltered protolith. Only the carbonate-altered basalt sample from MRO-006 yielded an IPAF value of 4.50, indicating minor carbonatization. The iron formation from MRO-007 yielded an IFRAIS value of 28.6, indicating intense hydrothermal alteration of the protolith. The alteration is calculated to be dominantly sericite (ISER = 65.7), with minor paragonite (IPARA = 5.74).

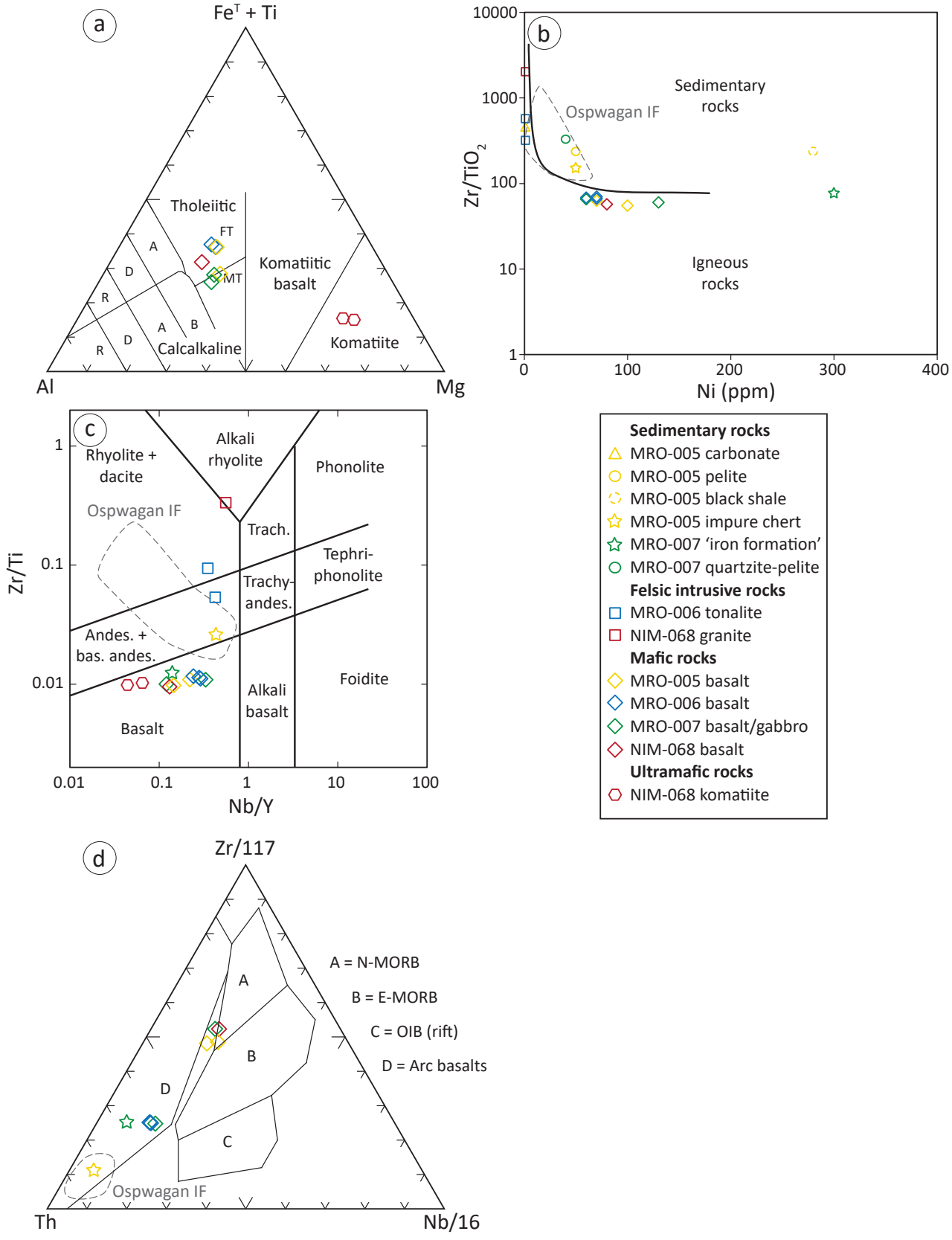

Figure GS2025-6-4: *Geochemical discrimination diagrams of samples from the study area:* ***a)*** *Al–Fe+Ti–Mg diagram (after Jensen and Pyke, 1982);* ***b)*** *Ni–Zr/TiO$_2$ diagram (after Couëslan, 2018; adapted from Winchester et al., 1980);* ***c)*** *Nb/Y–Zr/Ti diagram (after Pearce, 1996);* ***d)*** *Th–Zr–Nb diagram (after Wood et al., 1979). Abbreviations: A, andesite; Andes., andesite; B, basalt; bas., basaltic; D, dacite; E-MORB, enriched mid-ocean–ridge basalt; FT, high-Fe tholeiite; IF, iron formation; MT, high-Mg tholeiite; N-MORB, normal mid-ocean–ridge basalt; OIB, oceanic-island basalt; R, rhyolite; Trach., trachyte. Reference data for Ospwagan group iron formation from Zwanzig et al. (2007) and Couëslan (2021).*

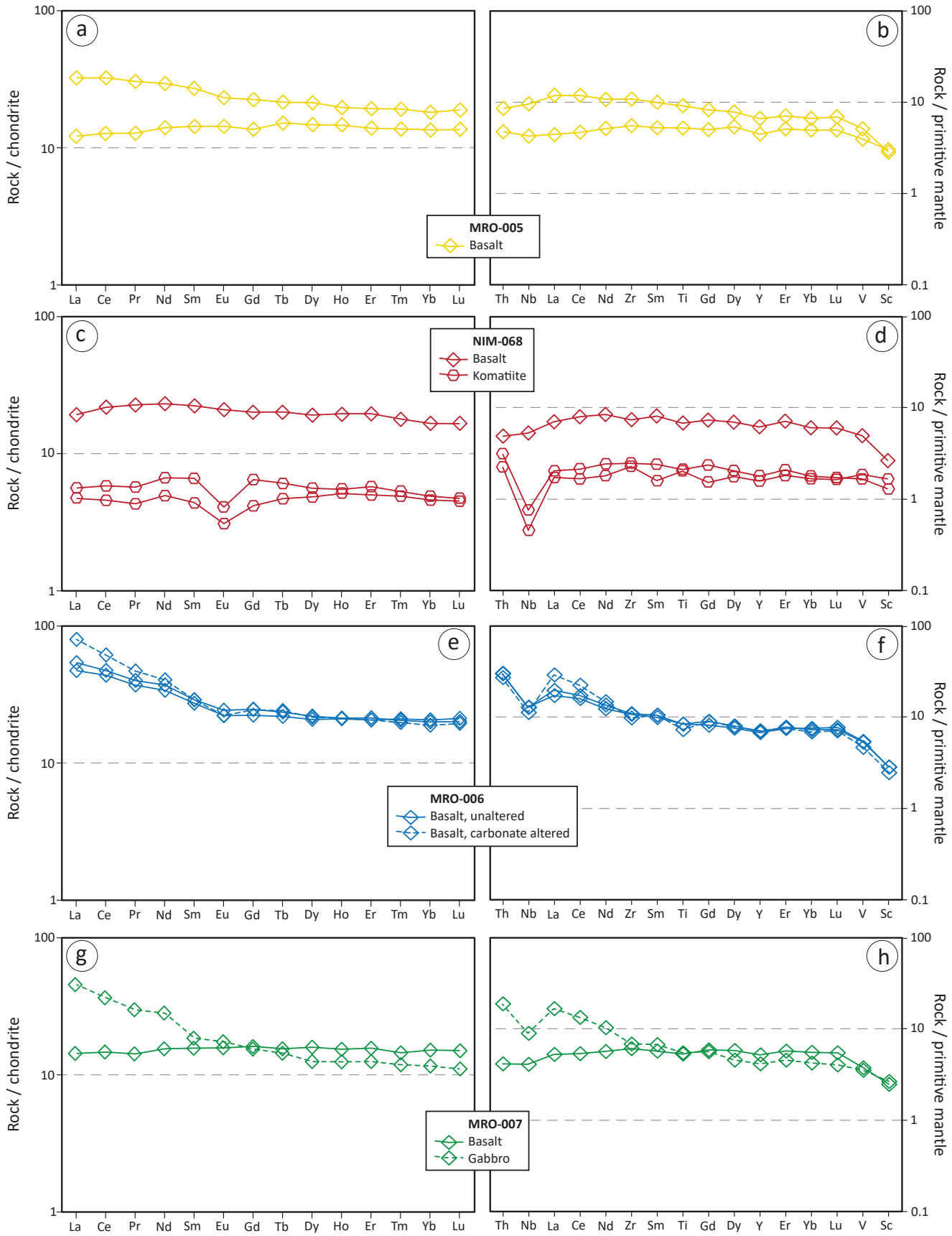

Figure GS2025-6-5: *Chondrite-normalized rare-earth element profiles (left column) and primitive mantle-normalized multi-element profiles (right column) of mafic and ultramafic rocks from the study area:* ***a), b)*** *basalt from drillhole MRO-005;* ***c), d)*** *basalt and komatiite from drillhole NIM-068;* ***e), f)*** *unaltered and altered basalt from drillhole MRO-006;* ***g), h)*** *basalt and gabbro from drillhole MRO-007. Normalizing values for chondrite and primitive mantle are from McDonough and Sun (1995).*

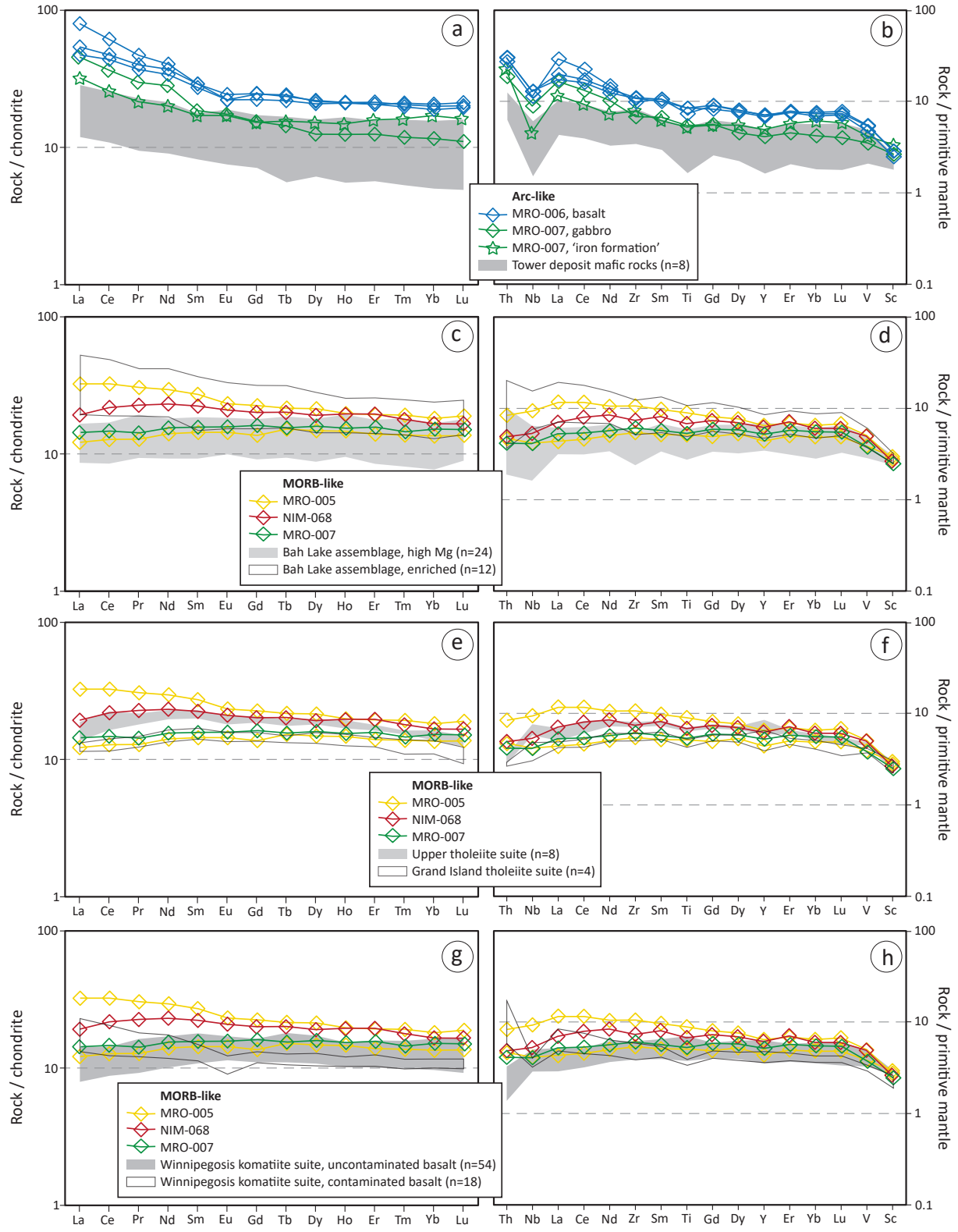

Figure GS2025-6-6: *Chondrite-normalized rare-earth element profiles (left column) and primitive mantle-normalized multi-element profiles (right column) of mafic rocks from the study area compared with other mafic rocks from the Thompson nickel belt and Winnipegosis komatiite belt:* ***a), b)*** *arc-affinity rocks from drillholes MRO-006 and MRO-007 compared with Tower deposit mafic rocks;* ***c), d)*** *MORB-affinity rocks from drillholes MRO-005, MRO-007 and NIM-068 compared with Bah Lake assemblage rocks;* ***e), f)*** *MORB-affinity rocks from drillholes MRO-005, MRO-007 and NIM-068 compared with the Upper tholeiite suite and the Grand Island tholeiite suite;* ***g), h)*** *MORB-affinity rocks from drillholes MRO-005, MRO-007 and NIM-068 compared with basalts from the Winnipegosis komatiite suite. Normalizing values for chondrite and primitive mantle are from McDonough and Sun (1995). Data sources: Bah Lake assemblage, Zwanzig (2005); Grand Island tholeiite suite, Burnham et al. (2009); Tower deposit mafic rocks, Couëslan (2018); Upper tholeiite suite, Burnham et al. (2009); Winnipegosis komatiite suite uncontaminated basalt, Ciborowski et al. (2017) and Waterton et al. (2017); Winnipegosis komatiite suite contaminated basalt, Burnham et al. (2009).*

The mafic igneous rocks in this study can be subdivided into two geochemical groups: one with relatively flat normalized REE and multi-element profiles ($[La/Yb]_N$ <1.8) suggestive of mid-ocean–ridge basalt (MORB)-affinity rocks; and the other with negative-sloping REE and multi-element profiles ($[La/Yb]_N$ >1.8), and prominent negative Nb anomalies suggestive of arc-affinity rocks. This subdivision is readily apparent on the Th-Zr-Nb diagram of Wood et al. (1979; Figure GS2025-6-4d). Several suites of MORB-affinity basalt occur in the region, including the Bah Lake volcanic assemblage of the TNB, and the Upper tholeiite suite, Grand Island suite and Winnipegosis suite of the WKB (Figure GS2025-6-6c–h). In contrast, arc-affinity basalt is only known from the sequence that hosts the Tower VMS deposit (Couëslan, 2018; Figure GS2025-6-6a, b).

Metamorphic petrology

Pelites

The two most commonly used bulk compositions for metamorphic studies are pelitic rocks and mafic rocks. Whereas mafic rocks are found in all of the examined drillcore, pelitic rocks are found only in holes MRO-005 and MRO-007 (Figure GS2025-6-1). The pelite from MRO-007 contains abundant muscovite and quartz, along with subordinate biotite, epidote, titanite and pyrite, and accessory carbonate and tourmaline. This mineral assemblage is not particularly informative for estimating metamorphic grade; however, the absence of chlorite and abundance of muscovite suggest peak metamorphic conditions of lower- to middle-amphibolite facies.

The pelite from drillhole MRO-005 contains the assemblage quartz-muscovite-biotite-garnet-staurolite-chlorite-plagioclase-ilmenite. Muscovite and biotite define a well-developed foliation, in which rare biotite 'fish' are wrapped by the fabric. Garnet and staurolite form poikiloblasts with inclusion trails indicating rotation and syntectonic growth (Figure GS2025-6-3b). Chlorite typically occurs as replacement of biotite and staurolite and locally crosscuts the foliation suggesting it is a relatively late, retrograde metamorphic mineral (Figure GS2025-6-3c). Local kink bands within the chlorite grains have boundaries parallel to the foliation, which suggests that deformation outlasted chlorite growth. The plagioclase occurs as relatively sparse grains that are intensely altered to sericite. The peak metamorphic assemblage of quartz-muscovite-biotite-garnet-staurolite-plagioclase-ilmenite is diagnostic of the middle-amphibolite facies in pelitic rocks.

Mafic rocks

Basalt samples from drillhole MRO-005 contain hornblende–plagioclase–quartz–Fe-Ti oxide–Fe sulphide±biotite ±cummingtonite. Where present, cummingtonite occurs as acicular to xenomorphic overgrowths on hornblende. Larger

Table GS2025-6-1: Normative mineral alteration indices calculated for mafic and ultramafic rocks from the study area using the NORMAT method of Piché and Jébrak (2004).

Sample	Rock type	IFRAIS[1]	IPARA[2]	ISER[3]	ICHLO[4]	IPYRO[5]	IPAF[6]
108-24-002	Metabasalt	100.00	0.00	0.00	0.00	0.00	N/A
108-24-005	Metabasalt	100.00	0.00	0.00	0.00	0.00	N/A
108-24-006	Metabasalt, carbonate-altered	100.00	0.00	0.00	0.00	0.00	4.50
108-24-008	Metabasalt	100.00	0.00	0.00	0.00	0.00	N/A
108-24-012	Metabasalt	100.00	0.00	0.00	0.00	0.00	N/A
108-24-013	Metabasalt	100.00	0.00	0.00	0.00	0.00	N/A
108-24-018	Metagabbro	100.00	0.00	0.00	0.00	0.00	N/A
108-24-019	Metabasalt	100.00	0.00	0.00	0.00	0.00	N/A
108-24-014	Komatiite	100.00	0.00	0.00	0.00	0.00	N/A
108-24-015	Komatiite	100.00	0.00	0.00	0.00	0.00	N/A
108-24-020	Iron formation	28.60	5.74	65.66	0.00	0.00	N/A

[1] Index of alkali-element depletion; lower numbers indicate an increase in the intensity of the depletion

[2] Index of paragonitization; higher numbers indicate increasing intensity

[3] Index of sericitization; higher numbers indicate increasing intensity

[4] Index of chloritization; higher numbers indicate increasing intensity

[5] Index of pyrophyllitization; higher numbers indicate increasing intensity

[6] Index of carbonatization; higher numbers indicate increasing intensity; samples with measured LOI <normative LOI = N/A

Abbreviations: LOI, loss-on-ignition; N/A, not applicable

hornblende grains contain rare cores of actinolite, which are interpreted as a relict, prograde metamorphic phase. Plagioclase occurs along with quartz as aggregates of xenomorphic grains. Local twinning indicates compositions near the oligoclase–andesine boundary as determined optically using a universal stage. The prograde assemblage of hornblende-plagioclase-quartz±cummingtonite±biotite is indicative of the amphibolite-facies for mafic rocks.

A single basalt sample was collected from drillhole NIM-068, which contains the mineral assemblage hornblende–plagioclase–quartz–titanite–Fe-Ti oxide–Fe sulphide. The plagioclase and quartz form a fine- to medium-grained, granoblastic groundmass. Optical determinations of abundant twining indicate a plagioclase composition of andesine. Titanite occurs as aggregates of xenomorphic grains along discontinuous laminations. The observed assemblage is characteristic of the amphibolite facies.

Basalt samples from drillhole MRO-006 contain hornblende–plagioclase–biotite–epidote–quartz–Fe-Ti oxide–Fe-sulphide±calcite. Larger hornblende grains contain rare cores of actinolite, which are interpreted as a relict, prograde metamorphic phase. The plagioclase is untwinned and typically intergrown with quartz in flattened aggregates/lenses. When present, the calcite is typically associated with the plagioclase-quartz lenses. The mineral assemblage hornblende-plagioclase-epidote-quartz±biotite is indicative of the lower- to middle-amphibolite facies for metabasites.

A gabbro sample from drillhole MRO-007 contains the assemblage actinolite–hornblende–plagioclase–epidote–quartz–biotite–titanite–Fe-Ti oxide. The hornblende typically occurs as overgrowths on, and along fractures within, the actinolite (Figure GS2025-6-3d). Plagioclase is untwinned and intergrown with quartz. The plagioclase-quartz segregations are commonly intergrown with epidote, biotite and acicular hornblende. The titanite typically occurs as polycrystalline aggregates enclosing Fe-Ti oxide. The mineral assemblage actinolite-hornblende-plagioclase-epidote-quartz is typical of lower-amphibolite–facies conditions near the greenschist-facies transition. A basalt sample from the same drillhole contains the assemblage hornblende–plagioclase–quartz–epidote–Fe-Ti oxide–Fe sulphide. Larger hornblende grains contain rare cores of actinolite, which is interpreted as a relict phase. Plagioclase is untwinned and is intergrown with quartz as polycrystalline aggregates. The aggregates contain sparse epidote and acicular hornblende. The metamorphic assemblage is typical of the lower- to middle-amphibolite facies for metabasites.

Phase-equilibria modelling and discussion of metamorphism

Phase-equilibria diagrams were calculated for select mafic rocks from each of the drillholes and pelite from dillhole MRO-005. The diagrams were calculated using the Theriak–Domino software package (de Capitani and Petrekakis, 2010) and the updated 2003 ds5.5 thermodynamic dataset of Holland and Powell (1998), and used activity models outlined in Tinkham and Ghent (2005), Pattison and Tinkham (2009), and Couëslan et al. (2011). The pelite was calculated in the system MnO-Na_2O-CaO-K_2O-FeO-MgO-Al2O_3-SiO2-H_2O-TiO_2 (MnNCKFMASHT), whereas the mafic rocks were calculated in the systems Na_2O-CaO-K_2O-FeO-MgO-Al_2O_3-SiO_2-H_2O-TiO_2-Fe_2O_3 (NCKFMASHTO), or NCF-MASHTO if whole-rock K_2O <0.5 wt. %. An Fe_2O_3/FeO ratio of 0.20 was used for all mafic rocks following Middlemost (1989).

The pelite sample from drillhole MRO-005 (108-24-007) contains the peak metamorphic assemblage quartz-muscovite-biotite-garnet-staurolite-plagioclase-ilmenite. The observed assemblage defines an area in modelled pressure-temperature (P-T) space of roughly 3.25–5.5 kbar and 550–650 °C (Figure GS2025-6-7a). The mineral assemblage observed in a basalt sample from the same drillhole (108-24-012) contains hornblende–plagioclase–quartz–Fe-Ti oxide. Actinolite is present as rare cores within larger hornblende grains but is interpreted as a relict, prograde phase. The observed peak metamorphic assemblage defines an area in the modelled P–T space of >3.75 kbar and >550 °C (Figure GS2025-6-7b). Although the observed assemblage from the basalt provides a poor constraint on the peak metamorphic pressure and temperature, it does overlap with the P-T conditions calculated for the peak assemblage in the pelite, which suggests agreement between the models.

A basalt sample (108-24-013) from drillhole NIM-068 contains a peak metamorphic assemblage of hornblende–plagioclase–quartz–titanite–Fe-Ti oxide. The observed assemblage defines a rather large field in modelled P-T space of roughly 2.0–6.8 kbar and 480–640 °C (Figure GS2025-6-7c).

Basalt sample 108-24-002 from drillhole MRO-006 contains a peak metamorphic assemblage of hornblende–biotite–plagioclase–quartz–epidote–Fe-Ti oxide. The observed assemblage is not predicted to occur in the modelled system without the presence of titanite. It is possible that trace amounts of titanite could be present in the rock and either were not identified or misidentified as epidote. Alternatively, titanite could be an artifact generated by the activity models used to calculate the phase equilibria. The observed assemblage plus titanite defines a relatively narrow field that covers a large part of the modeled P–T space from roughly 2–8 kbar and 480–650 °C (Figure GS2025-6-8a).

A metagabbro sample (108-24-018) from drillhole MRO-007 contains the mineral assemblage actinolite–hornblende–plagioclase–epidote–quartz–biotite–titanite–Fe-Ti oxide. No field with the observed assemblage is predicted in the modelled P–T space; however, the observed assemblage, minus Fe-Ti oxide, defines a field with relatively poor pressure constraints (roughly 2.0–6.5 kbar) but good temperature constraints (460–540 °C; Figure GS2025-6-8b). The presence of titanite as rims on Fe-Ti oxides in thin section indicates that titanite is a stable Ti-bearing phase in the assemblage. A small field with stable magnetite is present at approximately 2 kbar and 450 °C. It is possible that

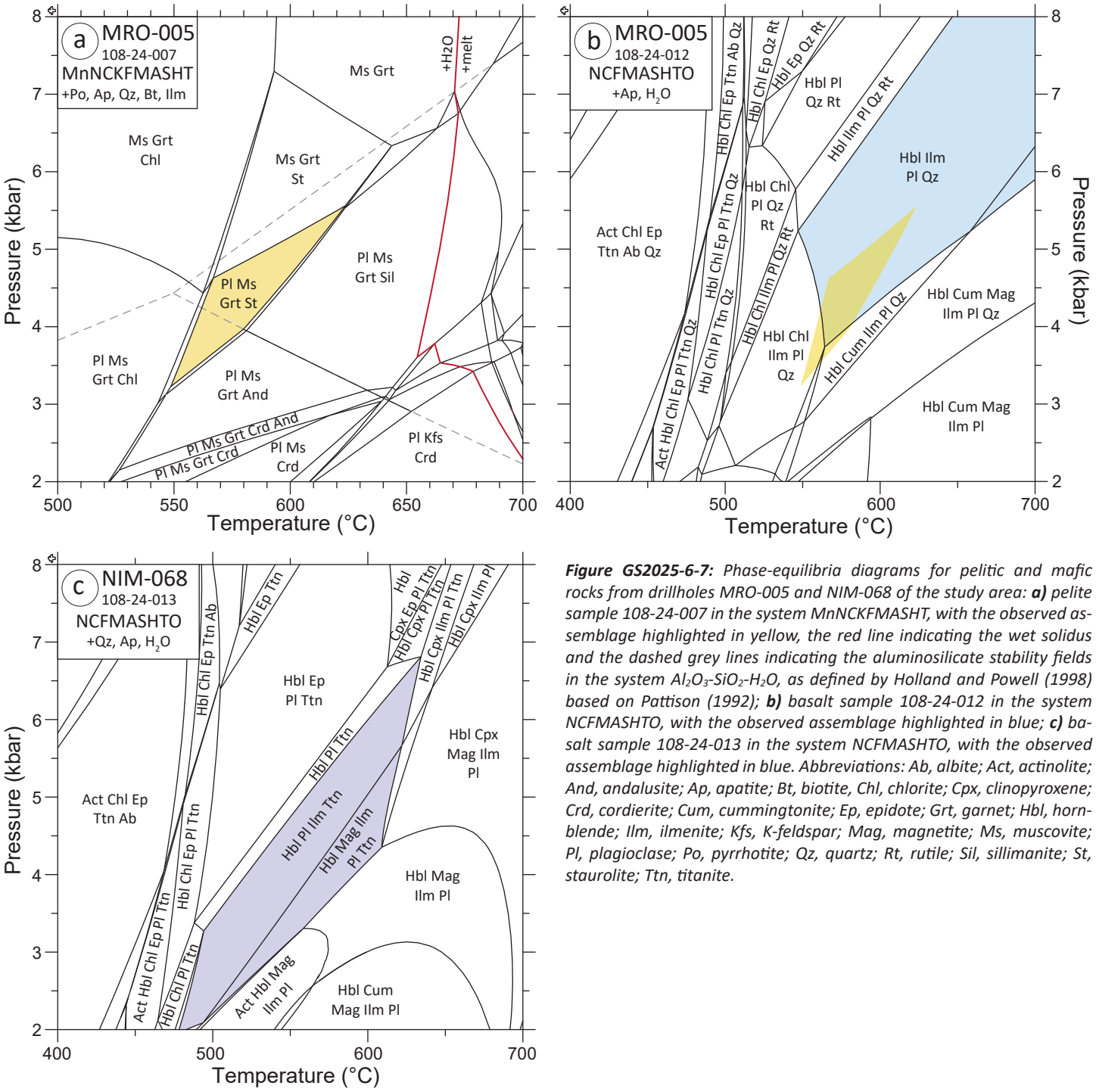

Figure GS2025-6-7: *Phase-equilibria diagrams for pelitic and mafic rocks from drillholes MRO-005 and NIM-068 of the study area:* ***a)*** *pelite sample 108-24-007 in the system MnNCKFMASHT, with the observed assemblage highlighted in yellow, the red line indicating the wet solidus and the dashed grey lines indicating the aluminosilicate stability fields in the system Al_2O_3-SiO_2-H_2O, as defined by Holland and Powell (1998) based on Pattison (1992);* ***b)*** *basalt sample 108-24-012 in the system NCFMASHTO, with the observed assemblage highlighted in blue;* ***c)*** *basalt sample 108-24-013 in the system NCFMASHTO, with the observed assemblage highlighted in blue. Abbreviations: Ab, albite; Act, actinolite; And, andalusite; Ap, apatite; Bt, biotite, Chl, chlorite; Cpx, clinopyroxene; Crd, cordierite; Cum, cummingtonite; Ep, epidote; Grt, garnet; Hbl, hornblende; Ilm, ilmenite; Kfs, K-feldspar; Mag, magnetite; Ms, muscovite; Pl, plagioclase; Po, pyrrhotite; Qz, quartz; Rt, rutile; Sil, sillimanite; St, staurolite; Ttn, titanite.*

relict magnetite from along the prograde path of metamorphism forms the oxide core to the titanite rims.

In general, rocks from the areas mapped as TNB appear to be metamorphosed to a slightly higher metamorphic grade than rocks from the WKB. The TNB rocks contain mineral assemblages typical of the middle-amphibolite facies, with the best peak P-T constraints provided by the pelite from hole MRO-005 at 3.25–5.5 kbar and 550–650 °C (Figure GS2025-6-7a). The WKB rocks contain epidote±actinolite-bearing mineral assemblages typical of the lower- to middle-amphibolite facies. Assuming that there is no metamorphic field gradient between drillholes MRO-006 and MRO-007, the metamorphic grade for these rocks could be further constrained by overlaying the observed mineral assemblages from samples 108-24-002 and 108-24-018 in P-T space (Figure GS2025-6-8c). The overlap between the fields defined by the observed assemblages indicate P-T conditions of roughly 2.5–4.5 kbar and 480–540 °C. In this scenario, a relatively sharp change in metamorphic grade could occur between the TNB rocks and the WKB rocks, possibly along a fault structure. However, it is equally possible that a continuous westward increase

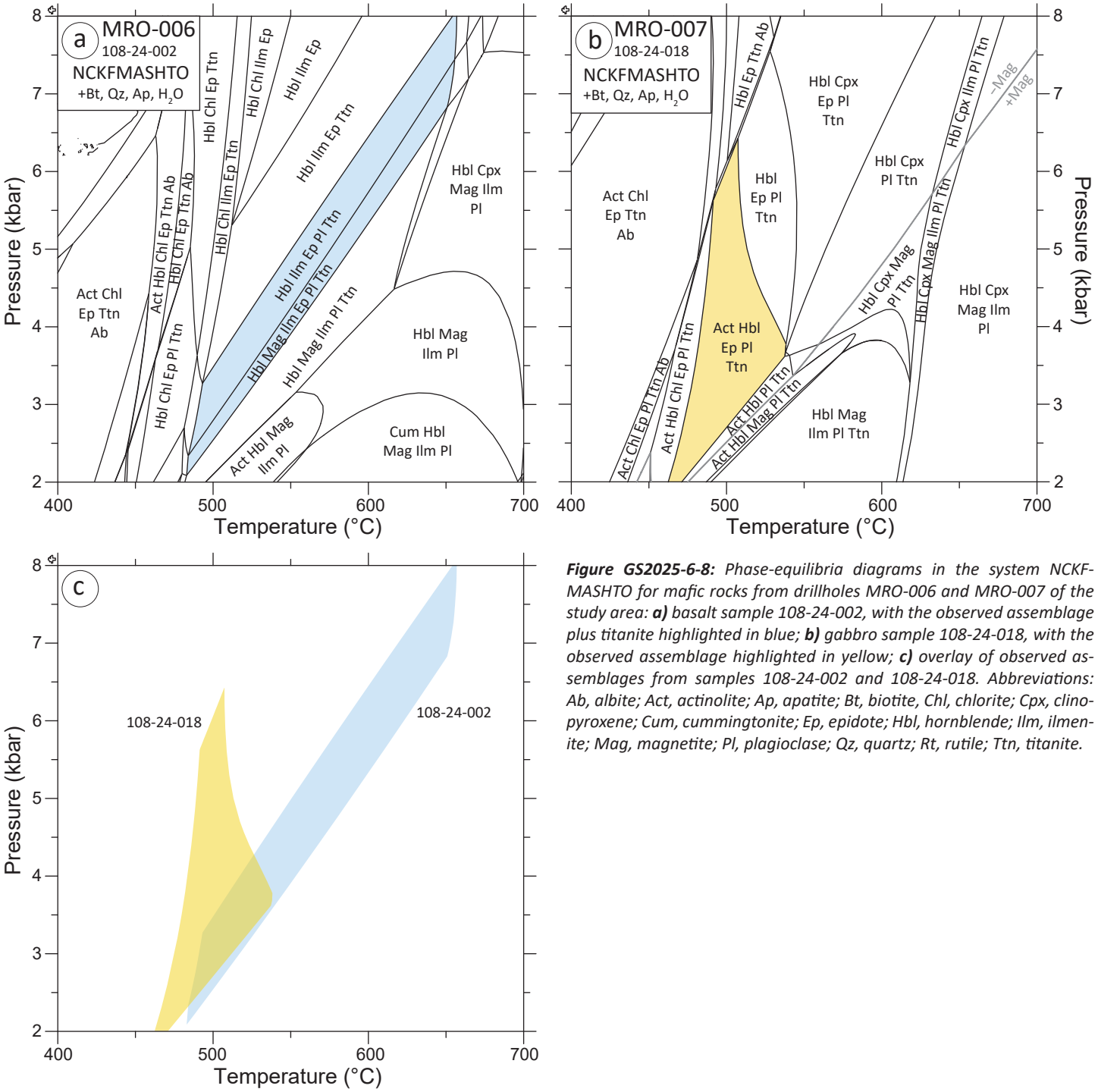

Figure GS2025-6-8: *Phase-equilibria diagrams in the system NCKFMASHTO for mafic rocks from drillholes MRO-006 and MRO-007 of the study area:* ***a)*** *basalt sample 108-24-002, with the observed assemblage plus titanite highlighted in blue;* ***b)*** *gabbro sample 108-24-018, with the observed assemblage highlighted in yellow;* ***c)*** *overlay of observed assemblages from samples 108-24-002 and 108-24-018. Abbreviations: Ab, albite; Act, actinolite; Ap, apatite; Bt, biotite, Chl, chlorite; Cpx, clinopyroxene; Cum, cummingtonite; Ep, epidote; Hbl, hornblende; Ilm, ilmenite; Mag, magnetite; Pl, plagioclase; Qz, quartz; Rt, rutile; Ttn, titanite.*

in metamorphic grade occurs from drillhole MRO-007 in the WKB (with the lowest P-T estimates and actinolite-hornblende-epidote–bearing assemblages), toward drillhole MRO-005 in the TNB (with notably higher P-T estimates, and actinolite- and epidote-free assemblages; Figure GS2025-6-1). This scenario would be similar to the exposed portions of the TNB, where metamorphic field gradients are steepest perpendicular to the strike of the belt (Couëslan and Pattison, 2012). Further refinement of the models may provide insight into this problem.

Economic considerations

Volcanogenic massive-sulphide deposits are an important mineral deposit type in the juvenile terranes of the Trans-Hudson orogen of Manitoba, where they are associated with arc-affinity volcanic rocks (Bailes and Galley, 1999; Syme et al., 1999; Tucker et al., 2005; Simard et al., 2010). The only known VMS deposit in the Superior boundary zone of Manitoba is the Tower deposit (Couëslan, 2018), which is also associated with juvenile arc-affinity volcanic rocks. Economic VMS deposits rarely occur

in isolation as demonstrated by the Flin Flon and Snow Lake mining camps. The identification of additional arc-affinity rocks approximately 15 km along strike of the Tower deposit suggests a larger area with potential to host VMS deposits than previously recognized. Intense sericitic alteration of basalt in drillhole MRO-007 suggests the potential development of at least localized, synvolcanic hydrothermal systems. Immediately above this zone of hydrothermal alteration is a siliceous rock with pyrite laminations that was previously interpreted as a quartzite (Couëslan, 2024). This unit should be revisited to see if it could be derived from felsic volcanic rocks.

The presence of arc-affinity volcanic rocks in what was previously mapped as the WKB raises many questions regarding current understanding of the Precambrian geology in this part of the province and the potential for VMS exploration. The arc rocks of the Tower deposit were interpreted as a klippe or erosional remnant of juvenile arc rocks that were thrust onto the Superior margin during the Trans-Hudson orogeny (Couëslan, 2018). Could the arc rocks in drillholes MRO-006 and MRO-007 be part of the same, or a similar, structure? Is the klippe model still valid, or could a belt of juvenile arc rocks have formed along the Superior margin? The WKB is interpreted to have formed in an evolving rift environment (Ciborowski et al., 2017; Waterton et al., 2017). Could rifting have progressed until the development of a juvenile arc was possible during closure of the rift basin? In this scenario, why would the arc rocks be preserved at the northern terminus of the belt rather than farther south, where the WKB (and presumably the rift basin) was substantially thicker? It is hoped that samples submitted for isotope geochemistry might help answer some of these questions; however, they may remain largely unanswered without additional information from drillcore.

Acknowledgments

The author thanks N. Richardson and C. Venturi from HudBay Minerals Inc. for their continued support of this project. Thanks to T. Martins, J. Macdonald and K. Reid for reviewing earlier drafts of the report.

References

Bailes, A.H. and Galley, A.G. 1999: Evolution of the Paleoproterozoic Snow Lake arc assemblage and geodynamic setting for associated volcanic-hosted massive sulphide deposits, Flin Flon Belt, Manitoba, Canada; Canadian Journal of Earth Sciences, v. 36, p. 1789–1805.

Burnham, O.M., Halden, N., Layton-Matthews, D., Lesher, C.M., Liwanag, J., Heaman, L., Hulbert, L., Machado, N., Michalak, D., Pacey, M., Peck, D.C., Potrel, A., Theyer, P., Toope, K. and Zwanzig, H. 2009: CAMIRO project 97E-02, Thompson Nickel Belt: final report, March 2002, revised and updated 2003; Manitoba Science, Technology, Energy and Mines, Manitoba Geological Survey, Open File OF2008-11, 434 p., plus appendices and GIS shape files for use with ArcInfo®.

Ciborowski, T.J.R., Minifie, M.J., Kerr, A.C., Ernst, R.E., Baragar, B. and Millar, I.L. 2017: A mantle plume origin for the Paleoproterozoic circum-Superior large igneous province; Precambrian Research, v. 294, p. 189–213.

Couëslan, C.G. 2016: Whole-rock lithogeochemistry, Sm-Nd isotope geochemistry, and U-Pb zircon geochronology for samples from the Paint and Phillips lakes area, Manitoba (parts of NTS 63O1, 8, 9, 63P5, 12); Manitoba Growth Enterprise and Trade, Manitoba Geological Survey, Data Repository Item DRI2016001, Microsoft® Excel® file.

Couëslan C.G. 2018: Geology of the Tower Cu-Zn-Ag-Au deposit, sub-Phanerozoic Superior boundary zone, central Manitoba (part of NTS 63G14); Manitoba Growth, Enterprise and Trade, Manitoba Geological Survey, Open File OF2018-4, 38 p.

Couëslan, C.G. 2021: Lithogeochemistry of iron formation, calcsilicate, marble, and mafic dikes from the Thompson nickel belt, central Manitoba (NTS 63O8, 9, 63P5, 12, 15); Manitoba Agriculture and Resource Development, Manitoba Geological Survey, Data Repository Item DRI2021016, Microsoft® Excel® file.

Couëslan, C.G. 2022: Characterization of ultramafic-hosting metasedimentary rocks and implications for nickel exploration at Phillips Lake, Thompson nickel belt, central Manitoba (part of NTS 63O1); Manitoba Natural Resources and Northern Development, Manitoba Geological Survey, Geoscientific Paper GP2022-1, 33 p., 4 appendices.

Couëslan, C.G. 2024: Investigation of volcanic rocks along the eastern margin of the sub-Phanerozoic Thompson nickel belt, central Manitoba (part of NTS 63J3); *in* Report of Activities 2024, Manitoba Economic Development, Investment, Trade and Natural Resources, Manitoba Geological Survey, p. 104–115.

Couëslan, C.G. and Pattison, D.R.M. 2012: Low-pressure regional amphibolite-facies to granulite-facies metamorphism of the Paleoproterozoic Thompson Nickel Belt, Manitoba; Canadian Journal of Earth Sciences, v. 49, p. 1117–1153.

Couëslan, C.G. and Janssens, J. 2025: Whole-rock lithogeochemistry and assays for samples along the eastern margin of the sub-Phanerozoic Thompson nickel belt, central Manitoba (part of NTS 63J3); Manitoba Business, Mining, Trade and Job Creation, Manitoba Geological Survey, Data Repository Item DRI2025012, Microsoft® Excel® file.

Couëslan, C.G., Pattison, D.R.M. and Tinkham, D.K. 2011: Regional low-pressure amphibolite-facies metamorphism at the Pipe II mine, Thompson nickel belt, Manitoba, and comparison of metamorphic isograds in metapelites and meta-iron formations; The Canadian Mineralogist, v. 49, p. 721–747.

de Capitani, C. and Petrakakis, K. 2010: The computation of equilibrium assemblage diagrams with Theriak/Domino software; American Mineralogist, v. 95, no. 7, p. 1006–1016.

Holland, T.J.B. and Powell, R. 1998: An internally-consistent thermodynamic dataset for phases of petrological interest; Journal of Metamorphic Geology, v. 16, no. 3, p. 309–344.

Jensen, L.S. and Pyke, D.R. 1982: Komatiites in the Ontario portion of the Abitibi belt; *in* Komatiites, N.T. Arndt and E.G. Nisbet (ed.), George Allen and Unwin, London, United Kingdom, p. 147–157.

Macek, J.J., Zwanzig, H.V. and Pacey, J.M. 2006: Thompson Nickel Belt geological compilation map, Manitoba (parts of NTS 63G, J, O, P and 64A and B); Manitoba Science, Technology, Energy and Mines, Manitoba Geological Survey, Open File Report, OF2006-33, digital map on CD, URL <https://www.manitoba.ca/iem/info/libmin/OF2006-33.zip> [August 2023].

McDonough, W.F. and Sun, S.-s. 1995: The composition of the Earth; Chemical Geology, v. 120, p. 223–253, URL <https://doi.org/10.1016/0009-2541(94)00140-4>.

Middlemost, E.A.K. 1989: Iron oxidation ratios, norms and the classification of volcanic rocks; Chemical Geology, v. 77, p. 19–26.

Nesbitt, R.W., Sun, S.-s. and Purvis, A.C. 1979: Komatiites: geochemistry and genesis; The Canadian Mineralogist; v. 17, p. 165–186.

Pattison, D.R.M. 1992: Stability of andalusite and sillimanite and the Al_2SiO_5 triple point: constraints from the Ballachulish aureole, Scotland; Journal of Geology, v. 100, p. 423–446.

Pattison, D.R.M. and Tinkham, D.K. 2009: Interplay between equilibrium and kinetics in prograde metamorphism of pelites: an example from the Nelson aureole, British Columbia; Journal of Metamorphic Geology, v. 27, p. 249–279.

Pearce, J.A. 1996: A user's guide to basalt discrimination diagrams; *in* Trace Element Geochemistry of Volcanic Rocks: Applications for Massive Sulphide Exploration, D.A. Wyman (ed.), Geological Association of Canada, Short Course Notes, v. 12, p. 79–113.

Piché, M. and Jébrak, M. 2004: Normative minerals and alteration indices developed for mineral exploration; Journal of Geochemical Exploration, v. 82, p. 59–77.

Simard, R.-L., McGregor, C.R., Rayner, N. and Creaser, R.A. 2010: New geological mapping, geochemical, Sm-Nd isotopic and U-Pb age data for the eastern sub-Phanerozoic Flin Flon Belt, west-central Manitoba (parts of NTS 63J3–6, 11, 12, 14, 63K1–2, 7–10); *in* Report of Activities 2010, Manitoba Innovation, Energy and Mines, Manitoba Geological Survey, p. 69–87, URL <https://www.manitoba.ca/iem/geo/field/roa10pdfs/GS-6.pdf> [July 2025].

Sproule, R.A., Lesher, C.M., Ayer, J.A., Thurston, P.C. and Herzberg, C.T. 2002: Spatial and temporal variations in the geochemistry of komatiites and komatiitic basalts in the Abitibi greenstone belt; Precambrian Research, v. 115, p. 153–186.

Syme, E.C., Lucas, S.B., Bailes, A.H. and Stern, R.A. 1999: Contrasting arc and MORB-like assemblages in the Paleoproterozoic Flin Flon belt, Manitoba, and the role of intra-arc extension in localizing volcanic-hosted massive sulphide deposits; Canadian Journal of Earth Sciences, v. 36, no. 11, p. 1767–1788, URL <https://doi.org/10.1139/e98-084>.

Tinkham, D.K. and Ghent, E.D. 2005: Estimating P-T conditions of garnet growth with isochemical phase diagram sections and the problem of effective bulk-composition; The Canadian Mineralogist, v. 43, p. 35–50.

Tucker, C., Barrie, C.T., Taylor, C. and Ames, D.E. 2005: Geology and metal contents of the Ruttan volcanogenic massive sulfide deposit, northern Manitoba, Canada; Mineralium Deposita, v. 39, p. 795–812.

Waterton, P., Pearson, D.G., Kjarsgaard, B., Hulbert, L., Locock, A., Parman, S. and Davis, B. 2017: Age, origin, and thermal evolution of the ultra-fresh ~1.9 Ga Winnipegosis Komatiites, Manitoba, Canada; Lithos, v. 268–271, p. 114–130.

Winchester, J.A., Park, R.G. and Holland, J.G. 1980: The geochemistry of Lewisian semipelitic schists from the Gairloch district, Wester Ross; Scottish Journal of Geology, v. 16, p. 165–179.

Wood, D.A., Joron, J.-L. and Treul, M. 1979: A re-appraisal of the use of trace elements to classify and discriminate between magma series erupted in different tectonic settings; Earth and Planetary Science Letters, v. 45, p. 326–336.

Zwanzig, H.V. 2005: Geochemistry, Sm-Nd isotope data and age constraints of the Bah Lake assemblage, Thompson Nickel Belt and Kisseynew Domain margin: relation to Thompson-type ultramafic bodies and a tectonic model (NTS 63J, O and P); *in* Report of Activities 2005, Manitoba Industry, Economic Development and Mines, Manitoba Geological Survey, p. 40–53.

Zwanzig, H.V., Macek, J.J. and McGregor, C.R. 2007: Lithostratigraphy and geochemistry of the high-grade metasedimentary rocks in the Thompson Nickel Belt and adjacent Kisseynew Domain, Manitoba: implications for nickel exploration; Economic Geology, v. 102, p. 1197–1216.

GS2025-7

Preliminary observations and whole-rock geochemistry of archived drillcore east of Stephens Lake, northeastern Manitoba (parts of NTS 54C, D)

by J. Macdonald

In Brief:

- Archival drillcore east of Stephens Lake was relogged to characterize the stratigraphy of the area
- Preliminary observations and geochemical data indicate these rocks are correlative with the north flank of the Kisseynew domain
- Widespread occurrences of ultramafic rocks may have implications for Ni mineralization

Citation:
Macdonald, J. 2025: Preliminary observations and whole-rock geochemistry of archived drillcore east of Stephens Lake, northeastern Manitoba (parts of NTS 54C, D); *in* Report of Activities 2025, Manitoba Business, Mining, Trade and Job Creation, Manitoba Geological Survey, p. 73–86.

Summary

In June 2025, a field project was initiated to review available geological information on poorly exposed Precambrian rocks east of Stephens Lake in northeastern Manitoba. These rocks are situated north of the Fox River belt and are correlated with the rocks of the Trans-Hudson orogen but have never been the focus of a detailed study to determine their affinity. Industry exploration efforts have targeted these rocks to pursue possible extensions of the Thompson nickel belt and to investigate source rocks for diamondiferous kimberlite indicators in glacial till, which makes assessing their affinity essential to understanding their mineral potential. Thirteen archival drillholes within this area were selected for relogging in the current work. Preliminary findings identify two broad geographic distributions of lithologies: southern holes contain variably migmatized graphitic greywacke and talc-rich ultramafic rocks that locally display a spinifex-like texture, whereas northern holes intersected variably hematized, mafic to ultramafic intrusive rocks, as well as a sequence of felsic to intermediate volcanic rocks and banded iron formation. Geochemical similarities between the metasedimentary rocks in the southern drillholes and those of the northern flank of the Kisseynew domain support a correlation between the two metasedimentary packages; moreover, volcanic arc and mafic to ultramafic intrusive rocks to the north may correlate with the Lynn Lake domain. Fifty samples were collected and will be variably submitted for petrographic thin-section preparation, whole-rock geochemistry, uranium-lead geochronology and samarium-neodymium isotopic analysis to aid in lithotectonic correlations.

Introduction

Little is known of the Precambrian geology north of the Superior province in the Hudson Bay Lowland of northeastern Manitoba. Rock exposures are sparse and Phanerozoic sedimentary rocks overlie much of the Precambrian bedrock. The rocks are interpreted to be correlative with rocks of the northern flank of the Kisseynew domain (KD; Haugh and Elphick, 1968; Corkery, 1985) but are isolated from the KD by an area of poor bedrock exposures and mixed Archean and Paleoproterozoic isotopic signatures that may mark a collisional zone between the Archean Superior craton and the Paleoproterozoic Churchill province (Figure GS2025-7-1; Hartlaub et al., 2005; Böhm et al., 2019). Bedrock mapping, whole-rock geochemistry and samarium-neodymium (Sm-Nd) isotopic data indicate that the rocks of the principal KD extend as far northeast as Rock Lake (Zwanzig and Böhm, 2004). To the northwest, the Owl River shear zone separates the mixed collisional zone from metasedimentary rocks of Archean provenance on Campbell Lake (Hartlaub et al., 2005). The Sm-Nd isotopic characteristics of metasedimentary rocks at Stephens Lake and north of the Fox River belt, referred to in this report as the Stephens Lake assemblage (SLA; Figure GS2025-7-1), indicate a Paleoproterozoic provenance (Rinne, 2018; Böhm et al., 2019).

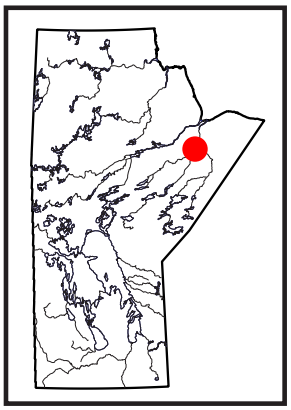

Bedrock mapping north of the Superior province was conducted primarily at Stephens Lake and the Nelson River prior to hydroelectric dam development in 1971 (Figure GS2025-7-1; Haugh and Elphick, 1968; Frohlinger, 1974; Corkery, 1985), and bedrock exposures are now minimal. Exploratory drillholes east of Stephens Lake targeted electromagnetic anomalies within these rocks (Figure GS2025-7-1; Assessment Files 74249, 74410, 74005, 74154, 74259, 91728 and 94676; Manitoba Economic Development, Investment, Trade and Natural Resources, Winnipeg) and intersected a diverse suite of rock types that are not commonly observed in the KD or at Stephens Lake. As the lack of bedrock exposures precludes a field mapping program, the current project involves two components:

- targeted sampling of the rare shoreline outcroppings of bedrock at Stephens Lake for whole-rock Sm-Nd and detrital uranium-lead (U-Pb) zircon analysis to assess provenance and depositional age

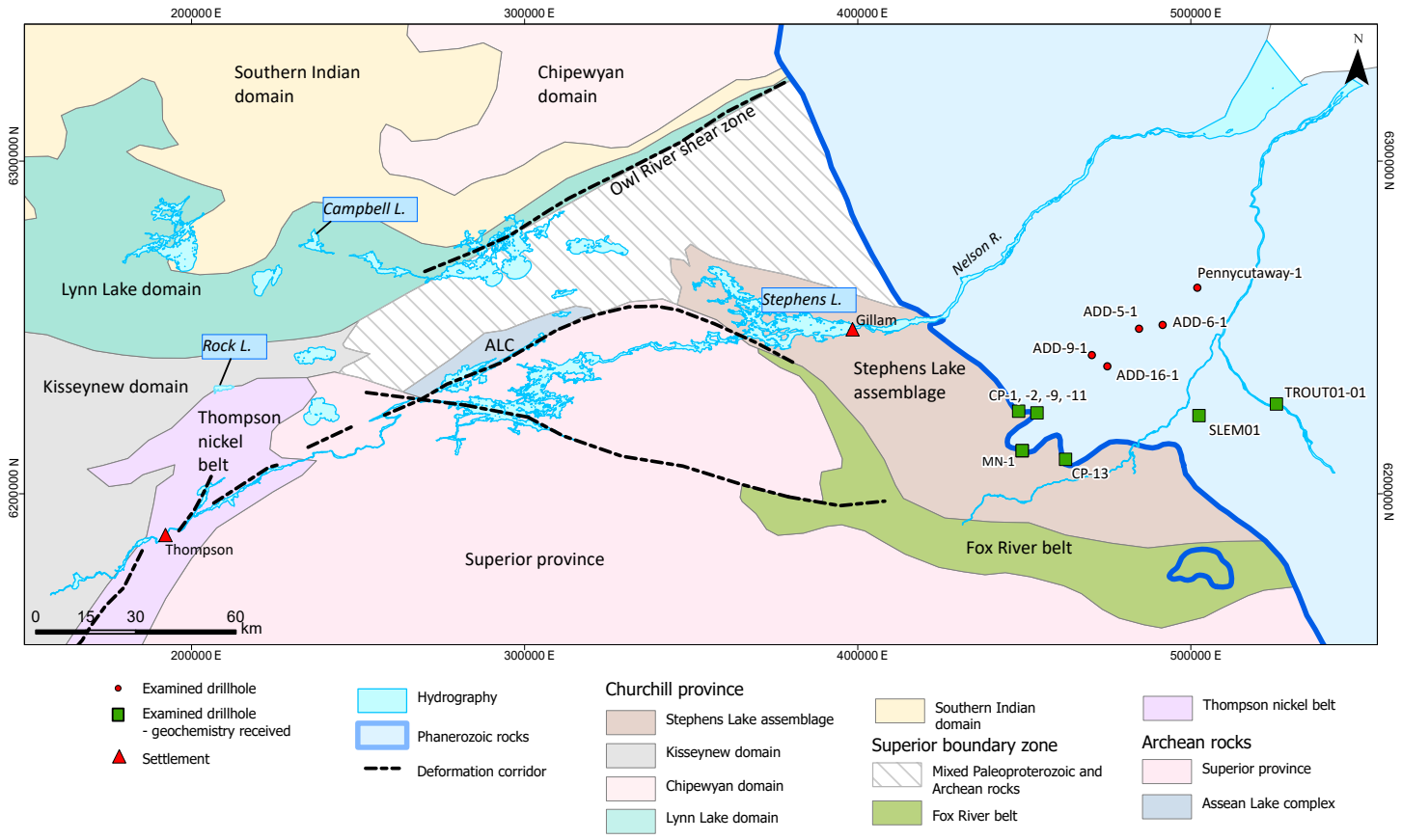

Figure GS2025-7-1: *Drillholes of the study area overlain on a simplified lithotectonic map of the Trans-Hudson orogen in east-central Manitoba (after Manitoba Geological Survey, 2024 and Hartlaub et al., 2005). Co-ordinates are in UTM zone 14, NAD83. Abbreviations: ACL, Assean Lake complex; L., lake.*

- relogging and sampling of selected industry drillholes collared east of Stephens Lake to draw potential correlations with regional lithotectonic packages

Only preliminary findings associated with relogging of the industry drillcore are presented in this report, as the Stephens Lake bedrock-sampling component could not be carried out due to road closures and hazardous conditions associated with wildfires this past summer.

Regional setting

During the Trans-Hudson orogeny (THO), a series of volcanic arcs and associated sedimentary basins belonging to Churchill province were accreted onto the southern margin of the Archean Hearne craton (ca. 1890 to 1830 Ma; Corrigan et al., 2009). The KD consists of synorogenic turbidites and continental sandstones deposited in a back-arc, intra-arc or fore-arc setting (Zwanzig, 1990; Ansdell et al., 1995; Zwanzig and Bailes, 2010) between 1890 and 1830 Ma (Machado et al., 1999; Lawley et al., 2020). The Burntwood group comprises the majority of the central KD and consists of migmatites and biotite gneisses that contain garnet, sillimanite and cordierite porphyroblasts and minor graphite (Zwanzig, 1990). High-grade metamorphism and intense deformation have made stratigraphic correlations within the Burntwood rocks unrecognizable (Zwanzig, 1990); however, a distinct layered amphibolite unit sits at the top of the Burntwood group and is locally associated with calcsilicate rock, iron-rich rock, ultramafic rock, impure marble and chert (Zwanzig, 1990), which are collectively referred to as the Granville complex (Murphy and Zwanzig, 2021). The Granville complex is thought to be in thrust contact with the top of the Burntwood group and to represent the ocean floor onto which the Burntwood group turbidites were deposited (Murphy and Zwanzig, 2021).

The continentally derived Sickle group stratigraphically overlies the Burntwood group on the northern flank of the KD at a contact that can be conformable or structural (Zwanzig, 1990; Ansdell et al., 1995). The Sickle group comprises migmatitic quartz-rich gneisses that commonly contain magnetite and potassium feldspar, and are thought to be derived from lithic sandstone, calcareous sandstone, arkose, conglomerate and argillaceous siltstone (Zwanzig, 1990). Abundant granitoid clasts (Stauffer, 1990) and ca. 1880 to 1833 Ma detrital zircons (Ansdell, 1993; David et al., 1996; Lawley et al., 2020) in the detritus indicate a proximal provenance from the bounding arc terranes and a maximum depositional age of ca. 1833 Ma (Murphy and Zwanzig, 2021).

At ca. 1830–1800 Ma, the northwestern margin of the Superior craton collided with the accreted terranes of the southern Churchill province (Corrigan et al., 2009). Peak metamorphic conditions in the KD reached upper-amphibolite– to granulite–facies (750 ±50 °C and 5.5 ±1 kbar; Gordon, 1989), caused widespread partial melting and were reached by ca. 1815 Ma (Gordon et al., 1990; Growdon, 2010). Mylonite zones and brittle faults offset the peak metamorphic isograds and postdate the period of folding and anatexis (Zwanzig, 1990). Felsic to mafic calcalkalic magmatism in the central KD occurred from ca. 1840 to 1800 Ma (Bickford et al., 1990; Gordon et al., 1990).

Drillcore descriptions

Approximately 1200 m of drillcore from 13 drillholes collared east of Stephens Lake were selected for relogging (Figure GS2025-7-1). All drillcore examined in the current work is archived at the core storage facilities of the Manitoba Geological Survey and the collar details are provided in the accompanying Data Repository Item DRI2025024 (Macdonald and Janssens, 2025)[1]. The examined drillholes were selected to maximize the number of different lithologies described and ensure the widest geographic distribution. Many of the drillholes (8 of 13) returned short intersections (<70 m) of one Precambrian rock type that do not allow for the characterization of genetic relationships between the rock types. Thus, correlations between individual drillholes are difficult. All rocks described here have been metamorphosed; however, the 'meta' prefix has been omitted for clarity.

Peridotite

Pervasively talc- and serpentine-altered rocks were intersected in three drillholes: CP-2, SLEM01 and TROUT01-01. These rocks are light green to grey and display two textural varieties: 1) coarse-grained domains of spinifex-like crystals completely replaced by variable amounts of serpentine, chlorite, actinolite and talc, and commonly associated with fine- to medium-grained magnetite disseminations (Figure GS2025-7-2a); and 2) massive aphanitic intervals that are talc rich and that host up to 10% fine- to medium-grained disseminated magnetite.

The pseudomorphous, spinifex-textured crystals typically lack a preferred orientation but are weakly aligned in one interval (~2.5 m). One ~60 cm interval contains medium- to coarse-grained orthocumulate olivines that are partially to completely serpentinized and set in a talc matrix. Magnetite-rich veins are locally abundant, have jagged, nonplanar margins and crosscut the aphanitic, talc-rich host at a variety of angles. A zone of massive pyrrhotite and pyrite was reported in drillhole TROUT01-01 during the initial drillcore logging (290.5–291.2 m; Assessment File 74249) but the drillcore containing this interval was not available for study during the current work.

Ultramafic rocks containing relict or pseudomorphous olivine and pyroxene are the dominant rock types in drillholes ADD-5-1, ADD-16-1 and ADD-9-1; however, intense alteration has obscured the primary mineralogy. Geochemistry and petrography may assist in differentiating the rocks described in this paragraph. These rocks are dark grey to light green or brick-red, medium to coarse grained and lack a pervasive foliation. Olivine (10–90% locally) is variably altered and has been partially to completely replaced by serpentine, chlorite or hematite. The presence of gradational variations in the abundance of the replaced crystals suggests cumulus crystallization of olivine (Figure GS2025-7-2b). Pseudomorphous, euhedral pyroxene (<1.2 cm) comprises 5–25% of the groundmass and has been strongly chlorite altered. Biotite is locally a major mineralogical component of the groundmass (up to 40%) and occurs as fine-grained crystals in a chlorite-rich groundmass, with local variations in the abundance of serpentine and talc. Magnetite is present throughout the replaced olivine crystals and altered groundmass as fine-grained disseminations (<10%) and locally infills a breccia as coarse, elongate crystals nucleated on the heterolithic fragments. Carbonate minerals (5–15%) occur as round aggregates of crystals that are pink in the cores. The matrix has locally been strongly hematite altered and coarse-grained (<3 cm wide), beige amphibole porphyroblasts (Fe-anthophylite?) appear to overgrow the hematized groundmass (Figure GS2025-7-2c). Serpentine-carbonate veins (<5–50 mm) hosting disseminated magnetite and crosscutting the altered rock are ubiquitous, and locally form a stockwork comprising up to 25% of the rock.

Anorthosite

The one locality in which this rock is observed in drillhole ADD-9-1 is within cumulate-textured peridotite. It is white to beige, very coarse grained and contains ~85–90% randomly oriented, beige plagioclase crystals (up to 3.5 cm wide; Figure GS2025-7-2d). Pseudomorphs consisting of hornblende and biotite comprise the remainder of the rock and developed after a medium-grained, subhedral primary phase. The upper contact of this rock is marked by a selvage of talc and serpentine ~25 cm across and wide fractures (>5 mm) that crosscut the rock are infilled with the same mineral assemblage. Abundant narrow fractures (<5 mm) are infilled with a soft, aphanitic mineral, translucent in appearance, and associated with a halo of brick-red hematite alteration 2–5 mm wide (Figure GS2025-7-2d).

Ultramafic schist

Drillhole SLEM01 intersected a ~8 m interval of texturally variable serpentine- and chlorite-rich rock immediately below the Paleozoic unconformity. Regolith is developed near the top of the interval and the rock is poorly preserved in the drillcore.

[1] MGS Data Repository Item DRI2025024, containing the data or other information sources used to compile this report, is available online to download free of charge at https://manitoba.ca/iem/info/library/downloads/index.html, or on request from minesinfo@gov.mb.ca, or by contacting the Resource Centre, Manitoba Business, Mining, Trade and Job Creation, 360-1395 Ellice Avenue, Winnipeg, Manitoba R3G 3P2, Canada.

Figure GS2025-7-2: *Drillcore photographs of mafic to ultramafic rocks east of Stephens Lake; all drillcore is NQ™ size (diameter = 4.76 cm):* ***a)*** *spinifex-like pseudomorphs in ultramafic rock (drillhole TROUT01-01, 213.8 m);* ***b)*** *selectively hematite-replaced cumulus olivine in altered peridotite (drillhole ADD-9-1, 113.55 m);* ***c)*** *pervasively hematite-altered ultramafic rock, with beige porphyroblasts overgrowing hematized groundmass (arrows; drillhole ADD-16-1, 94.8 m);* ***d)*** *hematite-altered peridotite (top row), and fractured and altered anorthosite (bottom row; drillhole ADD-9-1, 134.7 m);* ***e)*** *pegmatitic gabbro (top two rows) and diorite (bottom row; drillhole ADD-6-1, 130 m);* ***f)*** *basalt, with coarse-grained pyroxene (centre row) and irregular carbonate vein (bottom row; drillhole SLEM01, 185.5 m).*

The ultramafic schist is fine to medium grained and typically has a weak planar fabric defined by aligned chlorite, talc and lesser biotite. Serpentine is abundant along fracture planes and, at the top of the lithology, these bands are aligned subparallel in an anastomosing network.

Gabbro to pyroxenite

Pegmatitic gabbro is the dominant lithology in drillhole ADD-6-1 (Figure GS2025-7-2e). It is mottled black and white and lacks a foliation in hand sample. Diorite and granitic pegmatite dikes sharply crosscut it. Domains of differing grain size grade into one another over intervals ~2–4 m long, although the mineralogy of the different domains is similar. Subhedral to euhedral hornblende (80–85%) is randomly oriented in a matrix of plagioclase (~10–20%). Light brown, well-cleaved titanite crystals are locally observed in the pegmatitic portions and minor amounts of a fine-grained, bright green to yellow mineral (epidote?) are also locally observed along cleavage planes in hornblende or along grain boundaries. Chalcopyrite and pyrite are disseminated in trace amounts as fine-grained blebs. The rock has strong magnetic properties locally, and plagioclase crystals are weakly hematized.

Mafic intrusive rocks are present in three drillholes: SLEM01, CP-1 and ADD-9-1. These dark green to grey, medium-grained rocks are composed primarily of dark green amphibole (60–90%), light green pyroxene (10–30%) and interstitial chlorite, which are aligned to define a subtle, continuous foliation. Pyroxene phenocrysts up to 2.5 cm long are locally present and aligned with the foliation (Figure GS2025-7-2f). Fine-grained, interstitial plagioclase, up to 10% locally, occurs in the dark green amphibole groundmass. Sharp contacts are not observed between these rocks and their fine-grained mafic host, and it may be that they represent coarsely recrystallized basalt.

Basalt

Mafic volcanic rocks were intersected in drillhole SLEM01, where they are in contact with semipelitic greywacke, and in drillhole Pennycutaway-1, where they are in sheared contact with quartz porphyry and conformable contact with banded iron formation. These fine-grained rocks are dark green to grey and have a continuous foliation defined by the alignment of amphibole, plagioclase and, locally, pyroxene and chlorite. Garnet is locally present as medium-grained, equant crystals (up to 10%) in a biotite-altered groundmass. Primary features were not identified in the drillcore; however irregularly shaped carbonate veins with biotite- and diopside-bearing selvages may represent altered pillow selvages (Figure GS2025-7-2f). Fine-grained disseminations and millimetre-scale stringers of pyrrhotite are common.

Felsic to intermediate volcanic rocks

Felsic volcanic rocks that vary from light grey to blue are the dominant lithology in drillhole Pennycutaway-1 (Figure GS2025-7-3a–d). The rocks consist of a quartz- and plagioclase-rich groundmass hosting various proportions of lenticular to amoeboid lithic fragments (<5–20%; 5–30 mm) and plagioclase (2–15%; 2–5 mm), quartz (1–15%, 1–10 mm) and/or dark green amphibole (1–10%) phenocrysts (Figure GS2025-7-3a, b). Sericite-rich bands (2–5%, 1–4 cm wide) and amphibole-rich bands (1–5%, 1–8 cm wide) are present throughout. Garnet occurs as fine- to medium-grained crystals in amphibole-rich bands and as fine-grained aggregates of crystals in the quartzofeldspathic groundmass. Medium-grained euhedral magnetite (<8 mm) is locally hosted in the groundmass and trace amounts of pyrrhotite occur as fine-grained stringers that parallel the foliation. Arsenopyrite is locally associated with quartz veining or occurs as fine-grained disseminations in the groundmass (2–3% over 30 cm). Zones of alteration (<4 m wide) grade into the unaltered rock and contain biotite (15%), chlorite (<10%), andalusite (<10%) and garnet (1–8%); the presence of andalusite porphyroblasts (up to 15%) is also noted in a 1.6 m interval lacking a pervasively altered groundmass and in which they overgrow select compositional bands. Four varieties of lithic fragments (lapilli?) are observed:

- an aphanitic to fine-grained light grey rock that contains 15% K-feldspar and 5–15% dark green amphibole
- light green fragments with cores hosting 10% fine-grained, dark grey quartz and fine-grained epidote with aphanitic white rims
- a light pink and aphanitic rock with 10% fine-grained, dark green amphibole
- rare, round fragments (0.5–1.5 cm wide) that are dark grey and quartz rich, host fine-grained green inclusions and lack a reaction rim

A foliation is defined by the elongation of quartz phenocrysts, plagioclase phenocrysts and/or lithic fragments, and the alignment of amphibole and plagioclase in the groundmass. Variations in relative abundances of fragments and mineral constituents define compositional bands that are parallel to the foliation. Graded beds (5–15 cm wide) are locally present and have tops oriented downhole, as indicated by gradational increases in the abundance of biotite and amphibole. Lithic fragments are rotated in the foliation and have recrystallized tails. A sericite-rich mylonitic zone overprints the continuous foliation over a ~60 cm interval and marks a contact with basalt.

Quartz porphyry

This porphyritic unit is in sharp contact with amphibolite and banded iron formation in drillhole Pennycutaway-1 (Figure GS2025-7-3b, d). It comprises a dark grey to beige aphanitic and siliceous groundmass hosting anastomosing bands of fine-grained sericite (10–15%), dark green fine- to medium-grained amphibole (5–15%), medium-grained biotite (5–10%) and blue grey ‘quartz eyes’ (1–12%). These minerals are aligned to define a foliation that wraps the quartz eyes. Garnet occurs as fine-grained pinpricks in the amphibole-rich domains and as medium-grained (3–6 mm) crystals that are associated with quartz phenocrysts

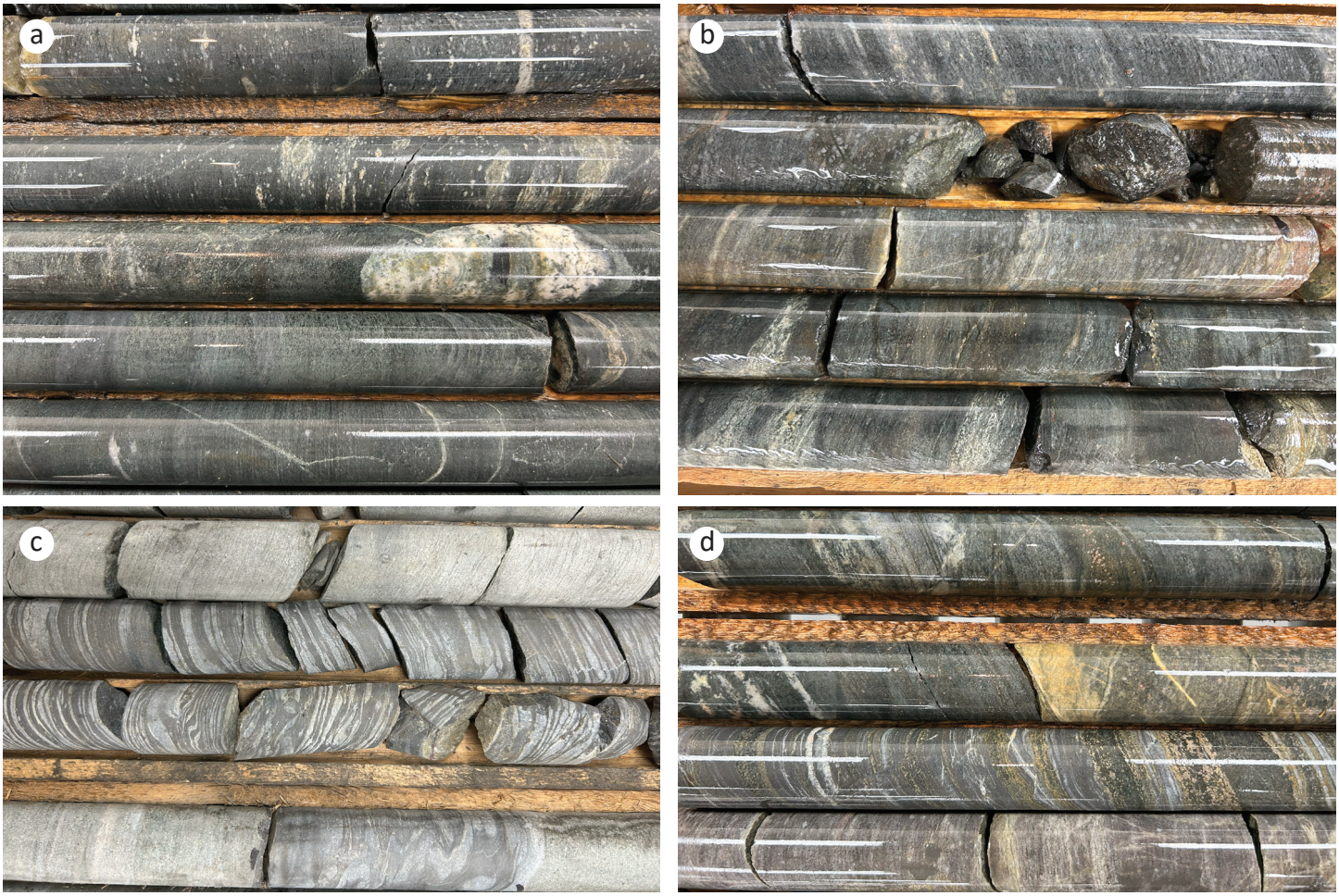

Figure GS2025-7-3: *Drillcore photographs of felsic to intermediate volcanic rocks east of Stephens Lake; all drillcore is AQ™ size (diameter = 2.70 cm):* ***a)*** *felsic to intermediate volcanic rock (drillhole Pennycutaway-1, 404.6 m);* ***b)*** *felsic to intermediate volcanic rock (top two rows), quartz porphyry (middle row) and basalt (bottom rows; Pennycutaway-1, 236.5 m);* ***c)*** *felsic to intermediate volcanic rock (top row) and banded iron formation (bottom three rows; Pennycutaway-1, 352.3 m);* ***d)*** *intercalated amphibolite (top two rows), banded iron formation and quartz porphyry (bottom two rows, respectively; Pennycutaway-1, 370.6 m).*

and overgrow the foliation. Cummingtonite is locally present as light brown to yellow, fine-grained equant crystals that selectively overgrow select beds with amphibole, garnet and biotite. Pyrrhotite (1–5%) occurs primarily as fine-grained stringers or in a net-texture, where it is most abundant.

Rhyolite

Light grey, aphanitic felsic dikes crosscut altered peridotite in drillhole ADD-16-1. The rock contains 1–4% fine-grained plagioclase crystals randomly oriented in an aphanitic siliceous groundmass. Fine-grained actinolite (~2%) is present throughout and hematite alteration permeates the matrix. A fragmental texture is locally present, in which ovoid fragments of this rock are aligned in an anastomosing matrix of foliated, medium-grained biotite.

Semipelitic greywacke

A muscovite-biotite schist was intersected in MN-1 and SLEM01 (Figure GS2025-7-4a) and interpreted to represent a semipelitic greywacke. These rocks are light blue to grey and have a prominent schistosity defined by layers of medium-grained muscovite (2–10%), biotite (2–10%) and local sillimanite knots (<1%–8%) in a matrix of quartz and plagioclase. Primary textures are not common, but variations in the relative proportions of the above minerals likely represent bedding. Garnet is observed in a few locations as medium-grained euhedral crystals set in biotite-rich folia. Where sillimanite is present, biotite is more abundant than muscovite. Pyrrhotite is present throughout the rock as millimetre-scale laminations along the schistosity planes. There are broad changes in the orientation of the schistosity over 1–10 m intervals and crenulations in the schistosity are commonly present.

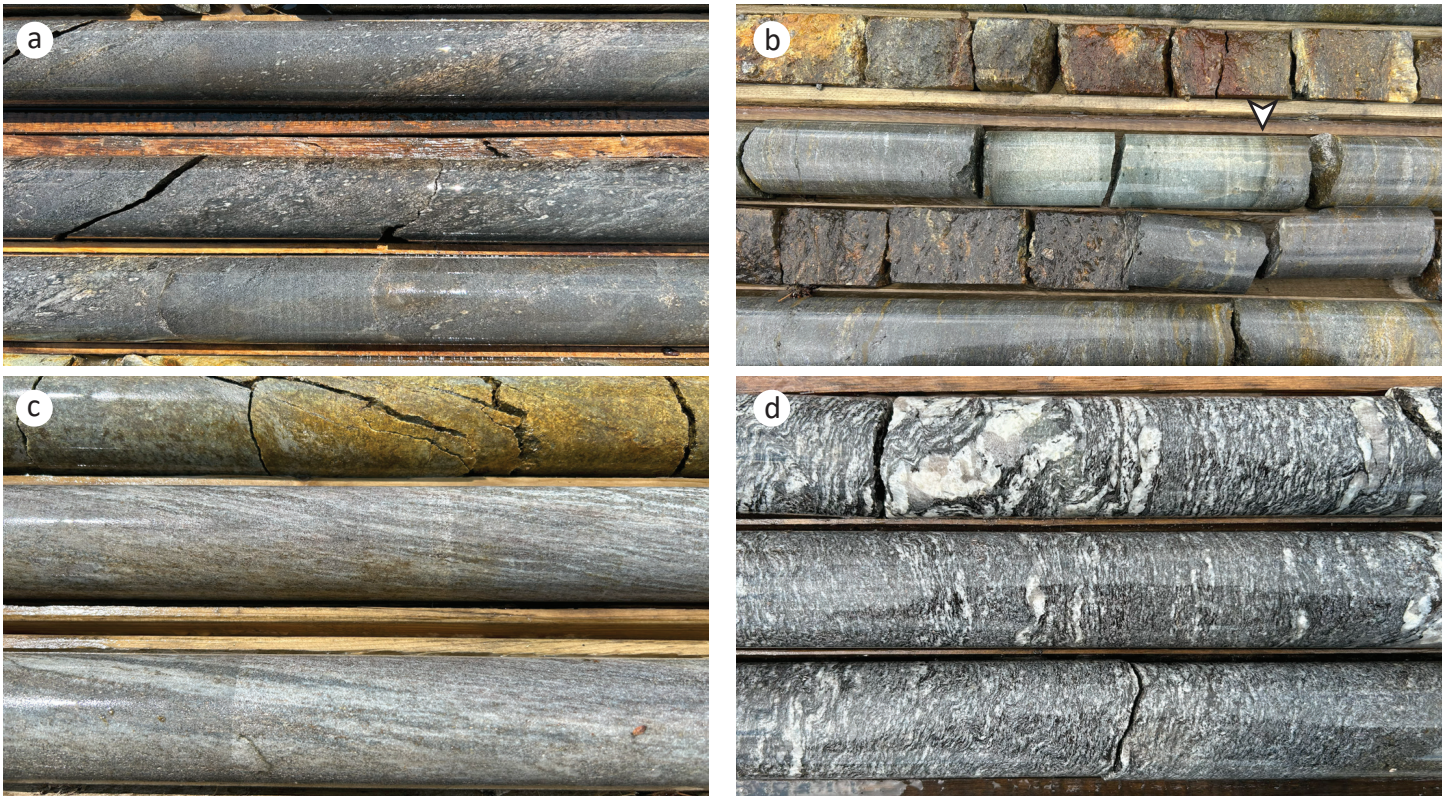

Figure GS2025-7-4: *Drillcore photographs of metasedimentary rocks east of Stephens Lake; all drillcore is NQ™ size (diameter = 4.76 cm):* ***a)*** *semipelitic greywacke, with beds of differing composition (drillhole SLEM01, 252.3 m);* ***b)*** *sulphidic and graphitic mudstone, with gradational contact on siliceous (chert?) layer (arrow; drillhole MN-1, 108.0 m);* ***c)*** *strained calcsilicate rock (drillhole MN-1, 214.0 m);* ***d)*** *migmatitic biotite-sillimanite gneiss (drillhole MN-1, 256.3 m).*

Feldspathic wacke

This texturally and mineralogically homogeneous rock was encountered in drillhole CP-9 over a 66 m drilled interval. It is light grey to blue, medium grained and has a continuous foliation defined by the alignment of quartz, plagioclase and biotite. Medium-grained quartz and plagioclase are present in roughly equal amounts, and fine- to medium-grained biotite (5–10%) occurs as aggregate clusters aligned with the foliation. Muscovite intergrown with biotite is locally present. Fracture networks impart a brecciated texture over intervals of ~1–2 m and are associated with weak pervasive silicification.

Mudstone

Sulphide- and graphite-bearing mudstone was encountered in drillhole MN-1 (Figure GS2025-7-4b). This rock is black, aphanitic to fine grained and is in gradational contact with the muscovite-biotite-quartz schist that is marked by a decrease in the abundance of quartz and feldspar and an increase in the abundance of biotite, graphite and sulphide minerals. The two rock types are intercalated in segments of 1–3 m over an interval ~10 m long. The groundmass of the rock is composed largely of biotite, which is aligned to define a foliation that is parallel to the overall trend of abundant discontinuous and chaotically folded layers (<1.5 cm wide) of pyrite, pyrrhotite and local chalcopyrite. Graphite occurs as fine-grained aligned flakes, wispy layers and rarely in massive to net-textured intergrowths with pyrrhotite. Pyrrhotite locally forms a net texture around fragments of the biotite matrix. Narrow (<20 cm), siliceous (cherty?) horizons contain up to 5% muscovite and are separated from the graphitic mudstone by narrow (<4 mm) gradational contacts (Figure GS2025-7-4b).

Calcsilicate rock

This rock is observed in drillhole MN-1 in sharp contact with the semipelitic greywacke. The rock is white to light green, with a banded and mottled texture that varies in orientation and

strain intensity locally. The banding is defined by differences in modal mineralogy and comprises a white, aphanitic and siliceous groundmass with bands of light green diopside (5–20%), discontinuous bands of pyrrhotite (5–8%), disseminated fine-grained cubic pyrite (2–3%) and trace amounts of blebby chalcopyrite (<8 mm across). Local patches of calcite (~2–4%) occur in the white matrix. Medium-grained biotite and muscovite form laminations locally, and flakes of bright green chlorite form the foliation in a few instances. Locally, crystals of a fine-grained, subhedral acicular amphibole (3–5%) are randomly oriented. Near the bottom of the drilled interval, the strain intensity increases and the compositional layering is replaced by a ribbon texture (Figure GS2025-7-4c).

Iron formation

Banded iron formation occurs in conformable contact with basalt and felsic to intermediate volcanic rocks in drillhole Pennycutaway-1 (Figure GS2025-7-3c). These rocks contain alternating laminae of aphanitic magnetite and quartz and locally host zones up to 2 m across comprising massive chlorite that hosts disseminations of medium-grained, euhedral magnetite (up to 20 vol. % of the rock) and ovoid domains of quartz set in an anastomosing network of fine- to medium-grained pyrite and pyrrhotite (up to 50 vol. % of the rock). Locally, the anastomosing networks of sulphide minerals host medium-grained euhedral magnetite. Randomly oriented, fine-grained flakes of chlorite can overgrow the magnetite-rich bands, and local patches of sericite and anthophyllite are present. Rootless and intrafolial isoclinal folds in the bands are common and local high-strain zones comprise a network of fine-grained magnetite anastomosing around lenticular domains of quartz. Light yellow, equant cummingtonite overgrows select quartz-rich laminations and gradationally increases in abundance nearing the adjacent magnetite lamina. Narrow intervals of the banded iron formation are intercalated with amphibolite and contain <10% quartz bands. Amphibole-rich bands (up to 7 cm wide) are common in these intervals and host fine-grained magnetite, garnet and cummingtonite (Figure GS2025-7-3d).

A texturally and mineralogically heterogeneous unit tentatively interpreted as iron formation was intersected over a ~20 m interval in drillhole MN-1. The strongly magnetic unit is dark grey to brown, hosted in the semipelitic greywacke and contains mineralogical bands overprinted by a weak continuous foliation. Rubbly, hand-split drillcore did not allow for the contact with the host to be observed. The rock contains fine-grained, light green pyroxene (20–30%); medium-grained biotite (10–20%); semi-massive to finely disseminated pyrrhotite (5–0%); banded and fine-grained, light red garnet (<1–8%); and trace amounts of a fine-grained, light brown amphibole locally. Conformable bands of blue-grey quartz (1–4 cm wide) can contain massive to net-textured pyrrhotite and medium-grained euhedral crystals of magnetite. Graphite is locally present (2–4%) as isolated flakes with the net-textured pyrrhotite or as semi-massive bands.

Migmatitic biotite-sillimanite gneiss

A migmatitic biotite-sillimanite gneiss was encountered in drillholes MN-1 and CP-13. This rock is light grey and characterized by a strong gneissosity defined by alternating bands of biotite and quartz and plagioclase (Figure GS2025-7-4d). The orientation of the gneissosity broadly changes over metre-scale intervals and parasitic, open to isoclinal folds are common. Quartz in the groundmass (~35%) is medium grained, elongate in the foliation and intergrown with fine-grained plagioclase (~25%). Biotite (10–20%) occurs as medium-grained bands that are aligned to define the foliation of the rock. Muscovite (<5%) is locally present as medium-grained crystals intergrown with biotite and can be euhedral with no preferred orientation, or anhedral and aligned with the gneissosity. Coarse-grained to pegmatitic leucosome comprises 5–20% of the rock as segregations up to 30 cm wide that are concordant with the gneissic fabric and lack an internal foliation. These domains consist of quartz, K-feldspar, plagioclase, and minor biotite and muscovite. Wider pods of leucosome (>1 cm wide) have sharp contacts with a well-developed margin of biotite-rich melanosome, whereas narrow pods (<1 cm) have diffuse margins that grade into the gneissosity and lack well-defined melanosome. The abundance of leucosome and biotite varies locally, with intervals up to 8 m long that lack leucosome and contain less biotite (<3%), which may represent primary compositional differences. Narrow mylonitic zones (<2 cm wide) with narrow strain gradients are rarely present, contain muscovite, and crosscut the leucosome and melanosome. One graphitic horizon (~60% graphite over 70 cm) contains concordant bands of pyrrhotite (<5 mm wide) that are set in the fine-grained graphitic matrix and constitute up to 10% of this interval.

Granite

This light grey to pink rock hosted in massive peridotite was intersected in drillhole ADD-5-1. It is fine-grained and has a strong continuous foliation defined by the alignment of K-feldspar (35–40%), quartz (25–30%), plagioclase (20–25%), biotite (3–4%) and hornblende (3–4%). Quartz ribbons are well developed and a light green aphanitic alteration of the rock matrix is observed over intervals of ~10 cm. The lower contact of the dike is marked by a ~60 cm interval of strongly foliated light beige, soft minerals that are host to elongate amphibolite boudins. The rock is crosscut by numerous inconsistently oriented fractures that are associated with narrow (<1 cm wide) selvages of pervasive hematite alteration.

Granodiorite

Dark-red, medium-grained and massive to weakly foliated granodiorite dikes are hosted as narrow intrusions (5–20 cm wide) and boudins in the altered peridotite of drillhole ADD-5-1. The dikes contain plagioclase (35–50%), quartz (10–35%), dark green amphibole (7–10%) and K-feldspar (5–10%), which are

weakly aligned to define the foliation. Trace amounts of a fine-grained disseminated black, metallic, nonmagnetic mineral are locally present. Alteration haloes of hematite can locally occur immediately adjacent to the granodiorite contacts (~1 cm from the contact) and are in sharp contact with an outer facies of epidote alteration (~5 cm from the contact). Coarse-grained, bladed, brown amphibole is present throughout the alteration halo. The dikes are crosscut by abundant millimetre-scale fractures mantled by a hematite selvage 3–5 mm wide, and in which biotite has crystallized along a central line.

Monzogranite

This rock observed in drillhole CP-11 is not in contact with any other lithology. The rock is light grey to pink and medium grained. The dominant mineralogical components are K-feldspar (40%), quartz (20%), plagioclase (20%), hornblende (5–10%), magnetite (2–8%), biotite (1–4%), garnet (<1%) and chalcopyrite (<1%). Quartz and feldspars do not show any preferred orientation in hand sample, but biotite and hornblende are aligned to define a weak foliation. Magnetite occurs as fine- to medium-grained disseminations and chalcopyrite is locally present as irregularly shaped blebs <6 mm across. Pegmatitic segregations (<50 cm) have a simple mineralogy of quartz, K-feldspar, plagioclase, muscovite and, locally, biotite; they also have narrow (<3 mm) gradational contacts with the granitoid host.

Diorite to quartz diorite

These rocks are observed in drillholes ADD-5-1, ADD-6-1 and Pennycutaway-1 (Figure GS2025-7-2e). They are light grey and medium grained, with a subtle continuous foliation defined by a weakly aligned groundmass of plagioclase (60–70%), quartz (10%), biotite (5–15%) and hornblende (3–15%), in which equant quartz or aligned plagioclase phenocrysts are locally present. Trace amounts of fine-grained red garnet locally occur along the amphibole grain boundaries.

Tonalite

This light grey to pink rock is observed in drillhole ADD-9-1. It is medium-grained and massive, and contains plagioclase (60%), quartz (30%), dark green amphibole (7%) and biotite (3%). It is crosscut by numerous fractures (~2–6 cm thick) that are infilled with light brown clay minerals. Biotite and amphibole are lightly hematized along grain boundaries. Contact relationships of this unit are not observed, but a narrow rim of brick-red hematite alteration is present within the dike, less than 5 mm from the dike contacts.

Pegmatite

Massive, pink granitic pegmatites (up to 60 cm wide) crosscut the gabbro and altered peridotite in drillholes ADD-5-1 and ADD-6-1 at sharp, planar contacts. The dikes are rich in megacrystic K-feldspar and contain lesser amounts of quartz, plagioclase, biotite and magnetite. In drillhole CP-9, one such pegmatite crosscuts the feldspathic wacke and hosts a clot of fine- to coarse-grained black tourmaline along its lower contact, which is locally intergrown with an unidentified fine-grained, silvery, mineral of metallic lustre and tabular habit.

Metamorphism

The metamorphic grade of the examined rocks indicates regional amphibolite-facies conditions. In the south, the metamorphic grade is best indicated in the mineral assemblages of the semipelitic greywacke (muscovite-biotite-sillimanite±garnet) and migmatitic biotite-sillimanite gneiss (biotite-sillimanite-melt), which indicate lower-amphibolite and upper-amphibolite– to granulite–facies conditions, respectively (Palin and Dyck, 2021). In the northern drillholes, amphibolite-facies conditions are suggested by the mineral assemblages of pegmatitic gabbro (hornblende-epidote-plagioclase) and banded iron formation (amphibole-garnet-biotite-magnetite). Muscovite-bearing mylonitic zones crosscut the migmatitic biotite-sillimanite gneiss in the south and the felsic to intermediate volcanic rocks in the north and may indicate localized metamorphic retrogression.

Geochemistry

Whole-rock lithogeochemistry results from samples collected in the southern drillholes (CP-1, CP-2, CP-9, CP-11, CP-13, SLEM01, MN-1 and TROUT01-01) are summarized here. A description of the analytical procedures and a full set of the initial geochemical results are available in the accompanying DRI (Macdonald and Janssens, 2025). Geochemistry results for the remainder of the drillholes (ADD series and Pennycutaway-1) are pending. As monzogranite was the only granitoid rock analyzed in the current dataset, discriminatory plots are not included; Nb, Ta, Yb, Y and Rb abundances of this rock indicate volcanic arc affinity (Pearce et al., 1984).

Whole-rock geochemical compositions of the complete dataset are plotted on a Zr/Ti versus Nb/Y volcanic rock discrimination diagram (Figure GS2025-7-5a). Rocks that plot as basaltic in composition are further discriminated by their Ti/V ratios (Figure GS2025-7-5b) and normal mid-ocean–ridge basalt (N-MORB) normalized trace-element profiles (Figure GS025-7-5c). Basalt and pyroxenite in drillhole SLEM01 have Ti/V ratios ranging from 28.9 to 31.4 (Figure GS2025-7-5b) and trace-element abundances indicative of E-MORB affinity (enrichment in Th and Nb and slight enrichment in Zr relative to Ti and Y; Figure GS2025-7-5c), whereas gabbro from CP-1 has characteristics indicative of volcanic arc affinity (Ti/V = 12.7; low trace-element abundances and relative depletions in Nb and Zr relative to Y; Figure GS2026-7-5b, c).

Peridotite samples are not plotted on Figure GS2025-7-5a due to Nb, Y and Zr abundances being below detection limits, but are included with basaltic rocks in the Ti/V and multi-element diagrams due to their high Cr and Ni contents (>2000 ppm Cr and

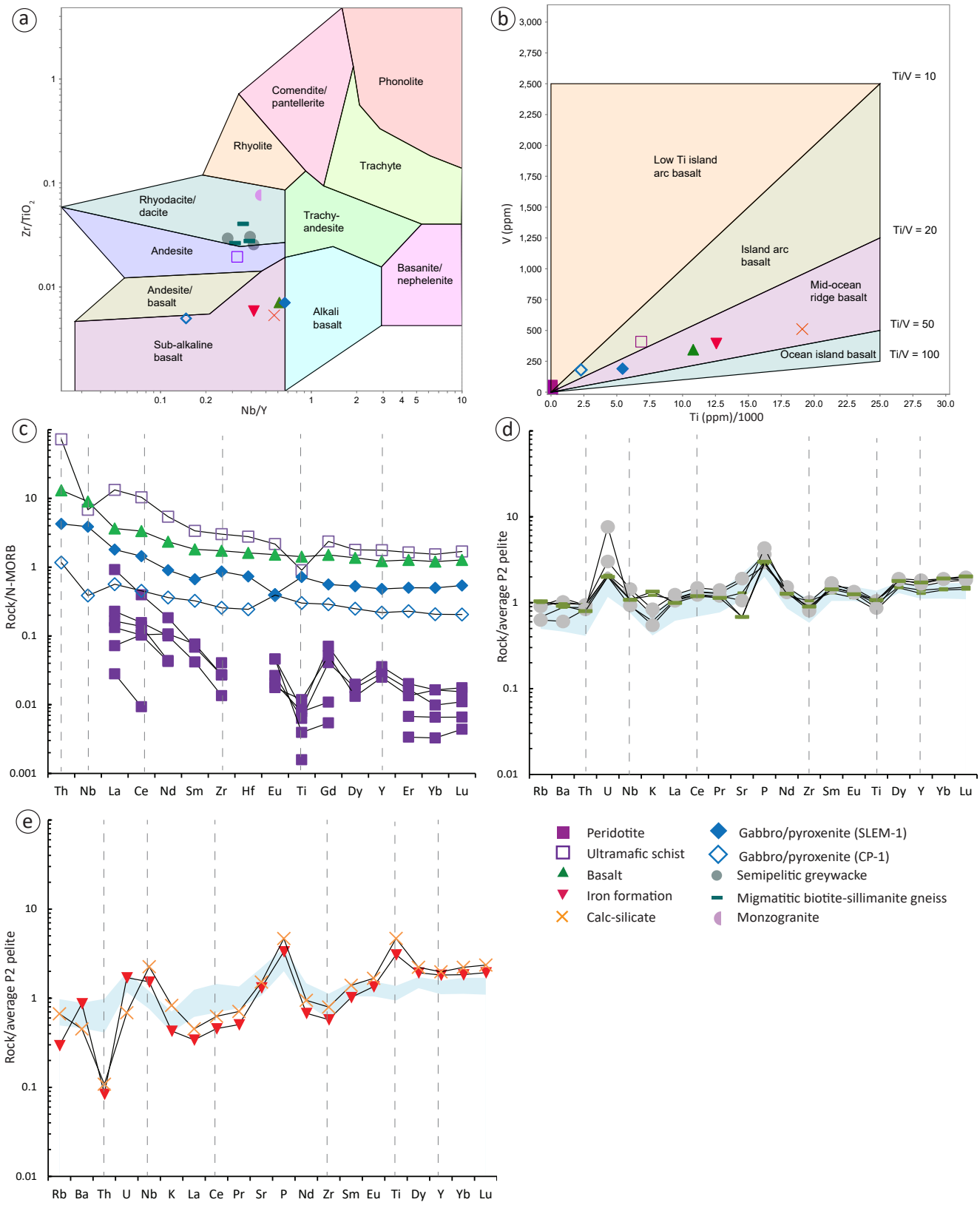

Figure GS2025-7-5: *Geochemical plots of whole-rock compositions in drillholes CP-1, CP-2, CP-9, CP-11, CP-13, SLEM01, MN-1 and TROUT01-01;* ***a)*** *Zr/Ti versus Nb/Y volcanic rock classification diagram (after Winchester and Floyd, 1977);* ***b)*** *Ti versus V basalt discrimination diagram (after Shervais, 1982);* ***c)*** *normal mid-ocean–ridge basalt (N-MORB) normalized multi-element plots of mafic to ultramafic rocks (element order after Murphy and Zwanzig, 2021; normalized values from Sun and McDonough, 1989);* ***d, e)*** *average P2 pelite-normalized multi-element plots (after Zwanzig et al., 2007) of semipelitic greywacke and migmatitic biotite-sillimanite, and of calcsilicate and iron formation, respectively, compared with characteristic pattern of Burntwood group metagreywacke-mudstone (light blue field) from Murphy and Zwanzig (2021).*

>1000 ppm Ni). Multi-element profiles of peridotite are largely incomplete due to the low trace-element abundances but display negatively sloped profiles with consistent depletions in Ti and Dy relative to Gd and Y (Figure GS-2025-7-5c). The Ti/V ratios range from 0.999 to 11.2, consistent with island-arc basalts; however major-element abundances in the peridotite samples indicate these rocks experienced significant alteration (loss-on-ignition >15%; Macdonald and Janssens, 2025); therefore, a more thorough analysis will be needed for geochemical characterization of the samples.

Murphy and Zwanzig (2021) showed that the metasedimentary rocks in the KD and the Superior boundary zone (Ospwagan, Burntwood and Sickle groups, and Granville complex) can be distinguished by multi-element profiles normalized against the average whole-rock composition of the P2 member of the Ospwagan group, as in Zwanzig et al. (2007; Figure GS2025-7-5d, e). The semipelitic greywacke and migmatitic biotite-sillimanite gneiss have parallel trace-element profiles that are characterized by depletions in Zr and Ti, and enrichments in U and P (Figure GS2025-7-5d). The semipelitic greywacke contains comparatively higher U relative to the migmatitic gneiss, which shows slight K enrichment and Sr depletion relative to the semipelitic greywacke in 2 of 3 samples. The calcsilicate and iron formation in drillhole MN-1 have different trace-element characteristics than the host semipelitic greywacke and display slightly positively sloped profiles, with prominent Th, La and Zr depletions and Nb, P and Ti enrichments (Figure GS2025-7-5e). The Zr/Ti and Nb/Y ratios of these two rocks also differ from those of the other metasedimentary lithologies and plot in the basaltic field (Figure GS2025-7-5a), with MORB-type Ti/V ratios (31.8 and 37.4, respectively; Figure GS2025-7-5b). These rocks did not preserve any distinctive primary features, but their geochemical composition suggests that they may have derived from a different provenance, or represent hydrothermally altered and metamorphosed basalts of MORB affinity.

Discussion

Two broad distributions of lithologies are identified in the current project: a southern domain, in which drillholes intersected primarily terrigenous metasedimentary rocks and mafic to ultramafic rocks (drillholes CP-1, CP-2, CP-9, CP-11, CP-13, SLEM01, MN-1 and TROUT01-01); and a northern domain, characterized by mafic to ultramafic intrusive rocks and a felsic to intermediate volcanic sequence intercalated with banded iron formation (drillholes ADD-5-1, ADD-6-1, ADD-9-1, ADD-16-1 and Pennycutaway-1). The lack of field relationships and sparse spacing of the observations limit potential tectonic interpretations; however, correlations may be drawn with the exposed and better studied rocks to the west. It should also be noted that the lithologies are likely not representative of the regions as the examined drillholes selectively targeted conductive and electromagnetic anomalies.

The lithological, metamorphic and trace-element characteristics of the semipelitic greywacke and migmatitic biotite-sillimanite gneiss in the southern drillholes (Stephens Lake assemblage) are similar to those of the Burntwood group (Murphy and Zwanzig, 2021), which comprises the majority of the central KD (Zwanzig, 1990). Furthermore, Nd-model ages of metasedimentary rocks on Stephens Lake and north of the Fox River belt (1.95 and 2.30 Ga, respectively; Rinne, 2018; Böhm et al., 2019) indicate derivation from Paleoproterozoic crust, like the KD. Samples of the semipelitic greywacke and migmatitic biotite-sillimanite gneiss from SLEM01 and MN-1, respectively, were collected for detrital zircon geochronology and should help to further constrain the provenance and timing of deposition in the SLA.

Several rock types described here are similar to those described in the Granville complex, which transects the northern flank of the KD (Murphy and Zwanzig, 2021):

- MORB-type mafic to ultramafic rocks
- mottled, white to brown calcsilicate rocks containing varying proportions of plagioclase, diopside, calcite and amphibole
- rusty, green to grey-brown iron formation that grades into, or is interlayered with, less sulphidic paragneiss, cherty layers, or mudstone

The multi-element profiles of the basalt, iron formation and calcsilicate rock reported here (Figure GS2025-7-5c, e) are like those of the Granville complex (Murphy and Zwanzig, 2021), further supporting a correlation between the two regions. On Stephens Lake, a layered amphibolite commonly marks the contact between graphitic turbidites and magnetiferous arkoses (inferred Burntwood and Sickle groups, respectively; Corkery, 1985), perhaps representing a continuation of the Granville complex through Stephens Lake as well.

The occurrence of gabbroic and volcanic rocks in the northern domain of the current study area may represent an eastern continuation of the Lynn Lake domain. In western Manitoba, the Lynn Lake domain bounds the northern flank of the KD and represents a series of juvenile oceanic volcanic arcs, associated sedimentary basins and plutons (Gilbert et al., 1980) that are host to numerous different deposit types (orogenic Au; Cu-Zn volcanogenic massive sulphide and magmatic Ni-Cu-Co). The pending geochemistry results from the northern drillholes (ADD series and Pennycutaway-1) will be compared to the well-documented geochemistry of the volcanic (Zwanzig, 1999) and intrusive (Yang, 2025) rocks of the Lynn Lake belt to elucidate any potential correlations.

Economic considerations

Nickel

Drillholes examined in the current work (Assessment Files 74154, 74249, 74410) targeted rocks thought to be extensions of the Thompson nickel belt (TNB); therefore, one of the cur-

rent project goals is to assess similarities between the rocks of the two regions. As Ni-Cu mineralization in the TNB is thought to be associated with the intrusion of ultramafic magmas into the sulphidic horizons in the Ospwagan group (Bleeker, 1990; Zwanzig et al., 2007; Lightfoot et al., 2017), exploration efforts focus largely on the identification of ultramafic rocks or the sulphidic horizons in the metasedimentary hostrocks (e.g., Zwanzig et al., 2007). The metasedimentary rocks in the current work are geochemically different than those of the Ospwagan group, and the available geological evidence does not support a correlation between the studied ultramafic rocks and those of the TNB. However, ultramafic rocks in the northern SLA are now identified over a distance of ~80 km, some of which are in close spatial association with sulphidic sedimentary rocks (i.e., drillhole SLEM01). No instances of ultramafic intrusion into the metasedimentary country rocks were observed but, presumably, interaction between the two rock types could lead to sulphide saturation and the precipitation of Ni-Cu sulphides. The historical assay results of the spinifex-like ultramafic rocks in drillhole TROUT01-01 were not encouraging (up to 66 ppb Pt; Assessment File 74249); however, proximal electromagnetic conductors were not tested with diamond drilling and the basal contact of the 180 m thick ultramafic intercept was not reached. Glacial drift prospecting in Thompson has identified indicator minerals associated with Ni-Cu deposits (McLeneghan et al., 2012, 2013) and may prove a useful exploration technique here if the ultramafic rocks are not overlain by Phanerozoic cover.

Diamonds

Diamonds are principally mined from kimberlite, a rare rock type that is associated with the margins of ancient terranes (e.g., the Superior craton) and often identified through drift prospecting of glacial till deposits. Kimberlite indicator minerals occur in the till deposits of the Fox and Hayes rivers areas south and east of the examined drillholes (Fedikow et al., 2001; Nielsen and Fedikow, 2002; Keller, 2019; Gauthier et al., 2021; Gauthier and Hodder, 2022), suggesting that these diamondiferous rocks may occur in northeastern Manitoba. Exploration programs in the area, which included some of the examined drillholes (Assessment Files 74005, 94676, 74259), targeted potential source kimberlites; however, the source of the anomalous indicator minerals was not identified.

Acknowledgments

The author thanks W. Sharpe and N. Palacios Montenegro for enthusiastic and capable field assistance while core logging in Thompson; E. Ralph, C. Epp and P. Belanger for thorough logistical support and assistance at the Midland drillcore storage facility; and C. Böhm for a discussion on the geology of the area and helping navigate archival sample data. The companies that donated the examined drillcore to the Manitoba Geological Survey (Selco Exploration Company Ltd., Valerie Gold Resources Ltd., BHP Billiton Diamonds Inc. and Arctic Star Diamond Corporation) are graciously thanked as well. Lastly, K. Reid and X.M. Yang are thanked for their constructive reviews and D. O'Hara is gratefully acknowledged for final editing and formatting of this report.

References

Ansdell, K.M. 1993: U-Pb zircon constraints on the timing and provenance of fluvial sedimentary rocks in the Flin Flon and Athapapuskow basins, Flin Flon Domain, Trans-Hudson Orogen, Manitoba and Saskatchewan; *in* Radiogenic age and isotopic studies: report 7, Geological Survey of Canada, Paper 93-02, p. 49–57.

Ansdell, K.M., Lucas, S.B., Connors, K.A. and Stern, R.A. 1995: Kisseynew metasedimentary gneiss belt, Trans-Hudson Orogen (Canada): back-arc origin and collisional inversion; Geology, v. 23, no. 11, p. 1039–1043.

Bickford, M.E., Collerson, K.D., Lewry, J.F., Van Schmus, W.R. and Chiarenzelli, J.R. 1990: Proterozoic collisional tectonism in the Trans-Hudson orogen, Saskatchewan; Geology, v. 18, p. 14–18.

Bleeker, W. 1990: New structural-metamorphic constraints on early Proterozoic oblique collision along the Thompson nickel belt, Manitoba, Canada; *in* The Early Proterozoic Trans-Hudson Orogen of North America, J.F. Lewry and M.R. Stauffer (ed.), Geological Association of Canada, Special Paper, v. 37, p. 57–73.

Böhm, C.O., Hartlaub, R.P., Heaman, L., Cates, N., Guitreau, M., Bourdon, B., Roth, A.S.G., Mojzsis, S.J. and Blichert-Toft, J. 2019: The Assean Lake complex: ancient crust at the northwestern margin of the Superior Craton, Manitoba, Canada; chapter 6.2 *in* Earth's Oldest Rocks, M. Van Kranendonk, V.C. Bennet and J.E. Hoffmann (ed.), Developments in Precambrian Geology, v. 15, p. 751–774, URL <https://doi.org/10.1016/S0166-2635(07)15096-9>.

Corkery, M.T. 1985: Geology of the lower Nelson River project area; Manitoba Energy and Mines, Geological Services, Geological Report 82-1, 66 p., plus 5 maps.

Corrigan, D., Pehrsson, S., Wodicka, N. and de Kemp, E. 2009: The Paleoproterozoic Trans-Hudson Orogen: a prototype of modern accretionary processes; *in* Ancient Orogens and Modern Analogues, J.B. Murphy, J.D. Keppie and A.J. Hynes (ed.), Geological Society of London, Special Publications, v. 327, p. 457–479.

David, J., Bailes, A.H. and Machado, N. 1996: Evolution of the Snow Lake portion of the Palaeoproterozoic Flin Flon and Kisseynew belts, Trans-Hudson Orogen, Manitoba, Canada; Precambrian Research, v. 80, no. 1–2, p. 107–124.

Fedikow, M A.F., Nielsen, E., Conley, G.G. and Lenton, P.G. 2001: Operation Superior: kimberlite indicator mineral survey results (2000) for the northern half of the Knee Lake Greenstone Belt, Northern Superior Province, Manitoba (NTS 53M/1, 2, 3, 7 and 53L/15); Manitoba Industry, Trade and Mines, Geological Survey, Open File Report 2001-5, 57 p., URL <https://www.manitoba.ca/iem/info/library/downloads/quaternary_and_surficial_geology.html> [October 2025].

Frohlinger, T.G. 1974: Geology of the Kettle Rapids–Long Spruce Rapids area, Manitoba Department of Mines, Resources and Environmental Management, Mineral Resources Division, Exploration and Geological Survey Branch, Summary of Geological Field Work, 1974, Geological Paper 2/74, p. 21–25, URL <https://www.manitoba.ca/iem/info/libmin/GP2-74.pdf> [September 2025].

Gauthier, M.S. and Hodder, T.J. 2022: Kimberlite-indicator-mineral data derived from glacial sediments (till) in the western Fox River greenstone belt area, northeastern Manitoba (NTS 53M15, 16); Manitoba Natural Resources and Northern Development, Manitoba Geological Survey, Data Repository Item DRI2022010, Microsoft® Excel® file, URL <https://manitoba.ca/iem/info/libmin/DRI2022010.xlsx> [September 2025].

Gauthier, M.S., Breckenbridge, A. and Hodder, T.J. 2021: Patterns of ice recession and ice stream activity for the MIS 2 Laurentide Ice Sheet in Manitoba, Canada; Boreas, v. 51, no. 2, p. 274–298.

Gilbert, H.P., Syme, E.C. and Zwanzig, H.V. 1980: Geology of the metavolcanic and volcaniclastic metasedimentary rocks in the Lynn Lake area; Manitoba Energy and Mines, Mineral Resources Division, Geological Paper 80-1, 118 p., URL <https://www.manitoba.ca/iem/info/libmin/GP80-1.zip> [September 2025].

Gordon, T.M. 1989: Thermal evolution of the Kisseynew sedimentary gneiss belt, Manitoba: metamorphism at an early Proterozoic accretionary margin; *in* Evolution of Metamorphic Belts, J.S. Daly, R.A. Cliff and B.W.D. Yardley (ed.), Geological Society, v. 43, p. 233–243.

Gordon, T.M., Hunt, P.A., Bailes, A.H. and Syme, E.C. 1990: U-Pb ages from the Flin Flon and Kisseynew belts, Manitoba: chronology of crust formation at an Early Proterozoic accretionary margin; *in* The Early Proterozoic Trans-Hudson Orogen of North America, J.F. Lewry and M.R. Stauffer (ed.), Geological Association of Canada, Special Paper, v. 37, p. 177–199.

Growdon, M. L. 2010: Crustal development and deformation of Laurentia during the Trans-Hudson and Alleghenian Orogenies; Ph.D. thesis, Indiana University at Bloomington, Indiana, 236 p.

Hartlaub, R.P., Böhm, C.O., Heaman, L.M. and Simonetti, A. 2005: Northwestern Superior craton margin, Manitoba: an overview of Archean and Proterozoic episodes of crustal growth, erosion and orogenesis (parts of NTS 54D and 64A); *in* Report of Activities 2005, Manitoba Industry, Economic Development and Mines, Manitoba Geological Survey, p. 54-60, URL <https://www.manitoba.ca/iem/geo/field/roa05pdfs/GS-07.pdf> [September 2025].

Haugh, I. and Elphick, S C. 1968: Kettle Rapids–Moose Lake area, Manitoba Mines and Natural Resources, Mines Branch, Geological Survey of Manitoba, Summary of Geological Fieldwork, 1968, Geological Paper 3/68, p. 29–37, URL <https://www.manitoba.ca/iem/info/libmin/GP3-68.pdf> [September 2025].

Keller, G.R. 2019: Manitoba Kimberlite Indicator Mineral Database (version 3.2); Manitoba Growth, Enterprise and Trade, Manitoba Geological Survey, zipped Microsoft™ Access™ 2016 Database, URL <https://www.gov.mb.ca/iem/geo/diamonds/MBKIMDB_32.zip> [October 2025].

Lawley, C.J.M., Yang, X.M., Selby, D., Davis, W., Zhang, S., Petts, D.C. and Jackson, S.E. 2020: Sedimentary basin controls on orogenic gold deposits: new constraints from U-Pb detrital zircon and Re-Os sulphide geochronology, Lynn Lake greenstone belt, Canada; Ore Geology Reviews, v. 126, p. 21.

Lightfoot, P.C., Stewart, R., Gribbin, G. and Mooney, S.J. 2017: Relative contribution of magmatic and post-magmatic processes in the genesis of the Thompson Mine Ni-Co sulfide ores, Manitoba, Canada; Ore Geology Reviews, v. 83, p. 258–286.

Macdonald, J. and Janssens, J. 2025: Whole-rock lithogeochemistry and assays for samples collected from archived drillcore east of Stephens Lake, northeastern Manitoba (parts of NTS 54C, D); Manitoba Business, Mining, Trade and Job Creation, Manitoba Geological Survey, Data Repository Item DRI2025024, file format Excel®, URL <https://www.manitoba.ca/iem/info/libmin/DRI2025024.xlsx> [October 2025].

Machado, N., Zwanzig, H.V. and Parent, M. 1999: U-Pb ages of plutonism, sedimentation, and metamorphism of the Paleoproterozoic Kisseynew metasedimentary belt, Trans-Hudson Orogen (Manitoba, Canada); Canadian Journal of Earth Sciences, v. 36, no. 11, p. 1829–1842.

Manitoba Geological Survey 2024: Bedrock geology of Manitoba; Manitoba Economic Development, Investment and Trade, Manitoba Geological Survey, Open File OF2024-4, scale 1:1 000 000.

McLeneghan, M.B., Kjarsgaard, I.M., Averill, S.A., Layton-Matthews, D., Crabtree, D. and Matile, G. 2012: Indicator mineral signatures of magmatic Ni-Cu deposits, Thompson Nickel Belt, Manitoba: Part 1 - bedrock data; Geological Survey of Canada, Open File 6766, 43 p.

McLeneghan, M.B., Kjarsgaard, I.M., Averill, S.A., Layton-Matthews, D., Crabtree, D., Matile, G., McMartin, I. and Pyne, M. 2013: Indicator mineral signatures of magmatic Ni-Cu deposits, Thompson Nickel Belt, Manitoba: Part 2 - till data; Geological Survey of Canada, Open File 7200, 148 p.

Murphy, L.A. and Zwanzig, H.V. 2021: Geology of the Wuskwatim–Granville lakes corridor, Kisseynew domain, Manitoba (parts of NTS 63O, P, 64A–C); Manitoba Agriculture and Resource Development, Manitoba Geological Survey, Geoscientific Report GR2021-2, 105 p., URL <https://www.manitoba.ca/iem/info/libmin/GR2021-2.zip> [September 2025].

Nielsen, E. and Fedikow, M.A.F. 2002: Kimberlite indicator-mineral survey, lower Hayes River; Manitoba Industry, Trade and Mines, Manitoba Geological Survey, Geoscientific Paper 2002-1, 39 p., URL <https://www.manitoba.ca/iem/info/libmin/GP2002-1.zip> [September 2025].

Palin, R.M. and Dyck, B. 2021: Metamorphism of pelitic (Al-rich) rocks; *in* Encyclopedia of Geology, 2nd edition, A. Alderton and S.A. Elias (ed.), Elsevier, London, United Kingdom, p. 445–456, URL <https://doi.org/10.1016/B978-0-08-102908-4.00081-3>.

Pearce, J., Harris, N. and Tindle, A.G. 1984: Trace element discrimination diagrams for the tectonic interpretation of granitic rocks; Journal of Petrology, v. 25, p. 956–983.

Rinne, M.L. 2018: Summary of key results and interpretations from the Fox River belt compilation project, northeastern Manitoba (parts of NTS 53M, N, O, 54B, C, D); Manitoba Growth, Enterprise and Trade, Manitoba Geological Survey, p. 25–36, URL <https://www.manitoba.ca/iem/geo/field/roa18pdfs/GS2018-3.pdf> [September 2025].

Shervais, J.W. 1982: Ti-V plots and the petrogenesis of modern and ophiolitic lavas; Earth and Planetary Science Letters, v. 59, no. 1, p. 101–118.

Stauffer, M.R. 1990: The Missi Formation: an Aphebian molasse deposit in the Reindeer Lake Zone of the Trans-Hudson Orogen, Canada; *in* The Early Proterozoic Trans-Hudson Orogen of North America, J.F. Lewry and M.R. Stauffer (ed.), Geological Association of Canada, Special Paper, v. 37, p. 121–141.

Sun, S.-s. and McDonough, W.F. 1989: Chemical and isotopic systematics of oceanic basalts: implications for mantle composition and processes; *in* Magmatism in the Ocean Basins, A.D. Saunders and M.J. Norry (ed.), Geological Society, London, Special Publications, v. 42, p. 313–345, URL <https://doi.org/10.1144/GSL.SP.1989.042.01.19>.

Winchester, J.A. and Floyd, P.A. 1977: Geochemical discrimination of different magma series and their differentiation products using immobile elements; Chemical Geology, v. 20, p. 325–343.

Yang, X.M. 2025: Geochemical data of 737 whole-rock samples from the Lynn Lake greenstone belt, northwestern Manitoba (parts of NTS 64C10–12, 14–16); Manitoba Business, Mining, Trade and Job Creation, Manitoba Geological Survey, Data Repository Item DRI2025004, Microsoft® Excel® file, URL <https://www.manitoba.ca/iem/info/libmin/DRI2025004.xlsx> [September 2025].

Zwanzig, H.V. 1990: Kisseynew gneiss belt in Manitoba: stratigraphy, structure, and tectonic evolution; *in* The Early Proterozoic Trans-Hudson Orogen of North America, J.F. Lewry and M.R. Stauffer (ed.), Geological Association of Canada, Special Paper, v. 37, p. 95–120.

Zwanzig, H.V. 1999: Updated trace element geochemistry of ca. 1.9 Ga metavolcanic rocks in the Paleoproterozoic Lynn Lake belt; Manitoba Industry, Trade and Mines, Geological Services, Manitoba Geological Survey, Open File Report 99-13, URL <https://www.manitoba.ca/iem/info/libmin/OF99-13.zip> [October 2025]

Zwanzig, H.V. and Bailes, A.H. 2010: Geology and geochemical evolution of the northern Flin Flon and southern Kisseynew domains, Kississing-File lakes area, Manitoba (parts of NTS 63K, N); Manitoba Innovation, Energy and Mines, Manitoba Geological Survey, Geoscientific Report 2010-1, 135 p., URL <https://www.manitoba.ca/iem/info/libmin/GR2010-1.zip> [September 2025].

Zwanzig, H.V. and Böhm, C.O. 2004: Northern extension of the Thompson Nickel Belt, Manitoba (NTS 64A3 and 4); *in* Report of Activities 2004, Manitoba Industry, Economic Development and Mines, Manitoba Geological Survey, p. 115–119, URL <https://www.manitoba.ca/iem/geo/field/roa04pdfs/GS-10.pdf> [September 2025].

Zwanzig, H.V., Macek, J.J. and McGregor, C.R. 2007: Lithostratigraphy and geochemistry of the high-grade metasedimentary rocks in the Thompson nickel belt and adjacent Kisseynew Domain, Manitoba: implications for nickel exploration; Economic Geology, v. 102, no. 7, p. 1197–1216, URL <https://doi.org/10.2113/gsecongeo.102.7.1197>.

GS2025-8

Preliminary results of a broadband magnetotelluric survey over the interior Reindeer zone of the Trans-Hudson orogen, northern Manitoba (parts of NTS 63O, P, 64B, C, F)

by B. Lee[1] and V. Tschirhart[1]

In Brief:

- A new broadband magnetotelluric dataset was collected along more than 500 km of roads between Lynn Lake and Gillam
- The data are being analysed and will be used to study the deep crustal structure beneath the region's historic mining districts

Citation:
Lee, B. and Tschirhart, V. 2025: Preliminary results of a broadband magnetotelluric survey over the interior Reindeer zone of the Trans-Hudson orogen, northern Manitoba (parts of NTS 63O, P, 64B, C, F); *in* Report of Activities 2025, Manitoba Business, Mining, Trade and Job Creation, Manitoba Geological Survey, p. 87–93.

Summary

As part of the Government of Canada's Critical Minerals Geoscience and Data Initiative, a new profile of broadband magnetotelluric (MT) data was collected in 2025 across the interior Reindeer zone of the Trans-Hudson orogen in northern Manitoba. The MT data generally have an apparent resistivity above 1000 ohm-metre (Ω•m) at periods shorter than 1 s. The apparent resistivity decreases at periods longer than 1 s, approaching 1 Ω•m along certain sections of a northwest-southeast profile. The MT impedance phase data are consistent with a decrease in apparent resistivity at greater depths. The presence of out-of-quadrant phases and large phase tensor skew angles suggest that the underlying electrical resistivity structure cannot be approximated as a two-dimensional model. Future work will use three-dimensional modelling to more accurately model the data. The resulting resistivity model will be interpreted in conjunction with existing geological and geophysical data to inform future mineral exploration activities in the region.

Introduction

The Geological Survey of Canada aims to support Canada's responsible development of natural resources through the Critical Minerals Geoscience and Data (CMGD) Initiative. A major aspect of the CMGD Initiative is to advance foundational geoscience data to accelerate responsible exploration of critical minerals within Canada that are necessary for developing future technologies. As part of the CMGD Initiative, a broadband magnetotelluric (MT) survey was conducted over the Trans-Hudson orogen (THO) in northern Manitoba. The study area was chosen because the role of deep crustal structure in mineral endowment is poorly understood in the prominent mining districts of the Thompson nickel belt and the Lynn Lake domain. The goal of this project is to use broadband MT data, along with existing geological and geophysical datasets, to provide new insights into crustal-scale geological controls on critical mineral occurrences.

Geophysical methods are crucial to understanding geological structures at inaccessible depths. Regional-scale geophysical studies have proven useful for imaging deeper structures correlated to near-surface mineralization (Heinson et al., 2018; Roots et al., 2022; Tschirhart et al., 2022; Adetunji et al., 2023). Previously, regional-scale seismic reflection and MT surveys have been conducted over the THO as part of the LITHOPROBE program (e.g., Lewry et al., 1994; White et al., 2000; Ferguson et al., 2005; Jones et al., 2005). These studies revealed the regional geophysical signatures of the THO, namely the seismic reflectivity and electrical resistivity of domains involved in the Paleoproterozoic continental collision and crustal accretion. In the current study, new MT data collected over the interior Reindeer zone of the THO, between Thompson and Lynn Lake, is analyzed.

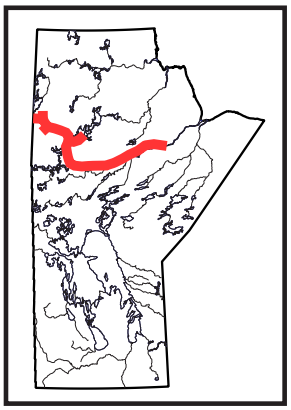

General geology

The THO provides a record of craton collision and mountain building between 1.92 and 1.80 Ga, now observed in the rock record from present-day Baffin Island to the north-central United States (Lewry and Stauffer, 1990; Ansdell, 2005; Corrigan et al., 2009). The THO can be broadly divided into Archean cratons (Superior, Wyoming, Rae, Sask and Hearne) and the Paleoproterozoic accretionary arc complexes of the Reindeer zone. The study area spans the Superior boundary zone, Kisseynew domain, Lynn Lake domain, Southern Indian domain and Chipewyan domain (Figure GS2025-8-1). The arc volcanic rocks of the Lynn Lake and Southern Indian domains were accreted to the Hearne craton margin ca. 1.92–1.86 Ga (e.g., Baldwin et al., 1987; Martins et al., 2022). The Superior boundary zone, which contains the Thompson nickel belt, contains Archean gneisses of the Superior craton

[1] Natural Resources Canada, Geological Survey of Canada, Ottawa, Ontario

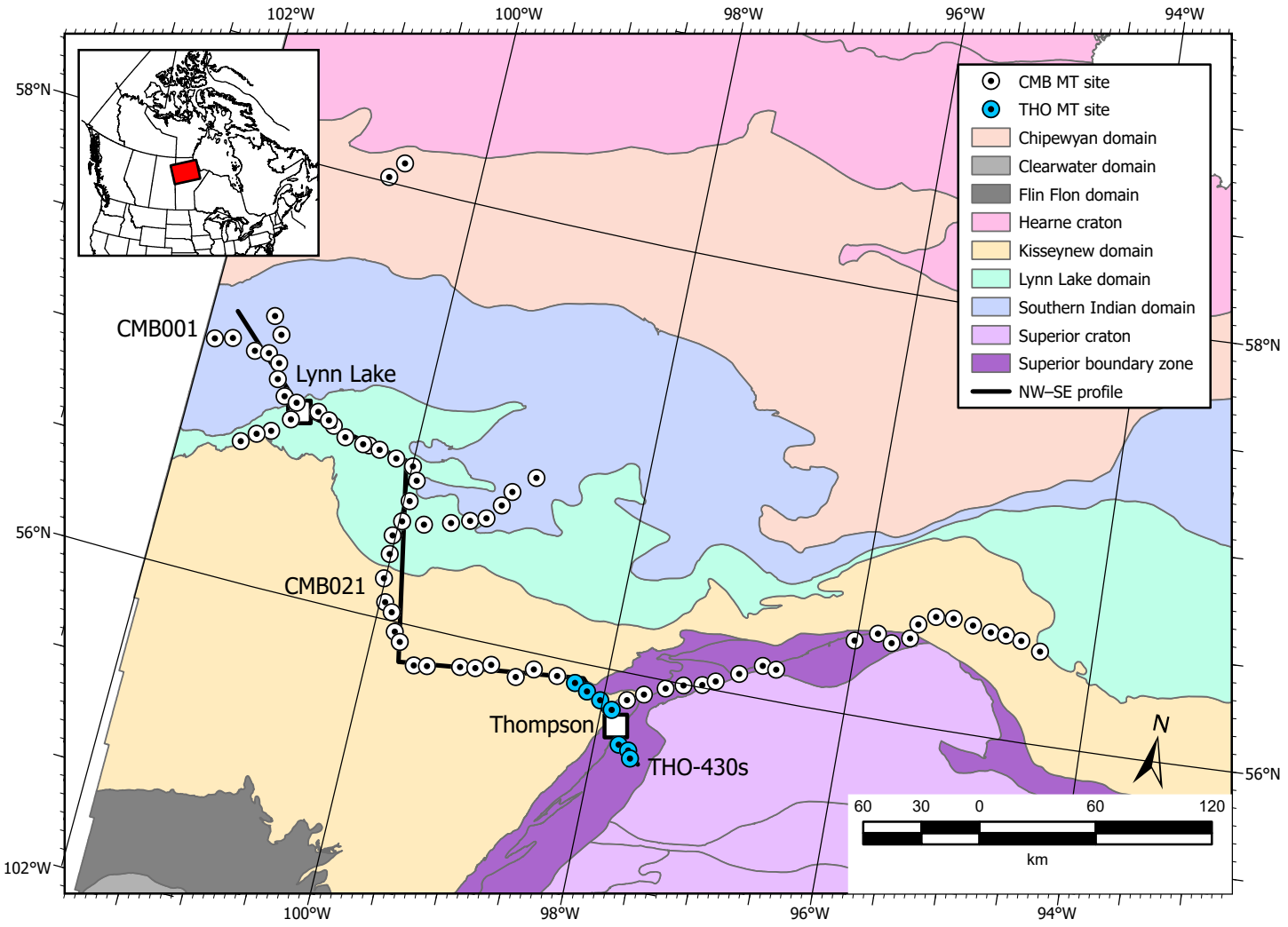

Figure GS2025-8-1:*Geological map of major lithotectonic domains in the study area. Thin grey lines indicate the boundaries of the subdomains within the Superior and Hearne cratons. White circles show locations of magnetotelluric (MT) sites deployed in 2025 and blue circles show MT sites deployed in 1994 as part of the LITHOPROBE program (Natural Resources Canada, 2022). Location of the northwest (NW)–southeast (SE) profile is shown with the names of three MT sites for reference (CMB001, CMB021, THO-430s; see Figures GS2025-8-2 to -6). Inset map shows the study area location within Manitoba. Geological data from Manitoba Geological Survey (2024).*

and Paleoproterozoic sedimentary units of the Ospwagan group, reworked during extensional magmatism on the Superior craton margin ca. 1.88–1.86 Ga (e.g., Bleeker, 1990; Zwanzig et al., 2007). The Kisseynew domain contains metasedimentary rocks intruded by felsic to intermediate plutons during basin inversion in the Manikewan Ocean ca. 1.85–1.84 Ga (e.g., Zwanzig, 1990). The Chipewyan domain consists predominantly of a continental-arc batholith that was emplaced ca. 1.86–1.85 Ga in the Hearne craton margin and also intruded the accreted arc assemblages of the Lynn Lake and Southern Indian domains (e.g., Meyer et al., 1992).

Methodology

Magnetotellurics is a passive electromagnetic geophysical method sensitive to the electrical conductivity of the Earth. Magnetotellurics is a flexible method that can be used in a variety of applications from shallow upper-crustal exploration to deep lower-crustal studies. The focus of this study was the crust from a depth of 0 to 50 km, similar in scope to previous MT studies performed over the THO. This is the first regional-scale study of the interior Reindeer zone aside from seven MT sites over the THO–Superior boundary zone deployed under the LITHOPROBE program (blue circles in Figure GS2025-8-1). The new MT data were collected by Quantec Geoscience from 69 sites in the winter of 2025. Data were measured overnight at each site and processed with the remote reference method. A second phase of data collection on the Chipewyan domain and crossing the THO–Hearne craton boundary is planned for the winter of 2026.

New broadband magnetotelluric data

The processed MT data are of overall high quality and are displayed as apparent resistivity and phase pseudosections in Figures GS2025-8-2 to -5. The vertical axis in the pseudosections corresponds to the signal period in seconds, which can

be considered a proxy for depth (i.e., longer period signals penetrate deeper into the Earth). As a routine exercise with MT data, some data points have been masked at the longest periods where the recording time was insufficient to obtain a precise estimate of apparent resistivity and phase. The displayed data are from MT sites along the northwest-southeast profile shown in Figure GS2025-8-1. The remaining sites to the east on the Kisseynew domain–Superior boundary zone will be analyzed in a future study.

Figure GS2025-8-2 shows the apparent resistivity of the xy component, corresponding to an electric field aligned with geographic north and a magnetic field aligned with geographic east. The apparent resistivity is generally high (>1000 Ω•m) at periods shorter than 1 s. A low apparent resistivity is observed at longer periods (>1 s) at sites on the Southern Indian domain and on

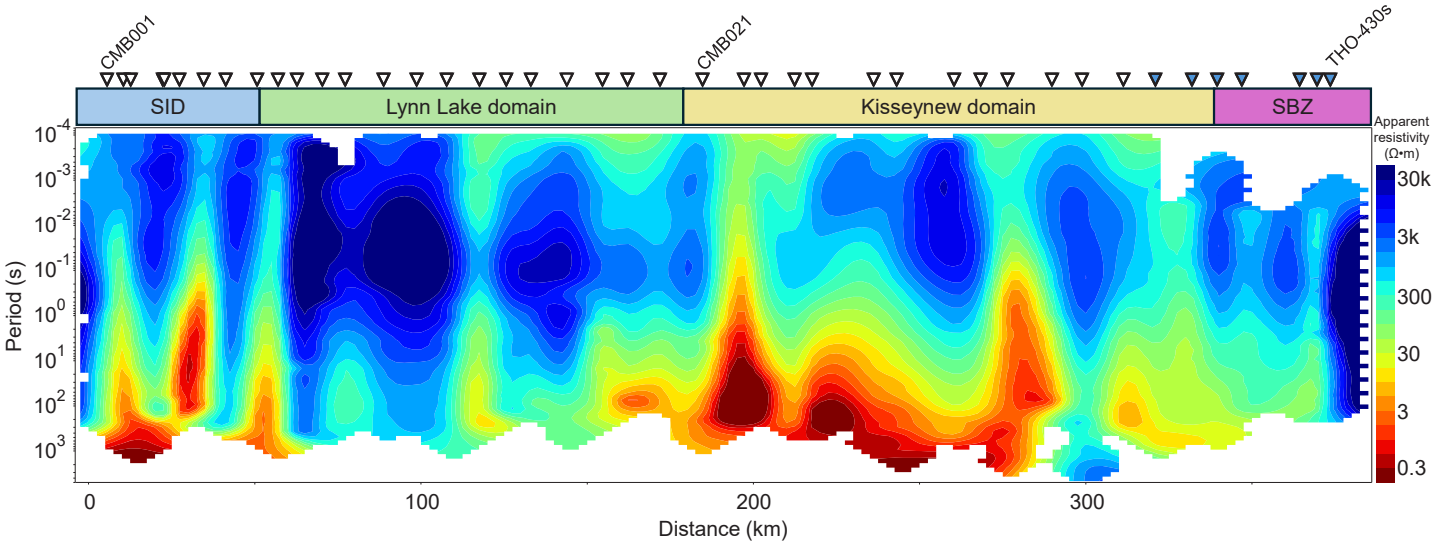

Figure GS2025-8-2: *Pseudosection of the xy component of magnetotelluric (MT) apparent resistivity along the profile shown in Figure GS2025-8-1. Cooler (blue) colours indicate higher apparent resistivity, warmer (red) colours indicate lower apparent resistivity. The xy component corresponds to an electric field aligned with geographic north and a magnetic field aligned with geographic east. Projected locations of MT sites are shown as inverted black triangles. Three MT sites are labelled for reference (CMB001, CMB021, THO-430s; see Figure GS2025-8-1 for locations). Abbreviations: Ω•m, ohm-metre; k, thousand; SBZ, Superior boundary zone; SID, Southern Indian domain.*

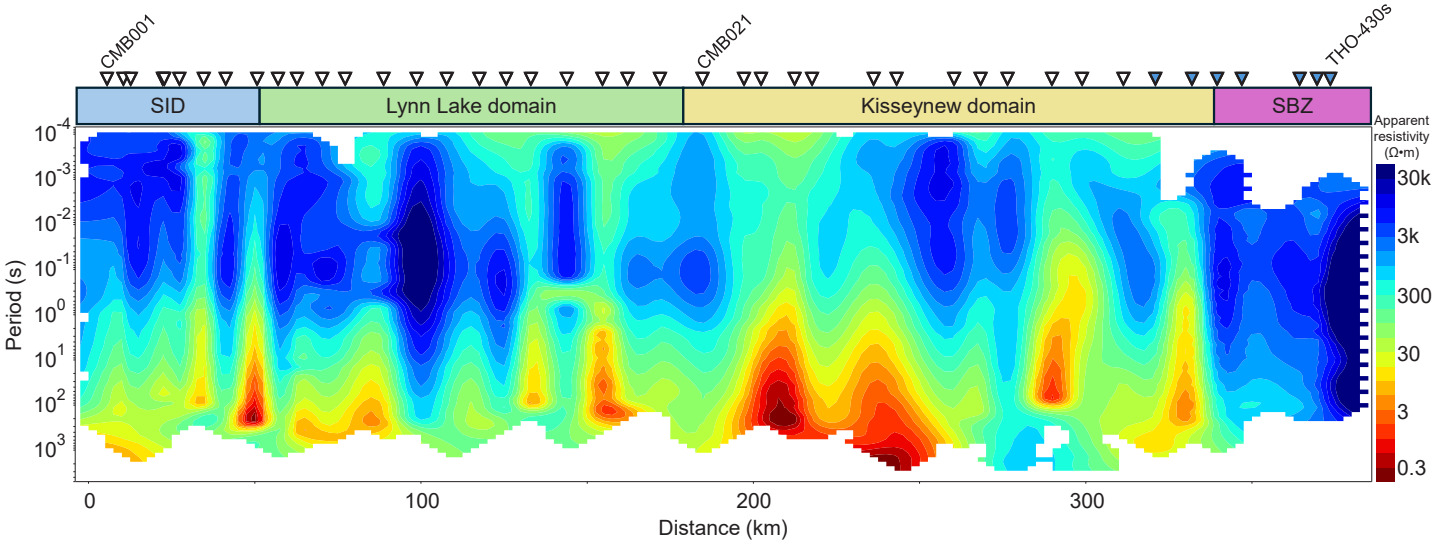

Figure GS2025-8-3: *Pseudosection of the yx component of magnetotelluric (MT) apparent resistivity along the profile shown in Figure GS2025-8-1. Cooler (blue) colours indicate higher apparent resistivity, warmer (red) colours indicate lower apparent resistivity. The yx component corresponds to an electric field aligned with geographic east and a magnetic field aligned with geographic north. Projected locations of MT sites are shown as inverted black triangles. Three MT sites are labelled for reference (CMB001, CMB021, THO-430s; see Figure GS2025-8-1 for locations). Abbreviations: Ω•m, ohm-metre; k, thousand; SBZ, Superior boundary zone; SID, Southern Indian domain.*

the Kisseynew domain (at approximately 0 to 60 km and 180 to 300 km, respectively; Figures GS2025-8-2 to -6). Figure GS2025-8-3 shows the apparent resistivity of the yx component, which is calculated from the electric field aligned with geographic east and the magnetic field aligned with geographic north. The same general trend can be seen as with the xy apparent resistivity, with high apparent resistivity at periods of shorter than 1 s and lower apparent resistivity at periods longer than 1 s.

Figures GS2025-8-4 and -5 show the phase angle computed for the xy and yx components, respectively. Note that 180 degrees has been added to the yx phase to simplify the comparison with the xy phase. Unlike the apparent resistivity data,

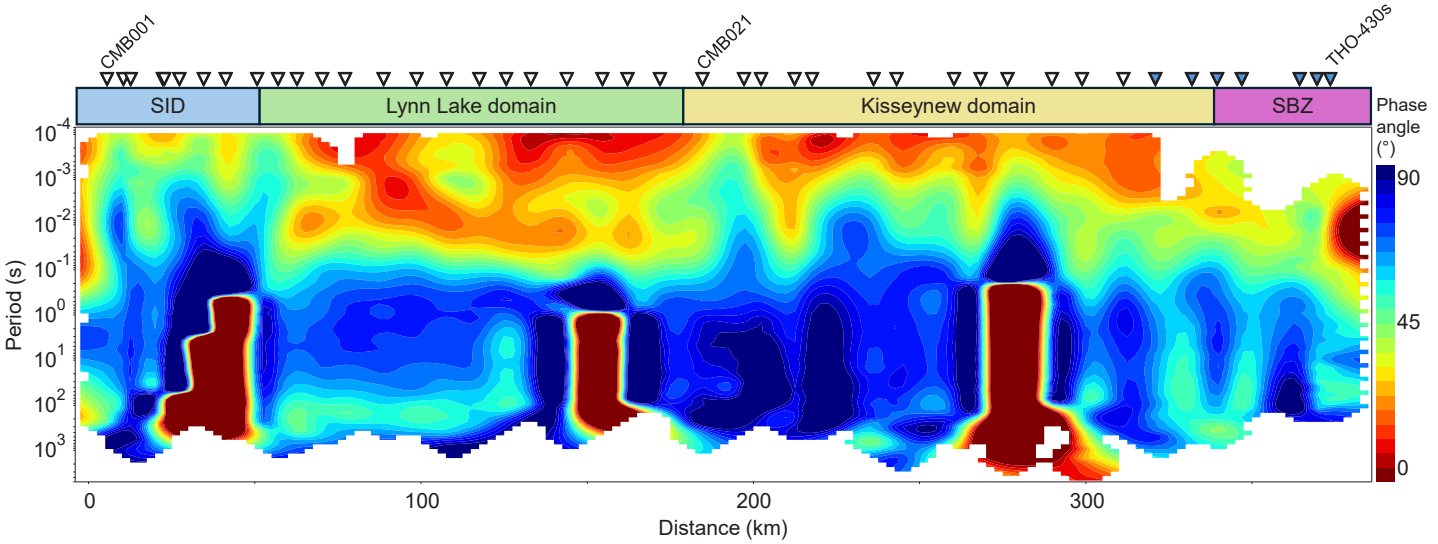

Figure GS2025-8-4: *Pseudosection of the xy component of magnetotelluric (MT) impedance phase angle along the profile shown in Figure GS2025-8-1. Cooler (blue) colours indicate higher phase angle, warmer (red) colours indicate lower phase angle. Phase angle between 45° and 90° indicates decreasing apparent resistivity with period, phase angle between 0° and 45° indicates increasing apparent resistivity with period. The xy component corresponds to an electric field aligned with geographic north and a magnetic field aligned with geographic east. Projected locations of MT sites are shown as inverted black triangles. Three MT sites are labelled for reference (CMB001, CMB021, THO-430s; see Figure GS2025-8-1 for locations). Abbreviations: SBZ, Superior boundary zone; SID, Southern Indian domain.*

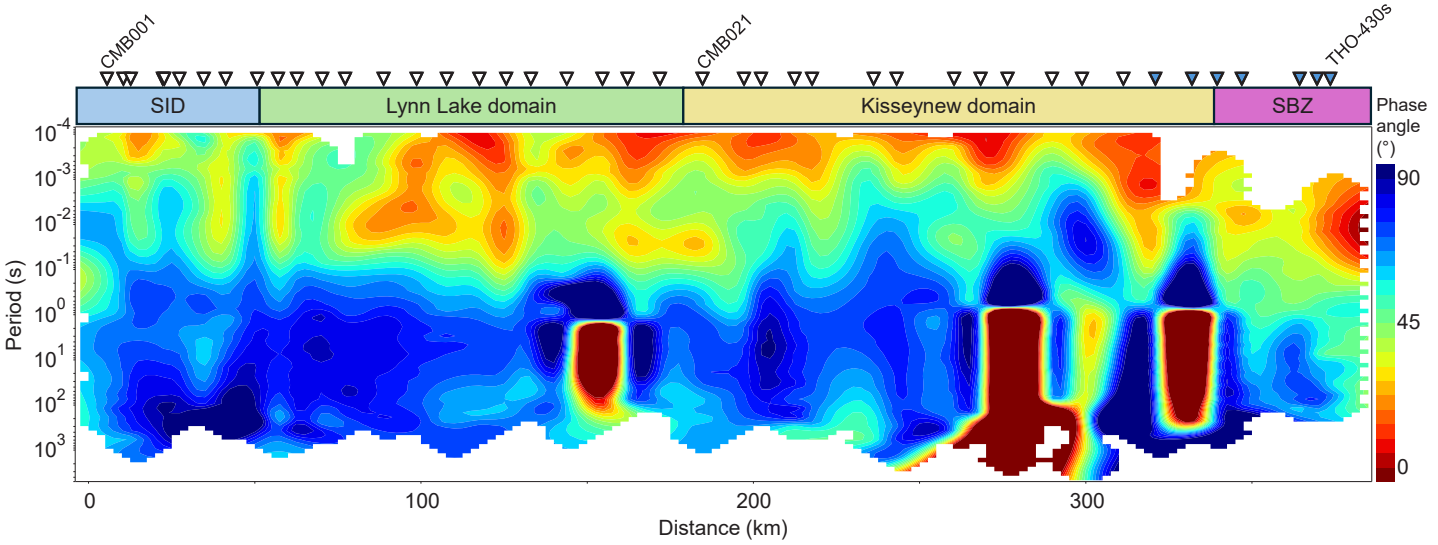

Figure GS2025-8-5: *Pseudosection of the yx component of magnetotelluric (MT) impedance phase angle along the profile shown in Figure GS2025-8-1. Cooler (blue) colours indicate higher phase angle, warmer (red) colours indicate lower phase angle. Phase angle between 45° and 90° indicates decreasing apparent resistivity with period, phase angle between 0° and 45° indicates increasing apparent resistivity with period. The yx component corresponds to an electric field aligned with geographic east and a magnetic field aligned with geographic north. Note that 180 ° has been added to the yx phase to simplify the comparison with the xy phase. Projected locations of MT sites are shown as inverted black triangles. Three MT sites are labelled for reference (CMB001, CMB021, THO-430s; see Figure GS2025-8-1 for locations). Abbreviations: SBZ, Superior boundary zone; SID, Southern Indian domain.*

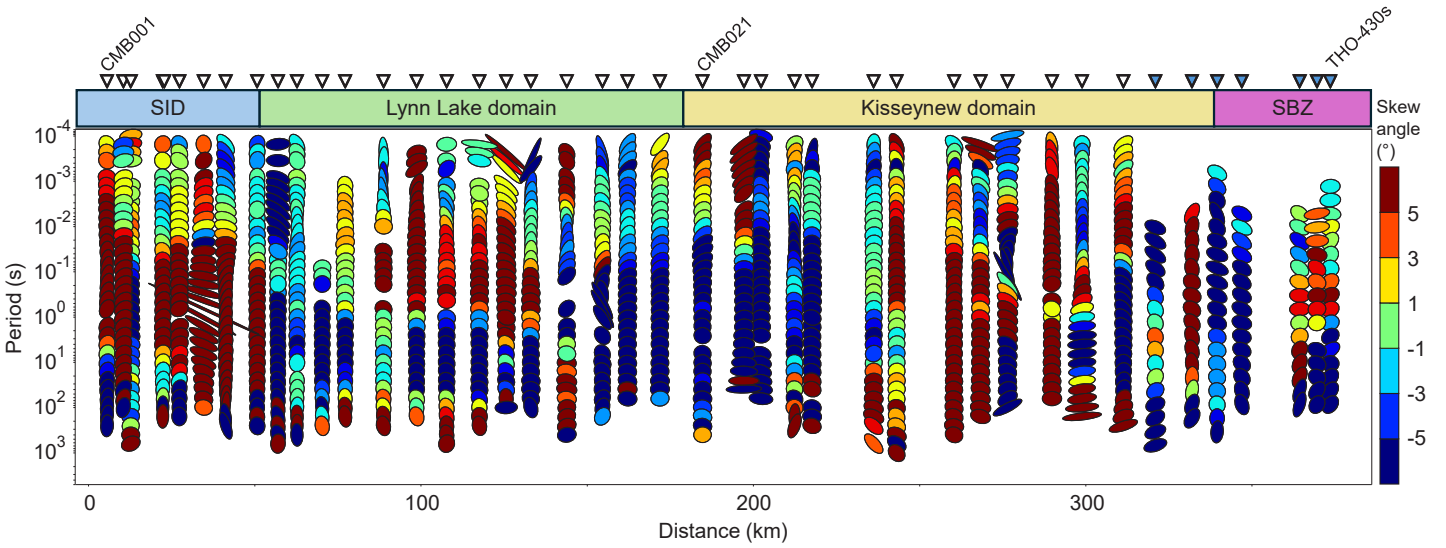

Figure GS2025-8-6: *Pseudosection of magnetotelluric (MT) phase tensor ellipses along the profile shown in Figure GS2025-8-1. Phase tensor ellipse fill colour corresponds to the skew angle (β), where β = 0 indicates 1-D geoelectrical structure. Length of ellipse principal axes corresponds to the degree of phase split in orthogonal directions, i.e., due to 2-D/3-D structure or electrical anisotropy. The ellipse at every second period is omitted for clarity. Projected locations of MT sites are shown as inverted black triangles. Three MT sites are labelled for reference (CMB001, CMB021, THO-430s; see Figure GS2025-8-1 for locations). Abbreviations: SBZ, Superior boundary zone; SID, Southern Indian domain.*

the phase data are not susceptible to local anomalies in electric field amplitude (i.e., static shifts), which appear as vertical stripes in the apparent resistivity pseudosections (e.g., at 150 km in Figure GS2025-8-3). The xy and yx phases are generally less than 45 degrees at periods shorter than 0.1 s, indicative of an increasing apparent resistivity as a function of period. At periods longer than 1 s, the xy and yx phases are mostly greater than 45 degrees, which represents decreasing apparent resistivity as a function of period. A few sites have phases outside of their typical quadrants (dark red in Figures GS2025-8-4, -5), a phenomenon known as out-of-quadrant phase, which can be caused by strong resistivity contrasts, complicated 3-D resistivity structure or electrical anisotropy (Heise and Pous, 2003; Lezaeta and Haak, 2003). Therefore, a 2-D anisotropic inversion code or 3-D inversion code is required to accurately model the out-of-quadrant phase data.

A pseudosection of the MT phase tensor data (Caldwell et al., 2004) is shown in Figure GS2025-8-6. The phase tensor provides information on the dimensionality of the MT data, which determines which type of modelling is appropriate for the dataset (2-D or 3-D). The phase tensor can be displayed as an ellipse at each period, with the principal axes oriented according to the direction of the regional induction current. For a 1-D Earth where there is no defined geoelectric strike direction, the principal axes are equal in length, and the ellipse is a circle. Alternatively, an elongated ellipse with principal axes of different lengths indicates the presence of 2-D/3-D structure or electrical anisotropy. In Figure GS2025-8-6, each phase tensor ellipse is filled with a colour corresponding to the skew angle (β), which is a measure of the phase tensor asymmetry. The skew angle for an ideal 2-D Earth is equal to zero; thus, many MT studies have used the skew angle to determine whether the underlying resistivity structure can be approximated as 2-D (Booker, 2014). If the 2-D approximation can be justified, then a 2-D inversion algorithm is suitable for modelling the MT data. The threshold of an acceptable skew angle for the 2-D approximation is subjective, but a threshold of $|\beta|<3^{\circ}$has been widely used, with some caveats (i.e., Booker, 2014). As seen in Figure GS2025-8-6, the majority of MT sites do not meet the condition of $|\beta|<3^{\circ}$, especially at the long periods, which are sensitive to the deepest resistivity structures. The sites and periods with a large skew magnitude are also spatially correlated with the previously shown out-of-quadrant phases in Figures GS2025-8-4 and -5. The orientations of phase tensor ellipse axes vary considerably between sites, which further suggests a 2-D approximation cannot be used for the entire study area as there is changing geoelectric structure between different geological domains. Therefore, a 3-D approach will be employed in future work as a 2-D analysis of the data would not produce reliable results.

Future work

After preliminary analysis of the newly collected MT data, the next step is to use an inversion algorithm to obtain an electrical resistivity model consistent with the MT data. As evidenced by the out-of-quadrant phases and high phase tensor skew angles, the regional resistivity structure cannot be approximated as 2-D. If carefully used, a 3-D inversion algorithm can be used to model MT data collected along a profile (e.g., Siripunvaraporn et al., 2005). The interpretation of the electrical resistivity model will be integrated with previous geological and geophysical data,

including a seismic reflection profile collected along the same highway above the Kisseynew, Lynn Lake and Southern Indian domains (White et al., 2000).

Economic considerations

A new broadband MT dataset has been collected over the interior Reindeer zone of the THO, which will help to elucidate the regional electromagnetic signature, similar to what the LITHOPROBE transects over other parts of the THO have done in the past. The new MT profile crosses the historic Lynn Lake and Thompson mining areas and will provide new information to de-risk future exploration activities in the area, including highlighting potential deep-seated structures that may be related to critical mineral endowment and pointing out additional areas of interest. The MT studies targeting the entire crustal depth range, such as those conducted as part of the Metal Earth program over the Superior Craton (Adetunji et al., 2023, 2025; Smith et al., 2023), have shown an improved knowledge of deep crustal features is crucial as they may be spatially and temporally linked to near-surface mineral occurrences.

Acknowledgments

The authors thank T. Martins for assistance in co-ordinating magnetotelluric site locations, as well as J. Marks, K. Reid and S.M. Ansari for their reviews, which improved this manuscript. The magnetotelluric data used in this study were collected by Quantec Geoscience. This study was supported by the Critical Minerals Geoscience and Data (CMGD) Initiative of the Geological Survey of Canada.

References

Adetunji, A.Q., Ferguson, I.J., Simmons, J.M., Ma, C., Cheraghi, S., Snyder, D.B. and Ayer, J.A. 2025: Trans-crustal geophysical responses beneath the supergiant Timmins-Porcupine orogenic gold camp, Canada; Journal of Geophysical Research: Solid Earth, v. 130, no. 3, art. e2024JB028839.

Adetunji, A.Q., Launay, G., Ferguson, I.J., Simmons, J.M., Ma, C., Ayer, J. and Lafrance, B. 2023: Crustal conductivity footprint of the orogenic gold district in the Red Lake greenstone belt, western Superior craton, Canada; Geology, v. 51, no. 4, p. 377–382.

Ansdell, K.M. 2005: Tectonic evolution of the Manitoba-Saskatchewan segment of the Paleoproterozoic Trans-Hudson orogen, Canada; Canadian Journal of Earth Sciences, v. 42, no. 4, p. 741–759.

Baldwin, D.A., Syme, E.C., Zwanzig, H.V., Gordon, T.M., Hunt, P.A. and Stevens, R.D. 1987: U–Pb zircon ages from the Lynn Lake and Rusty Lake metavolcanic belts, Manitoba: two ages of Proterozoic magmatism; Canadian Journal of Earth Sciences, v. 24, no. 5, p. 1053–1063.

Bleeker, W. 1990: New structural-metamorphic constraints on Early Proterozoic oblique collision along the Thompson Nickel Belt, Manitoba, Canada; *in* The Early Proterozoic Trans-Hudson Orogen of North America, J.F. Lewry and M.R. Stauffer (ed.), Geological Association of Canada, Special Paper 37, p. 57–73.

Booker, J.R. 2014: The magnetotelluric phase tensor: a critical review; Surveys in Geophysics, v. 35, no. 1, p. 7–40.

Caldwell, T.G., Bibby, H.M. and Brown, C. 2004: The magnetotelluric phase tensor; Geophysical Journal International, v. 158, no. 2, p. 457–469.

Corrigan, D., Pehrsson, S., Wodicka, N. and De Kemp, E. 2009: The Palaeoproterozoic Trans-Hudson Orogen: a prototype of modern accretionary processes; *in* Ancient Orogens and Modern Analogues, J.B. Murphy, J.D. Keppie and A.J. Hynes (ed.), Geological Society of London, Special Publications, v. 327, p. 457–479.

Ferguson, I.J., Stevens, K.M. and Jones, A.G. 2005: Electrical-resistivity imaging of the central Trans-Hudson orogen; Canadian Journal of Earth Sciences, v. 42, no. 4, p. 495–515.

Heinson, G., Didana, Y., Soeffky, P., Thiel, S. and Wise, T. 2018: The crustal geophysical signature of a world-class magmatic mineral system; Scientific Reports, v. 8, no. 1, art. 10608.

Heise, W. and Pous, J. 2003: Anomalous phases exceeding 90° in magnetotellurics: anisotropic model studies and a field example; Geophysical Journal International, v. 155, no. 1, p. 308–318.

Jones, A.G., Ledo, J. and Ferguson, I.J. 2005: Electromagnetic images of the Trans-Hudson orogen: the North American Central Plains anomaly revealed; Canadian Journal of Earth Sciences, v. 42, no. 4, p. 457–478.

Lewry, J.F. and Stauffer, M.R., ed. 1990: The Early Proterozoic Trans-Hudson orogen of North America; Geological Association of Canada, Special Paper 37, 505 p.

Lewry, J.F., Hajnal, Z., Green, A., Lucas, S.B., White, D., Stauffer, M.R., Ashton, K.E., Weber, W. and Clowes, R. 1994: Structure of a Paleoproterozoic continent-continent collision zone: a LITHOPROBE seismic reflection profile across the Trans-Hudson Orogen, Canada; Tectonophysics, v. 232, no. 1–4, p. 143–160.

Lezaeta, P. and Haak, V. 2003: Beyond magnetotelluric decomposition: induction, current channeling, and magnetotelluric phases over 90; Journal of Geophysical Research: Solid Earth, v. 108, no. B6, art. 2305.

Manitoba Geological Survey 2024: Bedrock geology of Manitoba; Manitoba Economic Development, Investment, Trade and Natural Resources, Manitoba Geological Survey, Open File OF2024-4, scale 1:1 000 000.

Martins, T., Rayner, N., Corrigan, D. and Kremer, P. 2022: Regional geology and tectonic framework of the Southern Indian domain, Trans-Hudson orogen, Manitoba; Canadian Journal of Earth Sciences, v. 59, no. 6, p. 371–388.

Meyer, M.T., Bickford, M.E. and Lewry, J.F. 1992: The Wathaman batholith: an Early Proterozoic continental arc in the Trans-Hudson orogenic belt, Canada; Geological Society of America Bulletin, v. 104, no. 9, p. 1073–1085.

Natural Resources Canada 2022: Lithoprobe THOT Transect MT; 108 sites from THOT thot92; magnetotelluric; *in* Geological Survey of Canada, Seismic and Magnetotelluric Data, Natural Resources Canada, URL <https://search.open.canada.ca/opendata> [October 2025].

Roots, E.A., Hill, G.J., Frieman, B.M., Wannamaker, P.E., Maris, V., Calvert, A.J., Craven, J.A., Smith, R.S. and Snyder, D.B. 2022: Magmatic, hydrothermal and ore element transfer processes of the southeastern Archean Superior Province implied from electrical resistivity structure; Gondwana Research, v. 105, p. 84–95.

Siripunvaraporn, W., Egbert, G. and Uyeshima, M. 2005: Interpretation of two-dimensional magnetotelluric profile data with three-dimensional inversion: synthetic examples; Geophysical Journal International, v. 160, no. 3, p. 804–814.

Smith, R.S., Naghizadeh, M., Cheraghi, S., Adetunji, A., Vayavur, R., Eshaghi, E., Hill, G.J., Snyder, D., Roots, E.A., Justina, F.D. and Fam, H.J.A. 2023: Geophysical transects in the Abitibi greenstone belt of Canada from the mineral-exploration-oriented Metal Earth project; The Leading Edge, v. 42, no. 4, p. 245–255.

Tschirhart, V., Potter, E.G., Powell, J.W., Roots, E.A. and Craven, J.A. 2022: Deep geological controls on formation of the highest-grade uranium deposits in the world: magnetotelluric imaging of unconformity-related systems from the Athabasca Basin, Canada; Geophysical Research Letters, v. 49, no. 15, art. e2022GL098208.

White, D.J., Zwanzig, H.V. and Hajnal, Z. 2000: Crustal suture preserved in the Paleoproterozoic Trans-Hudson orogen, Canada; Geology, v. 28, no. 6, p. 527–530.

Zwanzig, H.V. 1990: Kisseynew Gneiss Belt in Manitoba: stratigraphy, structure, and tectonic evolution; *in* The Early Proterozoic Trans-Hudson Orogen of North America, J.F. Lewry and M.R. Stauffer (ed.), Geological Association of Canada, Special Paper 37, p. 95–120.

Zwanzig, H.V., Macek, J.J. and McGregor, C.R. 2007: Lithostratigraphy and geochemistry of the high-grade metasedimentary rocks in the Thompson Nickel Belt and adjacent Kisseynew Domain, Manitoba: implications for nickel exploration; Economic Geology, v. 102, no. 7, p. 1197–1216.

GS2025-9

Expanded long-period magnetotelluric data coverage over the Trans-Hudson orogen in southwestern Manitoba (NTS 62N, O, J, G, F, K, parts of 63C, B)

by B.F.W. Chase[1], M.J. Unsworth[1], K. Moshtaghian[1], A. Redanz[1], J. Marks, A. Williamson[1], Z. Vestrum[1] and S. Palmers[1]

In Brief:

- Long-period magnetotelluric coverage in Manitoba was expanded southward to the US border
- The data will be used to produce a 3-D resistivity model of the lithosphere, and conductive anomalies will be interpreted within the mineral systems framework
- The data and resistivity model will serve as regional reconnaissance tools for mineral exploration in the province

Citation:
Chase, B.F.W., Unsworth, M.J., Moshtaghian, K., Redanz, A., Marks, J., Williamson, A., Vestrum, Z. and Palmers, S. 2025: Expanded long-period magnetotelluric data coverage over the Trans-Hudson orogen in southwestern Manitoba (NTS 62N, O, J, G, F, K, parts of 63C, B); *in* Report of Activities 2025, Manitoba Business, Mining, Trade and Job Creation, Manitoba Geological Survey, p. 94–103.

Summary

Information about the structure of the deep lithospheric mantle cannot be obtained from drilling and requires geophysical exploration. One of the most useful methods for this task is magnetotelluric exploration, which uses natural low-frequency radio signals to determine the electrical resistivity structure of the Earth to depths in excess of 200 km. The Manitoba Geological Survey, in collaboration with the University of Alberta, is continuing to develop a 3-D resistivity model of the deep lithospheric structure beneath the province. In 2024, long-period magnetotelluric (LMT) data were collected at 22 stations in west-central Manitoba. In 2025, LMT data were collected at an additional 13 stations in southwestern Manitoba with the goal of extending coverage over the boundary between the Trans-Hudson orogen and the Superior craton as far south as the border with the United States. The new LMT data will be combined with previously collected data in Saskatchewan and Manitoba to produce a 3-D resistivity model of the Trans-Hudson orogen beneath the provinces. The goal of developing the 3-D resistivity model is to improve the understanding of the deep lithospheric structure and how it may be used for predicting and analyzing the spatial distribution of mineralization. Ultimately, these LMT data and the resulting 3-D resistivity model would help to guide future mineral exploration in the province.

Introduction

The basement rocks of Manitoba include part of the eastern margin of the Trans-Hudson orogen (THO) and the boundary between the THO and the Superior craton (Figure GS2025-9-1). This part of Laurentia was assembled during the closure of the Manikewan Ocean in the Proterozoic ca. 1.9–1.8 Ga (Whitmeyer and Karlstrom, 2007). Terranes mapped in this region include the Flin Flon belt, the Lynn Lake–La Ronge belt and the Superior boundary zone and several subdomains of the Superior province (e.g., Superior craton; Figure GS2025-9-1). All of these terranes are associated with significant mineral endowment and host numerous active and historical mines. A relatively brief geological overview is provided by Chase et al. (2024) as part of prior data collection efforts in the THO. For more information, interested readers are directed to the work of Bleeker (1990), Lewry and Collerson (1990), Machado (1990), Weber (1990), Ansdell et al. (1995), Bleeker et al. (1995), Conners et al. (1999), Syme et al. (1999), Whalen et al. (1999), Percival et al. (2006, 2012), Zwanzig et al. (2007) and Clowes and Roy (2020).

The current understanding of the deep lithospheric structure of the THO is derived from geophysical studies that have used seismic, magnetotelluric (MT) and potential-field exploration methods (e.g., Jones et al., 2005; White et al., 2005). The depth of exploration in these previous studies has been largely limited to the crust. As a result, there is limited information about the deeper lithospheric mantle of the THO. Additionally, these geophysical studies have generally used 2-D approaches for data analysis, which provides limited information about the along-strike variability of the structure of the THO (e.g., White et al., 2002). In past studies, the structural complexity of the THO has led to differing interpretations of fundamental features such as the polarity of subduction (e.g., White et al., 2002). In the United States, 3-D modelling of deep-imaging, whole-lithosphere–scale geophysical data has helped improve understanding of the structure of the southern THO (from lat. 43 to 49°N) and has highlighted how the shallow complex crustal structure may overprint and obscure earlier structures at greater depths (Ye et al., 2019; Bedrosian and Finn, 2021). These data have provided greater insights into the tectonic evolution of the THO. Additionally, these geophysical data have suggested that several of the tectonic terranes associated with mineralization in Manitoba (e.g., the Flin Flon

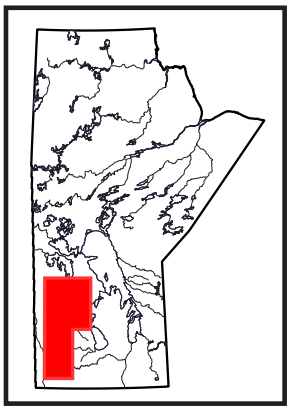

[1] Department of Physics, University of Alberta, Edmonton, Alberta

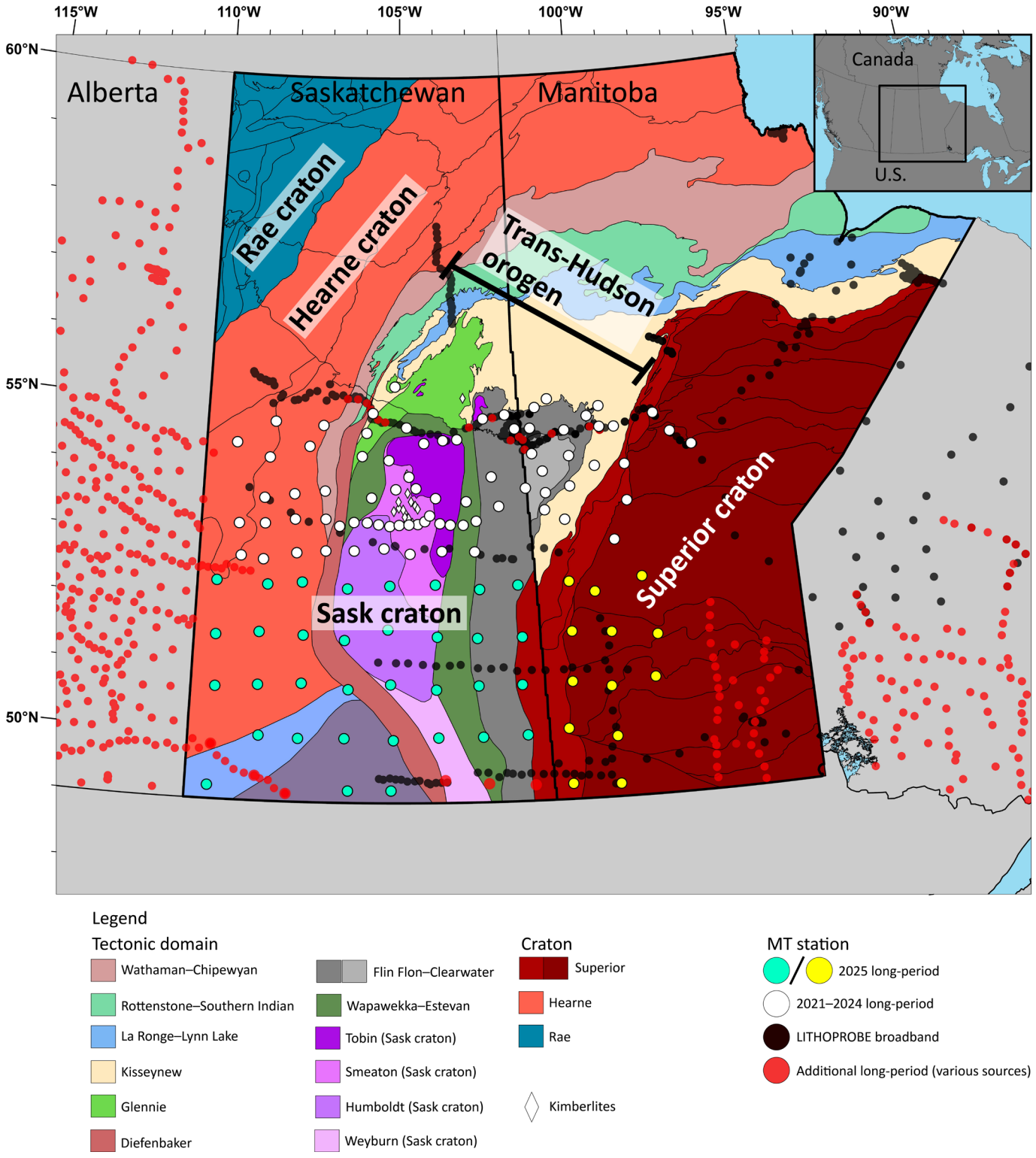

Figure GS2025-9-1: *Lithotectonic units of Manitoba and Saskatchewan. The Trans-Hudson orogen is composed of the various lithotectonic units between the Hearne and Superior cratons. Thin black lines indicate the boundaries of the subdomains within the Superior, Hearne and Rae cratons. Magnetotelluric (MT) data coverage is shown for the region (University of Alberta, unpublished data, 2024). Note that the additional long-period magnetotelluric (LMT) stations in Alberta represent stations where the data were collected for the LITHOPROBE program or by the University of Alberta, whereas in the rest of Canada, data were collected for the LITHOPROBE program and some smaller studies. The 2025 LMT stations in Manitoba are shown as yellow dots (also see Figure GS2025-9-4). The 2025 LMT stations in Saskatchewan, deployed as part of a companion survey, are shown as teal dots. The 2021–2024 LMT data were collected as part of the work of Chase and Unsworth (2024) and Chase et al. (2024). Data from the stations around the 2021–2025 LMT stations will also be used to create the 3-D resistivity model of the lithosphere of the Trans-Hudson orogen in this area. Manitoba lithotectonic units modified after Manitoba Geological Survey (2022). Saskatchewan lithotectonic units modified after Saskatchewan Energy and Resources (2021).*

terrane) continue south well into the United States (Bedrosian and Finn, 2021). This suggests that additional mineralization may be present further south in the basement beneath the Western Canada Sedimentary Basin. To improve the understanding of the structure of the THO and extent of additional mineralization in Canada, 3-D geophysical datasets with the capability of imaging the entire lithosphere are required.

The MT method is particularly well suited for imaging mineral systems because it is sensitive to conductive anomalies, which are commonly associated with the ore-related minerals and regions altered by the passage of mineralizing fluids during tectonic processes (e.g., Heinson et al., 2018; Kirkby et al., 2022; Chase and Unsworth, 2024). In particular, the long-period magnetotelluric (LMT) method is capable of imaging the entire lithosphere and the deep structure around regional mineral deposits and mining districts thus it was used for this project to help predict and analyze the spatial distribution of mineralization in Manitoba. Any major conductors identified in the lithosphere can be incorporated within a mineral systems framework to aid mineral exploration at a regional scale. The mineral systems framework is an emerging technique in exploration that is focused on understanding how mineralization develops from the deposit to the regional scale. In this framework, the individual deposit is treated as a small end-product of processes that operate on much larger spatial and temporal scales. A major focus of the mineral systems framework is determining the genesis, ascent and localization of mineralizing fluids throughout the lithosphere (McCuaig et al., 2010; McCuaig and Hronsky, 2014). In practice, to do this requires the use of regional deep-imaging geophysical methods. The data collected can then be used to determine which areas, both brownfield and greenfield, may have enhanced mineral potential. The LMT data are capable of imaging the entire lithosphere, and from a geophysical perspective, are well-suited for use in the mineral systems framework at the camp- to regional-scale (Figure GS2025-9-2).

The questions that the 2025 LMT dataset is intended to address include

- What is the electrical resistivity structure of the eastern margin of the THO and adjacent area of the Superior craton in Manitoba, extending as far south as the border with the United States?
- Are there additional low resistivity anomalies that may be associated with mineralization along the eastern margin of the THO?

Previous studies

The following section presents text first presented in Chase et al. (2024). Geophysical studies of the deep lithospheric structure of the THO in Canada have taken place since the 1980s through the LITHOPROBE program (Clowes et al., 1999). The LITHOPROBE program collected multiple seismic reflection, seismic refraction and MT profiles across the THO (Figure GS2025-9-1). The seismic datasets were used to delineate terrane boundary zones and determine the direction of subduction during closure of the Manikewan Ocean (e.g., Ansdell, 2005; White et al., 2005). The MT datasets were used in a similar manner and identified a northward extension of the North American central plains conductor, a crustal anomaly (or break) that is related to the suture zone observed in the THO both in the United States and Canada (Jones et al., 2005; Bedrosian and Finn, 2021). The MT data also showed that the North American central plains conductor was located beneath the La Ronge gold belt, suggesting a connection between deep conductive anomalies and mineral deposits (Jones et al., 2005). The LMT data collected in 2020–2022 (Figure GS2025-9-1) revealed a similar conductor beneath the Flin Flon region, suggesting that regional-scale conductors were likely associated with a major conductor in the lithospheric mantle beneath the Sask craton (Chase and Unsworth, 2024).

Introduction to the magnetotelluric method

In mineral exploration, airborne or ground-based electromagnetic (EM) surveys are routinely used to locate electrically conductive anomalies related to mineralization. As previously described in Chase et al. (2024), in these methods, the depth of investigation is determined by the skin depth, which is defined as

$$\delta = \frac{503}{\sqrt{\sigma f}} \quad (1)$$

where δ is the skin depth (metres), σ is the electrical conductivity (the inverse of resistivity) of the Earth (siemens/m) and f is frequency (hertz). These methods use a transmitter to generate the signals, and the depth of investigation is typically limited to a few hundred metres.

For deeper imaging, it is necessary to use natural lower-frequency EM signals to increase the depth of investigation (Equation 1). To do this, it is practical to use the MT method. While similar to many of the controlled-source EM methods used in exploration, the naturally occurring EM signals in MT are typically in the range of 10 000–0.0001 hertz (Hz; or 0.0001 to 10 000 seconds per cycle). In comparison, the frequencies for common controlled-source EM methods are in the range of 100 000–100 Hz. As a result, the MT method is capable of imaging considerably deeper than most controlled-source EM methods.

At frequencies above 1 Hz, these signals come from global lightning activity, and below 1 Hz they are primarily generated by interactions between the solar wind and the magnetosphere (Simpson and Bahr, 2005). The MT time-series data are Fourier transformed during processing into the frequency domain to give apparent resistivity curves, which show the resistivity of the subsurface as a function of frequency. Magnetotelluric exploration uses three distinct frequency bands, depending on the target depth. The first is audio magnetotellurics (AMT), which has the frequency range of 10 000–1 Hz, and it is useful for imaging the relatively shallow near surface, usually to depths of <1–2 km. It is often used in the mineral exploration industry for its ability to

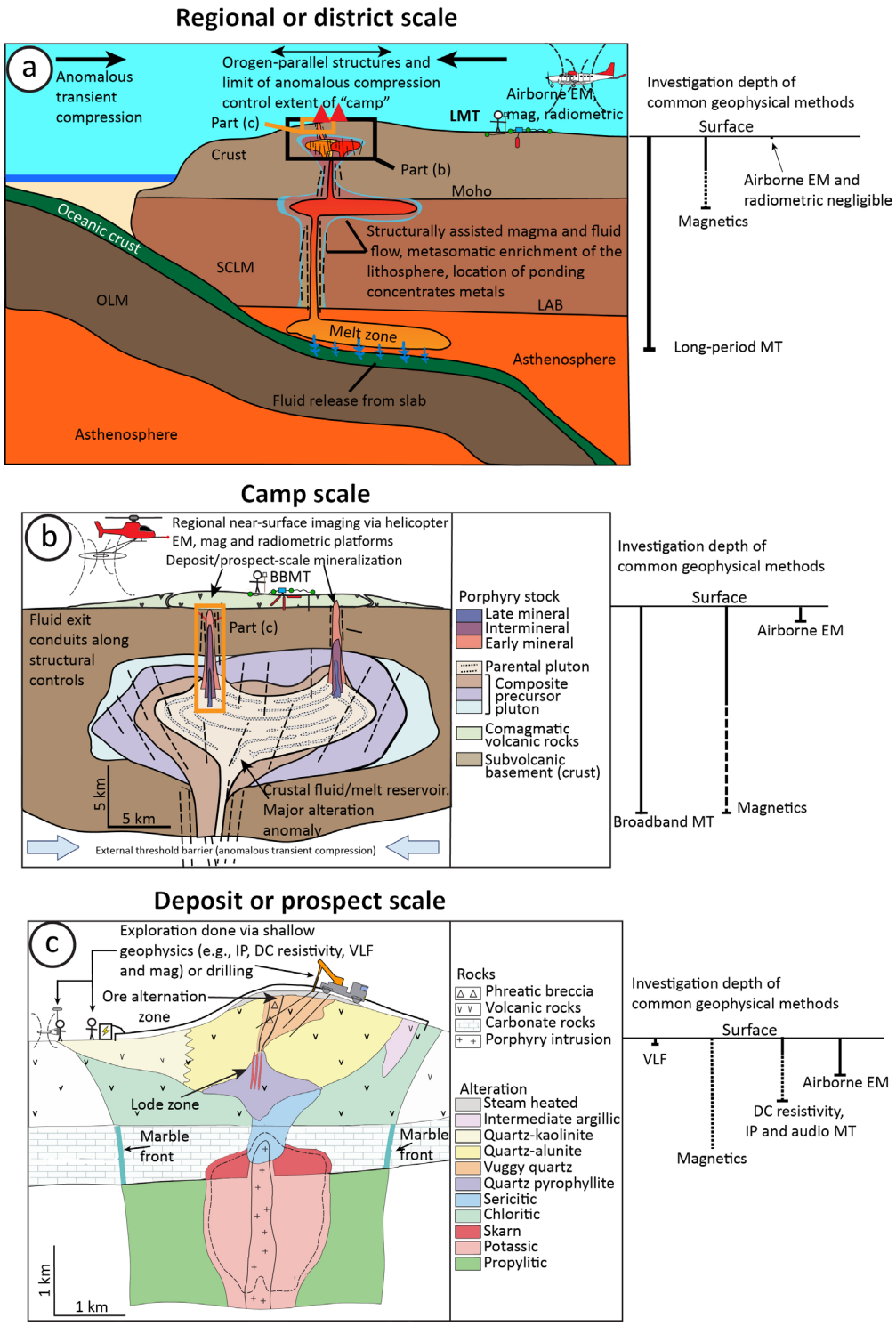

Figure GS2025-9-2: *General components and geophysical investigation criteria for the mineral systems framework at the* ***a)*** *regional or district scale,* ***b)*** *camp scale and* ***c)*** *deposit or prospect scale for an example porphyry deposit. At the tectonic regional scale, targets include major structures and fluid pathways exploited during tectonism as well as where these features are favourably situated and concentrated in discrete regions at the camp scale. At the camp scale, targets include major upper-crustal structures, alteration zones and centres of fluid concentration at deposit-scale depths. At the deposit scale, targets include ore zones (identifying and differentiating them from alteration haloes), ore-controlling structures and higher ore-grade zones. This scale commands the majority of expenditures and time during exploration. Geophysical methods, including the various magnetotelluric (MT) frequency bands, relevant to examining components of the mineral systems at each scale are shown with their typical depths of investigation. In this context, the long-period magnetotelluric (LMT) data collected here are best suited for analysis of mineral system criteria at the regional to camp scale. Black dashed lines denote hypothetical structures that acted as conduits for fluid movement. Adapted from McCuaig and Hronsky (2014) and Chase (2025). Abbreviations: BBMT, broadband magnetotelluric; DC, direct current; EM, electromagnetic; IP, induced polarization; LAB, lithosphere-asthenosphere boundary; mag, magnetics; Moho, Mohorovičić discontinuity; OLM, oceanic lithospheric mantle; SCLM, subcontinental lithospheric mantle; VLF, very low frequency.*

refine targets at somewhat greater depths than other EM methods are capable of imaging. The second is broadband magnetotellurics (BBMT), which has the frequency range of 1000–0.001 Hz. BBMT is useful for imaging the crust and upper mantle and is often used in mineral exploration at the camp scale. The final frequency band is for LMT and has a frequency range of 1–0.0001 Hz; it is capable of imaging the entire lithosphere. Long-period MT data are typically collected to produce regional backbone data products that can be used to refine search areas or to identify areas to be followed up on by higher-resolution geophysical methods.

In the field, MT instruments record two orthogonal electric field components and three orthogonal magnetic field components as a function of time (Figure GS2025-9-3a–c). In LMT systems, the magnetic fields are recorded with a single three-component fluxgate sensor, whereas in BBMT and AMT systems they are recorded using three separate induction coil sensors. Installation of an MT site is not labour intensive, and can be accomplished in 2–3 hours with a crew of 2–3 people. Installation is also minimally invasive, requiring only a few temporary holes to be dug so that various components of the system (e.g., magnetic sensors and electrodes) can be buried. Due to the distance between stations in regional LMT surveys, usually only 2–3 stations are installed per day. It is also important to select station locations that are away from cultural noise. Powerlines, water pumps, pipelines and cattle fences are common sources of electromagnetic noise that will negatively impact MT data.

Magnetotelluric fieldwork

In the summer of 2025, LMT data were recorded at 13 stations in southwestern Manitoba with an average station spacing of 50–70 km (Figures GS2025-9-1, -4). At each location, the LMT station recorded time-series data for 10–20 days. The data were recorded with Narod Geophysics Ltd.'s NIMS (Narod Intelligent Magnetotelluric System), LMT instruments owned by the University of Alberta. Following best practices for LMT data collection, the electrodes were buried 30–40 cm below the surface to avoid the effects of daily temperature variations and precipitation. Bentonite was placed in the electrode holes to improve electrical contact with the ground. Stations were time synchronized using GPS in order to allow for comparison of the time-series data and the removal of noise. The LMT stations were installed at least 500 m away from major infrastructure to minimize cultural noise. Each station produced 100–220 MB of time-series data. Data were successfully recovered at all 13 stations.

Magnetotelluric data analysis

After data processing, reliable apparent resistivity curves were obtained in the period range 5–10 000 s. Figure GS2025-9-5a–d provides examples of data from the 2025 LMT survey. At each station, the measured apparent resistivity at the highest frequencies (>10^{-1} Hz) is determined by the structure of the near surface. The shallow structure in the study area has an apparent resistivity in the range of 1–10 000 ohm-metre (Ω•m; as shown by the variability in the soundings in Figure GS2025-9-5). Apparent resistivity values at sites in the south (e.g., MGS202) are closer to 1 Ω•m, and they increase to 10 000 Ω•m as the sites get farther north (e.g., MGS503). This is expected as sites farther south are located above the thicker portions of the conductive Western Canada Sedimentary Basin in Manitoba. Farther north, the basin gets progressively thinner, and its influence on the data decreases. The northernmost sites register high apparent resistivity values, consistent with a shield environment and resistive crystalline upper-crustal rocks.

At mid-frequencies (10^{-1} to 10^{-3} Hz), results from the southern sites show progressively higher apparent resistivity values, consistent with the stable lithosphere of the Superior craton and border of the THO. In comparison, results from the northern sites show progressively lower apparent resistivity, albeit slowly.

At low frequencies (>10^{-3} Hz), apparent resistivity values at all sites trend toward lower values, likely corresponding to either deeper conductive features or the asthenosphere. A 2-D or 3-D resistivity structure is indicated by the XY and YX curves diverging as a function of frequency to some degree at all stations. If the resistivity structure was 1-D the curves would be coincident.

Future work

Long-period magnetotelluric data are measured as a function of frequency and need to be converted into a resistivity model as a function of depth and horizontal distance using a process called inversion. The LMT data collected in Manitoba show some 3-D characteristics (Figure GS2025-9-5), implying that a 3-D inversion approach must be used. The 3-D inversion models will be produced using the ModEM (Modular system for Electromagnetic inversion) algorithm of Kelbert et al. (2014). Computer resources will be provided by the Digital Research Alliance of Canada. Prior inversions on the data collected in 2024 from 22 stations showed that a number of crustal conductors are located in the west-central portion of the data grid, approximately 30–80 km east of The Pas, west-central Manitoba (Chase et al., 2024). One major lithospheric conductor is present beneath the Snow Lake mining district, and is similar to those observed by Chase and Unsworth (2024) beneath mineralization in the Flin Flon and La Ronge mineral belts. This suggests the deep crust and upper lithospheric mantle have a role in the genesis and ascent of mineralizing fluids in both regions.

The inversion of the new LMT data collected in Manitoba is still in progress. The planned research will combine the 2025 LMT data with the MT data collected by LITHOPROBE (Jones et al., 2005), Chase and Unsworth (2024) and Chase et al. (2024), together with the LMT data collected in Saskatchewan in 2025 (see Figure GS2025-9-1). The integrated dataset will be inverted to produce a resistivity model that includes as much of the previously collected data as possible and that covers the extent of the LMT data collected since 2021. The resulting 3-D resistivity model

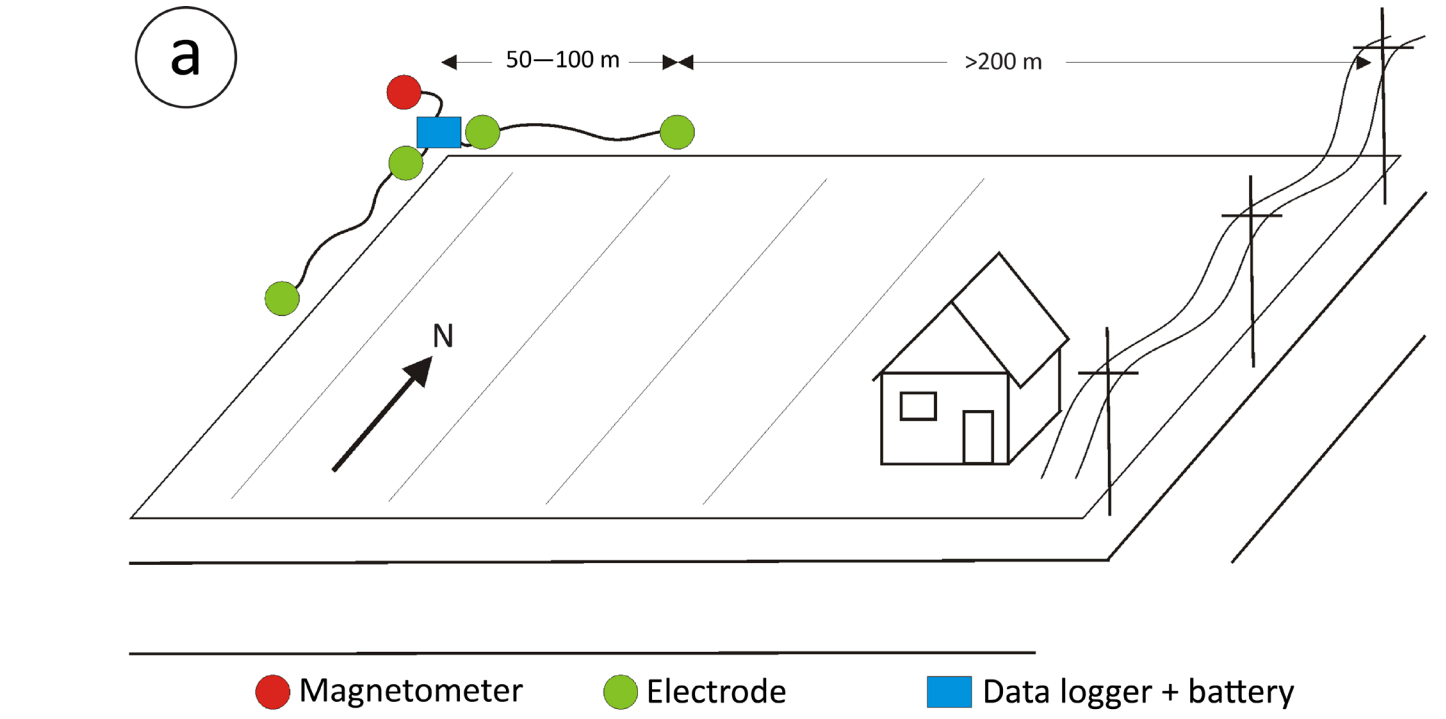

***Figure GS2025-9-3**: **a)** Layout of a long-period magnetotelluric (LMT) station. Installation only requires digging 4–6 temporary holes in the ground to a depth of 30–40 cm. The station typically occupies an area that is up to 100 by 100 m in size. Examples of an LMT system (Narod Geophysics Ltd.'s Narod Intelligent Magnetotelluric System [NIMS]) being **b)** deployed and **c)** recovered in the field in Manitoba.*

will be evaluated with a sensitivity analysis to determine which model features are required. This will be followed by a systematic interpretation of the 3-D resistivity model. Low-resistivity anomalies in this model will be quantitatively interpreted to determine the cause of the low-resistivity anomalies. Anomalies present in the crust will be evaluated using regional geology maps, drillcore and geophysical data, which will allow for a better understanding of the structural controls related to their formation and how they may relate to regional mineralization. The 3-D resistivity model will be interpreted within the mineral systems framework (e.g., McCuaig et al., 2010; McCuaig and Hronsky, 2014) to determine the factors that control the spatial distribution of mineralization. In the long term, it is hoped that partnerships with private-sector companies will allow for this grid to continue expanding north-

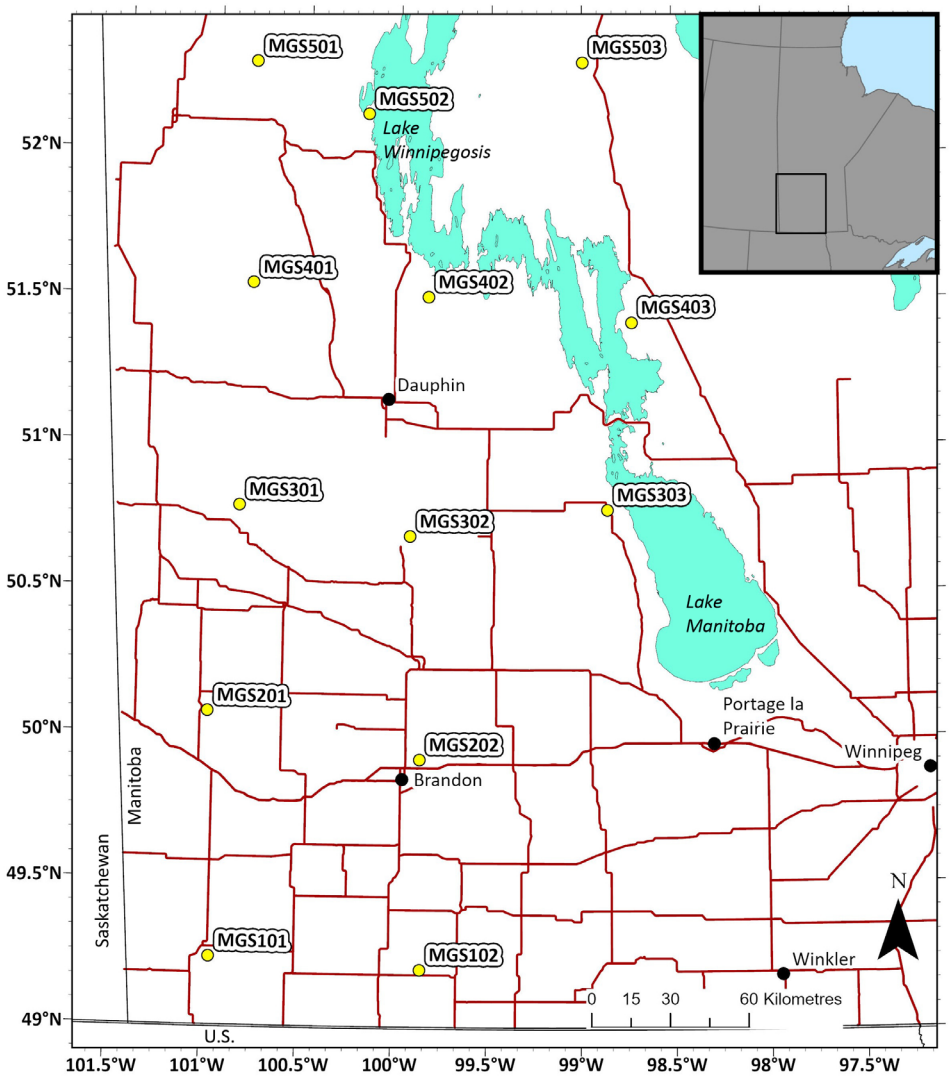

Figure GS2025-9-4: *Distribution of the long-period magnetotelluric (LMT) stations deployed in 2025 in southwestern Manitoba, shown as yellow dots here and in Figure GS2025-9-1. Provincial Trunk Highways shown as red lines. Inset map shows the location of the survey area at the Manitoba–Saskatchewan–United States border.*

ward where access is more challenging. The grid of LMT stations will also be combined with the EarthScope MT array in the contiguous United States (Murphy et al., 2023). This will produce a 3-D resistivity model of the lithosphere of the entire THO, which will offer improvements on tectonic evolution models for North America.

Economic considerations

The MT resistivity model developed by Chase and Unsworth (2024) for central Saskatchewan shows the presence of several major lithospheric conductors beneath the Flin Flon and La Ronge mineral belts. These conductors are connected to a conductive anomaly in the underlying lithospheric mantle, located beneath the Sask craton. These conductors were interpreted to be due to the presence of sulphide minerals and graphite films deposited by past episodes of fluid flow in the lithosphere. These sulphide minerals may be effective carriers of economically important base and precious metals (e.g., Tomkins and Evans, 2015; Walters et al., 2020). Thus, detection of these major conductors may help to locate areas favourable for mineralization and enhance the prospectivity of known areas. Ultimately, these conductors may help explain why economic mineralization is concentrated beneath the Flin Flon and La Ronge mineral belts. This may suggest that there are regional whole-lithosphere controls on the distribution of mineralization in this region of the THO. The LMT data collected in 2024 (Chase et al., 2024) will be used alongside the data collected in 2025 to evaluate if similar conductors are present in Manitoba and if they may be linked to potential mineralization. Critically, the new LMT data will be used to determine if potential mineralization may be present beneath the Western Canada Sedimentary Basin. At its northern reaches, where the basin rapidly thins, there may be additional targets

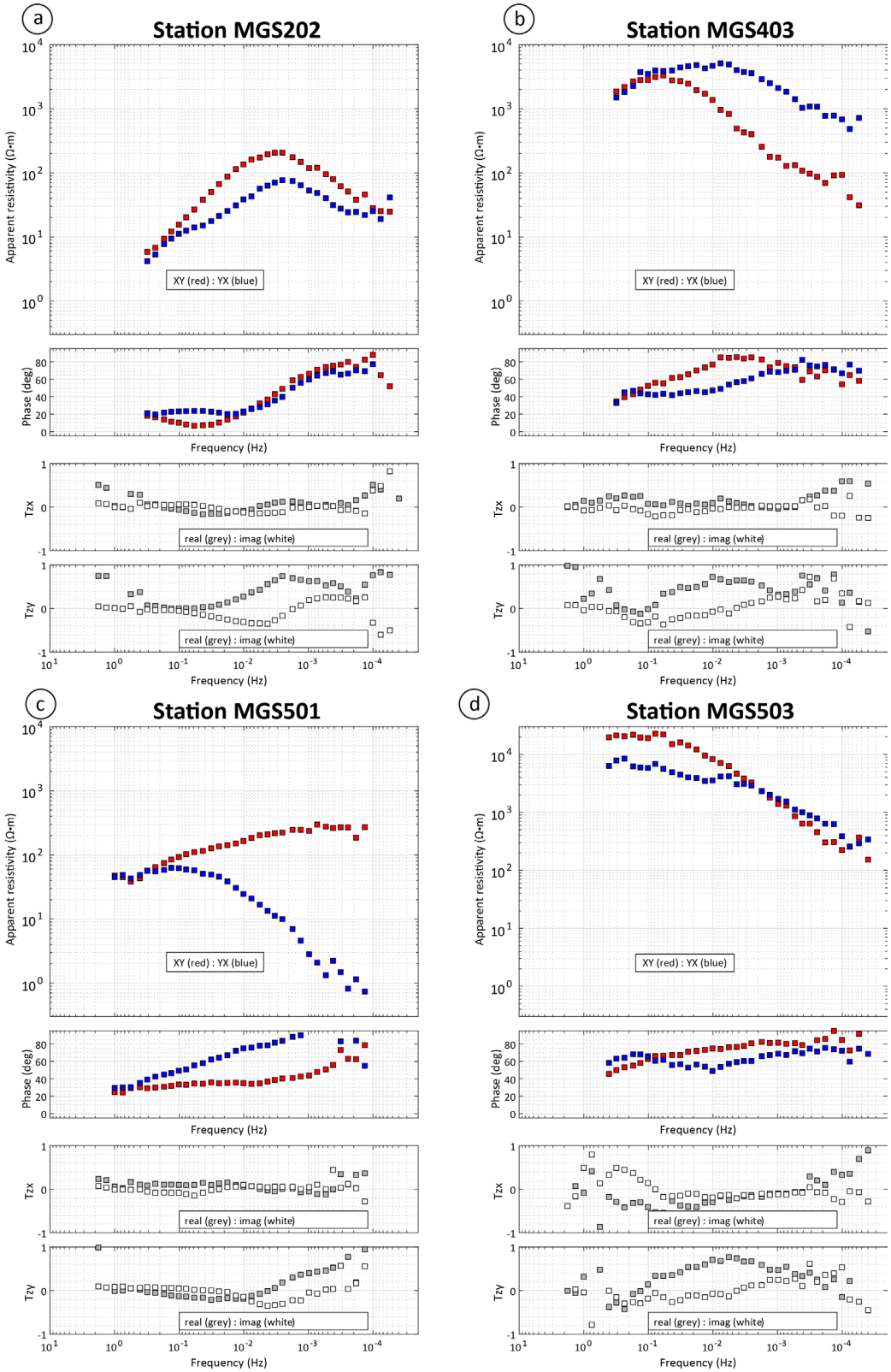

Figure GS2025-9-5: *Apparent resistivity and phase curves as a function of frequency for four long-period magnetotelluric (LMT) stations installed as part of this study:* ***a)*** *station MGS202;* ***b)*** *station MGS403;* ***c)*** *station MGS501;* ***d)*** *station MGS503. The apparent resistivity curves are obtained from the ratio of components of the electric and magnetic field measurements. The X and Y correspond to measurements of these fields in the north-south and east-west directions, respectively. Red curves are the transverse electric mode, which is highly sensitive to conductive features. Blue curves are the transverse magnetic mode, which is sensitive to both resistors and conductors, but the latter less so than the transverse electric mode. The functions labelled T_{zy} and T_{zx} are the components of the tipper (T) and are computed from the ratio of vertical (z) to horizontal (x and y) magnetic field components. The tipper is highly sensitive to conductive features. The real and imaginary (imag) components of the tipper are the in-phase and quadrature components, respectively. The locations of the stations chosen are shown in Figure GS2025-9-4. Abbreviations: Ω•m, ohm-metre; deg, degree; Hz, hertz.*

that are largely accessible but have escaped detection due to burial beneath relatively shallow sedimentary overburden.

Acknowledgments

The authors thank the Manitoba Geological Survey and T. Martins for their logistical support, assistance in survey planning, and communication with local communities about the survey. The authors thank M. Rinne and X.M. Yang for reviews of this report and D. O'Hara is thanked for the layout of the report. C. Epp, P. Belanger and E. Ralph are thanked for their assistance with vehicle, expediting and equipment maintenance. RnD Technical is thanked for technical editing assistance.

References

Ansdell, K.M. 2005: Tectonic evolution of the Manitoba-Saskatchewan segment of the Paleoproterozoic Trans-Hudson orogen, Canada; Canadian Journal of Earth Sciences, v. 42, no. 4, p. 741–759, URL <https://doi.org/10.1139/e05-035>.

Ansdell, K.M., Lucas, S.B., Connors, K. and Stern, R.A. 1995: Kisseynew metasedimentary gneiss belt, Trans-Hudson orogen (Canada): back-arc origin and collisional inversion; Geology, v. 23, no. 11, p. 1039–1043, URL <https://doi.org/10.1130/0091-7613(1995)023<1039:KMGBTH>2.3.CO;2>.

Bedrosian, P.A. and Finn, C.A. 2021: When Wyoming became superior: oblique convergence along the southern Trans-Hudson orogen; Geophysical Research Letters, v. 48, no. 13, art. e2021GL092970, URL <https://doi.org/10.1029/2021GL092970>.

Bleeker, W. 1990: New structural-metamorphic constraints on Early Proterozoic oblique collision along the Thompson nickel belt, northern Manitoba; *in* The Early Proterozoic Trans-Hudson Orogen of North America, J.F. Lewry and M.R. Stauffer (ed.), Geological Association of Canada, Special Paper 37, p. 57–74.

Bleeker, W., Nagerl, P. and Machado, N. 1995: The Thompson nickel belt, Manitoba: some new U-Pb ages; Geological Association of Canada–Mineralogical Association of Canada, Joint Annual Meeting, May 17–19, 1996, Victoria, British Columbia, Program with Abstracts, v. 20, p. A8.

Chase, B.F.W. 2025: Tectonic studies of the lithosphere of Laurentia using magnetotelluric data and the implications for diamond resources; Ph.D. thesis, University of Alberta, Edmonton, Alberta, 326 p.

Chase, B.F.W. and Unsworth, M.J. 2024: Magnetotelluric evidence for the formation of the layered Sask Craton by flat slab subduction; Earth and Planetary Science Letters, v. 647, art. 119027, URL <https://doi.org/10.1016/j.epsl.2024.119027>.

Chase, B.F.W., Marks, J., Williamson, A., Maki, A., Moshtaghian, K. and Unsworth, M.J. 2024: Initial results from a long-period magnetotelluric survey in the Flin Flon, Snow Lake and The Pas area, west-central Manitoba (NTS 63F, G, J, K, parts of 63B, I, N); *in* Report of Activities 2024, Manitoba Economic Development, Investment, Trade and Natural Resources, Manitoba Geological Survey, p. 145–152, URL <https://www.manitoba.ca/iem/geo/field/roa24pdfs/GS2024-17.pdf> [July 2025].

Clowes, R.M. and Roy, B. 2020: Crustal structure of the metasedimentary Kisseynew domain and bounding volcanic–plutonic domains, Trans-Hudson orogen, Canada; Canadian Journal of Earth Sciences, v. 58, no. 3, p. 268–285, URL <https://doi.org/10.1139/cjes-2020-0062>.

Clowes, R., Cook, F., Hajnal, Z., Hall, J., Lewry, J., Lucas, S. and Wardle, R. 1999: Canada's LITHOPROBE Project (collaborative, multidisciplinary geoscience research leads to new understanding of continental evolution); Episodes Journal of International Geoscience, v. 22, no. 1, p. 3–20, URL <https://doi.org/10.18814/epiiugs/1999/v22i1/002>.

Connors, K.A., Ansdell, K.M. and Lucas, S.B. 1999: Coeval sedimentation, magmatism, and fold-thrust development in the Trans-Hudson orogen: propagation of deformation into an active continental arc setting, Wekusko Lake area, Manitoba; Canadian Journal of Earth Sciences, v. 36, no. 2, p. 275–291, URL <https://doi.org/10.1139/e98-090>.

Heinson, G., Didana, Y., Soeffky, P., Thiel, S. and Wise, T. 2018: The crustal geophysical signature of a world-class magmatic mineral system; Scientific Reports, v. 8, art. 10608, URL <https://doi.org/10.1038/s41598-018-29016-2>.

Jones, A.G., Ledo, J. and Ferguson, I.J. 2005: Electromagnetic images of the Trans-Hudson orogen: the North American Central Plains anomaly revealed; Canadian Journal of Earth Sciences, v. 42, no. 4, p. 457–478, URL <https://doi.org/10.1139/e05-018>.

Kelbert, A., Meqbel, N., Egbert, G.D. and Tandon, K. 2014: ModEM: a modular system for inversion of electromagnetic geophysical data; Computers & Geosciences, v. 66, p. 40–53, URL <https://doi.org/10.1016/j.cageo.2014.01.010>.

Kirkby, A., Czarnota, K., Huston, D.L., Champion, D.C., Doublier, M.P., Bedrosian, P.A., Duan, J. and Heinson, G. 2022: Lithospheric conductors reveal source regions of convergent margin mineral systems; Scientific Reports, v. 12, no. 1, art. 8190, URL <https://doi.org/10.1038/s41598-022-11921-2>.

Lewry, J.F. and Collerson, K.D. 1990: Trans-Hudson orogen: extent, subdivisions, and problems; *in* The Early Proterozoic Trans-Hudson Orogen of North America, J.F. Lewry and M.R. Stauffer (ed.), Geological Association of Canada, Special Paper 37, p. 1–14.

Machado, N. 1990: Timing of collisional events in the Trans-Hudson orogen: evidence from U-Pb geochronology for the New Quebec orogen, the Thompson belt and the Reindeer zone (Manitoba and Saskatchewan); *in* The Early Proterozoic Trans-Hudson Orogen of North America, J.F. Lewry and M.R. Stauffer (ed.), Geological Association of Canada, Special Paper 37, p. 433–441.

Manitoba Geological Survey 2022: Bedrock geology of Manitoba; Manitoba Natural Resources and Northern Development, Manitoba Geological Survey, Open File OF2022-2, scale 1:1 000 000.

McCuaig, T.C. and Hronsky, J.M.A. 2014: The mineral system concept: the key to exploration targeting; *in* Building Exploration Capability for the 21st Century, K.D. Kelly and H.C. Golden (ed.), Society of Economic Geologists, Special Publication 18, p. 153–175.

McCuaig, T.C., Beresford, S. and Hronsky, J. 2010: Translating the mineral systems approach into an effective exploration targeting system; Ore Geology Reviews, v. 38, no. 3, p. 128–138, URL <https://doi.org/10.1016/j.oregeorev.2010.05.008>.

Murphy, B.S., Bedrosian, P. and Kelbert, A. 2023: Geoelectric constraints on the Precambrian assembly and architecture of southern Laurentia; *in* Laurentia: Turning Points in the Evolution of a Continent, S.J. Whitmeyer, M.L. Williams, D.A. Kellett and B. Tikoff (ed.), Geological Society of America, Memoir 220, p. 203–220, URL <https://doi.org/10.1130/2022.1220(13)>.

Percival, J.A., Sanborn-Barrie, M., Skulski, T., Stott, G.M., Helmstaedt, H. and White, D.J. 2006: Tectonic evolution of the western Superior Province from NATMAP and Lithoprobe studies; Canadian Journal of Earth Sciences, v. 43, no. 7, p. 1085–1117, URL <https://doi.org/10.1139/e06-062>.

Percival, J.A., Skulski, T., Sanborn-Barrie, M., Stott, G.M., Leclair, A.D., Corkery, M.T. and Boily, M. 2012: Geology and tectonic evolution of the Superior Province, Canada; *in* Tectonic Styles in Canada: the LITHOPROBE Perspective, J.A. Percival, F.A. Cook and R.M. Clowes (ed.), Geological Association of Canada, Special Paper 49, p. 321–378.

Saskatchewan Energy and Resources 2021: Geological domains for the province of Saskatchewan, CSRS NAD83 Zone 13; *in* Mining and Petroleum GeoAtlas, Saskatchewan Ministry of Energy and Resources, URL <https://gisappl.saskatchewan.ca/Html5Ext/index.html?viewer=GeoAtlas> [September 2022].

Simpson, F. and Bahr, K. 2005: Practical Magnetotellurics; Cambridge University Press, Cambridge, United Kingdom, 254 p.

Syme, E.C., Lucas, S.B., Bailes, A.H. and Stern, R.A. 1999: Contrasting arc and MORB-like assemblages in the Paleoproterozoic Flin Flon belt, Manitoba, and the role of intra-arc extension in localizing volcanic-hosted massive sulphide deposits; Canadian Journal of Earth Sciences, v. 36, no. 11, p. 1767–1788, URL <https://doi.org/10.1139/e98-084>.

Tomkins, A.G. and Evans, K.A. 2015: Separate zones of sulfate and sulfide release from subducted mafic oceanic crust; Earth and Planetary Science Letters, v. 428, p. 73–83, URL <https://doi.org/10.1016/j.epsl.2015.07.028>.

Walters, J.B., Cruz-Uribe, A.M. and Marschall, H.R. 2020: Sulfur loss from subducted altered oceanic crust and implications for mantle oxidation; Geochemical Perspective Letters, v. 13, p. 36–41, URL <https://doi.org/10.7185/geochemlet.2011>.

Weber, W. 1990: The Churchill-Superior boundary zone, southeast margin of the Trans-Hudson orogen: a review; *in* The Early Proterozoic Trans-Hudson Orogen of North America, J.F. Lewry and M.R. Stauffer (ed.), Geological Association of Canada, Special Paper 37, p. 41–55.

Whalen, J.B., Syme, E.C. and Stern, R.A. 1999: Geochemical and Nd isotopic evolution of Paleoproterozoic arc-type magmatism in the Flin Flon belt, Trans-Hudson orogen, Canada; Canadian Journal of Earth Sciences, v. 36, no. 2, p. 227–250, URL <https://doi.org/10.1139/e98-026>.

White, D.J., Lucas, S.B., Bleeker, W., Hajnal, Z., Lewry, J.F. and Zwanzig, H.V. 2002: Suture-zone geometry along an irregular Paleoproterozoic margin: the Superior boundary zone, Manitoba, Canada; Geology, v. 30, no. 8, p. 735–738, URL <https://doi.org/10.1130/0091-7613(2002)030<0735:SZGAAI>2.0.CO;2>.

White, D.J., Thomas, M.D., Jones, A.G., Hope, J., Németh, B. and Hajnal, Z. 2005: Geophysical transect across a Paleoproterozoic continent–continent collision zone: the Trans-Hudson orogen; Canadian Journal of Earth Sciences, v. 42, no. 4, p. 385–402, URL <https://doi.org/10.1139/e05-002>.

Whitmeyer, S.J. and Karlstrom, K.E. 2007: Tectonic model for the Proterozoic growth of North America; Geosphere, v. 3, no. 4, p. 220–259, URL <https://doi.org/10.1130/GES00055.1>.

Ye, G., Unsworth, M., Wei, W., Jin, S. and Liu, Z. 2019: The lithospheric structure of the Solonker suture zone and adjacent areas: crustal anisotropy revealed by a high-resolution magnetotelluric study; Journal of Geophysical Research: Solid Earth, v. 124, no. 2, p. 1142–1163, URL <https://doi.org/10.1029/2018JB015719>.

Zwanzig, H.V., Macek, J.J. and McGregor, C.R. 2007: Lithostratigraphy and geochemistry of the high-grade metasedimentary rocks in the Thompson nickel belt and adjacent Kisseynew domain, Manitoba: implications for nickel exploration; Economic Geology, v. 102, no. 7, p. 1197–1216, URL <https://doi.org/10.2113/gsecongeo.102.7.1197>.

GS2025-10

Preliminary investigation into the natural hydrogen generation potential of Precambrian rocks beneath the Williston Basin, southwestern Manitoba (parts of NTS 62G, J, K, O, 63B, C, G, K)

by M.P.B. Nicolas, D. Coutts[1] and O.H. Ardakani[1]

In Brief:

- Precambrian samples were analysed and used to calculate their hydrogen generation potential by the radiolysis pathway
- Results will be integrated into a basin-scale hydrogen generation model lead by the Geological Survey of Canada

Citation:
Nicolas, M.P.B., Coutts, D. and Ardakani, O.H. 2025: Preliminary investigation into the natural hydrogen generation potential of Precambrian rocks beneath the Williston Basin, southwestern Manitoba (parts of NTS 62G, J, K, O, 63B, C, G, K); *in* Report of Activities 2025, Manitoba Business, Mining, Trade and Job Creation, Manitoba Geological Survey, p. 104–109.

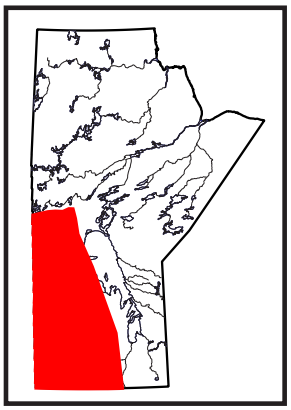

Summary

Molecular hydrogen (H_2) in the continental crust is generated through two main reaction pathways: 1) rock-water interactions (i.e., serpentinization) and 2) water radiolysis from the radioactive decay of U- and Th-rich minerals. Samples of Precambrian drillcore from the crystalline basement of the Williston Basin in Manitoba were collected and analyzed for whole-rock lithogeochemistry to confirm lithology and their hydrogen generation potential was assessed using a Monte Carlo radiolysis model. Helium (He) is a critical mineral also formed through the radiolysis reaction and can be used as a proxy for natural hydrogen exploration. From this small, limited sample set, hydrogen generation rates from radiolysis (reported as minimum/mean/maximum) are estimated to be 0.05/7.84/88.40 mol H_2/km^3/year for felsic rocks, 0.03/6.16/37.30 mol H_2/km^3/year for intermediate rocks, 0.001/2.86/25.30 mol H_2/km^3/year for mafic rocks and 0.06/6.31/28.90 mol H_2/km^3/year for iron formation. Refinement and further interpretations of the hydrogen generation potential of the basement will be integrated into a larger hydrogen generation model for the Western Canada Sedimentary Basin, a project led by the Geological Survey of Canada.

Introduction

Elevated hydrogen values (1.46–8.50 mol. % H_2) have been identified in oil and gas wells in Manitoba's Williston Basin sedimentary strata (Figure GS2025-10-1; Nicolas, 2024). The source of the hydrogen trapped within these sedimentary reservoirs is uncertain. Molecular hydrogen as free gas is rare in nature due to its high reactivity with other elements, its small molecule size, which makes it difficult to trap and accumulate (Zgonnik, 2020; Ballentine et al., 2025), and its consumption by subsurface microbiomes (Stevens and McKinley, 1995; Sherwood Lollar et al., 2007). Hydrogen is primarily generated in the crust through rock-water redox reactions (i.e., serpentinization), water radiolysis from the radioactive decay of U and Th hosted in minerals (Sherwood Lollar et al., 2014; Ballentine et al., 2025) or from high thermal maturity and decomposition of organic matter (Mahlstedt et al., 2022; Boreham et al., 2023). In southwestern Manitoba, beneath the sedimentary rocks of the Williston Basin, Precambrian rocks are likely the best source of hydrogen, along with highly organic-rich shale within the sedimentary strata being a possible source and/or caprock.

For this study, samples of Precambrian crystalline basement beneath the sedimentary cover were collected from several drillcore that penetrated the Precambrian basement (Figure GS2025-10-1). These samples were cut into thin sections and the geochemistry was determined to allow for an evaluation of the mineralogy and chemical composition of each sample, which allows for an estimation of hydrogen generation potential via radiolysis. This work is part of a larger project led by the Geological Survey of Canada (Calgary, Alberta) to model the hydrogen generation potential of the crystalline basement of the Western Canada Sedimentary Basin (WCSB).

Methodology and results

To select drillcore for sampling, an inventory of all the Precambrian drillcore was compiled from Bezys and Conley (1998) and McGregor (2011) and through searches conducted on the Manitoba Oil and Gas Information System (MOGWIS; Manitoba Business, Mining, Trade and Job Creation, internal database) and geoLOGIC systems ltd.'s geoSCOUT™. Only drillcore from within the Williston Basin that was stored at the Manitoba Geological Survey Midland Sample and Core Library (Winnipeg, Manitoba) were selected for further consideration. If only one drillcore was identified in a large area, it was tagged for sampling. If more than one drillcore from a small area was identified, only one drillcore

[1] Natural Resources Canada, Geological Survey of Canada, Calgary, Alberta

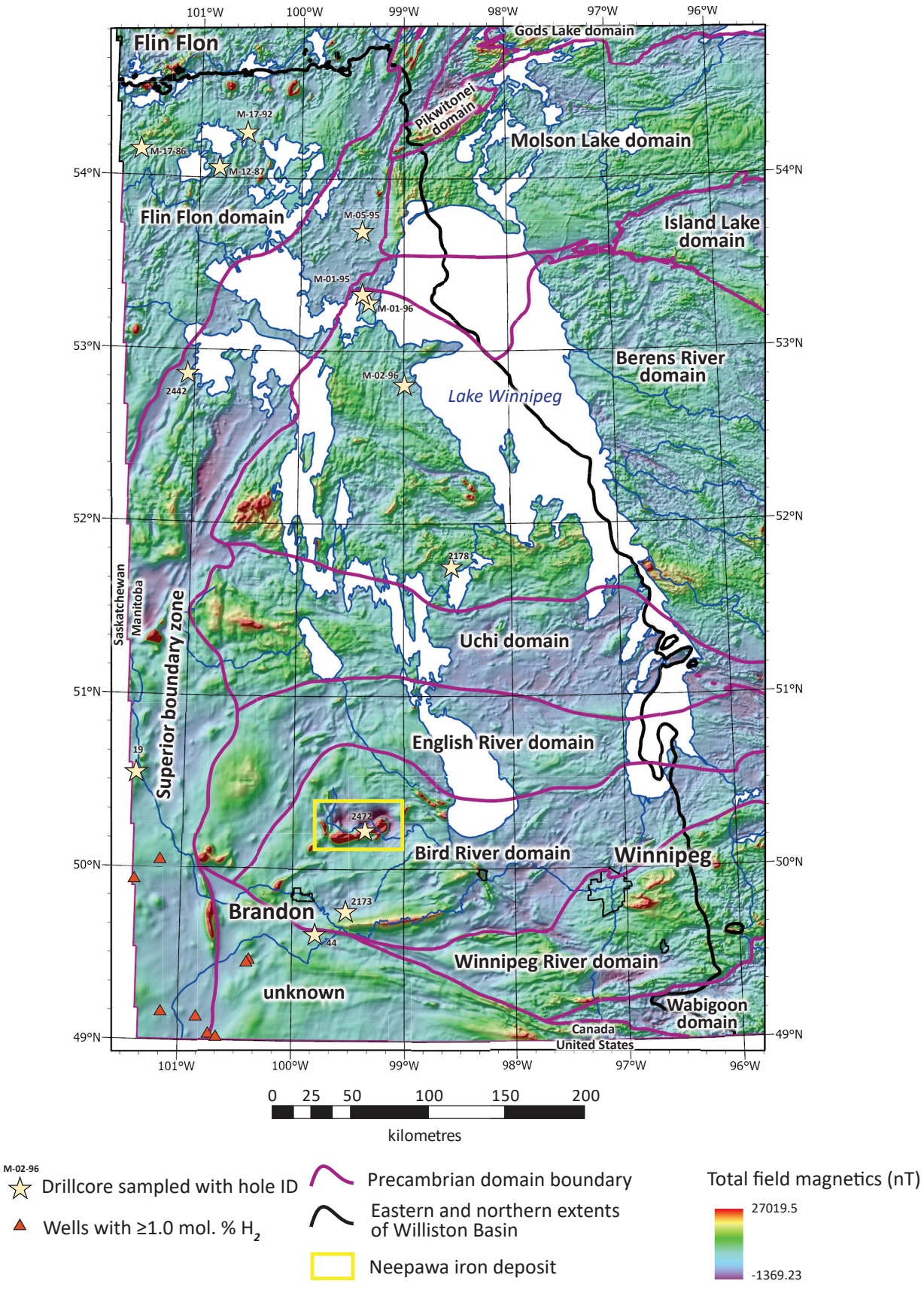

Figure GS2025-10-1: *Shaded total field magnetic anomaly map of the Williston Basin in southwestern Manitoba (Manitoba Business, Mining, Trade and Job Creation, 2025) showing the Precambrian domain boundaries (from McGregor, 2013), hydrogen gas shows in oil and gas wells (Nicolas, 2024) and the locations of the drillcore sampled for this study. Abbreviation: nT, nanotesla.*

with the thickest and best preserved Precambrian section was selected for sampling. In the areas with less drillcore availability, especially in the southern half of the study area, and to ensure a good geographic distribution of samples, all Precambrian drillcore in those areas were selected for sampling; this resulted in an unintentional sample bias toward felsic rock lithologies. In addition, only a very short drillcore section (<50 cm) of the Neepawa iron formation, at L.S. 15. Sec. 29, Twp. 14, Rge. 14, W 1st Mer. (abbreviated 15-29-14-14W1), was available for sampling. Due to its high iron content and hydrogen generation potential, this was a core of particular interest from a hydrogen modelling perspective.

For each drillcore, one to three samples were selected in the Precambrian portion based on lithological variations. If the lithology in the drillcore was similar throughout, one sample interval was selected. If a drillcore showed varying lithologies or major changes in grain size (e.g., granite versus pegmatite), one sample location per major lithological or grain-size change was selected. In addition, if a drillcore was particularly long, multiple samples from similar lithologies were selected but they were taken far apart from each other. A sample size of 3–4 cm long and a half to one-third of the core diameter was cut using a rock saw, or a broken piece of core was taken, if available. Sample depths were recorded and photographs of the core and the cut samples were taken.

A total of 22 samples were sent to the Geological Survey of Canada (Calgary, Alberta) for further selection and processing. From those samples, a smaller suite of 16 samples was selected based on lithological uniqueness. If the same core had multiple samples from various depths, only those which appeared to be different lithologies were sent for further processing, and the other samples were kept in archive for future consideration. A thin section of each sample was made and a subsample was sent for geochemical characterization at Activation Laboratories Ltd. (Ancaster, Ontario). The proportions of major, minor and trace elements were measured using inductively coupled plasma–optical emission spectroscopy (ICP-OES) and inductively coupled plasma–mass spectroscopy (ICP-MS), following fusion digestion with lithium metaborate/tetraborate. The lithogeochemistry results for the 16 samples are reported in Nicolas et al. (2025[1]). The geochemistry results were used to classify each sample based on their composition (felsic, >63% SiO_2; intermediate, 52–63% SiO_2; mafic, 45–52% SiO_2; ultramafic, <52% SiO_2) or, in instances of intense metamorphism/alteration, a possible original lithological interpretation. This information was then used to assign a lithology to the samples in the model (Table GS2025-10-1).

Hydrogen generation potential through the radiolysis reaction pathway was calculated using 'Radiolysis', an R package (D. Coutts, O. Warr, O. Ardakani and B. Sherwood Lollar, unpublished paper, 2025), for the 16 samples, which follows the Monte Carlo methods of Warr et al. (2023). Each sample was modelled individually to determine a realistic range of hydrogen generation rates. The model of Warr et al. (2023) and subsequent code of D. Coutts, O. Warr, O. Ardakani and B. Sherwood Lollar (unpublished paper, 2025) require inputs for U, Th and K concentrations, rock properties (density and porosity) and fluid density. These are input as truncated normal distributions (minimum/maximum/mean/standard deviation). In this case, U, Th and K concentrations were not modelled as truncated distribution (i.e., a standard deviation of zero, minimum and maximum concentrations set at 0 and 100, respectively, and a mean of the distribution set to the measured concentration) as these values were determined by lithogeochemical analysis. Rock properties (porosity and grain density) were taken from summarized data of Enkin (2018) for matching lithologies. Fluid density was given an appropriate range following Warr et al. (2023), which was set at 1.1 g/cm^3, with a standard deviation of 0.5 g/cm^3, and minimum and maximum values of 1 and 1.37 g/cm^3, respectively. The sample parameters used for modelling and the estimated hydrogen generation rates via radiolysis are presented in Table GS2025-10-1. The Monte Carlo models consisted of 1000 simulations per sample. These results are further summarized by grouping the output simulations based on composition (e.g., felsic, mafic) and finding the minimum, mean and maximum hydrogen generation rates.

Discussion

This initial analysis of Precambrian core demonstrates some relationships between hydrogen potential and lithology (Figures GS2025-10-2, -3), however, this sample set is small and limited in lithological variability, adding bias to the results. The U and Th content is higher in felsic rock samples, with a mean range of 1.38–21.18 combined ppm, which is expected due to magmatic differentiation (Whitfield et al., 1959; Sheng et al., 2025). Sample 106-25-M1786-67 is anomalous as it has a combined U and Th mean value of 66.6 ppm, which skews the results for felsic lithologies. This high value could be due to the presence of a single columbite grain; this will be verified in the thin section. Intermediate and mafic rocks samples have higher Fe and Mg values (5.87–12.34 wt. % Fe_2O_3 + MgO for intermediate; 9.78–23.96 wt. % Fe_2O_3 + MgO for mafic) and generally lower U and Th values (0.85–4.37 combined ppm for intermediate; 0.27–1.63 combined ppm for mafic), with no significant difference between intermediate and mafic rocks. However, sample 106-25-M296-157 is classified as an intermediate sample due to its SiO_2 content but plots similar to felsic rocks in the variation diagram in Figure GS2025-10-2; this inconsistency is likely due to alteration

[1] GS Data Repository Item DRI2025022, containing the data or other information sources used to compile this report, is available online to download free of charge at https://manitoba.ca/iem/info/library/downloads/index.html, or on request from minesinfor@gov.mb.ca, or by contacting the Resource Centre, Manitoba Business, Mining, Trade and Job Creation, 360-1395 Ellice Avenue, Winnipeg, Manitoba R3G 3P2, Canada.

Table GS2025-10-1: Sample parameters used for modelling and the hydrogen generation potential of samples by radiolysis calculated using the 'Radiolysis' R package; each sample was treated as an individual Monte Carlo model. Samples from Precambrian drillcore from beneath the Williston Basin, southwestern Manitoba. For all samples, fluid density was set at 1.1 g/cm^3 with a standard deviation (SD) of 0.5 g/cm^3, and a minimum (min) and maximum (max) value of 1 and 1.37 g/cm^3, respectively; minimum and maximum concentrations of U, Th and K were set at 1 and 100, respectively, with a standard deviation of zero. Abbreviation: IUGS, International Union of Geological Sciences.

Hole ID	Sample ID	Sample description	IUGS[1] classification	Model lithology	U (ppm)	Th (ppm)	K (wt. %)	H_2 generation (mol/km^3/year)			
					Mean	Mean	Mean	Min	Max	Mean	SD
44	106-25-44-3824	Granodiorite	Felsic	Granodiorite	0.65	3.37	1.81	0.05	13.10	3.77	2.39
19	106-25-19-4452	Granite gneiss	Felsic	Orthogneiss	1.12	6.55	2.58	0.37	8.35	2.83	1.58
2178	106-25-2178-318	Granite (altered)	Felsic	Granite	0.96	10.80	3.05	0.18	13.70	4.39	2.38
M-01-96	106-25-M196-166	Alkali granite	Felsic	Granite	0.54	0.84	1.41	0.05	4.36	1.42	0.80
M-05-95	106-25-M595-145	Sericitized granite	Felsic	Granite	1.77	3.22	9.59	0.28	26.10	8.39	4.99
M-12-87	106-25-M1287-95	Granodiorite	Felsic	Granodiorite	2.15	9.36	3.55	0.12	33.30	8.97	5.62
M-12-87	106-25-M1287-103	Granite biotite gneiss with pegmatite inclusion	Felsic	Orthogneiss	5.26	5.17	3.60	0.71	15.80	5.39	2.78
M-17-86	106-25-M1786-66	Granite biotite gneiss	Felsic	Orthogneiss	3.18	2.69	1.81	0.38	8.82	2.89	1.58
M-17-86	106-25-M1786-67	Pegmatitic granite	Felsic	Granite	36.40	30.20	6.80	1.17	88.40	30.70	17.30
M-17-92	106-25-M1792-64	Pegmatitic granite	Felsic	Granite	4.08	17.10	6.76	0.33	32.70	9.67	5.46
2472	106-25-2472-764	Iron formation	Iron formation	Metasedimentary - siliciclastic	1.25	4.19	3.81	0.06	28.90	6.31	4.48
M-02-96	106-25-M296-157	Syenodiorite (altered)	Intermediate	Diorite	0.73	3.64	7.67	0.08	37.30	10.40	6.91
2442	106-25-2442-1125	Diorite	Intermediate	Diorite	0.18	0.67	1.39	0.03	7.12	1.92	1.29
2173	106-25-2173-973	Mafic tectonite (metabasalt?)	Mafic	Metavolcanic - mafic	0.68	0.54	2.04	0.03	9.26	2.35	1.62
2173	106-25-2173-976	Mafic tectonite (meta-syenodiorite or meta-trachy-andesite?)	Mafic[2]	Metavolcanic - mafic	1.02	0.61	6.33	0.06	25.30	6.17	4.46
M-01-95	106-25-M195-149	Pyroxene-hornblende gabbro	Mafic	Gabbro	0.05	0.22	0.08	0.00	0.22	0.07	0.04

[1] With the exception of sample 106-25-2472-764

[2] IUGS classification indicates intermediate composition, but other geochemical signatures suggest an original mafic composition more similar to sample 106-25-2173-973.

and leaching, which was visible in the hand sample, suggesting the original rock composition may have been more felsic.

Hydrogen generation rates from radiolysis for this sample set is shown in Figure GS2025-10-3 and are estimated to be (reported as minimum/mean/maximum) 0.05/7.84/88.40 mol H_2/km^3/year for felsic rocks, 0.03/6.16/37.30 mol H_2/km^3/year for intermediate rocks, 0.001/2.86/25.30 mol H_2/km^3/year for mafic rocks, and 0.06/6.31/28.90 mol H_2/km^3/year for iron formation. Intermediate, mafic and iron formation samples will be dominated by the rock-water interaction pathway of hydrogen generation, therefore the generation rates for those samples using the radiolysis model are expected to be lower. Samples with higher concentrations of U and Th, such as felsic to some intermediate rocks, indicate that radiolysis would be the dominant pathway of hydrogen generation, which is further demonstrated by the output of the Monte Carlo models. There are currently no accessible and efficient numeric models to estimate hydrogen generation rates through water-rock interactions for hydrogen prospectivity. Knowing which samples are more likely to generate hydrogen by a specific pathway, or combination thereof, will help provide parameters and inform mathematical models toward the gross estimation of hydrogen generation over time.

A detailed discussion on the hydrogen generative potential of these samples is beyond the scope of this report. These results will be incorporated into a WCSB-wide model, a project led by the Geological Survey of Canada.

Economic considerations

Understanding natural hydrogen generation and occurrences as a potential resource in Manitoba is important to the economic growth of the province. While hydrogen is still a new economic consideration for most of the world (Ballentine et al., 2025), breaking down and evaluating the science behind hydrogen generation in a region—such as the hydrogen generation capacity of the Canadian Shield—is critical to inform future exploration decisions and drill target identification, minimizing risk and maximizing success. Along with hydrogen source rocks,

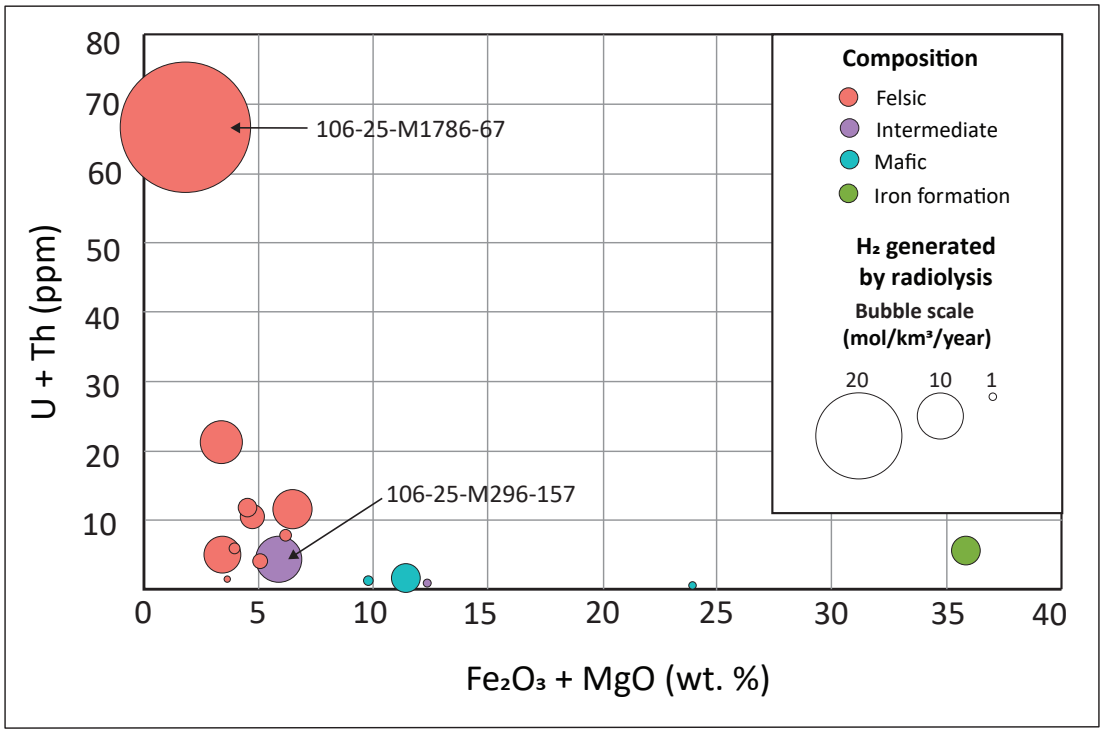

Figure GS2025-10-2: *Variation diagram showing the differentiation of U + Th as a function of the Fe_2O_3 + MgO content of the sample and their respective modelled hydrogen generation rates. Samples from Precambrian drillcore from beneath the Williston Basin, southwestern Manitoba. Felsic lithologies have >63% SiO_2, intermediate lithologies have 52–63% SiO_2, mafic lithologies have 45–52% SiO_2. Iron formation is highlighted on its own. Sample 106-25-M1786-67 is considered anomalous due to the likely presence of a columbite grain, and sample 106-25-M296-157 showed evidence of alteration and leaching.*

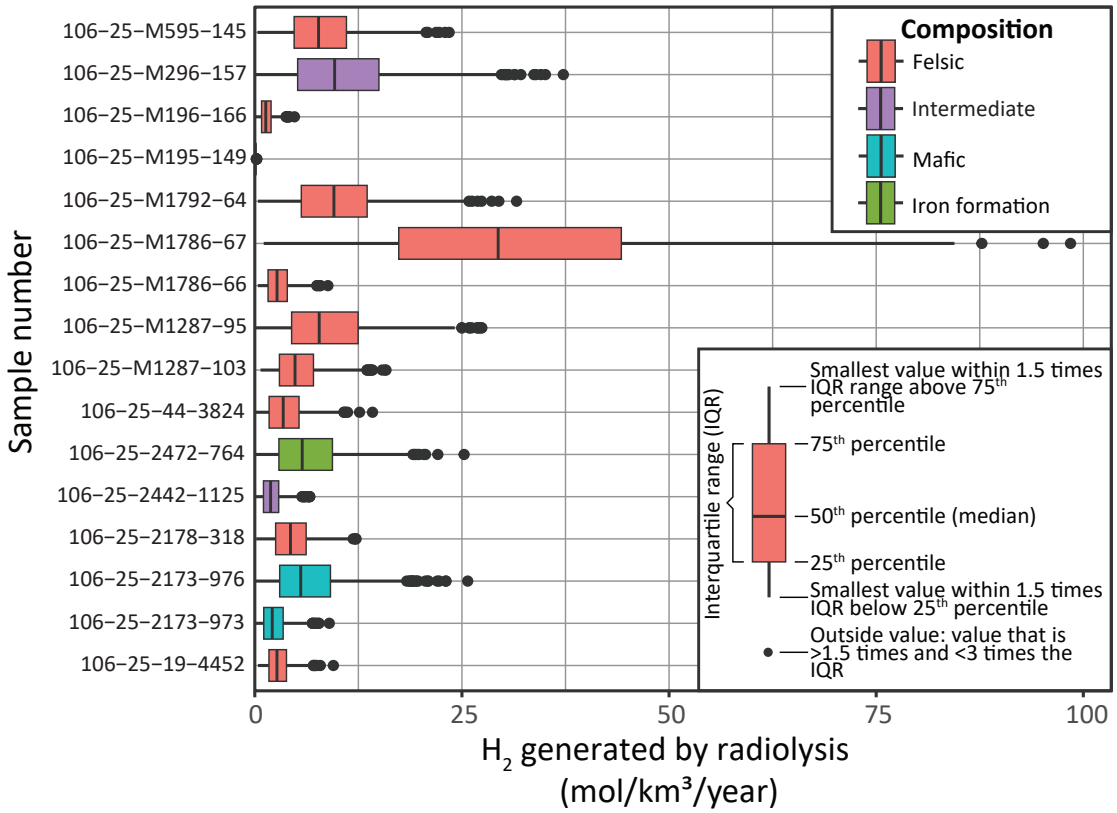

Figure GS2025-10-3: *Boxplot of sample bulk rock compositions and their modelled hydrogen generation rates. Samples from Precambrian drillcore from beneath the Williston Basin, southwestern Manitoba.*

an understanding of the Williston Basin's reservoirs and seals / cap rocks is necessary for derisking and characterizing the hydrogen system. It is important to emphasize one of the byproducts of the radiolysis process is helium, a critical mineral, which can be used as a proxy in natural hydrogen exploration.

Acknowledgments

The authors would like to thank C.G. Couëslan from the Manitoba Geological Survey (MGS) for his assistance in identifying the Precambrian lithologies in some of the drillcore; J. Janssens from the MGS for cutting, labelling and taking photos of the drillcore and samples, and the layout of Data Repository Item DRI2025022; and C. Epp and P. Belanger from the MGS Midland Sample and Core Library for assembling and preparing the drillcore for viewing. The authors would like to acknowledge C.G. Couëslan and T.J. Hodder (MGS) for their critical and constructive review of this report.

References

Ballentine, C.J., Karolytė, R., Cheng, A., Sherwood Lollar, B., Gluyas, J.G. and Daly, M.C. 2025: Natural hydrogen resource accumulation in the continental crust; Nature Reviews Earth & Environment, v. 6, no. 5, p. 342–356, URL <https://doi.org/10.1038/s43017-025-00670-1>.

Bezys, R.K. and Conley, G.G. 1998: Manitoba stratigraphic database and the Manitoba stratigraphic map series; Manitoba Energy and Mines, Geological Services, Open File Report OF98-7, CD-ROM.

Boreham, C.J., Edwards, D.S., Feitz, A.J., Murray, A.P., Mahlstedt, N. and Horsfield, B. 2023: Modelling of hydrogen gas generation from overmature organic matter in the Cooper Basin, Australia; The APPEA Journal, v. 63, no. 2, p. S351–S356, URL <https://doi.org/10.1071/aj22084>.

Enkin, R.J. 2018: Canadian rock physical property database: first public release; Geological Survey of Canada, Open File 8460, 1 .zip file, URL <https://doi.org/10.4095/313389>.

Mahlstedt, N., Horsfield, B., Weniger, P., Misch, D., Shi, X., Noah, M. and Boreham, C. 2022: Molecular hydrogen from organic sources in geological systems; Journal of Natural Gas Science and Engineering, v. 105, art. 104704, URL <https://doi.org/10.1016/J.JNGSE.2022.104704>.

Manitoba Business, Mining, Trade and Job Creation, 2025: Geoscience service; *in* GIS Map Gallery, Manitoba Business, Mining, Trade and Job Creation, Manitoba Geological Survey, URL <https://rdmaps.gov.mb.ca/Html5Viewer/index.html?viewer=MapGallery_Geology.MapGallery> [October 2025].

McGregor, C.R. 2011: GIS compilation of drillcore logs from Manitoba Geological Survey drilling programs, 1968-2007; Manitoba Innovation, Energy and Mines, Manitoba Geological Survey, Open File Report 2011-2, 1 DVD-ROM.

McGregor, C.R. 2013: Digital compilation of sub-Phanerozoic Precambrian geology in Manitoba; Manitoba Innovation, Energy and Mines, Manitoba Geological Survey, Open File Report 2012-2, 1 DVD-ROM.

Nicolas, M.P.B. 2024: Geologic hydrogen in the Williston and Hudson Bay basins, southwestern and northeastern Manitoba (parts of NTS 53, 54, 62, 63); *in* Report of Activities 2024, Manitoba Economic Development, Investment, Trade and Natural Resources, Manitoba Geological Survey, p. 164–171.

Nicolas, M.P.B., Coutts, D. and Ardakani, O.H. 2025: Lithogeochemistry of Precambrian core samples from beneath the Williston Basin, southwestern Manitoba (parts of NTS 62G, J, K, O, 63B, C, G, K); Manitoba Business, Mining, Trade and Job Creation, Manitoba Geological Survey, Data Repository Item DRI2025022, Microsoft® Excel® file.

Sheng, J.-R., Jiang, D.-S., Erdmann, S., Deng, G.-X., Duan, H.-C., Jackson, M., Devos, G., Moynier, F., Guo, H.-H. and Huang, F. 2025: Fluid-mediated uranium isotope fractionation in magmatic systems; Geochemical Perspectives Letters, v. 36, p. 1–7.

Sherwood Lollar, B., Onstott, T.C., Lacrampe-Couloume, G. and Ballentine, C.J. 2014: The contribution of the Precambrian continental lithosphere to global H_2 production; Nature, v. 516, no. 7531, p. 379–382, URL <https://doi.org/10.1038/nature14017>.

Sherwood Lollar, B., Voglesonger, K., Lin, L.-H., Lacrampe-Couloume, G., Telling, J., Abrajano, T.A., Onstott, T.C. and Pratt, L.M. 2007: Hydrogeologic controls on episodic H_2 release from Precambrian fractured rocks–energy for deep subsurface life on Earth and Mars; Astrobiology, v. 7, no. 6, p. 971–986, URL <https://doi.org/10.1089/ast.2006.0096>.

Stevens, T.O. and McKinley, J.P. 1995: Lithoautotrophic microbial ecosystems in deep basalt aquifers; Science, v. 270, no. 5235, p. 450–455, URL <https://doi.org/10.1126/science.270.5235.450>.

Warr, O., Song, M. and Sherwood Lollar, B. 2023: The application of Monte Carlo modelling to quantify in situ hydrogen and associated element production in the deep subsurface; Frontiers in Earth Science, v. 11, p. 1–14.

Whitfield, J.M., Rogers, J.J.W. and Adams, J.A.S. 1959: The relationship between the petrology and the thorium and uranium contents of some granitic rocks; Geochimica et Cosmochimica Acta, v. 17, p. 248–271.

Zgonnik, V. 2020: The occurrence and geoscience of natural hydrogen: a comprehensive review; Earth-Science Reviews, v. 203, art. 103140, URL <https://doi.org/10.1016/J.EARSCIREV.2020.103140>.

GS2025-11

Effects of drill-cutting size and age on the reliability of measuring helium and other volatiles in samples, southwestern Manitoba (parts of NTS 62K6, 7, 11)

by M.P.B. Nicolas, C.M. Smith[1] and M.P. Smith[1]

In Brief:

- Volatile analysis of legacy drill cuttings was done on four oil wells
- Helium and hydrocarbons are found consistently throughout the Stony Mountain Fm. to Interlake Gp. Interval
- Comparisons of RVS results from drill cuttings from the 1970's to 2000's can be made with confidence

Citation:
Nicolas, M.P.B., Smith, C.M. and Smith, M.P. 2025: Effects of drill-cutting size and age on the reliability of measuring helium and other volatiles in samples, southwestern Manitoba (parts of NTS 62K6, 7, 11); *in* Report of Activities 2025, Manitoba Business, Mining, Trade and Job Creation, Manitoba Geological Survey, p. 110–119.

Summary

Drill cuttings from four legacy oil wells were sampled for volatile analysis using Rock Volatiles Stratigraphy (RVS). This testing was conducted to 1) evaluate the helium and hydrocarbon potential of the interval analyzed, and 2) assess how drill-cutting size, age of samples and drill-cutting technology influence the reliability of RVS results. The sampled wells are located at L.S. 2, Sec. 14, Twp. 18, Rge. 29, W 1st Mer. (abbreviated 2-14-18-29W1), 2-14-16-28W1, 12-34-15-26W1 and 2-7-16-26W1 in southwestern Manitoba. These wells were selected based on stratigraphy and geographic location, as well as age and size of drill cuttings. In this study, cuttings from the 1970s and 1990s, sampled from the Ordovician Stony Mountain Formation to Silurian Interlake Group interval, were compared. The volatile compounds measured included C1–C10 hydrocarbons, carbon dioxide, water and helium. This study found that reliable RVS results can be obtained from drill cuttings of different age and size. Low but consistent helium and hydrocarbon concentrations were identified in all samples. The ubiquity of helium and hydrocarbons in these samples suggests that the lack of identified accumulations in this interval is not related to source, generation, migration or quantity, but rather a need to identify, and explore for, reservoirs, seals and traps.

Introduction

A review of helium occurrences in southwestern Manitoba oil and gas wells indicated encouraging helium occurrences in the subsurface (Nicolas, 2018); some indicative of concentrations of economic interest. The highest and most notable values ranged from 0.3 to 2.0 mol. % helium and occurred mostly in lower Paleozoic horizons. To better understand these results, two follow-up studies were conducted to measure fluids trapped in micropore spaces in legacy drill cuttings from lower Paleozoic horizons, reported in Nicolas et al. (2023b, 2024a). For these studies, the Manitoba Geological Survey (MGS) in partnership with Advanced Hydrocarbon Stratigraphy, Inc. (AHS) studied the volatile fraction of fluids in drill cuttings from four oil wells drilled in the lower Paleozoic using a Rock Volatiles Stratigraphy (RVS) system. The analysis measured fluid, gas, hydrocarbon, rock and reservoir properties to evaluate for helium prospectivity in Manitoba and provide additional insights into local hydrocarbon systems.

The RVS system is an innovative analytical approach that provides information on the fluid history of a stratigraphic unit, and when combined with other wells, offers constraints on pore-space fluid composition and geology of an area. Nicolas et al. (2023b) described the methodology of the RVS system. The insights provided from prior RVS results detail a complex subsurface fluid system, with prolific helium generation, migration and multistratal accumulations, and a highly prospective unexplored hydrocarbon system in Devonian strata in southwestern Manitoba.

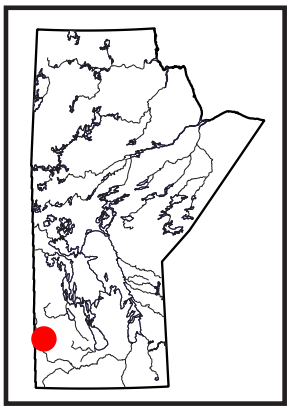

Throughout these studies, drill-cutting size has been an important factor for interpreting results. Coarser-grained drill cuttings are expected to preserve fluids in microporosity better than finer-grained drill cuttings. An attenuation of the results in fine-grained drill cuttings can occur, but when comparing trends from one well to another, that attenuation is recognizable (see Nicolas et al., 2024a for discussion on attenuation of results). AHS has done rock volatile analysis on hundreds of legacy oil wells where the age of cuttings or core appeared to not affect RVS results or the ability to get insight into the fluid system and reservoir properties of the sampled sections (Smith and Smith, 2020; Smith et al., 2021a, b, 2022a, b, 2023a, b, c; Nicolas et al., 2023b, 2024a), however a direct test of this assumption has not been completed.

[1] Advance Hydrocarbon Stratigraphy, Inc., Tulsa, Oklahoma

This study is two-fold: 1) identify potential helium and hydrocarbon prospects in Paleozoic horizons that act as reservoirs for migrating fluids from deeper, leaky reservoirs; and 2) test the effect of drill-cutting size and age and drill-cutting technology on the reliability of RVS results in Manitoba. For this study, a suite of 100 samples were collected over a short stratigraphic interval from four wells (25 samples per well) in a geographic area where the effects of the Superior boundary zone were deemed to be equal (Figure GS2025-11-1; Table GS2025-11-1).

Methodology

Drill cuttings from four historical petroleum exploration wells in southwestern Manitoba were selected for testing using the RVS system. The four wells sampled for this study are 1) ASM-BTO et al Gamber Prov. 100/02-14-018-29W1/00 (oil and gas well licence 2534, Manitoba Business, Mining, Trade and Job Creation, Winnipeg) at 2-14-18-29W1; 2) ASM-BTO et al Ft. Ellice Prov. 100/02-14-016-28W1/00 (oil and gas well licence 2536) at 2-14-16-28W1; 3) Chel TRC Teck Birtle Prov. 100/12-34-015-26W1/00 (oil and gas well licence 4383) at 12-34-15-26W1; and 4) Husky South Birtle 100/02-07-016-26W1/00 (oil and gas well licence 4744) in 2-7-16-26W1. The two older wells, oil and gas well licences 2534 and 2536, were drilled in 1974, and the two younger wells, oil and gas well licences 4383 and 4744, were drilled in 1993 and 1997, respectively.

The older wells had drill cuttings that were coarser grained (granule to pebble size), than those from the younger wells, which typically were medium-grained sand-sized cuttings (Figure GS2025-11-2a–d). Sampling was limited to 25 samples per well and covered the stratigraphic interval from the Stony Mountain Formation to the top of the Interlake Group, and in some wells, to the base of the Ashern Formation.

As is with all drill cuttings, the sample intervals are predetermined at the time of drilling. For the two older wells, the predetermined minimum sampling interval was 3.05 m (10 ft.) per sample vial; to collect 25 samples and cover the target stratigraphic horizons, sampling for this study was limited to one sample every 6.10 m (20 ft.). For the two newer wells, the predetermined sampling interval was 5 m, which was followed for this study. As a result, the older wells have a gap in their representative sample intervals compared to the newer wells.

The samples were sent to the AHS laboratory in Tulsa, Oklahoma, for analysis by their proprietary cryotrap mass spectrometer (CT-MS) system specially designed to analyze for C1–C10 hydrocarbons, helium, formation water, CO_2, sulphur gasses, organic acids and mechanical strength. The same volatiles were measured and the same analytical methods were used on these samples as those described in Nicolas et al. (2023b).

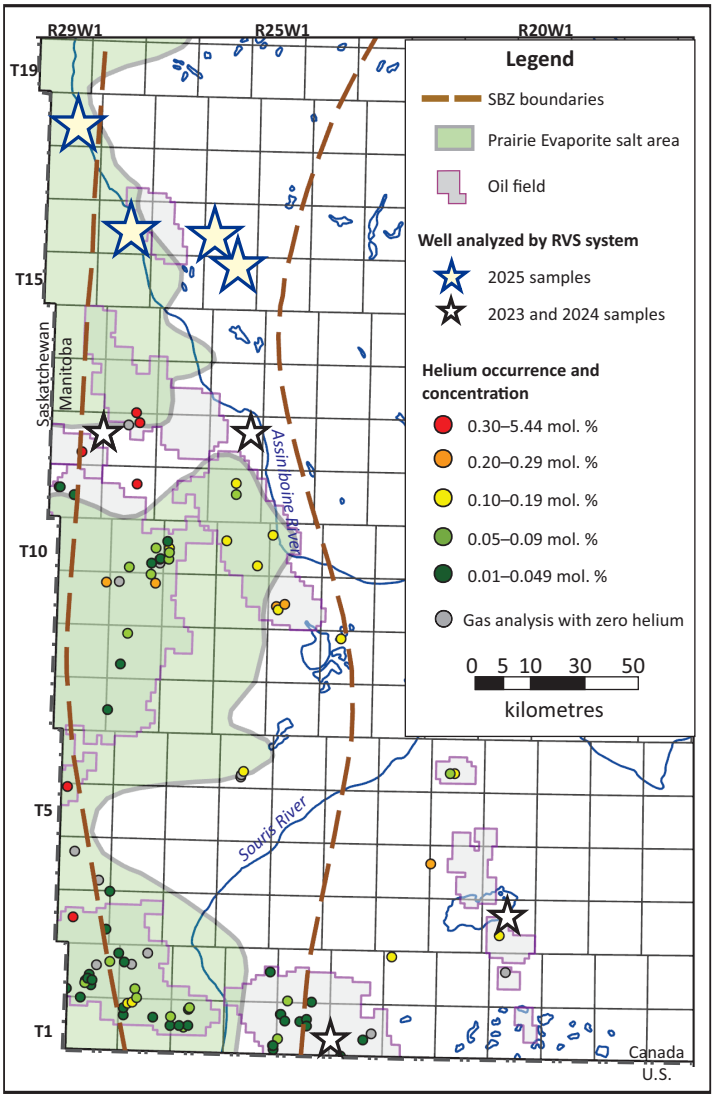

Figure GS2025-11-1: *Map of southwestern Manitoba showing the 1) locations of wells sampled in 2023, 2024 and 2025 and analyzed by the Rock Volatiles Stratigraphy (RVS) system, 2) distribution of gas analyses and helium occurrences (modified from Nicolas, 2018), and 3) locations of oil fields (Fulton-Regula, 2024). Abbreviation: SBZ, Superior boundary zone.*

Rock Volatiles Stratigraphy results

The entirety of the RVS data is available in Data Repository Item DRI2025021 (Nicolas et al., 2025[1]). A wide range of information can be extracted from the RVS data. However, this report focuses only on the data used to evaluate helium and hydrocarbon prospectivity, as well as selected data for other fluids, such as hydrocarbons, water and CO_2, as they provide additional information about the overall fluid dynamics of the basin.

[1] MGS Data Repository Item DRI2025021, containing the data or other information sources used to compile this report, is available online to download free of charge at https://manitoba.ca/iem/info/library/downloads/index.html, or on request from minesinfo@gov.mb.ca, or by contacting the Resource Centre, Manitoba Business, Mining, Trade and Job Creation, 360-1395 Ellice Avenue, Winnipeg, Manitoba R3G 3P2, Canada.

Table GS2025-11-1: List of wells sampled in southwestern Manitoba for Rock Volatiles Stratigraphy analysis. Abbreviations: PDC, polycrystalline diamond compact; TVD, true vertical depth.

Unique well identifier (UWI)	Oil and gas well licence	Easting (Zone 14, NAD83)	Northing (Zone 14, NAD83)	Year drilled	Total depth (m TVD)	Sample depth range (m TVD)	Sample interval	Stratigraphy	Comments
100/02-14-018-29W1/00	2534	332007.76	5601016.20	1974	1332.3	1149.10–999.74	~6 m (20 ft.)	Stony Mountain Fm. to Interlake Gp.	Salt-gel, starch and diesel fuel drilling mud used in deeper section; drilled with mill-tooth drill bit
100/02-14-016-28W1/00	2536	341353.60	5581038.45	1974	1284.7	1091.18–941.83	~6 m (20 ft.)	Stony Mountain Fm. to Ashern Fm.	Salt-gel and starch drilling mud used in deeper sections; drilled with mill-tooth drill bit
100/12-34-015-26W1/00	4383	358339.73	5576471.07	1993	1318.0	1110–990	5 m	Stony Mountain Fm. to Ashern Fm.	Gel chem drilling mud; drill bit undetermined but likely PDC drill bit
100/02-07-016-26W1/00	4744	354459.10	5579086.17	1997	1345.0	1145–1025	5 m	Stony Mountain Fm. to Interlake Gp.	Gel chem drilling mud; drilled with tungsten carbide button drill bit

Oil and gas well at 2-14-18-29W1 (licence 2534)

Drill cuttings collected from the well at 2-14-18-29W1 were sampled from 1149.10 m true vertical depth (TVD) in the Stony Mountain Formation up to 999.74 m TVD in the upper Interlake Group. Samples represent a 3.05 m (10 ft.) section and for this study every second vial was sampled, equating to every 6.10 m (20 ft.). Figure GS2025-11-3 shows the data logs for select analyses, including helium, as they relate to stratigraphy.

Oil and gas well at 2-14-16-28W1 (licence 2536)

Drill cuttings collected from the well at 2-14-16-28W1 were sampled from 1091.18 m TVD in the Stony Mountain Formation up to 941.83 m TVD at the base of the Ashern Formation. Each sample is representative of a 3.05 m (10 ft.) section and samples were taken every 6.10 m (20 ft.). Figure GS2025-11-4 shows the data logs for select analyses, including helium, as they relate to stratigraphy and lithology. For this well, the lithology descriptions and estimated porosity for each sampled interval are shown in Figure GS2025-11-4; this information was compiled from the technical well file (oil and gas well licence 2536).

Oil and gas well at 12-34-15-26W1 (licence 4383)

Drill cuttings collected from the well at 12-34-15-26W1 were sampled from 1110 m TVD in the Stony Mountain Formation to 990 m TVD at the base of the Ashern Formation. Samples collected represent 5 m intervals. Figure GS2025-11-5 shows the data logs for select analyses, including helium, as they relate to stratigraphy.

Oil and gas well at 2-7-16-26W1 (licence 4744)

Drill cuttings collected from the well at 2-7-16-26W1 were sampled from 1145 m TVD in the Stony Mountain Formation to 1025 m TVD in the upper Interlake Group. Samples collected represent 5 m intervals. Figure GS2025-11-6 shows the data logs for select analyses, including helium, as they relate to stratigraphy.

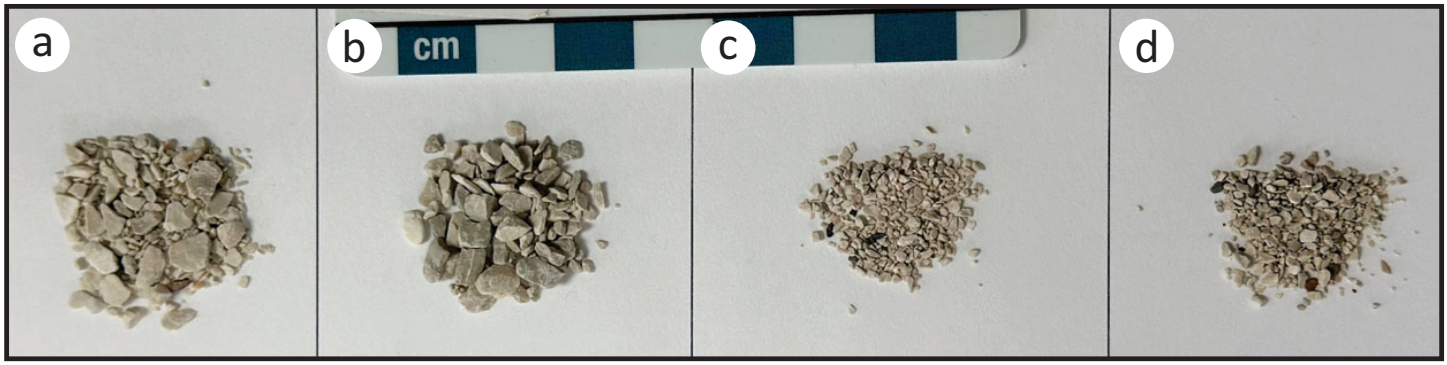

Figure GS2025-11-2: *Grain-size variations in the drill cuttings for the four wells in southwestern Manitoba sampled for this study:* ***a)*** *L.S. 2, Sec. 14, Twp. 18, Rge. 29, W 1st Mer. (abbreviated 2-14-18-29W1; oil and gas well licence 2534) at 1018.03–1021.08 m true vertical depth (TVD; sample 106-25-2534-4),* ***b)*** *2-14-16-28W1 (oil and gas well licence 2536) at 1008.90–1011.94 m TVD (sample 106-25-2536-12),* ***c)*** *12-34-15-26W1 (oil and gas well licence 4383) at 1045 m TVD (sample 106-25-4383-12),* ***d)*** *2-7-16-26W1 (oil and gas well licence 4744) at 1075 m TVD (sample 106-25-4744-11). The older (1970s) wells with coarser drill cuttings are shown in (a) and (b) and the newer (1990s) wells with finer drill cuttings are shown in (c) and (d).*

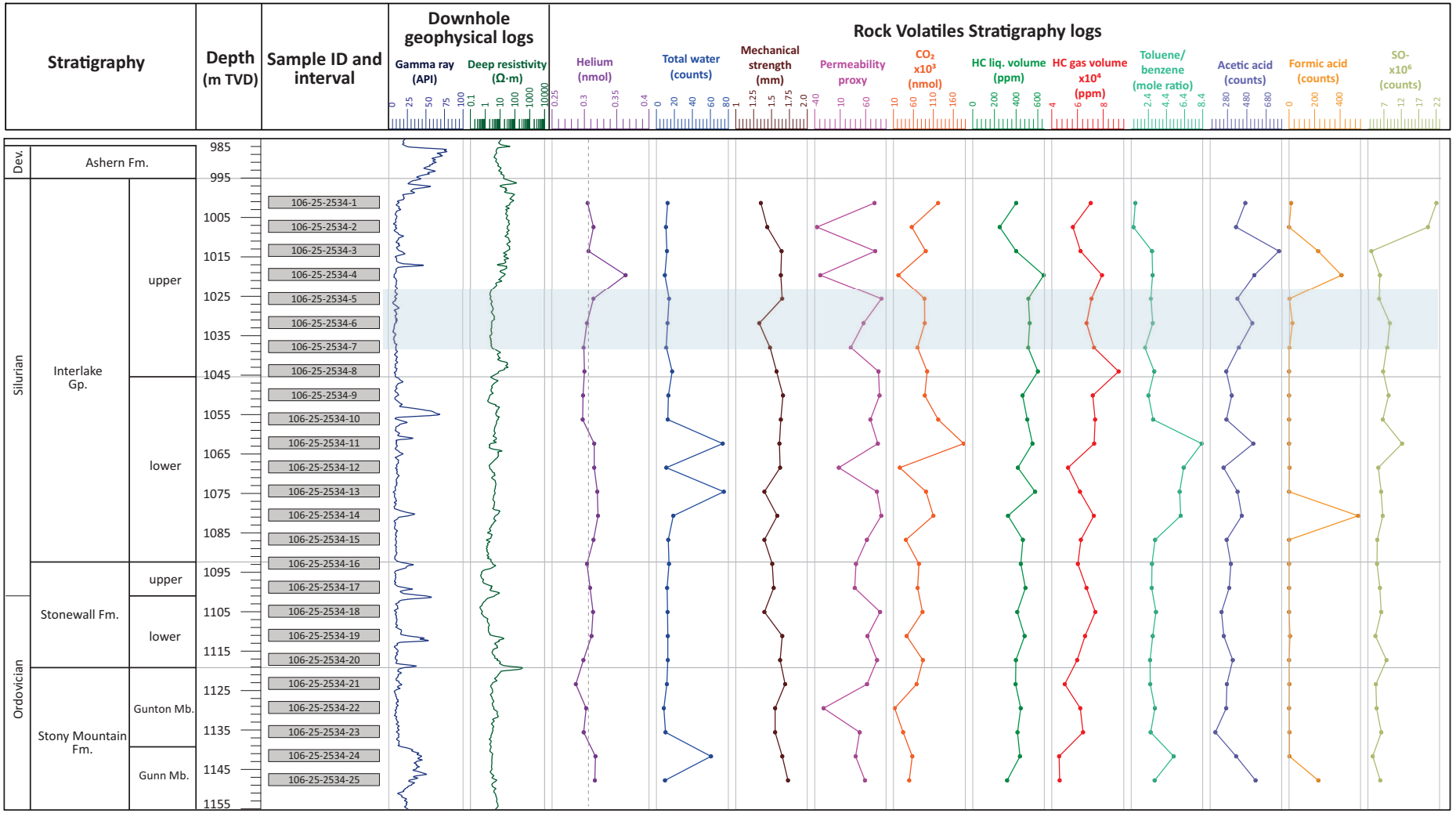

Figure GS2025-11-3: *Stratigraphy and Rock Volatiles Stratigraphy data logs for the oil and gas well at L.S. 2, Sec. 14, Twp. 18, Rge. 29, W 1st Mer. (2-14-18-29W1, southwestern Manitoba; oil and gas well licence 2534), including select downhole geophysical logs. Samples covered a 3.05 m (10 ft.) interval every 6.10 m (20 ft.). Dashed grey vertical line in helium track is the average value (0.306 nanomoles [nmol]) for all wells in this study combined. Mechanical strength of the sample increases from left to right on the mechanical strength log; the permeability proxy log indicates increased permeability from left to right. Blue-shaded band represents an interval of higher porosity and coarser-grained dolomitic textures that correlates to the shaded band in Figure GS2025-11-4. Abbreviations: Ω, ohm; Dev., Devonian; HC, hydrocarbon; liq., liquid; TVD, true vertical depth.*

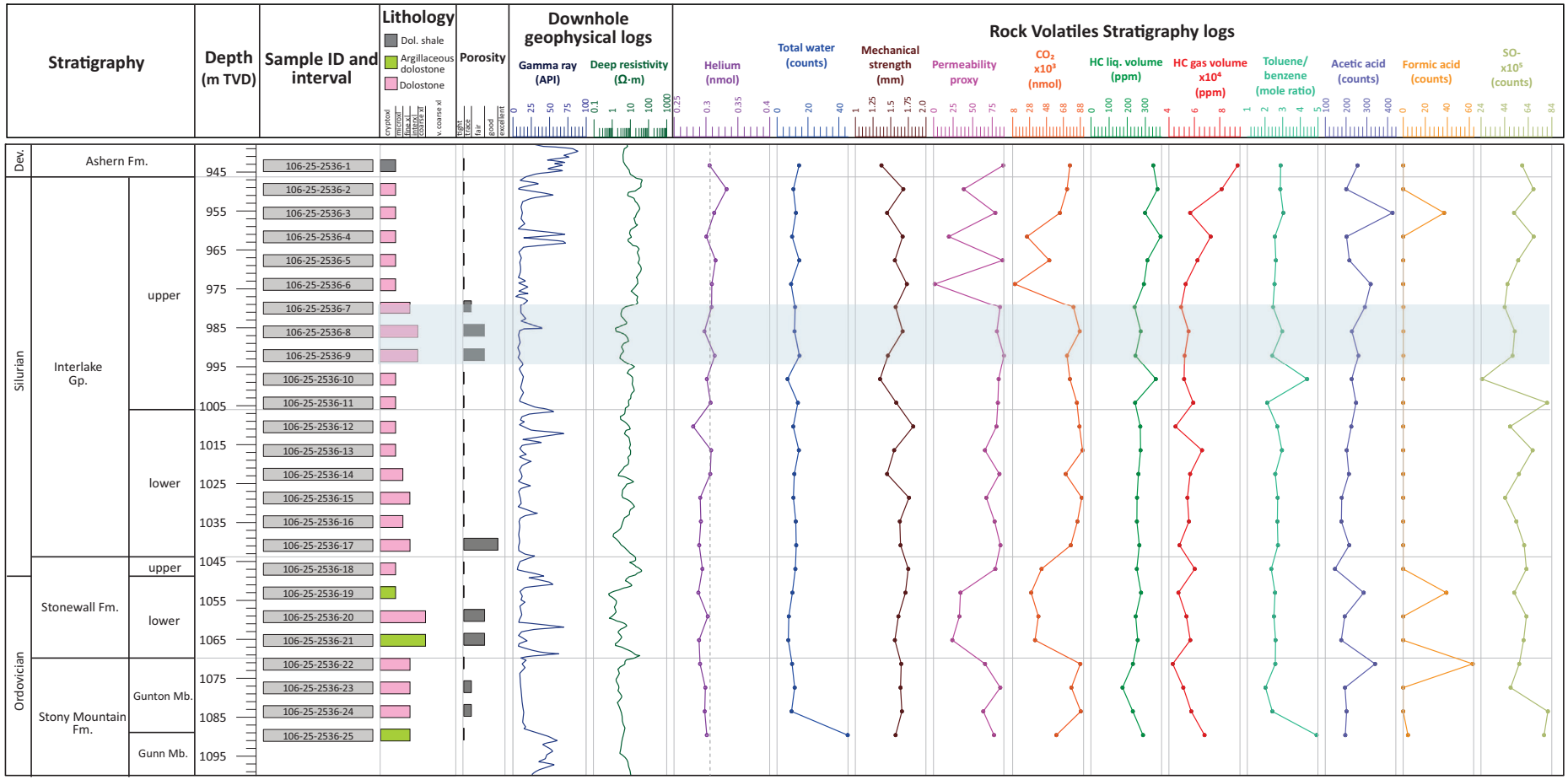

Figure GS2025-11-4: *Stratigraphy, lithology, porosity and Rock Volatiles Stratigraphy data logs for the oil and gas well at L.S. 2, Sec. 14, Twp. 16, Rge. 28, W 1st Mer. (2-14-16-28W1, southwestern Manitoba; oil and gas well licence 2536), including select downhole geophysical logs. Samples covered a 3.05 m (10 ft.) interval every 6.10 m (20 ft.). Dashed grey vertical line in helium track is the average value (0.306 nanomoles [nmol]) for all wells in this study combined. Mechanical strength of the sample increases from left to right on the mechanical strength log; the permeability proxy log indicates increased permeability from left to right. Blue-shaded band represents an interval of higher porosity and coarser-grained dolomitic textures. Abbreviations: Ω, ohm; coarse xl, coarse crystalline; cryptoxl, cryptocrystalline; Dev., Devonian; Dol., dolomitic; fine xl, fine crystalline; HC, hydrocarbon; interxl, intercrystalline; liq., liquid; microxl, microcrystalline; TVD, true vertical depth; v., very.*

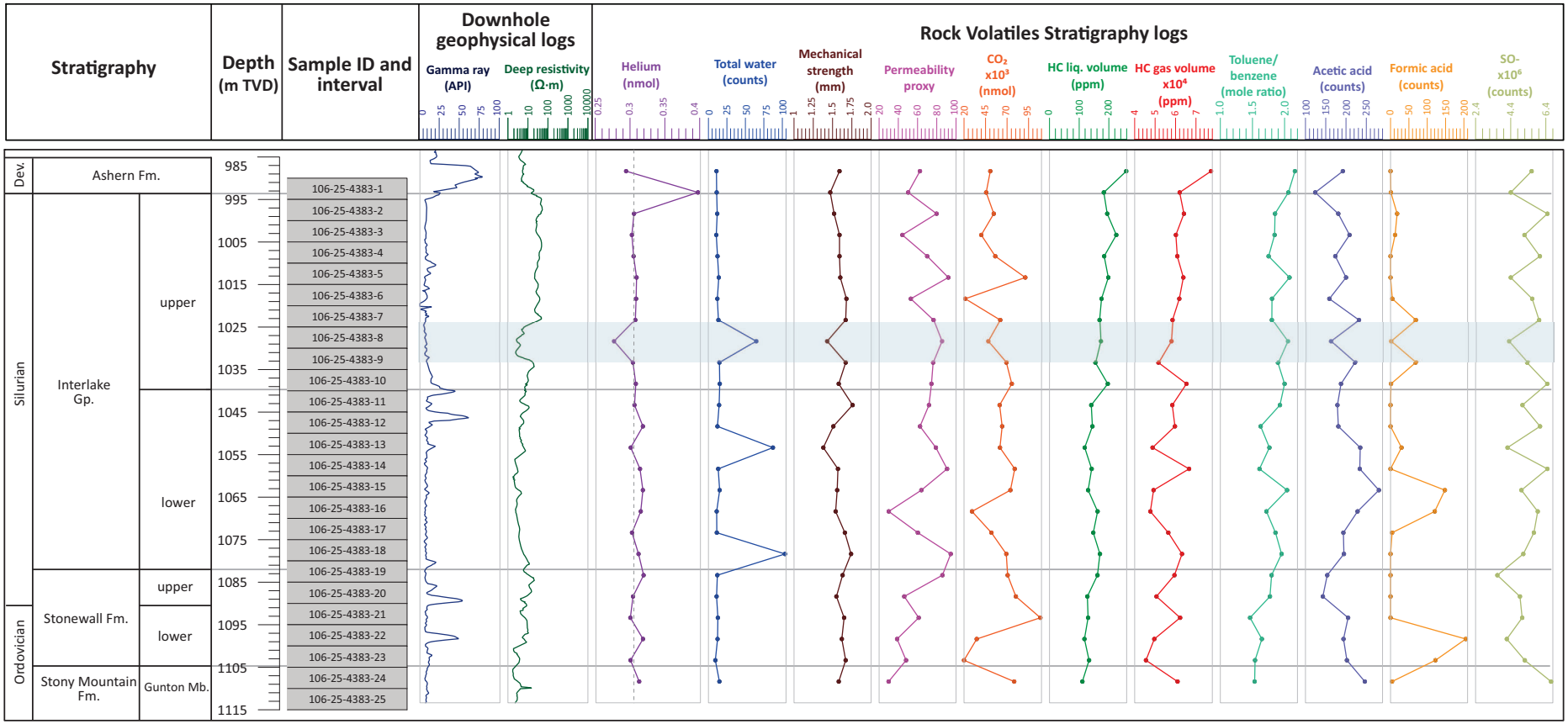

Figure GS2025-11-5: *Stratigraphy and Rock Volatiles Stratigraphy data logs for the oil and gas well at L.S. 12, Sec. 34, Twp. 15, Rge. 26, W 1st Mer. (12-34-15-26W1, southwestern Manitoba; oil and gas well licence 4383), including select downhole geophysical logs. Samples covered a 5.0 m interval. Dashed grey vertical line in helium track is the average value (0.306 nanomoles [nmol]) for all wells in this study combined. Mechanical strength of the sample increases from left to right on the mechanical strength log; the permeability proxy log indicates increased permeability from left to right. Blue-shaded band represents an interval of higher porosity and coarser-grained dolomitic textures that correlates to the shaded band in Figure GS2025-11-4. Abbreviations: Ω, ohm; Dev., Devonian; HC, hydrocarbon; liq., liquid; TVD, true vertical depth.*

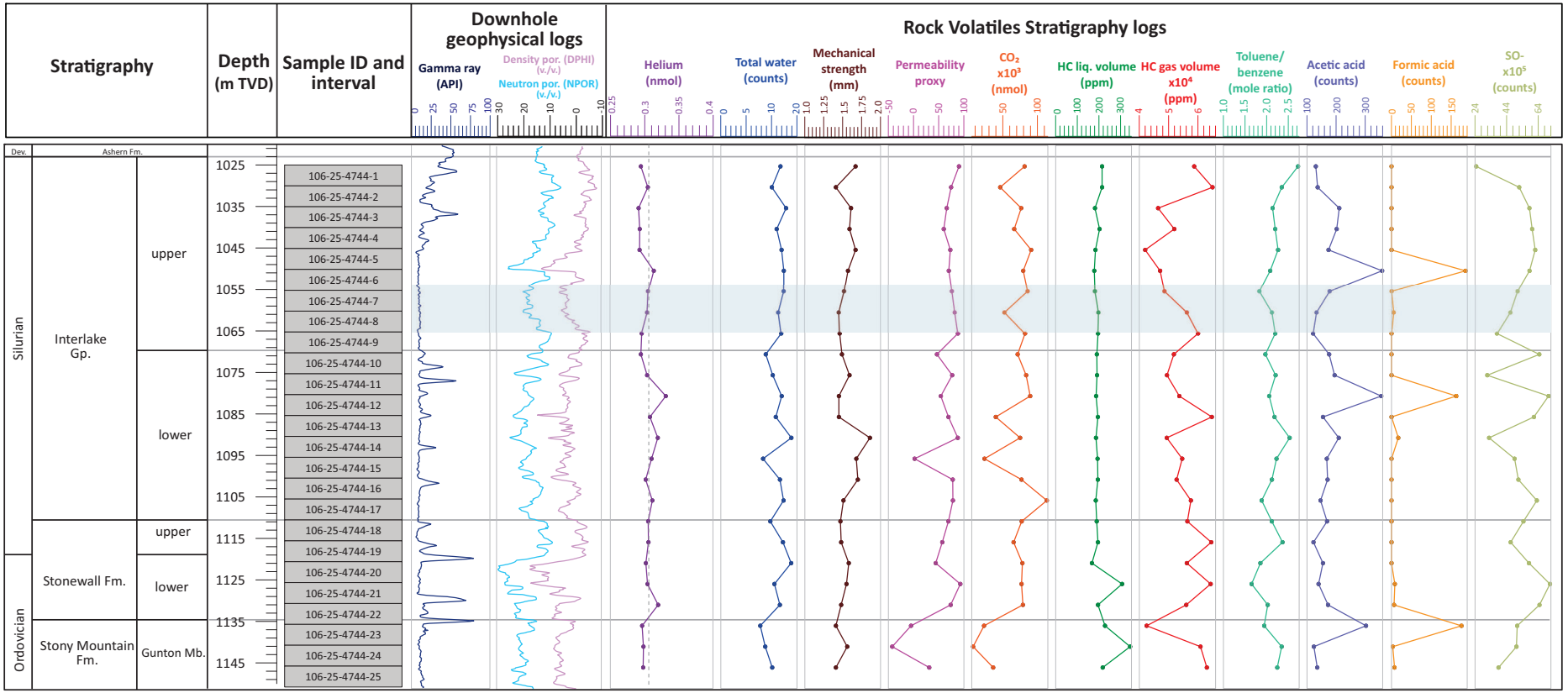

Figure GS2025-11-6: *Stratigraphy and Rock Volatiles Stratigraphy data logs for the oil and gas well at L.S. 2, Sec. 7, Twp. 16, Rge. 26, W 1st Mer. (2-7-16-26W1, southwestern Manitoba; oil and gas well licence 4744), including select downhole geophysical logs. Samples covered a 5.0 m interval. Dashed grey vertical line in helium track is the average value (0.306 nanomoles [nmol]) for all wells in this study combined. Mechanical strength of the sample increases from left to right on the mechanical strength log; the permeability proxy log indicates increased permeability from left to right. Blue-shaded band represents an interval of higher porosity and coarser-grained dolomitic textures that correlates to the shaded band in Figure GS2025-11-4. Abbreviations: Ω, ohm; Dev., Devonian; DPHI, density porosity; HC, hydrocarbon; liq., liquid; por., porosity; NPOR, neutron porosity; TVD, true vertical depth.*

Discussion

Stratigraphic homogeneity

The four wells used in this study are geographically close to each other to minimize the stratigraphic variability between each well. The strong similarities in the gamma-ray and resistivity logs, as well as the uniform thickness of each formation and member supports the assumption of stratigraphic homogeneity to minimize structural and lithological variations at the sample level (Stony Mountain Formation to Ashern Formation). As such, the lithology and porosity logs from well 2-14-16-28W1 (Figure GS2025-11-4) can be used as a proxy for the other three wells.

An example of this is a thick interval with higher porosity and coarser-grained dolomitic textures in the well at 2-14-16-28W1, shown by the blue-shaded band in Figure GS2025-11-4. Using the geophysical signature of the resistivity log as a correlation tool, this same blocky signature of lower resistivity can be found at similar stratigraphic positioning in the other three wells (blue-shaded bands in Figures GS2025-11-3, -5, -6). It is also equivalent to an interval with higher density and neutron log responses in the well at 2-7-16-26W1. This correlation indicates minor variations in the vertical positioning of this interval within the upper Interlake Group, as well as negligible variations in thickness of that unit. These differences are likely due to local facies changes and/or diagenetic porosity variations. Neither of these factors are of significance at the scale of the helium system being evaluated here.

Helium

In comparison to the RVS profiles in Nicolas et al. (2023b, 2024a), the sections analyzed are much smaller, which limits broader, large-scale observations. Despite this, none of these sections show any helium occurrences above the 0.7 nanomole (nmol) helium threshold for potential economic accumulations. This suggests that 1) helium migrating through the system is low in concentration, diffuse and/or flushed due to high permeability, 2) helium is not accumulating to any significant degree within the studied intervals, or 3) any helium generated from the Precambrian crystalline basement is trapped in deeper strata (e.g., Winnipeg Formation) or baffled, limiting the migration upward in these locations.

The helium values in all four wells are similar with an overall average of 0.306 nmol; this average is shown by the dashed grey vertical line on the helium tracks in Figures GS2025-11-3 to -6. Even though the variations from the average line are small, it is possible to identify some trends. These trends become more apparent when compared to the more pronounced trends in the helium tracks in Nicolas et al. (2023b, 2024a), particularly in the uppermost upper Interlake Group, lower Interlake Group and lower Stonewall Formation.

In previous studies, the upper strata in the upper Interlake Group commonly showed an abrupt increase in helium to approximately 2.0 nmol (Nicolas et al., 2023a, b). Although a large spike in helium is absent in this study, there is a small notable increase in the average helium value, up to a maximum of 0.3965 nmol, in the Interlake Group. In the upper Interlake Group section, this study's samples displayed similar trend lines between wells, including a small increase in the upper quarter of the upper Interlake Group section. In previous Manitoba studies, the lower Interlake Group had consistently shown above average helium values, commonly above the 0.7 nmol economic threshold. A similar pattern occurs in the lower Stonewall Formation where a small increase midway through the section consistently occurs in this and previous studies.

Radiolysis is the dominant pathway for helium generation and is also an important pathway for hydrogen generation. Nicolas et al. (2025b) modelled the hydrogen generation rate by radiolysis from Precambrian basement rocks by analyzing the lithogeochemistry of core samples (Nicolas et al., 2025a). One of the samples was from a core located at 16-18-18-29W1, just a few kilometres west of the well at 2-14-18-29W1. The geochemistry of that core sample (a granitic gneiss) indicated moderately low hydrogen generation for a felsic rock, attributed to high-grade metamorphism and weathering that reduced uranium and thorium concentrations. Lower concentrations of radioactive elements from this area may result in lower helium quantities migrating into the overlying stratigraphic section. This hypothesis is based on a single Precambrian sample, however, the Precambrian lithology in the other wells in this area is unknown, making extrapolations and assumptions on Precambrian helium contribution to the system difficult.

Hydrocarbons

All four wells indicate hydrocarbons throughout the sections studied, with hydrocarbon liquid and gas volume traces mimicking each other. The ratio of toluene/benzene is a proxy measurement used to identify zones in which large volumes of oil may have migrated. Values ≥3 are considered possible indicators, and values ≥5 are considered likely indicators, since such ratios are rare in produced crude oils. Elevated ratios suggest fractionation, with the larger, more polar toluene molecule retained in the rock matrix. Acetic and formic acid measurements can further indicate oil–water contacts (Rossini, 1960; Smith, 1968; Lord et al., 2018). The correlations of these five geochemical tracks suggest a hydrocarbon system present in the strata.

In particular, the well at 2-14-18-29W1 suggests a hydrocarbon system migrating within the lower Interlake Group as shown by the high toluene/benzene ratio between 1085 and 1055 m TVD. Coincident acetic acid and formic acid peaks at the base of that interval at 1077 m TVD suggest some accumulation may have occurred and a weak oil–water contact formed. The water content increase between 1060.70 and 1078.99 m TVD also follows this rationale. The high hydrocarbon liquid and gas volume values in the lower Interlake Group support this, how-

ever, high values also extend the hydrocarbon column higher in the strata, up to the upper Interlake Group. This may suggest a multilevel hydrocarbon system, with slow migration dominating the lower Interlake Group—slow enough to allow an oil–water contact signature to be preserved—but with accumulation of oil and gas higher up in the section. A similar hydrocarbon interpretation can be made in the same strata section in the 12-34-15-26W1 and 2-7-16-26W1 wells, but the former may be richer in lighter hydrocarbons (gas fraction).

An overall gradual increase in hydrocarbons (liquid and gas) was noted in all wells within the study area, reaching a maximum just below the Ashern Formation, similar to the findings of Nicolas et al. (2023b, 2024a). This suggests the Devonian Ashern Formation is acting as a regional sealing unit by minimizing, dampening or preventing vertical migration of hydrocarbon fluid; this is somewhat expected since the Ashern Formation is dominantly a dolomitic shale. These hydrocarbon fluids were noted, in all study area wells, to have higher concentrations than those measured for the same interval in prior studies (Nicolas et al., 2023a, b, 2024a, b). In the experience of AHS, this persistence of good quality light hydrocarbons in a sample set is what indicates proximity to a hydrocarbon resource. All the samples in this suite have this persistent signature.

In the study area, oil production is currently limited to the shallower Devonian Torquay Formation to Mississippian Bakken Formation intervals, and exploration for deeper oil resources is sparse. Previous RVS studies in Manitoba consistently indicate hydrocarbon opportunities in deeper Devonian strata, indicative of unexplored resources below current known production. At a minimum, these results indicate hydrocarbons are in this system, but economic accumulations can only be confirmed through targeted exploration.

Drill-cutting age and size

To evaluate drill-cutting age and size and their effect on RVS results, the RVS logs need to be viewed in a broader context. If results from an older well agree with those of a new well, when all else is equal, then age and size do not matter. For example, helium values show no accumulation, with background helium values that are comparable across wells regardless of the age and size of the drill cuttings. This is supported by comparing the mean and standard deviation of helium values for wells from the 1970s (2-14-18-29W1 and 2-14-16-28W1) and for wells from the 1990s (12-35-15-26W1 and 2-7-16-26W1). The wells from the 1970s have a mean concentration of 0.3057 ±0.0132 nmol and the wells from the 1990s have a mean of 0.3069 ±0.0157 nmol. A similar observation is observed with total water, mechanical strength, permeability, CO_2 and sulphate (SO-) proxy. Given that mechanical strength and permeability are directly measured from the rock and there is stratigraphic homogeneity in this suite of samples, similarities are expected. If the drill-cutting size were an issue for readings, then it would be expected for the results from older wells to deviate consistently from newer wells, however, this is not the case here. In Nicolas et al. (2023b), an attenuation of readings in newer (from the 2000s) drill cuttings that are fine grained was observed, but overall trends compared to older coarse drill cuttings were the same.

Conclusions

In the wells from this study, helium is present but no accumulations of interest occur in the Interlake Group, Stonewall Formation or Stony Mountain Formation. The same conclusion can be made for hydrocarbons. These observations do not preclude the possibility of economic concentrations above or below the sampled intervals. The ubiquity of helium and hydrocarbons in these samples indicate that the absence of economic accumulations in Ordovician and Silurian strata are not related due to limitations in source, generation, migration or quantity, but rather a need to identify reservoirs, seals and traps.

When comparing datasets from wells from the 1970s and 1990s, drill-cutting age and size does not affect the quality of RVS data or the ability to interpret and understand fluid systems. Even though attenuation of results (i.e., lower measurements) may occur in newer wells with fine-grained cuttings, overall trends of volatiles preserved in the micropores are the same as those from older, coarse-grained cuttings. Being aware that attenuation may be a factor is important when doing well-to-well comparisons with drill-cuttings–derived data. This awareness allows drill cuttings from the 1970s to 2000s to be compared directly to each other. In conclusion, these results broadly show that comparisons between drill cuttings of different ages and sizes can be made with confidence.

Economic considerations

The RVS data from these four Manitoba wells indicate that helium and hydrocarbons are present in the stratigraphic system from the Ordovician Stony Mountain Formation to Silurian Interlake Group, but not in economic concentrations. Nonetheless, the consistent detection of both fluids highlights the potential for larger accumulations of helium or hydrocarbons in unexplored horizons above or below the interval tested.

The helium in the Ordovician and Silurian strata appears to occur independently of hydrocarbons and can be produced on its own basis, as green helium. Green helium is a highly attractive target for investment and exploration, particularly in the growing market for environmentally sustainable resources.

Acknowledgments

The authors would like to thank C. Epp and P. Belanger from the Manitoba Geological Survey for their assistance with the drill cuttings. The authors would like to acknowledge P.J. Fulton-Regula and P.E. Fraino (Manitoba Geological Survey) for their critical review of this report.

References

Fulton-Regula, P. 2024: Manitoba's designated oil fields and pools 2024 (NTS 62F/1-3, 6-11, 14-16; 62K/1-3, 6-8); Manitoba Economic Development, Investment, Trade and Natural Resources, Manitoba Geological Survey, URL <https://www.manitoba.ca/iem/petroleum/f_p_codes/pool_book_2024.pdf> [October 2025].

Lord, D., Allen, R., Rudeen, D., Wocken, C. and Aulich, T. 2018: DOE/DOT crude oil characterization research study, task 2 test report on evaluating crude oil sampling and analysis methods, revision 1 - winter sampling; Sandia National Laboratories, Report SAND2018-5909, 177 p.

Nicolas, M.P.B. 2018: Summary of helium occurrences in southwestern Manitoba; *in* Report of Activities 2018, Manitoba Growth, Enterprise and Trade, Manitoba Geological Survey, p. 110–118.

Nicolas, M.P.B., Coutts, D. and Ardakani, O.H. 2025a: Lithogeochemistry of Precambrian core samples from beneath the Williston Basin, southwestern Manitoba (parts of NTS 62G, J, K, O, 63B, C, G, K); Manitoba Business, Mining, Trade and Job Creation, Manitoba Geological Survey, Data Repository Item DRI2025022, Microsoft® Excel® file.

Nicolas, M.P.B., Coutts, D. and Ardakani, O.H. 2025b: Preliminary investigation into the natural hydrogen generation potential of Precambrian rocks beneath the Williston Basin, southwestern Manitoba (parts of NTS 62G, J, K, O, 63B, C, G, K); *in* Report of Activities 2025, Manitoba Business, Mining, Trade and Job Creation, Manitoba Geological Survey, p. 104–109.

Nicolas, M.P.B., Smith, C.M. and Smith, M.P. 2023a: Rock Volatiles Stratigraphy data from drill cuttings from three wells in southwestern Manitoba (parts of NTS 62F2, K3); Manitoba Economic Development, Investment, Trade and Natural Resources, Manitoba Geological Survey, Data Repository Item DRI2023014, Microsoft® Excel® file.

Nicolas, M.P.B., Smith, C.M. and Smith, M.P. 2023b: Volatiles analysis of drill cuttings to evaluate the helium prospectivity of southwestern Manitoba (parts of NTS 62F2, K3); *in* Report of Activities 2023, Manitoba Economic Development, Investment, Trade and Natural Resources, Manitoba Geological Survey, p. 93–104.

Nicolas, M.P.B., Smith, C.M. and Smith, M.P. 2024a: Rock volatiles analysis of drill cuttings to evaluate the helium and hydrocarbon prospectivity of southwestern Manitoba (parts of NTS 62F2, K3); *in* Report of Activities 2024, Manitoba Economic Development, Investment, Trade and Natural Resources, Manitoba Geological Survey, p. 153–163.

Nicolas, M.P.B., Smith, C.M. and Smith, M.P. 2024b: Rock Volatiles Stratigraphy data from drill cuttings from four oil wells in southwestern Manitoba (parts of NTS 62F2, K3); Manitoba Economic Development, Investment, Trade and Natural Resources, Manitoba Geological Survey, Data Repository Item DRI2024008, Microsoft® Excel® file.

Nicolas, M.P.B., Smith, C.M. and Smith, M.P. 2025: Rock Volatiles Stratigraphy data from drill cuttings from four oil wells in southwestern Manitoba (parts of NTS 62K6, 7, 11); Manitoba Business, Mining, Trade and Job Creation, Manitoba Geological Survey, Data Repository Item DRI2025021, Microsoft® Excel® file.

Rossini, F.D. 1960: Hydrocarbons in petroleum; Journal of Chemical Education, v. 37, no. 11, p. 554–561.

Smith, C.M. and Smith, M.P. 2020: Evaluating failure: extracting relevant volatile geochemical information from legacy geological materials from dry holes and under performing wells; GeoGulf Transactions, v. 70, p. 297–309.

Smith, C.M., Cammack, J., Smith, T.M., Gordon, P.S. and Smith, M.P. 2023b: Helium and low-hydrocarbon reservoir in San Juan County, Utah: unconventional methods to detect reservoir zonations and gas-water contacts, part 2; The Rocky Mountain Association of Geologists, North American Helium Conference, March 22–23, 2023, Westminster, Colorado, Program Book, p. 69–70.

Smith, C.M., Mercer, D., Smith, T.M., Liaw, V., Gordon, P.S. and Smith, M.P. 2021a: A volatiles analysis case study evaluating the petroleum system, pay zones, seals, chemical compartments, and potential pay zones from a Gulf of Mexico well in Main Pass Field using legacy, oil based mud and PDC bit cuttings, with tie ins to wireline and seismic data; GeoGulf Transactions, v. 71, p. 265–279.

Smith, C., Pool, S., Dinterman, P., Moore, J., Vance, J., Smith, T., Gordon, P. and Smith, M. 2021b: Evaluating the liquids potential and distribution of West Virginia's Marcellus liquids fairway, Houston, Texas; SPE/AAPG/SEG Unconventional Resources Technology Conference, July 26–28, 2021, Houston, Texas, abstract, 1 p., URL <https://doi.org/10.15530/urtec-2021-5540>.

Smith, C.M., Smith, M.P., Gordon, P.S., Smith, T.M. and Duncan, E. 2023c: Advanced Hydrocarbon Stratigraphy (AHS) use of proprietary Rock Volatile Stratigraphy (RVS) system to analyze cuttings samples of Great Bear Pantheon's exploration wells on the North Slope; Society of Petroleum Engineers, Western Regional Meeting, May 22–25, 2023, Anchorage, Alaska, paper presented, p. 1–19.

Smith, C.M., Smith, M.P., Gordon, P.S., Smith, T.M., Flynn, J., Priddell, T. and Yurkowski, M. 2022a: Rock Volatiles Analyses of the B.A. Saskatchewan Landing Core — detailed fluid, reservoir, and cap rock insights from the C1-C10 hydrocarbons, organic acids, CO_2, formation water, helium, various sulfur gases, and mechanical strength: implications for helium system analysis; Saskatchewan Geological Society, Twenty-ninth Williston Basin Petroleum Conference, Dr. Don Kent Core Workshop Volume, Special Publication No. 27, p. 1–9.

Smith, C.M., Smith, T.M., Gordon, P.S. and Smith, M.P. 2022b: Rock Volatiles Stratigraphy analysis of helium in 60+ year old cores from the Keyes Dome Field in Oklahoma: implications for helium exploration and development; Society of Applied Geoscientists and Engineers, 2nd SAGE Applied Geoscience and Engineering Symposium, June 30, 2022, Lafayette, Louisiana, abstract.

Smith, C., Yurkowski, M., Flynn, J., Kohlruss, D., Smith, T., Gordon, P.S. and Smith, M. 2023a: Understanding the subsurface helium system of Saskatchewan with a focus on traps/seals via volatiles analysis of helium and other compounds in legacy cores; The Rocky Mountain Association of Geologists, North American Helium Conference, March 22–23, 2023, Westminster, Colorado, Program Book, p. 50–51.

Smith, H.M. 1968: Qualitative and quantitative aspects of crude oil composition; U.S. Department of the Interior, Bureau of Mines, Bulletin 642, 136 p.

GS2025-12

Geochemistry of the Carman Sand and lower unit sand of the Winnipeg Formation, southern Manitoba (parts of NTS 62H, P)

by V.L. Markstrom

Summary

Silica sand derived from two layers of the Winnipeg Formation, the lower unit sand and the Carman Sand, have significant potential for economic development due to their high silica content. As part of an ongoing project on the Winnipeg Formation, the Manitoba Geological Survey (MGS) has reconstructed the Carman Sand isopach and structure maps to better reflect geological boundaries. New isopach and structure maps were constructed for the basal sandstone, a blanket-type sandstone that forms the base of the lower unit. These maps were used to assess the distribution differences between the lowermost sandstone layer and the interbedded shale and sand that make up the rest of the lower unit. The isopach map illustrates that the thickest part of the basal sandstone occurs near the Dauphin area of the province and is thinnest north of the City of Winnipeg. Geochemical analysis of 20 Winnipeg Formation samples was completed to evaluate the difference between the two sand layers with the highest economic potential: the Carman Sand and lower unit sand. Concentrations of SiO_2 from the Carman Sand samples ranged from 95.74 to 99.68%, with only minor spatial and stratigraphic variations. The lower unit sand had a larger SiO_2 concentration range of 65.55–98.22%, consistent with previous research.

In Brief:

- Mapping of the basal sandstone of the Winnipeg Formation in southern Manitoba shows variability in distribution of sand
- Results from geochemical analysis illustrates the difference between the two most economically viable sand layers in the Winnipeg Formation

Citation:
Markstrom, V.L. 2025: Geochemistry of the Carman Sand and lower unit sand of the Winnipeg Formation, southern Manitoba (parts of NTS 62H, P); *in* Report of Activities 2025, Manitoba Business, Mining, Trade and Job Creation, Manitoba Geological Survey, p. 120–127.

Introduction

The Winnipeg Formation is composed mostly of interlayered quartz-rich sandstones and arenaceous shales (McCabe, 1978). McCabe (1978) and Markstrom (2024) include detailed information on the geology of the Winnipeg Formation. There are multiple sand-bearing layers within the Winnipeg Formation (McCabe, 1978), with previous research identifying the lower unit sand and Carman Sand as those of highest economic potential (Figure GS2025-12-1). The sand from the lower unit has been characterized through sieve and geochemical analyses (Watson, 1985; Gale et al., 1993; Lapenskie, 2016) and is primarily used to produce glass (Watson, 1985). The Carman Sand has yet to be extracted for industrial use due to difficulties extracting the unconsolidated sand (Watson, 1985) from the subsurface. However, renewed interest in the economic potential of the Carman Sand has led to recent exploration and geological investigations in south-central Manitoba (Markstrom, 2024).

Quantifying the differences between the lower unit sand and the Carman Sand will provide a better understanding of the depositional setting of the Winnipeg Formation. This will help with exploration of these deposits and potentially locate other areas of high economic potential for silica sand. This project will also contribute toward formalizing the stratigraphic nomenclature in Manitoba, and a better understanding of the stratigraphic positioning of these sand layers. Additionally, geochemical characterization of the sand beds will inform exploration decisions and the economic development of both sand beds.

This study is a continuation of the Winnipeg Formation project introduced in Markstrom (2024). The goals for this year were to

1) update and construct new isopach and structure maps based on data collected from Markstrom (2024);
2) conduct whole-rock geochemical analysis on the Carman Sand and lower unit sand;
3) assess the stratigraphic and spatial variability within the Carman Sand; and
4) compare results from Carman Sand samples with lower unit sand samples to illustrate differences between the layers.

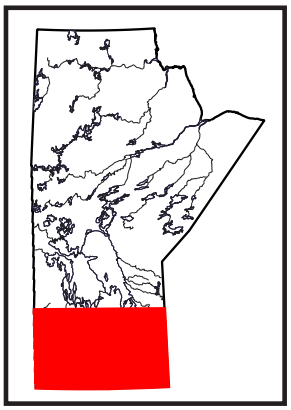

Methodology

Isopach and structure maps of the Carman Sand were updated (Markstrom, 2024) and new maps were constructed for the basal sandstone. These maps were made using drillcore data from the Williston Basin Targeted Geoscience Initiative (TGI) database (TGI Williston Basin Working Group, 2008b)

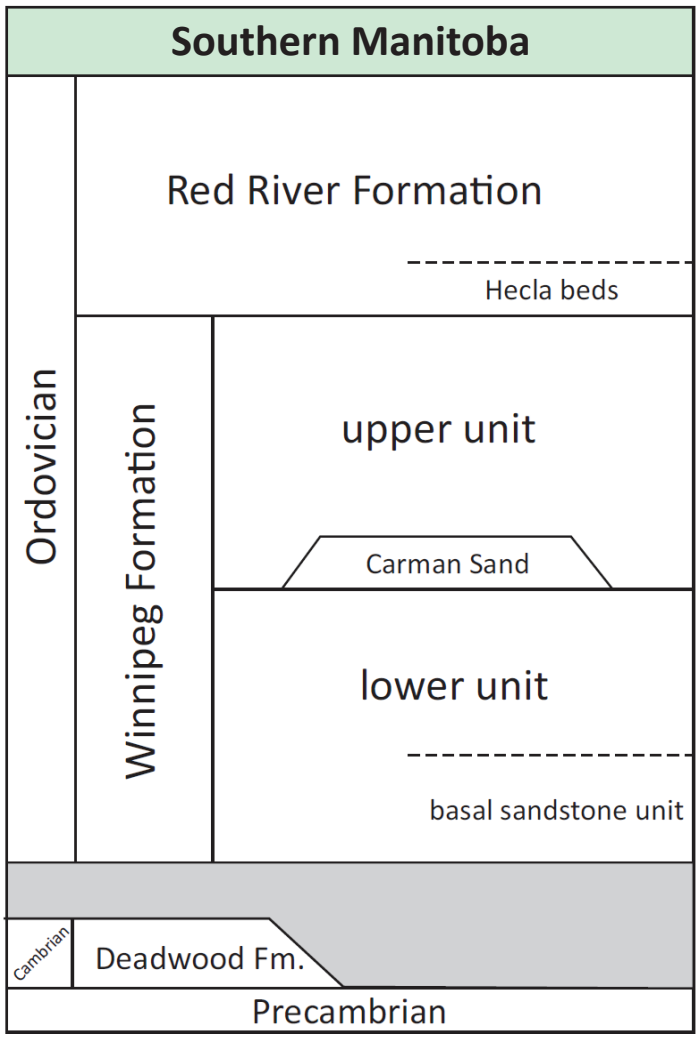

Figure GS2025-12-1: *Stratigraphic column of the lower Paleozoic of southern Manitoba in the Williston Basin (Markstrom, 2024).*

and the Manitoba Stratigraphic Database (MSD; Bezys and Conley, 1999) as well as borehole data from the Integrated Mining and Quarrying System (iMaQs; Manitoba Business, Mining, Trade and Job Creation, 2025). The Natural Neighbours geoprocessing tool was used in Esri® ArcGIS® Pro to generate these maps, which were cropped to the Phanerozoic edge of the Williston Basin.

A total of 20 samples were collected from drillcore and outcrop for geochemical analysis, sample information can be found in Table 1_2 of Data Repository Item DRI2025028 (Markstrom, 2025[1]). Thirteen Carman Sand samples from four drillcore in south-central Manitoba were provided by SiO Silica, Inc. for analysis (Figure GS2025-12-2a). Two lower unit samples were cut and collected from drillcore 11-29-1-25 (oil and gas well licence 2543, Manitoba Business, Mining, Trade and Job Creation, Winnipeg) at the MGS Midland Sample and Core Library (core library) in Winnipeg, Manitoba (Figure GS2025-12-2b). Five samples were collected from the lower unit sand from one outcrop near Seymourville, Manitoba (Figure GS2025-12-2c, d) with site access provided by Canadian Premium Sand Inc. Only one site was sampled because the geochemical composition of the lower unit has been documented previously by several authors (Watson, 1985; Gale et al., 1993; Lapenskie, 2016). At the core library, a fraction of all samples were oven dried, crushed in a steel jaw crusher and pulverizer and milled to <200 mesh for geochemical analysis. Whole-rock total digestion (lithium metaborate/tetraborate fusion) followed by inductively coupled plasma–optical emission spectroscopy (ICP-OES) and inductively coupled plasma–mass spectrometry (ICP-MS) was conducted on all samples by Activation Laboratories Ltd. (Ancaster, Ontario). The OREAS® 21f (quartz sand) certified reference material was also submitted for analysis to validate the quality of the geochemical data. Sieve analysis was also conducted on four samples by the Central Lab of the Materials Engineering Branch, Manitoba Infrastructure (Winnipeg, Manitoba). The results can be found in Table 2_1 to 2_5 of Markstrom (2025), however, due to the small sample size the results will not be discussed in this report.

Results

Isopach maps

The updated Carman Sand isopach map (Figure GS2025-12-3) shows a modified bed boundary that better reflects interpreted geological boundaries as compared with Markstrom (2024). Additionally, an isopach map of the lower unit basal sandstone was constructed (Figure GS2025-12-4). This isopach map illustrates that the basal sandstone is thickest near Dauphin Lake and east of Lake Manitoba and thins toward the northern and southeastern edges of the Winnipeg Formation (Figure GS2025-12-4). The southern extent of the lower unit basal sandstone overlaps with parts of the overlying Carman Sand in places (Markstrom, 2024). The thinnest part of the basal sandstone is located just north of the City of Winnipeg. Structure maps for the Carman Sand and basal sandstone are consistent with previous research and did not significantly differ from the TGI maps (TGI Williston Basin Working Group, 2008a).

Geochemistry

The total digestion (lithium metaborate/tetraborate fusion) geochemical analysis of Carman Sand (n = 13) indicates that the sand is composed of 95.74–99.68 wt. % SiO_2. There are minor variations in SiO_2 concentrations between samples from drillcore Den 269-1 but no obvious correlation with depth. The SiO_2 values from drillcore Den 245-1 have a greater variability in SiO_2 concentration compared to drillcore Den 269-1, but no obvious correlation with depth either. The chemical impurities within the Carman

[1] MGS Data Repository Item DRI2025028, containing the data or other information sources used to compile this report, is available online to download free of charge at https://manitoba.ca/iem/info/library/downloads/index.html, or on request from minesinfo@gov.mb.ca, or by contacting the Resource Centre, Manitoba Business, Mining, Trade and Job Creation, 360-1395 Ellice Avenue, Winnipeg, Manitoba R3G 3P2, Canada.

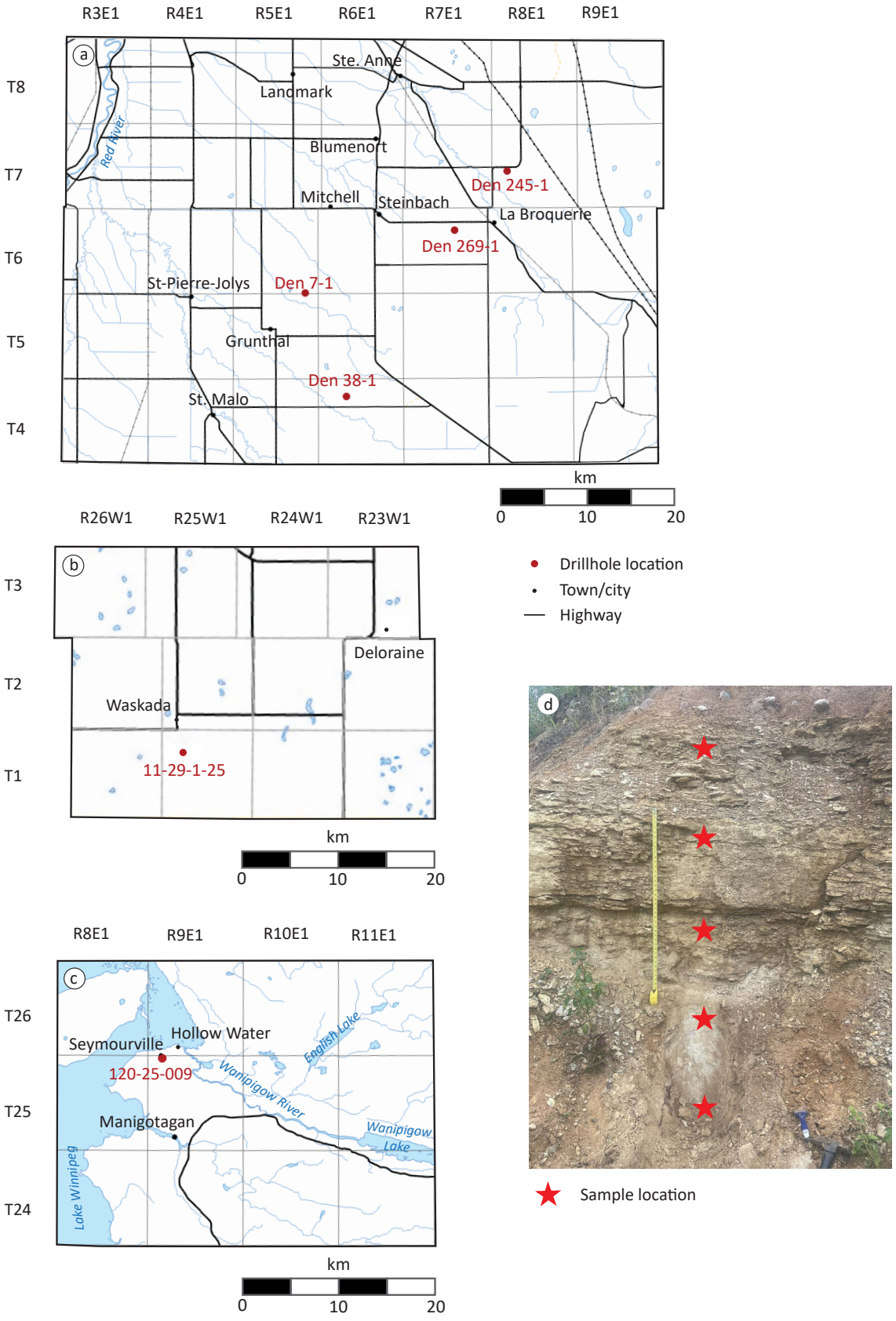

Figure GS2025-12-2: *Location of drillhole and outcrop sample locations in southern Manitoba:* ***a)*** *drillhole locations for the Carman Sand samples;* ***b)*** *location of drillhole 11-29-1-25;* ***c)*** *site 120-25-009 – Seymourville;* ***d)*** *stratigraphic position of Winnipeg Formation lower unit sand samples that were collected at site 120-25-009. Measuring tape shows 1 m.*

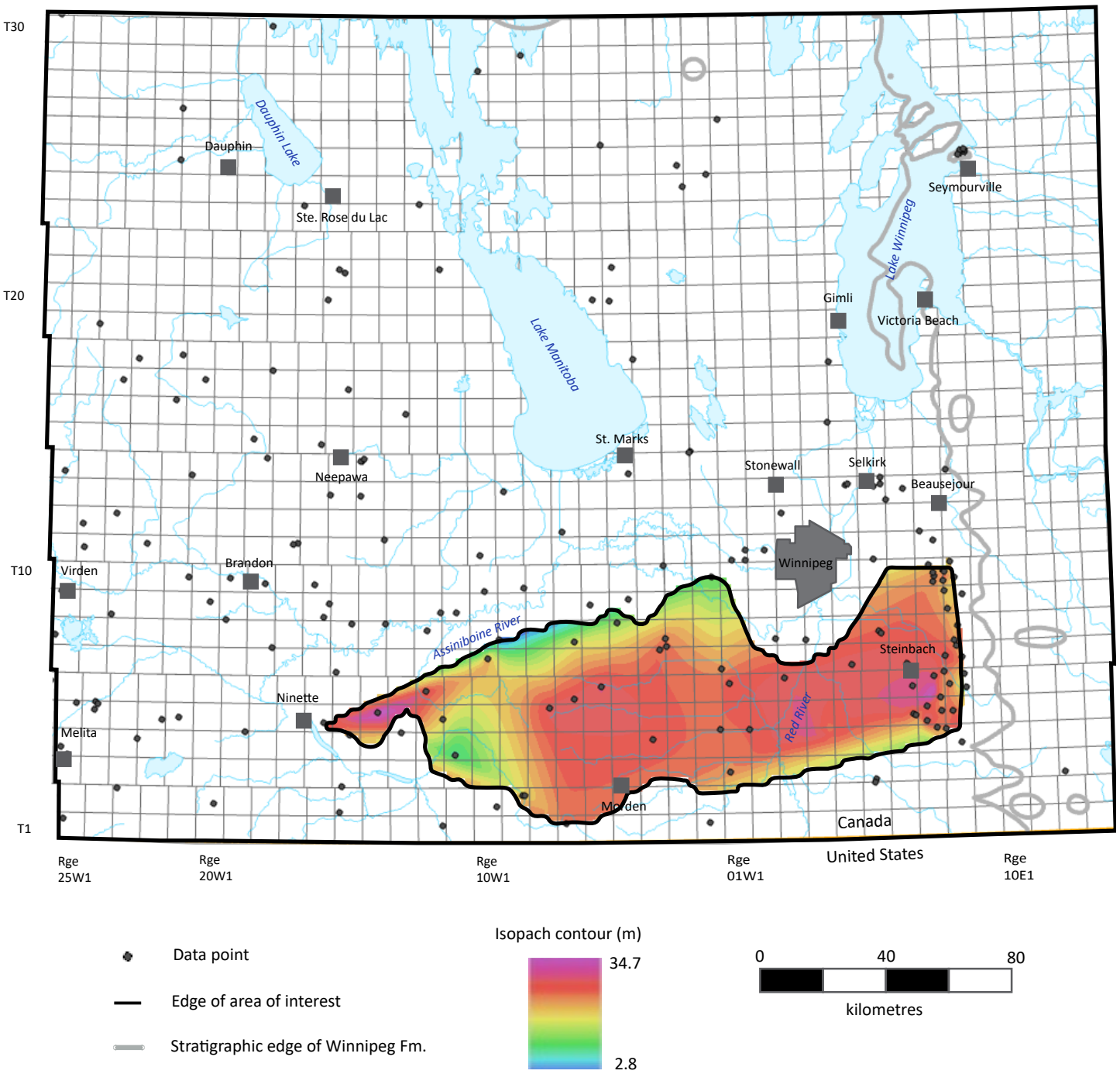

Figure GS2025-12-3: *Isopach map of the Carman Sand of the Winnipeg Formation in southern Manitoba. This preliminary map was constructed using a computer-generated model constrained to the project dataset. Data points from TGI Williston Basin Working Group (2008b). Basemap was created using ArcGIS® software by Esri. ArcGIS® is the intellectual property of Esri and is used herein under license. Copyright © Esri. All rights reserved. For more information about Esri software, please visit <https://esri.ca/>.*

Sand are primarily Al_2O_3, Fe_2O_3, MgO, CaO and TiO_2. Most of the Carman Sand samples have concentrations of total impurities between 0.83 to 1.92 wt. %. However, sample 120-25-Den245_1-174 has a higher concentration of total impurities, 3.32 wt. %, and has the lowest SiO_2 concentration (95.74 wt. % SiO_2) of the Carman Sand samples.

The lower unit sand samples from the Seymourville site and drillcore 11-29-1-25 (n = 7) have a greater range in SiO_2 concentrations, 65.55–98.22 wt. %, compared to the Carman Sand samples. The lower unit sand samples collected from the Seymourville site have no apparent correlation between SiO_2 concentration and the stratigraphic position of the sample. The impurities in the

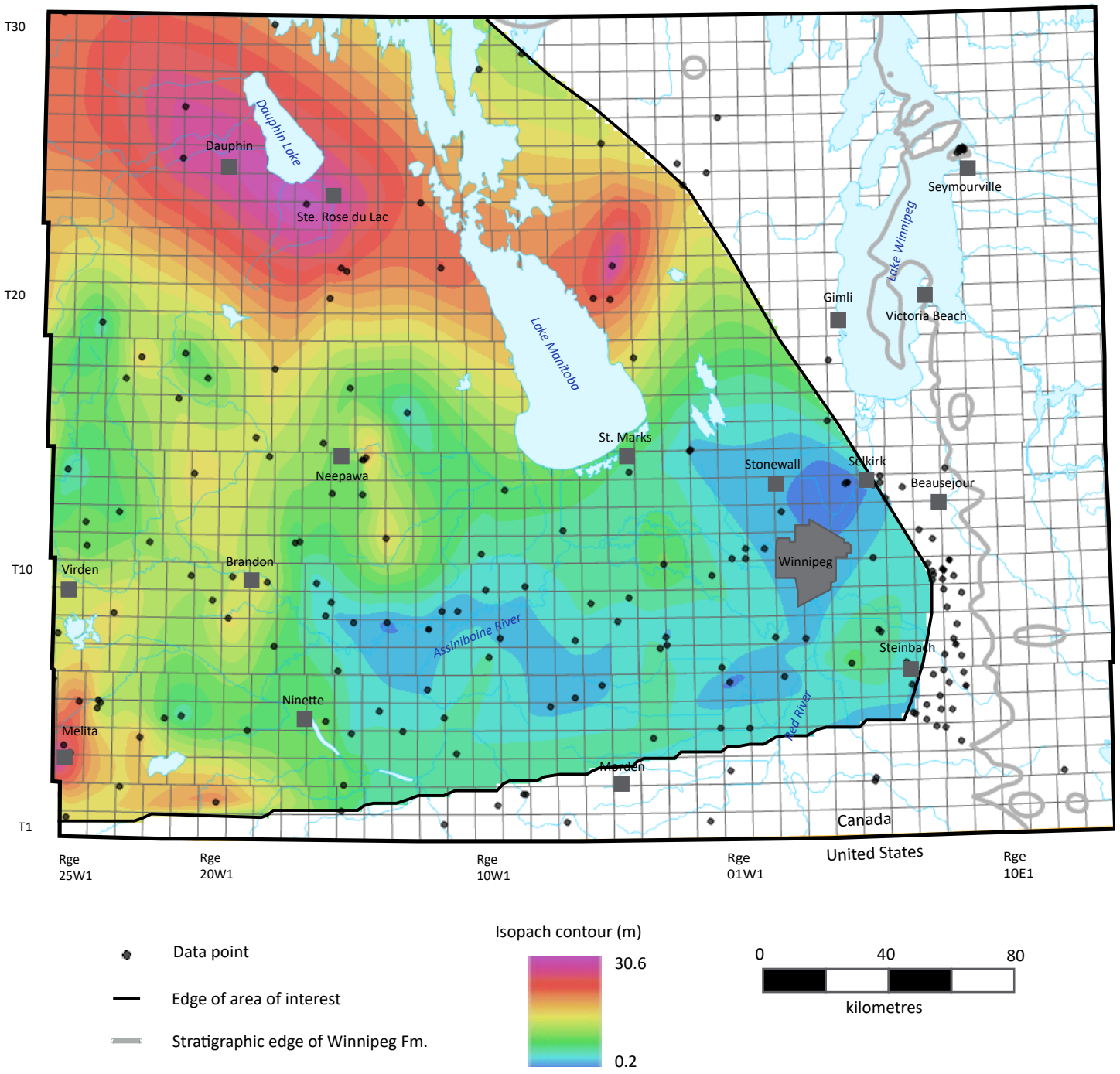

Figure GS2025-12-4: *Isopach map of the basal sandstone of the Winnipeg Formation in southern Manitoba. This preliminary map was constructed using a computer-generated model constrained to the project dataset. Data points from TGI Williston Basin Working Group (2008b). Basemap was created using ArcGIS® software by Esri. ArcGIS® is the intellectual property of Esri and is used herein under license. Copyright © Esri. All rights reserved. For more information about Esri software, please visit <https://esri.ca/>.*

lower unit sand samples are primarily Al_2O_3, Fe_2O_3, MgO, CaO, TiO_2 and K_2O and the samples have a greater range in total impurities (between 1.44 and 23.52 wt. %) compared to the Carman Sand samples (0.83–3.32 wt. %). The observed trends in chemical composition of the lower unit sand are consistent with previous research (Watson, 1985; Gale et al., 1993; Lapenskie, 2016).

Discussion

Isopach maps

The basal sandstone isopach map (Figure GS2025-12-4) was compared against the entire lower unit isopach map constructed by Markstrom (2024) to identify any differences in distribution

between the lowermost sandstone and the interbedded sand and shale that make up the rest of the lower unit. Since the basal sandstone has been correlated with the lower part of the Black Island Member in Saskatchewan (McCabe, 1978), identifying its distribution in Manitoba may prove useful for future stratigraphic work and help formalize the nomenclature of the Winnipeg Formation.

The limited data suggests the basal sandstone is thickest near Dauphin Lake and east of Lake Manitoba (Figure GS2025-12-4). When compared to the isopach map of the entire lower unit (Figure GS2025-12-5), it is apparent that the Dauphin Lake area is composed primarily of the basal sandstone with little of the lower unit interbedded sand and shale. A similar pattern is seen in the Melita area where most of the lower unit is com-

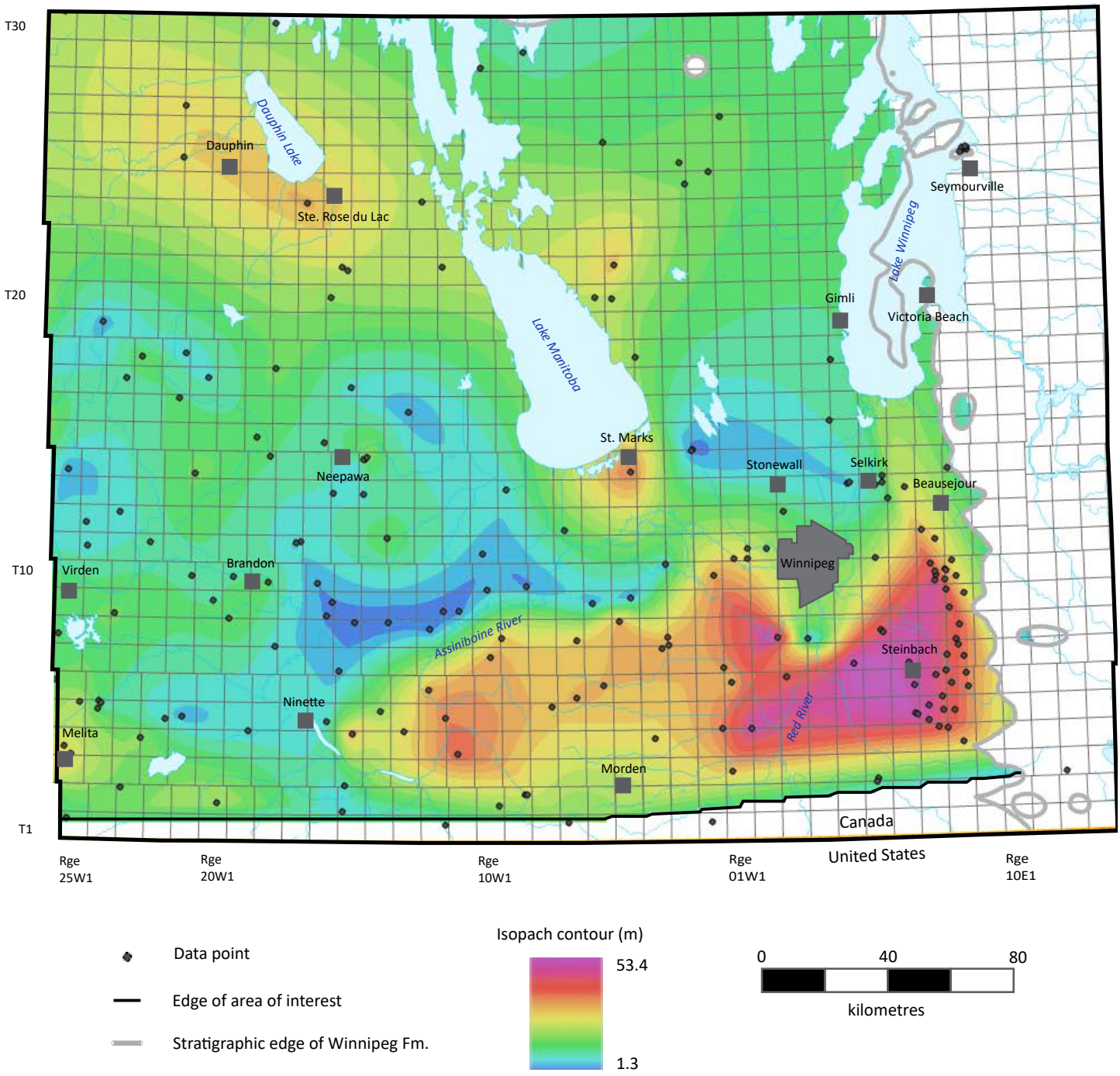

Figure GS2025-12-5: *Isopach map of the lower unit of the Winnipeg Formation in southern Manitoba (Markstrom, 2024). This preliminary map was constructed using a computer-generated model constrained to the project dataset. Data points from TGI Williston Basin Working Group (2008b). Basemap was created using ArcGIS® software by Esri. ArcGIS® is the intellectual property of Esri and is used herein under license. Copyright © Esri. All rights reserved. For more information about Esri software, please visit <https://esri.ca/>.*

posed of a thick section of basal sandstone, and the rest of the lower unit is almost absent. The opposite trend can be observed in the south-central portion of the province. The basal sandstone appears thinnest in an area roughly between Brandon and Selkirk; therefore, most of the lower unit present in this area is likely composed of the lower unit layers of sand and shale. It is important to note that parts of the overlying Carman Sand spatially overlap in this area.

Geochemistry

The SiO_2 concentrations of the seven Carman Sand samples from drillhole Den 269-1 have little variation regardless of their drillcore depth. This implies that stratigraphically the geochemical composition is consistent throughout the Carman Sand at this location. In samples from a location nearby, drillhole Den 245-1, there is some variability depending on depth interval. The lowest SiO_2 concentration in the Carman Sand, 95.74 wt. % in drillcore Den 245-1, was measured at the top of the drillcore but samples below have concentrations around 97–98 wt. % SiO_2. Only one sample was collected from each of the Den 7-1 and Den 38-1 drillcore, therefore, the stratigraphic variability at these locations cannot be verified.

The results from this analysis show there is minor spatial variability in SiO_2 concentrations of the Carman Sand when comparing the average results from drillcore Den 269-1 (average 98.55 wt. % SiO_2), Den 245-1 (average 97.52 wt. % SiO_2), Den 38-1 (99.68 wt. % SiO_2) and Den 7-1 (97.41 wt. % SiO_2). Due to the low sample population and limited sampling sites in this study, it is difficult to constrain the stratigraphic and spatial variability of SiO_2 that may be occurring in the Carman Sand. In order to address this shortfall, additional data from more localities of the Carman Sand are needed. In contrast, the lower unit sand has a much larger variability in SiO_2 concentrations. Although the average SiO_2 concentration for the lower unit sand (87.66 wt. % SiO_2) is lower than the Carman Sand average (98.23 wt. % SiO_2), samples 120-25-009-01 and 120-25-11_29_1_25-1924.45 have concentrations within the range observed for the Carman Sand. At the Seymourville site, the SiO_2 concentrations vary significantly, which is consistent with previous research (Watson, 1985). However, no trend between SiO_2 concentration and stratigraphic position of the samples is apparent.

Future work

Future research on the Winnipeg Formation will include additional geochemical analyses of the Carman Sand. Samples within a larger spatial and stratigraphic context will better confirm and constrain any changes within the units. Sieve analysis will also be conducted on additional lower unit sand and Carman Sand samples to characterize grain distributions and further assess differences between the two sand layers. Passive seismic studies will be conducted to better understand the geometry of the Winnipeg Formation and the topography of the Precambrian basement. This information is important because the Precambrian topography could have had a direct impact on the thickness and spatial distribution of different units within the Winnipeg Formation.

Economic considerations

There are many industrial uses for silica sand but its industrial application is greatly affected by composition and grain-size characteristics. The 20 samples tested in this study do not meet the specifications for high-quality glass production (Vatalis et al., 2015). However, it is important to note that the none of the samples were cleaned or refined before analysis and it is difficult to confirm industrial usage for each sand layer. Higher SiO_2 concentrations might be achievable for the Carman Sand and lower unit sand depending on the cleaning methods used.

Acknowledgments

The author would like to thank Sio Silica, Inc. and Canadian Premium Sand Inc. for site and sample access. Logistical and field support from C. Epp, E. Ralph and P. Belanger (Manitoba Geological Survey) is appreciated. Reviews of this report were provided by T.J. Hodder and M.S. Gauthier (Manitoba Geological Survey).

References

Bezys, R.K. and Conley, G.G. 1999: Manitoba Stratigraphic Database and the Manitoba Stratigraphic Map Series; Manitoba Energy and Mines, Geological Services, Open File Report OF98-7, 1 CD-ROM.

Gale, G.H., Halden, N.M. and Mejia, S. 1993: High purity silica studies-geochemical and mineralogical studies of Winnipeg Formation silica sands; *in* Report of Activities 1993, Manitoba Energy and Mines, Geological Services, p. 146–148.

Lapenskie, K. 2016: Preliminary investigations into the high-purity silica sand of the Winnipeg Formation, southern Manitoba; *in* Report of Activities 2016, Manitoba Growth, Enterprise and Trade, Manitoba Geological Survey, p. 176–180.

Manitoba Business, Mining, Trade and Job Creation 2025: iMaQs, Manitoba's Integrated Mining and Quarrying System; Manitoba Business, Mining, Trade and Job Creation, URL <https://manitoba.ca/iem/mines/imaqs/index.html> [January 2025].

Markstrom, V.L. 2024: Distribution of the lithological units of the Winnipeg Formation, southern Manitoba (NTS 62F–K, N–P); *in* Report of Activities 2024, Manitoba Economic Development, Investment, Trade and Natural Resources, Manitoba Geological Survey, p. 185–191.

Markstrom, V.L. 2025: Sieve and geochemical analyses data from samples of the Winnipeg Formation in southern Manitoba (parts of NTS 62H, P); Manitoba Business, Mining, Trade and Job Creation, Manitoba Geological Survey, Data Repository Item DRI2025028, Microsoft® Excel®.

McCabe, H.R. 1978: Reservoir potential of the Deadwood and Winnipeg formations, southwestern Manitoba; Manitoba Department of Mines, Resources and Environmental Management, Mineral Resources Division, Geological Paper GP78-3, 54 p.

TGI Williston Basin Working Group 2008a: Ordovician Winnipeg Formation: structure contour; Manitoba Science, Technology, Energy and Mines, Manitoba Geological Survey, Stratigraphic Map SM2008-OW-I, scale 1:1 000 000, URL <https://www.gov.mb.ca/iem/geo/willistontgi/mapfiles/pdfs/055_ord_winnipeg_fm_str.pdf> [September 2025].

TGI Williston Basin Working Group 2008b: TGI II Williston Basin database service, lower Paleozoic data; Manitoba Science, Technology, Energy and Mines, Manitoba Geological Survey, URL <https://www.manitoba.ca/iem/geo/willistontgi/database.html> [September 2025].

Vatalis, K.I., Charalambides, G. and Benetis, N.P. 2015: Market of high purity quartz innovative applications; Procedia Economics and Finance, v. 24, p. 734–742.

Watson, D.M. 1985: Silica in Manitoba; Manitoba Energy and Mines, Geological Services, Economic Geology Report ER84-2, 35 p.

GS2025-13

Pilot study of lithium concentrations in mudstone intervals from the Manitoba Potash Corporation core at 3-29-20-29W1, southwestern Manitoba (part of NTS 62K11)

by P.E. Fraino

In Brief:

- Nine mudstone intervals within the Duperow Formation were sampled for Lithium concentrations
- Variable but elevated lithium concentrations of 15.6 – 100 ppm (four-acid digestion) and 17 – 112 ppm (sodium peroxide fusion) were reported
- Geochemistry from core indicate mudstone intervals may be contributors to lithium for basin brines

Citation:
Fraino, P.E. 2025: Pilot study of lithium concentrations in mudstone intervals from the Manitoba Potash Corporation core at 3-29-20-29W1, southwestern Manitoba (part of NTS 62K11); *in* Report of Activities 2025, Manitoba Business, Mining, Trade and Job Creation, Manitoba Geological Survey, p. 128–134.

Summary

The first lithium concentration data from mudstone intervals in the Upper Devonian Duperow Formation in southwestern Manitoba were obtained from powdered core samples collected from the Manitoba Potash Corporation (MPC) core drilled at L.S. 3, Sec. 29, Twp. 20, Rge. 29, W 1st Mer. (abbreviated 3-29-20-29W1). Lithium concentrations ranged from 15.6 to 112 ppm depending on the digestion method used (four acid and sodium peroxide fusion). Elevated lithium concentrations were identified in mudstones across multiple members of the Duperow Formation, including the lower, middle and upper Wymark Member and Seward Member. These preliminary results suggest that lithium enrichment in mudstones of the Duperow Formation are not restricted to a single stratigraphic interval and that they may contribute to lithium-bearing brines throughout the formation in southwestern Manitoba.

Introduction

Deep formational brines in sedimentary basins are increasingly drawing attention due to their high concentrations of dissolved metals, particularly lithium (Li; Dugamin et al., 2023). A focus of exploration has been directed toward these brines as potential unconventional sources of Li, a crucial critical element for electric mobility, stationary energy storage, consumer electronics and industrial applications (Bibienne et al., 2020; Dugamin et al., 2021, 2023; Butler et al., 2025). Although elevated Li concentrations in formational waters are now widely recognized across various basins and formations in the world (Dugamin et al., 2023), the origin of the Li-enriched fluids remains poorly understood. One of the main contributors to Li-enrichment is attributed to mudstone deposits composed of clay minerals, whereby Li can be stored through structural substitution or surface adsorption that is then released during long-term diagenetic processes and water–rock interactions with formation waters within the pore space (Kadi et al., 2023; Butler et al., 2025; Lazowski et al., 2025).

In the Williston Basin, the Upper Devonian Duperow Formation presents a compelling opportunity to evaluate this Li source potential. The Duperow Formation is predominantly a mixed carbonate–evaporite succession, consisting of interbedded limestone, dolostone and anhydrite, deposited in restricted marine to sabkha environments (Cen, 2009; Eggie et al., 2012b; Bates et al., 2016; Nicolas and Chow, 2018). Although less abundant, mudstone intervals are present in the Duperow Formation and can be correlated basin wide for hundreds of kilometres in Manitoba, Saskatchewan and North Dakota (Wilson and Pilatzke, 1987; Cen, 2009; Bates, 2016). Previous studies from Saskatchewan have reported elevated Li concentrations ranging from 1 to 120 ppm in core from the Duperow Formation, with the mudstone/dolomudstone intervals having higher Li concentrations (30 to 120 ppm) relative to evaporite and carbonate-rich lithofacies (Jensen et al., 2020; Jensen and Kohlruss, 2023). Therefore, these mudstone intervals are hypothesized to be an important intraformational Li source for the Duperow Formation in the Williston Basin (Jensen and Kohlruss, 2023; Bishop and Robbins, 2025). As a result, the Li concentrations of nine mudstone intervals in the most complete core of the Duperow Formation in southwestern Manitoba, the MPC core located in 3-29-20-29W1 (oil and gas well licence 3884, Manitoba Business, Mining, Trade and Job Creation, Winnipeg; Figure GS2025-13-1), were determined. The objectives of this pilot study were to

1) assess the Li concentration using two different analytical methods; and
2) investigate whether the Li concentrations in the Duperow Formation vary stratigraphically.

These objectives form the basis of a preliminary evaluation of the mudstone intervals to determine if they are one of the primary contributors to Li enrichment in brines in southwestern Manitoba.

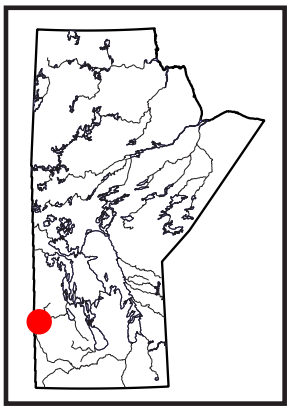

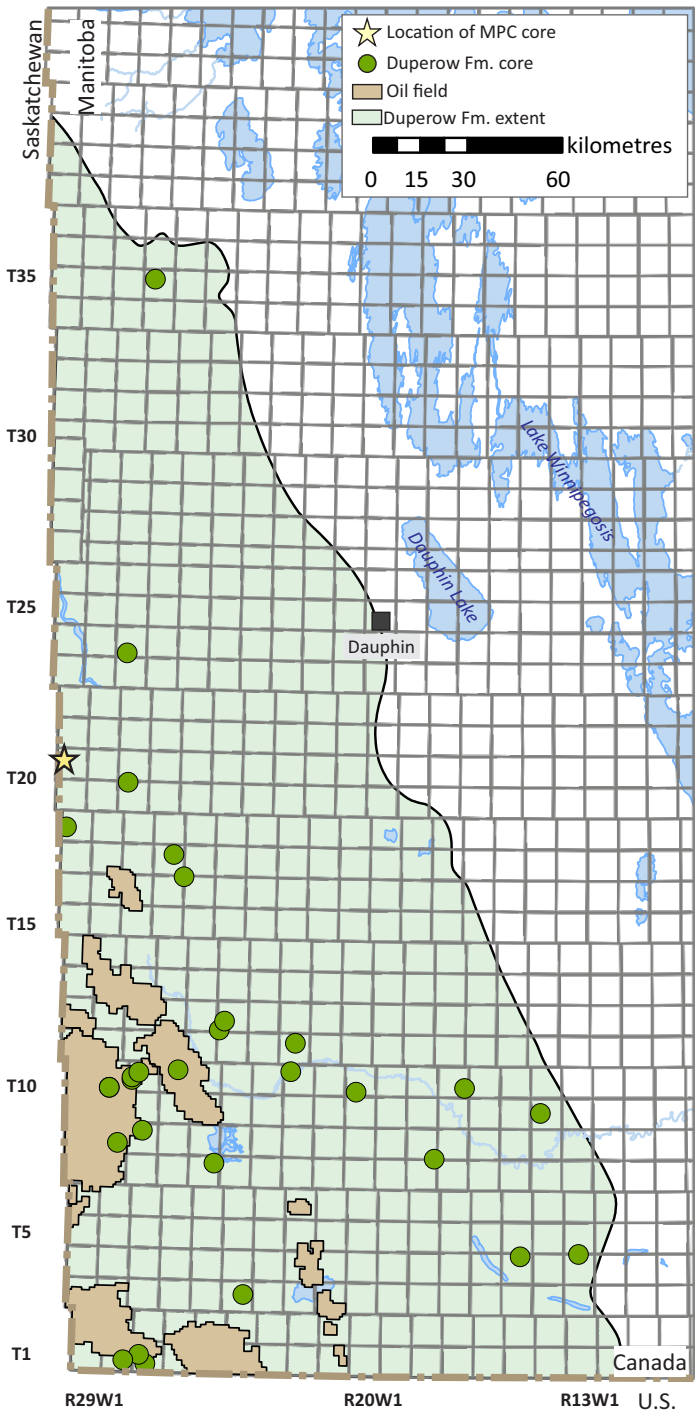

Figure GS2025-13-1: *Study area in southwestern Manitoba with the Duperow Formation core locations. Yellow star denotes the location of the Manitoba Potash Corporation (MPC) core.*

Duperow Formation stratigraphy in the MPC core

The Upper Devonian Duperow Formation was deposited within the intracratonic Elk Point Basin of the Western Canada Sedimentary Basin (Nicolas and Barchyn, 2008). In southwestern Manitoba, the Duperow Formation records deposition in a shallow-water, restricted, back-reef setting on the eastern platform, sheltered from open marine circulation by the Leduc reef complex in Alberta (Eggie et al., 2012a; Bates et al., 2016). These conditions led to the development of laterally extensive, carbonate–evaporite cycles, recognized across southern Saskatchewan, Manitoba, Montana and North Dakota (Wilson, 1967; Wilson and Pilatzke, 1987).

In the MPC core, the Duperow Formation is fully preserved, spanning 153.36 m in thickness (Figure GS2025-13-2). The Duperow Formation is subdivided into the Saskatoon, Wymark and Seward members. The Saskatoon Member (15.26 m thick) consists of burrow and mottled dolomudstone, fossiliferous wackestone to framestone, and laminated anhydrite beds, representing deposition in a subtidal, slightly restricted marine setting. The overlying Wymark Member is the thickest (97.78 m) and is informally subdivided into the lower, middle and upper units. The Wymark Member consists of interbedded lime mudstone, floatstone, laminated dolostone and massive anhydrite organized into metre-scale, shallowing-upward cycles reflecting transitions from subtidal to supratidal environments. The uppermost Seward Member (40.32 m thick) includes the regionally mappable Seward shale and consists of laminated and mottled dolomudstone with fossiliferous wackestone interbeds (Nicolas and Chow, 2018).

The members and informal unit (lower, middle and upper Wymark Member) subdivisions of the Duperow Formation can be correlated across the basin due to the presence of marker beds that typically consist of a fissile mudstone interval, providing a consistent petrophysical well log pick for regional correlation (Figure GS2025-13-2; Bates, 2016). In addition to these key marker beds, several other mudstone intervals are observed within the lower, middle and upper units in the Wymark Member, as well as within the Seward Member. However, the Saskatoon Member within the MPC core does not contain argillaceous, siliciclastic mudstone intervals, and consequently this member was not sampled.

Geochemical methodology and dataset

Nine mudstone samples from the MPC core were selected for geochemical analysis to assess Li concentrations and associated major-, minor- and trace-element trends. Approximately 8 g of each sample were pulverized to a grain size of <63 µm to ensure analytical homogeneity and minimize grain-size–related biases during digestion. Two digestion methods were employed to compare Li concentrations, four acid and sodium peroxide fusion.

Samples were submitted to Activation Laboratories Ltd. (Ancaster, Ontario) to be analyzed. The four-acid digestion consists of dissolving the powdered material using hydrofluoric acid, nitric acid, perchloric acid and hydrochloric acid, followed by analysis using inductively coupled plasma–mass spectrometry (ICP-MS) and inductively coupled plasma–optical emission spectrometry (ICP-OES). This digestion approach yields near-total elemental recovery for most mineral matrices, although some

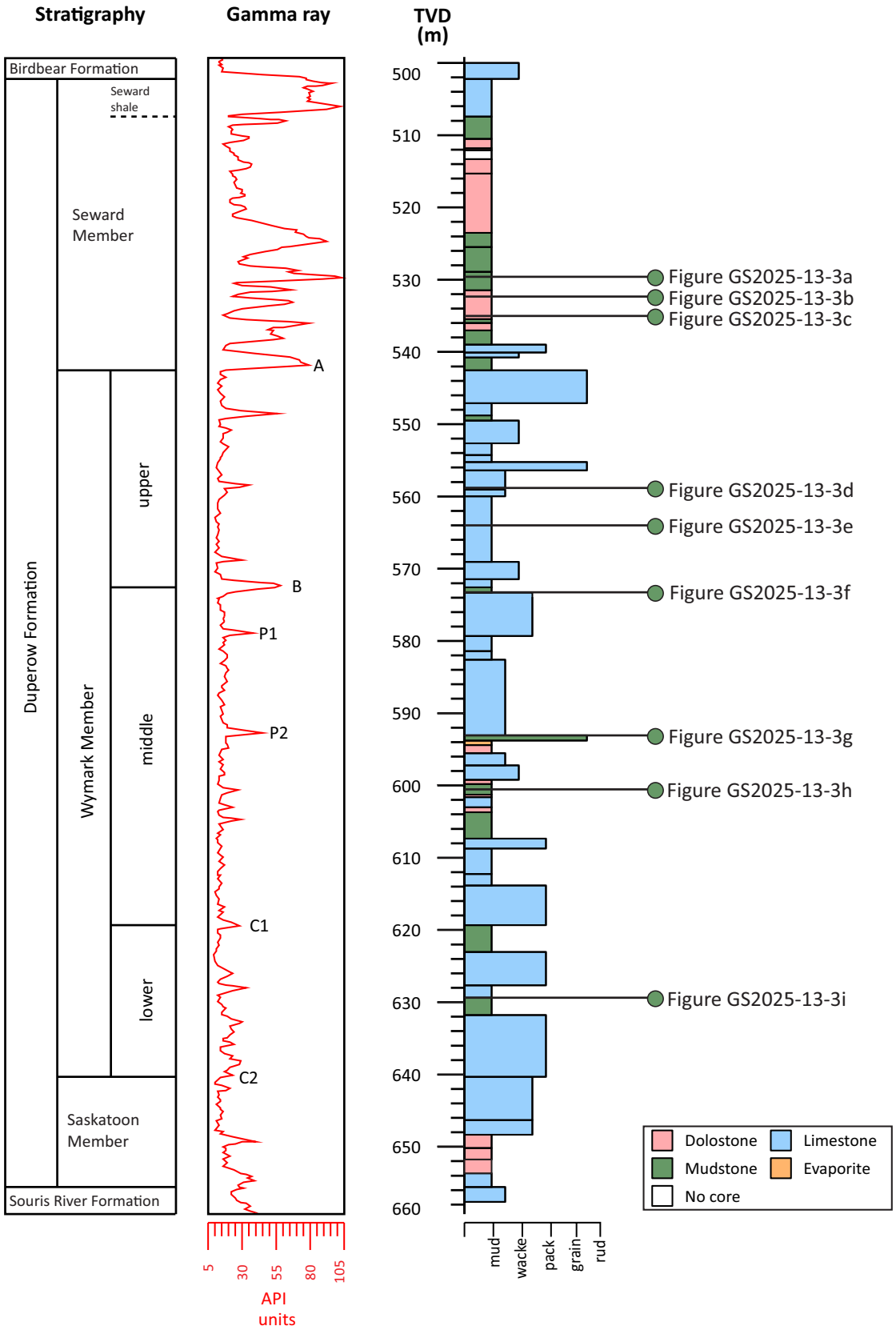

Figure GS2025-13-2: *Core log for the Duperow Formation in the Manitoba Potash Corporation (MPC) core, drilled at L.S. 3, Sec. 29, Twp. 20, Rge. 29, W 1st Mer., showing stratigraphy, gamma-ray downhole wireline geophysics and lithology; prominent basin-wide marker beds (A, B, P1, P2, C1 and C2) are labelled on the gamma-ray track (modified from Nicolas and Chow, 2018). Sample locations for core shown in Figure GS2025-13-3 are labelled in the stratigraphic column. Abbreviations: grain, grainstone; mud, mudstone; pack, packstone; rud, rudstone; TVD, true vertical depth; wacke, wackestone.*

highly refractory phases may remain partially undissolved. The sodium peroxide fusion method fully dissolves all mineral phases, including refractory components. Subsequent analysis by ICP-MS allows for accurate determination of trace-element concentrations, including Li. To verify analytical precision and accuracy, the certified reference material OREAS 750, a Li-bearing pegmatite ore, was included as an internal standard. Recovery values from this reference material were consistent with certified values, confirming the reliability of Li measurements obtained from both analytical methods.

The entirety of the geochemical data is available in MGS Data Repository Item DRI2025023 (Fraino, 2025[1]).

Mudstone interval characteristics

The mudstone intervals observed in the MPC core are typically light grey to olive green in colour and are characterized on geophysical logs by high gamma-ray signatures (Figures GS2025-13-2, -3). Individual mudstone beds range in thickness from approximately 1 to 50 cm. In hand specimen, these mudstones are generally fissile and fragmented (Figure GS2025-13-3c, e, i). Intervals commonly appear as massive with subtle mottling or evidence of low-intensity bioturbation and lack any sedimentary structures (Figure GS2025-13-3f). Rounded, dark grey anhydrite nodules, typically less than 1 mm in diameter, are common throughout several of these intervals (Figure GS2025-13-3a, b, d, i). In some instances, mudstone intervals consist of angular to semirounded clasts within a mudstone or dolomudstone matrix. These clasts are sand to pebble sized and consist primarily of massive dolomudstone to mudstone, some of which preserve primary planar laminations (Figure GS2025-13-3).

Mudstone beds consistently overlie laminated anhydrite–dolostone or massive anhydrite beds and, in turn, are overlain by fossiliferous wackestone or nodular calcareous mudstone (Bates et al., 2016).

Lithium concentrations from mudstone intervals

Lithium concentrations in the nine mudstone samples from the MPC core were determined to range from 15.6 to 100 ppm by four-acid digestion, and from 17 to 112 ppm by sodium peroxide fusion. These results indicate that Li enrichment was observed across all sampled intervals, with values varying by stratigraphic position and lithological composition.

At 569.7 m true vertical depth (TVD), the highest Li concentrations were recorded, with values of 100 ppm (four-acid) and 112 ppm (sodium peroxide fusion). Reported as '(four-acid digestion/sodium peroxide fusion digestion)', other samples with notable elevated Li concentration values include 559.5 m TVD (50.9/60 ppm), 534.4 m TVD (49.7/58 ppm), 594.4 m TVD (44.4/49 ppm), 574.0 m TVD (41.7/51 ppm) and 629.3 m TVD (28.1/32 ppm). Lower concentrations were observed in samples from 532.47 m TVD (15.6/17 ppm), 604.3 m TVD (21.6/25 ppm) and 529.6 m TVD (25.7/26 ppm; Figure GS2025-13-3). Although Li concentrations measured by four-acid and sodium peroxide fusion digestion methods show similar trends across samples, the sodium peroxide fusion method consistently yielded higher values. Notably, the difference in Li concentration between the two methods increases with overall Li content. In samples with higher Li concentrations, the discrepancy between the two digestion methods is more pronounced (Figure GS2025-13-3a–i), suggesting that the sodium peroxide fusion method more effectively captures Li bound in resistant mineral phases. Furthermore, the intervals with the highest Li concentrations also exhibit elevated concentrations of SiO_2, K_2O and Al_2O_3 (Fraino, 2025). This is consistent with the presence of clay minerals, which are known to host Li via structural substitution and surface adsorption (Dugamin et al., 2023), although further analysis needs to be conducted to understand the mineralogy of these intervals.

Lithium concentration comparison to Saskatchewan

Preliminary Li concentration values from the MPC core in southwestern Manitoba are broadly consistent with those reported from equivalent stratigraphic intervals in southeastern Saskatchewan. On the Saskatchewan side, multiple stratigraphic horizons within the Duperow Formation have been shown to host elevated Li in both brines and analyzed core samples. Core analyses have reported Li concentrations of up to 120 ppm in mudstone intervals, whereas produced water analyses have documented values from 25 to 259 mg/L, with a median Li concentration of 115 mg/L (Jensen and Rostron, 2018; Jensen, 2020; Jensen et al., 2020; Jensen and Kohlruss, 2023; Bishop and Robbins, 2025). These elevated concentrations occur in several discrete intervals, supporting the interpretation that Li enrichment is stratigraphically widespread across the formation (Rostron et al., 2023). The Manitoba core results extend these findings eastward into previously unsampled parts of the basin. Elevated Li concentrations were recorded in mudstone intervals from core throughout the Duperow Formation, including the lower, middle and upper Wymark Member and the Seward Member. This suggests that Li-bearing lithofacies may be continuous across provinces. These results provide the first core-based geochemical evidence from Manitoba that the Duperow Formation may host Li-enriched brines comparable in character and distribution to those found in Saskatchewan.

Future work

Based on the results from this pilot study of mudstone intervals from the MPC core, future work will include the following expanded objectives:

[1] MGS Data Repository Item DRI2025023, containing the data or other information sources used to compile this report, is available online to download free of charge at https://manitoba.ca/iem/info/library/downloads/index.html, or on request from minesinfo@gov.mb.ca, or by contacting the Resource Centre, Manitoba Business, Mining, Trade, and Job Creation, 360-1395 Ellice Avenue, Winnipeg, Manitoba R3G 3P2, Canada.

Figure GS2025-13-3: *Photographs of the nine mudstone sampled sections in the Manitoba Potash Corporation (MPC) 3-29-20-29W1 core:* ***a–c)*** *Seward Member;* ***d–e)*** *upper Wymark Member;* ***f–h)*** *middle Wymark Member;* ***i)*** *lower Wymark Member. Note that the Saskatoon Member within the MPC core does not have any argillaceous, siliciclastic mudstone intervals, thus it was not sampled. See Figure GS2025-13-2 for sample locations along the core. Lithium concentration from each sample is shown in blue and green for four-acid and sodium peroxide fusion digestion methods, respectively. Samples are presented in stratigraphic ascending order (true vertical depth is shown in black).*

1) targeted sampling of mudstone (calcareous, dolomitic and clastic) intervals from additional Duperow Formation cores across southwestern Manitoba to assess lateral variability

3) assessment of clay mineralogy using X-ray diffraction (XRD) to evaluate the relationship between specific clay types, bulk mineralogy and Li concentrations derived from trace-element analysis

4) where appropriate, use of Raman spectroscopy to complement XRD by confirming Li-hosting mineral phases

Future work will also explore the relationship between Li and associated major, minor, and trace elements reported in Fraino (2025). Although this report only focused on mudstone intervals, continuous sampling of the MPC core conducted in the summer of 2025 also included other lithofacies. These samples will be analyzed for whole-rock lithogeochemistry to determine the broader distribution of Li across different lithofacies. Having this information will help constrain the temporal variability of Li enrichment within the Duperow Formation and support the assessment of its potential as a Li-bearing brine system in southwestern Manitoba.

Economic considerations

With global demand for Li continuing to rise due to its essential role in battery technologies, sedimentary basin–hosted brines are increasingly being recognized as economically viable sources of Li (Dugamin et al., 2021). Although no analyses of Li concentrations in water presently exist for the Duperow Formation in southwestern Manitoba, Li concentrations from core samples provide an indirect indication of the potential for Li-bearing brines within the formation. The first set of Li concentrations from core is presented in this report and suggests that mudstone intervals within the Duperow Formation contain elevated Li concentrations. These preliminary results highlight the potential role of fine-grained lithologies as a contributor to intraformational Li enrichment in the Duperow Formation in southwestern Manitoba.

Acknowledgments

The author would like to thank C. Epp, P. Belanger and E. Ralph (Manitoba Geological Survey) for their assistance with co-ordinating the logistics of core retrieval. Junior geological assistant, J. Gellert (University of Manitoba) is thanked for sample collection and preparation for lithogeochemical analysis and J. Janssens (Manitoba Geological Survey) is thanked for helping to layout the Data Repository Item 2025023 that accompanies this report. Reviews of this report were provided by T. Martins and M.P.B. Nicolas (Manitoba Geological Survey).

References

Bates, K. 2016: Stratigraphy, sedimentology and petroleum potential of the Upper Devonian Duperow Formation, southwest Manitoba; M.Sc. thesis, University of Manitoba, Winnipeg, Manitoba, 228 p.

Bates, K., Chow, N. and Nicolas, M.P.B. 2016: Preliminary results from sedimentological investigations and petroleum evaluation of the Upper Devonian Duperow Formation, southwestern Manitoba; *in* Report of Activities 2016, Manitoba Growth, Enterprise and Trade, Manitoba Geological Survey, p. 157–167.

Bibienne, T., Magnan, J.-F., Rupp, A. and Laroche, N. 2020: From mine to mind and mobiles: society's increasing dependence on lithium; Elements, v. 16, no. 4, p. 265–270.

Bishop, B.A. and Robbins, L.J. 2025: Overview of brine-hosted lithium mineral resources, distribution, and genesis in the Western Canada Sedimentary Basin; The Canadian Journal of Mineralogy and Petrology, early publication.

Butler, K.L., Munk, L.A., Boutt, D.F., Morris, N., Kennedy, J., Saha, P., Blake, M.R., Custado, M.J. and Ibarra, D.E. 2025: The origin and enrichment of sedimentary basin lithium brines: a case study from the Upper Devonian Leduc Formation, Alberta Basin, Canada; Economic Geology, v. 120, no. 3, p. 649–662.

Cen, X.C. 2009: Stratigraphy, sedimentology and reservoir characterization of an inner platform carbonate-evaporite sequence: the Late Devonian Duperow Formation of southwestern Saskatchewan, Canada; M.Sc. thesis, University of Regina, Regina, Saskatchewan, 116 p.

Dugamin, E.J.N., Cathelineau, M., Boiron, M.C., Richard, A. and Despinois, F. 2023: Lithium enrichment processes in sedimentary formation waters; Chemical Geology, v. 635, p. 1–19.

Dugamin, E.J.N., Richard, A., Cathelineau, M., Boiron, M.C., Despinois, F. and Brisset, A. 2021: Groundwater in sedimentary basins as potential lithium resource: a global prospective study; Scientific Reports, v. 11, art. 21091.

Eggie, L., Chow, N. and Nicolas, M.P.B. 2012a: Lithofacies analysis and reservoir potential of the Duperow Formation (Upper Devonian), Williston Basin, southwestern Manitoba; Canadian Society of Petroleum Geologists–Canadian Society of Exploration Geophysicists–Canadian Well Logging Society, Joint Annual Meeting (GeoConvention 2012), May 14–18, 2012, Calgary, Alberta, abstract, 2 p.

Eggie, L., Chow, N. and Nicolas, M.P.B. 2012b: Sedimentology of the Wymark Member (middle unit) of the Upper Devonian Duperow Formation, southwestern Manitoba (NTS 62F14, 15, 16); *in* Report of Activities 2012, Manitoba Innovation, Energy and Mines, Manitoba Geological Survey, p. 160–171.

Fraino, P.E. 2025: Lithogeochemistry of the Duperow Formation in the Manitoba Potash Corporation core at 3-29-20-29W1, southwestern Manitoba (part of NTS 62K11); Manitoba Business, Mining, Trade and Job Creation, Manitoba Geological Survey, Data Repository Item DRI2025023, Microsoft® Excel® file.

Jensen, G. 2020: Investigating the lithium potential of brines in Saskatchewan: new results from brine and core sampling; Canadian Society of Petroleum Geologists–Canadian Society of Exploration Geophysicists–Canadian Well Logging Society, Joint Annual Meeting (GeoConvention 2020), September 21–23, 2020, virtual, abstract, 2 p.

Jensen, G. and Kohlruss, D. 2023: Lithium concentrations in the Duperow and Red River formations: results from four cores in southeastern Saskatchewan; *in* Summary of Investigations 2023, Volume 1, Saskatchewan Geological Survey, Saskatchewan Ministry of Energy and Resources, Miscellaneous Report 2023-4.1, Paper A-4, 14 p., 1 appendix.

Jensen, G., Pollard, A. and Rostron, B.J. 2020: Lithium concentration in the Duperow Formation: preliminary results of geochemical analysis of core samples from two wells in southeastern Saskatchewan; *in* Summary of Investigations 2020, Volume 1, Saskatchewan Geological Survey, Saskatchewan Ministry of Energy and Resources, Miscellaneous Report 2020-4.1, Paper A-2, 8 p., 1 appendix.

Jensen, G.K.S. and Rostron, B.J. 2018: Investigating the mineral potential of brines in Saskatchewan: new results from the brine sampling project for 2018; *in* Summary of Investigations 2018, Volume 1, Saskatchewan Geological Survey, Saskatchewan Ministry of Energy and Resources, Miscellaneous Report 2018-4.1, Paper A-5, 8 p.

Kadi, S., Kula, T., Erkoyum, H., Helvaci, C., Eren, M. and Demiral, B. 2023: Mineralogy, geochemistry, and genesis of lithium-bearing argillaceous sediments associated with the Neogene Bigadiç borate deposits, Balıkesir, western Anatolia, Türkiye; Applied Clay Science, v. 242, p. 1–20.

Lazowski, C.N., Melnyk, S., Gutierrez-Rueda, D., Wang, J., Tarhan, L.G., Hauck, T.E., Alessi, D.S., Konhauser, K.O. and Gingras, M.K. 2025: Characterizing the potential of wind-blown lithium sediments: a case study from Devonian evaporites of the Western Canada Sedimentary Basin; Geological Society of America Bulletin, early publication.

Nicolas, M.P.B. and Barchyn, D. 2008: Williston Basin Project (Targeted Geoscience Initiative II): summary report on Paleozoic stratigraphy, mapping and hydrocarbon assessment, southwestern Manitoba; Manitoba Science, Technology, Energy and Mines, Manitoba Geological Survey, Geoscientific Paper GP2008-2, 21 p.

Nicolas, M.P.B. and Chow, N. 2018: Stratigraphy, lithology and petroleum potential of the Upper Devonian Duperow Formation in the Manitoba Potash Corporation core at 3-29-20-29W1, southwestern Manitoba (part of NTS 65K1); *in* Report of Activities 2018, Manitoba Innovation, Energy and Mines, Manitoba Geological Survey, p. 125–135.

Rostron, B.J., Hillier, C., Mauerer, Z., Caplan, M. and Kreis, L.K. 2023: Spatial distribution of lithium in saline brines (Duperow aquifer) in southeast Saskatchewan; Canadian Energy Geoscience Association–Canadian Society of Exploration Geophysicists, Joint Annual Meeting (GeoConvention 2023), May 15–17, 2023, Calgary, Alberta, abstract, 3 p.

Wilson, J.L. 1967: Carbonate-evaporite cycles in lower Duperow Formation of Williston Basin; Bulletin of Canadian Petroleum Geology, v. 15, p. 230–312.

Wilson, J.L. and Pilatzke, R.H. 1987: Carbonate-evaporite cycles in the lower Duperow Formation of the Williston Basin; *in* Williston Basin: Anatomy of a Cratonic Oil Province, J.A. Peterson, D.M. Kent, S.B. Anderson, R.H. Pilatzke and M.W. Longman (ed.), Rocky Mountain Association of Geologists, p. 119–146.

GS2025-14

Electrofacies-based characterization of heterogeneity in the Wymark Member, Duperow Formation, southwestern Manitoba (parts of NTS 62F, G)

by P.E. Fraino

In Brief:

- Electrofacies classification in the Duperow Formation (Wymark Member) was conducted to delineate lithological variability
- Five electrofacies were defined five distinct lithologies
- The workflow provides a continuous and scalable method to assess heterogeneity and lithological trends in subsurface datasets

Citation:
Fraino, P.E. 2025: Electrofacies-based characterization of heterogeneity in the Wymark Member, Duperow Formation, southwestern Manitoba (parts of NTS 62F, G); *in* Report of Activities 2025, Manitoba Business, Mining, Trade and Job Creation, Manitoba Geological Survey, p. 135–144.

Summary

An electrofacies-based characterization of lithological variability and heterogeneity in petrophysical well log data was conducted on the Wymark Member of the Duperow Formation in southwestern Manitoba. Five electrofacies were delineated, each corresponding to a characteristic log response that is interpreted to represent limestone, dolostone, dolomitic limestone, mudstone and evaporite. These were assigned based on distinctive log responses and compared to available nearby core to validate the lithological expression of these electrofacies. Units within the Wymark Member each exhibit a distinct distribution of electrofacies and associated interpreted lithologies: the lower unit of the Wymark Member electrofacies is characterized by laterally continuous limestone intervals with minor dolostone and dolomitic limestone; the middle unit of the Wymark Member is the thickest and most heterogeneous, characterized by thick dolostone and dolomitic limestone that laterally transition into limestone toward the northern and eastern regions of the study area; and the upper unit of the Wymark Member electrofacies comprises laterally continuous limestone interbedded with thinner, discontinuous dolostone lenses and widespread anhydrite–mudstone seal intervals. These heterogeneous units provide important context for predicting reservoir distribution within the Wymark Member. The electrofacies classification workflow used in this study provides a tool for delineating heterogeneity in data-limited areas and can be applied to other intervals within the Duperow Formation to improve geological characterization.

Introduction

The Upper Devonian Duperow Formation in southwestern Manitoba is a regionally extensive carbonate–evaporite succession deposited within the Williston Basin (Wilson and Pilatzke, 1987). Brine exploration has recently targeted the Duperow Formation as an important interval for the critical mineral lithium. The formation is composed of metre-scale, carbonate–evaporite cycles that were deposited in subtidal, intertidal and supratidal settings that form distinctive brining-upward packages (Wilson and Pilatzke, 1987; Cen and Salad Hersi, 2006; Eggie, 2012; Eggie et al., 2012a; Bates, 2016; Nicolas and Chow, 2018)

Within the Duperow Formation, the Wymark Member is the thickest member, reaching up to 119 m in Manitoba. This member is of particular interest as lithium-rich brine is present in equivalent strata to the west, in Saskatchewan. The Wymark Member is informally subdivided into three units: the lower, middle and upper units. These units comprise interbedded dolostone, limestone, dolomitic limestone, anhydrite and mudstone, forming a heterogeneous lithological framework. This heterogeneity significantly influences reservoir quality, fluid flow and the development of internal baffles and barriers. Therefore, accurately characterizing the distribution and stacking of these lithologies is important for assessing reservoir compartmentalization and predicting brine accumulation zones.

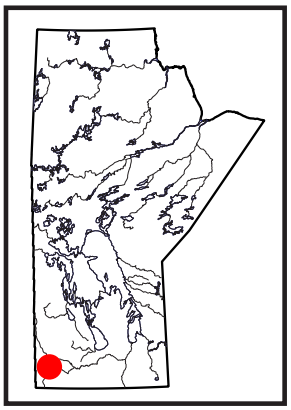

Traditional core-based facies analysis provides invaluable lithological and textural information but is limited by the sparse and discontinuous nature of core. To overcome these limitations, electrofacies classification derived from petrophysical well log curves, specifically digital Log ASCII Standard (LAS) files, was used in this report as a complementary tool to delineate lithologies observed in core descriptions. The objectives of this study are to

1) delineate key electrofacies curve signatures corresponding to major lithologies in the Wymark Member; and
2) identify spatial and temporal variability across the three units of the Wymark Member (lower, middle and upper units).

This integrated electrofacies-based approach refines the understanding of the internal architecture of the Wymark Member and offers a scalable workflow that can be applied to other members of

the Duperow and other formations, and to raster data to improve regional mapping and correlations across Manitoba when limited core data are available.

Previous work

Previous studies on the Upper Devonian Duperow Formation in southwestern Manitoba have focused primarily on establishing a stratigraphic framework, characterizing diagenesis and assessing hydrocarbon potential. Regional mapping and stratigraphic correlation were significantly advanced through the Targeted Geoscience Initiative (TGI), Phase II by Bezys and Bamburak (2004) and Nicolas and Barchyn (2008). They extended the formal member-level stratigraphy of the Duperow Formation from Saskatchewan into Manitoba. Subsequent work by Eggie (2012), Eggie et al. (2012a, b), Bates (2016) and Bates et al. (2016) included logging 10 core and conducting detailed petrographic and stable isotope analyses (Sr, O, C) to investigate depositional facies, diagenesis and formation evolution to assess the hydrocarbon potential. More recently, the entire Duperow Formation was logged in the Manitoba Potash Corporation (MPC) core (oil and gas well licence 3884, Manitoba Business, Mining, Trade and Job Creation, Winnipeg) located in L.S. 3, Sec. 29, Twp. 20, Rge. 29, W 1st Mer. (abbreviated 3-29-20-29W1) by Nicolas and Chow (2018). Interest in the Duperow Formation has since expanded with the emergence of lithium exploration, and as a result, previous work on facies architecture, diagenesis and reservoir properties now provides a crucial foundation for evaluating its potential to host lithium-bearing brines. Lastly, the first core-derived lithium concentration data have been reported from the MPC core in Fraino (2025), which highlights the role of intraformational, lithium-enriched mudstone intervals as a potential contributor to lithium in formation waters.

Stratigraphy

The Upper Devonian (Frasnian age) Duperow Formation is a carbonate and evaporite succession up to 260 m thick in the subsurface of the Williston Basin of northern North Dakota, southern Saskatchewan and southwestern Manitoba (Dunn, 1975; Pilatzke et al., 1987; Wilson and Pilatzke, 1987; Nicolas and Barchyn, 2008; Cen, 2009; Eggie, 2012). In Saskatchewan, the Duperow Formation reaches thicknesses between 125 and 260 m, whereas in southwestern Manitoba it thins to 122–195 m (Figure GS2025-14-1). The Duperow Formation conformably overlies the Souris River Formation and, in turn, is overlain by the Birdbear Formation (Nicolas and Barchyn, 2008). In North Dakota and Saskatchewan, the Duperow Formation is divided into four members: Saskatoon, Elstow, Wymark and Seward. These members are distinguished based on regionally extensive marker beds visible in geophysical logs and core. However, in eastern Saskatchewan and southwestern Manitoba, the Elstow Member is not distinguishable from the Saskatoon Member, and only the latter is recognized in this report. The Wymark Member is informally subdivided into lower, middle and upper units. The Seward

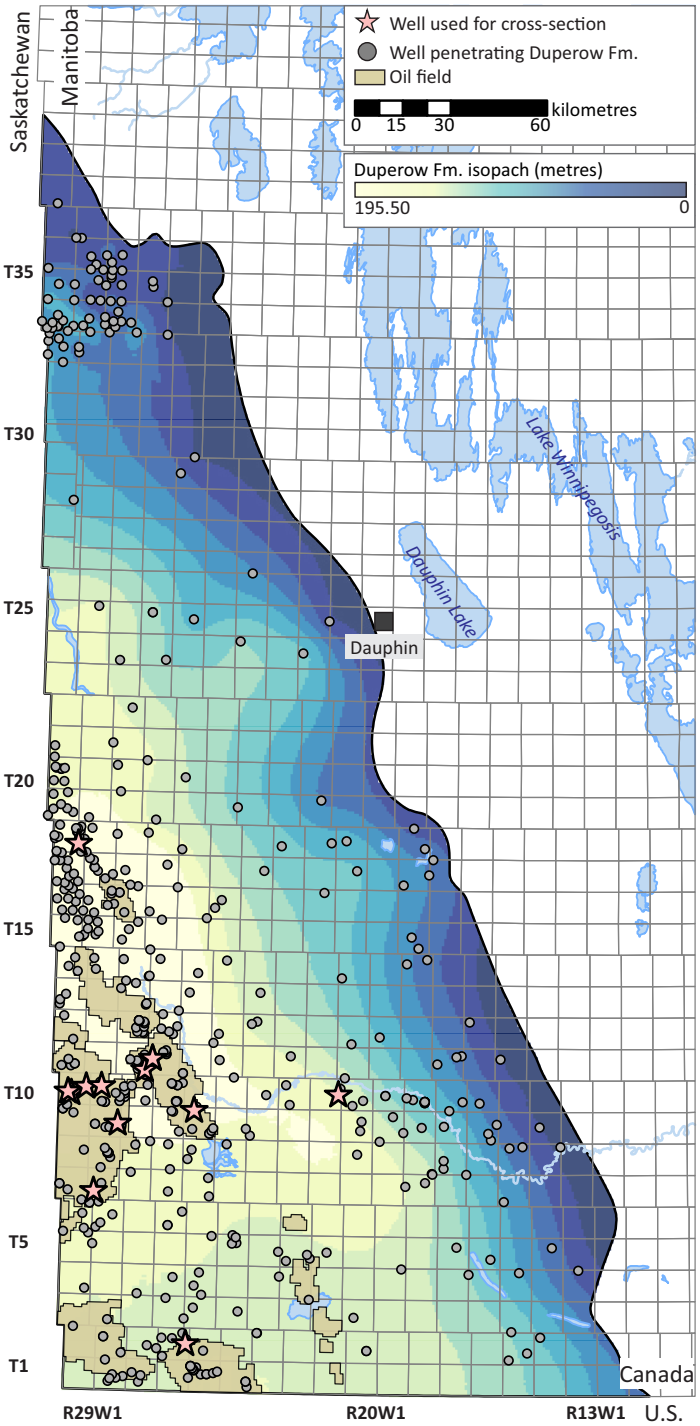

Figure GS2025-14-1: *Isopach map of the Duperow Formation in the study area in southwestern Manitoba, showing all wells that penetrated the Duperow Formation and the wells with Log ASCII Standard log files that were used in the cross-sections for this study (Figures GS2025-14-5, -6; geoLOGICS ltd.'s geoSCOUT™). Data points from geoSCOUT™ were processed using ArcGIS®. Isopach basemap was created using ArcGIS® software by Esri. ArcGIS® is the intellectual property of Esri and is used herein under license. Copyright © Esri. All rights reserved. For more information about Esri software, please visit <https://esri.ca/>.*

Member consists of a discontinuous basal evaporite, the Flat Lake Evaporite, and the upper laterally extensive Seward shale (Nicolas and Barchyn, 2008). In this report, the Wymark Mem-

ber and its informal units (lower, middle and upper units) are the intervals of interest (Figure GS2025-14-2).

Dataset and electrofacies methodology

In Manitoba, a total of 515 wells penetrate the Duperow Formation, of which 329 wells include a suite of digital LAS log files that were available in geoLOGIC systems ltd.'s geoSCOUT™. For this report, 35 wells with LAS log files were analyzed for their gamma-ray (GR), neutron porosity calibrated to a limestone matrix (Nphi), density porosity calibrated to a limestone matrix (Dphi), photoelectric factor (PEF), bulk density (RHOB) and deep resistivity (RT) curves (Figure GS2025-14-2).

Electrofacies are distinctive groupings of log-curve responses that can be used to infer different lithologies within a wellbore (Davies, 2018). In this study, electrofacies were distinguished primarily using PEF, Nphi and Dphi curves, supported by GR, RHOB and RT curves. A rules-based classification scheme was developed by calibrating lithologies recognized in core to their characteristic log responses in carbonate–evaporite systems (Figure GS2025-14-2). This involved applying numeric cutoff values, starting with known PEF curve values, which provides the clearest separation between lithologies. Dolostone and mudstone intervals exhibit low PEF values (<3.3), whereas limestone and evaporite intervals display higher PEF values (>4.5). Intermediate values (3.3–4.5) are associated with transitional dolomitic limestone. Porosity curves (Nphi and Dphi) were then used to refine these groupings, followed by GR, RHOB and RT curves.

These combined curve relationships define the 'rules' of the electrofacies classification and are illustrated in the example log panel (Figure GS2025-14-2). This process was carried out for each of the 35 wells in the study area, and the resulting electrofacies assignments were compared across wells to ensure consistency and reproducibility. The lithologies applied in this scheme were confirmed by direct observation in Wymark Member core (Figure GS2025-14-3) and then extended to nearby wells. To improve accuracy, intervals were further refined using combined-log pattern recognition, ensuring that subtle variations not captured by simple cutoff values were incorporated into the electrofacies assignments.

To complement the rules-based classification, principal component analysis (PCA) was applied to the variables used for the rules-based electrofacies determination (GR, Nphi, Dphi, RHOB, PEF and RT curves) using a Python code (Figure GS2025-14-4). Prior to analysis, each variable within the dataset was standardized by subtracting the mean and dividing by the standard deviation for each curve. This ensured that all petrophysical logs contributed equally to the PCA, preventing variables with larger numerical ranges from dominating the results. The PCA reduces the number of variables into a few components that capture the majority of the variance in the dataset (see Grunsky, 2010; Jolliffe and Cadima, 2016), allowing log responses of different lithologies to be more easily understood (e.g., Lee et al., 2002; Perez et al., 2003). When plotted, intervals assigned to different electrofacies should theoretically form distinct groupings, confirming that the rules-based cutoffs are an accurate reflection of observed variance within the dataset, which is reflective of lithological changes. In this study, PCA therefore is used as a validation step instead of for classification, demonstrating that the electrofacies defined by rules and supported by core calibration are indeed distinct through PCA.

Electrofacies classification

In the Wymark Member of the Duperow Formation, five electrofacies were identified and are interpreted to represent five lithologies commonly observed in core, including limestone, dolostone, dolomitic limestone, mudstone and evaporite (Figures GS2025-14-2, -3). Each electrofacies exhibits a distinct log response; the responses are summarized in Table GS2025-14-1 and show clear groupings in the PCA space (Figure GS2025-14-4).

Electrofacies 1 is identified by low gamma-ray (<20 API units) and high PEF (>4.5) values, and relatively consistent RT values (<52 Ω•m), RHOB values between 2300 and2710 kg/m^3, and Nphi and Dphi logs that track each other at 2–10%. Based on log responses, this is interpreted to be limestone intervals that correspond to subtidal lithologies, including calcareous mudstone, wackestone-packstone and stromatoporoid framestone lithofacies (Eggie, 2012; Eggie et al., 2012a, b; Bates, 2016; Bates et al., 2016; Figure GS2025-14-3).

Electrofacies 2 consists of low gamma-ray values (<25 API units), low PEF values (<3.3) and high Nphi and Dphi values (>15%) compared to other electrofacies, RHOB values between 2100 and 2810 kg/m^3 and RT values of <50 Ω•m. Electrofacies 2 is interpreted to correspond to dolostone intervals that, in core, appear as intertidal laminated or massive dolostone with pervasive intercrystalline pore space in comparison to limestone lithologies (Bates, 2016; Figure GS2025-14-3).

Electrofacies 3 consists of low GR values (<35 API units), intermediate PEF values (3.3–4.5), high Nphi and Dphi values (5–15%) compared to other electrofacies, RHOB values between 2170 and 2750 kg/m^3 and RT values of <36 Ω•m. Electrofacies 3 is interpreted to be dolomitic limestone intervals as these are intermediate or transitional log responses, falling between the dolostone and limestone responses described above. In core, these are often laminated and partially recrystallized (Figure GS2025-14-3).

Electrofacies 4 and 5 comprise thinner intervals (<5 m thick) in contrast to electrofacies 1, 2 and 3. Electrofacies 4 is characterized by the highest gamma-ray values (>50 API units), low PEF values (<3.3), low RHOB values (<2500 kg/m^3), near zero Nphi and Dphi values and RT values between 1 and 10. Electrofacies 4 corresponds to mudstone intervals and, in core, this electrofacies represents fine-grained, clay-rich mudstone (Figure GS2025-14-3). Whereas electrofacies 5 consists of low GR values (<25 API units), high PEF values (>4.5), high RHOB values (>2800 kg/m^3), highest RT values (>200 Ω•m) and low Dphi and Nphi val-

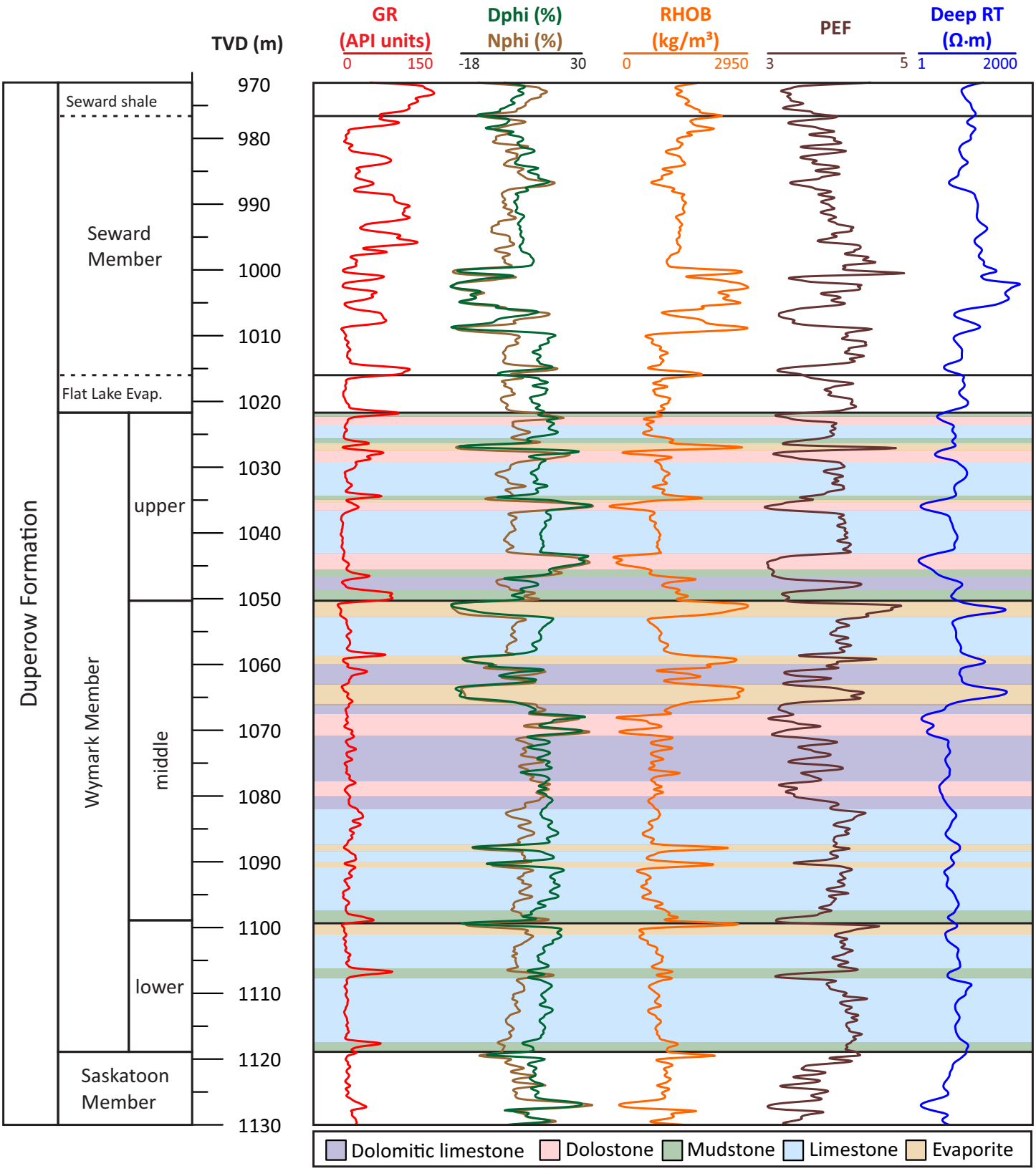

Figure GS2025-14-2: *Stratigraphy and petrophysical well logs for the well at L.S. 15, Sec. 32, Twp. 9, Rge. 29, W 1st Mer. (abbreviated 15-32-9-29W1; oil and gas well licence 5270, Manitoba Business, Mining, Trade and Job Creation, Winnipeg) in southwestern Manitoba with the assigned rules-based electrofacies (dolomitic limestone, dolostone, limestone, evaporite and mudstone). Abbreviations: Ω, ohm; dec, decimal; Dphi, density porosity calibrated to a limestone matrix; Evap., Evaporite; GR, gamma ray; Nphi, neutron porosity calibrated to a limestone matrix; PEF, photoelectric factor; RHOB, bulk density; RT, resistivity; TVD, true vertical depth.*

Figure GS2025-14-3: *Example core logs displaying the typical stacking of lithologies in the* ***a)*** *lower unit of the Wymark Member from the oil and gas well at L.S. 4, Sec. 27, Twp. 11, Rge. 22, W 1st Mer. (abbreviated 4-27-11-22W1; oil and gas well licence 1228, Manitoba Business, Mining, Trade and Job Creation, Winnipeg),* ***b)*** *middle unit of the Wymark Member from the oil and gas well at 7-18-10-20W1 (oil and gas well licence 2456), and* ***c)*** *upper unit of the Wymark Member from the oil and gas well at 13-4-10-20W1 (oil and gas well licence 1456).*

ues (~0%). This electrofacies corresponds to evaporite intervals that, in core, represent supratidal, anhydrite intervals although some thinner intervals likely represent anhydrite nodules enveloped within the carbonate electrofacies described above (Figure GS2025-14-3).

The PCA results confirm that the electrofacies derived from rules-based classification form distinct groupings in multivariate space (Figure GS2025-14-4). The principal component 1 (PC1) space accounts for 47.6% of the variance, primarily reflecting Nphi, Dphi, RHOB and RT curves, whereas PC2 space explains 25.3% and captures variation in GR, with PEF and RHOB having the same loading for PC2 (Figure GS2025-14-4a). Dolostone, limestone, mudstone and evaporite intervals interpreted from electrofacies analysis plot as isolated groupings due to their contrasting petrophysical properties, whereas dolomitic limestone shows partial overlap with both limestone and dolostone, reflecting its transitional composition (Figure GS2025-14-4b). The purpose of this analysis is not to redefine the electrofacies, but to provide an independent statistical validation that the rules-based groups are robust and correspond to lithologies observed in core.

Electrofacies trends and heterogeneity

Using the electrofacies classification and interpreted lithological intervals described above, five distinct vertical and lateral electrofacies variations are observed in the Wymark Member across the study area. Although all five electrofacies occur in the lower, middle and upper units of the Wymark Member, their distribution and occurrence vary spatially and temporally within each unit (e.g., Figure GS2025-14-2). These variations influence reservoir connectivity (Figures GS2025-14-5, -6).

The lower unit of the Wymark Member (13.1–34.9 m thick) is dominated by limestone (averages 14 m thick), with subordinate dolostone and dolomitic limestone intervals (average 3.4 m thick), which are more common along the southern and western margins of the study. The lower unit of the Wymark Member forms two laterally extensive, limestone intervals, separated by a thinner and laterally continuous mudstone interval (1 m thick)

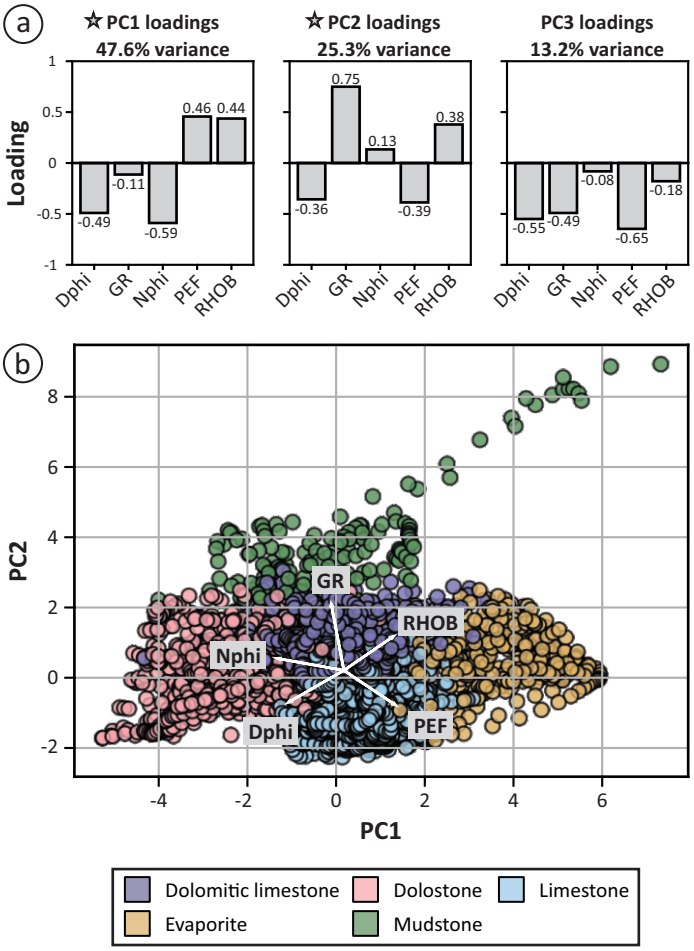

Figure GS2025-14-4: a) *Principal component analysis (PCA) loadings for the first three principal components (principal component 1 (PC1)–PC3), which together explain the majority (86.1%) of the variance in the petrophysical datasets. Grey stars denote the loadings used for (b).* ***b)*** *PCA biplot of PC1 versus PC2 with samples classified by identified electrofacies. The petrophysical data loadings are shown by the arrows. Abbreviations: Dphi, density porosity calibrated to a limestone matrix; GR, gamma ray; Nphi, neutron porosity calibrated to a limestone matrix; PEF, photoelectric factor; RHOB, bulk density.*

and an anhydrite interval (1 m thick). The spatial electrofacies heterogeneity in this unit is relatively low, as the limestone intervals are continuous; however, subtle lateral and vertical lithofacies transitions or diagenesis overprint within these intervals may affect reservoir continuity.

The middle unit of the Wymark Member (39–68.9 m thick) is the thickest and most heterogeneous interval. The basal interval consists of limestone (averages 15 m thick), which is overlain by a characteristic succession of dolostone and dolomitic limestone (average 25 m thick). Dolostone is common along Twp. 2–15, Rge. 26–29, W 1st Mer., transitioning into limestone toward the northern and eastern parts of the study area. In contrast, dolomitic limestone interfingers with dolostone southward and thickens toward the north (Figure GS2025-14-5). Along the west–east transect (Figure GS2025-14-6), dolomitic limestone occurs as localized intervals enveloped within dolostone intervals that thin to less than 2 m thick and transition into limestone intervals to the east (35 m thick east of the study area). The heterogeneity within the middle unit of the Wymark Member reflects variations in depositional conditions and this heterogeneity influenced laterally extensive electrofacies transitions across the study area. Similar to the lower unit of the Wymark Member, limestone, dolostone and dolomitic limestone intervals are commonly capped by evaporite and mudstone intervals.

The upper unit of the Wymark Member (18.3–30.3 m thick) is primarily composed of limestone interbedded with laterally continuous mudstone (averages 1.5 m thick) and anhydrite intervals (averages 1.6 m thick). Unlike the middle unit of the Wymark Member, dolostone intervals occur as discontinuous lenses (average 7.4 m thick) enveloped within limestone intervals (average 13 m thick) that extend for tens of kilometres. Therefore, the heterogeneity is defined by the spatial extent of the dolostone intervals.

Throughout the Wymark Member, limestone, dolomitic limestone and dolostone intervals are commonly overlain by anhydrite intervals, which in turn are capped by mudstone intervals that develop laterally continuous, internal baffles. The vertically stacked carbonate–anhydrite–mudstone successions reflect repeated brining-upward cycles, marking a transition from open-marine to restricted supratidal, evaporitic conditions (Nicolas and Chow, 2018; Figure GS2025-14-3).

Electrofacies analysis identifies the most porous intervals, based on Nphi and Dphi curves, to occur within thick, laterally extensive dolostone and dolomitic limestone intervals, particularly in the middle unit of the Wymark Member. Although porosity curves (Nphi and Dphi) are calibrated to a limestone matrix, based on core analysis, dolostone consistently shows better-developed, intercrystalline pore networks, compared to limestone lithologies, with up to 28% porosity reported from routine core analysis (Eggie, 2012; Eggie et al., 2012b; Bates, 2016; Bates et al., 2016). In contrast, limestone intervals in the lower, middle and upper units of the Wymark Member consist of lateral continuous intervals with variable porosity.

Conclusion and future work

Electrofacies classification is effective at delineating lithology and heterogeneity within the Wymark Member. This methodology allows for consistent identification of lithology despite variability across wells in areas with limited or absent core data. The application of electrofacies cutoffs to well logs captured key lithological transitions between wells and enabled the detailed interpretation of potential reservoir and seal lithology distribution within the Wymark Member. These electrofacies trends are directly relevant to lithium-brine exploration, as variability in electrofacies stacking, continuity and seal development may influence brine migration, fluid compartmentalization and the vertical isolation of individual reservoir zones. Understanding

Table GS2025-14-1: *Electrofacies classification scheme used in this study, showing diagnostic ranges for gamma rays (GR), photoelectric factor (PEF), bulk density (RHOB), resistivity (RT), and neutron (Nphi) and density (Dphi) porosities calibrated to a limestone matrix. Abbreviation: Ω, ohm.*

Electrofacies	Lithology	GR (API units)	PEF	RHOB (kg/m³)	RT (Ω•m)	Nphi (%)	Dphi (%)
1	Limestone	<20	>4.5	2300 to 2710	<52	2 to 10	2 to 10
2	Dolostone	<25	<3.3	2100 to 2810	<50	>15	>15
3	Dolomitic limestone	<35	3.3 to 4.5	2170 to 2750	<36	5 to 15	5 to 15
4	Mudstone	>50	<3.3	<2500	1 to 10	~ 0	~ 0
5	Evaporite	<25	>4.5	>2800	>200	~ 0	~ 0

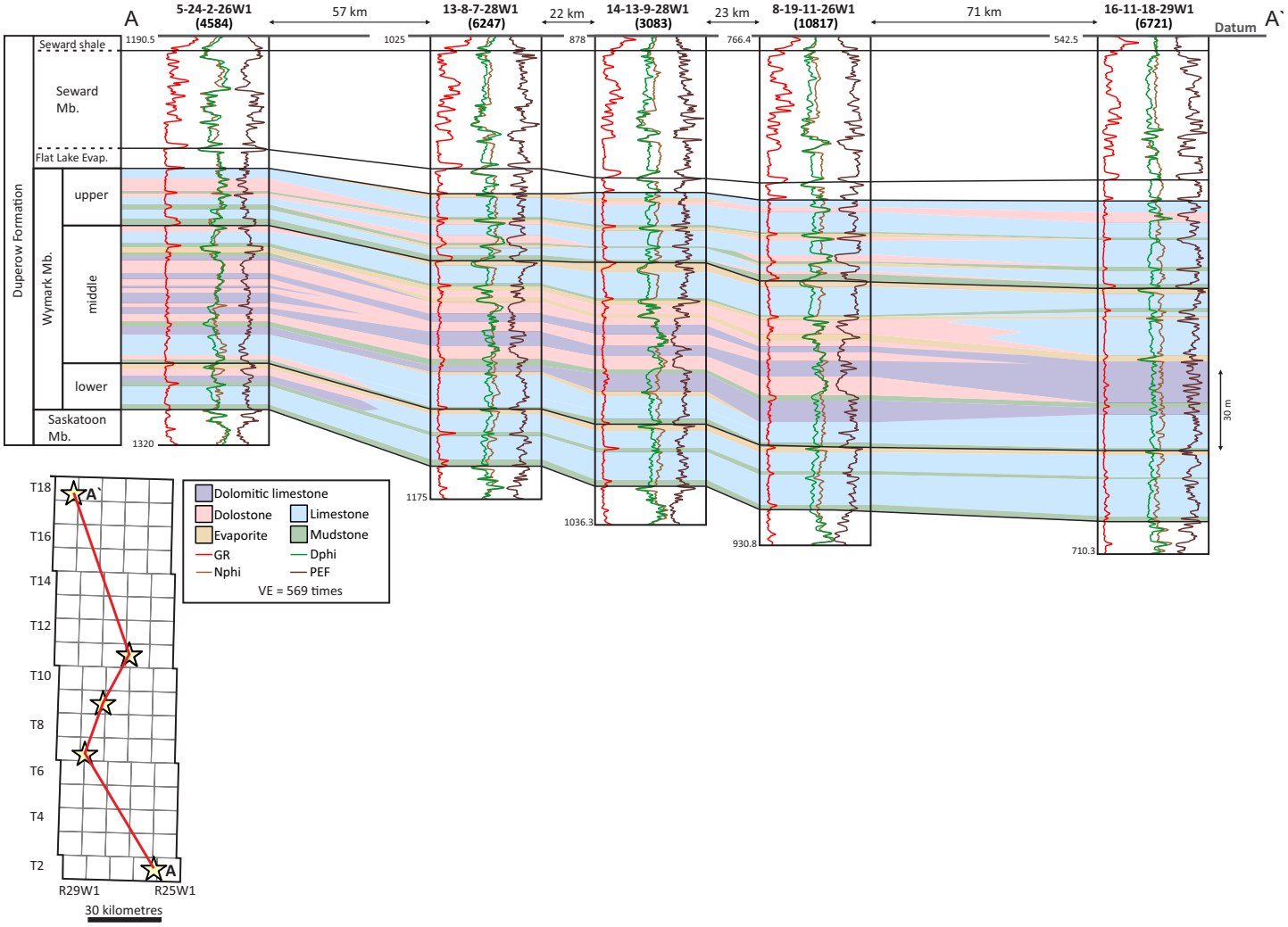

Figure GS2025-14-5: *Regional cross-section correlation from south (A) to north (A') for the Duperow Formation in southwestern Manitoba, with assigned electrofacies. Oil and gas licence number (Manitoba Business, Mining, Trade and Job Creation, Winnipeg) is denoted under the well number at the top of each petrophysical log. For simplicity, only gamma-ray (GR), neutron porosity calibrated to a limestone matrix (Nphi), density porosity calibrated to a limestone matrix (Dphi) and photoelectric factor (PEF) petrophysical well logs are shown in the correlation. Top and bottom depth for each well is shown as true vertical depth in metres. Top of the Duperow Formation is used as the datum. The well at L.S. 8, Sec. 19, Twp. 11, Rge. 26, W 1st Mer. (abbreviated 8-19-11-26W1) has also been included in cross-section B–B' (Figure GS2025-14-6). Abbreviations: Evap., Evaporite; VE, vertical exaggeration.*

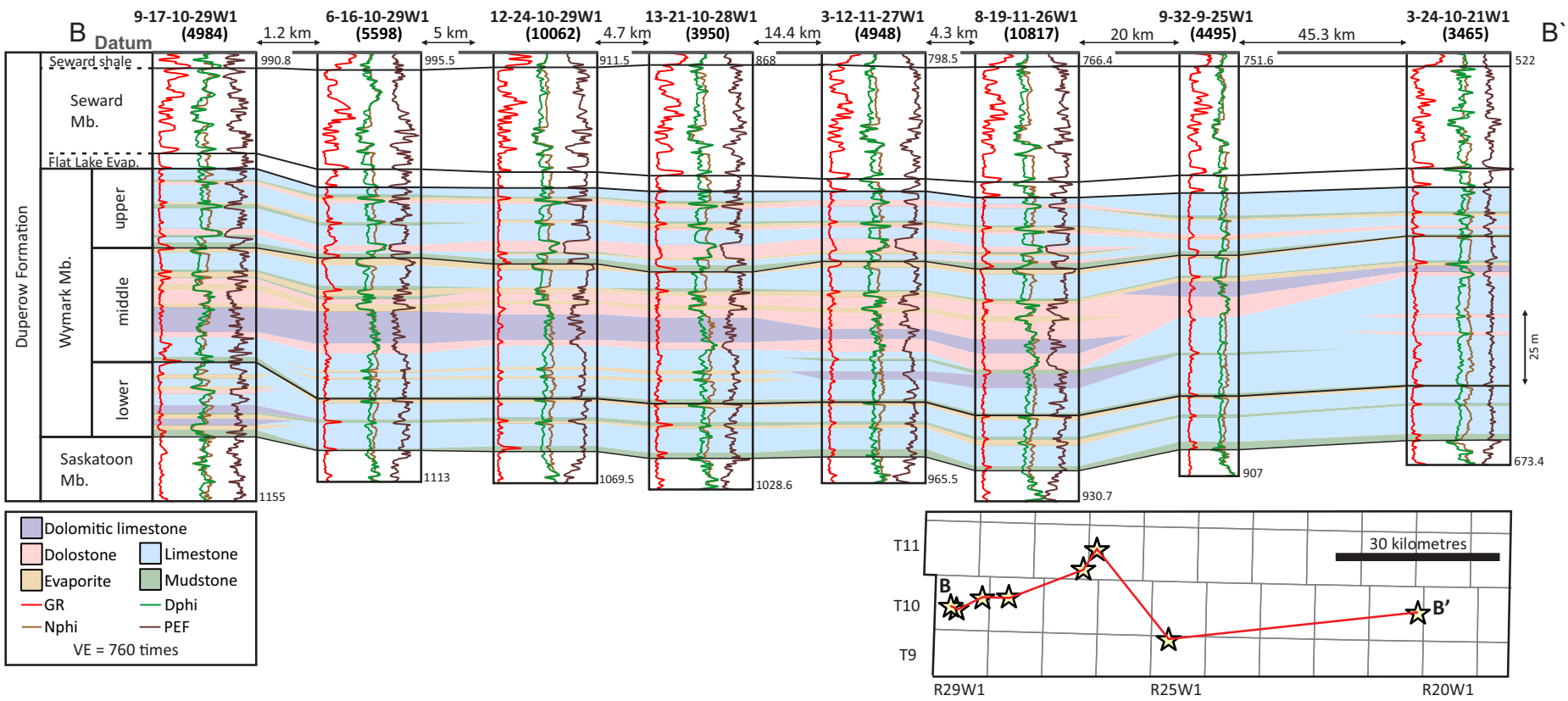

Figure GS2025-14-6: *Regional cross-section correlation from west (B) to east (B') for the Duperow Formation in southwestern Manitoba, with assigned electrofacies. Oil and gas licence number (Manitoba Business, Mining, Trade and Job Creation, Winnipeg) is denoted under the well number at the top of the each petrophysical log. For simplicity, only gamma-ray (GR), neutron porosity calibrated to a limestone matrix (Nphi), density porosity calibrated to a limestone matrix (Dphi) and photoelectric factor (PEF) petrophysical well logs are shown in the correlation. Top and bottom depth for each well is shown as true vertical depth in metres. Top of the Duperow Formation is used as the datum. The well at L.S. 8, Sec. 19, Twp. 11, Rge. 26, W 1st Mer. (abbreviated 8-19-11-26W1) has also been included in cross-section A–A' (Figure GS2025-14-5). Abbreviations: Evap., Evaporite; VE, vertical exaggeration.*

and mapping the spatial arrangement of these electrofacies is thus critical for targeting zones with the greatest resource potential.

The workflow developed can be extended to build a more comprehensive understanding of electrofacies distribution and depositional architecture across the Duperow Formation. Future work will focus on integrating electrofacies with core descriptions to better identify electrofacies and lithological extents across southwestern Manitoba.

Economic considerations

As Manitoba expands its critical mineral strategy, lithium is becoming a key exploration focus within the province's deeper Paleozoic formations. The Duperow Formation represents a strategic target for potentially hosting lithium-bearing brines. Although the formation is well-studied in adjacent jurisdictions for hydrocarbons and, more recently, from a lithium-brine perspective, its potential in Manitoba remains largely underexplored. As such, understanding depositional trends and electrofacies distribution within the Wymark Member, as presented in this report, is essential to advancing lithium-brine exploration in southwestern Manitoba.

Acknowledgments

The author would like to thank C. Epp, P. Belanger and E. Ralph (Manitoba Geological Survey) for their assistance with coordinating the logistics of core retrieval. The author would like to thank P.J. Fulton-Regula and M.P.B. Nicolas (Manitoba Geological Survey) for proving constructive feedback on an earlier version of this report and T.J. Hodder (Manitoba Geological Survey) for providing feedback on the statistical analysis.

References

Bates, K. 2016: Stratigraphy, sedimentology and petroleum potential of the Upper Devonian Duperow Formation, southwest Manitoba; M.Sc. thesis, University of Manitoba, Winnipeg, Manitoba, 228 p.

Bates, K., Chow, N. and Nicolas, M.P.B. 2016: Preliminary results from sedimentological investigations and petroleum evaluation of the Upper Devonian Duperow Formation, southwestern Manitoba; *in* Report of Activities 2016, Manitoba Growth, Enterprise and Trade, Manitoba Geological Survey, p. 157–167.

Bezys, R.K. and Bamburak, J.D. 2004: Lower to Middle Paleozoic stratigraphy of southwestern Manitoba; Manitoba Industry, Economic Development and Mines, Manitoba Geological Survey, May 25–28, 2004, Winnipeg, Manitoba, WCSB/TGI II Field Trip Guidebook, 72 p.

Cen, X.C. 2009: Stratigraphy, sedimentology and reservoir characterization of an inner platform carbonate-evaporite sequence: the Late Devonian Duperow Formation of southwestern Saskatchewan, Canada; M.Sc. thesis, University of Regina, Regina, Saskatchewan, 116 p.

Cen, X.C. and Salad Hersi, O. 2006: Sedimentology, microfacies analysis, and depositional setting of the Late Devonian Duperow Formation, southeastern Saskatchewan; *in* Summary of Investigations 2006, Volume 1, Saskatchewan Geological Survey, Saskatchewan Industry Resources, Miscellaneous Report 2006-4.1, Paper A-10, 18 p.

Davies, J.C. 2018: Electrofacies in reservoir characterization; *in* Handbook of Mathematical Geosciences, Fifty Years of IAMG, B.S. Daya Sagar, Q. Cheng and F. Agterberg (ed.), Springer International Publishing AG, Cham, Switzerland, p. 211–223.

Dunn, C.E. 1975: The upper Devonian Duperow Formation in southeastern Saskatchewan; Saskatchewan Department of Mineral Resources, Saskatchewan Geological Survey, Report No. 179, 151 p.

Eggie, L. 2012: Sedimentology and petroleum reservoir potential of the middle unit of the Wymark Member in the Upper Devonian Duperow Formation, southwestern Manitoba; B.Sc. thesis, University of Manitoba, Winnipeg, Manitoba, 145 p.

Eggie, L., Chow, N. and Nicolas, M.P.B. 2012a: Lithofacies analysis and reservoir potential of the Duperow Formation (Upper Devonian), Williston Basin, southwestern Manitoba; Canadian Society of Petroleum Geologists–Canadian Society of Exploration Geophysicists–Canadian Well Logging Society, Joint Annual Meeting (GeoConvention 2012), May 14–18, 2012, Calgary, Alberta, abstract, 2 p.

Eggie, L., Chow, N. and Nicolas, M.P.B. 2012b: Sedimentology of the Wymark Member (middle unit) of the Upper Devonian Duperow Formation, southwestern Manitoba (NTS 62F14, 15, 16); *in* Report of Activities 2012, Manitoba Innovation, Energy and Mines, Manitoba Geological Survey, p. 160–171.

Fraino, P.E. 2025: Pilot study of lithium concentrations in mudstone intervals from the Manitoba Potash Corporation core at 3-29-20-29W1, southwestern Manitoba (part of NTS 62K11); *in* Report of Activities 2025, Manitoba Business, Mining, Trade and Job Creation, Manitoba Geological Survey, p. 128–134.

Grunsky, E.C. 2010: The interpretation of geochemical survey data; Geochemistry: Exploration, Environment, Analysis, v. 10, no. 1, p. 27–74.

Jolliffe, I.T. and Cadima, J. 2016: Principal component analysis: a review and recent developments; Philosophical Transactions of the Royal Society A: Mathematical, Physical and Engineering Sciences, v. 374, no. 2065, art. 20150202.

Lee, S.H., Kharghoria, A. and Datta-Gupta, A. 2002: Electrofacies characterization and permeability predictions in complex reservoirs; SPE Reservoir Evaluation & Engineering, v. 5, no. 03, p. 237–248.

Nicolas, M.P.B. and Barchyn, D. 2008: Williston Basin Project (Targeted Geoscience Initiative II): summary report on Paleozoic stratigraphy, mapping and hydrocarbon assessment, southwestern Manitoba; Manitoba Science, Technology, Energy and Mines, Manitoba Geological Survey, Geoscientific Paper GP2008-2, 21 p.

Nicolas, M.P.B. and Chow, N. 2018: Stratigraphy, lithology and petroleum potential of the Upper Devonian Duperow Formation in the Manitoba Potash Corporation core at 3-29-20-29W1, southwestern Manitoba (part of NTS 65K1); *in* Report of Activities 2018, Manitoba Innovation, Energy and Mines, Manitoba Geological Survey, p. 125–135.

Perez, H.H., Datta-Gupta, A. and Mishra, S. 2003: The role of electrofacies, lithofacies, and hydraulic flow units in permeability predictions from well logs: a comparative analysis using classification trees; SPE Annual Technical Conference and Exhibition, October 5–8, 2003, Denver, Colorado, paper SPE-84301-MS.

Pilatzke, E.H., Fischer, D.W. and Pilatzke, C.L. 1987: Overview of Duperow (Devonian) production in the Williston Basin; *in* Williston Basin: Anatomy of a Cratonic Oil Province, J.A. Peterson, D.M. Kent, S.B. Anderson, R.H. Pilatzke and M.W. Longman (ed.), Rocky Mountain Association of Geologists, p. 423–432.

Wilson, J.L. and Pilatzke, R.H. 1987: Carbonate-evaporite cycles in the lower Duperow Formation of the Williston Basin; *in* Williston Basin: Anatomy of a Cratonic Oil Province, J.A. Peterson, D.M. Kent, S.B. Anderson, R.H. Pilatzke and M.W. Longman (ed.), Rocky Mountain Association of Geologists, p. 119–146.

GS2025-15

Compilation of saline water analysis data from oil and gas wells and a case study of Duperow Formation data, southwestern Manitoba (parts of NTS 62F–K, N, O, 63C)

by E. Enaworu

In Brief:

- Saline water analysis data have been compiled into a user-friendly digital format
- Duperow Formation saline aquifers are dominated by sodium, potassium and chloride ions
- Total Dissolved Solids (TDS) concentrations and other water properties can inform hydrogeological evaluation of saline water aquifers

Citation:
Enaworu, E. 2025: Compilation of saline water analysis data from oil and gas wells and a case study of Duperow Formation data, southwestern Manitoba (parts of NTS 62F–K, N, O, 63C); *in* Report of Activities 2025, Manitoba Business, Mining, Trade and Job Creation, Manitoba Geological Survey, p. 145–154.

Summary

As part of an ongoing project initiated by the Manitoba Geological Survey (MGS) in 2023, this report details the completion of the compilation of water analysis data from oil and gas wells in southwestern Manitoba. In addition, the Duperow Formation data were used as a case study to show the usefulness of the compiled data in characterizing the saline aquifers of southwestern Manitoba. Preliminary results from the Duperow Formation classified the saline aquifers into highly saline to brine with sodium and potassium (combined) and chloride ions as the dominant salinity drivers. The dominance has led to the classification of the Duperow Formation water as a sodium-chloride–type formation water. The major cations and anions that contributed to the total dissolved solids (TDS) for each well were identified. Cations, anions and TDS concentrations varied amongst the stratigraphic members, with the lowest TDS value of 13 201 ppm occurring in the Seward Member and the highest value of 240 763 ppm reported in the middle Wymark Member. The water analysis data for the Duperow Formation suggests it has a relationship with the dolomitization and anhydrite formation observed in previous studies. Other data analyses trends and patterns were used to establish correlations/relationships that could possibly be used to predict water chemistry and petrophysical properties for areas without data or poor-quality data.

Introduction

In 2023, the MGS started compiling saline water analysis data for the subsurface saline aquifer formations located in southwestern Manitoba. This compilation entailed compiling saline water analysis data spanning over 70 years from oil and gas wells into a user-friendly digital format (Manitoba Business, Mining, Trade and Job Creation, 2025).

This study brings to the fore the completed compilation of saline water analysis data from 744 oil and gas wells in southwestern Manitoba. Multiple wells recorded multiple samples from different intervals in the well. For each sample, various information was captured, including oil and gas well licence number, unique well identifier (UWI), well name, location, bottom-hole latitude, bottom-hole longitude, DST number, sampling point, oil field name, depth intervals tested, subsurface formation assigned at the time of sampling, geological age, nature of liquid, total dissolved solids (TDS), primary salinity, secondary salinity, primary alkalinity, secondary alkalinity, chloride salinity, sulphate salinity, and cation and anion concentrations, among others. Water petrophysical properties such as conductivity, resistivity, density, pH, specific gravity, hardness and turbidity were also captured, when the information was available in the original reports.

This report details 1) the concluding phase (phase four) of the compiled saline water analysis data project for southwestern Manitoba, first introduced in Enaworu and Nicolas (2024), and 2) a case study using a subset of saline water analysis data from the Duperow Formation to evaluate data quality, relationships and trends.

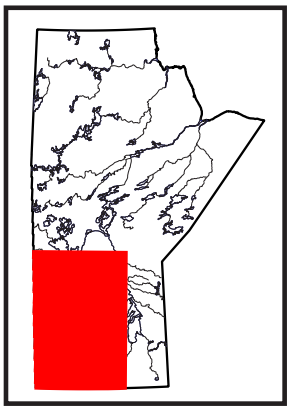

Geology and stratigraphy

The Williston Basin consists of several geological formations deposited throughout the Paleozoic to Cenozoic eras. Within these geological formations are several saline aquifers, which vary in depth, TDS and ion concentrations, and water physical properties from one location to the next. The economic potential and growing need for saline aquifers due to their potential use as key sources for minerals/metals, carbon capture and storage and geothermal energy has spurred serious interest in the Williston Basin.

There are several Devonian formations deposited within the Williston Basin but the Duperow Formation was chosen for a case study because of its potential for lithium. The formation extends

to other provinces, such as eastern Saskatchewan, but the case study only focused on the subsurface Duperow Formation in Manitoba. In southwestern Manitoba, the Duperow Formation is 122–195 m thick and thins laterally from the west to the east and consists of carbonate–evaporite successions. It is characterized by a thick stratigraphic interval composed of limestone, evaporite and dolostone units deposited within a semiconstrained, back-reef depositional setting in the Devonian Elk Point Basin; the Devonian Elk Point Basin extended and incorporated the Williston Basin as its southeastern sector (Anna et al., 2013; Chow et al., 2014; Eggie and Chow, 2024).

The Duperow Formation consists of three distinct members—from oldest to youngest—Saskatoon, Wymark and Seward members (Figure GS2025-15-1). The Wymark Member is the thickest member and has been stratigraphically divided from oldest to youngest into the lower, middle and upper units (Nicolas and Chow, 2018; Eggie and Chow, 2024). Eggie et al. (2012), Bates (2016) and Bates et al. (2016) identified three key lithofacies associations in the Duperow Formation—subtidal, intertidal and supratidal.

A recent study using petrophysical analysis of well logs in southwestern Manitoba defined the vertical and lateral arrangement of the carbonate cycles in the Duperow Formation (Fraino, 2025a; Fraino and Nicolas, 2025). Preliminary isopach maps in Fraino and Nicolas (2025) indicate differences in the thicknesses of these cycles with the thickest successions identified in Twp. 10–20, Rge. 20–29, W 1st Mer. Fraino and Nicolas (2025) also showed that facies-controlled diagenetic processes including dolomitization and dissolution contributed significantly to the enhancement of porosity and permeability within the Duperow Formation. Consequently, intervals rich in dolomite situated in intertidal and subtidal deposits were identified as being good intervals for brine aquifers because of their favourable reservoir properties.

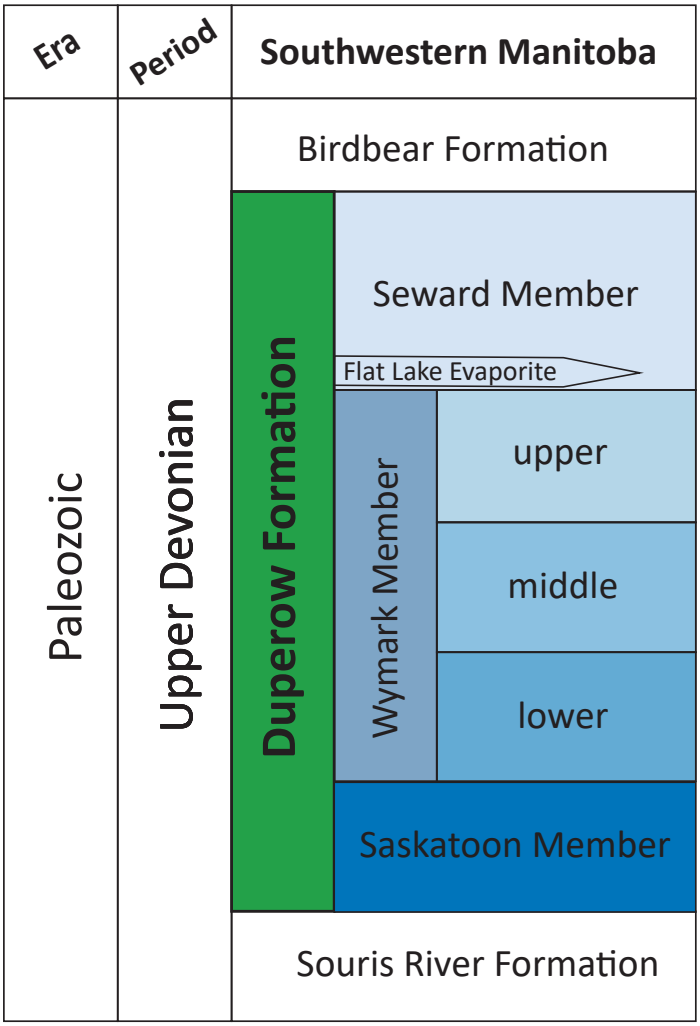

Figure GS2025-15-1: *Stratigraphy of the Upper Devonian Duperow Formation (modified from Nicolas and Barchyn, 2008).*

Hydrogeology

Palombi (2008) reported that within the central portion of the Williston Basin, the movement of fluids occur typically up-dip to the northeast, with vertical fluid movement noted toward the edge of the basin. Salt dissolution has been recognized as a major factor enhancing upward flow, with the Prairie Evaporite posing as a hydraulic barrier separating aquifers. The lower Paleozoic aquifer formation waters tend to follow a similar up-dip and northeast flow pattern heading toward subcrop and outcrop areas (Palombi, 2008).

Based on hydrochemical analyses of the waters within the saline aquifers of the Williston Basin across Saskatchewan and Manitoba, Palombi (2008) categorized the water composition into four types: type 1 (calcium-sulphate), type 2 (sodium-chloride), type 3 (sodium-bicarbonate) and type 4 (sodium-sulphate). Type 2 (sodium-chloride) is stated as being the most prevalent. For the lower Paleozoic aquifers, Palombi (2008) found that plots of major cations such as sodium against TDS revealed strong linear correlations, until approximately 200 g/L where Na concentrations began to drop. On the other hand, calcium within these aquifers exhibited a U-shaped trend with TDS. In terms of anion fractions, sulphate ions exhibited strong negative exponential relationships with TDS.

Palombi (2008) also noted in the Duperow Formation that variations in TDS values are uniform with other Paleozoic aquifers and they ranged from 5 to 330 g/L in northern (Twp. 46, Rge. 9, W 2nd Mer.) and southern (Twp. 6, Rge. 8, W 2nd Mer.) Saskatchewan, respectively.

The secondary porosity and permeability that occurs from dolomitization can increase reservoir rock quality. The occurrence of dolomitized units in the Duperow Formation has enhanced porosity and permeability and may lead to higher potential for petroleum (Bates et al., 2016) as well as improved fluid movement in these units. However, intercrystalline porosity may be reduced locally because of the effect of anhydrite and fine-crystalline gypsum cement (Eggie and Chow, 2024). There-

fore, a sound knowledge of the dolomitization process and diagenetic and facies trends are key to predicting the distribution and location of the reservoir rock intervals with the best quality in the Duperow Formation (Eggie and Chow, 2024).

Methodology

This study was grouped into two stages, the completion of the compilation stage and the analysis stage, which used a subset of data from the Duperow Formation.

Compilation stage

The compilation stage was grouped into four phases, phases 1–3 were reported by Enaworu and Nicolas (2024) and this report focuses on phase four, which involved four main steps:

1) The original data were verified, which included identifying and removing data outliers and duplicates, verifying errors of omissions against original data and rectifying them, and standardizing units of measurement across the dataset and screening out parameters that were out of range.
2) Stratigraphic names and geological ages were assigned to each sampled interval. When sample depth and stratigraphic unit information was not available, the total depth and oldest formation penetrated were assigned to these wells. This step was accomplished using formation tops and bases within the software geoSCOUT™ by geoLOGIC systems ltd. Due to frequent inaccuracies provided on water analysis laboratory reports, this step was required to ensure the stratigraphic information was accurate and consistent across all wells and official Manitoba stratigraphic assignments were used.
3) The surface and bottom-hole geographic co-ordinates were assigned using data from the Manitoba Oil and Gas Well Information System (MOGWIS; Manitoba Business, Mining, Trade and Job Creation, internal database). All UTMs were recorded in Zone 14, NAD83, for both surface and bottom-hole co-ordinates for each well and converted to longitude and latitude using ArcGIS® Pro software by Esri®.
4) The dataset was checked to ensure that all oil and gas wells with saline water analysis data were included.

These steps were taken to ensure the reliability of the data, reduce human error and confirm that the dataset was ready for various statistical analyses, regulatory purposes and hydrogeological characterization.

A location map of all the oil and gas wells with saline water analysis data included in the dataset is shown in Figure GS2025-15-2.

Analysis stage

The analysis stage used a small subset of the compiled data to test the data quality and generate and analyze trends. These steps were part of the data quality checking and screening process, which is necessary to ensure consistency, accuracy and effective usability of the dataset. The following steps were undertaken:

1) Duperow Formation data were extracted from the compiled saline water analysis dataset (Figure GS2025-15-2). The Duperow Formation was selected for this test because of its potential for lithium; elevated lithium levels in the Duperow Formation have been reported in Manitoba (e.g., Fraino, 2025b, c) and in other provinces such as Saskatchewan (e.g., Rostron et al., 2002; Bishop and Robbins, 2023; Jensen et al., 2020).
2) Duperow Formation data quality was verified using cross-plots of TDS against ion concentrations (sodium, calcium, chloride, etc.) and physical properties (conductivity, resistivity and density).
3) Water salinity was classified into fresh, slightly saline, moderately saline, highly saline and brine using the criteria in Table GS2025-15-1.

Results

The saline water analysis dataset has 744 oil and gas wells, some with several sample intervals, and associated saline water analysis reports. From this dataset, a subset of nine wells with 12 sample intervals and associated saline water analysis data for the Duperow Formation were identified (Figure GS2025-15-2) and extracted for evaluation. A selection of physical properties and chemical analysis results from this subset are presented in Table GS2025-15-2 and Figures GS2025-15-3 to -5.

The chemical composition of water samples from the Duperow Formation varied across the 12 sample points and stratigraphic members. The TDS values ranged from 13 201 ppm to 240 763 ppm indicating highly saline to brine waters (Tables GS2025-15-1, -2). The highest TDS value was recorded in a sample from oil and gas well licence 763 (Manitoba Business, Mining, Trade and Job Creation, Winnipeg) at L.S. 7, Sec. 27, Twp. 10, Rge. 26, W 1st Mer. (abbreviated 7-27-10-26W1). The second highest TDS concentration (199 318 ppm) was recorded from the same well but at a different sample interval. Other well locations with high TDS values (>100 000 ppm) are oil and gas well licences 1783 (13-4-10-22W1), 19 (16-18-18-29W1), 640 (3-17-12-24W1) and 2452 (15-20-3-25W1). Oil and gas well licence 1876 (5-3-4-25W1) had the lowest value of 13 201 ppm.

Table GS2025-15-1: Salinity classification scale (Barlow, 2003; U.S. Geological Survey Water Science School, 2018).

Salinity classification	Total dissolved solids (ppm)
Fresh	<1000
Slightly saline	1000 to 3000
Moderately saline	3000 to 10 000
Highly saline	10 000 to 35 000
Brine	>35 000

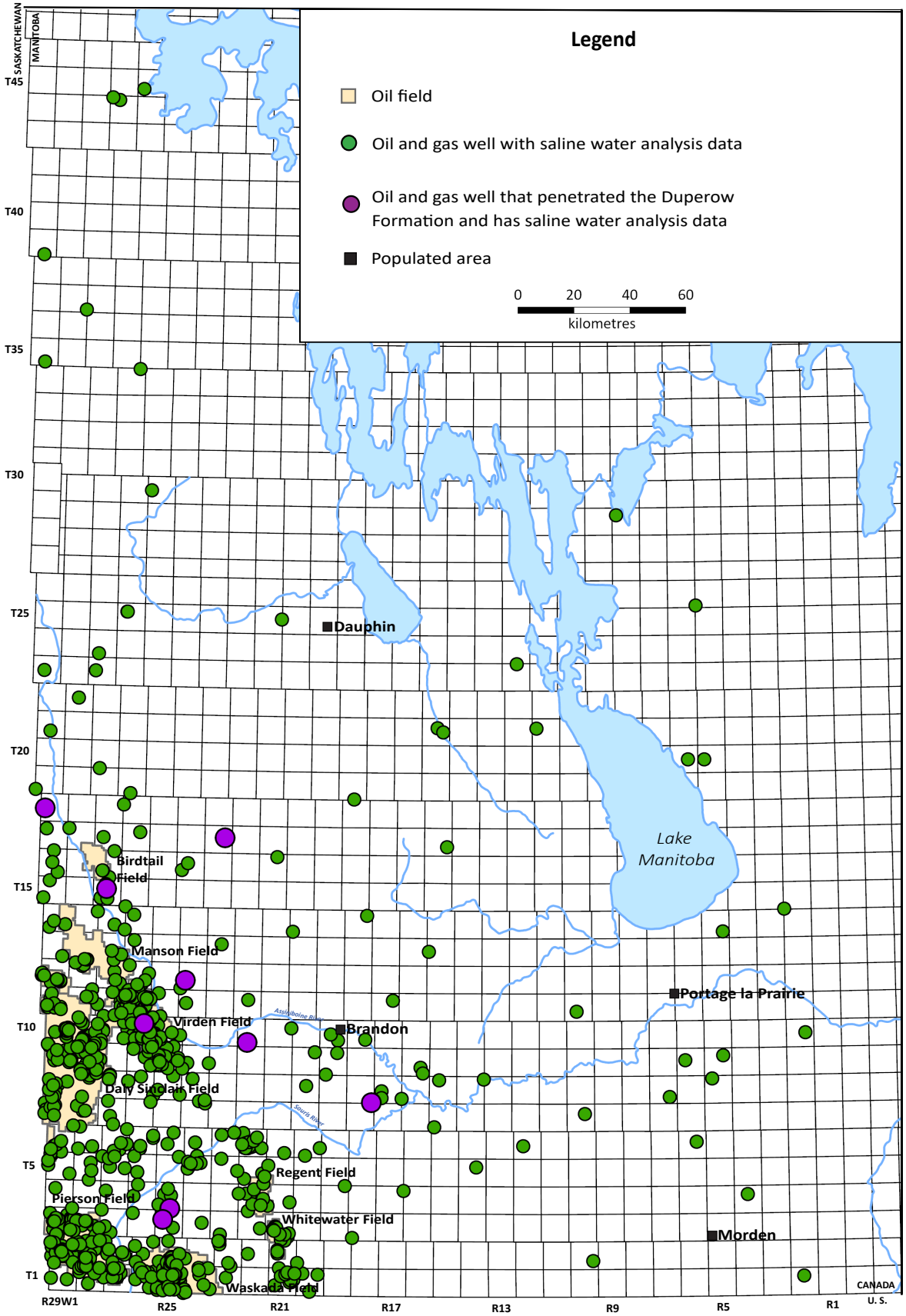

Figure GS2025-15-2: *Locations of oil fields, 744 oil and gas wells with saline water analysis data and the nine oil and gas wells that were used for the Duperow Formation case study, southwestern Manitoba (modified from Enaworu and Nicolas, 2024). Location based on bottom-hole co-ordinates. Oil field boundaries are from Fulton-Regula (2024) and well locations from Manitoba Business, Mining, Trade and Job Creation (2025).*

Table GS2025-15-2: *Oil and gas well licence (Manitoba Business, Mining, Trade and Job Creation, Winnipeg) and location information linked to stratigraphic information and salinity classification for samples from the Duperow Formation in southwestern Manitoba (Manitoba Business, Mining, Trade and Job Creation, 2025).*

Oil and gas well licence	Bottom-hole longitude (NAD 83)	Bottom-hole latitude (NAD 83)	Location	Sample depth (m TVD)		KB (m asl)	Sample elevation (m bsl)		Stratigraphy		TDS (ppm)	Salinity classification
				Top	Bottom		Top	Bottom	Top	Bottom		
44	99.793964W	49.622682N	3-1-8-18W1	517.86	525.17	415.90	101.96	109.27	Seward Mb.	Seward Mb.	67 754	Brine
1876	100.779305W	49.272270N	5-3-4-25W1	1070.46	1071.07	462.70	607.76	608.37	Seward Mb.	Seward Mb.	13 201	Highly saline
2452	100.813461W	49.235660N	15-20-3-25W1	1130.50	1138.73	468.80	661.70	669.93	Seward Mb.	Seward Mb.	172 919	Brine
640	100.728729W	50.006604N	3-17-12-24W1	694.94	701.34	472.70	222.24	228.64	Seward Mb.	Flat Lake Evaporite	140 740	Brine
763	100.928778W	49.864542N	7-27-10-26W1	801.62	812.29	442.00	359.62	370.29	Upper Wymark Mb.	Upper Wymark Mb.	199 318	Brine
1235	100.545342W	50.467187N	6-23-17-23W1	588.26	595.58	567.50	20.76	28.08	Middle Wymark Mb.	Middle Wymark Mb.	27 537	Highly saline
763	100.928778W	49.864542N	7-27-10-26W1	842.77	853.44	442.00	400.77	411.44	Middle Wymark Mb.	Middle Wymark Mb.	240 763	Brine
19	101.456467W	50.547884N	16-18-18-29W1	676.96	681.53	486.80	190.16	194.73	Middle Wymark Mb.	Lower Wymark Mb.	155 156	Brine
1783	100.414289W	49.811008N	13-4-10-22W1	668.12	720.24	422.80	245.32	297.44	Middle Wymark Mb.	Lower Wymark Mb.	149 339	Brine
640	100.728729W	50.006604N	3-17-12-24W1	769.62	781.81	472.70	296.92	309.11	Middle Wymark Mb.	Lower Wymark Mb.	92 943	Brine
247	101.13402W	50.294247N	9-21-15-27W1	722.99	733.04	469.40	253.59	263.64	Lower Wymark Mb.	Lower Wymark Mb.	31 963	Highly saline
640	100.728729W	50.006604N	3-17-12-24W1	798.58	810.77	472.70	325.88	338.07	Saskatoon Mb.	Saskatoon Mb.	87 411	Brine

Abbreviations: 3-1-8-18W1, L.S. 3, Sec. 1, Twp. 8, Rge. 18, W 1st Mer.; bsl, below sea level; KB, kelly bushing; TDS, total dissolved solids; TVD, true vertical depth

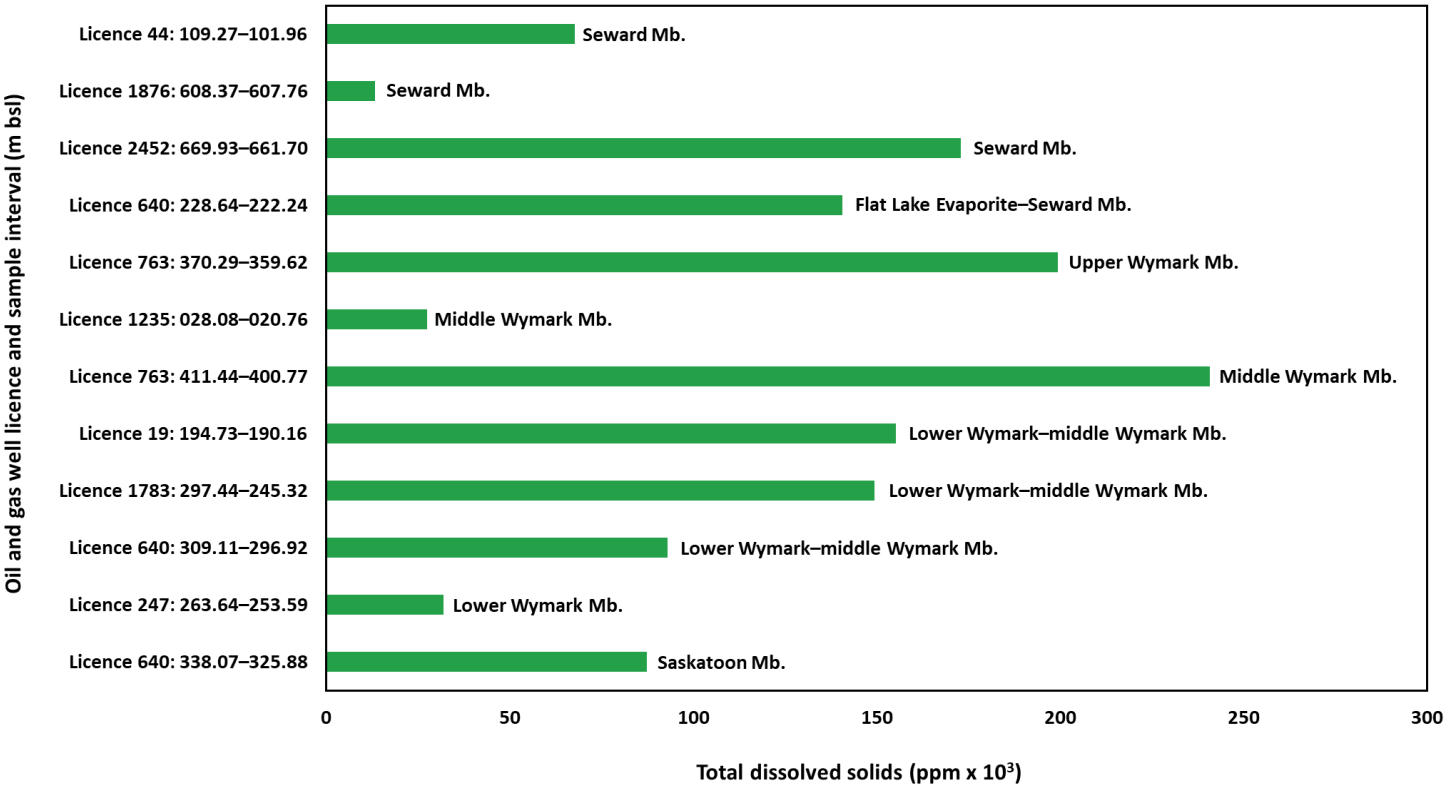

Figure GS2025-15-3: *Bar chart showing the total dissolved solids for each Duperow Formation sample with the stratigraphic assignment of each interval indicated, listed in order from the oldest (bottom) to youngest (top) strata (Manitoba Business, Mining, Trade and Job Creation, 2025). Oil and gas well licences are also included (Manitoba Business, Mining, Trade and Job Creation, Winnipeg). Abbreviation: bsl, below sea level.*

From Figure GS2025-15-3 there is no general trend/pattern in TDS concentrations with respect to sample depth or stratigraphy, as some member units recorded both high and low TDS concentrations. The middle Wymark Member reported high values in some locations and low values in other locations. A similar trend occurs in the Seward Member, which recorded the lowest value for the Duperow Formation but still reported one of the highest values in another well location. This same trend is seen for the lower–middle Wymark Member interval. Each of the Saskatoon Member, upper Wymark Member and Flat Lake Evaporite–Seward Member intervals only had an individual TDS value from a single sample interval.

The percentage contribution of each ion to the overall TDS for the Duperow Formation is seen in Figure GS2025-15-4, where $Na^+ + K^+$ and Cl^- contributed an average of over 30% and 50%, respectively, to overall TDS concentrations within the Duperow Formation. The ions $Na^+ + K^+$ and Cl^- combined contributed more than every other ion toward the TDS values for every sample. The ions Ca^{2+} and SO_4^{2-} report low average percentage contributions of 3.1% and 6.7%, respectively, whereas Mg^{2+} recorded the lowest average percentage contribution of 0.9%.

Figure GS2025-15-5a–c shows a strong correlation between TDS and conductivity, resistivity and density with a coefficient of determination (R^2) of 0.99 for all properties.

Ion concentrations vary within the Duperow Formation (Figure GS2025-15-5d–h), the $Na^+ + K^+$ concentration ranges from 3.6×10^3 to 84.9×10^3 ppm, whereas Cl^- concentrations range from 3.2×10^3 to 146.0×10^3 ppm. Both $Na^+ + K^+$ and Cl^- produced a good correlation with TDS, with a R^2 of 0.99. The cation concentrations for Ca^{2+} range from 0.67 x10^3 to 5.78×10^3 ppm and Mg^{2+} from 0.21×10^3 to 2.50×10^3 ppm, whereas anion concentrations of SO_4^{2-} range from 1.85×10^3 to 6.28×10^3 ppm. Weaker correlations with TDS concentrations are observed for Ca^{2+}, Mg^{2+} and SO_4^{2-}, with R^2 of 0.64, 0.79 and 0.65, respectively; there are also some scattered/inconsistent points (Figure GS2025-15-5e, f, h).

Overall, the data shows that there is no evidence of freshwater influence but the water is rich in major ions ($Na^+ + K^+$, Ca^{2+}, Mg^{2+}, Cl^- and SO_4^{2-}).

Discussion of Analysis

Based on the subset of data, the water within the aquifers of the Duperow Formation are classified as highly saline to brine (Tables GS2025-15-1, -2). The upper and middle Wymark Member have the highest TDS values (Figure GS2025-15-3) with Na^+, K^+ and Cl^- ions contributing the most to these high TDS numbers (Figure GS2025-15-4). Also, the dominance of Na^+ and Cl^- ions indicate a type 2 (Na-Cl) formation water (Khan, 2006; Palombi,

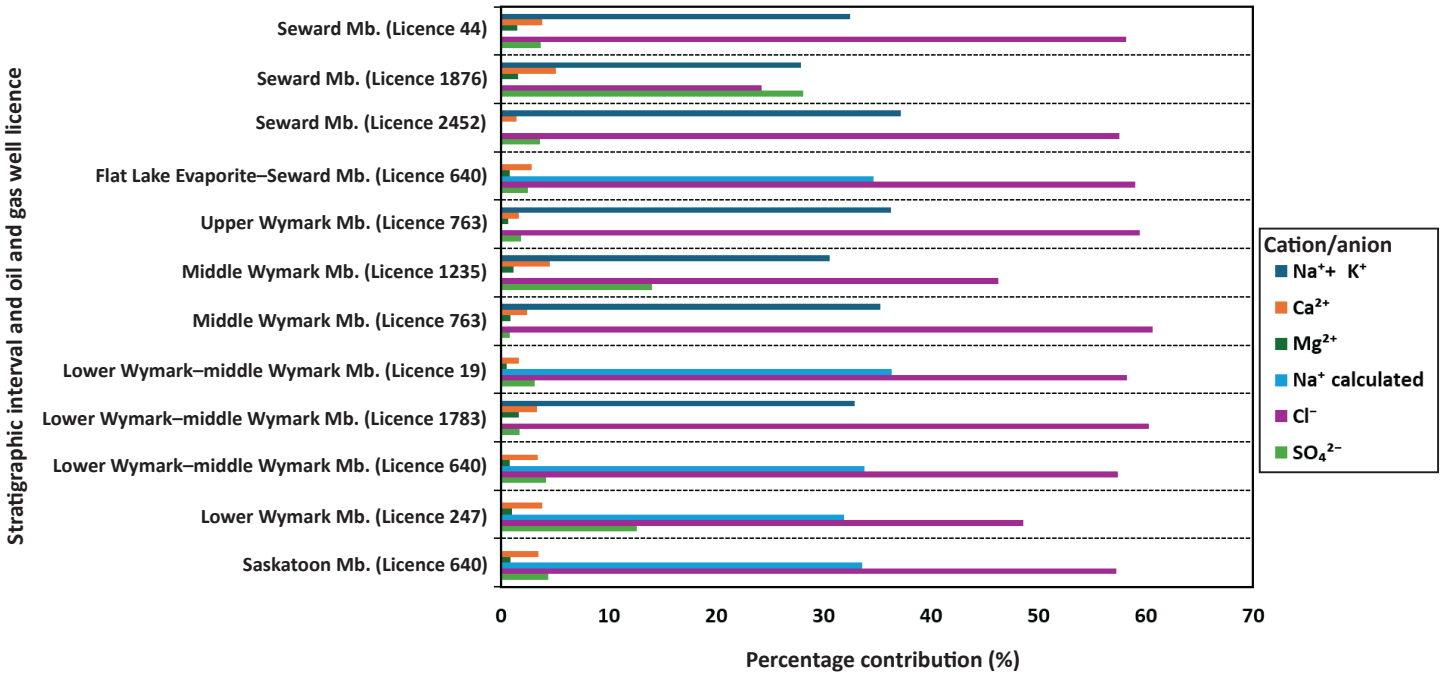

Figure GS2025-15-4: *Bar chart showing the percentage contribution of select cations and anions to each Duperow Formation sample, listed in stratigraphic order from the oldest (bottom) to youngest (top; Manitoba Business, Mining, Trade and Job Creation, 2025). Oil and gas well licences are also included (Manitoba Business, Mining, Trade and Job Creation, Winnipeg).*

2008). The K^+ ions combining with Na^+ could mean that K^+ occurs in much lower concentrations.

In Figure GS2025-15-5a and b, TDS shows a strong positive correlation with conductivity but an inverse relationship or negative correlation with resistivity. Conductivity increases with increasing TDS values as there are more dissolved salts and hence ions to carry electric charge. Resistivity decreases with increasing TDS values, as resistivity is a measure of how strongly the fluid resists an electrical current, more ions in solution means lower resistivity.

The plot of TDS versus density shows a good positive correlation and regression coefficient value (R^2 = 0.99; Figure GS2025-15-5c). This relationship is expected as higher TDS values mean more ions in solution (Na^+, K^+, Cl^-) without an increase in volume, and hence the density of the fluid increases.

In Figure GS2025-15-5d and g, there is a strong correlation between TDS and $Na^+ + K^+$ and Cl^- ion concentrations. As $Na^+ + K^+$ and Cl^- ions are the major drivers of the salinity, this relationship between $Na^+ + K^+$ and TDS is not unexpected and is consistent with Palombi (2008).

Weak correlations between TDS and Mg^{2+}, Ca^{2+} and SO_4^{2-} ion concentrations (Figure GS2025-15-5e, f, h) might be caused by secondary geochemical processes such as anhydrite precipitation and active dolomitization. This is corroborated with the stratigraphy and lithology of the Duperow Formation, where the presence and occurrence of anhydrite and dolomitization affects the porosity and permeability of the formation (Bates et al., 2016; Chow et al., 2019; Fraino and Nicolas, 2025). Although these correlations are noted, further work is required to determine if these ion concentrations are due to the presence of primary dolomites and anhydrites or are caused by secondary geochemical processes such as anhydrite precipitation and dolomitization.

Conclusion

A saline water analysis dataset has been created from the technical well files of 744 oil and gas wells in southwestern Manitoba. From this dataset, a subset of data points for the Devonian Duperow Formation has enabled the classification of the water within this aquifer into highly saline–brine types. With Na^+, K^+ and Cl^- ions as the dominant salinity drivers, the water has been further classified into a type 2 (Na-Cl) formation water. This has established the baseline water chemistry for this formation. Correlations between TDS and major ion concentrations and other physical properties was illustrated and can be used to inform hydrogeological evaluation of saline water aquifers. The correlations with high R^2 values, signifying a better fit, could be used to predict water chemistry in sampled intervals with poor water chemistry data or no data.

The procedures used in this study will be used to inform future studies of other saline aquifers within the Williston Basin in Manitoba. They will also assist in exploring for critical minerals and pore-space resource, informing regulatory decisions on

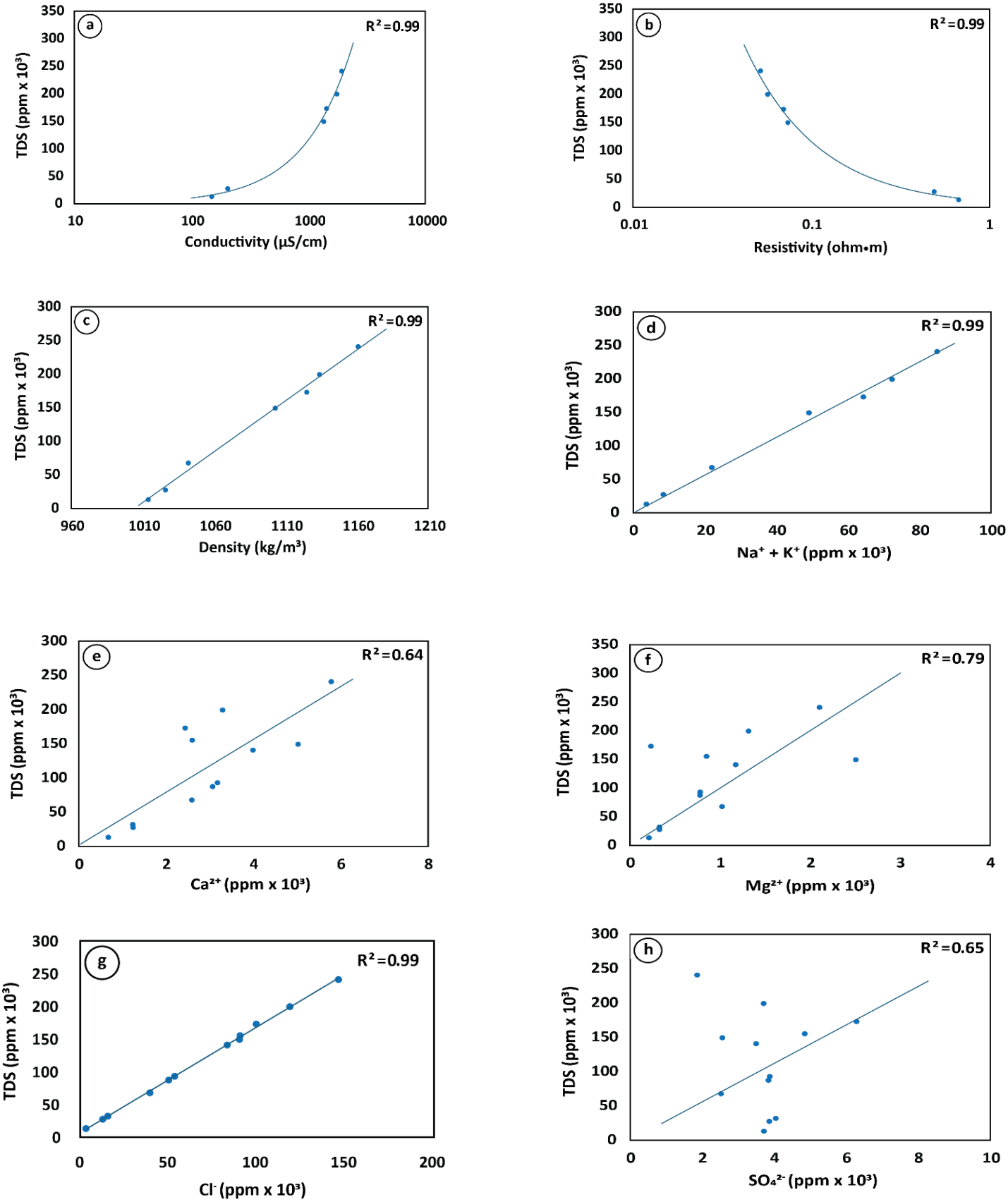

Figure GS2025-15-5: *Duperow Formation sample data cross-plots of total dissolved solids (TDS) concentration as it relates to water properties,* ***a)*** *conductivity,* ***b)*** *resistivity and* ***c)*** *density, and cation/anion concentrations,* ***d)*** *$Na^+ + K^+$,* ***e)*** *Ca^{2+},* ***f)*** *Mg^{2+},* ***g)*** *Cl^- and* ***h)*** *SO_4^{2-} (Manitoba Business, Mining, Trade and Job Creation, 2025). Abbreviation: S, siemen.*

land-use planning and helping to ensure the success of captured carbon and storage (CCS) projects and mitigate any associated risks. This information will also be used for future hydrogeological studies.

Future work

Going forward, this dataset will be used to create maps and conduct targeted hydrogeological investigations, including

- investigating weak correlations and inconsistent relationship patterns observed between TDS and ion concentrations and physical properties, which will increase the understanding of the hydrogeochemical processes occurring within saline aquifers;
- creating water property and chemistry maps by formation, which will provide a better understanding of the changes in water chemistry and physical properties in saline aquifers; and
- providing continued support for regulatory development and pore-space resource compliance to ensure accurate reporting and reservoir evaluation and maintenance of baseline hydrogeological data reporting.

Publication of the compiled dataset is planned for late 2025–early 2026, with the intent to update the dataset as new water analyses are reported.

Economic considerations

The saline aquifers of the Duperow Formation possess brine and pore-space resource potential. The occurrence of higher ion concentrations and the confirmed classification of the groundwater within the Duperow Formation to be highly saline–brine (predominantly brine) indicates it could serve as a source of industrial elements and compounds. For example,

- magnesium, which can be combined with sodium hydroxide to produce magnesium hydroxide for use in the chemical industry and for flame-retardant applications;
- calcium and sulphate ions under certain temperature conditions could be reprecipitated into gypsum or anhydrite, which are useful for cement and plaster production; and
- sodium chloride, which can be reprecipitated and used as a preservative (rock salt).

The dataset from the Duperow Formation serves as baseline data that would inform metal brine exploration, enhance well design and inform fluid migration models, CCS projects and potential geothermal projects. Work continues to quantify and map the concentrations of the valuable minerals in the Williston Basin.

Acknowledgments

The author would like to thank V. Fu, A. Abdelrahman and S. Sidhu (Mining, Oil and Gas Branch), M.P.B. Nicolas, P.E. Fraino, H. Adediran and J. Janssens (Manitoba Geological Survey) for their advice, suggestions, data access and software support. The author would like to acknowledge V. Markstrom, P.J. Fulton-Regula and M.P.B. Nicolas for their thorough review of this report.

References

Anna, L.O., Pollastro, R. and Gaswirth, S.B. 2013: Williston Basin Province—stratigraphic and structural framework to a geologic assessment of undiscovered oil and gas resources; Chap. 2 *in* Assessment of Undiscovered Oil and Gas Resources of the Williston Basin Province of North Dakota, Montana, and South Dakota, 2010 U.S. Geological Survey, Digital Data Series 69–W, 17 p.

Barlow, P.M. 2003: Ground water in freshwater-saltwater environments of the Atlantic coast; U.S. Geological Survey, Circular 1262, 113 p., URL <https://pubs.usgs.gov/circ/2003/circ1262/pdf/circ1262.pdf> [October 2025].

Bates, K. 2016: Stratigraphy, sedimentology and petroleum potential of the Upper Devonian Duperow Formation, southwest Manitoba; M.Sc. thesis, University of Manitoba, Winnipeg, Manitoba, 228 p.

Bates, K.B., Chow, N. and Nicolas, M.P.B. 2016: Preliminary results from sedimentological investigations and petroleum evaluation of the Upper Devonian Duperow Formation, southwestern Manitoba; *in* Report of Activities 2016, Manitoba Growth, Enterprise and Trade, Manitoba Geological Survey, p. 157–167.

Bishop, B.A. and Robbins, L.J. 2023: Overview of potential lithium sources in the WCSB; Canadian Energy Geoscience Association–Canadian Society of Exploration Geophysicists, Joint Annual Meeting (GeoConvention 2023), May 15–17, 2023, Calgary, Alberta, abstract.

Chow, N., Bates, K., Eggie, L., McDonald, D. and Nicolas, M.P.B. 2014: Sedimentological controls on the resource potential of the Devonian Winnipegosis and Duperow Formations in Manitoba; AAPG Eastern Section 43rd Annual Meeting, September 27–30, 2014, London, Ontario, abstract.

Chow, N., Bates, K., Eggie, L. and Nicolas, M.P.B. 2019: Sedimentology and petroleum evaluation of the Upper Devonian Duperow Formation, southwestern Manitoba; Canadian Society of Petroleum Geologists Core Conference, May 16–17, 2019, Calgary, Alberta, Abstracts, p. 105–109.

Eggie, L. and Chow, N. 2024: The middle Wymark Member of the Duperow Formation in SW Manitoba: sedimentology and paragenesis of an underexplored reservoir unit; Canadian Energy Geoscience Association–Canadian Society of Exploration Geophysicists, Joint Annual Meeting (GeoConvention 2024), June 17–19, 2024, Calgary, Aberta, abstract.

Eggie, L., Chow, N. and Nicolas, M.P.B. 2012: Sedimentology of the Wymark Member (middle unit) of the Upper Devonian Duperow Formation, southwestern Manitoba (NTS 62F14, 15, 16); *in* Report of Activities 2012, Manitoba Innovation, Energy and Mines, Manitoba Geological Survey, p. 160–171.

Enaworu, E. and Nicolas, M.P.B. 2024: Compilation of saline water analysis data from oil and gas wells, southwestern Manitoba (NTS 62F, G, J, K, N); *in* Report of Activities 2024, Manitoba Economic Development, Investment, Trade and Natural Resources, Manitoba Geological Survey, p. 181–184.

Fraino, P.E. 2025a: Electrofacies-based characterization of heterogeneity in the Wymark Member, Duperow Formation, southwestern Manitoba (parts of NTS 62F, G); *in* Report of Activities 2025, Manitoba Business, Mining, Trade and Job Creation, Manitoba Geological Survey, p. 135–144.

Fraino, P.E. 2025b: Lithogeochemistry of the Duperow Formation in the Manitoba Potash Corporation core at 3-29-20-29W1, southwestern Manitoba (part of NTS 62K11); Manitoba Business, Mining, Trade and Job Creation, Manitoba Geological Survey, Data Repository Item DRI2025023, Microsoft® Excel® file.

Fraino, P.E. 2025c: Pilot study of lithium concentrations in mudstone intervals from the Manitoba Potash Corporation core at 3-29-20-29W1, southwestern Manitoba (part of NTS 62K11); *in* Report of Activities 2025, Manitoba Business, Mining, Trade and Job Creation, Manitoba Geological Survey, p. 128–134.

Fraino, P.E. and Nicolas, M.P.B. 2025: Carbonate-evaporite cycles in the Upper Devonian Duperow Formation: a geological framework for lithium brine resource assessment in southwestern Manitoba; Canadian Energy Geoscience Association–Canadian Society of Exploration Geophysicists, Joint Annual Meeting (GeoConvention 2025), May 12–14, 2025, Calgary, Alberta, abstract.

Fulton-Regula, P. 2024: Manitoba's designated oil fields and pools 2024 (NTS 62F/1-3, 6-11, 14-16; 62K/1-3, 6-8); Manitoba Economic Development, Investment, Trade and Natural Resources, Manitoba Geological Survey.

Jensen, G.K.S., Pollard, A. and Rostron, B.J. 2020: Lithium concentration in the Duperow Formation: preliminary results of geochemical analysis of core samples from two wells in southeastern Saskatchewan; *in* Summary of Investigations 2020, Volume 1, Saskatchewan Geological Survey, Saskatchewan Ministry of Energy and Resources,

Miscellaneous Report 2020-4.1, Paper A-2, 8 p., 1 appendix.

Khan, D.K. 2006: Hydrogeological characterization of the Weyburn CO_2 project area and gradient-free inverse conditioning of heterogenous aquifer models to hydraulic head data; Ph.D. thesis, University of Alberta, Edmonton, Alberta, 238 p.

Manitoba Business, Mining, Trade and Job Creation 2025: Petroleum technical well files; *in* GIS Map Gallery, Manitoba Business, Mining, Trade and Job Creation, Mining, Oil and Gas Branch, URL <https://www.manitoba.ca/iem/petroleum/gis/technical.html> [September 2025].

Nicolas, M.P.B. and Barchyn, D. 2008: Williston Basin Project (Targeted Geoscience Initiative II): summary report on Paleozoic stratigraphy, mapping and hydrocarbon assessment, southwestern Manitoba; Manitoba Science, Technology, Energy and Mines, Manitoba Geological Survey, Geoscientific Paper GP2008-2, 21 p.

Nicolas, M.P.B. and Chow, N. 2018: Stratigraphy, lithology and petroleum potential of the Upper Devonian Duperow Formation in the Manitoba Potash Corporation core at 3-29-20- 29W1, southwestern Manitoba (part of NTS 65K1); *in* Report of Activities 2018, Manitoba Growth, Enterprise and Trade, Manitoba Geological Survey, p. 125–135.

Palombi, D.D. 2008: Regional hydrogeological characterization of the northeastern margin in the Williston Basin; M.Sc. thesis, University of Alberta, Edmonton, Alberta, 196 p.

Rostron, B.J., Kelley, L.I., Kreis, L.K. and Holmden, C. 2002: Economic potential of formation brines: interim results from the Saskatchewan Brine Sampling Program; *in* Summary of Investigations 2002, Volume 2, Saskatchewan Geological Survey, Saskatchewan Industry Resources, Miscellaneous Report 2002-4.2, Paper C-1, 29 p.

U.S. Geological Survey Water Science School 2018: Saline water and salinity; U.S. Geological Survey, URL <https://www.usgs.gov/water-science-school/science/saline-water-and-salinity> [October 2025].

GS2025-16

Critical minerals in oil and produced water, Manson oil field, southwestern Manitoba (parts of NTS 62F14, 15, K2, 3)

by P.J. Fulton-Regula

In Brief:

- One emulsion sample was analysed for oil and water properties, and metal concentrations in each fraction
- Oil from the Manson Field Melita-Reston-Amaranth-Lodgepole D pool is possibly migrated Lodgepole Formation oil
- Critical mineral concentrations were found in the analysed sample

Citation:
Fulton-Regula, P.J. 2025: Critical minerals in oil and produced water, Manson oil field, southwestern Manitoba (parts of NTS 62F14, 15, K2, 3); *in* Report of Activities 2025, Manitoba Business, Mining, Trade and Job Creation, Manitoba Geological Survey, p. 155–161.

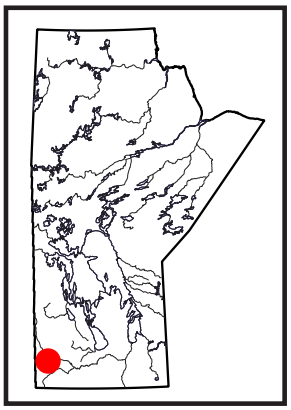

Summary

To assess the metal content of produced fluid from the Manson oil field, an oil and water emulsion sample was collected from the well at L.S. 12, Sec. 1, Twp. 13, Rge. 27, W 1st Mer. (abbreviated 12-1-13-27W1; oil and gas well licence 9990) in the Melita-Reston-Amaranth-Lodgepole undifferentiated D (17 22D) pool in the Manson Field. The oil fraction returned an oil density (API gravity 29.1 °) and a sulphur concentration (1.76 wt. %) consistent with past sampling in the Manson Field but with V (6.60 ppm), Ni (4.58 ppm), Pb (2.47 ppm), Zn (1.58 ppm) and Cu (0.18 ppm) metal occurrences. The water fraction returned values consistent with known Mississippian Lodgepole Formation and Jurassic aquifers in the project area and had low Li concentrations (2.54 ppm) consistent with those previously reported for the Lodgepole to Lower Amaranth formations in Manitoba. The sample results suggest the oil found in the 17 22D pool likely migrated from the Mississippian Lodgepole Formation, and that metals such as V, Ni, Pb, Zn and Cu could have been carried by that oil. Further work is required to map metal concentrations within Manitoba's oil fields and to evaluate the carrying capacity of Manitoba's oil for critical minerals.

Introduction

In 2016, the Manitoba Geological Survey began a study on the Manson Field in southwestern Manitoba (Figure GS2025-16-1). This study was conducted to understand unusual stratigraphic discrepancies identified when doing downhole geophysical log correlations. To date, the study has focused on describing and sampling drillcore, conducting detailed geophysical log correlations and determining formation tops to better understand the complex geology of the project area (Fulton-Regula, 2024b). The next step for this study was to acquire and test the produced fluid from a well in the Manson Field.

Manitoba has produced over 80 million m^3 (as of October 1, 2025, from Manitoba Oil and Gas Well Information System [MOGWIS], Manitoba Business, Mining, Trade and Job Creation internal database) of oil since 1951 from 13 oil fields. Oil has been produced from pools between the Devonian Torquay Formation and the Lower Melita Member of the Melita Formation (Figure GS2025-16-2).

A review of the Manitoba Business, Mining, Trade and Job Creation's petroleum technical well files (Manitoba Business, Mining, Trade and Job Creation, 2025b) and reservoir documents (Manitoba Business, Mining, Trade and Job Creation, 2025c) was completed to collate the results of oil analyses submitted to the Government of Manitoba under *The Oil and Gas Act*. Through this search, only standard oil analyses were found with no metal analyses reported. A compilation of standard oil analyses indicate that oil follows a linear trend from light (low density <875.7 kg/m^3; high API gravity >29.6 °) low sulphur oil of the Bakken and Torquay formations in the Daly Sinclair Field, to heavy (high density >875.7 kg/m^3; low API gravity <29.6 °) high sulphur oil of the Melita Formation in smaller pools in Other Areas (Figure GS2025-16-3a, b). The plots of API gravity versus sulphur weight percent (wt. % S) suggest an overall increase in oil sulphur content and oil density with reducing stratigraphic depth. Oil analyses from the Manson Field indicate the oil produced from this field has absolute densities from 804 to 890.5 kg/m^3 (at 15–16.8 °C after cleaning; API gravity 44.47–27.30 °) and high sulphur values from 2.19 to 17.9 mg/kg (0.22–1.79 wt. % S). These high sulphur values coincide with the observation of minor amounts of primary and secondary pyrite, sphalerite and chalcopyrite in some core samples (Fulton-Regula, 2024b).

The high sulphur values in the oil and the presence of secondary sulphides in core prompted an independent assessment of the oil, water and metal contents of produced fluid from the Manson Field. The analytical results from one emulsion sample of produced oil and water from the well at 12-1-13-27W1 (oil and gas licence 9990, Manitoba Business, Mining, Trade and Job Creation, Winni-

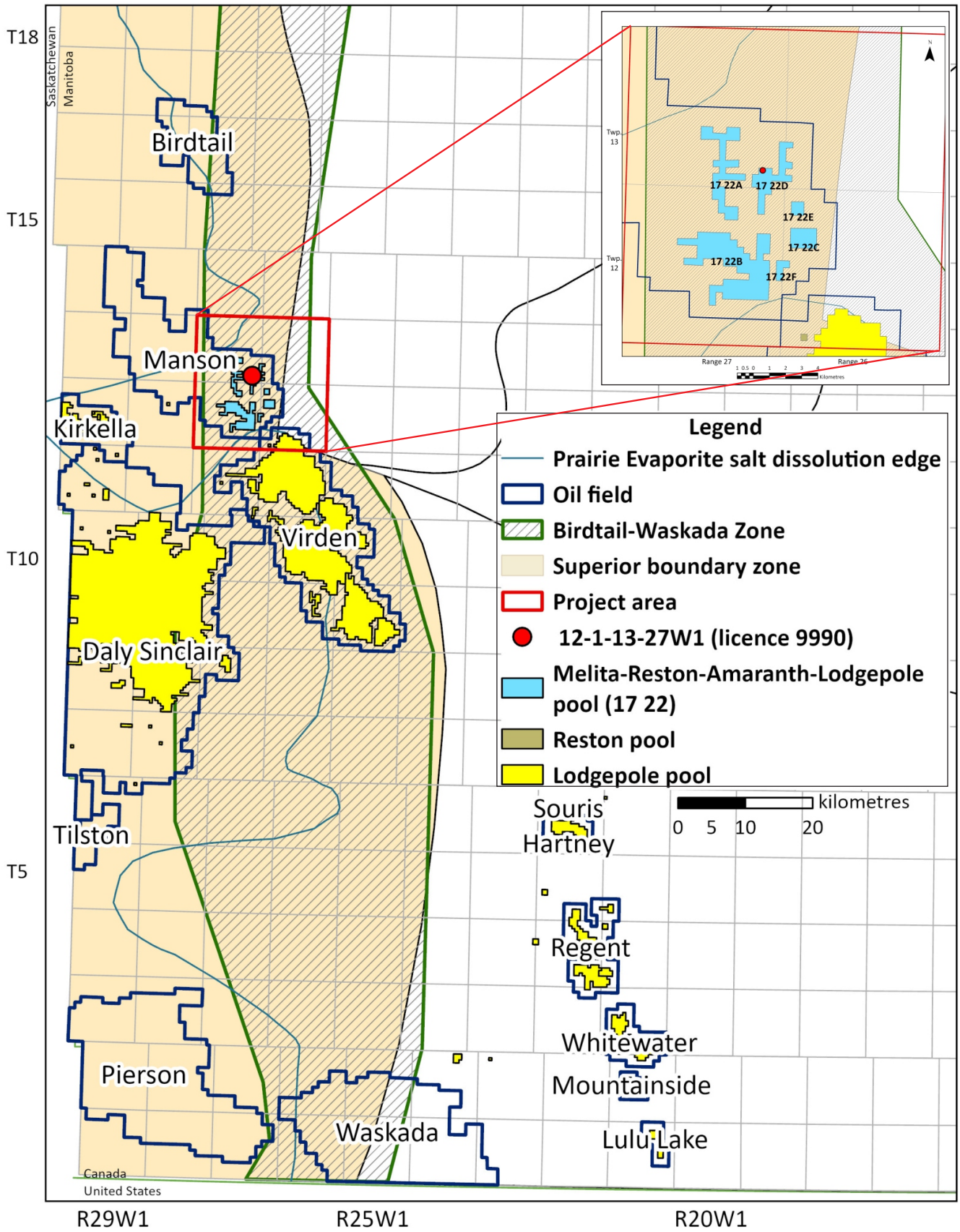

Figure GS2025-16-1: *Location map showing the project area and oil field boundaries (Fulton-Regula, 2024a) in southwestern Manitoba in relation to the Superior boundary zone (Manitoba Geological Survey, 2024), Birdtail-Waskada Zone (McCabe, 1967, 1971; Nicolas and Barchyn, 2008; Nicolas, 2012) and Prairie Evaporite salt dissolution edge (Nicolas, 2015). Inset map shows Manson 17 22 oil pools (Fulton-Regula, 2024a) and the location of the well sampled for fluid analysis.*

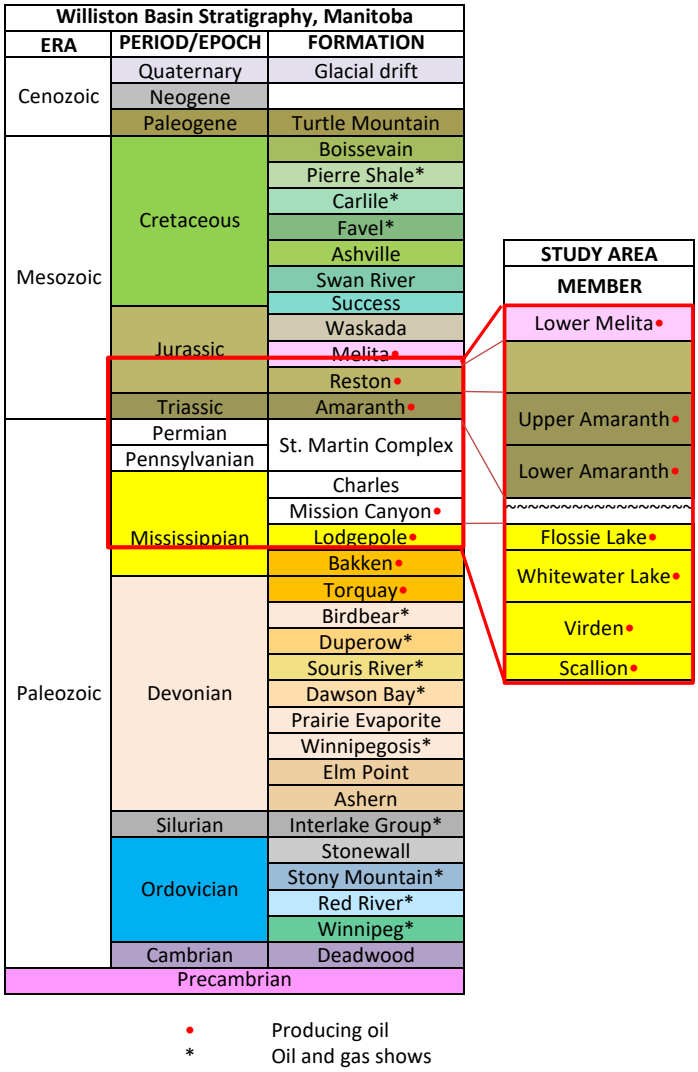

Figure GS2025-16-2: *Stratigraphic column (adapted from Manitoba Business, Mining, Trade and Job Creation, 2025a) for the Williston Basin in southwestern Manitoba and the study area. Formations/members producing oil or with oil and gas shows are indicated.*

peg) in the Melita-Reston-Amaranth-Lodgepole undifferentiated D (17 22D) pool are presented in this report.

Project area and sample location

The project area is located in southwestern Manitoba along the northeastern edge of the Phanerozoic Williston Basin in parts of the Virden and Manson oil fields, in Twp. 12–13, Rge. 26–27, W 1st Mer. (Figure GS2025-16-1). Underlying the Phanerozoic strata in this area are rocks of Precambrian age, which fall within the Superior boundary zone (SBZ; Manitoba Geological Survey, 2024), a major crustal suture or fault (Figure GS2025-16-1). On a seismic survey from the SBZ, Dietrich and Magnusson (1998) and Dietrich et al. (1999) observed reactivated faults that originated in the Precambrian basement and extended into the overlying Phanerozoic strata as far upsection as Mississippian strata. Overlying the SBZ is a Devonian feature referred to as the Birdtail-Waskada Zone (BWZ). The BWZ is the result of preferential dissolution of the Prairie Evaporite caused by effects from the underlying SBZ on the overlying strata (McCabe, 1967, 1971; Nicolas and Barchyn, 2008; Nicolas, 2012). The SBZ and the BWZ underlie the oil fields in southwestern Manitoba and under the project area (Figure GS2025-16-1).

The oil pools within this area have produced 2.1 million m^3 oil and 26.9 million m^3 water since 1956 from three separate zones (as of September 2, 2025, MOGWIS). The oldest production comes from the Lodgepole Formation pools of the Virden Field. More recent production comes from the Bakken-Torquay and Melita-Reston-Amaranth-Lodgepole pools of the Manson Field and a Reston pool in the Virden Field. In the project area, Bakken-Torquay pools have produced 71 900 m^3 oil and 351 600 m^3 water, Reston pools have produced 49 m^3 oil and 839 m^3 water and Melita-Reston-Amaranth-Lodgepole pools have produced 978 000 m^3 oil and 22 800 m^3 water (as of September 2, 2025, MOGWIS).

The well at 12-1-13-27W1 was selected for further analysis because minor quantities of chalcopyrite were observed in core. This well is located over the SBZ and BWZ, where salt from the Prairie Evaporite has been completely dissolved (Nicolas, 2015). This vertical well was drilled by Elcano Exploration Inc. in 2014. It was cored from 537.0 to 550.8 m true vertical depth (TVD), cased for production from surface to 590 m TVD and tubulars were installed from surface to 550.78 m TVD. The well was perforated at 539.0–541.4 and 542.0–545.0 m TVD. As of August 17, 2025, this well had produced 3531.9 m^3 oil and 3839.7 m^3 water (MOGWIS). This well is currently operated by 10101906 Manitoba Ltd. (MOGWIS).

Methodology

Producing wells in the study area were assessed for their oil to water ratio and presence of sulphides in core. Wells with an oil-water ratio of 1 (50% oil, 50% water) were selected as possible candidates for further testing. In June 2025, a sample of oil and water emulsion fluid was taken from the wellhead at 12-1-13-27W1. Wellhead sampling was chosen to minimize the interaction and mixing between the produced fluid from different wells and the well, flowline and battery infrastructure. This produced fluid was collected in glass jars, the temperature recorded and, after 24 hours, the fluid refrigerated. The sample was sent for analysis to Core Laboratories Canada Ltd. (Core Lab; Calgary, Alberta).

At Core Lab, the oil portion of the emulsion sample was tested using a routine oil analysis for density, API gravity, sulphur, viscosity, water, sediment, pour point, colour and by inductively coupled plasma–atomic emission spectrometry (ICP-AES) for metals. The water portion of the sample was tested by extended water analysis at Core Lab for cations, anions, pH, resistivity, refractive index, specific gravity and calculated total dissolved solids (TDS). The water portion of the sample was then sent to ALS Environmental (Calgary, Alberta) and tested for Li and total

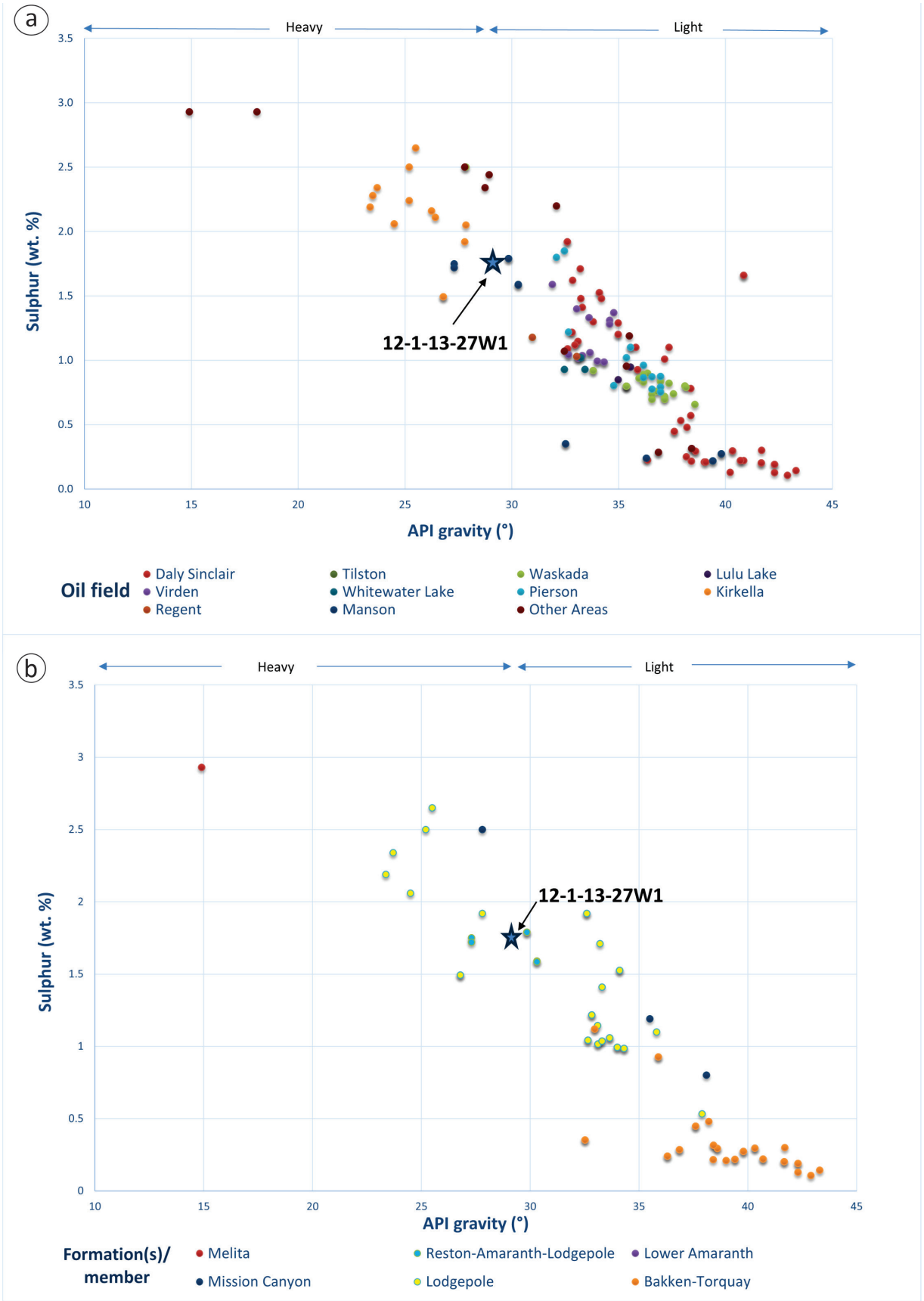

Figure GS2025-16-3: a) *Chart of oil API gravity versus sulphur content by oil field;* ***b)*** *chart of oil API gravity versus sulphur content by producing formation(s)/member (Fulton-Regula, 2025; Manitoba Business, Mining, Trade and Job Creation, 2025b, c). Heavy high sulphur oil on the left and light low sulphur oil on the right. The oil sample from the well at L.S. 12, Sec. 1, Twp. 13, Rge. 27, W 1st Mer. (abbreviated 12-1-13-27W1; oil and gas well licence 9990), southwestern Manitoba, is denoted by a star.*

metals by collision/reaction cell, inductively coupled plasma–mass spectrometry (CRC ICP-MS). Neither the bottom sediment nor impurities from the oil and water samples were tested, nor was the effect of cleaning the oil sample in the lab evaluated.

Results

The full oil and water emulsion fluid analyses results can be found in Data Repository Item DRI2025026 (Fulton-Regula, 2025[1]). Table GS2025-16-1 shows a summary of selected chemical analyses results. The oil API gravity versus sulphur wt. % analysis results from this well are plotted in Figure GS2025-16-3 with oil analysis results from other producing areas in Manitoba.

Discussion

Oil density and sulphur content

The density and sulphur content for 12-1-13-27W1 oil is consistent with other oil density and sulphur reports for the Melita-Reston-Amaranth-Lodgepole pools in the Manson Field (Figure GS2025-16-3). These results indicate oil from the Melita-Reston-Amaranth-Lodgepole pools is lighter (higher API gravity) with a lower sulphur content than Melita Formation oil, but heavier (lower API gravity) with a higher sulphur content than Bakken Formation oil (Figure GS2025-16-3). The sample from this study plots within the range of values seen in the Lodgepole

Table GS2025-16-1: Select metal and compound concentrations in the sample from L.S. 12, Sec. 1, Twp. 13, Rge. 27, W 1st Mer. (abbreviated 12-1-13-27W1; oil and gas well licence 9990), southwestern Manitoba. Conversions used: 1 kg/m^3 = 0.001 g/ml; mg/L = solution density × mg/kg; 1 mg/L = 1 ppm; absolute density (g/mL) = specific gravity.

Fluid	API gravity at 15.6 °C (°)	Specific gravity at 15.6 °C	Calculated absolute density[1] (g/mL)	pH at 25 °C	Resistivity at 25 °C (Ohm-metres)	TDS (g/L)	Element/ compound	Concentration (ppm)	Concentration (mg/kg)
Water	n/a	1.0256	1.0256	7	0.203	35.535	Li	2.54	–
							Na^+	11432	–
							K^+	187	–
							Mg^{2+}	361	–
							Ca^{2+}	1050	–
							SO_4^-	3487	–
							HCO_3^-	1505	–
							S	n/a	–
							V	<1.00	–
							Ni	<1.00	–
							Zn	<6.00	–
							Cu	<1.00	–
							Pb	<0.10	–
Oil	29.1	n/a	0.8804	n/a	n/a	n/a	Li	n/a	n/a
							Na^+	22.46	21.9
							K^+	n/a	n/a
							Mg^{2+}	0.10	0.1
							Ca^{2+}	2.67	2.6
							SO_4^-	n/a	n/a
							HCO_3^-	n/a	n/a
							S	15.50	17.6
							V	6.60	7.5
							Ni	4.58	5.2
							Zn	1.58	1.8
							Cu	0.18	0.2
							Pb	2.47	2.8

[1] After cleaning

Abbreviations: TDS, total dissolved solids; n/a, not analyzed

[1] MGS Data Repository Item DRI2025026, containing the data or other information sources used to compile this report, is available online to download free of charge at https://manitoba.ca/iem/info/library/downloads/index.html, or on request from minesinfo@gov.mb.ca, or by contacting the Resource Centre, Manitoba Business, Mining, Trade and Job Creation, 360-1395 Ellice Avenue, Winnipeg, Manitoba R3G 3P2, Canada.

Formation, between the heavy (lower API gravity) and higher sulphur oil of the Lodgepole Formation in the Kirkella Field and the lighter (higher API gravity) and lower sulphur content of the Lodgepole Formation oil in the Virden Field. This suggests oil from the Melita-Reston-Amaranth-Lodgepole pools in the Manson Field may be migrated Lodgepole Formation oil.

Water composition

The concentration of 35.535 g/L TDS for the produced water is consistent with the findings of Palombi (2008) for the Mississippian Lodgepole Formation and Jurassic aquifers in this area. The concentrations for the cations Na^+, K^+ and Mg^{2+} are also consistent with the recorded values in Palombi (2008) for Mississippian and Jurassic aquifers within the Williston Basin. The Ca^{2+}, SO_4^- and HCO_3^- concentrations are low but fall within the wide variability in concentrations discussed in Palombi (2008) for Mississippian and Jurassic aquifers in the Williston Basin.

Metal concentrations in water and oil

Analyses of the metal concentrations in the produced fluid sample appear to show a preference for some metals to be concentrated in the water fraction whereas others are concentrated in the oil fraction. The Na^+ and Mg^{2+} concentrations are preferentially higher in the water fraction whereas V, Ni, Pb, Cu and Zn concentrations are preferentially higher in the oil fraction (Table GS2025-16-1).

The Li concentration of the water fraction is 2.54 ppm. This is consistent with the findings of Nicolas (2017), where values of 0.258–7.320 ppm were reported in brines from the Lodgepole to the Amaranth formations in Manitoba.

The oil fraction has concentrations of V at 6.60 ppm, Ni at 4.58 ppm, Pb at 2.47 ppm, Zn at 1.58 ppm and Cu at 0.18 ppm. It is common for Ni, Pb, Zn and Cu to occur as contaminants from oil field machinery but they are also known to occur in uncontaminated crude oils (Reynolds, 2001; Mohammad et al., 2012; Fetter et al., 2019; Sanz-Robinson and William-Jones, 2019). The well at 12-1-13-27W1 was completed using J55 coiled steel tubing, which does not contain Ni, Cu, Pb or Zn (American Petroleum Institute, 2023), and it was drilled in 2014 prior to the production of 3531.9 m^3 oil and 3839.7 m^3 water. The oil extracted from this well appears to be uncontaminated by wellbore operations or by oil field machinery. The metals found in this oil are thought to originate from the oil source, the rocks along the oil migration pathway and/or the reservoir. This is supported by the presence of sulphide minerals in core. In order to evaluate the variability of metals within oils in the region, additional sampling from other oil fields is recommended.

Conclusions

These test results confirm low concentrations of Li are present in produced water in the Manson Field and critical metals such as V, Ni, Zn and Cu are present in the produced oil from the 17 22D pool in the Manson Field. In addition, the oil found in the 17 22D pool may be Mississippian Lodgepole Formation oil, and critical metals such as V, Ni, Zn and Cu may be carried by Lodgepole Formation oil in the Manitoba subsurface.

Future work

The presence of critical minerals in the oil fraction of this sample suggests critical minerals may occur in produced fluids and within sedimentary rocks in Manitoba's Williston Basin. The following next steps are recommended:

1) Further research to understand
   a) critical mineral leaching into crude oil and precipitation as a function of temperature, pH, density, percent sulphur and pressure;
   b) the resource potential of critical minerals in crude oil; and
   c) the metal content of crude oil as an exploration tool for critical minerals in sedimentary strata.
2) Further sampling and analysis of oil samples for critical minerals by field and pool.
3) Mapping of metal concentrations in crude oil to determine the association of critical minerals as a function of depth, temperature, pH, percent sulphur, density and proximity to structural features, such as the SBZ and faults.

Economic considerations

This study has shown the critical minerals V, Ni, Zn and Cu can be found in crude oil from the 17 22D pool in the Manson Field. The presence of critical minerals in this oil suggests there may be opportunities to explore for critical minerals, using produced fluids to identify target areas within the sedimentary strata in southwestern Manitoba. The minerals V, Ni, Zn and Cu are used in a wide variety of applications from catalysts and coatings to steel manufacture, superconductors, battery technology, electrical power transmission, electronics and many other applications.

Acknowledgments

The author thanks the staff at 10101906 Manitoba Ltd., Manitoba Regulatory Services and the Manitoba Geological Survey. Specifically, B. Rinn (10101906 Manitoba Ltd.), W. Baker and M. Langlois (Manitoba Regulatory Services) for enabling the collection and delivery of this sample, C. Epp and P. Belanger for logistical support and M.P.B. Nicolas and E. Enaworu (Manitoba Geological Survey) and J. Dawson for their edits to this report.

References

American Petroleum Institute 2023: API Specification 5CT, Casing and Tubing, 10th edition; American Petroleum Institute, 262 p.

Dietrich, J.R. and Magnusson, D.H. 1998: Basement controls on Phanerozoic development of the Birdtail-Waskada salt dissolution zone, Williston Basin, southwestern Manitoba; *in* Eighth International Williston Basin Symposium, J.E. Christopher, C.F. Gilboy, D.F. Paterson and S.L. Bend (ed.), Saskatchewan Geological Society, October 19–21, 1998, Regina, Saskatchewan, Special Publication 13, p. 166–174.

Dietrich, J.R., Majorowicz, J.A. and Thomas, M.D. 1999: Williston Basin profile, southeast Saskatchewan and southwest Manitoba: a window on basement-sedimentary cover interaction; Geological Survey of Canada, Open File 3824, 1 sheet.

Fetter, N., Blichert-Toft, J., Telouk, P. and Albarede, F. 2019: Extraction of Pb and Zn from crude oil for high-precision isotopic analysis by MC-ICP-MS; Chemical Geology, v. 511, no. 20, p. 112–122.

Fulton-Regula, P. 2024a: Manitoba's designated oil fields and pools 2024 (NTS 62F/1-3, 6-11, 14-16; 62K/1-3, 6-8); Manitoba Economic Development, Investment, Trade and Natural Resources, Manitoba Geological Survey.

Fulton-Regula, P.J. 2024b: Preliminary observations from the Manson Field's Reston-Amaranth-Lodgepole oil reservoir, southwestern Manitoba (part of NTS 62K); *in* Report of Activities, 2024; Manitoba Economic Development, Investment, Trade and Natural Resources, Manitoba Geological Survey, p. 192–199.

Fulton-Regula, P.J. 2025: Oil and water analysis of produced fluid, Manson oil field, southwestern Manitoba (part of NTS 62K3); Manitoba Business, Trade and Job Creation, Manitoba Geological Survey, Data Repository Item DRI2025026, Microsoft® Excel® file.

Manitoba Business, Mining, Trade and Job Creation 2025a: Stratigraphic column for southwestern Manitoba; *in* GIS Map Gallery, Manitoba Business, Mining, Trade and Job Creation, Mining, Oil and Gas Branch, URL <https://www.manitoba.ca/iem/petroleum/pubcat/stratcolumn.pdf> [September 2025].

Manitoba Business, Mining, Trade and Job Creation 2025b: Petroleum technical well files; *in* GIS Map Gallery, Manitoba Business, Mining, Trade and Job Creation, Mining, Oil and Gas Branch, URL <https://www.manitoba.ca/iem/petroleum/gis/technical.html> [September 2025].

Manitoba Business, Mining, Trade and Job Creation 2025c: Reservoir documents; *in* GIS Map Gallery, Manitoba Business, Mining, Trade and Job Creation, Mining, Oil and Gas Branch, URL <https://www.manitoba.ca/iem/petroleum/reservoir/index.html> [December 2016].

Manitoba Geological Survey 2024: Bedrock geology of Manitoba; Manitoba Economic Development, Investment, Trade and Natural Resources, Manitoba Geological Survey, Open File OF2024-4, scale 1:1 000 000.

McCabe, H.R. 1967: Tectonic framework of Paleozoic formations in Manitoba; Canadian Mining and Metallurgical Bulletin, v. 60, no. 663, p. 765–774.

McCabe, H.R. 1971: Stratigraphy of Manitoba, an introduction and review; *in* Geoscience Studies in Manitoba, A.C. Turnock (ed.), Geological Association of Canada, Special Paper 9, p. 167–187.

Mohammad, I.A., Abdallah, R.I., El-Naggar, A.Y., Mashalay, M.M. and Salem, A.A. 2012: Characterization of four Egyptian crude oils; Nature and Science, v. 10, no. 5, p. 72–79.

Nicolas, M.P.B. 2012: Stratigraphy and regional geology of the Late Devonian-Early Mississippian Three Forks Group, southwestern Manitoba (NTS 62F, parts of 62G, K); Manitoba Innovation, Energy and Mines, Manitoba Geological Survey, Geoscientific Report 2012-3, 1 DVD-ROM.

Nicolas, M.P.B. 2015: Potash deposits in the Devonian Prairie Evaporite, southwestern Manitoba (parts of NTS 62F, K); *in* Report of Activities 2015, Manitoba Mineral Resources, Manitoba Geological Survey, p. 97–105.

Nicolas, M.P.B. 2017: Preliminary investigation of the potential for lithium in groundwater in sedimentary rocks in southwestern Manitoba; *in* Report of Activities 2017, Manitoba Growth, Enterprise and Trade, Manitoba Geological Survey, p. 183–190.

Nicolas, M.P.B. and Barchyn, D. 2008: Williston Basin Project (Targeted Geoscience Initiative II): summary report on Paleozoic stratigraphy, mapping and hydrocarbon assessment, southwestern Manitoba; Manitoba Geological Survey, Geoscientific Paper GP2008-2, 21 p.

Palombi, D.D. 2008: Regional hydrogeological characterization of the northeastern margin in the Williston Basin; M.Sc. thesis, University of Alberta, Edmonton, Alberta, 196 p.

Reynolds, J.G. 2001: Nickel in petroleum refining; Petroleum Science and Technology, v. 19, no. 7–8, p. 979–1007.

Sanz-Robinson, J. and William-Jones, A.E. 2019: Zinc solubility, speciation and deposition: a role for liquid hydrocarbons as ore fluids for Mississippi Valley Type Zn-Pb deposits; Chemical Geology, v. 520, p. 60–68.

GS2025-17

Preliminary investigations into the rare-earth elements in the Carlile Formation and Pierre Shale across southwestern Manitoba (parts of NTS 62G, K)

by V.L. Markstrom

In Brief:

- Geological investigations into the Upper Cretaceous shales in Manitoba and collecting samples for future geochemical analysis
- Characterizing rare earth element concentrations within the Carlile Formation and the Pierre Shale contributes to the economic development of these critical minerals

Citation:
Markstrom, V.L. 2025: Preliminary investigations into the rare-earth elements in the Carlile Formation and Pierre Shale across southwestern Manitoba (parts of NTS 62G, K); *in* Report of Activities 2025, Manitoba Business, Mining, Trade and Job Creation, Manitoba Geological Survey, p. 162–166.

Summary

Rare-earth elements (REEs) are essential for many modern technologies and are in high economic demand. Recent research has highlighted the potential economic development of secondary sources of REEs, including enriched sedimentary basin deposits. In Manitoba, anomalously high concentrations of REEs have been previously documented in the Upper Cretaceous Pierre Shale, but further work is required to confirm, constrain and characterize the elevated REE concentrations in Manitoba's Upper Cretaceous shales. During the 2025 field season, a total of 34 samples were collected from the Boyne Member of the Carile Formation and the Gammon Ferruginous and Pembina members of the Pierre Shale from four sites across southwestern Manitoba. Over the next year, geochemical analysis will be conducted on these samples to assess the REE potential in the Carlile Formation and the Pierre Shale. Investigating the REE enrichment within the strata is critical for improving the understanding of these types of shale deposits and contributing to the economic development of REEs in Manitoba.

Introduction

The growing demand for REEs has led to increased interest in exploring alternative sources for these critical minerals. While most REEs are currently produced from hard rock deposits, recent studies have highlighted the potential of sedimentary basins as secondary sources. In particular, modern deep-sea sedimentary basin deposits in the western North Pacific Ocean have shown up to 5000 ppm total REEs and yttrium (REYs; Tanaka et al., 2020, 2023). Li et al. (2023) determined that REEs were primarily hosted within the bioapatite of disseminated skeletal elements found within the ocean sediments of the Indian Ocean Basin. Recent efforts have been made to identify, explore and understand the mechanism of REE accumulation in modern deep-sea sediments. These global findings have drawn attention to older sedimentary successions that may have preserved anomalous REE concentrations.

In Manitoba, the Upper Cretaceous strata consist of a thick package of oceanic sedimentary rocks with a depositional environment that may be analogous to modern ocean basins, sediments of which contain economic REE concentrations. In fact, preliminary studies found REE contents exceeding 3000 ppm within the Upper Cretaceous Gammon Ferruginous Member of the Pierre Shale (Bamburak and Nicolas, 2010; Bamburak et al., 2012, 2013, 2014), thus suggesting these shale deposits may be a potential resource.

Following these preliminary findings in Manitoba, more work was needed to understand the mechanisms of REE enrichment within fine-grained, basinal mudstone and shale deposits and the depositional controls that led to these elevated REE concentrations. The goal of this project is to

1) confirm elevated REE concentrations in the Boyne Member of the Carlile Formation and the Gammon Ferruginous and Pembina members of the Pierre Shale across southwestern Manitoba; and
2) characterize and compare the REE geochemistry of these three members.

This report includes a description of the field sites and sample locations that form the foundation for the geochemical sampling program for this study. This will help to further evaluate the potential of Upper Cretaceous shales as a resource for REEs in Manitoba.

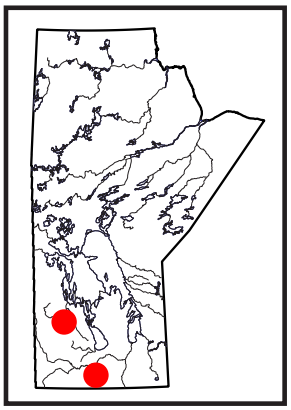

Previous work

Elevated total REE (TREE) concentrations in the Gammon Ferruginous Member were first described by Bamburak and Nicolas (2010), based on samples collected from various sites in the Pembina Hills area and at one site along the Vermilion River on Riding Mountain near Dauphin, Manitoba. This study also noted high concentrations of other elements, such as Pt, Pd, Cu, Ni, V and Zn. In a follow-up investigation, Bamburak et al. (2012) constrained REE concentrations in drill cuttings

from Relative Daly Sinclair HZNTL 8-31-7-29W1 well (oil and gas well licence 7639, Manitoba Business, Mining, Trade and Job Creation, Winnipeg). Samples from the Morden and Boyne members of the Carlile Formation, as well as the Gammon Ferruginous and Pembina members of the Pierre Shale were analyzed. The chondrite-normalized REE plot from this report shows that all four members have similar REE signatures.

In 2013, the Gammon Ferruginous Member was measured to contain up to 3178 ppm TREEs, 0.124% heavy rare-earth elements (HREEs) and 0.225% light rare-earth elements (LREEs; Bamburak et al., 2013). Bamburak et al. (2014) further suggested that the REEs in the Gammon Ferruginous Member are likely hosted in bioapatite derived from microscopic fossil fragments. More recently, elevated but highly variable REE concentrations have also been measured in some macrofossils from the overlying Pembina Member. The average TREE concentration is similar to previous research, suggesting that the REEs in Manitoba's Upper Cretaceous shale strata are hosted within the bioapatite in fossilized material (Markstrom, 2023). However, a recent publication by Nicolas and Bamburak (2025) reported lower TREE concentrations (150–350 ppm) in samples of the Boyne, Gammon Ferruginous and Pembina members that were collected near Dauphin, suggesting variability in REE enrichment across southwestern Manitoba.

Geological setting

The Carlile Formation was deposited during the Santonian to early Campanian (Late Cretaceous Period) and is primarily composed of chalky, calcareous and noncalcareous grey to black shale. The Carlile Formation has two members, the Morden and Boyne members, separated by a sharp unconformable contact (Nicolas, 2009). The Boyne Member is characterized by grey, variably calcareous shale and is subdivided into a lower calcareous unit and an upper chalky unit. The Boyne Member records deposition during a relative sea-level rise associated with the transgressive stage of the Niobrara cyclothem, with the upper chalky unit deposited during the late stage of the transgression (McNeil and Caldwell, 1981; Shaw et al., 2017). The Boyne Member is unconformably overlain by the Gammon Ferruginous or Pembina members of the Pierre Shale (McNeil and Caldwell, 1981; Nicolas, 2009; Muehlbauer et al., 2014).

The Pierre Shale is primarily composed of black shale deposited during the late Campanian and interpreted to be deposited during the regressive stage of the Niobrara cyclothem (McNeil and Caldwell, 1981; Shaw et al., 2017). The Pierre Shale has been divided into the Gammon Ferruginous, Pembina, Milwood, Odanah and Coulter members. The Gammon Ferruginous Member is characterized by uniform dark grey, noncalcareous shale with reddish-brown ferruginous and sideritic concretions. It is absent in certain parts of the province and has an unconformable contact with the overlying Pembina Member. The Pembina Member is characterized by calcareous black shale, interbedded with a series of yellow-grey bentonite beds (McNeal and Caldwell, 1981). The Pembina Member has a conformable contact with the overlying Milwood Member of the Pierre Shale (Nicolas, 2009).

Current investigations

During the 2025 field season, three sites in the Pembina Hills region and one site along the Vermilion River on Riding Mountain were visited (Figure GS2025-17-1a, b). A total of 34 shale samples were collected from the Boyne, Gammon Ferruginous and Pembina members. Site location and stratigraphic position of samples taken can be seen in Figures GS2025-17-2 and -3.

Site 120-25-003 – Spencer's Ditch

The outcrop at the Spencer's Ditch site is a 13 m thick exposure on an east ravine wall located at L.S. 15, Sec. 31, Twp. 3, Rge. 6, W 1st Mer. (abbreviated 15-31-3-6W1). The outcrop consists of an approximately 9.3 m thick exposure of the Boyne Member, a 0.25 m thick exposure of the Gammon Ferruginous Member and a 3.5 m thick exposure of the Pembina Member. This site has been studied previously and was sampled by Bamburak et al. (2013). For this project, two measured sections were chosen, and a total of six samples were collected from this site: one from the Boyne Member, one from the Gammon Ferruginous Member and four samples from the Pembina Member (Figure GS2025-17-2a, b).

Site 120-25-006 – Glencross

The Glencross site is an approximately 6 m thick roadcut exposure at SW7-2-5W1. Although the Boyne and Gammon Ferruginous members have been recognized at this site in the past, both members have been eroded and only the Pembina Member was present at the time of sampling in 2025. A total of seven samples of the Pembina Member were collected from this site (Figure GS2025-17-2c).

Site 120-25-007 – Roseisle

The Roseisle site is a series of roadcut exposures, the outcrop visited for this study is located at 16-10-6-8W1. The outcrop is approximately 20 m thick, but only 3.5 m on the westernmost side was accessible. Although the Pembina Member has been recognized at this site in the past, only the Boyne Member was present during the 2025 field season. A total of three Boyne Member samples were collected at this site (Figure GS2025-17-2d).

Site 120-25-008 – Vermilion River

This site is located at 15-15-23-20W1 along the Vermilion River. The outcrop is approximately 35 m thick and has a 3 m thick exposure of the Gammon Ferruginous Member and an approximately 32 m thick exposure of the Pembina Member. This site has been sampled for previous studies by Bamburak et al. (2014) and Nicolas and Bamburak (2025). Due to the large size of the outcrop, two measured sections were chosen, one at ground level and one at the top of the outcrop. The lower section has the Gammon Ferruginous Member–Pembina Member contact

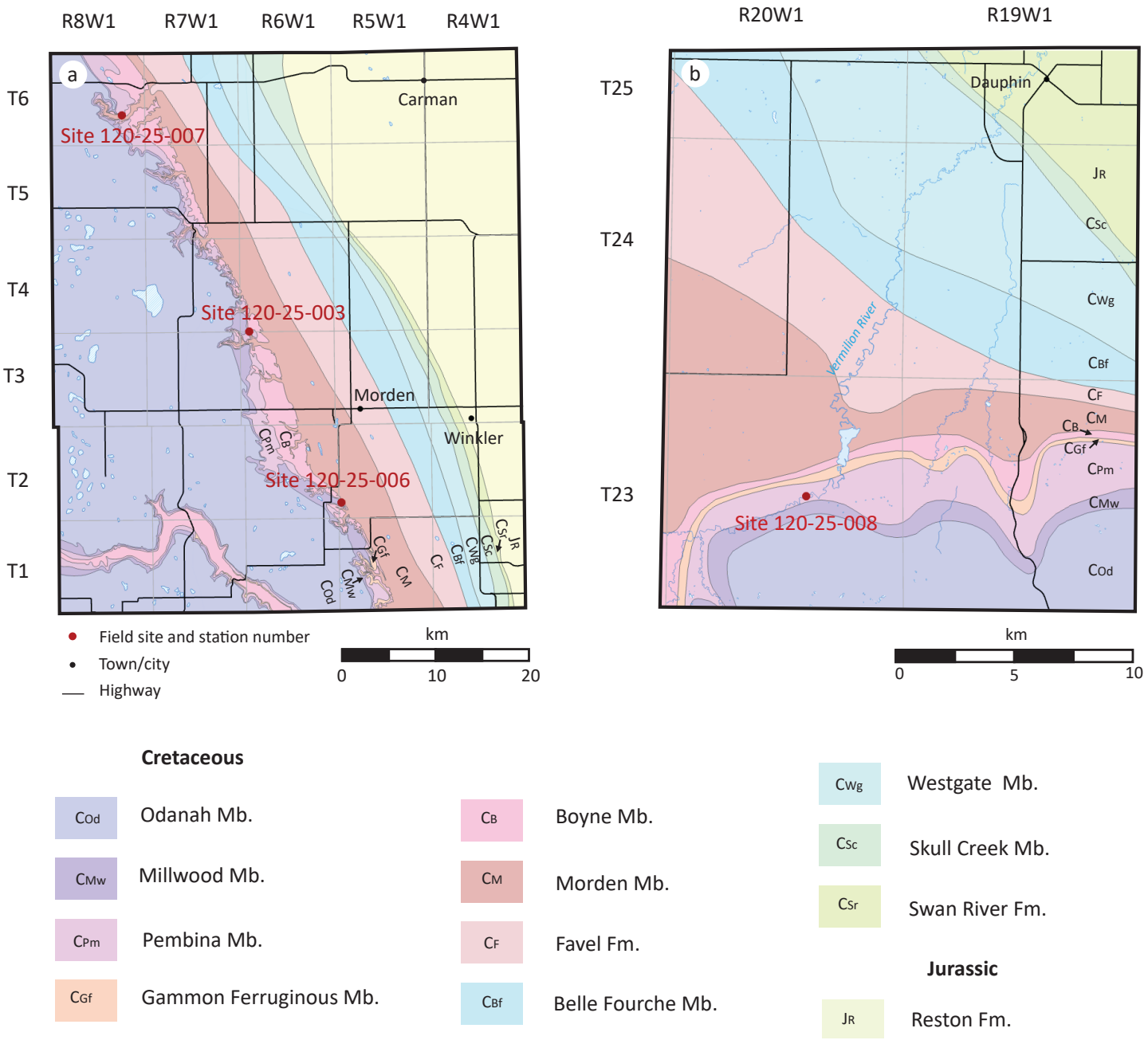

Figure GS2025-17-1: *Bedrock geology map (modified from Nicolas et al., 2010) showing field sites visited in the 2025 field season:* ***a)*** *Pembina Hills area,* ***b)*** *Riding Mountain area, southwestern Manitoba.*

and eight samples were collected, four samples from each member (Figure GS2025-17-3a). Two Pembina Member samples were taken between the two sections (Figure GS2025-17-3a). Eight samples were taken from the upper section, all of which were from the Pembina Member (Figure GS2025-17-3b).

Future work

Samples collected during the 2025 field season have been submitted to Activation Laboratories Ltd. (Ancaster, Ontario) for analysis; results are pending. The samples will be analyzed using lithium metaborate-tetraborate fusion digestion followed by inductively coupled plasma–optical emission spectroscopy (ICP-OES) and inductively coupled plasma–mass spectrometry (ICP-MS) to determine REE concentrations. These results will be used to assess the distribution of elevated REE concentrations across southwestern Manitoba. Additional sampling from other sites across the Manitoba escarpment will expand the spatial and stratigraphic scope of this project. The results of this study and others in Manitoba will be compared to other REE-enriched organic-rich shales reported in the literature, as well as modern REE-enriched deep-sea sites in the Indian Ocean Basin. This comparison will lead to a better understanding of REE deposits and the mechanisms of REE enrichment in ocean sediments.

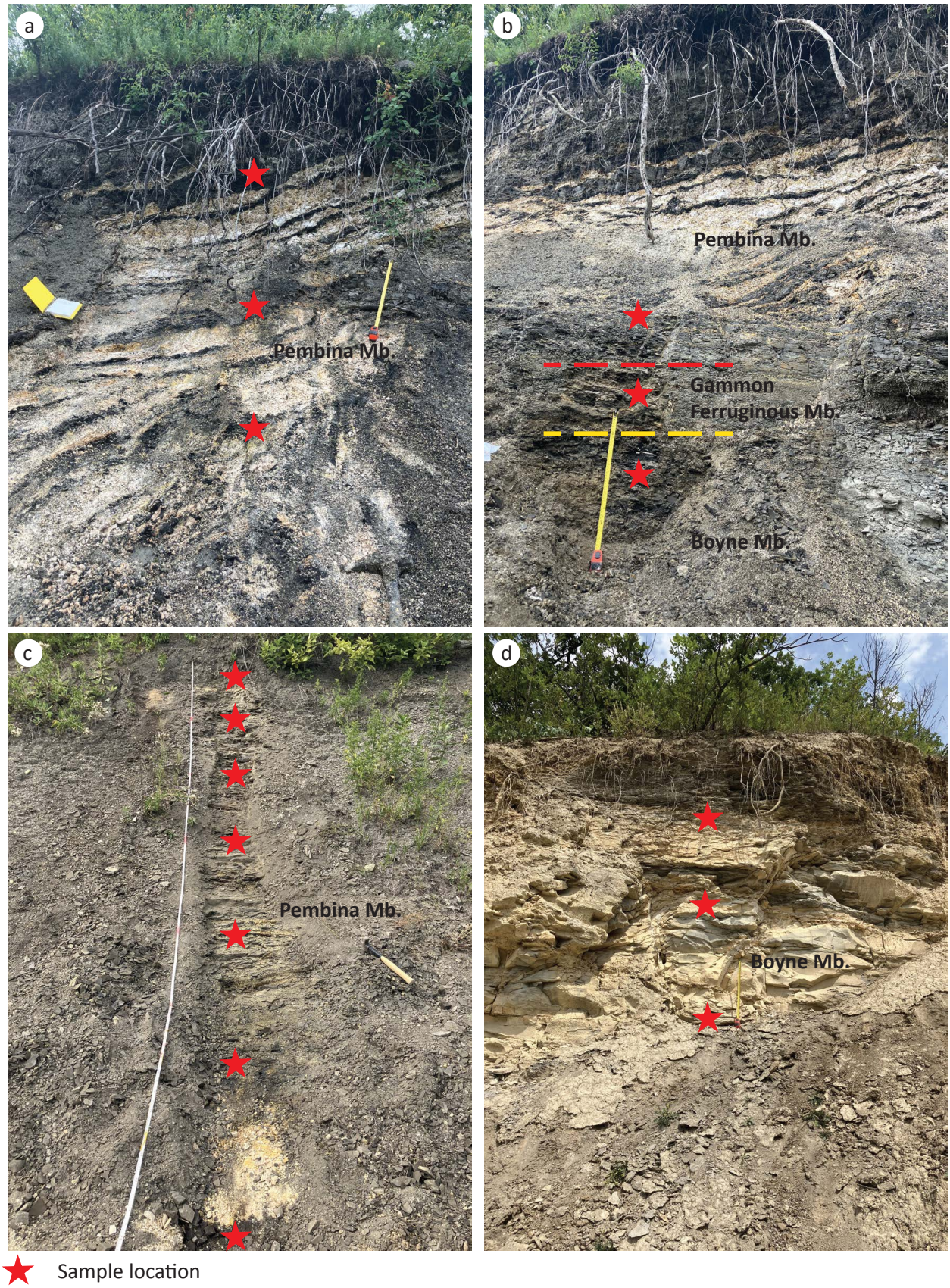

Figure GS2025-17-2: *Stratigraphic position of samples collected at* ***a)*** *the upper section at site 120-25-003 – Spencer's Ditch, 0.5 m measuring tape for scale;* ***b)*** *the lower section at site 120-25-003 – Spencer's Ditch, 0.5 m measuring tape for scale;* ***c)*** *site 120-25-006 – Glencross, 6.2 m measuring tape for scale; and* ***d)*** *site 120-25-007 – Roseisle, 0.5 m measuring tape for scale. The yellow dashed line indicates approximate contact between the Boyne and Gammon Ferruginous members and the red dashed line indicates approximate contact between the Gammon Ferruginous and Pembina members.*

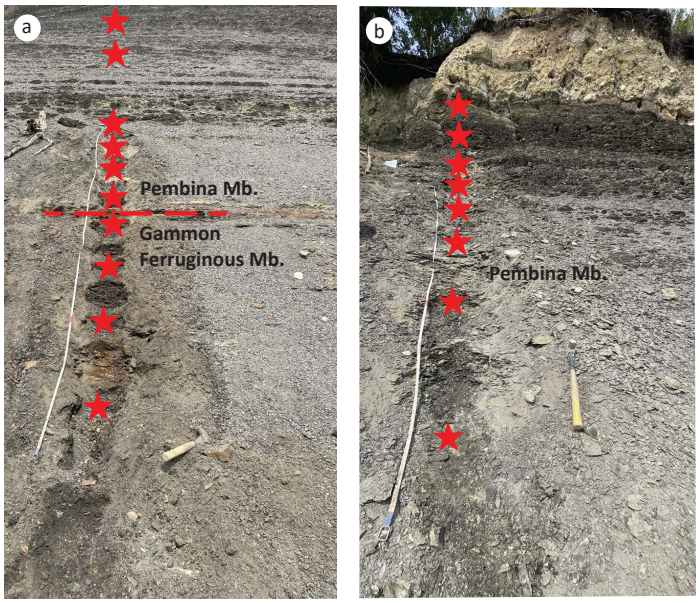

★ Sample location

Figure GS2025-17-3: *Stratigraphic position of samples collected at site 120-25-008 – Vermilion:* ***a)*** *lower section, 6 m measuring tape for scale;* ***b)*** *upper section, 4.3 m measuring tape for scale. Samples from both sections were collected every metre. Red dashed line indicates approximate contact between the Gammon Ferruginous and Pembina members.*

Economic considerations

Rare-earth elements are listed as critical minerals because they are critical to modern technology. They have a wide range of industrial uses, including the production of magnets, lasers, camera lenses, hybrid/electric vehicle batteries, computer hard drives, monitors and phones. As demand for these products increases, exploration for new sources of REEs is increasing and the importance of sources like REE-enriched sedimentary deposits will continue to rise. Studying deposits in the rock record, like the Upper Cretaceous shales of southwestern Manitoba, may provide valuable insight into the development of secondary REEs resources in the province.

Acknowledgments

The author thanks J. Gellert (University of Manitoba) for providing enthusiastic field assistance, as well as C. Epp, E. Ralph and P. Belanger (Manitoba Geological Survey) for thorough logistical field support. Reviews of this report were provided by P.E. Fraino and M.P.B. Nicolas of the Manitoba Geological Survey.

References

Bamburak, J.D. and Nicolas, M.P.B. 2010: Gammon Ferruginous Member of the Cretaceous Pierre Shale in southwestern Manitoba: distribution and mineral potential (parts of NTS 62F, G, J, K, N, O, 63C); *in* Report of Activities 2010, Manitoba Innovation, Energy and Mines, Manitoba Geological Survey, p. 170–177.

Bamburak, J.D., Hatcher, J. and Nicolas, M.P.B. 2012: Chemostratigraphy, paleontology and mineral potential of the Gammon Ferruginous Member of the Cretaceous Pierre Shale in southwestern Manitoba (parts of NTS 62F, G, H, J, K, N, O, 63C, F); *in* Report of Activities 2012, Manitoba Innovation, Energy and Mines, Manitoba Geological Survey, p. 141–150.

Bamburak, J.D., Martins, T., Nicolas, M.P.B. and Yang, X.M. 2014: Update on the rare-earth element potential of the Gammon Ferruginous Member of the Upper Cretaceous Pierre Shale in southwestern Manitoba; *in* Report of Activities 2014, Manitoba Mineral Resources, Manitoba Geological Survey, p. 172–180.

Bamburak, J.D., Nicolas, M.P.B., Hatcher, J. and Yang, X.M. 2013: Rare-earth element potential of the Gammon Ferruginous Member of the Upper Cretaceous Pierre Shale in southwestern Manitoba; *in* Report of Activities 2013, Manitoba Mineral Resources, Manitoba Geological Survey, p. 123–128.

Li, J., Shi, X., Huang, M., Yu, M., Bi, D., Song, Z., Shen, F., Liu, J., Zhang, Y., Wang, H. and Sun, Y. 2023: The transformation and accumulation mechanism of rare earth elements in deep-sea sediments from the Wharton Basin, Indian Ocean; Ore Geology Reviews, v. 161, art. 105655.

Markstrom, V.L. 2023: Thermoregulation in Late Cretaceous marine reptiles of Manitoba; M.Sc. thesis, University of Manitoba, Winnipeg, Manitoba, 105 p.

McNeil, D.H. and Caldwell, W.G.E. 1981: Cretaceous rocks and their foraminifera in Manitoba Escarpment; Geological Association of Canada, Special Paper 21, 439 p.

Muehlbauer, R., Kelly, D.C., Bamburak, J.D. and Nicolas, M.P.B. 2014: Late Cretaceous (Santonian–Campanian) marine microfossils of the Manitoba escarpment, southwestern Manitoba; *in* Report of Activities 2014, Manitoba Mineral Resources, Manitoba Geological Survey, p. 181–186.

Nicolas, M.P.B. 2009: Williston Basin Project (Targeted Geoscience Initiative II): summary report on Mesozoic stratigraphy, mapping and hydrocarbon assessment, southwestern Manitoba; Manitoba Science, Technology, Energy and Mines, Manitoba Geological Survey, Geoscientific Paper GP2009-1, 19 p.

Nicolas, M.P.B. and Bamburak, J.D. 2025: Whole rock geochemistry results from Cretaceous outcrops along the Vermillion River and drill cuttings from an oil well, southwestern Manitoba (parts of NTS 62F11 and 62K16); Manitoba Business, Mining, Trade and Job Creation, Manitoba Geological Survey, Data Repository Item DRI2025020, Microsoft® Excel® file.

Nicolas, M.P.B., Matile, G.L.D., Keller, G.R. and Bamburak, J.D. 2010: Phanerozoic geology of southern Manitoba; Manitoba Innovation, Energy and Mines, Manitoba Geological Survey, Stratigraphic Map SM2010-1, 2 sheets, scale 1:600 000.

Shaw, D.J., Nicolas, M.P.B. and Chow, N. 2017: Stratigraphy and geochemistry of the Cretaceous Boyne Member, Carlile Formation, in the Manitoba Potash Corporation core at 3-29-20-29W1, southwestern Manitoba (parts of NTS 65K1); *in* Report of Activities 2017, Manitoba Growth, Enterprise and Trade, Manitoba Geological Survey, p. 173–182.

Tanaka, E., Mimura, K., Nakamura, K., Ohta, J., Yasukawa, K. and Kato, Y. 2023: Rare-earth elements in deep-sea sediments in the South Pacific Gyre: source materials and resource potentials; Geochemistry, Geophysics, Geosystems, v. 24, no. 3, art. e2022GC010681.

Tanaka, E., Nakamura, K., Yasukawa, K., Mimura, K., Fujinaga, K., Iijima, K., Nozaki, T. and Kato, Y. 2020: Chemostratigraphy of deep-sea sediments in the western North Pacific Ocean: implications for genesis of mud highly enriched in rare-earth elements and yttrium; Ore Geology Reviews, v. 119, art. 103392.

GS2025-18

Drone photogrammetry acquisition in support of geological field mapping in recently burnt forested terrain, west-central Manitoba (part of NTS 63K13)

by J. Marks

In Brief:

- Photogrammetry was effective in recently burned forested terrain
- The data was of sufficient quality and detail to aid potential future geological mapping projects
- Contributing to more efficient geological mapping approaches supports resource development and economic growth

Citation:
Marks, J. 2025: Drone photogrammetry acquisition in support of geological field mapping in recently burnt forested terrain, west-central Manitoba (part of NTS 63K13); *in* Report of Activities 2025, Manitoba Business, Mining, Trade and Job Creation, Manitoba Geological Survey, p. 167–173.

Summary

A photogrammetry survey was flown near Flin Flon, west-central Manitoba, to assess its effectiveness for geological field mapping. The objective of this study was to create a repeatable procedure and evaluate its viability for future implementation elsewhere. Recently burnt terrain provided ideal conditions for the photogrammetry survey, as the area was previously covered by a dense vegetation canopy. Two separate flight heights were chosen to assess whether higher resolution data justifies the additional time required to collect it. The 90 m above ground level (agl) dataset provided comparable data to the 50 m agl dataset, and covered approximately 2.8 times more area after normalizing total flight time between the datasets. Furthermore, the 90 m digital terrain model correlates well with previously noted fault and outcrop locations, which are key aspects of geological mapping. A replicable process was created and can be used as an approach for future projects in similar conditions.

Introduction

A drone-based photogrammetry survey was conducted by the Manitoba Geological Survey (MGS) to assess the efficacy of using its data to aid geological field mapping efforts. The primary objective was to determine if photogrammetry could provide enhanced, high-quality datasets to aid in geological mapping. Recently burnt forested areas provide ideal conditions for photogrammetric surveys due to the reduction of the ground vegetation and canopy cover, which typically hinders photogrammetric terrain model generation by obstructing the view of the ground surface (Wallace et al., 2016).

The study area, located 15 km east of Flin Flon, was selected for its burnt forest conditions and its potential for future geological field mapping, while also having some pre-existing geological information for comparison purposes (Gale and Babek, 2002). The area was sectioned into two overlapping flight blocks, each with subsequent subblocks to allow for a complete flight within a single battery charge (Figure GS2025-18-1). To assess the trade-off between coverage and data quality, the two flight blocks were flown at different heights; block A at 90 m and block B at 50 m above ground level (agl), which corresponds to a predicted ground sample distance (GSD) of 2.4 and 1.3 cm/pixel, respectively. The methodology was designed to compare the resolutions at different flight heights, measured by GSD, and to determine if the additional time required for higher resolution data collection was justified for geological mapping purposes.

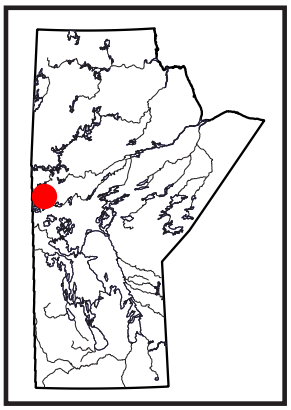

Methodology and survey design

Both blocks were flown with a SZ DJI Technology Co., Ltd. Mavic 3 Enterprise drone, using its wide-angle lens and integrated DJI D-RTK2 real-time kinematic (RTK) system. Utilization of an RTK system eliminated the need for ground control points (GCPs), while still maintaining sufficient positional accuracy (Pugh et al., 2021; Alkan, 2024). Survey parameters were selected to balance flight efficiency and data quality, while ensuring adequate GSD and image overlap. For all flights:

- all images were captured at a nadir orientation (camera angle of 90°);
- overlap was set to 80% frontal and 75% side to ensure sufficient image redundancy and robust 3-D model generation (Lopes Bento et al., 2022);
- azimuth was set to 90° to optimize flight efficiency by flying crosswind to the predominant north-south winds in the area (Chu et al., 2021); and
- terrain-following modes were used to maintain constant flight height agl, which improves overall data accuracy by providing more consistent GSD throughout flights (Singh et al., 2023).

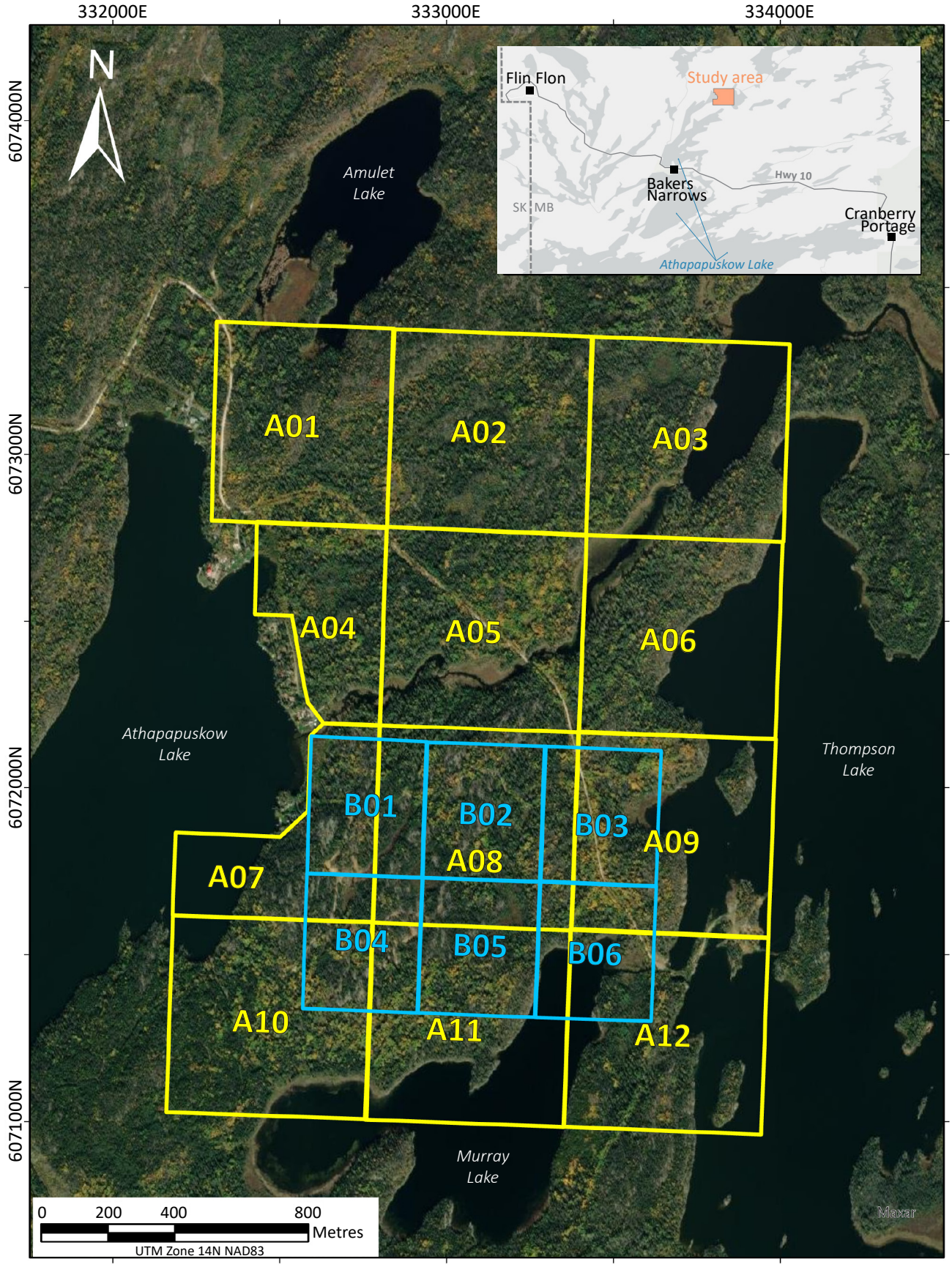

Figure GS2025-18-1: *Locations of flight blocks A and B. Blue and yellow polygons indicate outlines of subblocks within each flight block. Inset shows the location of the study area within west-central Manitoba. Satellite imagery from Esri® (2023), © Maxar 2021.*

Table GS2025-18-1 shows additional flight parameters used for each survey block. A lower flight height for block B facilitated a slower flight speed to mitigate increased risk of photograph motion blur.

The drone imagery was processed using OpenDroneMap™ WebODM™, an open-source photogrammetry software. Subblocks were processed separately, generating four primary outputs for each:

1) orthomosaic
2) digital surface model (DSM)
3) digital terrain model (DTM)
4) 3-D point cloud

Orthomosaic resolution was set to match the GSD and images were not resized prior to processing. The DSM and DTM resolutions were set to 5 cm/pixel. The DTM was created by filtering the DSM using a simple morphological filter (SMF), with the goal of isolating the ground surface by attempting to remove all nonground objects. The DTM datasets were stitched together postprocessing using Esri® ArcGIS® Pro to obtain a combined dataset for each survey block.

Results

The results of the survey showed that block A covered approximately 2.8 times more area than block B after normalizing for total flight time. Both blocks yielded low 3-D root mean square errors (RMSEs) and good position accuracy indicating the collection of high-quality data (Table GS2025-18-2), which is supported by the precise mapping of the road through the study area (black dotted line in Figure GS2025-18-2). Absolute accuracy is not provided as GCPs were not utilized.

Artifacts are present in low-elevation areas within both blocks, contributing to areas of missing data in block A (white areas in Figure GS2025-18-2). These artifacts are due to the presence of water (blue lines in Figure GS2025-18-2), which classically hinders aerial photogrammetric processing (Acharya et al., 2021). Even though most vegetation was removed by the fire, some ground vegetation and canopy cover remained. The SMF filtered most of this vegetation well, but some areas of dense canopy persisted in block A's dataset (black arrows in Figure GS2025-18-2). Additionally, decimetre-scale ground vegetation is present throughout both datasets, however, it does not significantly impact the quality of the data overall.

Table GS2025-18-1: Additional flight parameters for flight blocks A and B. Abbreviations: agl, above ground level; GSD, ground sample distance.

Parameter	Block A	Block B
Flight height (agl)	90	50
Flight speed (m/s)	10	7.5
Estimated line spacing (m)	32	18
Predicted GSD (cm/pixel)	2.4	1.3

Table GS2025-18-2: Parameters resulting from data processing for flight blocks A and B. Abbreviations: CE90, circular error at 90% confidence; GSD, ground sample distance; LE90, linear error at 90% confidence.

Parameter	Block A	Block B
Flight time (h:min)	4:43	2:53
Total area (km^2)	4.099	0.909
Average GSD (cm/pixel)	2.325	1.600
3-D root mean square error	0.114	0.058
Relative horizontal accuracy, CE90 (m)	0.098	0.057
Relative vertical accuracy, LE90 (m)	0.183	0.109

A comparison between block A and block B data reveals that block B has a cleaner dataset overall (Figure GS2025-18-3). This is due to its lower GSD and relatively denser point cloud. When comparing the DTMs, block B features appear sharper and ground vegetation is less prevalent (dashed ellipses in Figure GS2025-18-3a, b), resulting in a more accurate ground surface representation. Block B data also provided slightly higher resolution orthomosaics (Figure GS2025-18-3c, d).

Despite these differences, the datasets are quite similar at this scale. All significant topographical features visible in block B are also present in block A, suggesting that no significant information is gained from the former (Figure GS2025-18-3a–d). These similarities are likely related to the smaller difference between the calculated GSDs of the two datasets (Table GS2025-18-2), than in their predicted GSDs (Table GS2025-18-1), as GSD is a direct measurement of spatial resolution. Variations between predicted and calculated GSDs are generally caused by unexpected variations in flight height (Kozmus Trajkovski et al., 2020).

Discussion

The DTM produced for block A provides an accurate representation of the topography in the study area. Such models can provide a valuable resource for identifying geomorphological or structural features. For example, DTM data show a distinct northeast-southwest topographical trend in block A (Figure GS2025-18-2). This correlates well with mapped outcrops (Gale and Babek, 2002), which are associated with local elevation highs and show a similar directional trend (black outlined polygons in Figure GS2025-18-4). Another example is the presence of a prominent northeast-trending lineation in the northeastern portion of block A, which strongly correlates to a structural fault interpreted by Gale and Babek (2002; Figures GS2025-18-2, -4). Features such as these become clearly visible in high-resolution DTM data, which can be more difficult to identify with traditional methods, and can help provide a foundation for detailed geological mapping.

This study also highlighted the critical role of site selection for photogrammetry. Some areas of surviving canopy cover were not removed by the SMF due to their size and density (Figures GS2025-18-2, -3a, b), demonstrating the challenge that photogrammetric processing has when trying to accurately

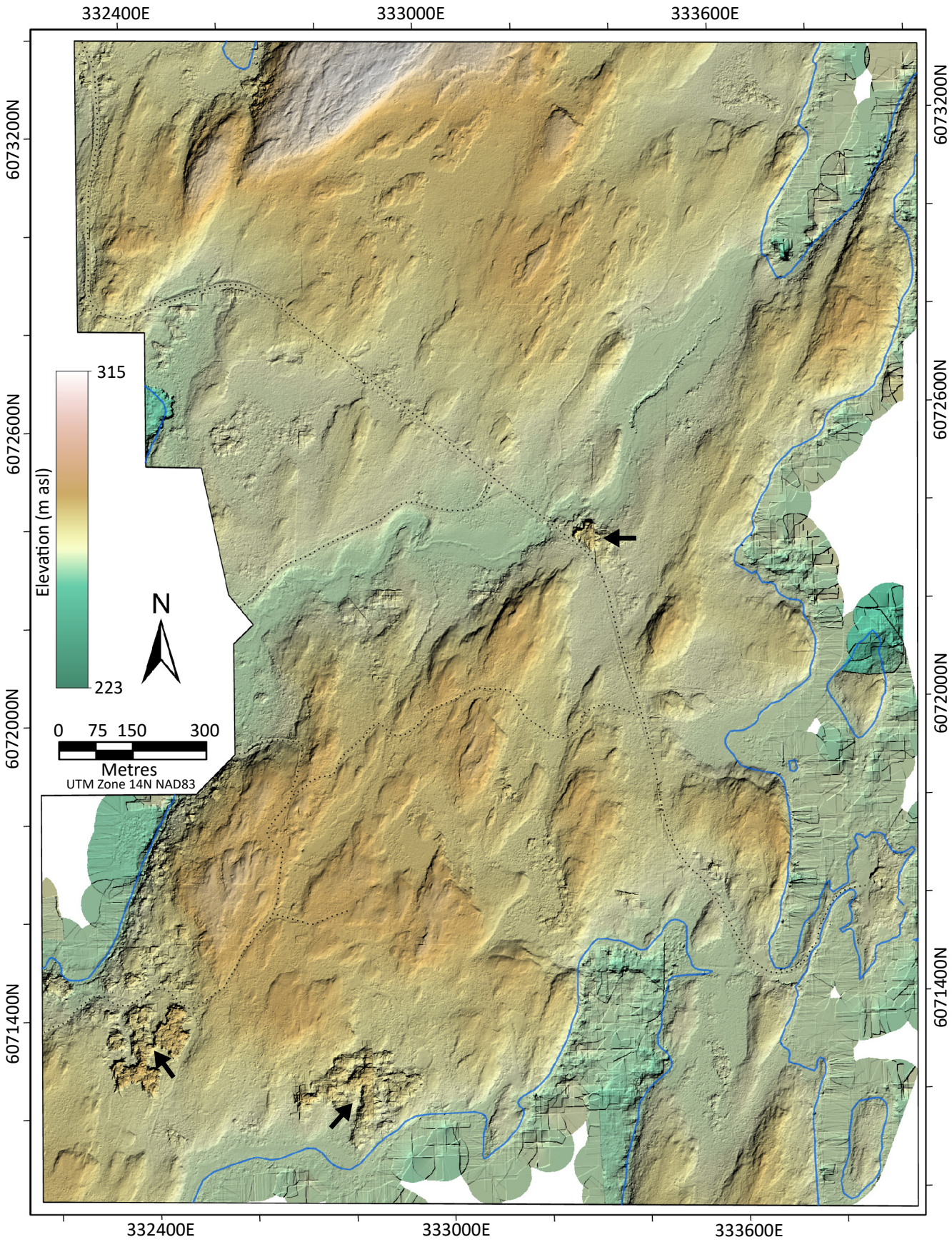

Figure GS2025-18-2: *Results showing digital terrain model (DTM) for flight block A in shaded relief. Dotted lines highlight roads distinguishable within the DTM data. Black arrows indicate areas of vegetation that persisted through simple morphological filtering. Blue lines outline approximate water body boundaries (from Gale and Babek, 2002). White areas represent areas of missing data.*

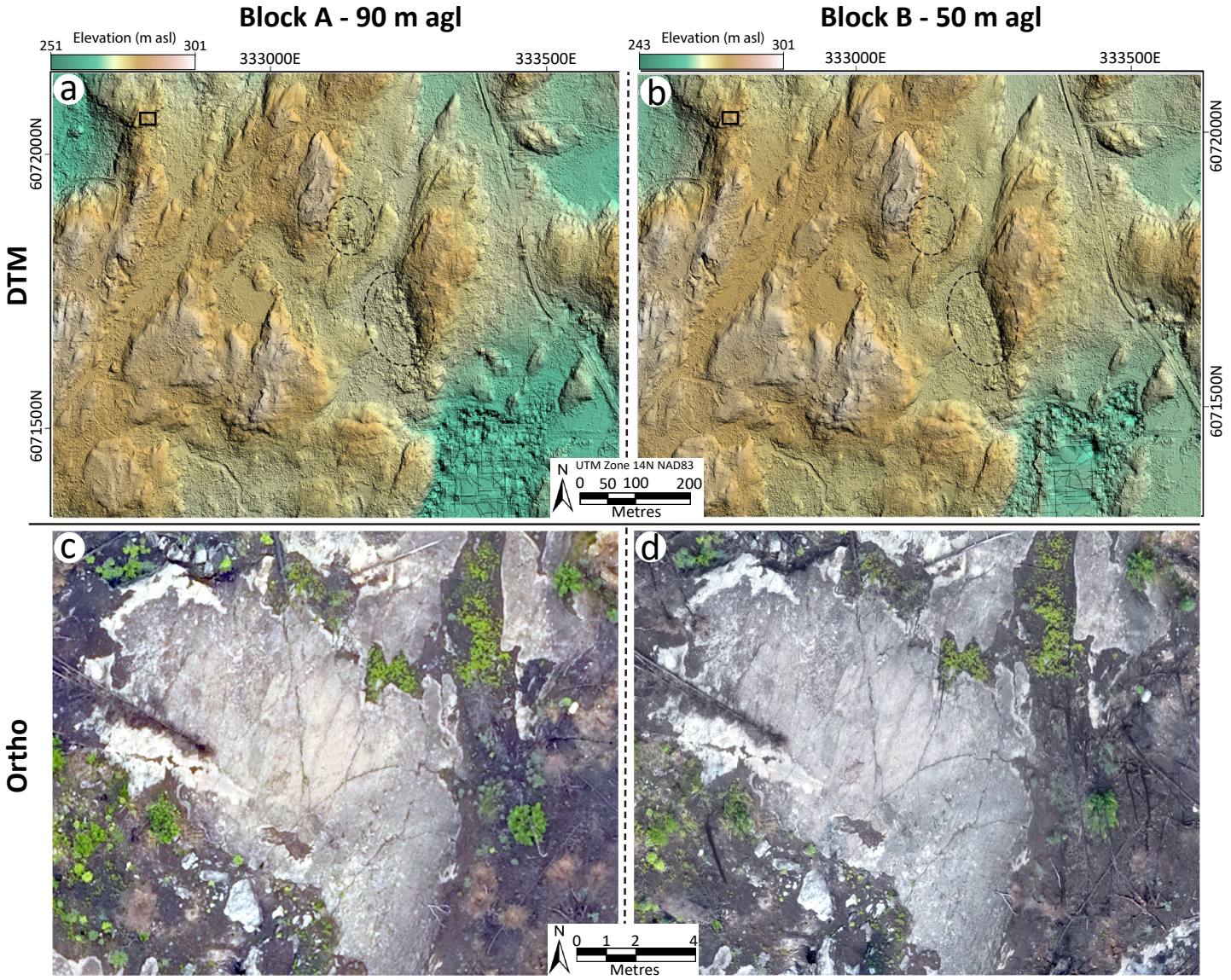

Figure GS2025-18-3: *Comparison of digital terrain model (DTM) and orthomosaic (ortho) data for flight blocks A and B:* ***a)*** *block A DTM, 90 m above ground level (agl);* ***b)*** *block B DTM, 50 m agl;* ***c)*** *block A orthomosaic, 90 m agl;* ***d)*** *block B orthomosaic, 50 m agl. Dashed ellipses in a) show locations of vegetation within block A that persisted after filtering. Dashed ellipses in b) show the vegetation was filtered out in block B. Black square in a) and b) indicates the location within the DTM of the orthomosaics in c) and d).*

model the ground surface. These challenges can be mitigated by increasing image overlap or performing additional flights at different heights and camera angles, thus increasing the chance of generating ground points beneath the canopy surface (Pessacg et al., 2022). However, these methods would significantly decrease data collection efficiency, and increase time required for processing. This reinforces the value of conducting this study in recently burnt forested terrain, as it allowed for the efficient production of high-quality data by minimizing the challenges typically associated with photogrammetry in forested terrain.

Economic considerations

Geological mapping is a vital tool with many applications. For Manitoba, it plays a fundamental role for informing land-use decisions, understanding geological features and the tectonic evolution of terrains through time, and assessing the economic potential of a region. Geological mapping is also used by the exploration and mining industry, providing critical data for resource exploration and economic planning. Increased forest fire activity this past summer provided potential target areas for photogrammetry surveys in terrain that is now better exposed. These surveys can offer rapid and effective means to acquire data to aid geological field mapping. Acquiring these types of data is particularly relevant given the increasing global demand for critical minerals and Manitoba's critical minerals strategy, which highlights the need for accelerated geological investigations to support resource development and economic growth. The successful application of this survey framework provides a replica-

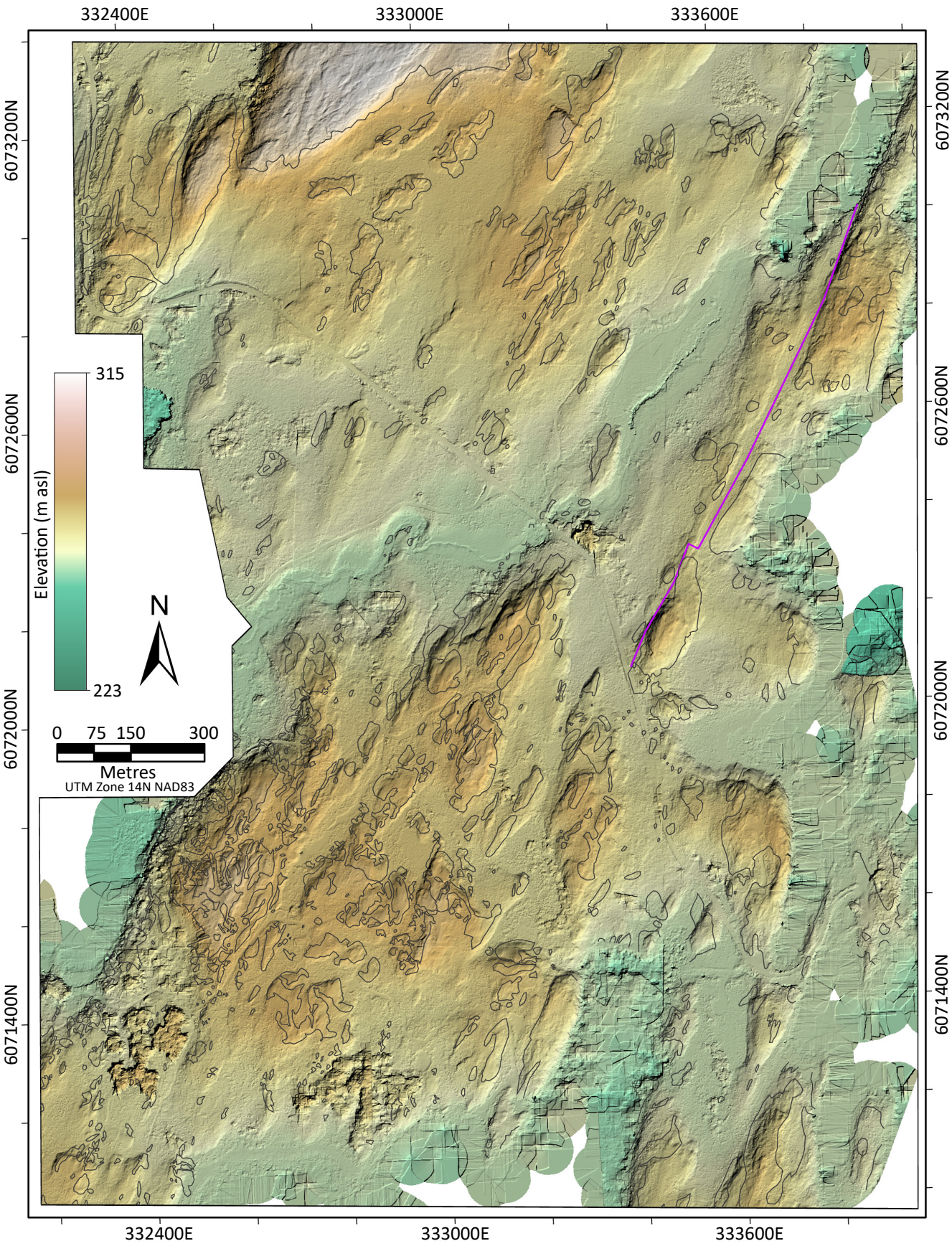

Figure GS2025-18-4: *Flight block A digital terrain model in shaded relief, annotated with the locations of outcrops and a fault (from Gale and Babek, 2002). Black polygons outline outcrop locations. Purple line shows location of an interpreted fault.*

ble approach for future projects, contributing to more efficient approaches to geological mapping.

Acknowledgments

The author acknowledges K.D. Reid from the Manitoba Geological Survey for his geological insights and his part in generating the project. D. Koop is thanked for graciously providing accommodations during the fieldwork, and W. Sharpe (summer student, University of Manitoba) is thanked for his assistance with data collection. Lastly, C. Epp, E. Ralph and P. Belanger (Manitoba Geological Survey) are thanked for their roles in equipment expediting and maintenance.

References

Acharya, B.S., Bhandari, M., Bandini, F., Pizarro, A., Perks, M., Joshi, D.R., Wang, S., Dogwiler, T., Ray, R.L., Kharel, G. and Sharma, S. 2021: Unmanned aerial vehicles in hydrology and water management: applications, challenges, and perspectives; Water Resources Research, v. 57, no. 11, art. e2021WR029925.

Alkan, M.N. 2024: High-precision UAV photogrammetry with RTK GNSS: eliminating ground control points; Hittite Journal of Science and Engineering, v. 11, no. 4, p. 139–147.

Chu, T., Starek, M.J., Berryhill, J., Quiroga, C. and Pashaei, M. 2021: Simulation and characterization of wind impacts on sUAS flight performance for crash scene reconstruction; Drones, v. 5, no. 3, art. 67.

Esri® 2023: World imagery map, April 05, 2021; Esri, no scale given, URL <https://services.arcgisonline.com/ArcGIS/rest/services/World_Imagery/MapServer> [September 2025].

Gale, G.H. and Babek, L.B. 2002: Geology of the Baker Patton Complex, Flin Flon, Manitoba (parts of NTS areas 63K 12, 13); Manitoba Industry, Trade and Mines, Manitoba Geological Survey, Geoscientific Map MAP2002-1, scale 1:10 000.

Kozmus Trajkovski, K., Grigillo, D. and Petrovič, D. 2020: Optimization of UAV flight missions in steep terrain; Remote Sensing, v. 12, no. 8, art. 1293.

Lopes Bento, N., Araújo E Silva Ferraz, G., Alexandre Pena Barata, R., Santos Santana, L., Diennevan Souza Barbosa, B., Conti, L., Becciolini, V. and Rossi, G. 2022: Overlap influence in images obtained by an unmanned aerial vehicle on a digital terrain model of altimetric precision; European Journal of Remote Sensing, v. 55, no. 1, art. 2054028.

Pessacg, F., Gómez-Fernández, F., Nitsche, M., Chamo, N., Torrella, S., Ginzburg, R. and De Cristóforis, P. 2022: Simplifying UAV-based photogrammetry in forestry: how to generate accurate digital terrain model and assess flight mission settings; Forests, v. 13, no. 2, art. 173.

Pugh, N.A., Thorp, K.R., Gonzalez, E.M., Elshikha, D.E.M. and Pauli, D. 2021: Comparison of image georeferencing strategies for agricultural applications of small unoccupied aircraft systems; The Plant Phenome Journal, v. 4, no. 1, art. e20026.

Singh, C.H., Mishra, V. and Jain, K. 2023: High-resolution mapping of forested hills using real-time UAV terrain following; ISPRS Annals of the Photogrammetry, Remote Sensing and Spatial Information Sciences, v. X-1/W1-2023, p. 665–671.

Wallace, L., Lucieer, A., Malenovský, Z., Turner, D. and Vopěnka, P. 2016: Assessment of forest structure using two UAV techniques: a comparison of airborne laser scanning and structure from motion (SfM) point clouds; Forests, v. 7, no. 3, art. 62.

GS2025-19

Till sampling strategies and surficial geology mapping in the Bird River greenstone belt area, southeastern Manitoba (parts of NTS 52L5, 6, 11, 12)

by T.J. Hodder and J. Janssens

In Brief:

- Updating surficial geology mapping of Bird River greenstone belt area
- Till sampling strategies discussed for winnowed tills in bedrock-dominated terrain

Citation:
Hodder, T.J. and Janssens, J. 2025: Till sampling strategies and surficial geology mapping in the Bird River greenstone belt area, southeastern Manitoba (parts of NTS 52L5, 6, 11, 12); *in* Report of Activities 2025, Manitoba Business, Mining, Trade and Job Creation, Manitoba Geological Survey, p. 174–180.

Summary

Quaternary geology investigations in the Bird River greenstone belt area, southeastern Manitoba, are providing updates to the surficial geology mapping at a 1:50 000 scale. Till prospecting in the region is complicated by a relative scarcity of glacial sediments combined with postglacial sediment winnowing processes by glacial Lake Agassiz. Till is preserved mostly as bedrock lee-side (down-ice) deposits, which are relatively easily identified with light detection and ranging (LiDAR) datasets. The degree of sediment winnowing by glacial Lake Agassiz needs to be assessed in the field before a 'till' sample can be taken, as in some cases all of the fines have been winnowed—resulting in a till-derived sandy gravel that no longer reflects primary derivation from bedrock. Ongoing mapping efforts, combined with a paleo–ice-flow reconstruction and till composition studies, will provide an updated framework for till prospecting in the region.

Introduction

The Bird River greenstone belt (BRGB) is situated within the Bird River domain of the Superior Province and is host to a variety of mineral deposits including rare-element–bearing pegmatites and Ni-Cu–platinum group element (PGE) and Cr-PGE deposits (Martins et al., 2023). The Manitoba Geological Survey (MGS) is conducting a multidisciplinary Precambrian and Quaternary geology project to better understand the geological setting of these deposits and the glacial dispersal signature down-ice of these deposits (Martins et al., 2023; Hodder and Lian, 2024). As part of this ongoing work, the scope of the Quaternary geology investigations has been expanded to include updating the surficial geology mapping for the BRGB area (Figure GS2025-19-1), which is detailed within this report along with advice for till sampling in the region based on lessons learned to date.

Surficial geology mapping

Previous mapping

The surficial geology of southeastern Manitoba was mapped at a 1:100 000 scale during the National Geoscience Mapping Program (NATMAP; Southern Prairies and Greater Winnipeg projects; Matile and Fulton, 1994; Matile et al., 1998). This ambitious mapping project used local road and trail access, with limited fixed-wing airplane support in the BRGB area, to obtain field data (Matile et al., 1998). The surficial geology maps produced for the BRGB area indicate that the dominate surficial material consists of discontinuous till and associated glaciofluvial deposits (Mann, 2004a, b), which are defined in the legend vaguely as "gravelly silt to sand diamicton, sand and gravel; 1–30 m thick; low-relief deposits between bedrock outcrops making up 25–75% of the area; sandy till interbedded and interspersed with nearly equal and often greater amounts of sandy glaciofluvial sediments, as well as minor glaciolacustrine sediments." By this definition, these previously mapped till and glaciofluvial polygons can consist of up to 75% bedrock, which is problematic for an area such as the BRGB that is a bedrock-dominated terrain (e.g., Figure GS2025-19-2a, b). Instead, this surficial geology should have been mapped as complex units (e.g., map code Tv.GFv or GFv.Tv; Deblonde et al., 2024) or bedrock (map code R). Using this methodology, the mapped polygons are labelled by the predominant unit first and all other map units that encompass >20% of a polygon are included in the remainder of the label (Deblonde et al., 2024). As such, an unknown proportion of the NATMAP 'till' polygons (code Tp; Figure GS2025-19-2a) should have been mapped as bedrock-dominated terrains (e.g., Figure GS2025-19-2b, c). Problematically, as happens during regional compilation, the overly simplified polygons were identified by their map units (noncalcareous sand diamicton; Matile and Keller, 2004, 2007) and not their full complexity as suggested by the written description in the legend,

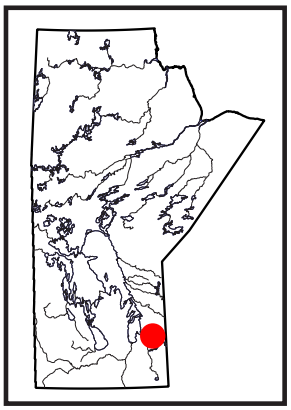

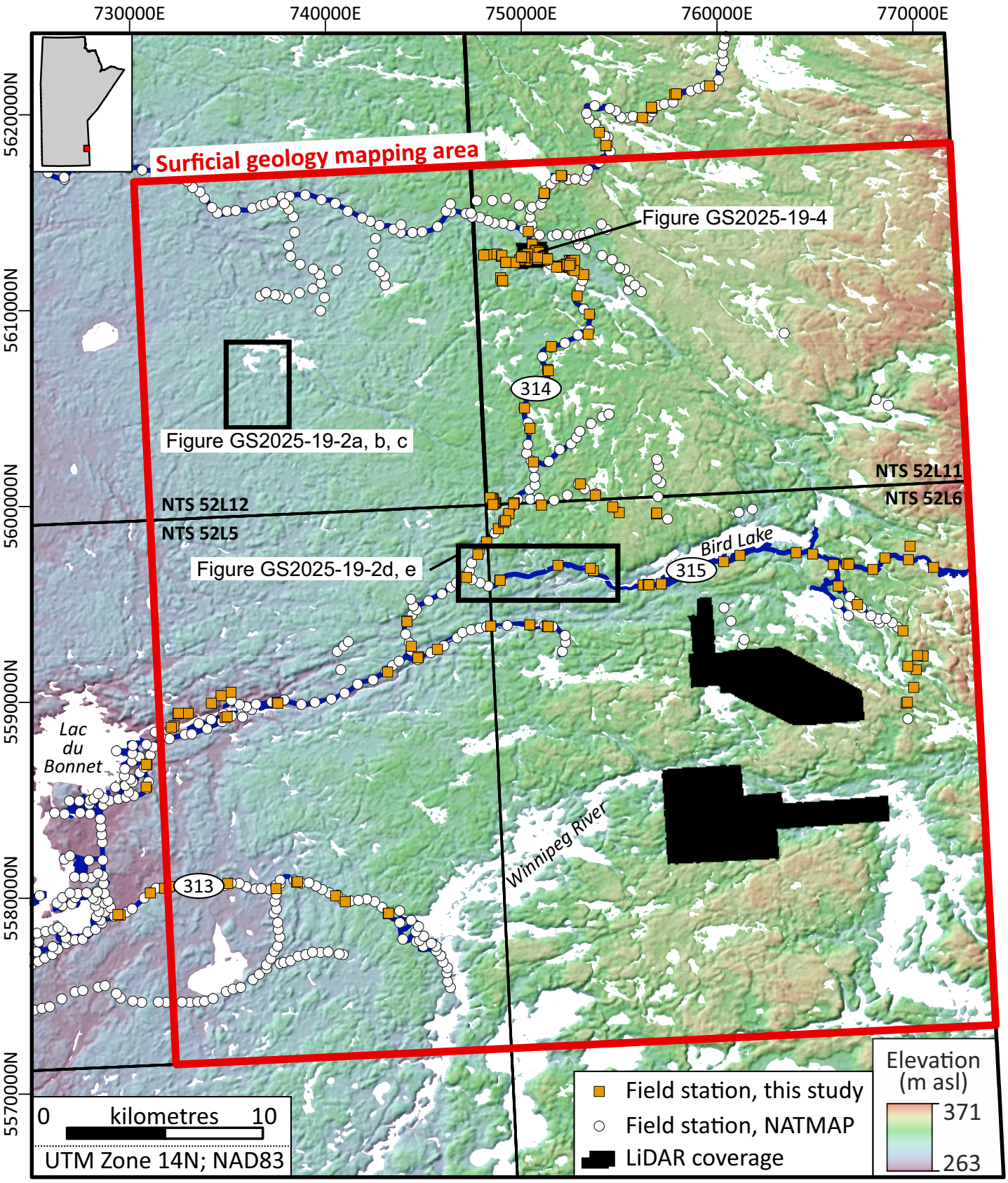

Figure GS2025-19-1: *Region currently being mapped at a 1:50 000 scale focused on the Bird River greenstone belt area of southeastern Manitoba. National Geoscience Mapping Program (NATMAP) field stations from Matile et al. (2023). Background image was generated from Medium Resolution Digital Elevation Model (Natural Resources Canada, 2025). Abbreviation: LiDAR, light detection and ranging.*

compounding the problem. Indeed, 1:50 000 scale mapping by Henderson and Way Nee (1998) just to the north concurs that most of the area is bedrock dominated.

Testing the accuracy of existing mapping

The existing mapping for the BRGB area is a reflection of a problematic mapping approach and regions that are clearly bedrock-dominated terrain have mostly been mapped as complex till (Tp) polygons (Figure GS2025-19-2a, b). The mapping issues are not restricted to bedrock-dominated terrain and persist in areas with relatively thicker sediments (Figure GS2025-19-2d, e). For example, along PR314 east of the junction with PR315, most of the previously mapped 'Tp' polygons (discontinuous till and associated glaciofluvial deposits; Figure GS2025-19-2d) consist of glaciolacustrine sediments, glaciofluvial sediments or bedrock based on fieldwork conducted in the area and new mapping (Figure GS2025-19-2e). Fieldwork conducted in 2022–2024 in the BRGB area has indicated that the current surficial geology mapping is insufficient for till prospecting or land-use planning purposes and is not an accurate reflection of field-based observations collected during NATMAP and this study (Hodder and Martins, 2023).

Current mapping

Parts of NTS 52L5, 6, 11 and 12 are being remapped at a 1:50 000 scale (Figures GS2025-19-1, -2). Considering the limited amount of ground-truthing completed for this area, the mapping approach will first use satellite imagery and digital elevation models to map bedrock and organic deposits. Next, the remaining Quaternary deposits will be differentiated based on interpretation of imagery and digital elevation models alongside field-based observations. This work is being completed to more accurately reflect the surficial geology of the region as a bedrock-dominated landscape instead of a till-dominated landscape (e.g., Figure GS2025-19-2). Fieldwork and preliminary surficial geology mapping indicate that till deposits are rarely mappable at the 1:50 000 scale in the BRGB area.

Till sampling strategies

The BRGB of southeastern Manitoba is a bedrock-dominated terrain with a thin, discontinuous cover of Quaternary sediments over much of the region. Till deposition was generally restricted to the down-ice side (or lee-side) of bedrock outcrops (Figure GS2025-19-3a). Following retreat of the Laurentide Ice Sheet from southern Manitoba, the area was inundated by glacial Lake Agassiz. This large ice-dammed lake experienced numerous lake level changes throughout its history (e.g., Thorleifson, 1996; Fisher and Breckenridge, 2022). This dynamic lake modified previously deposited sediments through wave and current processes, while also depositing nearshore and offshore sediments throughout most of Manitoba. In the BRGB area, till deposits were winnowed by these lacustrine processes and an extensive boulder and cobble lag developed at surface; at these sites, till needs to be sampled from below this lag (Figure GS2025-19-3b, d). In some cases, generally in areas of thinner Quaternary sediments, the till has been completely reworked by lacustrine processes and the deposit is now a till-derived sandy gravel (Figure GS2025-19-3c, e). Furthermore, till deposits seem to be highly localized and can exhibit lateral thickness variations at the outcrop scale. Thus, the local topography needs to be carefully considered to find the optimal sampling location, where till is the thickest, and could require several digging attempts. The relative scarcity of till across the BRGB means that sampling using a defined grid spacing is not possible; till sampling programs need to focus on identifying lee-side deposits where the least modified till is found. It is recommended to sample lee-side deposits, where possible, along lines oriented approximately northwest-southeast, which is perpendicular to the dominant ice-flow direction(s) based on field-based mapping (Hodder and Lian, 2024), at a defined spacing suitable for the study objectives.

High-resolution digital elevation models, such as those derived from LiDAR, are advantageous for identifying till sampling targets and mapping geomorphology and they provide valuable information regarding bedrock structure; thus, LiDAR acquisition is highly recommended for mineral exploration programs in the BRGB area at the property scale. For example, access to LiDAR around the F.D. no. 5 pegmatite and Eagle pegmatites was obtained after completing fieldwork (e.g., Figure GS2025-19-4a, b). From a LiDAR-derived digital elevation model, the lee-side till deposits discovered in the field (e.g., Figure GS2025-19-4c) are easily identifiable and additional potential till sampling localities can be mapped quickly, which saves significant time in the field. Interestingly, the streamlined bedrock mapped with LiDAR, including the F.D. no. 5 outcrop, is predominantly oriented toward the south-southwest. This is not in agreement with the last ice-flow event the region experienced (230–250°; Hodder and Lian, 2024), but instead with the penultimate ice-flow event mapped across the region, toward the south-southwest (205–228°; Hodder and Lian, 2024), as evidenced by striations mapped on a protected face of the F.D. no. 5 pegmatite indicating a 212° ice-flow direction (Figure GS2025-19-4d). This new information was only observable with the LiDAR dataset and suggests that the penultimate ice-flow event was possibly more erosive compared to the last ice-flow event the BRGB experienced, which is important information to consider when interpreting sediment-landform relationships.

Future work

Ongoing work is focusing on 1:50 000 scale surficial geology mapping of the BRGB area. This mapping, along with till compositional studies and ice-flow mapping, will provide an updated framework for till prospecting in the region.

Economic considerations

Surficial geology maps provide important information on the distribution of sediments across a region and the processes that

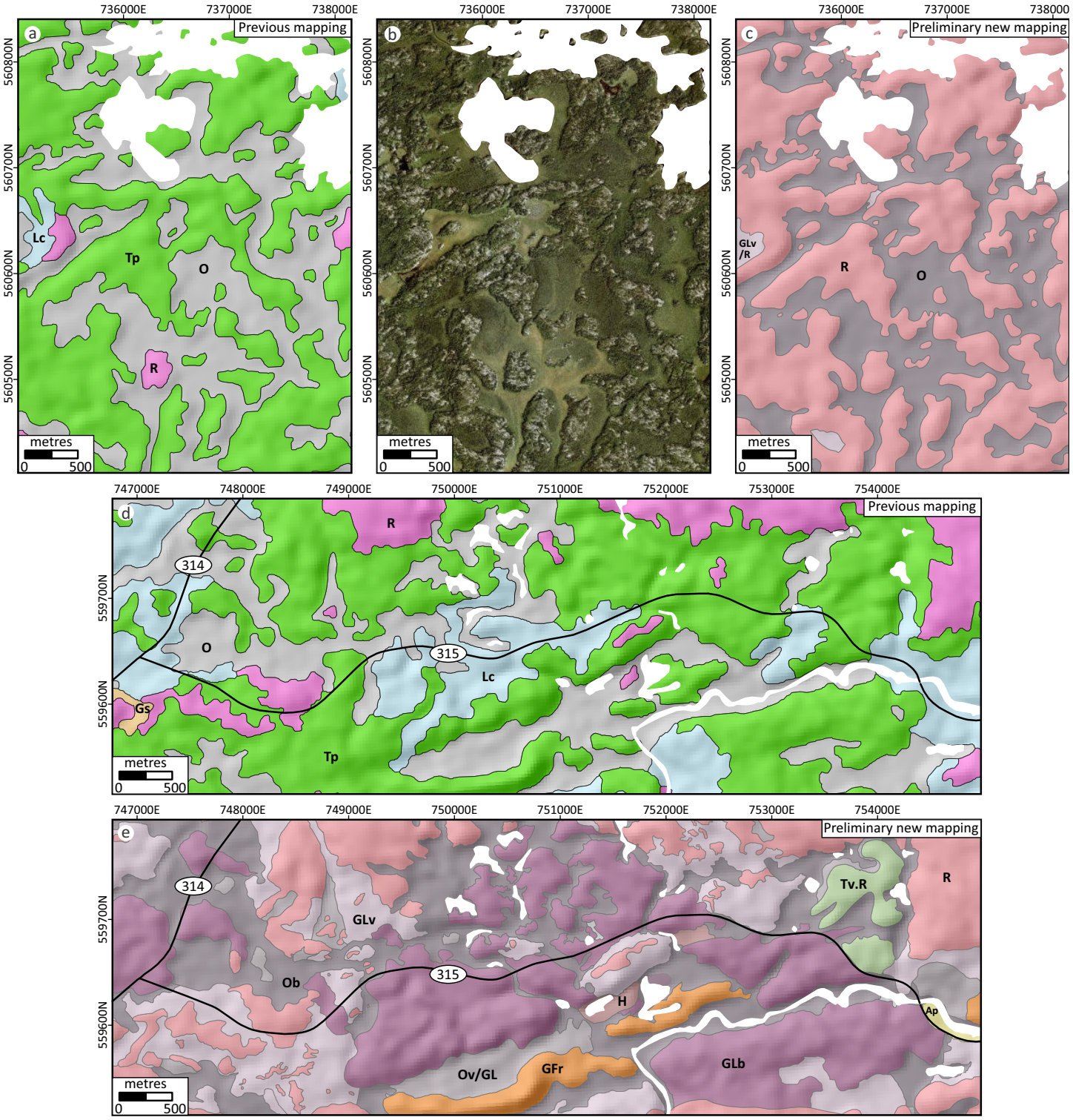

Figure GS2025-19-2: *Example of mapping in progress for this study and a comparison to previous mapping:* ***a)*** *previous 1:100 000 scale surficial geology mapping in the area (Mann, 2004b);* ***b)*** *aerial photograph of the mapping area with visible bedrock outcrops;* ***c)*** *preliminary new 1:50 000 scale surficial geology mapping of the area shown in (a) and (b);* ***d)*** *previous 1:100 000 scale surficial geology mapping in the area (Mann, 2004b);* ***e)*** *preliminary updated 1:50 000 scale surficial geology mapping of the area shown in (d). Basemap imagery in (b) was created using ArcGIS® software by Esri. ArcGIS® is the intellectual property of Esri and is used herein under license. Copyright © Esri. All rights reserved. For more information about Esri software please visit <https://esri.ca/>. Abbreviations: Ap, alluvial floodplain sediment; GFr, esker sediment; GL, glaciolacustrine deposit; GLb, glaciolacustrine blanket sediment; GLv, glaciolacustrine veneer sediment; Gs, subaqueous outwash; H, anthropogenic deposit; Lc, lacustrine clay to silty clay; O, organic deposit; Ob, organic blanket deposit; Ov, organic veneer deposit; R, bedrock; Tp, discontinuous till and associated glaciofluvial sediment, predominantly derived from igneous and metamorphic rocks; Tv.R, till veneer deposit and bedrock.*

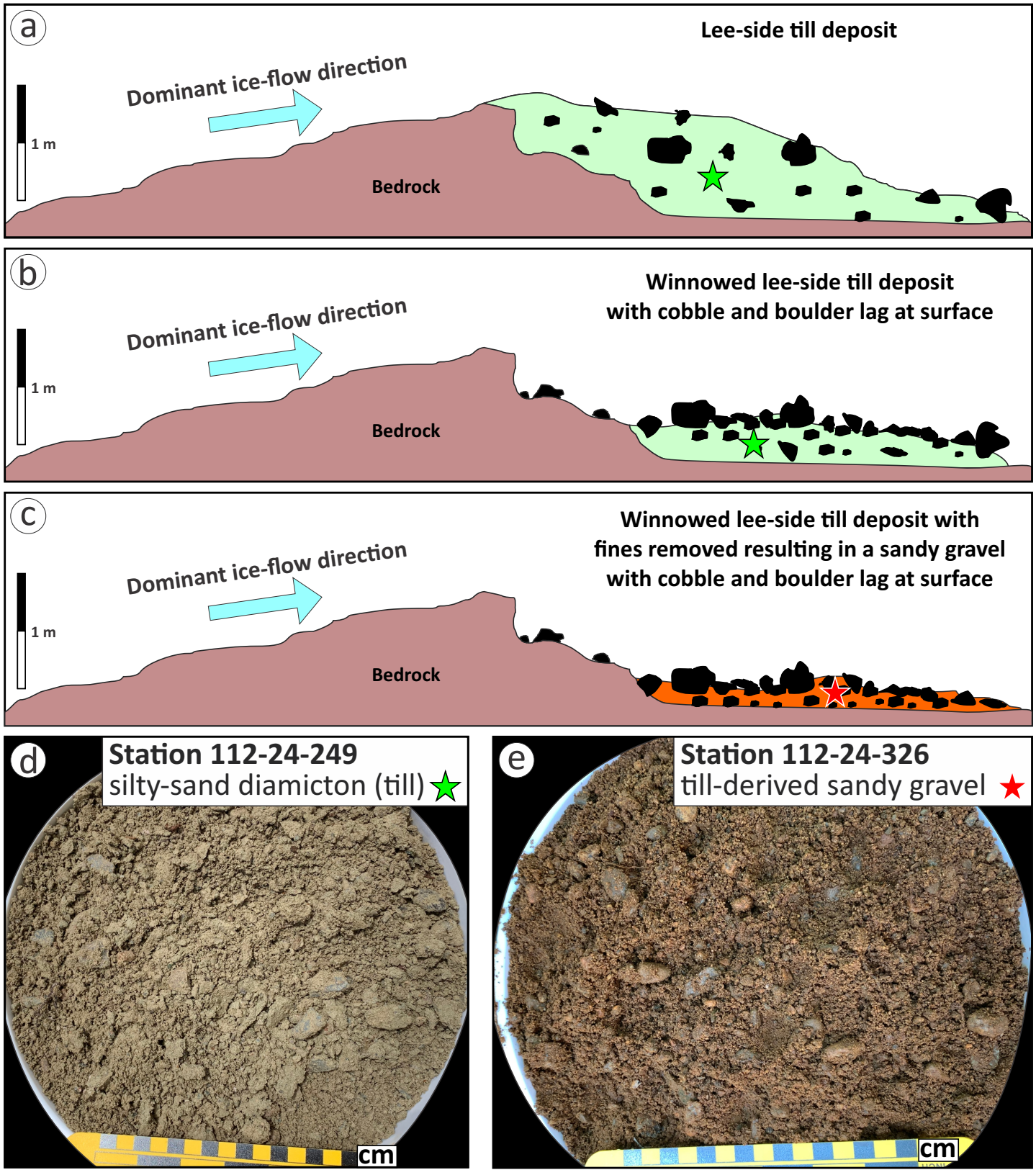

Figure GS2025-19-3: *Schematic of lee-side sediment deposits and sediment examples:* ***a)*** *unmodified lee-side till deposit;* ***b)*** *lee-side till deposit that has been winnowed by glaciolacustrine processes and is now cladded by an extensive cobble and boulder lag at surface;* ***c)*** *lee-side till deposit that has been winnowed by glaciolacustrine processes to the point that fines have been removed and a sandy gravel cladded by an extensive cobble and boulder lag at surface remains;* ***d)*** *example of till uncovered beneath the lag in the geological setting depicted in (b);* ***e)*** *example of a sandy gravel uncovered beneath the lag in the geological setting depicted in (c).*

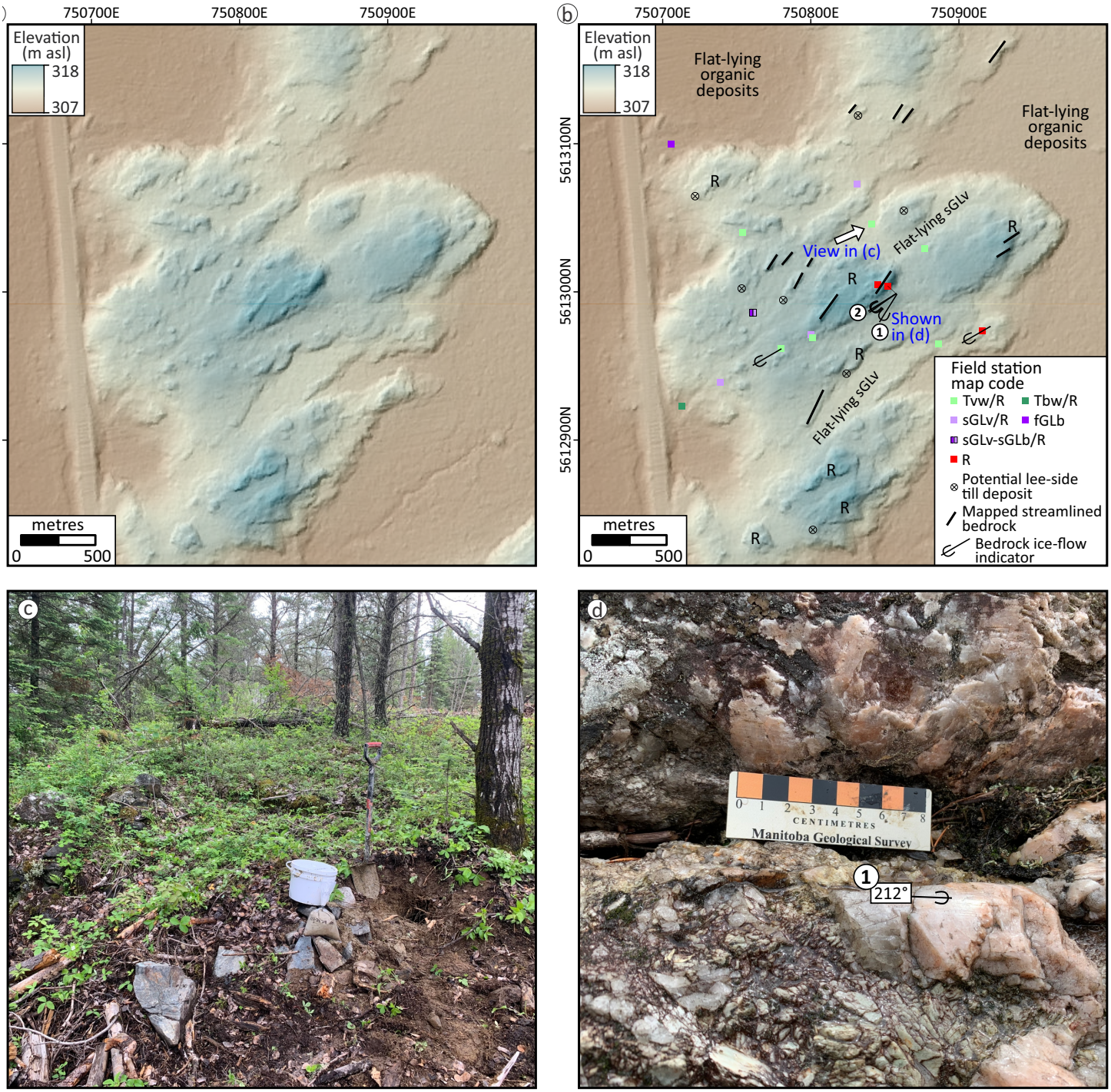

Figure GS2025-19-4: *Imagery and photographs of the F.D. no. 5 pegmatite area:* ***a)*** *light detection and ranging (LiDAR) imagery;* ***b)*** *annotated LiDAR imagery of the area with field stations and potential lee-side till deposits identified;* ***c)*** *lee-side till deposit in the area;* ***d)*** *fine striations oriented toward 212° on a protected face of the F.D. no. 5 outcrop. Background LiDAR-derived digital elevation model imagery from New Age Metals Inc. (unpublished data, 2025). Abbreviations: fGLb, fine-grained glaciolacustrine blanket sediment; sGLb, sandy glaciolacustrine blanket sediment; sGLV, sandy glaciolacustrine veneer sediment; R, bedrock; Tbw, till blanket sediment, winnowed; Tvw, till veneer sediment, winnowed.*

deposited these sediments. When combined with a better understanding of the direction(s), timing and nature of major and minor ice-flow events in the region, the surficial geology maps provide an updated framework for till prospecting in the Bird River greenstone belt area. Till indicator-mineral and matrix geochemistry datasets collected during this study provide information on the mineral potential across the region and the dispersal signature from known deposits is also being investigated. These datasets can be used to facilitate mineral exploration across the region.

Acknowledgments

The authors thank A. Martin for mapping support throughout this project. Logistical support from C. Epp, E. Ralph and

P. Belanger is appreciated. M.S. Gauthier is thanked for field assistance and discussions in 2025. The authors thank V.L. Markstrom and M.S. Gauthier for their reviews of this report.

References

Deblonde, C., Campbell, J.E., Chow, W., Cocking, R.B., Huntley, D.H., Parent, M., Rice, J.M., Robertson, L., Smith, I.R., Weatherston, A. and Zawadzka, K. 2024: Surficial Data Model: the science language of the integrated Geological Survey of Canada data model for surficial geology maps; Geological Survey of Canada, Open File 8236, ver. 2.5.1, 1 .zip file.

Fisher, T.G. and Breckenridge, A. 2022: Relative lake level reconstructions for glacial Lake Agassiz spanning the Herman to Campbell levels; Quaternary Science Reviews, v. 294, art. 107760, URL <https://doi.org/10.1016/j.quascirev.2022.107760>.

Henderson, P.J. and Way Nee, V.J. 1998: Surficial geology, Bissett, Manitoba; Geological Survey of Canada, Map 1897A, scale 1:50 000.

Hodder, T.J. and Lian, O.B. 2024: Reconnaissance-scale Quaternary geology investigations to support lithium exploration in southeastern Manitoba (parts of NTS 52L, M, 62P, 63A); *in* Report of Activities 2024, Manitoba Economic Development, Investment, Trade and Natural Resources, Manitoba Geological Survey, p. 200–208.

Hodder, T.J. and Martins, T. 2023: Current Quaternary geology investigations in southeastern Manitoba and implications for mineral exploration (parts of NTS 52L, 62P, 63A); *in* Report of Activities 2023, Manitoba Economic Development, Investment, Trade and Natural Resources, Manitoba Geological Survey, p. 105–119.

Mann, J.D. 2004a: Surficial geology, Big Whiteshell Lake, Manitoba–Ontario; Geological Survey of Canada, Map 2054A and Manitoba Industry, Economic Development and Mines, Manitoba Geological Survey, Geoscientific Map MAP2003-6, scale 1:100 000.

Mann, J.D. 2004b: Surficial geology, Nopiming, Manitoba–Ontario; Geological Survey of Canada, Map 2051A and Manitoba Industry, Economic Development and Mines, Manitoba Geological Survey, Geoscientific Map MAP2003-3, scale 1:100 000.

Martins, T., Rinne, M.L., Breasley, C. and Adediran, H. 2023: Preliminary results from field investigations in the Bird River domain of the Archean Superior province, Manitoba (parts of NTS 52L5, 6, 11, 12); *in* Report of Activities 2023, Manitoba Economic Development, Investment, Trade and Natural Resources, Manitoba Geological Survey, p. 4–13.

Matile, G.L.D. and Fulton, R.J. 1994: Southern prairies NATMAP, a progress report (NTS 62F, 62H); *in* Report of Activities 1994, Manitoba Energy and Mines, Geological Services, p. 182–183.

Matile, G.L.D. and Keller, G.R. 2004: Surficial geology of southern Manitoba (south of 53°); Manitoba Industry, Economic Development and Mines, Manitoba Geological Survey, Surficial Geology Compilation Map SG-SMB, scale 1:500 000.

Matile, G.L.D. and Keller, G.R. 2007: Surficial geology of Manitoba; Manitoba Science, Technology, Energy and Mines, Manitoba Geological Survey, Surficial Geology Compilation Map SG-MB, scale 1:1 000 000.

Matile, G.L.D., Thorleifson, L.H., Grant, N., Burt, A. and Mann, J. 1998: Geology of the Winnipeg region NATMAP project (NTS 62H/W, 62I and 52L/W); *in* Report of Activities 1998, Manitoba Energy and Mines, Geological Services, p. 161–171.

Matile, G.L.D., Thorleifson, L.H., Martin, A.B. and Hodder, T.J. 2023: Quaternary field site data collected during the 1997–1998 NATMAP field seasons, southeastern Manitoba (parts of NTS 52L, 62H, I); Manitoba Economic Development, Investment, Trade and Natural Resources, Manitoba Geological Survey, Data Repository Item DRI2023010, Microsoft® Excel® file.

Natural Resources Canada 2025: Medium Resolution Digital Elevation Model; Natural Resources Canada, CanElevation Series, URL <https://open.canada.ca/data/en/dataset/18752265-bda3-498c-a4ba-9dfe68cb98da> [July 2025].

Thorleifson, L.H. 1996: Review of Lake Agassiz history; *in* Sedimentology, Geomorphology and History of the Central Lake Agassiz Basin, J.T. Teller, L.H. Thorleifson, G.L.D. Matile and W.C. Brisbin (ed.), Geological Association of Canada–Mineralogical Association of Canada, Joint Annual Meeting, May 27–29, 1996, Winnipeg, Manitoba, Field Trip Guidebook B2, p. 55–84.

GS2025-20

Complex Quaternary geology around Grunthal, south-central Manitoba (parts of NTS 62H7)

by M.S. Gauthier

Summary

Herein, the stratigraphy from several representative gravel pits near Grunthal, Manitoba, is described. The subtill 'buried' granular-aggregate deposits in the two studied pits were likely deposited as proglacial outwash, at fluctuating distances from the ice margin. Timing of deposition is still questionable, as the granular aggregates were likely deposited during ice-margin retreat in an earlier interstadial and/or interglacial period(s). Current data suggest there is no obvious link between gravel or till composition and provenance, and deposits were likely formed in complex environments by water and ice flowing from the northwest, north and northeast.

In Brief:

- Buried gravel in the Grunthal area was deposited during pre-Holocene ice-margin retreat
- There may have been multiple phases of deposition

Citation:
Gauthier, M.S. 2025: Complex Quaternary geology around Grunthal, south-central Manitoba (parts of NTS 62H7); *in* Report of Activities 2025, Manitoba Business, Mining, Trade and Job Creation, Manitoba Geological Survey, p. 181–190.

Introduction

In south-central Manitoba, near Grunthal (Figure GS2025-20-1), there are significant economic granular-aggregate deposits. These deposits have been mapped as both kame-deltas deposited in proglacial Lake Agassiz (Fenton, 1974; Thorleifson and Matile, 1993) or within an older proglacial lake formed during the penultimate retreat of ice (Matile and Conley, 1979), or as eskers (Matile and Conley, 1979; C.R. Harington, G.A. Young, A. Telka and G.L.D. Matile, unpublished poster, 2007). Interestingly, the deposits do not have a topographic expression, making it difficult to map the lateral extent of existing deposits, and to predict the location of additional aggregate resources (Gauthier and Rentz, 2024; Marks and Rentz, 2024; Rentz et al., 2024).

According to local aggregate producers around Grunthal, diamict (~0–5 m thick) regionally drapes gravel or sand (~0–30 m thick; C.R. Harington, G.A. Young, A. Telka and G.L.D. Matile, unpublished poster, 2007). The diamict cover, if interpreted as till, would suggest that the granular-aggregate deposits were formed either under the ice, or were buried by subsequent deposition of sediment by ice; and hence they are older than the Holocene deglaciation. Interestingly, mammal fossils and spruce wood have been extracted below the water level, from an unknown source or sources (Nielsen and Matile, 2002; C.R. Harington, G.A. Young, A. Telka and G.L.D. Matile, unpublished poster, 2007), which further questions the formation and age(s) of these deposits.

Herein, the stratigraphy from several representative gravel pits near Grunthal is described. The goal is to evaluate whether the buried granular-aggregate deposits are of the same formation and age, and hence whether it's possible to better map these buried deposits.

Previous work

A Quaternary stratigraphic framework for southeastern Manitoba was initially developed by Fenton (1974). This framework consisted of four laterally discontinuous tills that were identified at surface; initially interpreted to represent one southwest-trending advance of ice from the Quebec–Labrador sector of the Laurentide Ice Sheet (LIS), and three southeast-trending advances and readvances of ice from the Keewatin sector of the LIS during the last glacial period (Fenton, 1974; Teller and Fenton, 1980). Recent stratigraphic study of the Roseau River area, 23 km to the south of Grunthal, confirmed the advance and retreat of ice along the southern margin of the LIS during the last interstadial (Gauthier et al., 2025). There, sands were deposited in both fluvial and shallow ice-marginal lake (glacial Lake Vita) environments, prior to the more significant advance of ice sometime after 30.4 ±2.3 ka. As such, the study area was glaciated at least twice during the last glacial cycle with ice-free conditions during parts of interstadial Marine Isotope Stage 3 (57–29 ka). It should be noted that the above history accounts for just ~11 m of the 70–90 m of Quaternary sediments in the region (Keller and Matile, 2021).

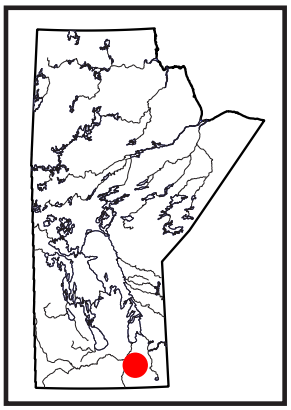

Plausible depositional environments for granular-aggregate deposition

To evaluate whether the buried granular-aggregate deposits near Grunthal are correlative, first, the depositional environment(s) in which they formed in needs to be determined, as well as their

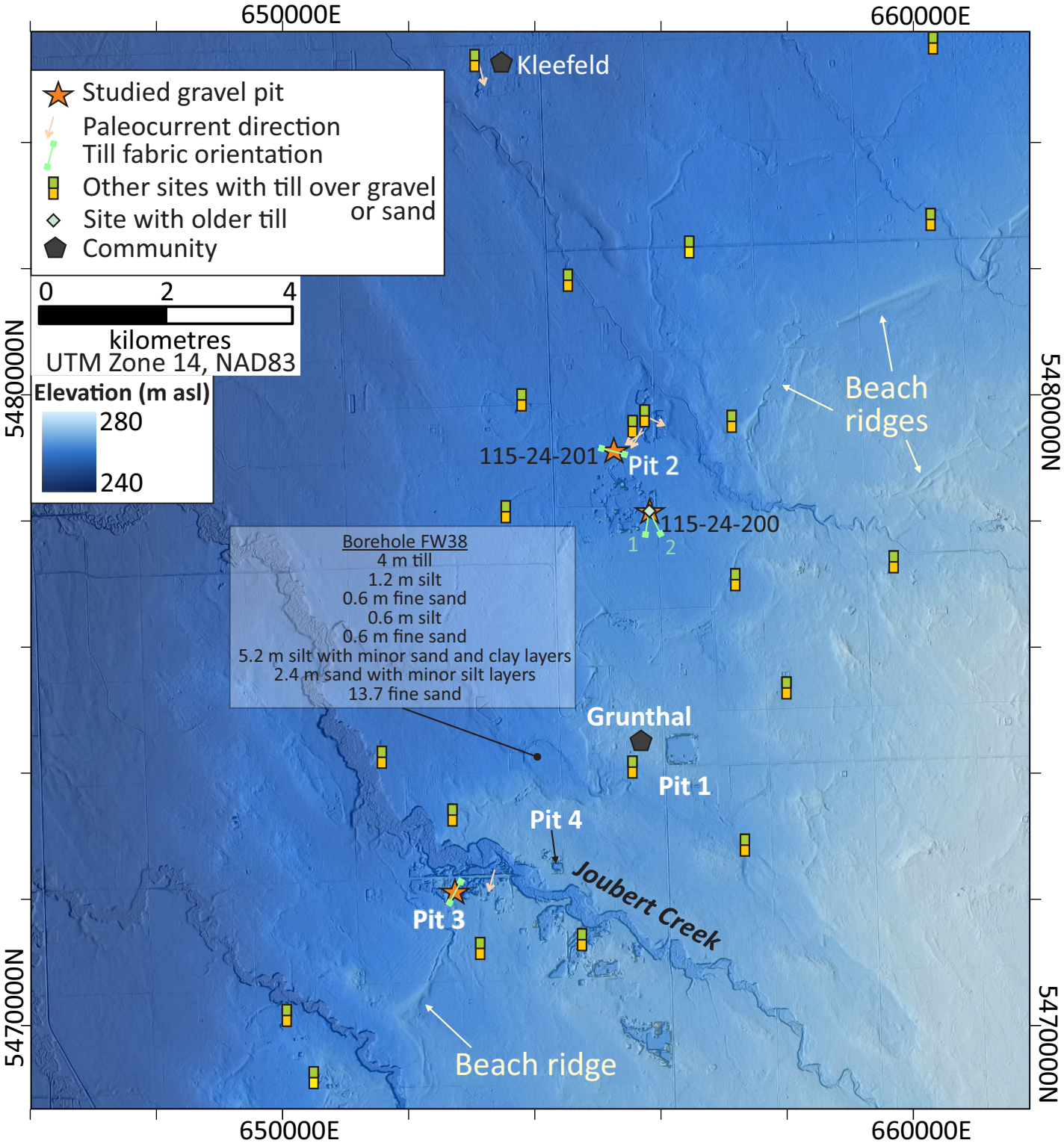

Figure GS2025-20-1: *The area around the town of Grunthal, south-central Manitoba, includes at least eight aggregate pits in deposits that have no topographic relief—only studied pits are labelled. Northeast-trending beach ridges separate the upper sand and till landscape (to the southeast) from the lower glaciolacustrine clay landscape (to the northwest). The background hillshade is derived from light detection and ranging (LiDAR) imagery (Manitoba Government, 2020). Borehole data is from Fenton (1974).*

stratigraphic relationships to other Quaternary sediments. The majority of the granular aggregate in Manitoba is from sediments that were deposited within environments related to the glaciers that crossed the province (James F. MacLaren Limited, 1980). In general, granular-aggregate deposits are formed either in front of a glacier, as proglacial fluvial outwash or proglacial lacustrine sediment, or under the glacier, as subglacial glaciofluvial sediment.

The distance from the ice margin affected the sediment supply and presumably flow rate as well; meaning that deposits with higher proportions of gravel—especially coarser gravel—were likely deposited closer to the ice margin. Geology and sediment provenance also played a factor, as the softer Paleozoic and Mesozoic bedrock breaks down faster into smaller grain sizes than the harder Precambrian shield bedrock (Figure GS2025-20-2).

Study area

The Grunthal area, south-central Manitoba, lies between ~257 and 267 m asl and is situated just east of the low-lying (240 m asl) Red River valley of central Manitoba (Figure GS2025-20-1). The local rise in topography is due to the thickness of Quaternary sediment (40 to 60 m in this poorly studied area; Keller and Matile, 2021) and not bedrock topography. Eight major aggregate pits have no topographic expression (Figure GS2025-20-1), attesting to the buried nature of the deposits. Most of the study area is mapped as till covered by a thin veneer of glaciolacustrine and/or glaciofluvial sediments, or as fine- to medium-grained sand deposited in moderate to shallow levels of glacial Lake Agassiz (Matile, 2004). The study area was glaciated by the Red River ice stream during the end of the last glaciation (Matile and Conley, 1979; Dredge and Cowan, 1989; Patterson, 1997; Harris et al., 2020; Gauthier et al., 2022), and by ice of unknown source at least twice prior to that (Fenton, 1974; Matile et al., 2023a;

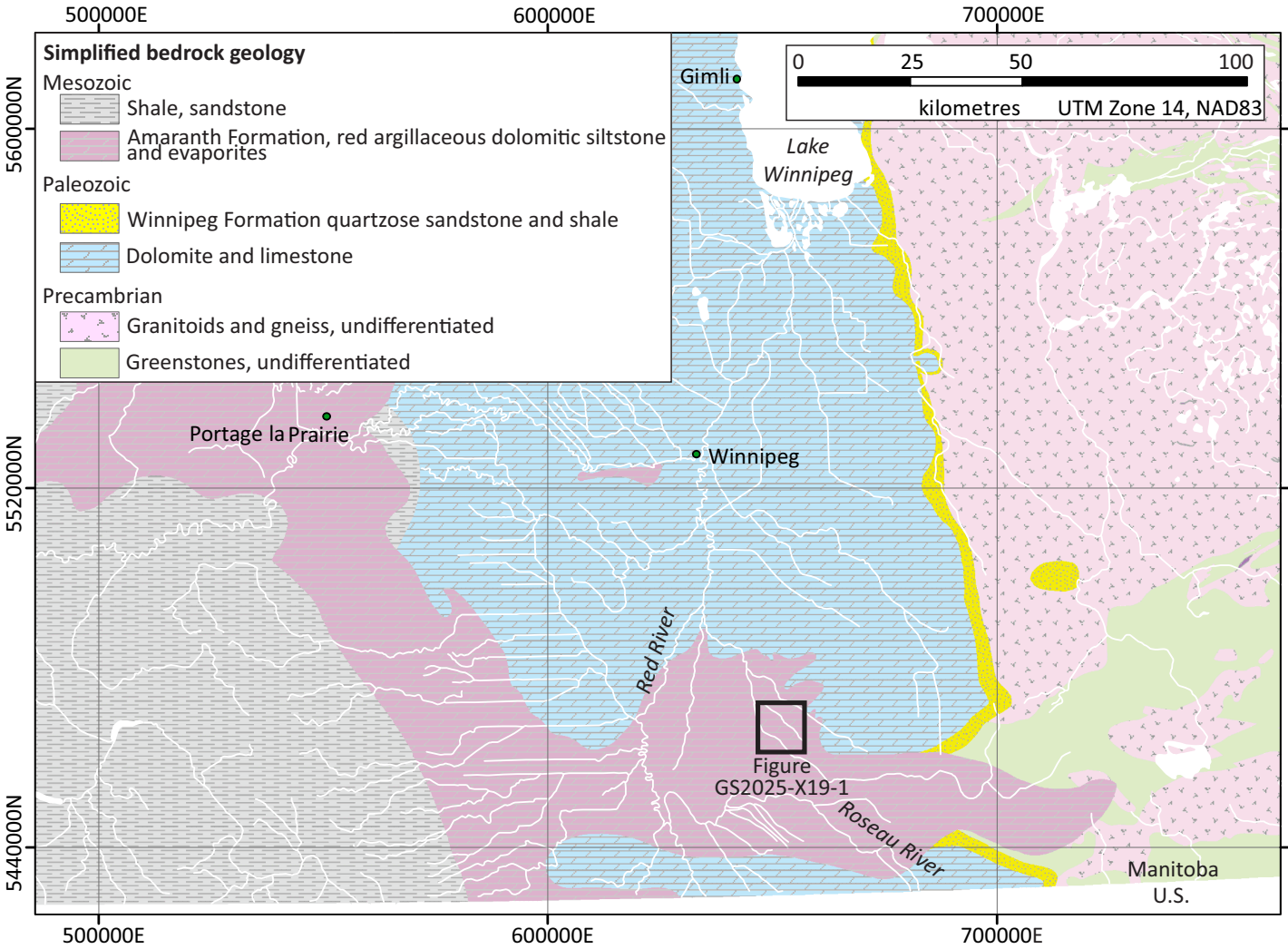

Figure GS2025-20-2: *Regional bedrock geology surrounding the study area (black square), modified from Manitoba Geological Survey (2024).*

Gauthier et al., 2025). The region was then covered by glacial Lake Agassiz, which formed beach ridges at the surface in higher areas and deposited clay in low-lying areas (Figure GS2025-20-1).

Methods

Two active gravel pits, north and southwest of Grunthal, Manitoba, were visited to investigate the Quaternary stratigraphy (pits 2 and 3; Figure GS2025-20-1). Lithofacies were defined based on texture, colour, sedimentary structures, clast content, stratigraphic position and the nature of contacts. Diamict and gravel samples were taken to compare with regional data (Thorleifson and Matile, 1993; Gauthier and Hodder, 2023). Clast-fabric measurements were conducted within the diamicts interpreted as tills, to determine the strain direction, which allows for an interpretation of the orientation of the ice flow that deposited the sediment (Holmes, 1941; Andrews and Smith, 1970). Fabric sites were chosen based on uniformity of diamict, where no sand lenses or discontinuous bedding was present. Clasts were carefully excavated and measured from within a 'box' consisting of three vertical faces of different orientations, over a maximum distance of 30 by 30 by 30 cm. Accepted clasts included in these analyses 1) were free to rotate in the matrix at the time of deposition (not clast supported or close to much larger clasts), 2) were rod-, tabular-rectangle– or wedge-shaped (ratio of the a:b axis was 1.5 or greater), 3) had a plunge of the a-axis less than 60° (average plunge of 18° with a standard deviation of 11°), and 4) had a plunge of the b-axis less than 60° (cf. Holmes, 1941). Clast-fabric data were represented graphically using Rockware® StereoStat v. 1.6.1. Ice-flow interpretations were assigned to the data based on stereonet patterns and rose-diagram patterns, in addition to the eigenvector of the largest eigenvalue or V_1 (Mark, 1974).

Results

Pit 1

The geology at this site is currently inaccessible, covered by colluvium or groundwater. According to a groundwater well record just north of the pit, the area consists of a till blanket (~1.5 m thick) over gravel (Manitoba Environment and Climate Change, unpublished data, 2025). A visit by the Manitoba Geological Survey (MGS) in 1979 noted "till that laterally transitions into or overlays interbedded and faulted fine-grained sand, coarse-grained sand and clay diamict" (site GM096; G.L.D. Matile and G.G. Conley, unpublished field notes associated with Matile and Conley, 1979).

Pit 2

The pit 2 area currently encompasses ~4.6 km^2 with several inactive and active pits (Figure GS2025-20-3). This study has identified four lithofacies at pit 2, ~3.3 km north of Grunthal, Manitoba (Figure GS2025-20-4). It must be noted, however, that the stratigraphic column represents a composite stratigraphy based on multiple exposures; the surface geology changes within as little as 200 m (Gauthier and Rentz, 2025[1]). The lowermost lithofacies (P2-A) is below groundwater. According to the pit operator in 2024, the dredged lithofacies contained ~12–24 m of sand and gravel (Figure GS2025-20-4a, b), with a few patchy 'clay' layers within that contained charcoal and wood. At several sites, P2-A is overlain by gravel or gravel and sand (up to ~2.5 m thick; lithofacies P2-B; Figure GS2025-20-4c, d). The gravel is poorly sorted, matrix to clast supported, and contains 40–90% fine pebble– to cobble-sized clasts in a medium- to very coarse grained sand matrix. Some clasts are striated, indicating a glacial origin. Lithofacies P2-B can be massive, and in one spot contains cross-beds, 0.8–1.0 m thick, that dip 18° to 232° and 26° to 210° (Figure GS2025-20-4c). A 0–2.7 m thick, laminated and overconsolidated diamict (lithofacies P2-C) overlies the gravel (Figure GS2025-20-4d, e). The diamict is light yellow–brown with a clayey–silty sand matrix and 15–20% clasts (Gauthier and Rentz, 2025). The clasts are granule to large cobble sized, sometimes faceted, and dominantly carbonate (74.8 ct. %; Figure GS2025-20-4f).

Lithofacies P2-C is interpreted as a subglacial traction till, based on the consolidated nature, texture, clast shape, clast fabric and lateral continuity (cf. Evans, 2018). A spread-unimodal clast fabric (S_1 = 0.66, n = 32) was measured from lithofacies P2-C and interpreted to have formed by west-northwest or east-southeast flowing ice (286–106°; Figure GS2025-20-4a; Gauthier and Rentz, 2025, Table 7.2). The high carbonate content suggests that ice flow was likely to the east-southeast (106°). The uppermost lithofacies (P2-D) is a 0.15–0.60 m thick sandy gravel to gravelly sand (site 115-24-201; Gauthier and Rentz, 2025).

Interestingly, there are two other diamicts interpreted as till in the pit 2 area at site 115-24-200 (Figure GS2025-20-3; Gauthier and Rentz, 2025*).* There, an upper (1.5 m thick) grey-brown till with a silty sand matrix and 5% clasts overlies a lower (>0.6 m thick) light olive–brown till with a clayey–sandy silt matrix and 5–10% clasts (Gauthier and Rentz, 2025). Both tills are highly overconsolidated and have a blocky and friable structure with oxidation staining along joints. These tills have measured clast fabrics interpreted to have been formed by ice flowing to the south-southeast (~158°) and south (~189°), respectively, and are relatively less calcareous (65.4–68.4 ct. % carbonate clasts; Gauthier and Rentz, 2025).

Pit 2 area preliminary interpretation

Pit 2 area consists of complex changes in surficial sediments over as little as 200 m (Figure GS2025-20-3). These changes

[1] MGS Data Repository Item DRI2025025, containing the data or other information sources used to compile this report, is available online to download free of charge at https://manitoba.ca/iem/info/library/downloads/index.html, or on request from minesinfo@gov.mb.ca, or by contacting the Resource Centre, Manitoba Business, Mining, Trade and Job Creation, 360-1395 Ellice Avenue, Winnipeg, Manitoba R3G 3P2, Canada.

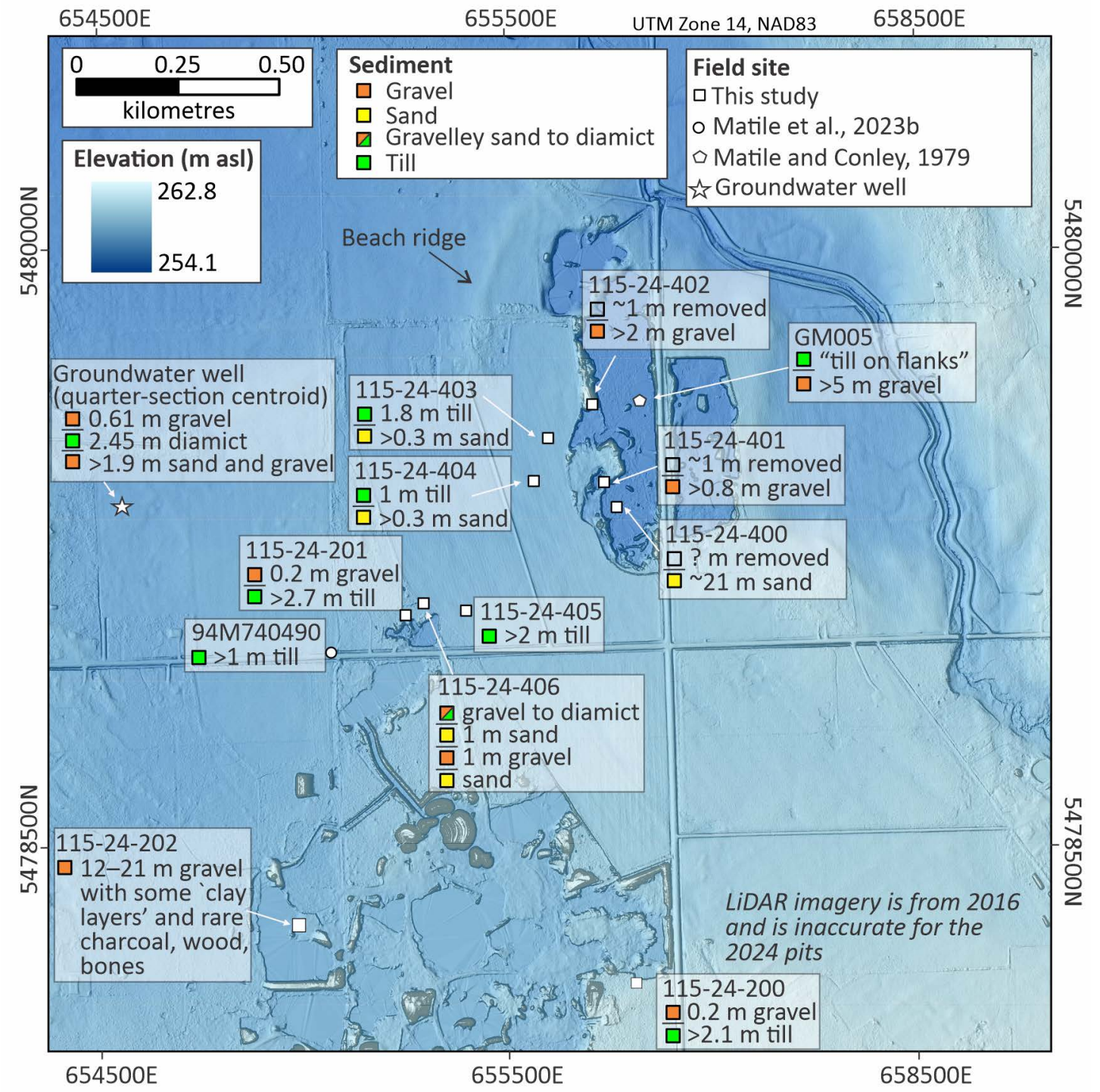

Figure GS2025-20-3: *Pit 2 area, ~3.3 km north of Grunthal, Manitoba, encompasses ~4.6 km² with complex surficial geology. Sites shown are from 2024 fieldwork (Gauthier and Rentz, 2025), historical data (Matile and Conley, 1979; Matile et al., 2023b) and groundwater well data (Manitoba Environment and Climate Change, unpublished data, 2025). The background hillshade is derived from light detection and ranging (LiDAR) imagery (Manitoba Government, 2020).*

have no topographic expression, suggesting that while glacial Lake Agassiz modified the surface (planed/denuded) it did not deposit sediments in the area. Instead, the landscape appears to be a patchy fragmented mosaic of whatever sediments were previously deposited. The composition of the pit 2 younger till is similar to that of the underlying gravel, perhaps signifying that the gravel has the same source as the till. In contrast, the paleo–ice-flow directions suggest different source areas for the till and gravel. Clearly, more work is needed to untangle the geological history of this area.

Pit 3

Pit 3, ~3.3 km southwest of Grunthal (Figure GS2025-20-1), was studied in the field in 2022 (sites 115-22-303 and 115-22-304,

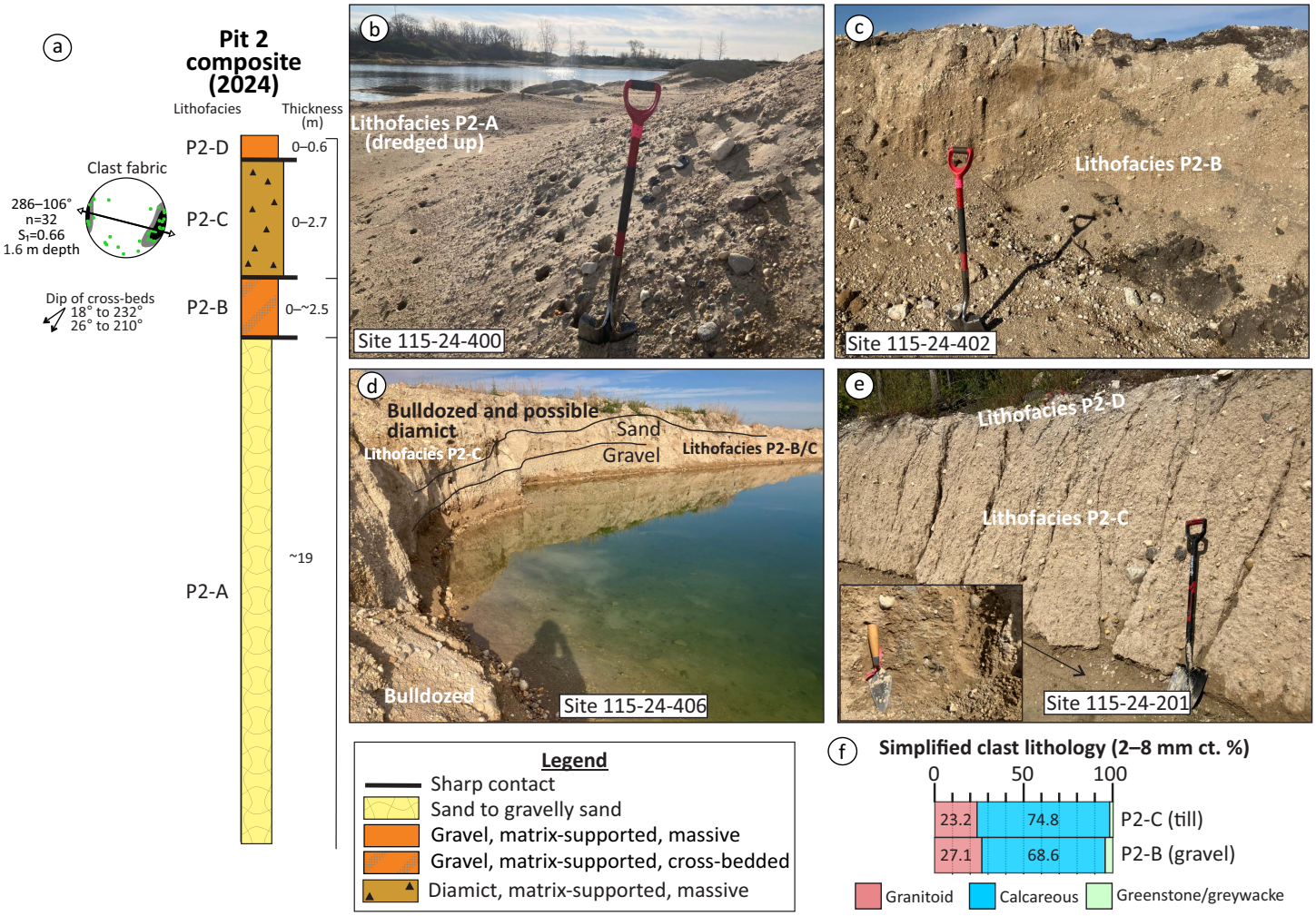

Figure GS2025-20-4: *Stratigraphic section showing the composite lithofacies for the pit 2 area* ***(a)****, which includes sand and gravel* ***(b)****, massive to cross-bedded gravel* ***(c, d)****, a calcareous diamict interpreted as a till* ***(e, f)*** *and a thin sandy gravel to gravelly sand (top of e).*

Gauthier and Hodder, 2023). This study has identified five lithofacies at pit 3 (Figure GS2025-20-5a). The lowermost lithofacies (P3-A) is a clast-supported, poorly sorted, imbricated, horizontal to chaotically bedded gravel, >5 m thick, with a fine-grained sand matrix and 40–60% subrounded to rounded clasts that are granule to large cobble sized (Figure GS2025-20-5b, c). According to the pit operator, lithofacies P3-A has a regionally variable thickness (0–30 m) and sporadically contains megafauna fossils. At the studied site, P3-A is overlain by a sand-filled channel, about 8 m wide and up to 2 m deep (lithofacies P3-B; Figure GS2025-20-5b). The sand is fine to medium grained and has beds 1–10 cm thick that drape the channel structure (Figure GS2025-20-5d). Overlying lithofacies P3-B is 0.3 m of clast-supported, poorly sorted gravel with a fine-grained sand matrix and 60% rounded to subrounded clasts that are granule to large cobble sized (lithofacies P3-C), similar to lithofacies P3-A (Figure GS2025-20-5d). The lower contact of lithofacies P3-C is sharp and undulatory. Preliminary analyses, from just one sample, show that the clasts are derived equally from the Precambrian shield (49%) and Paleozoic carbonate rocks (51%; Figure GS2025-20-5f). There are a few smaller sand-filled channels at similar elevations around the pit, though most of the pit exposes only gravel. A 1.25 m thick, laminated and overconsolidated diamict (lithofacies P3-D) overlies the gravel (Figure GS2025-20-5e). The diamict is light olive-brown with a silty sand matrix and 15% clasts (sample 115-22-304-A01, Gauthier and Hodder, 2023). The clasts are granule to medium pebble sized, sometimes faceted, and more calcareous than those within the underlying gravel (67.1 versus 50.6 ct. %; Figure GS2025-20-5f; Gauthier and Hodder, 2023).

Lithofacies P3-D is interpreted as a subglacial traction till, based on the consolidated nature, texture, clast shape, clast fabric and lateral continuity (cf. Evans, 2018). The lower contact with the gravel and sand is transitional over 0.3 m, indicating erosion and incorporation of the underlying unit into the till. A spread-unimodal clast fabric (S_1 = 0.67, n = 31) was measured from lithofacies P3-D and interpreted to have been formed by south-southwest flowing ice (~209°; Figure GS2025-20-5a; Gauthier and Hodder, 2023). The uppermost lithofacies (P3-E) exposed in the pit is a 0.25 m thick sandy soil that over-

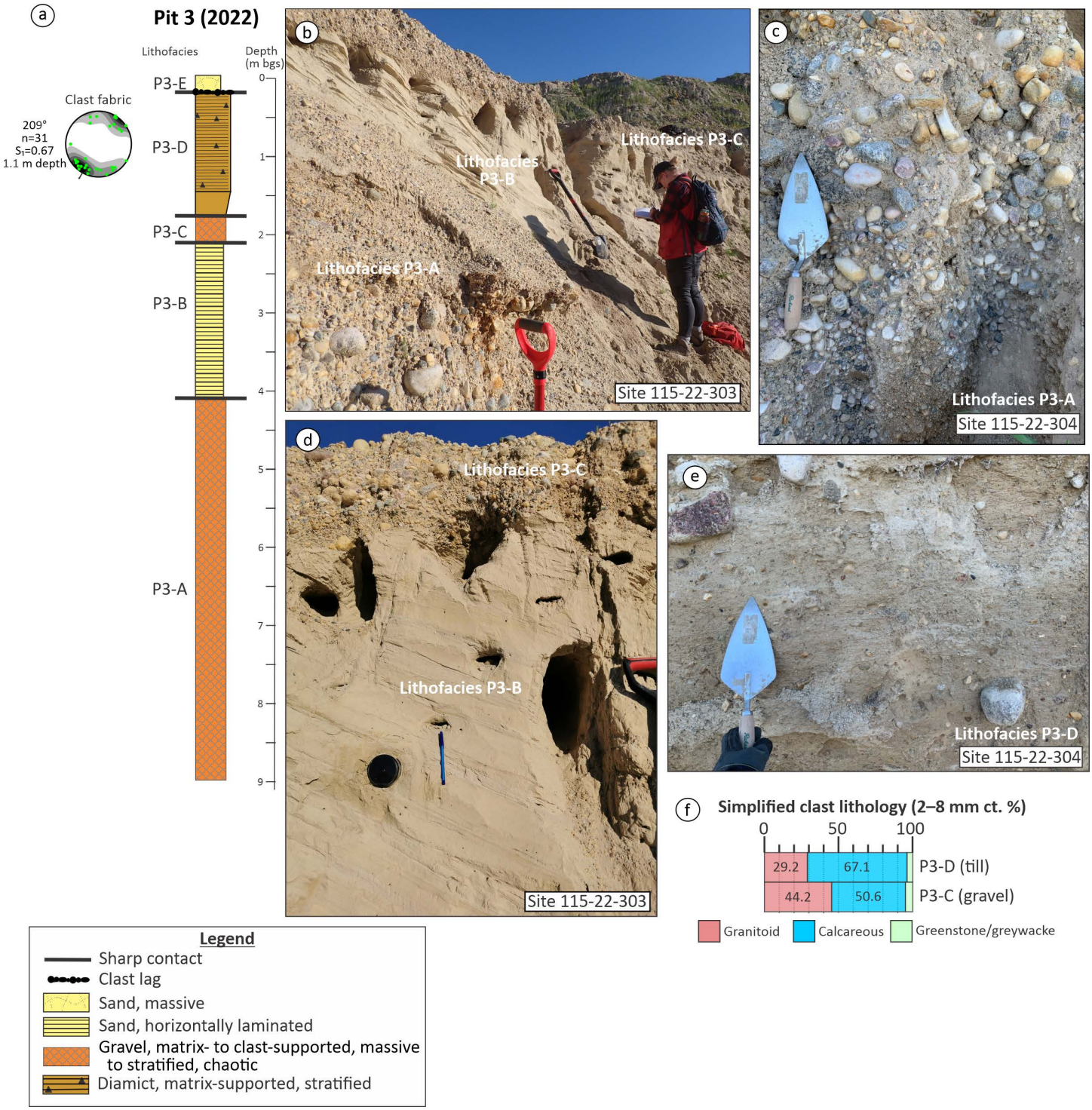

Figure GS2025-20-5: *Stratigraphic section* ***(a)*** *for Pit 3, ~3.3 km southwest of Grunthal, Manitoba, which exposes thick gravels* ***(b–d)****, with a sandy channel fill (b, d). The eastern side of the pit preserves the original surface, where laminated diamict* ***(e)*** *overlies gravel; the diamict is more calcareous than the gravel* ***(f)****. Details are in Gauthier and Hodder (2023, Appendices 1–8, sites 115-22-303 and 115-22-304). Abbreviation: bgs, below ground surface.*

lies a 0.05 m thick layer of clasts that vary from fine-pebble to large-cobble size (Gauthier and Hodder, 2023, Figure 24).

Pit 3 interpretation

The composition of the Pit 3 till is different than that of the underlying gravel. The elevated Precambrian shield clast concentration in the buried gravel suggests the source of this gravel was situated to the east or northeast (cf. Figure GS2025-20-2). The clast-supported, poorly sorted, subangular–subrounded, imbricated, horizontally to chaotically bedded nature of the gravel (sites 115-22-303 and 115-22-305) together with the mixed clast lithologies, requires a glacial source for the gravel. While these

near-surface subtill gravels have variably been attributed as esker sediments (C.R. Harington, G.A. Young, A. Telka and G.L.D. Matile, unpublished poster, 2007) or kame-delta sediments (Fenton, 1974), it is suggested the gravel was likely deposited as proglacial outwash during ice-margin retreat during an earlier interstadial or interglacial period.

Pit 4

The geology at this site is inaccessible, as it is an inactive and partially reclaimed pit. According to a groundwater well record just to the southeast, the area consists of a till plain (~4.0 m thick) over gravel (Manitoba Environment and Climate Change, unpublished data, 2025).

Other sites

A compilation of previous work shows at least seven additional sites in the study area where till overlies gravel or sand (G.L.D. Matile and G.G. Conley, unpublished field notes associated with Matile and Conley, 1979), and one borehole with till overlying >24 m of sorted sediments (Figure GS2025-20-1; Fenton, 1974, FW38). Subtill sediments vary over short distances; dominantly sand to gravelly sand to gravel, well to poorly sorted and clast to matrix supported. Three sites expose crossbeds, with an apparent dip of 16° towards 196° near pit 3 (Figure GS2025-20-6), towards 130° near pit 2 (historical site GM005, Matile and Conley, 1979), and towards 170° near Kleefeld (historical site GM003, Matile and Conley, 1979; Figure GS2025-20-1). An additional borehole, ~7 km east-northeast of Grunthal, encountered 4 m of fine sand over 8.5 m of clay, 1.8 m of till, 2.7 m of silt, 1.5 m of sand and another 7.3 m of till (site FW39, Fenton, 1974). It should be stressed that till does not always overlie the presumably older sorted sediments; they are sometimes at surface in both the Grunthal and Roseau River areas (Gauthier and Hodder, 2023; Gauthier et al., 2025).

Regional boreholes

Two rotosonic boreholes drilled in the 1990s, ~13 km south and ~15 km southeast of Grunthal, encountered 68–70 m of Quaternary sediments overlying bedrock (drillholes Q and R, originally discussed in Thorleifson and Matile [1993] with data and stratigraphy released in Matile et al. [2023a]). These boreholes drilled into approximately four different diamict packages, interpreted as tills, separated by proglacial or nonglacial lacustrine, pond or fluvial sediments. In those two spots, sand was encountered below till at 10.5 and 19 m, respectively, whereas gravel was not encountered. Thus, while the correlation to the Grunthal gravel(s) is uncertain, it's clear the study area has a depositional record that spans multiple glacial-interglacial cycles.

Figure GS2025-20-6: *This aggregate pit wall exposes 4 m of gravelly sand, the lower half of which is cross-bedded (dip indicated by black arrow); situated just east of Pit 3 (Figure GS2025-20-1).*

Discussion

The buried granular-aggregate deposits near Grunthal have variably been attributed as Holocene (Fenton, 1974; Thorleifson and Matile, 1993) or older (Matile and Conley, 1979) kame-delta sediments and/or Late Wisconsin or older esker sediments (Matile and Conley, 1979; C.R. Harington, G.A. Young, A. Telka and G.L.D. Matile, unpublished poster, 2007). The clast-supported, poorly sorted, subangular–subrounded, imbricated, horizontally to chaotically bedded nature of the gravels, together with the mixed clast lithologies, confirm a glacial source(s) for the gravel. Spatially variable changes in matrix support, sorting and rounding of clasts likely reflects varying distances of deposition from the ice margin, and variable re-entrainment of sediments, allowing for the possibility of multiple granular deposits from different environments of deposition. Any faunal evidence (e.g., C.R. Harington, G.A. Young, A. Telka and G.L.D. Matile, unpublished poster, 2007) favours a proglacial, rather than subglacial, source—unless the fossils are badly weathered and clearly travelled. The more fossils found, the more likely they are to be in situ or near to that.

Timing of deposition is still questionable, as the granular aggregates were likely deposited during ice-margin retreat in an earlier interstadial and/or interglacial period(s).

Provenance of deposits?

As previous work confirms, there are multiple patchy fragmented tills at surface (Fenton, 1974; Teller and Fenton, 1980; Gauthier and Hodder, 2023), and it's unclear how many different near-surface buried granular-aggregate deposits there are. Theoretically, the lower the carbonate clast concentration, the higher likelihood of an eastern or northeastern provenance, where Precambrian rocks outcrop (45–48 km east to northeast of Grunthal; Figure GS2025-20-2; Manitoba Geological Survey, 2024). The clast fabrics measured on tills herein are interpreted to suggest ice flowed to the east-southeast (pit 2, overconsolidated), south-southwest (pit 3) and south-southeast and south (pit 2, very overconsolidated and stained). There is no clear correlation with till-carbonate content, much as reported in Gauthier and Hodder (2023, Figure 7) where surface tills contain between 60.4 and 96.2 ct. % Paleozoic clasts. The five paleocurrent measurements from granular deposits suggest glacial meltwater similarly flowed to the south, southwest and possibly southeast. Interestingly, the gravels where paleocurrent flow was to the southwest (pit 2) do not have the highest Precambrian shield clast concentration measured (31.4 ct. % versus 49.4 ct. % at pit 3). As such, paleocurrent and paleo–ice-flow directional data suggest that both the tills and the gravels contain a mix of compositions, with no obvious correlation to source. As such, the specific source of granular aggregate is still questionable; likely reflecting re-entrainment of previously deposited sediments combined with distally derived sediment by water and ice flowing from the northwest, north and northeast.

Future work

Surficial mapping studies that incorporate new field observations, legacy datasets and high-resolution LiDAR elevation models are needed to better understand the type, genesis and relative age of surface and near-surface sediments. Chronological studies that consider the age(s) of these deposits, such as optical or radiocarbon dating, are also necessary. This will be essential for the discovery of new buried aggregate deposits in the area.

Economic considerations

Granular aggregate is a vital part of Manitoba's economy, as it provides essential materials for the construction and maintenance of Manitoba's infrastructure. With the increasing scarcity of aggregate resources in south-central Manitoba, it is imperative to be able to effectively identify and map the buried extent of shallow-buried aggregate resources. The Grunthal area contains high-quality reserves of granular aggregate of unknown extent. Understanding the geological origin of these known deposits is the first step to be able to effectively identify and map the extent of new granular-aggregate deposits.

Acknowledgments

The author thanks C. Epp and P. Benger for help sorting samples at the Manitoba Geological Survey Midland Sample and Core Library, and R. Boychecko for allowing the collection of samples from the aggregate pits. J. Janssens is thanked for assistance in identifying and counting till-sample clasts.

References

Andrews, J.T. and Smith, D.I. 1970: Statistical analysis of till fabric: methodology, local and regional variability (with particular reference to the north Yorkshire till cliffs); Quarterly Journal of the Geological Society of London, v. 125, p. 503–542.

Dredge, L.A. and Cowan, W.R. 1989: Quaternary geology of the southwestern Canadian Shield; *in* Quaternary Geology of Canada and Greenland, R.J. Fulton (ed.), Geological Survey of Canada, Geology of Canada, no. 1, p. 214–248.

Evans, D.J.A. 2018: Till: A Glacial Process Sedimentology; John Wiley & Sons Ltd, Chichester, United Kingdom, 390 p.

Fenton, M.M. 1974: The Quaternary stratigraphy of a portion of southeastern Manitoba, Canada; Ph.D. thesis, Western University, London, Ontario, 793 p.

Gauthier, M.S. and Hodder, T.J. 2023: Quaternary site data, till composition and ice-flow indicators in the Roseau River area, southeastern Manitoba (parts of NTS 62H2, 7); Manitoba Economic Development, Investment, Trade and Natural Resources, Manitoba Geological Survey, Open File OF2023-3, 10 p., 8 appendices.

Gauthier, M.S. and Rentz, J. 2024: 2023 aggregate field visits: Quaternary site data, composition, and ice-flow indicators from gravel pits in southern Manitoba (parts of NTS 62H15, I13, P5); Manitoba Economic Development, Investment, Trade and Natural Resources, Manitoba Geological Survey, Data Repository Item DRI2024007, Microsoft® Excel® file, 1 appendix.

Gauthier, M.S. and Rentz, J. 2025: 2024 granular-aggregate field visits—Quaternary site data, sample composition and ice-flow indicators—in southern Manitoba (parts of NTS 62H7, 10, 15, 16, 62I2, 6); Manitoba Business, Mining, Trade and Job Creation, Manitoba Geological Survey, Data Repository Item DRI2025025, Microsoft® Excel® file, 2 appendices.

Gauthier, M.S., Breckenridge, A. and Hodder, T.J. 2022: Patterns of ice recession and ice stream activity for the MIS 2 Laurentide Ice Sheet in Manitoba, Canada; Boreas, v. 51, no. 2, p. 274–298.

Gauthier, M.S., Hodder, T.J., Dalton, A.S., Brewer, V., Lian, O.B., Finkelstein, S.A., Schaarschmidt, M. and Merghetti, A. 2025: South-central Laurentide Ice Sheet dynamics and the formation of proglacial Lake Vita during MIS 3; Quaternary Research, v. 123, p. 83–105.

Harris, K.L., Manz, L. and Lusardi, B.A. 2020: Quaternary stratigraphic nomenclature, Red River valley, North Dakota and Minnesota: an update; North Dakota Geological Survey, Miscellaneous Series No. 95, 249 p.

Holmes, C.D. 1941: Till fabric; Geological Society of America Bulletin, v. 52, p. 1299–1354.

James F. MacLaren Limited 1980: Mineral aggregate study of the southern Interlake region, volume 1; Manitoba Department of Energy and Mines, Mineral Resources Division, Open File 80-2, 51 p., 21 maps, 7 appendices

Keller, G.R. and Matile, G.L.D. 2021: Drift thickness of southern Manitoba; Manitoba Agriculture and Resource Development, Manitoba Geological Survey, Geoscientific Map MAP2021-2, scale 1:1 000 000.

Manitoba Geological Survey 2024: Bedrock geology of Manitoba; Manitoba Economic Development, Investment, Trade and Natural Resources, Manitoba Geological Survey, Open File OF2024-4, scale 1:1 000 000.

Manitoba Government 2020: Southern Manitoba LiDAR data; Manitoba Government, URL <https://mli.gov.mb.ca/dems/index_external_lidar.html> [January 2020].

Mark, D.M. 1974: On the interpretation of till fabrics; Geology, v. 2, no. 2, p. 101–104.

Marks, J. and Rentz, J. 2024: Preliminary results of a multi-electrode resistivity survey of a buried gravel deposit in the Rural Municipality of Taché, southeastern Manitoba (part of NTS 62H15); *in* Report of Activities 2024, Manitoba Economic Development, Investment, Trade and Natural Resources, Manitoba Geological Survey, p. 226–232.

Matile, G.L.D. 2004: Surficial geology, Sandilands, Manitoba; Geological Survey of Canada, Map 2059A, and Manitoba Industry, Economic Development and Mines, Manitoba Geological Survey, Geoscientific Map MAP2003-11, scale 1:100 000.

Matile, G.L.D. and Conley, G.G. 1979: Quaternary geology and sand and gravel resources of the Rural Municipality of Hanover; Manitoba Department of Energy and Mines, Mineral Resources Division, Aggregate Report AR80-4, scale 1:50 000.

Matile, G.L.D., Thorleifson, H.L. and Gauthier, M.S. 2023a: Rotosonic borehole stratigraphy, southeast Manitoba (parts of NTS 52E west and 62H east); Manitoba Economic Development, Investment and Trade, Manitoba Geological Survey, DRI2023005, Microsoft® Excel® file.

Matile, G.L.D., Thorleifson, H.L., Martin, A.B. and Hodder, T.J. 2023b: Quaternary field site data collected during the 1993–1994 NATMAP field seasons, southeastern Manitoba (parts of NTS 52E, 62A, H); Manitoba Economic Development, Investment, Trade and Natural Resources, Manitoba Geological Survey, Data Repository Item DRI2023009, Microsoft® Excel® file.

Nielsen, E. and Matile, G.L.D. 2002: Quaternary geology of southeastern Manitoba; *in* Institute on Lake Superior Geology: Proceedings, 2002, Institute on Lake Superior Geology, 48th Annual Meeting, May 12–16, 2002, Kenora, Ontario, v. 48, pt. 2, p. 23–35.

Patterson, C.J. 1997: Southern Laurentide ice lobes were created by ice streams: Des Moines Lobe in Minnesota, USA; Sedimentary Geology, v. 111, no. 1–4, p. 249–261.

Rentz, J., Marks, J., Frederiksen, A. and Guerard, R. 2024: Geophysical imaging of a buried gravel deposit in the Rural Municipality of Taché, southeastern Manitoba (part of NTS 62H15); *in* Report of Activities 2024, Manitoba Economic Development, Investment, Trade and Natural Resources, Manitoba Geological Survey, p. 219–225.

Teller, J.T. and Fenton, M.M. 1980: Late Wisconsinan glacial stratigraphy and history of southeastern Manitoba; Canadian Journal of Earth Sciences, v. 17, p. 19–35.

Thorleifson, L.H. and Matile, G.L.D. 1993: Till geochemistry and indicator mineral reconnaissance of southeastern Manitoba; Geological Survey of Canada, Open File 2750, 2 diskettes.

GS2025-21

Current mapping and assessment of granular-aggregate deposits in Manitoba

by J.W. Rentz, B. Wheadon and J. Janssens

Summary

The Manitoba Geological Survey is updating the mapping and assessment of granular-aggregate resources in the province. Earlier granular-aggregate mapping efforts in Manitoba were largely completed in the 1970s to mid-1990s and provided a baseline understanding of this resource in the province. These previous data are being concatenated and organized using an updated database structure and areas are being remapped using detailed elevation models and new field-based observations. A new quantitative matrix has been assembled to classify the economic potential for granular-aggregate deposits as high, medium and low, to protect mineral-rich lands under the legal requirements of *The Planning Act* of Manitoba. Since 2023, the focus has primarily been on updating the mapping of granular-aggregate resources in the Winnipeg Metropolitan Region.

In Brief:

- Aggregate maps for the Winnipeg metropolitan region are continuing to be updated with integration of historic and new data
- A new standardized database and mapping system is being developed to integrate historic and recent data
- New quantitative resource potential matrices are being developed to classify aggregate deposits for land-use planning

Citation:

Rentz, J.W., Wheadon, B. and Janssens, J. 2025: Current mapping and assessment of granular-aggregate deposits in Manitoba; *in* Report of Activities 2025, Manitoba Business, Mining, Trade and Job Creation, Manitoba Geological Survey, p. 191–194.

Introduction

The Manitoba Geological Survey (MGS) reinitiated the granular-aggregate program with the goal of re-evaluating and updating the previous mapping efforts (Rentz, 2023). The program focuses on identifying new potential deposits using field data, digital elevation models and high-resolution imagery. A new database structure is being developed to combine both historical and newly acquired data into a central database. Since the program's reinitiation, the focus has been on the Winnipeg Metropolitan Region, with site visits to historical and new locations (Figure GS2025-21-1), concatenating historical granular-aggregate data into a single database, as well as developing new database structures. A resource-potential framework has been developed to classify deposits as high, medium and low, in line with Section 8 of *The Planning Act* of Manitoba (Government of Manitoba, 2011), which restricts development on mineral-rich lands.

Current work

Concatenation and quality assurance–quality control of historical data

Granular-aggregate deposit and field-sediment data have been stored in various forms over time. An internal Microsoft® Access® database has been one focus of data quality assurance–quality control (QA-QC). To ensure data-point location accuracy, the points captured in this database were cross-referenced with hardcopy published maps. Once the spatial validity of the points was confirmed, each data point was given a unique identifier to differentiate exposure points with duplicate station identifiers. Lastly, a schema was generated to both account for this duplication and ensure that data within the internal database were accurate.

During cross-referencing of the points with the hardcopy maps, it was discovered that there was a substantial amount of field-station data that was not included in the original database. Approximately 3550 of these stations were identified, which resulted in a review of supporting documents including reports and field notes to compile any associated data. These data are in the process of being digitized and added to the new standardized database.

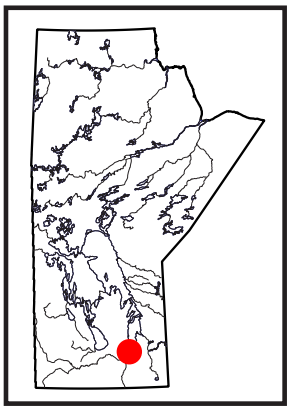

Development of a standardized point and polygon structure

To improve consistency, a standardized database structure was developed for capturing and presenting granular-aggregate exposure point and polygon data. The exposure-point structure is designed to capture field observations whereas the polygon structure is designed to summarize data at a 1:20 000 map scale.

It is important to note that granular-aggregate deposits in Manitoba often have variable sedimentology within one 'deposit'. At the same time, it is not desirable to take a sample of every single sediment type in every place. As such, a methodology is being developed to provide a consistent way

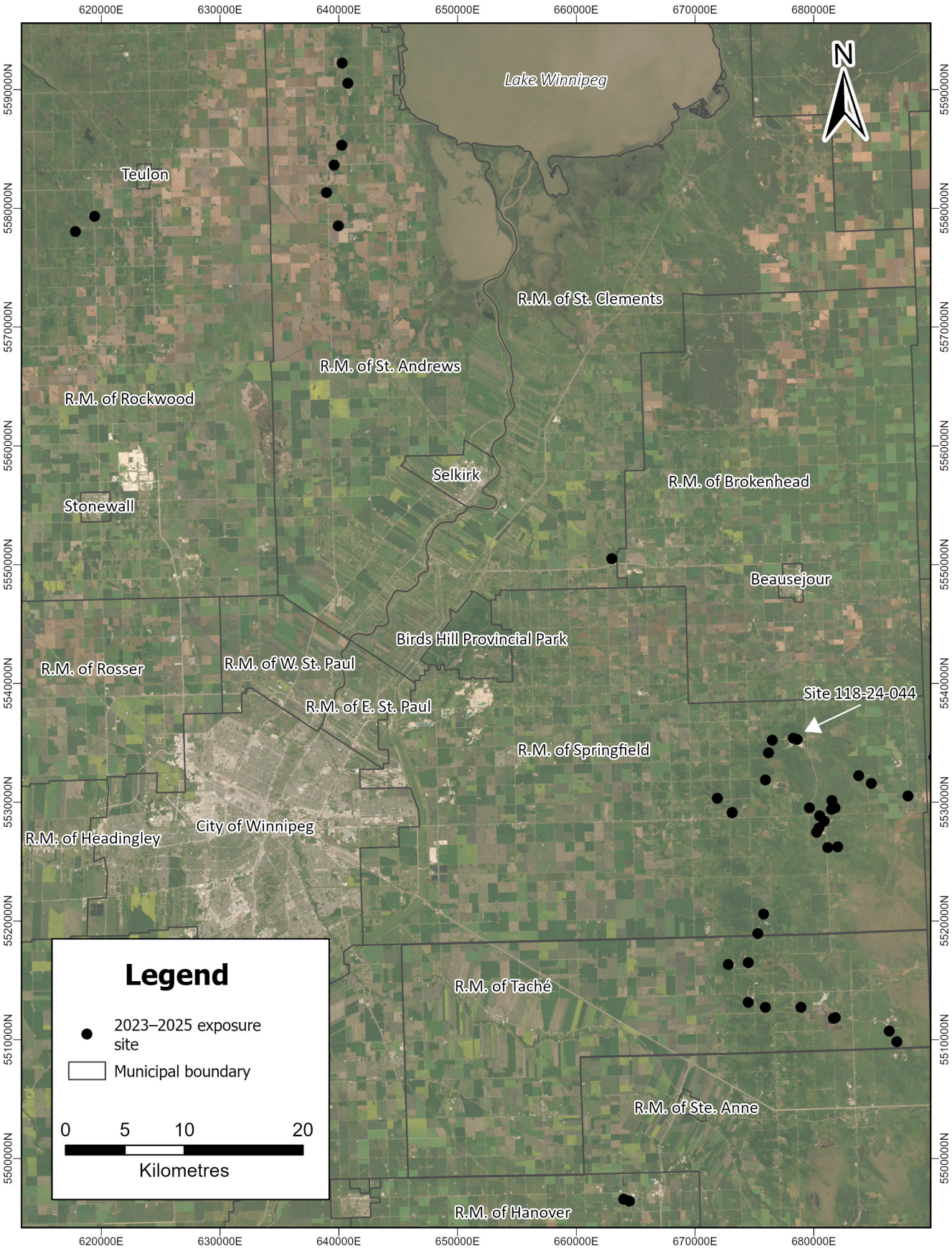

Figure GS2025-21-1: *Orthoimagery of the majority of the Winnipeg Metropolitan Region showing new exposure sites visited from 2023 to 2025 (Gauthier and Rentz, 2024; M.S. Gauthier and J.W. Rentz, unpublished data, 2025). Orthoimagery provided by Esri, Maxar, Earthstar Geographics and the GIS User Community. Abbreviations: E., East; R.M., Rural Municipality; W., West.*

to manage field data and create granular-aggregate maps. A full schema is planned to be released in future reports.

Resource potential evaluation

Section 8 of *The Planning Act* of Manitoba requires that economically valuable mineral resources be protected from land uses that limit exploration and development (Government of Manitoba, 2011). To meet these legal requirements, the MGS historically applied a rating of high, medium or low potential for granular aggregate. To ensure consistency moving forward, new quantitative matrices have been developed to assess the significance of both surface and buried granular-aggregate deposits using a weighted-point system. The parameters inputted into the weighted-point matrix include gravel content, fines content, shale and deleterious lithology content and deposit thickness. For buried deposits, the ease of extractability, the overburden thickness and water table depth are also included. Once completed, a full schema on the new resource potential matrices is planned to be released in future reports.

Preliminary map updates

The reinitiation of Manitoba's granular-aggregate program includes digital updating using more detailed remotely sensed imagery, namely orthophotos and publicly available light detection and ranging (LiDAR) digital elevation models (e.g., ATLIS Geomatics, 2016). Preliminary map updates are underway for the rural municipalities of Rockwood, St. Andrews, St. Clements, Springfield and Taché. Within these areas, a total of 71 exposure sites were visited in 2023–2025 (Figure GS2025-21-1; Gauthier and Rentz, 2024; M.S. Gauthier and J.W. Rentz, unpublished data, 2025). Many exposure sites were very close to each other at the ground level and overlap of some sites does exist at the scale of Figure GS2025-21-1, the aim of which is to show the overall scope of sites visited in these municipalities. The exposure sites were evaluated using the new standard field-data forms and granular-aggregate point data structure. Gravel (>4.75 mm) content, overburden information, aggregate thickness/exploration depth, groundwater depth, clast percentage, clast-size ranges, simplified clast lithology and a general field description were recorded at each site. An example of demarked stratigraphy at an exposure site is given in Figure GS2025-21-2. The intent of

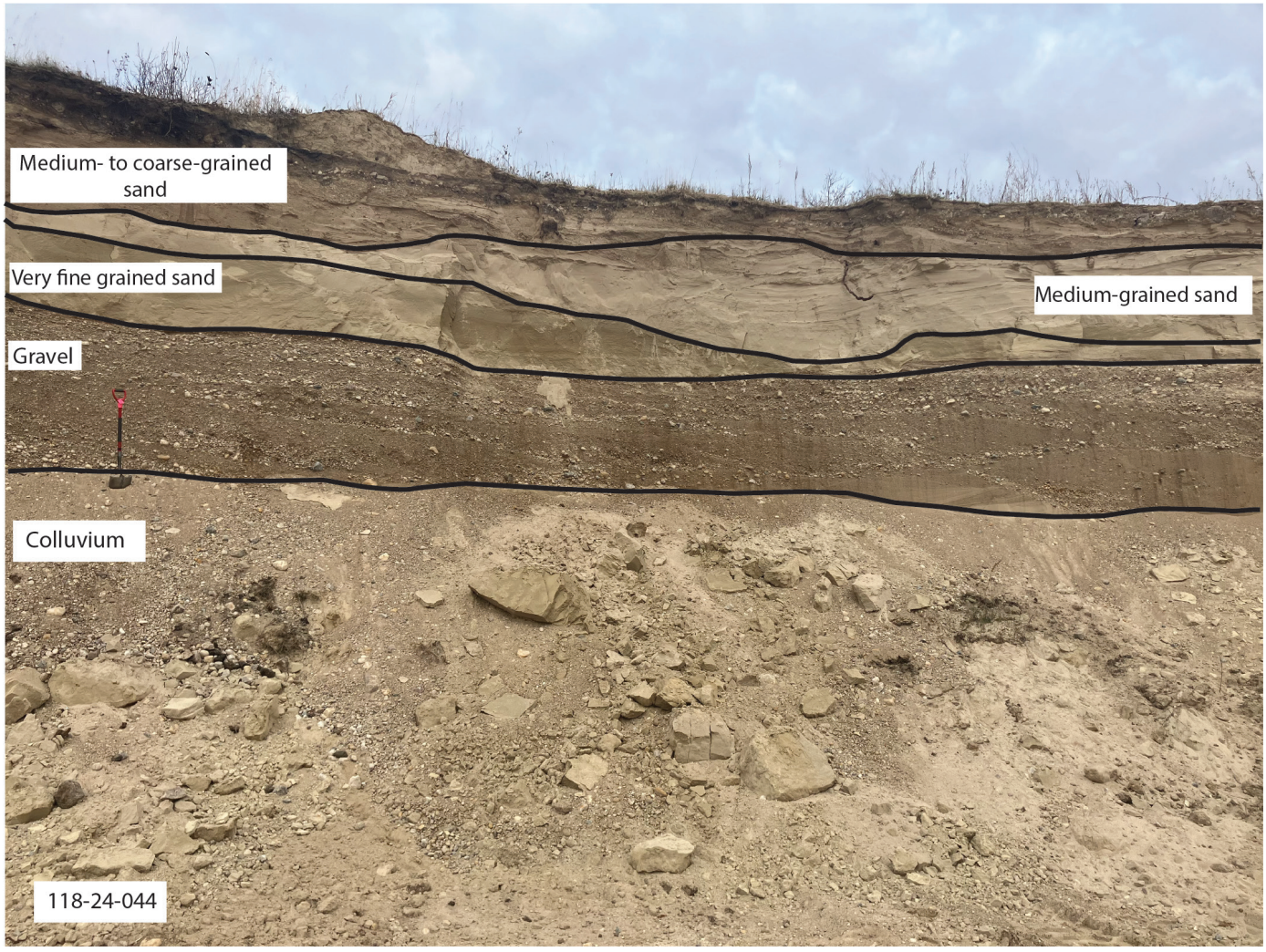

Figure GS2025-21-2: *Example of a currently producing gravel pit visited in the Rural Municipality of Springfield. The different stratigraphic layers are denoted at this exposure, site 118-24-044 (see Figure GS2025-21-1 for location). Shovel for scale is 1.2 m in length.*

these updates is to provide stakeholders with updated granular-aggregate information that can assist land-use planning.

Future work

Future granular-aggregate mapping will continue in the Winnipeg Metropolitan Region. Priorities will include both the implementation and finalization of the exposure point and granular-aggregate polygon standardizations, as well as finalizing the resource potential framework for land-use planning.

Economic considerations

Granular aggregate is an essential resource for road construction, foundation construction, railroad base and concrete/asphalt formation. The increasing demand for granular aggregate, especially from the Winnipeg Metropolitan Region, dictates that additional resources need to be identified.

Acknowledgments

The authors wish to thank the stakeholders and gravel pit operators who have assisted the Manitoba Geological Survey with site visits and providing valuable regional and site-specific knowledge. The authors acknowledge M.S. Gauthier and T.J. Hodder (Manitoba Geological Survey) for their critical review of this report.

References

ATLIS Geomatics 2016: Netley-Grassmere LiDAR DEM; Manitoba Infrastructure, URL <https://mli.gov.mb.ca/dems/index_external_lidar.html> [July 2023].

Gauthier, M.S. and Rentz, J.W. 2024: 2023 aggregate field visits: Quaternary site data, composition, and ice-flow indicators from gravel pits in southern Manitoba (parts of NTS 62H15, I13, P5); Manitoba Economic Development, Investment, Trade and Natural Resources, Manitoba Geological Survey, Data Repository Item DRI2024007, Microsoft® Excel® file, 1 appendix.

Government of Manitoba 2011: *The Planning Act* (C.C.S.M. c. P80), Provincial Planning Regulation, M.R. 81/2011; Government of Manitoba, URL <https://web2.gov.mb.ca/laws/regs/current/081-2011.php?lang=en> [October 2023].

Rentz, J.W. 2023: Manitoba's aggregate program: past, present, future; *in* Report of Activities 2023, Manitoba Economic Development, Investment, Trade and Natural Resources, Manitoba Geological Survey, p. 124–130.

GS2025-22

Exploring the use of geoanalytics to enhance landscape-integrated geochemical interpretations of lake sediments at the regional scale in northern Manitoba (NTS 64F, G, J, K)

by M.M Bodnar[1], A. Voinot[2], M. Leybourne[3], M.S. Gauthier and M. Trott[4]

In Brief:

- High quality lake sediment geochemistry data from northwestern Manitoba was recently re-analysed covering ~52,660 square kilometers
- Machine learning-enhanced critical mineral prospectivity maps are being developed by investigating the relationship between lake sediment geochemistry and surficial sediments

Citation:
Bodnar, M.M., Voinot, A., Leybourne, M., Gauthier, M. and Trott, M. 2025: Exploring the use of geoanalytics to enhance landscape-integrated geochemical interpretations of lake sediments at the regional scale in northern Manitoba (NTS 64F, G, J, K); *in* Report of Activities 2025, Manitoba Business, Mining, Trade and Job Creation, Manitoba Geological Survey, p. 195–202.

Summary

The objective of this study is to apply novel machine-learning prospectivity algorithms to recently reanalyzed lake-sediment geochemistry datasets in northern Manitoba. This investigation will involve the compilation and synthesizing of the current body of information available on the surficial geology and Quaternary processes, which are critical components influencing chemical signals in the lake-sediment dataset. In addition, other factors that may influence the lake-sediment chemistry, such as bedrock geology, will be incorporated. Initial findings of the data compilation and literature review suggest there is a notable control on spatial expression of chemical patterns caused predominantly by glaciolacustrine sediment coverage.

Introduction

Geochemical surveys at regional scale are designed to cover vast regions with an appropriate sampling density. Traditionally, this would involve an area covering several 1:250 000 scale National Topographic System (NTS) map sheets, with a sampling density of approximately 0.01 to 0.5 samples per square kilometre (Hosseini-Dinani et al., 2019). Results were then used to delineate prospective areas for further mineral exploration. Large regions of northern Manitoba were surveyed under the National Geochemical Reconnaissance Program starting in 1975 and largely concluded by the late 1980s. The original lake-sediment analytical results used atomic adsorption spectroscopy (AAS) and colorimetric analytical methods.

In the 40 to 50 years since the original analysis, significant advancements in analytical chemistry have been achieved and the archived lake-sediment sample material was reanalyzed in 2022 and 2023 using modern analytical methods. The original archived sample material was analyzed by Bureau Veritas facilities in Vancouver, British Columbia. A total of 65 elements were determined using inductively coupled plasma–mass spectrometry (ICP-MS) following digestion of 0.5 g of material by a modified aqua regia (1 HNO_3: 1 HCl: 1 H_2O). Additionally, 35 elements were determined by instrumental neutron activation analysis (INAA) of a 30 g sample (Amor et al., 2024a, b; Bourdeau, 2024). The reanalysis of lake-sediment data within the study area was completed in 2023 (Amor et al., 2024a). The final goal of the study is to generate landscape-integrated geochemical prospectivity maps enhanced by the application of machine learning (ML) algorithms to delineate areas of critical-mineral potential.

Study area

The study area encompasses a total of 3852 sites over an area of approximately 52 680 km^2 across four 1:250 000 scale NTS map sheets of northwestern Manitoba (Figure GS2025-22-1a, b). The area of interest is located 16 km north of the town of Lynn Lake and includes the First Nation communities of Tadoule Lake and Lac Brochet.

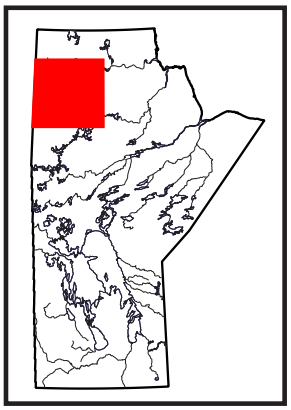

Methodology

There are four core components of this study: 1) geochemistry, 2) surficial geology and landscape-process history, 3) bedrock geology and mineralization and 4) machine-learning strategy. Geochemistry of the surface environment will be evaluated based on the available lake-sediment chemical data.

[1] Department of Geological Sciences and Geological Engineering, Queens University, Kingston, Ontario, matthew.bodnar@queensu.ca
[2] Natural Resources Canada, Geological Survey of Canada–Central, Ottawa, Ontario, alexandre.voinot@nrcan-rncan.gc.ca
[3] Department of Geological Sciences and Geological Engineering, Queens University, Kingston, Ontario, m.leybourne@queensu.ca
[4] Vrify Technology Inc., Vancouver, British Colombia, mcleantrott@vrify.com

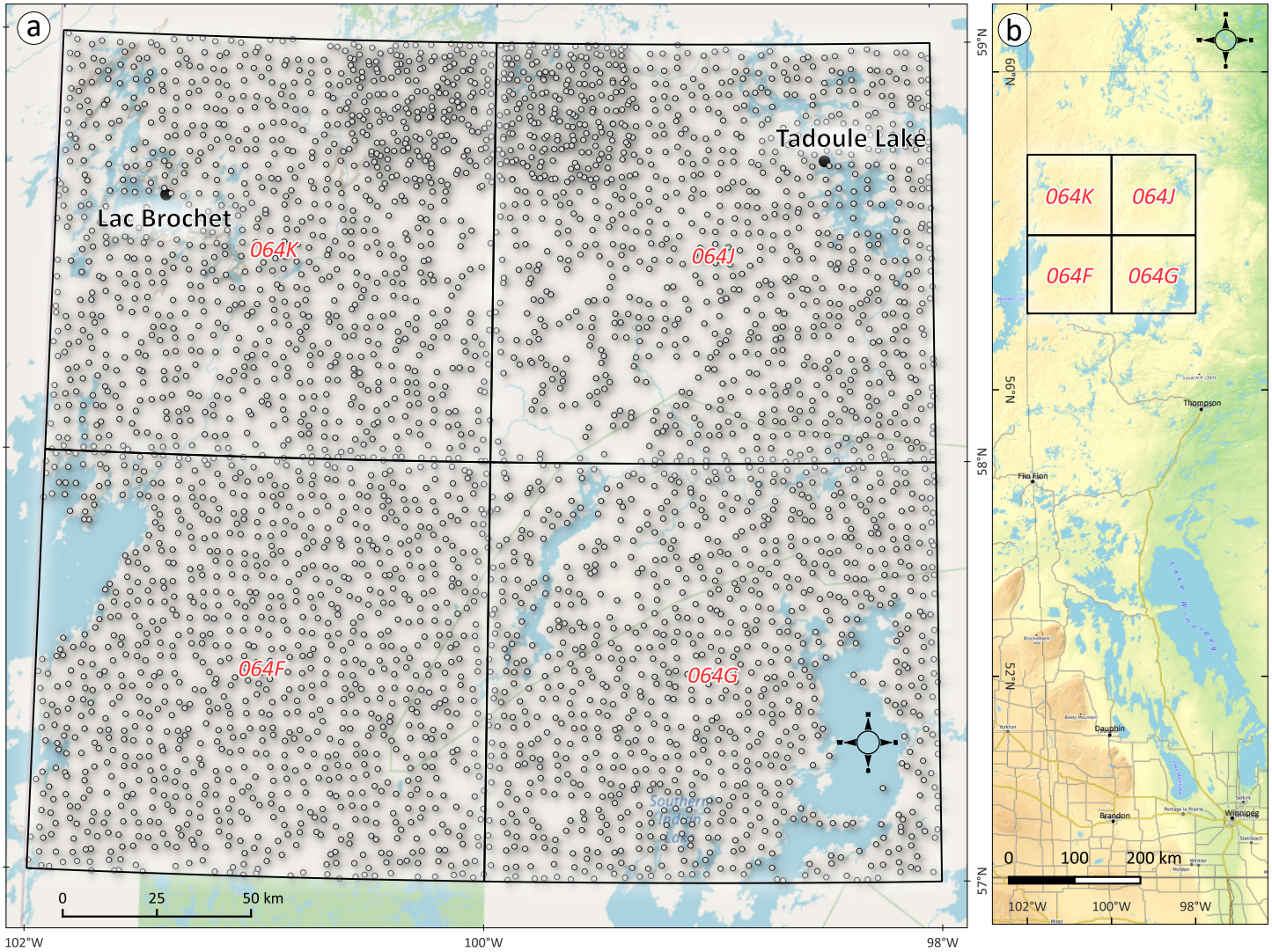

Figure GS2025-22-1: *Study area (NTS 64F, G, J, K) in northern Manitoba showing* ***a)*** *the location of lake-sediment samples (white dots) collected by the Geological Survey of Canada in the mid-1970s and 1980s;* ***b)*** *regional location within the province of Manitoba. Base maps sourced from Open Street Map (www.openstreetmap.com) and U.S. Geological Survey (2014).*

These chemical maps are indirect detection tools of potential mineral resources for the region but can be critical indicators of potential when combined with geophysical or other remote sensing data. The lake-sediment chemistry will be complemented by the integration of bedrock and/or till chemical data that is available in the literature.

The landscape surface, or biosphere, serves as the medium in which the lake-sediment sample is hosted. The character, distribution and movement or modification through time should be considered during the interpretation of the chemical data. Relevant terrain mapping and glacial history research will be included in the interpretation of the data and subsequent ML-enhanced prospectivity strategies. Other relevant factors, such as the organic content of each sample, regional hydrology and landforms potentially impacting migration of chemical elements (e.g., watersheds) will also be considered.

Bedrock geology is the primary origin of chemical signals in surficial sediments. It is important to understand the nature, chemistry and distribution of major rock units that may have been eroded by glacial ice or meltwaters. Bedrock geology mapping will be compiled and all documented mineral occurrences will be interrogated in preparation for the machine-learning prospectivity workflows that follow.

A selection of supervised and unsupervised ML algorithms will be evaluated for their suitability to lake-sediment geochemical datasets. Supervised algorithms such as linear regression, logistic regression, decision trees/random forest and gradient boosting will be considered for cases where map values may be predicted based on a set of known factors (e.g., predicting landscape/landform type from Sentinel-2 [European Space Agency, 2025] spectral data and topography). Unsupervised algorithms, such as clustering (e.g., hierarchical density-based spatial clustering of applications with noise [HDBSCAN]) and dimensionality reduction (e.g., principal component analysis), will also be leveraged for pattern recognition and predictive modeling where data labels are available or readily known. Finally, the cumulative

workflow will aim to apply the ML algorithms to identify subtle signatures embedded within a wide range of geological and ecological data inputs that have a direct impact on lake-sediment chemistry. Whenever possible, the data-driven strategy will be described in written scripts using Python coding language, in Python notebook(s) or in GIS software plug-in extensions for public use.

The current priority is the synthesis of available surficial geology maps and interpretation of landscape modification since the Pleistocene. The landscape and surficial materials will directly drive how the geochemical data is interpreted and will also provide a fundamental understanding of data layers that become available for later ML-model design.

Remote sensing and spectral analysis

Remote sensing satellites can map vast regions of the Earth quickly and consistently. This study will make use of Sentinel-2 multispectral data acquired from the Copernicus Browser web platform operated by the European Space Agency. This dataset comprises tiles of multiband spectral raster data split into individual raster images of each spectral band. The raw data will be processed to remove data that reflects biomass or vegetation signals and isolate bare soil or mineral signals (Rikimaru et al., 2002; Phiri et al., 2020; Mzid et al., 2021). The base soil index shown in the figure below (Figure GS2025-22-2a, b) was developed for a different landscape, ecology and climate to that present in the study area and, therefore, additional landscape features, such as recent wildfire residues, must be considered when evaluating results (M. Rinne, pers. comm., 2025). The final processed datasets will be evaluated individually in relationship to other landscape variables, digital elevation models (DEMs) and Quaternary geology, but will also be included in future ML workflows.

Digital elevation modelling

The morphology of the landscape surface provides significant insight into past processes. Access to a high-resolution and accurate surface map based on remotely acquired data is fundamental for predictive terrain mapping. Light detection and ranging (LiDAR) point-cloud datasets (LAZ file format) are considered the most valuable in terms of detailed (0.5–1 m resolution) terrain mapping; however, the acquisition of LiDAR data is costly and resource intensive. Commercial satellite-based alternatives acquired from public and private sources, such as the Airbus

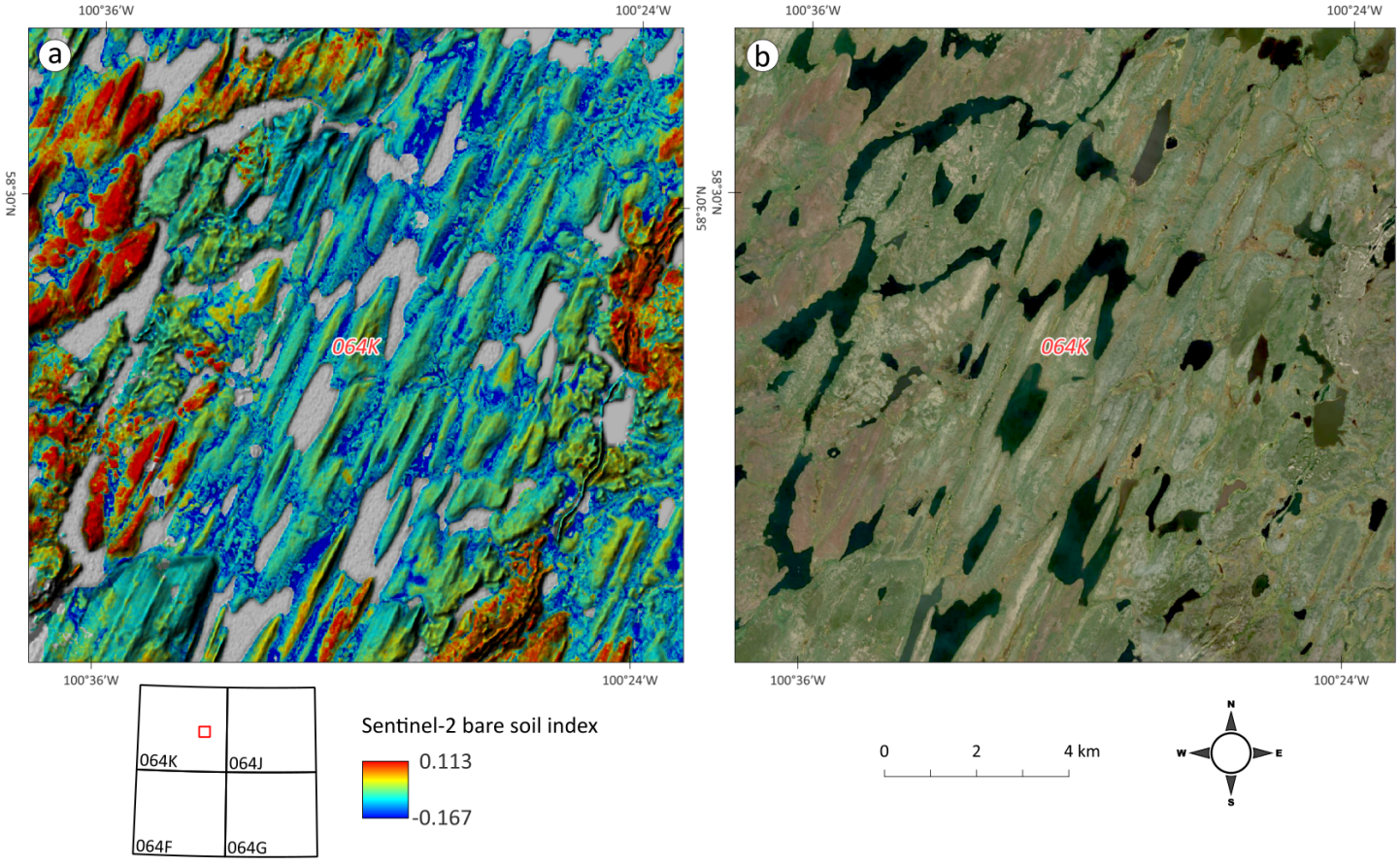

Figure GS2025-22-2: *Image of a small region along the eastern margin of NTS area 64K in northern Manitoba, showing* ***a)*** *the bare soil index calculated from Sentinel-2 spectral data overlaid on a hillshade Copernicus DEM at 30 m resolution, in which the red colours are most likely bare soil and the dark blue, least likely to be bare soil;* ***b)*** *satellite imagery of the same area. Data over waterbodies have been masked. Copernicus Sentinel-2 data (European Space Agency, 2025) processed by the European Space Agency (ESA) and accessed from the Copernicus Browser at https://browser.dataspace.copernicus.eu/. Figure produced using Copernicus WorldDEM-30 (© DLR e.V. 2010-2014 and © Airbus Defence and Space GmbH 2014-2018 provided under COPERNICUS by the European Union and ESA; all rights reserved). Image from Microsoft® Bing™ Maps service 2025).*

WorldDEM™ 5 m digital terrain model (DTM) or Maxar GeoEye-1 half-metre multispectral satellite imagery, can provide reasonable (1–30 m resolution) data for terrain analysis at a much lower fixed cost than LiDAR. However, it should be noted that these are not true bare earth ground-surface elevations and can be affected by thick and tall vegetation. Thus, optically-derived photogrammetric surface models are not as reliable for terrain analysis but can potentially be improved using mathematical models (Liu et al., 2014).

This study makes use of data from the Shuttle Radar Topography Mission (SRTM) distributed by the U.S. Geological Survey (U.S. Geological Survey, 2014) and the Copernicus products distributed by the European Space Agency (European Space Agency, 2025) to provide a continuous base layer for geographic interpretation (Figure GS2025-22-3). Each raster dataset has a cell size of approximately 30 by 30 m, making it suitable for large-scale regional interpretations. Additional detailed mapping may be completed with the acquisition of a commercially available product such as WorldDEM Neo data, which features a pixel resolution of up to 5 m and is suitable for vegetated areas as it utilizes modern technology (i.e., interferometric synthetic aperture radar) that can achieve near bare-earth elevations (Airbus Defence and Space, 2025).

In recent years, digital archeologists have been publishing innovative processing algorithms designed to be applied to LiDAR datasets to enhance subtle small-scale features thought to represent evidence of past human activity (Kokalj and Hesse, 2017). These same DEM processing algorithms will be applied to the DEM assembled for this study area to enhance subtle features (a few hundred metres minimum due to 30 m pixel resolution). A

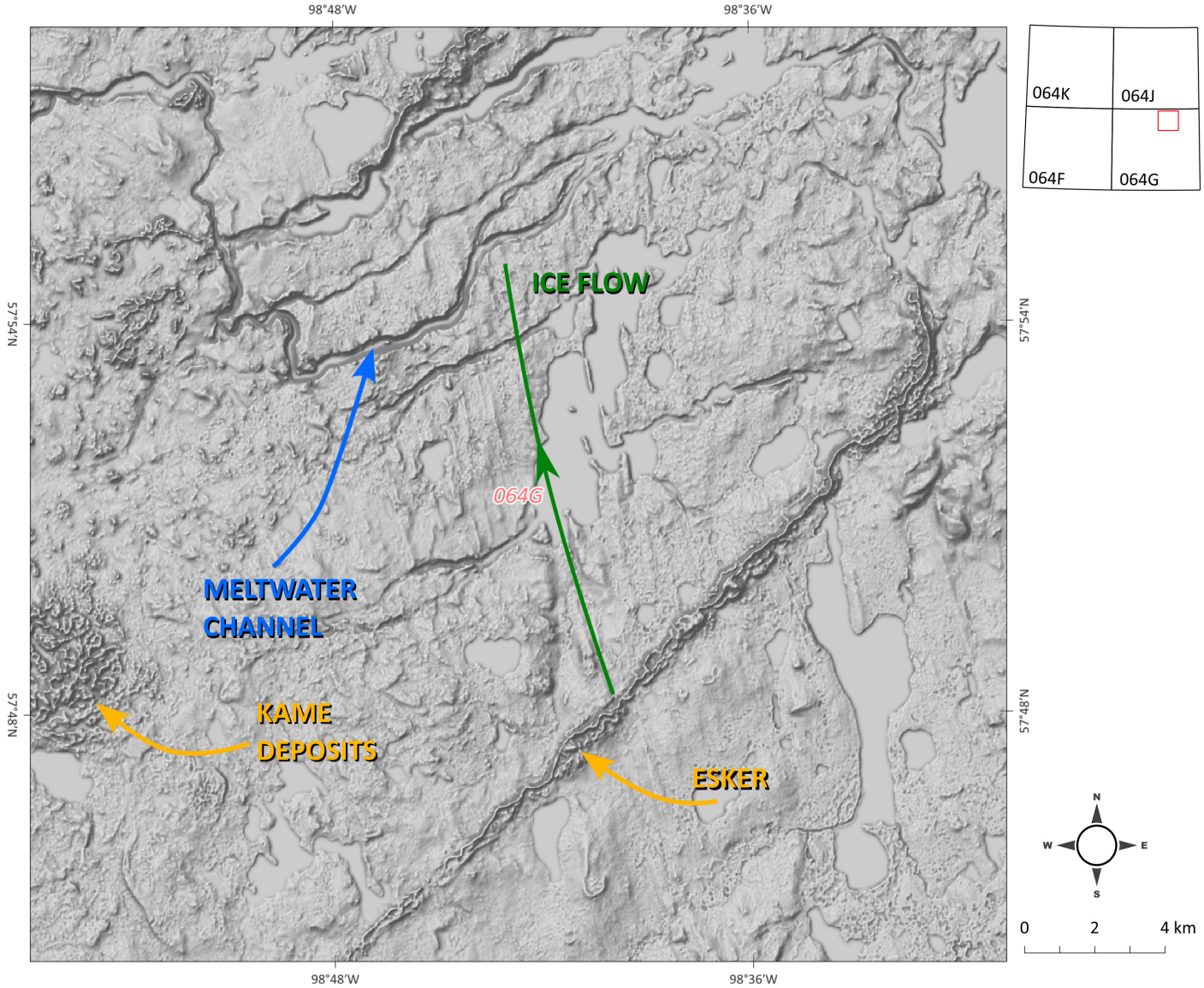

Figure GS2025-22-3: *Image of a small portion of NTS area 064G in northern Manitoba (location shown on inset) from the Copernicus 30 m DEM. The image illustrates streamlined landforms that indicate an ice-flow event (oriented approximately north-south), followed by the deposition of esker and kame deposits, and finally major erosional channels that were created as proglacial waterbodies migrated in response to fluctuations in ice position and accumulations of glacial deposits. Figure produced using Copernicus WorldDEM-30 (© DLR e.V. 2010-2014 and © Airbus Defence and Space GmbH 2014-2018 provided under COPERNICUS by the European Union and ESA; all rights reserved).*

future consideration for the DEM data layer is to generate apparent drainage catchments for waterbodies as a potential metric for use in machine-learning modelling.

Surficial landforms and Quaternary history

The surficial sediments that overlie bedrock are the most important variable in the interpretation of lake-sediment chemistry. The lake sediment is an accumulation of fine- to very fine-grained silt, clay and organic material thought to be representative of the waterbody catchment area. The chemistry of the glacial sediments is a first-order factor in the lake-sediment chemistry results and can potentially be directly related to its bedrock source, albeit influenced by mixing through the various phases of glacial transport. It is important to reiterate that landforms developed from the earliest phases of ice advance and retreat (e.g., esker and kame deposits, beachlines and glaciolacustrine basins) may often, but not always, be adjusted by subsequent phases of advancing ice. This will contribute to local chemical heterogeneity that is reflective of the reworking processes associated with glacial melt and retreat, which can obscure the original bedrock signal. Lastly, it is important to consider surficial sediment thickness when interpreting regional geochemical data. Regions with thicker surficial sediments generally have less chemical relation to the underlying bedrock (Cummings and Russell, 2018). The most southeastern area of the study is generally recognized as being overlain by glaciolacustrine sediment that, in certain locations, is observed to reach at least 5 m in thickness (T. Hodder, pers. comm., 2025).

In glaciated terrains, the surficial landforms are primarily related to erosion and deposition by ice or to proglacial water bodies that formed as glaciers waxed and waned. A large volume of research has been conducted across northern Manitoba and southern Nunavut to map major landforms and interpret glacial events (Trommelen et al., 2014; Gauthier et al., 2019; Amor et al., 2024a; Hodder et al., 2024). These studies have demonstrated that there has been a complex multiphase regime of ice-flow advance and retreat in the region, with ice advances from the north and southeast at different times in the past (Figure GS2025-22-4). However, it should be noted that the ice-flow

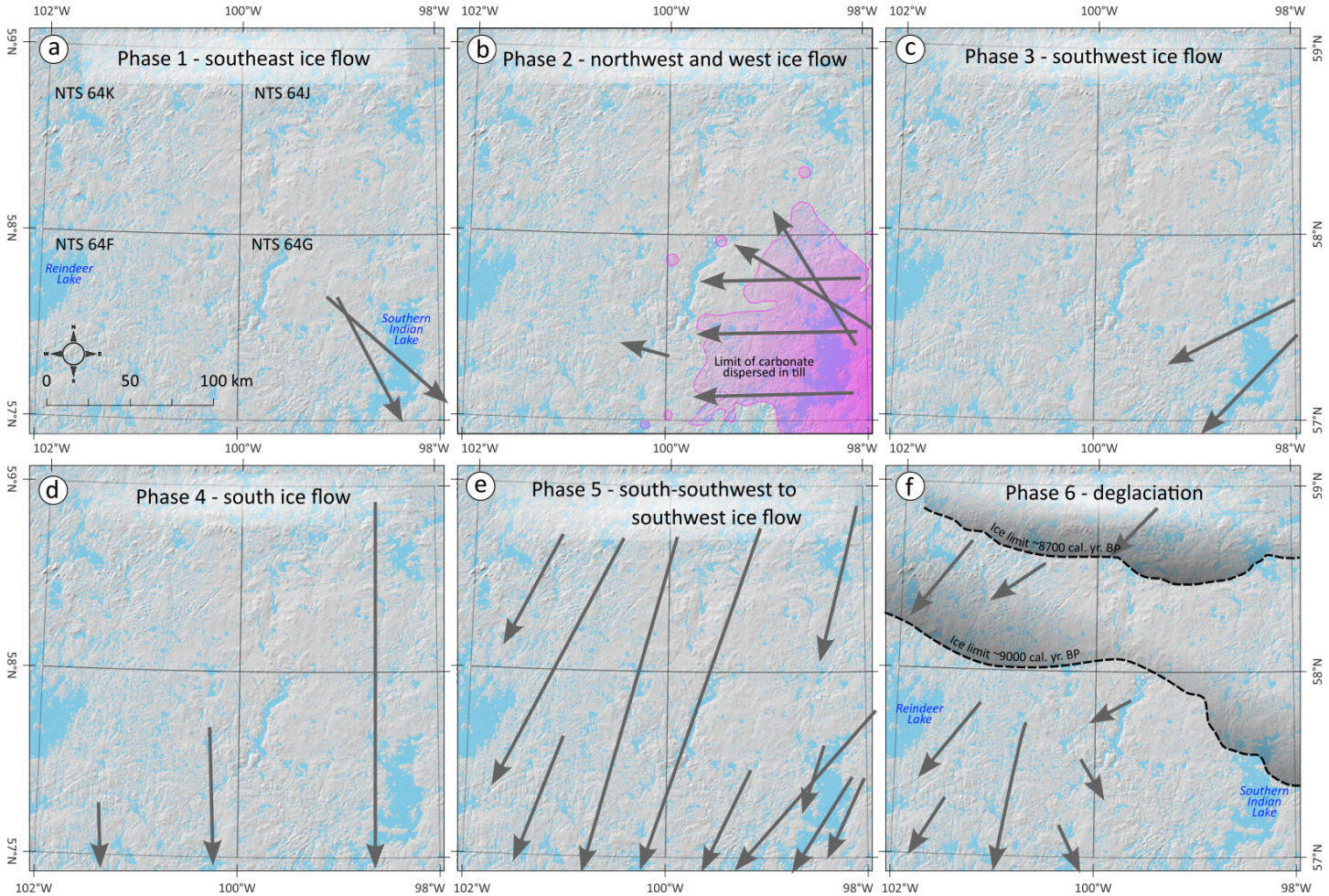

Figure GS2025-22-4: *Series of maps illustrating the phases of ice flow across the study area in northern Manitoba based on field mapping and satellite-image interpretation:* ***a)*** *ice flow in phase 1predominantly from the north;* ***b)***, ***c)*** *resurgence of ice from the east-southeast in phases 2 and 3 presumed to have transported carbonate clast-rich till over much of NTS area 064G;* ***d)*** *return of ice flow southward in phase 4;* ***e)*** *southwestward ice flow in phase 5;* ***f)*** *final phase of glacial retreat. Figure modified from Gauthier et al., 2019; Amor et al, 2024a. Base hillshade topography produced using Copernicus WorldDEM-30 (© DLR e.V. 2010-2014 and © Airbus Defence and Space GmbH 2014-2018 provided under COPERNICUS by the European Union and ESA; all rights reserved).*

history is not thought to be consistent across all four NTS areas that are the focus of this study.

The compilation and synthesis of literature pertaining to the Quaternary history of the area is ongoing and is being undertaken in conjunction with representatives at the Manitoba Geological Survey (MGS) and the Geological Survey of Canada (GSC). Currently all data from the literature is being compiled in a QGIS workspace, including all published spatial vector data. Where required, older vector data based on coarse resolution data will be remapped to the resolution of the Copernicus 30 m DEM. It is important to complete this process before applying a machine-learning modelling strategy since all core variables should initially be adequately quantified and the data problem well defined.

A compilation of relict beach ridges observed remotely is being undertaken with the support of the MGS. Surface maps from previous investigations are being synthesized (e.g., Figure GS2025-22-5a, b; Dredge and Nixon, 1981, 1982; Dredge et al., 1982a, b; Nixon et al., 1982; Richardson et al., 1982; DiLabio et al., 1986; Kaszycki and Way Nee, 1989). The relict beach ridges are a direct indicator of the limits of past proglacial lakes that formed at the margin of the Laurentide Ice Sheet, such as glacial Lake Agassiz (Teller, 1987). These large proglacial lakes received significant sediment input from the melting ice sheet, and silt and clay deposited within these lakes certainly contribute to masking the geochemical signals. Preserved beach ridges are most well developed near the centre of the area covered by the four NTS map sheets, indicating a period of time character-

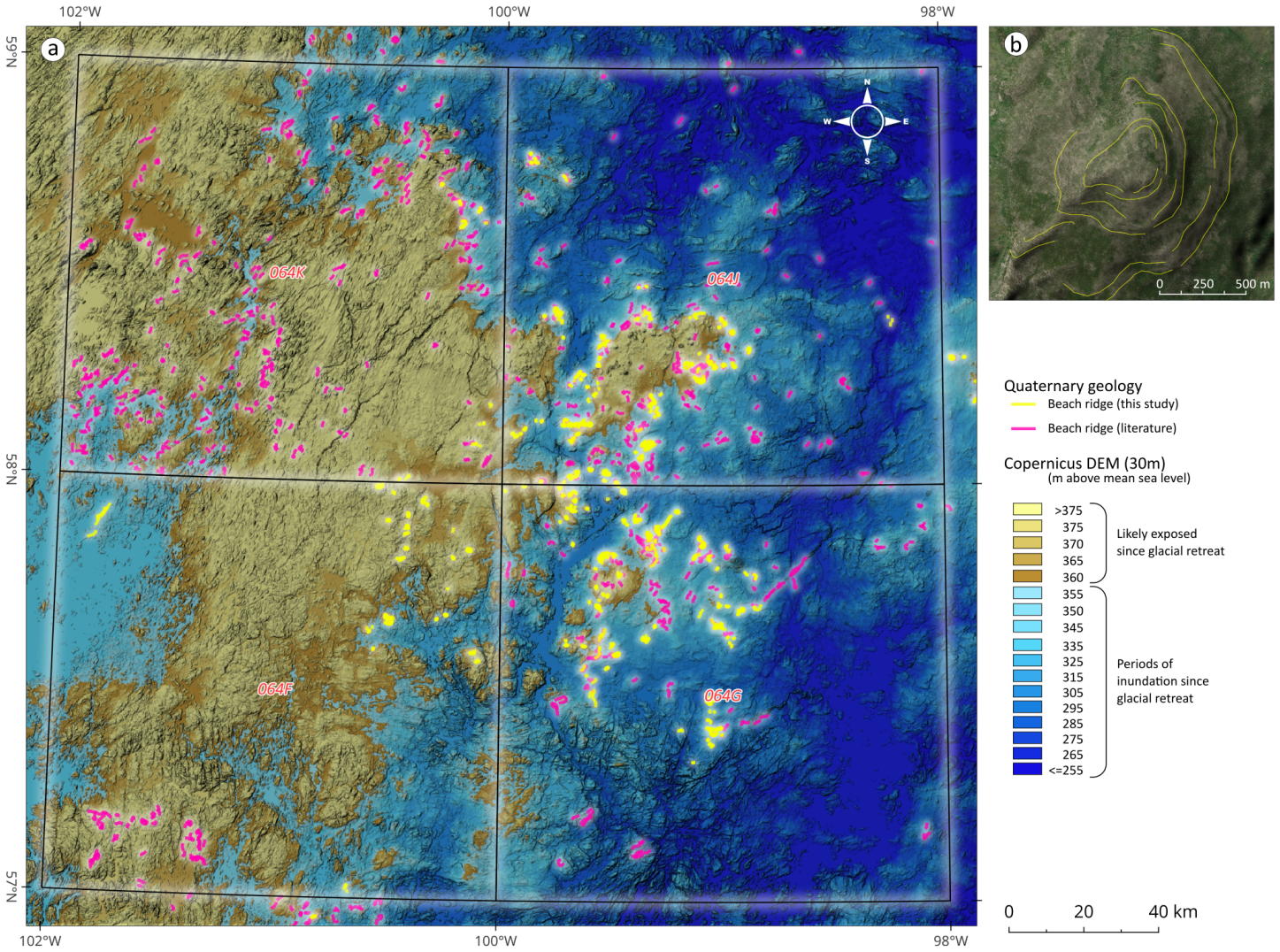

Figure GS2025-22-5: a) *Map of the study area in northern Manitoba showing the Copernicus 30 m DEM (European Space Agency, 2025). Beach ridges mapped in this study are shown as yellow polylines and beach ridges compiled from literature are shown as pink polylines. The majority of identified beach ridges cluster around 350–360 m elevation. The patterns of beach-ridge development may assist in delineating areas that were not exposed to extended periods of inundation and glaciolacustrine sedimentation. The digital elevation model was colour adjusted such that the brown to blue transition occurs at ~355 m elevation, which aligned with the mean elevation of the majority of visible beach ridges and may represent limits of subaerial exposure at ca. 8000 years ^{14}C BP.* ***b)*** *Satellite image showing a small mound with several relict beach ridges; yellow lines are interpreted as beach-ridge segments. Base hillshade topography produced using Copernicus WorldDEM-30 (© DLR e.V. 2010-2014 and © Airbus Defence and Space GmbH 2014-2018 provided under COPERNICUS by the European Union and ESA; all rights reserved). Image from Microsoft Bing Maps service 2025.*

ized by sustained proglacial lake levels (Figure GS2025-22-5a, b). Although beach ridges themselves are not a significant control of lake-sediment geochemistry, the patterns of beach-ridge development may assist in delineating local areas that were not exposed to extended periods of inundation and glaciolacustrine sedimentation. An intended outcome of the project is to also synthesize published surficial geology maps of the study area.

Geochemical data

The exploratory data analysis of the geochemical dataset has been limited, as additional work will require classifying surficial material into groups (or domains) and identifying the hydromorphic and mechanical dispersion vectors; however, preliminary analysis indicates chemical patterns that are of interest. For example, a map of lake-sediment nickel concentration reveals a relationship with mapped beaches, with samples recovered from elevations above the reconstructed beach ridges showing overall lower nickel values (Figure GS2025-22-6a, b). This pattern suggests glaciolacustrine sediments associated with Lake Agassiz may be more clay rich or organic rich and act as a more effective metal-retention medium. This will be explored further in the future, along with additional compilations of the INAA results and the original survey results to achieve a complete database that will assist in completing the research program.

Economic considerations

The work described herein plays a small part in the final goal of applying machine-learning–enhanced and landscape-integrated geochemical prospectivity to mapping for critical minerals in a remote region of northern Manitoba. This work builds on geochemical sampling, recent Quaternary mapping and sample reanalysis, the aim of which is to generate sophisticated maps of commodity and deposit-style prospectivity as a support to critical-mineral exploration. Mineral prospectivity maps are an important tool for mineral exploration and can also be used for effective land-use planning.

Acknowledgments

The authors thank all members of the Geological Survey of Canada and the Manitoba Geological Survey who have contributed to the launch of this study. In particular, B. McClenaghan is thanked for conceiving this project and providing early encouragement.

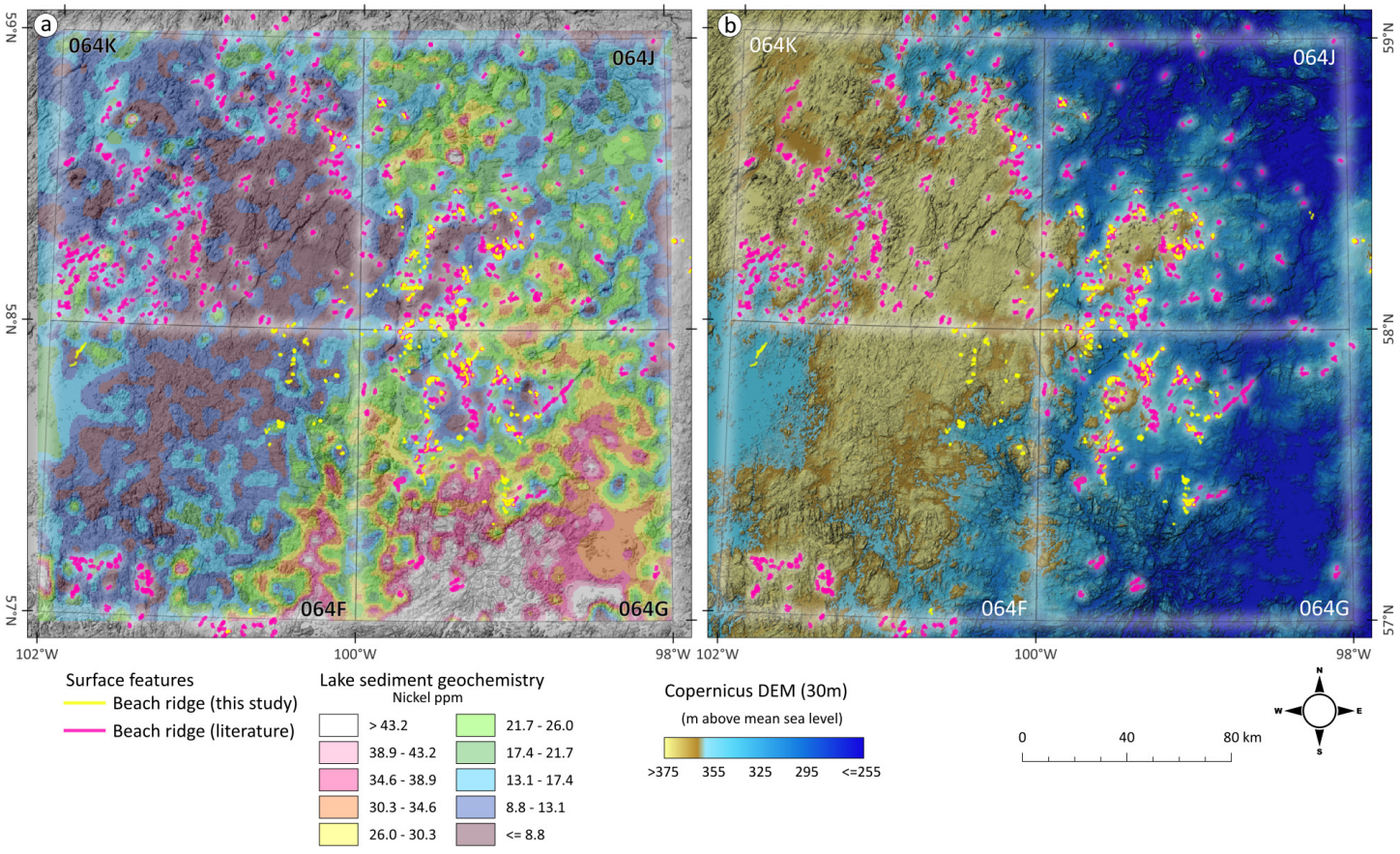

***Figure GS2025-22-6: S**eries of maps of the study area in northern Manitoba showing **a)** nickel concentration in lake-sediment samples (after aqua-regia digestion); **b)** a reconstruction of Lake Agassiz in the map area. There is a notable spatial relationship between these features, where nickel concentrations in lake sediment without paleolake coverage tend to be lower. Base hillshade topography produced using Copernicus WorldDEM-30 (© DLR e.V. 2010-2014 and © Airbus Defence and Space GmbH 2014-2018 provided under COPERNICUS by the European Union and ESA; all rights reserved).*

References

Airbus Defence and Space 2025: WorldDEM™ Neo–the next level of elevation data; Airbus, satellite imagery, URL <https://space-solutions.airbus.com/imagery/3d-elevation-and-reference-points/worlddem-neo/> [October 2025].

Amor, S.D., Couëslan, C.G., Gauthier, M.S., Martins, T., McCurdy, M.W., Day, S.J.A. and Adcock, S.W. 2024a: Regional lake-sediment geochemical data from northern Manitoba (NTS 064-G): reanalysis data and QA/QC evaluation; Geological Survey of Canada, Open file 9197, 1 .zip file, 27 p., URL <https://doi.org/10.4095/pmnwznphzq>.

Amor, S.D., Couëslan, C.G., Gauthier, M.S., Martins, T., McCurdy, M.W., Day, S.J.A. and Adcock, S.W. 2024b: Regional lake-sediment geochemical data from northern Manitoba (NTS 064-J and 064-K): reanalysis data and QA/QC evaluation; Geological Survey of Canada, Open File 9187, I .zip file, 28 p., URL <https://doi.org/120.4095/pj2gglxa5s>.

Bourdeau, J.E. 2024: Regional lake-sediment geochemical data from northwestern Manitoba (NTS 064-F): re-analysis data and QA/QC evaluation; Geological Survey of Canada, Open File 8948, I .zip file, 13 p., URL <https://doi.org/10.4095/332376>.

Cummings, D.I. and Russell, H.A.J. 2018: Glacial dispersal trains in North America; Journal of Maps, v. 14, no. 2, p. 476–485.

DiLabio, R.N.W., Kaskycki, C.A., Way Nee, V. and Nielsen, E. 1986: Surficial geology, Granville Lake, Manitoba; Geological Survey of Canada, Open File 1258, scale 1:125 000, URL <https://doi.org/10.4095/130050>.

Dredge, L.A. and Nixon, F.M. 1981: Surficial geology, Nejanilini Lake, Manitoba; Geological Survey of Canada, Preliminary Map 7-1980, scale 1:250 000, URL <https://doi.org/10.4095/109308>.

Dredge, L.A. and Nixon, F.M. 1982: Surficial geology, Shethanei Lake, Manitoba; Geological Survey of Canada, Preliminary Map 6-1980, scale 1:250 000, URL <https://doi.org/10.4095/109307>.

Dredge, L.A., Nixon, F.M. and Richardson, R.J. 1982a: Surficial geology, Kasmere Lake, Manitoba; Geological Survey of Canada, Preliminary Map 19-1981, scale 1:250 000.

Dredge, L.A., Nixon, F.M. and Richardson, R.J. 1982b: Surficial geology, Tadoule Lake, Manitoba; Geological Survey of Canada, Preliminary Map 17-1981, scale 1:250 000.

European Space Agency 2025: Copernicus Sentinel-2 imagery; European Space Agency, satellite imagery, URL <https://www.esa.int/Applications/Observing_the_Earth/Copernicus> [October 2025].

Gauthier, M.S., Hodder, T.J., Ross, M., Kelley, S.E., Rochester, A. and McCausland, P. 2019: The subglacial mosaic of the Laurentide Ice Sheet: a study of the interior region of southwestern Hudson Bay; Quaternary Science Reviews, v. 214, p. 1–27, URL <https://doi.org/10.1016/j.quascirev.2019.04.015>.

Hodder, T.J., Gauthier, M.S., Ross, M., Kelley, S.E., Lian, O.B., Dalton, A.S. and Finkelstein, S.A. 2024: Unravelling the fragmented sediment–landform assemblage in an area of thick Quaternary sediment, western Hudson Bay Lowland, Canada; Canadian Journal of Earth Sciences, v. 61, no. 11, p. 1156–1183, URL <https://doi.org/10.1139/cjes-2024-0018>.

Hosseini-Dinani, H., Mokhtari, A.R., Shahrestani, S. and De Vivo, B. 2019: Sampling density in regional exploration and environmental geochemical studies: a review; Natural Resources Research, v. 28, no. 3, p. 967–994.

Kaszycki, C.A. and Way Nee, V.J. 1989: Surficial geology, Brochet, Manitoba; Geological Survey of Canada, Open File 1331, scale 1:250 000, URL <https://doi.org/10.4095/129085>.

Kokalj, Ž. and Hesse, R. 2017: Airborne laser scanning raster data visualization. A guide to good practice; ZRC SAZU, Založba ZRC, Ljubljana, first edition,90 p., URL <https://doi.org/10.3986/9789612549848>.

Liu, J.-k., Liu, D. and Alsdorf, D. 2014: Extracting ground-level DEM from SRTM DEM in forest environments based on mathematical morphology; IEEE Transactions on Geoscience and Remote Sensing, v. 52, no. 10, p. 6333–6340, URL <https://doi.org/10.1109/TGRS.2013.2296232>.

Mzid, N., Pignatti, S., Huang, W. and Casa, R. 2021: An analysis of bare soil occurrence in arable croplands for remote sensing topsoil applications; Remote Sensing, v. 13, no. 3, art. 474, 24 p., URL <https://doi.org/10.3390/rs/3030474>.

Nixon, F.M., Dredge, L.A. and Richardson, R.J. 1982: Surficial geology, Munroe Lake, Manitoba; Geological Survey of Canada, Preliminary Map 20-1981, scale 1:250 000.

Phiri, D., Simwanda, M., Salekin, S., Nyirenda, V.R., Murayama, Y. and Ranagalage, M. 2020: Sentinel-2 data for land cover/use mapping: a review; Remote Sensing, v. 12, no. 14, 35 p., URL <https://doi.org/10.3390/rs12142291>.

Richardson, R.J., Dredge, L.A. and Nixon, F.M. 1982: Surficial geology, Whiskey Jack Lake, Manitoba; Geological Survey of Canada, Preliminary Map 18-1981, scale 1:250 000.

Rikimaru, A., Roy, P.S. and Miyatake, S. 2002: Tropical forest cover density mapping; Tropical Ecology, v. 43, no. 1, p. 39–47.

Teller, J.T. 1987: Proglacial lakes and the southern margin of the Laurentide Ice Sheet; *in* North America and Adjacent Oceans During the Last Deglaciation, W.F. Ruddiman and H.E. Wright, Jr. (ed.); Geological Society of America, v. K-3, p. 39–69, URL <https://doi.org/10.1130/DNAG-GNA-K3.39>.

Trommelen, M.S., Ross, M. and Ismail, A. 2014: Ribbed moraines in northern Manitoba, Canada: characteristics and preservation as part of a subglacial bed mosaic near the core regions of ice sheets; Quaternary Science Reviews, v. 87, p. 135–155.

U.S. Geological Survey 2014: USGS EROS archive - digital elevation - Shuttle Radar Topography Mission (SRTM) 1 arc-second global; U.S. Geological Survey, 30 m cell, zipped hgt format, URL <https://doi.org/10.5066/F7PR7TFT>.

PUBLICATIONS

Data Repository Items

DRI2025001

Laser-ablation inductively coupled plasma–mass spectrometry analyses of detrital zircon grains from metasedimentary rocks of the Thompson nickel belt, Manitoba (parts of NTS 63O1; 63P5, 12)

by C.G. Couëslan

DRI2025002

Quaternary stratigraphy from the Gillam area, northeastern Manitoba: additional 2022 and 2023 data (NTS 54D5, 7, 8; 64A2)

by M.S. Gauthier and T.J. Hodder

Microsoft® Excel® file supplements:

Gauthier, M.S. 2024: Till-clast–lithology data, Gillam area, northeastern Manitoba (parts of NTS 54C, D, 64A), Manitoba Economic Development, Investment, Trade and Natural Resources, Manitoba Geological Survey, DRI2024006, Microsoft® Excel® file, 1 appendix.

DRI2025003

Geochemical data of whole-rock samples collected in the 2024 summer from the Lynn Lake greenstone belt, northwestern Manitoba (parts of NTS 64C11–12, 14–16)

by X.M. Yang

DRI2025004

Geochemical data of 737 whole-rock samples from the Lynn Lake greenstone belt, northwestern Manitoba (parts of NTS 64C10–12, 14–16)

by X.M. Yang

Microsoft® Excel® file supplements:

Yang, X.M. 2024: Precise U-Pb zircon age and geochemical constraints on the geodynamic settings of the Falcon Lake intrusive complex and S-type Caddy Lake granite intrusion in the western Superior province,southeastern Manitoba (parts of NTS 52E11, 14); *in* Report of Activities 2024, Manitoba Economic Development, Investment, Trade and Natural Resources, Manitoba Geological Survey, p. 49–65.

DRI2025005

Till-matrix geochemistry data from the 2022–2024 field seasons in southeastern Manitoba (parts of NTS 52L, 62P, 63A)

by T.J. Hodder

DRI2025006

Gold and indicator-mineral data derived from glacial sediments (till) in southeastern Manitoba (parts of NTS 52L, M, 62P, 63A)

by T.J. Hodder

Microsoft® Excel® file supplements:

Hodder, T.J. and Lian, O.B. 2024: Reconnaissance-scale Quaternary geology investigations to support lithium exploration in southeastern Manitoba (parts of NTS 52L, M, 62P,63A); *in* Report of Activities 2024, Manitoba Economic Development, Investment, Trade and Natural Resources, Manitoba Geological Survey, p. 200–208.

DRI2025007

Field-based ice-flow–indicator data between the North Knife River and the Seal River, and in the Gross Lake area, far northeastern Manitoba (parts of NTS 54L10, 11, 12, 13, 14, 15 and 54M5, 6, 12)

by M.S. Gauthier

Microsoft® Excel® file supplements:

Gauthier, M. S. and Bergen, S. 2024: Quaternary site data, till composition and ice-flow indicators between the North Knife River and the Seal River, and in the Gross Lake area, far northeastern Manitoba (parts of NTS 54L10–15, 54M5, 6, 12; *in* Report of Activities 2024, Manitoba Economic Development, Investment, Trade and Natural Resources, Manitoba Geological Survey, p. 209–218.

DRI2025008

Whole-rock lithogeochemistry, assay, and Sm-Nd isotope geochemistry for the Armstrong assemblage and spatially associated rocks from the Armstrong and Natawahunan lakes area, central Manitoba (NTS 63P10, 11, 14)

by C.G. Couëslan and J. Janssens

DRI2025009

Whole rock geochemistry results from field work in the Cat Lake–Winnipeg River pegmatite field, southeastern Manitoba (parts of NTS 52L5, 6, 11, 12, 14)

by T. Martins, C. Nambaje and J. Janssens

Microsoft® Excel® file supplements:

Nambaje, C., Martins, T., McFarlane, C.R.M., Kaczmer, M., Rinne, M.L. and Groat, L. 2024:Preliminary results from field investigations in the Cat Lake–Winnipeg River pegmatite field, southeastern Manitoba (parts of NTS 52L5, 6, 11, 12); *in* Report of Activities 2024, Manitoba Economic Development, Investment, Trade and Natural Resources, Manitoba Geological Survey, p. 10–26.

DRI2025010

Whole-rock lithogeochemistry for select samples from the northwestern Burntwood Lake area, Kisseynew domain, west-central Manitoba (part of NTS 63N7, 8, 10)

by C.G. Couëslan and J. Janssens

Microsoft® Excel® file supplements:

Couëslan, C.G. and Friesen, M.A. 2024:Bedrock mapping in the northwestern Burntwood Lake area, Kisseynew domain, west-central Manitoba (part of NTS 63N7); *in* Report of Activities 2024, Manitoba Economic Development, Investment, Trade and Natural Resources, Manitoba Geological Survey, p. 116–126.

DRI2025011

Whole-rock lithogeochemistry and assays for samples from the Halfway Lake area, Thompson nickel belt, central Manitoba (parts of NTS 63O1, 2)

by C.G. Couëslan and J. Janssens

Microsoft® Excel® file supplements:

Couëslan, C.G. 2023:Logging of archived drillcore and re-interpretation of stratigraphy from the Halfway Lake area, Thompson nickel belt, central Manitoba (parts of NTS 63O1, 2); *in* Report of Activities 2023, Manitoba Economic Development, Investment, Trade and Natural Resources, Manitoba Geological Survey, p. 27–39.

DRI2025012

Whole-rock lithogeochemistry and assays for samples along the eastern margin of the sub-Phanerozoic Thompson nickel belt, central Manitoba (part of NTS 63J3)

by C.G. Couëslan and J. Janssens

Microsoft® Excel® file supplements:

Couëslan, C.G. 2024: Investigation of volcanic rocks along the eastern margin of the sub-Phanerozoic Thompson nickel belt, central Manitoba (part of NTS 63J3); *in* Report of Activities 2024, Manitoba Economic Development, Investment, Trade and Natural Resources, Manitoba Geological Survey, p. 104–115.

DRI2025013

Whole-rock lithogeochemistry of samples from the Suwannee River syenite intrusion, west-central Manitoba (part of NTS 64B4)

by C.G. Couëslan, J. Janssens, T. Martins

Microsoft® Excel® file supplements:

Martins, T. and Couëslan, C.G. 2022: Critical minerals scoping study of the Suwannee River syenite intrusion, west-central Manitoba (part of NTS 64B4); *in* Report of Activities 2022, Manitoba Natural Resources and Northern Development, Manitoba Geological Survey, p. 36–41.

DRI2025014

Lithogeochemistry of samples from the Thompson nickel belt, central Manitoba (parts of NTS 63P5, 12; 63O8)

by C.G. Couëslan and J. Janssens

DRI2025017

Gold, rare element and other indicator-mineral data derived from glacial sediments (till) in between the North Knife River and the Seal River, and in the Gross Lake area, far northeastern Manitoba (parts of NTS 54L10–15, 54M5, 6, 12)

by M.S. Gauthier

Microsoft® Excel® file supplements:

Gauthier, M. S. and Bergen, S. 2024: Quaternary site data, till composition and ice-flow indicators between the North Knife River and the Seal River, and in the Gross Lake area, far northeastern Manitoba (parts of NTS 54L10–15, 54M5, 6, 12); *in* Report of Activities 2024, Manitoba Economic Development, Investment, Trade and Natural Resources, Manitoba Geological Survey, p. 209–218.

Gauthier, M. S. 2025: Field-based ice-flow–indicator data between the North Knife River and the Seal River, and in the Gross Lake area, far northeastern Manitoba (parts of NTS 54L10, 11, 12, 13, 14, 15 and 54M5, 6, 12); Manitoba Business, Mining, Trade and Job Creation, Manitoba Geological Survey, Data Repository Item DRI2025007, Microsoft® Excel® file.

DRI2025015

Geochemistry from the File Lake and Wekusko Lake area (parts of NTS 63K16, 63J13)

by K.D. Reid

Microsoft® Excel® file supplements:

Reid, K.D. 2024: Geochronological update of sedimentary, volcanic and plutonic rocks in the Snow Lake area, north-central Manitoba (parts of NTS 63J13, 63K16); *in* Report of Activities 2024, Manitoba Economic Development, Investment, Trade and Natural Resources, Manitoba Geological Survey, p. 92–97.

DRI2025016

Bedrock geochemistry from Wekusko Lake and Niblock Lake (parts of NTS 63J13, 14)

by K.D. Reid

Microsoft® Excel® file supplements:

Reid, K.D. 2023: Geological investigations in the areas of Niblock Lake and Crowduck Bay (Wekusko Lake), north-central Manitoba (parts of NTS 63J13, 14); *in* Report of Activities 2023, Manitoba Economic Development, Investment, Trade and Natural Resources, Manitoba Geological Survey, p. 64–72.

DRI2025018

Whole rock geochemistry from wall rock and Li-bearing pegmatites from the Cat Lake-Winnipeg River pegmatite field, southeastern Manitoba (parts of NTS 52L6, 11)

by T. Martins, S. Chinaglia and J. Janssens

DRI2025019

Bedrock geochemical data from the Bird River domain, southeastern Manitoba (parts of NTS 52L5, 6, 11, 12)

by M.L. Rinne and T. Martins

Microsoft® Excel® file supplements:

Nambaje, C., Martins, T., McFarlane, C.R.M., Kaczmer, M., Rinne, M.L. and Groat, L. 2024: Preliminary results from field investigations in the Cat Lake–Winnipeg River pegmatite field, southeastern Manitoba (parts of NTS 52L5, 6, 11, 12); *in* Report of Activities 2024, Manitoba Economic Development, Investment, Trade and Natural Resources, Manitoba Geological Survey, p. 10–26.

Martins, T., Rinne, M.L., Breasley, C. and Adediran, H. 2023: Preliminary results from field investigations in the Bird River domain of the Archean Superior province, Manitoba (parts of NTS 52L5, 6, 11, 12); *in* Report of Activities 2023, Manitoba Economic Development, Investment, Trade and Natural Resources, Manitoba Geological Survey, p. 4–13.

DRI2025020

Whole rock geochemistry results from Cretaceous outcrops along the Vermillion River and drill cuttings from an oil well, southwestern Manitoba (parts of NTS 62F11 and 62K16)

by M.P.B. Nicolas and J.D. Bamburak

DRI2025021

Rock Volatiles Stratigraphy data from drill cuttings from four oil wells in southwestern Manitoba (parts of NTS 62K6, 7, 11)

by M.P.B. Nicolas, C.M. Smith and M.P. Smith

Microsoft® Excel® file supplements:

Nicolas, M.P.B., Smith, C.M. and Smith, M.P. 2025: Effects of drill-cutting size and age on the reliability of measuring helium and other volatiles in samples, southwestern Manitoba (parts of NTS 62K6, 7, 11); *in* Report of Activities 2025, Manitoba Business, Mining, Trade and Job Creation, Manitoba Geological Survey, p. 110–119.

DRI2025022

Lithogeochemistry of Precambrian core samples from beneath the Williston Basin, southwestern Manitoba (parts of NTS 62G, J, K, O, 63B, C, G, K)

by M.P.B Smith, D. Coutts and O.H. Ardakani

Microsoft® Excel® file supplements:

Nicolas, M.P.B., Coutts, D. and Ardakani, O.H. 2025: Preliminary investigation into the natural hydrogen generation potential of Precambrian rocks beneath the Williston Basin, southwestern Manitoba (parts of NTS 62G, J, K, O, 63B, C, G, K); *in* Report of Activities 2025, Manitoba Business, Mining, Trade and Job Creation, Manitoba Geological Survey, p. 104–109.

DRI2025023

Lithogeochemistry of the Duperow Formation in the Manitoba Potash Corporation core at 3-29-20-29W1, southwestern Manitoba (part of NTS 62K11)

by P.E. Fraino

Microsoft® Excel® file supplements:

Fraino, P.E. 2025: Pilot study of lithium concentrations in mudstone intervals from the Manitoba Potash Corporation core at 3-29-20-29W1, southwestern Manitoba (part of NTS 62K11); *in* Report of Activities 2025, Manitoba Business, Mining, Trade and Job Creation, Manitoba Geological Survey, p. 128–134.

DRI2025024

Whole-rock lithogeochemistry and assays for samples collected from archived drillcore east of Stephens Lake, northeastern Manitoba (parts of NTS 54C, D)

by J. Macdonald

Microsoft® Excel® file supplements:

Macdonald, J. 2025: Preliminary observations and whole-rock geochemistry of archived drillcore east of Stephens Lake, northeastern Manitoba (parts of NTS 54C, D); *in* Report of Activities 2025, Manitoba Business, Mining, Trade and Job Creation, Manitoba Geological Survey, p. 73–86.

DRI2025025

2024 granular-aggregate field visits—Quaternary site data, sample composition and ice-flow indicators—in southern Manitoba (parts of NTS 62H7, 10, 15, 16, 62I2, 6)

by M.S. Gauthier

Microsoft® Excel® file supplements:

Gauthier, M.S. 2025: Complex Quaternary geology around Grunthal, south-central Manitoba (parts of NTS 62H7); *in* Report of Activities 2025, Manitoba Business, Mining, Trade and Job Creation, Manitoba Geological Survey, p. 181–190.

DRI2025026

Oil and water analysis for one sample of produced fluid, Manson oil field, southwestern Manitoba (part of NTS 62K3)

by P.J. Fulton-Regula

Microsoft® Excel® file supplements:

Fulton-Regula, P.J. 2025: Critical minerals in oil and produced water, Manson oil field, southwestern Manitoba (parts of NTS 62F14, 15, K2, 3); in Report of Activities 2025, Manitoba Business, Mining, Trade and Job Creation, Manitoba Geological Survey, p. 155–161.

DRI2025028

Sieve and geochemical analyses data from samples of the Winnipeg Formation in southern Manitoba (parts of NTS 62H, P)

by V.L. Markstrom

Microsoft® Excel® file supplements:

Markstrom, V.L. 2025: Geochemistry of the Carman Sand and lower unit sand of the Winnipeg Formation, southern Manitoba (parts of NTS 62H, P); *in* Report of Activities 2025, Manitoba usiness, Mining, Trade and Job Creation, Manitoba Geological Survey, p. 120–127.

DRI2025029

Whole-rock lithogeochemistry and assays for drillcore samples from the Halfway Lake area, Thompson nickel belt, central Manitoba (parts of NTS 63O1, 2)

by C.G. Couëslan

Microsoft® Excel® file supplements:

Couëslan, C.G. 2025: Lithogeochemistry and isotopic analyses of rocks from the Halfway Lake area, Thompson nickel belt, central Manitoba (parts of NTS 63O1, 2); in Report of Activities 2025, Manitoba Business, Mining, Trade and Job Creation, Manitoba Geological Survey, p. 33–47.

DRI2025030

Till geochemistry in between the North Knife River and the Seal River, and in the Gross Lake area, far northeastern Manitoba (parts of NTS 54L10–15, 54M5, 6, 12)

by M.S. Gauthier

DRI2025031

Gamma-ray spectrometric data of granitoid rocks and related rocks from the terrane boundary zone between the Bird River and Winnipeg River domains, southeastern Manitoba (parts of NTS 52L3–6, 62I8)

by X.M. Yang, D.R. Lentz and T. Martins

Microsoft® Excel® file supplements:

Yang, X.M., Lentz, D.R. and Martins, T. 2025: Unveiling high-heat–production granites in the terrane boundary zone between the Bird River and Winnipeg River domains, southeastern Manitoba (parts of NTS 52L3–6, 62I8): a gamma-ray spectrometry approach; *in* Report of Activities 2025, Manitoba Business, Mining, Trade and Job Creation, Manitoba Geological Survey, p. 7–19.

GeoFiles

GeoFile 4-2024

Compilation on lithogeochemistry from Precambrian rocks in Manitoba

by Manitoba Geological Survey

GeoFile 8-2024

Manitoba till-matrix geochemistry compilation: visible gold grains in the heavy mineral (<2 mm) size fraction

by M.S. Gauthier

GeoFile 7-2025

Manitoba till-matrix geochemistry compilation: total carbonate of the silt plus clay (<63 µm) size-fraction

by M.S. Gauthier

GeoFile 8-2025

Manitoba till-matrix geochemistry compilation: visible gold grains in the heavy mineral (<2 mm) size fraction

by M.S. Gauthier

GeoFile 2-2025

Manitoba till-matrix geochemistry compilation: silt plus clay (<63 µm) size fraction by inductively coupled plasma–mass spectrometry after an aqua-regia or modified aqua-regia digestion

by M.S. Gauthier

Open Files

OF2024-3

The Tanco pegmatite: geological setting, internal zonation, mineralogy and mining of a world-class rare-element pegmatite deposit

by T. Martins, C. Breasley, L. Groat, R. Linnen, C. Deveau and S. Rankmore

OF20254-5

Palynological analyses of subtill sediments from eleven sites in the western Hudson Bay Lowland region of Manitoba (parts of NTS 54B, 54C, 54E, 54F)

by A.S. Dalton, S.A. Finkelstein, T.J. Hodder and M.S. Gauthier

OF2025-1

Quaternary site, till composition and ice-flow indicator data for the Little Churchill to Churchill rivers area, northeastern Manitoba (part of NTS 54E)

by T.J. Hodder and M.S. Gauthier

OF2025-2

Quaternary site, till composition and ice-flow indicator datasets in the Nelson River Estuary–Black Duck River area, northeastern Manitoba (parts of NTS 54A, B, C, F)

by T.J. Hodder and M.S. Gauthier

EXTERNAL PUBLICATIONS

Breasley, C.M., Martins, T., Linnen, R. L. and Groat, L.A. in press: Compositional evolution of tourmalines and exploration implications in the petalite subtype Prof pegmatite, Revelstoke, British Columbia, Canada; Canadian Journal of Mineralogy and Petrology.

Breasley, C.M., Martins, T., Linnen, R. L., Deveau, C., Groat, L. Al., Koopmans, L., Landry, E. and Moser, D. 2025: The geochemistry, origins and metallurgical implications of different textural types of spodumene-quartz intergrowths (SQUI) from the Tanco pegmatite, Manitoba, Canada; Ore Geology Reviews, URL <https://doi.org/10.1016/j.oregeorev.2025.106577>.

Cawood, T.K., Beyer, S., and Martins, T. 2025: How to form large LCT pegmatites: Clues from the western Superior Province of Canada; Society of Geology Applied to Mineral Deposits biennial meeting, August 3–7, 2025, Colorado, USA, abstract and oral presentation.

Cardenas-Vera, A., Santos, A.C., Bravo, J., Annesley, I.R., Martins, T. and Partin, C.A. 2025: A synthesis of known pegmatite fields in the Wollaston Domain and their REE potential, northern Saskatchewan: what we know and what we aim to know; Geological Association of Canada–Mineralogical Association of Canada, annual meeting 2025, May 11–14, 2025, Ottawa, Ontario, abstract and oral presentation.

Chinaglia, S., Miles, A, Martins, T., Goodenough, K. and Groat, L. 2025: Multi-Stage Fluid Alteration of the Agua Santa Pegmatite (Brazil): Implications for Mineral Zonation and Exploration; Society of Economic Geologists (SEG) conference, September 26–29, 2025, Brisbane, Australia, Abstract and poster presentation.

Chingalia, S., Miles, A., Martins, T., Goodenough, K., and Groat, L. 2025: Insights into the magmatic and metasomatic evolution of the Eagle pegmatite (Manitoba, Canada) from textural analyses; Volcanic and Magmatic Studies Group– Mineral Deposits Studies Group, first joint conference, January 5–9, 2025, Dublin, Ireland, abstract and poster presentation.

Couëslan, C., Martins, T., Chakhmouradian, A., Hnatiuk and T., Friesen, M. 2025: The Trans-Hudson alkaline-carbonatite suite: An alkaline-carbonatite province in the Reindeer zone of Manitoba; Prospectors and Developers Association of Canada, annual convention, March 2–5, 2025, Toronto, Ontario, presentation.

Couëslan, C., Chakhmouradian, A., Martins, T., Hnatiuk, T., Friesen, M. and Böhm, C. 2025: The Trans-Hudson alkaline-carbonatite suite: An alkaline-carbonatite province in the Reindeer Zone of Manitoba; Geological Association of Canada–Mineralogical Association of Canada, annual meeting 2025, annual meeting 2025, May 11–14, 2025, Ottawa, Ontario, abstract and oral presentation.

Dias, F., Ribeiro, R., Gonçalves, F., Lima, A., Roda-Robles, E. and Martins, T. in press: K-Feldspar geochemistry as an indicator of lithium mineralization in the B Barroso–Alvão Aplite-Pegmatite Field, Northern Portugal; Canadian Journal of Mineralogy and Petrology.

Fraino, P. E. and Nicolas, M.P.B. 2025: Carbonate-Evaporite Cycles in the Upper Devonian Duperow Formation: A Geological Framework for Lithium Brine Resource Assessment in Southwestern Manitoba; Canadian Energy Geoscience Association–Canadian Society of Exploration Geophysicists Annual Convention (Geoconvention 2025), May 12–14, 2025, Calgary, Alberta.

Gauthier, M. S., Hodder, T. J., Hathaway, J., Ross, M., Schaarschmidt, M., Lian, O. B. and Finkelstein, S. A. in press: Extending the western Hudson Bay Lowland Quaternary stratigraphy, in Manitoba Canada, to at least Marine Isotope Stage 10; Canadian Journal of Earth Sciences.

Gauthier, M. S., Hodder, T. J., Dalton, A. S., Brewer, V., Lian, O. B., Finkelstein, S. A., Schaarschmidt, M. and Merghetti, A. 2025: South-central Laurentide Ice Sheet dynamics and the formation of proglacial Lake Vita during MIS 3; Quaternary Research, v. 123, p. 83–105, URL <https://doi.org/10.1017/qua.2024.34>.

Groat, L.A., Martins, T. and Linnen, R. 2025: Lithium Resources in Canada; 2025 Goldschmidt Conference, July 6–11, 2025, Prague, Czech Republic, abstract and poster presentation.

Martins, T. 2025: Impact of the TGI programs for the advancement of geological knowledge in Manitoba; Geological Association of Canada–Mineralogical Association of Canada, annual meeting 2025, annual meeting 2025, May 11–14, 2025, Ottawa, Ontario, oral presentation.

Martins, T., McFarlane, C.R.M., Nambaje, C., Roush, J. and Groat, L.A. 2025: Voluminous lithium mineralization in the Cat Lake-Winnipeg River pegmatite field, Manitoba, Canada: insights for its origin and tectonic processes; Goldschmidt Conference, July 6–11, 2025, Prague, Czech Republic, abstract and poster presentation.

McFarlane, C.R.M., Roush, J. and Martins, T. 2025: The role of garnet in LCT pegmatite petrogenesis; Geological Association of Canada–Mineralogical Association of Canada, annual meeting 2025, May 11–14, 2025, Ottawa, Ontario, abstract and oral presentation.

Nambaje, C., McFarlane, C.R.M., Martins, T. Roush, J. and Groat, L.A. 2025: Exploration of rare-element pegmatites: Insights from the Cat Lake-Winnipeg River pegmatite field, Manitoba, Canada; Geological Association of Canada–Mineralogical Association of Canada, annual meeting 2025, May 11–14, 2025, Ottawa, Ontario, abstract and oral presentation.

Nicolas, M.P.B. 2025: Geologic hydrogen potential mapping in Manitoba's sedimentary basins; Canadian Energy Geoscience Association–Canadian Society of Exploration Geophysicists Annual Convention (Geoconvention 2025), May 12–14, 2025, Calgary, Alberta, oral presentation and extended abstract.

Nicolas, M.P.B., Smith, C. and Smith, M. 2025: Understanding the subsurface helium system in Manitoba and evaluating the potential for economic concentrations by analysing entrained volatiles in legacy cuttings; Rocky Mountain Association of Geologists, North American Helium and Hydrogen Conference 2025, April 9-10, 2025, Denver, Colorado, oral presentation and abstract volume.

Nicolas, M.P.B., Smith, C. and Smith, M. 2025: Understanding the subsurface helium system in Manitoba and evaluating the potential for economic concentrations by analysing entrained volatiles in legacy cuttings; Canadian Society of Exploration Geophysicists Annual Convention (Geoconvention 2025), May 12–14, 2025, Calgary, Alberta, oral presentation and extended abstract.

Parsa, M., Lawley, C. J. M., Cawood, T., Martins, T., Cumani, R., Zhang, S.E., Thompson, A., Schetselaar, E, Beyer, S., Lentz, D.R., Harris, J., Fam, H. J. A. and Voinet, A. 2025: Pan-Canadian Predictive Modeling of Lithium-Cesium-Tantalum Pegmatites with Deep Learning and Natural Language Processing; Natural Resources Research, v.34, p. 639–668, URL < https://doi.org/10.1007/s11053-024-10438-x>.

Pastula, C., Partin, C.A., McDonald, B., Hodder, T. and Martins, T. 2025: Using whole rock geochemistry and detrital zircon U-Pb geochronology of the Omarolluk Formation of Nunavut and omars of Manitoba to test the 'omar hypothesis'; Geological Association of Canada–Mineralogical Association of Canada, annual meeting 2025, May 11–14, 2025, Ottawa, Ontario, abstract and oral presentation.

Roda-Robles, E, Garate-Olave, I., Lima, A., Martins, T., Santos-Loyola, N. and Errandonea-Martin, J. 2025: From igneous to hydrothermal stages: Lithium mineralization types in the Central Iberian Zone (Spain & Portugal) and its implications for the European Variscan Belt; Goldschmidt Conference, July 6–11, 2025, Prague, Czech Republic, abstract and keynote presentation.

Roush, J., McFarlane, C.R.M., Martins and Groat, L.A. 2025: Monazite and holmquistite from host rock at the Eagle Pegmatite, Cat Lake pegmatite field, southeastern Manitoba – Evidence of exsolved pegmatitic fluids and metasomatism; Geological Association of Canada–Mineralogical Association of Canada, annual meeting 2025, May 11–14, 2025, Ottawa, Ontario, abstract and poster presentation.

Santos, A.C., Cardenas-Vera, A., Bravo, J., Annesley, I.R., Martins, T. and Partin, C.A. 2025: Towards understanding enrichment mechanisms of REE-bearing pegmatites at Fraser Lakes Zone B and Kulyk Lake in northern Saskatchewan, Canada; Geological Association of Canada–Mineralogical Association of Canada, annual meeting 2025, May 11–14, 2025, Ottawa, Ontario, abstract and oral presentation.

Silva, D., Groat, L.A., Martins, T. and Linnen, R. 2025: Unusual K/Rb and Li-Rb-Cs trends in muscovite and feldspars indicate multi-stage anatectic origin for pegmatites in the Wekusko Lake pegmatite field, central Manitoba, Canada; Goldschmidt Conference, July 6–11, 2025, Prague, Czech Republic, abstract and oral presentation.

Silva, D., Groat, L. Martins, T. and Linnen, R. 2025: Magmatic and tectonic controls on crystal fabric in spodumene-rich pegmatites: a case study from Wekusko Lake, Manitoba, Canada; Volcanic and Magmatic Studies Group– Mineral Deposits Studies Group, first joint conference, January 5–9, 2025, Dublin, Ireland, abstract and oral presentation.

Strong, J.W.D., Couëslan, C.G., McFarlane, C.R.M., Ross, K., Marsh, J., Simmons, J. and Thurston, P. 2025: Crustal reworking and Eo-Paleoarchean metamorphism of the northern Pikwitonei domain, Superior Province: U-Pb-Hf-TE analysis of 3.9–3.2 Ga detrital zircon; Chemical Geology, v. 690, art. 122886, URL <https://doi.org/10.1016/j.chemgeo.2025.122886>.

Yang, X.M. 2025: Fertility of gabbroic intrusions in the Paleoproterozoic Lynn Lake Greenstone Belt, Manitoba, Canada: Insights from field relationships, geochemical and metallogenic characteristics; Minerals, v. 15, art. 448, URL <https://doi.org/10.3390/min15050448> [May 2025].

Yang, X.M., Lentz, D.R., Yousefi, F. and Lawley, C.J.M. 2025: Linking Alkali-Lime Index (ALI) to Rittmann Serial Index (s): Insights into magmatic alkalinity and petrogenesis of alkaline rocks [abstract]; Geological Association of Canada–Mineralogical Association of Canada, Joint Annual Meeting, Ottawa, Ontario, May 11–14, 2025, program with abstracts, oral presentation; Geoscience Canada, v. 52, p. 261, URL <https://doi.org/10.12789/geocanj.2025.52.223> [September 2025].

Yousefi, F., Lentz, D.R. and Yang, E. 2025a: Geochemical Characteristics of Pantellerite and Comendite: Insights into petrogenesis and metallogenesis of peralkaline A-type granites with implications for their sources [abstract]; Geological Association of Canada–Mineralogical Association of Canada, Joint Annual Meeting, Ottawa, Ontario, May 11–14, 2025, Program with Abstracts, oral presentation; Geoscience Canada, v. 52, p. 263, URL < https://doi.org/10.12789/geocanj.2025.52.223> [September 2025].

Yousefi, F., Lentz, D.R. and Yang, X.M. 2025b: Petrogenesis and geochemical features of peralkaline A-type granites: reconciling insights from comendite and pantellerite - peralkaline rhyolitic systems [abstract]; Goldschmidt 2025 Conference, Prague, the Czech Republic, July 6–11, 2025, program with abstracts, poster presentation, URL <https://conf.goldschmidt.info/goldschmidt/2025/meetingapp.cgi/Paper/29781> [August 2025].